ROOT ADAPTATIONS TO MULTIPLE STRESS FACTORS

EDITED BY: Idupulapati Madhusudana Rao, Zhi Chang Chen and Manny Delhaize
PUBLISHED IN: Frontiers in Plant Science

frontiers Research Topics

frontiers

ISSN 1664-8714
ISBN 978-2-88966-514-3
DOI 10.3389/978-2-88966-514-3

About Frontiers

Frontiers is more than just an open-access publisher of scholarly articles: it is a pioneering approach to the world of academia, radically improving the way scholarly research is managed. The grand vision of Frontiers is a world where all people have an equal opportunity to seek, share and generate knowledge. Frontiers provides immediate and permanent online open access to all its publications, but this alone is not enough to realize our grand goals.

Frontiers Journal Series

The Frontiers Journal Series is a multi-tier and interdisciplinary set of open-access, online journals, promising a paradigm shift from the current review, selection and dissemination processes in academic publishing. All Frontiers journals are driven by researchers for researchers; therefore, they constitute a service to the scholarly community. At the same time, the Frontiers Journal Series operates on a revolutionary invention, the tiered publishing system, initially addressing specific communities of scholars, and gradually climbing up to broader public understanding, thus serving the interests of the lay society, too.

Dedication to Quality

Each Frontiers article is a landmark of the highest quality, thanks to genuinely collaborative interactions between authors and review editors, who include some of the world's best academicians. Research must be certified by peers before entering a stream of knowledge that may eventually reach the public - and shape society; therefore, Frontiers only applies the most rigorous and unbiased reviews.
Frontiers revolutionizes research publishing by freely delivering the most outstanding research, evaluated with no bias from both the academic and social point of view. By applying the most advanced information technologies, Frontiers is catapulting scholarly publishing into a new generation.

What are Frontiers Research Topics?

Frontiers Research Topics are very popular trademarks of the Frontiers Journals Series: they are collections of at least ten articles, all centered on a particular subject. With their unique mix of varied contributions from Original Research to Review Articles, Frontiers Research Topics unify the most influential researchers, the latest key findings and historical advances in a hot research area! Find out more on how to host your own Frontiers Research Topic or contribute to one as an author by contacting the Frontiers Editorial Office: frontiersin.org/about/contact

ROOT ADAPTATIONS TO MULTIPLE STRESS FACTORS

Topic Editors:
Idupulapati Madhusudana Rao, International Center for Tropical Agriculture (CIAT), Colombia
Zhi Chang Chen, Fujian Agriculture and Forestry University, China
Manny Delhaize, Australian National University, Australia

Citation: Rao, I. M., Chen, Z. C., Delhaize, M., eds. (2021). Root Adaptations to Multiple Stress Factors. Lausanne: Frontiers Media SA.
doi: 10.3389/978-2-88966-514-3

Table of Contents

frontiers in Plant Science

EDITORIAL
published: 15 January 2021
doi: 10.3389/fpls.2020.626960

Editorial: Root Adaptations to Multiple Stress Factors

Idupulapati Madhusudana Rao[1,2]*, *Emmanuel Delhaize*[3†] *and Zhi Chang Chen*[4]

[1] International Center for Tropical Agriculture (CIAT), Cali, Colombia, [2] International Centre of Insect Physiology and Ecology (icipe), Nairobi, Kenya, [3] Commonwealth Scientific and Industrial Research Organisation (CSIRO) Agriculture and Food, Canberra, ACT, Australia, [4] Root Biology Center, Fujian Agriculture and Forestry University, Fuzhou, China

Keywords: abiotic stress, metabolic changes, gene regulation, protein regulation, root architecture, root plasticity, deep rooting, yield

Editorial on the Research Topic

Root Adaptations to Multiple Stress Factors

The unfavorable soil (low supply of nutrients, high levels of toxic elements, salinity, compaction) and climatic (drought, waterlogging, high temperature, low temperature) conditions reduce plant and crop productivity (Pereira, 2016). Low fertility soils, and extreme weather events resulting from climate change, are a major threat to global food security (Evans, 2009). Plants have evolved sophisticated adaptive mechanisms to withstand the multiple abiotic stresses to which they are exposed (Lamers et al., 2020).

Most studies on plant adaptation to abiotic stress conditions are undertaken by applying a single stress condition and analyzing the different physiological, biochemical and molecular aspects of plant acclimation (Araújo et al., 2015). This contrasts to the conditions that occur in nature where crops and other plants are routinely subjected to a combination of different abiotic stresses (Mittler, 2006). A good example of combined soil stress is the co-occurrence of aluminum (Al) toxicity and phosphorus (P) deficiency in acid soils, particularly in the tropics (Rao et al., 2016). An example of a combined climatic stress is the co-occurrence of drought and heat stresses during summer (Hammer et al., 2020). The effect of combined stress factors on crops and plants is not always additive due to the nature of interactions between the stress factors which dictate the final outcome (Mickelbart et al., 2015; Magalhaes et al., 2018).

Plants depend on their root system responses for their survival in nature, and their yield and nutritional quality in agriculture (Gregory et al., 2009). Root systems are complex, and a variety of traits have been identified over the past decade that contribute to adaptation to multiple stress factors (Chen et al., 2019; Lynch, 2019). As an example of research on multiple stresses, recent studies now suggest that Al resistance can exert pleiotropic effects on P acquisition, potentially expanding the role of Al resistance on plant adaptation to acid soils (Magalhaes et al., 2018). Thus, pleiotropy could be a genetic linkage between Al resistance and low P tolerance. Understanding the mechanisms by which plants adapt to combined stress factors is critical for creating efficient genetic and agronomic strategies to develop cultivars for the sustainable intensification of production systems for meeting the growing demand for food.

This e-book on the Research Topic of "Root Adaptations to Multiple Stress Factors" contains 11 articles that addressed the way root systems respond to individual and combined abiotic stress factors, including soil and climatic stress conditions. It includes studies focused on the adaptations occurring in roots from the molecular, biochemical, physiological, morphological to agroecological levels that contribute to plant performance and crop yield.

OPEN ACCESS

Edited by:
Honghong Wu,
Huazhong Agricultural University, China

Reviewed by:
Jian Sun,
Jiangsu Normal University, China
Lan Zhu,
Huazhong Agricultural University, China

****Correspondence:***
Idupulapati Madhusudana Rao
i.rao@cgiar.org

†Present address:
Emmanuel Delhaize,
Research School of Biology, Australian National University, Canberra, ACT, Australia

Specialty section:
This article was submitted to Plant Abiotic Stress, a section of the journal Frontiers in Plant Science

Received: *07 November 2020*
Accepted: *16 December 2020*
Published: *15 January 2021*

Citation:
Rao IM, Delhaize E and Chen ZC (2021) Editorial: Root Adaptations to Multiple Stress Factors. Front. Plant Sci. 11:626960. doi: 10.3389/fpls.2020.626960

MULTIPLE STRESS TOLERANCE IN ACID SOILS

On tropical, acidic soils, Al toxicity, low P availability and drought stress are the major limitations to yield stability. Molecular breeding based on a small suite of pleiotropic genes, particularly those with moderate to major phenotypic effects, could help circumvent the need for complex breeding designs and large population sizes aimed at selecting transgressive progeny accumulating favorable alleles controlling polygenic traits. The underlying question is two-fold: do common tolerance mechanisms to Al toxicity, P deficiency and drought exist? And if they do, will they be useful in a plant breeding program that targets stress-prone environments. Barros et al. critically reviewed the literature and found candidate signaling and/or regulatory proteins that may play a role in regulating plant adaptations to Al toxicity, P deficiency and drought stress.

SINGLE OR MULTIPLE ABIOTIC STRESS FACTORS

Using RNA-seq, Ojeda-Rivera et al. performed a transcriptional dissection of wild-type and *stop1* root responses, individually or in combination, to toxic levels of Al^{3+}, low P availability, low pH and iron (Fe) excess. They found that the level of STOP1 is post-transcriptionally and coordinately upregulated in the roots of seedlings exposed to single or combined stresses. The accumulation of STOP1 correlated with the transcriptional activation of stress-specific and common gene sets that are activated in the roots of wild-type seedlings but not in *stop1* mutant. Results from this study suggested that perception of different environmental cues converges in at two levels via STOP1 signaling: post-translationally through the regulation of STOP1 turnover, and transcriptionally, via the activation of STOP1-dependent gene expression pathways that enables the root to better adapt to abiotic stress factors present in acidic soils.

ALUMINUM AND PROTON RHIZOTOXICITIES

Al and proton rhizotoxicities are major stresses of acid soil syndrome that limit world food production. Although Al and proton rhizotoxicities are co-existing in acid soils, it remains unclear about the relationship between genetic architecture and their regulated molecular mechanisms for adapting to acid soil. Nakano et al. provided a new insight into the genetic architecture that is complex and distinct in regulation of Al and proton tolerance. They used integrated analyses of genome-wide association study (GWAS), genomic prediction (GP) and co-expression genes network analyses and successfully identified multiple loci controlling each tolerance. This study also showed that rare-allele mutations are more important for generating Al tolerance variation than for proton tolerance variation.

HEAT, DROUGHT, AND SALINITY STRESS TOLERANCE

Velinov et al. described the role of an undescribed homolog of the *Aspergillus nidulans* NudC gene, named *NMig1* (for Nuclear Migration 1), in the root growth and multiple abiotic stress tolerance of *Arabidopsis thaliana*. Transgenic plants overexpressing *NMig1* had enhanced root growth and branching, and accumulate less reactive oxygen species under heat shock, drought and high salinity. This study provided novel insights into the role of NudC family in the protection of plants against abiotic stress. The authors suggested that the NudC genes could be considered as potentially important target genes in breeding more resilient crops with improved root architecture under abiotic stress. Zhao et al. performed a comprehensive analysis of the Ankyrin-repeat (ANK) gene family in soybean and included a phylogenetic tree, a description of the chromosomal localizations and gene structures. By analyzing the expression profiles of these genes, *GmANK114* was found to be highly induced by drought, salt, and abscisic acid in soybean. They further demonstrated that the over-expression of *GmANK114* in both Arabidopsis and soybean confers drought and salt tolerance.

LOW NITROGEN AND LOW PHOSPHORUS STRESS

Nitrogen (N) and phosphorus (P) are two major limiting factors for plant growth and development. The lack or excess of these two elements leads to morphological and metabolic alterations in root, yet the physiological and molecular mechanisms remain widely unexplored. Nadeem et al. reviewed the advances in abiotic stress responses of foxtail millet with a focus on its low N and low P adaptive responses in comparison to other crops. Foxtail millet is a drought tolerant crop but it responds to low N by developing a smaller root system and to low P by developing a larger root system. This unique response of foxtail millet is completely different to what is reported from studies on maize, rice, or other cereals and highlights that species can differ markedly from one another in their responses to nutrient stress.

LOW PHOSPHORUS TOLERANCE

Low P availability limits crop growth and yield on acid soils. It is well-known that root-associated acid phosphatases (APase) play an important role in extracellular organic P utilization. Zhu et al. investigated the dynamic changes of intracellular and root-associated APase activities under both Pi sufficient and deficient conditions. They identified 38 GmPAP genes in soybean and found that the expression of GmPAP7a and GmPAP7b were highly induced by Pi starvation in both roots and leaves, indicating that these two PAPs play key role in adaptation responses of soybean under Pi starvation.

WELL-WATERED AND WATER STRESSED

A generalized response of plant tissues to various biotic and abiotic stresses, including water stress, is the accumulation of reactive oxygen species, but their role in stress adaptation is not well-understood. Combining spatial growth analysis within the growth zone of well-watered and water-stressed maize primary roots with manipulation of levels of reactive oxygen species (using transgenic and biochemical approaches), Voothuluru et al. showed that apoplastic reactive oxygen species regulate cell production and root elongation in both well-watered and water-stressed conditions. They also demonstrated that the normally regulated increase in apoplastic H_2O_2 in water-stressed roots is causally related to down-regulation of cell production and root elongation.

COMBINED ARSENIC AND HYPOXIA STRESS

Kumar et al. tested the effect of individual and combined stress factors of hypoxia and arsenic (As) stress on root architecture of Arabidopsis. They found that the severe but reversible root growth arrest under stress, is linked to massive nutritional disorder, in particular P deficiency, and profound changes in transcripts related to the maintenance of the root apical meristem and root hair development. They suggested a scenario of how the root growth arrest and acclimation develops which later on upon reaeration allows for resumption of root growth.

MONITORING ROOT GROWTH *IN SITU*

Root studies are usually cumbersome and labor intensive and most of the existing methodologies are destructive and when *in situ*, are very expensive. Currently, the progress in developing sensors and sensing platforms has empowered us to collect much more root phenotypic data than what was possible just a few years ago. The novel Rootsnap sensor platform and the methods reported by Ahmed et al. are important tools for an enhanced capability in remotely measuring root traits. The developed Rootsnap sensor presents an easily assembled and cost-effective means of monitoring root growth *in situ*. The authors found a significant positive correlation of root length density estimates from this method compared with a root scanning method.

ROOT PLASTICITY

Root phenotypic plasticity has been proposed as a target for the development of more productive crops in variable environments. However, the plasticity of root anatomical and architectural responses to environmental cues is highly complex, and the consequences of these responses for plant fitness are poorly understood. Schneider and Lynch reviewed the published work on root phenotypic plasticity and indicated that it is dependent on specific agro-ecologies and management practices. The genetic control of plasticity is in general highly quantitative and is dependent on many loci having small effects. Further research efforts are needed to understand the fitness landscape of plastic responses including understanding plasticity in different environments, environmental signals that induce plastic responses, and the genetic architecture of plasticity before it is widely adopted in breeding programs.

CONCLUSION

Major advances have been made in the elucidation of root adaptive responses to individual and combined abiotic stress factors. Identification of *bona fide* molecular mechanisms responsible for combined stress factors is an important step in further identification of genes responsible and breeding of crops with improved resistance to multiple abiotic stress factors that are prevalent in low fertility soils of the tropics that are exposed frequently to unfavorable climatic conditions. Improved knowledge of how roots adapt to multiple stresses will allow researchers to define what is required at the root-soil interface for crops to tolerate the challenges imposed by these multiple stresses.

AUTHOR CONTRIBUTIONS

IR was the main contributor while ZC and ED helped revise the editorial. All authors contributed to the article and approved the submitted version.

ACKNOWLEDGMENTS

We are grateful to authors, reviewers, and the Frontiers Editorial Office for their contribution in creating the e-book on this Research Topic.

REFERENCES

Araújo, S. S., Beebe, S., Crespi, M., Delbreil, B., González, E. M., Gruber, V., et al. (2015). Abiotic stress responses in legumes: Strategies used to cope with environmental challenges. *Crit. Rev. Plant Sci.* 34, 237–280. doi: 10.1080/07352689.2014.898450

Chen, Y., Palta, J. A., Wu, P., and Siddique, K. H. M. (2019). Crop root systems and rhizosphere interactions. *Plant Soil* 439, 1–5. doi: 10.1007/s11104-019-04154-2

Evans, L. T. (2009). *The Feeding of the Nine Billion: Global Food Security for the 21st Century*. London: Chatham House.

Gregory, P. J., Bengough, A. G., Grinev, D., Schmidt, S., Thomas, W. B., Wojciechowski, T., et al. (2009). Root phenomics of crops: opportunities and challenges. *Funct. Plant Biol.* 36, 922–929. doi: 10.1071/FP09150

Hammer, G., Mc Lean, G., van Oosterom, E., Chapman, S., Zheng, B., Wu, A., et al. (2020). Designing crops for adaptation to the drought and high-temperature risks anticipated in future climates. *Crop Sci.* 60, 605–621. doi: 10.1002/csc2.20110

Lamers, J., van der Meer, T., and Testerink, C. (2020). How plants sense and respond to stressful environments. *Plant Physiol.* 182, 1624–1635. doi: 10.1104/pp.19.01464

Lynch, J. (2019). Root phenotypes for improved nutrient capture: an underexploited opportunity for global agriculture. *New Phytol.* 223, 548–564. doi: 10.1111/nph.15738

Magalhaes, J. V., Pineros, M. A., Maciel, L. S., and Kochian, L. V. (2018). Emerging pleiotropic mechanisms underlying aluminum resistance and phosphorus acquisition on acidic soils. *Front. Plant Sci.* 9:1420. doi: 10.3389/fpls.2018.01420

Mickelbart, M. V., Hasegawa, P. M., and Bailey-Serres, J. (2015). Genetic mechanisms of abiotic stress tolerance that translate to crop yield stability. *Nat. Rev. Genet.* 16, 237–251. doi: 10.1038/nrg3901

Mittler, R. (2006). Abiotic stress, the field environment and stress combination. *Trends Plant Sci.* 11, 15–19. doi: 10.1016/j.tplants.2005.11.002

Pereira, A. (2016). Plant abiotic stress challenges from the changing environment. *Front. Plant Sci.* 7:1123. doi: 10.3389/fpls.2016.01123

Rao, I. M., Miles, J. W., Beebe, S. E., and Horst, W. J. (2016). Root adaptations to soils with low fertility and toxicities. *Ann. Bot.* 118, 593–605. doi: 10.1093/aob/mcw073

Conflict of Interest: The authors declare that the research was conducted in the absence of any commercial or financial relationships that could be construed as a potential conflict of interest.

frontiers in Plant Science

REVIEW
published: 28 February 2020
doi: 10.3389/fpls.2020.00187

Adaptation of Foxtail Millet (*Setaria italica* L.) to Abiotic Stresses: A Special Perspective of Responses to Nitrogen and Phosphate Limitations

*Faisal Nadeem[1], Zeeshan Ahmad[1], Mahmood Ul Hassan[1], Ruifeng Wang[1], Xianmin Diao[2] and Xuexian Li[1]**

[1] MOE Key Laboratory of Plant-Soil Interactions, Department of Plant Nutrition, China Agricultural University, Beijing, China, [2] Institute of Crop Sciences, Chinese Academy of Agricultural Sciences, Beijing, China

OPEN ACCESS

Edited by:
Zhichang Chen, Fujian Agriculture and Forestry University, China

Reviewed by:
Mian Gu, Nanjing Agricultural University, China
Jiang Tian, South China Agricultural University, China

***Correspondence:**
Xuexian Li
steve@cau.edu.cn

Specialty section:
This article was submitted to Plant Abiotic Stress, a section of the journal Frontiers in Plant Science

Received: *11 December 2019*
Accepted: *07 February 2020*
Published: *28 February 2020*

Citation:
Nadeem F, Ahmad Z, Ul Hassan M, Wang R, Diao X and Li X (2020) Adaptation of Foxtail Millet (Setaria italica L.) to Abiotic Stresses: A Special Perspective of Responses to Nitrogen and Phosphate Limitations. Front. Plant Sci. 11:187. doi: 10.3389/fpls.2020.00187

Amongst various environmental constraints, abiotic stresses are increasing the risk of food insecurity worldwide by limiting crop production and disturbing the geographical distribution of food crops. Millets are known to possess unique features of resilience to adverse environments, especially infertile soil conditions, although the underlying mechanisms are yet to be determined. The small diploid genome, short stature, excellent seed production, C_4 photosynthesis, and short life cycle of foxtail millet make it a very promising model crop for studying nutrient stress responses. Known to be a drought-tolerant crop, it responds to low nitrogen and low phosphate by respective reduction and enhancement of its root system. This special response is quite different from that shown by maize and some other cereals. In contrast to having a smaller root system under low nitrogen, foxtail millet enhances biomass accumulation, facilitating root thickening, presumably for nutrient translocation. The low phosphate response of foxtail millet links to the internal nitrogen status, which tends to act as a signal regulating the expression of nitrogen transporters and hence indicates its inherent connection with nitrogen nutrition. Altogether, the low nitrogen and low phosphate responses of foxtail millet can act as a basis to further determine the underlying molecular mechanisms. Here, we will highlight the abiotic stress responses of foxtail millet with a key note on its low nitrogen and low phosphate adaptive responses in comparison to other crops.

Keywords: foxtail millet, abiotic stresses, nitrogen limitation, phosphate starvation, transporter

INTRODUCTION

Abiotic and biotic environmental stresses reduce plant growth and yield below optimum levels. According to an FAO report released in 2007, only 3.5% of the global area is not affected by environmental constraints, contributing to 50–70% of crop yield reduction (Boyer, 1982; Mittler, 2006). Being sessile in nature, plants encounter these environmental challenges while obtaining

the carbon, water, and nutrients necessary for development, growth, and biomass production. The dynamic and complex responses of plants to abiotic stresses can be elastic (reversible) or plastic (irreversible) (Cramer, 2010; Skirycz and Inze, 2010). Plant growth is based on cell proliferation, which requires the persistent availability of nutrients, water, and energy; hence, plants survive through acclimatory responses to nutrient, water, light, and temperature fluctuations.

Roots are vital for optimum crop production because, as well as their water and nutrient uptake functionality, they provide anchorage of plants to soils, store essential elements, and have symbiotic relationships with microorganisms present in the rhizosphere (Bechtold and Field, 2018). Drought, soil salinity, and nutrient toxicity and deficiency are frequent stresses directly encountered by plant roots, leading them to modify or alter their growth as per environmental signaling. The geochemical processes of rock weathering replenish soils with nutrients, except for nitrogen, which originates primarily from atmospheric nitrogen (N) fixation. The natural impoverishment of some nutrients leads to their deficiencies in soils. Nutrient limitation is a limiting factor in crop growth and production that originates from a combination of natural and anthropogenic processes (Sanchez and Salinas, 1981; Giehl and von Wirén, 2014).

N is an important macronutrient governing crop productivity through the regulation of growth and development. N exists in soils heterogeneously, either as inorganic forms, i.e., nitrate and ammonium, or organic forms, like amino acids, peptides, and lipids. Organic forms of nitrogen persist in specific habitats such as boreal and tropical ecosystems. Nitrate and ammonium are the predominant forms of N in most soils, and their availability is controlled by soil physical properties, leaching, and microbial activities, more often than not resulting in formation of N-depletion zones in soils (Miller and Cramer, 2004; Jones and Kielland, 2012; Werdin-Pfisterer et al., 2012); upon N limitation, plants develop physiological alterations to enhance nitrogen acquisition (Good et al., 2004; Hermans et al., 2006; Nacry et al., 2013) or farmers apply synthetic fertilizers to ensure yield. The latter often leads to the deterioration of soil physical properties on the one hand, whereas it results in N losses through leaching (polluting ground-water reservoirs), runoff (deposition in fresh-water bodies, causing eutrophication), NH_3-volatilization, and denitrification on the other hand. Excessive N deposition negatively influences air quality and ecosystem health by impacting human health, unbalancing greenhouse gas emissions, disturbing soil and water chemistry, and narrowing biological diversity (Tilman et al., 2006; Guo et al., 2009; Sutton et al., 2011; Stevens et al., 2015; Liu et al., 2016). Hence, to counter (1) environmental risks and economic losses associated with N-fertilization, and (2) the scarcity of N in natural soils, it is worth investigating the morphological, physiological, and molecular adaptive alterations adopted by plants to survive in N-limiting environments.

Phosphorus (P), a key component of nucleic acid and phospholipids, is another macronutrient that is essential for plant growth and development. It exists in soils either as inorganic phosphorus (Pi) interacting strongly with divalent and trivalent cations or as organophosphates releasing phosphorus for root uptake upon hydrolysis. In traditional agricultural systems, farmers either rely on the inherent fertility of the soil or the addition of manures and phosphate fertilizers to supply Pi for plant growth (Syers et al., 2008). However, the acquisition of phosphorus from soils is challenging for plants because of the low solubility of phosphates of aluminum, iron, and calcium (Schachtman et al., 1998). Pi also has high sorption capacity to soil particles; thus, its uptake by plants depends upon their ability to find immobile Pi in soils. Hence, the unavailability of P in soils and agricultural intensification have resulted in a dependency on the application of Pi fertilizers to increase crop yield (Cordell et al., 2009).

Different plants have evolved differential responses to cope with N, P, and other abiotic stresses. Research on the abiotic stress responses of plants has come to the forefront but now needs to be extended beyond maize, rice, wheat or *Arabidopsis thaliana* to enhance crop diversity. Foxtail millet (*Setaria italica* L.), thought to be native of South Asia, is one of the oldest cultivated millets around the globe. The cultivation of foxtail millet for human consumption dates back to 4000 years ago (Baltensperger, 1996). China, Russia, India, Africa, and the United States are the regions where it is widely grown. It is being cultivated for food and fodder throughout Eurasia and the Far East. It is primarily grown for hay in the United States and can produce 2.47–8.65 tones ha^{-1} aboveground biomass (Schonbeck and Morse, 2006). Its C/N ratio is 44, and it contains 48 kg ha^{-1} N in aboveground biomass (Creamer and Baldwin, 1999). It produces high yield with low levels of prussic acid (Sheahan, 2014). In contrast to other millets, foxtail millet can be grown in cooler and droughty regions in spite of having a shallow root system (Hancock Seed, 2014). It is a water-efficient crop: it requires 1/3 less water than maize and can produce one ton of forage in 2½ inch moisture (Koch, 2002). Foxtail millet is also a preferred choice for the restoration of steep slopes or mine lands because it grows fast and produces more biomass than annual rye (Burger et al., 2009).

Since the release of genome sequences of foxtail millet by the Joint Genome Institute (JGI) of the United States Department of Energy, the importance of this species has been increasingly growing. Owing to its close relationship with bioenergy crops like switch grass (*Panicum virgatum*), Napier grass (*Pennisetum purpureum*), and pearl millet (*Pennisetum glaucum*), foxtail millet is also considered as a model system for biofuel grasses (Doust et al., 2009). Bennetzen et al. (2012) and Zhang et al. (2012) have compiled two full reference genome sequences along with high-density linkage maps with another foxtail millet line and green foxtail and have examined the evolution and mechanisms of C_4 photosynthesis in foxtail millet. The availability of the foxtail millet genome provides an important resource for studying C_4 photosynthesis in the context of carbon, N, and P metabolism and nutrient use efficiency. The molecular basis of drought tolerance can also be investigated through drought-associated genes (Zhang et al., 2012). Intensive studies are expected to be conducted on foxtail millet as a model crop for plant nutrient use efficiency, which may benefit agricultural sustainability and food security by enhancing crop diversity (Doebley, 2006). Therefore, the current review will be focusing on

the abiotic stress responses of foxtail millet, with special emphasis on its responses to low N and Pi (**Figure 1**).

FOXTAIL MILLET: A MODEL CROP FOR STRESS BIOLOGY

Foxtail millet is a herbicide (Zhu et al., 2006) and is a drought and salt-tolerant crop (Jayaraman et al., 2008; Krishnamurthy et al., 2014; Sudhakar et al., 2015). Foxtail millet produces 1 g of dry mass at the cost of 257 g of water, which is far less than that required by maize and wheat (Li and Brutnell, 2011). Auxin response factors (ARFs) regulate embryogenesis, leaf expansion and senescence, and lateral root and fruit development by controlling the expression of auxin response genes (Wilmoth et al., 2005). Since ARF1 isolation (Regad et al., 1993), ARFs have been identified in plant species like *Arabidopsis,* rice, tomato, potato, maize, carrot, wheat, tobacco, and barley. In maize, ARF proteins are involved in the transformation of lipid composition indirectly (Verwoert et al., 1995), and overexpression of *ZmARF1* in *Arabidopsis* enhances growth rates by increasing leaf and seed size (Yuan et al., 2013). Similarly, overexpression of *ZmARF2* in *Arabidopsis* produces larger leaves and seeds and taller plants due to enhanced cell expansion (Wang et al., 2012). ARF proteins play roles in biotic and abiotic stress tolerance in crop plants. Identification of ARF/ARL gene family members in foxtail millet and rice, together with characterization of their structure, organization, duplication and divergence and expression patterns in different tissues, has been reported (Muthamilarasan et al., 2016). A total of 25 ARF genes were identified in foxtail millet diverged from a common ancestor. More efforts are required to investigate ARF genes in specific tissue under a specific stress condition to gain clear clues on tissue-specific and/or stress-inducible promoters. WRKYs are one of the largest transcription factor families and contain W-box in their promoter region to control gene expression and regulation in plants (Eulgem et al., 2000). Comprehensive computational approaches have also been used to identify WRKY genes in foxtail millet. Differential expression patterns of candidate *SiWRKY* genes under abiotic stresses suggest their stress-related regulatory functions (Muthamilarasan et al., 2015).

Foxtail millet responds to abiotic stresses through enhanced biochemical activities like higher levels of antioxidants, reactive oxygen species, and their scavenging enzymes, enzyme activities of catalase and superoxides, and synthesis of osmolytes and their stress-related proteins (Lata et al., 2011b). Aldo-Keto reductases (AKRs) are known to be cytosolic, monomeric oxidoreductases catalyzing NADPH-dependent reduction activities on carbonyl

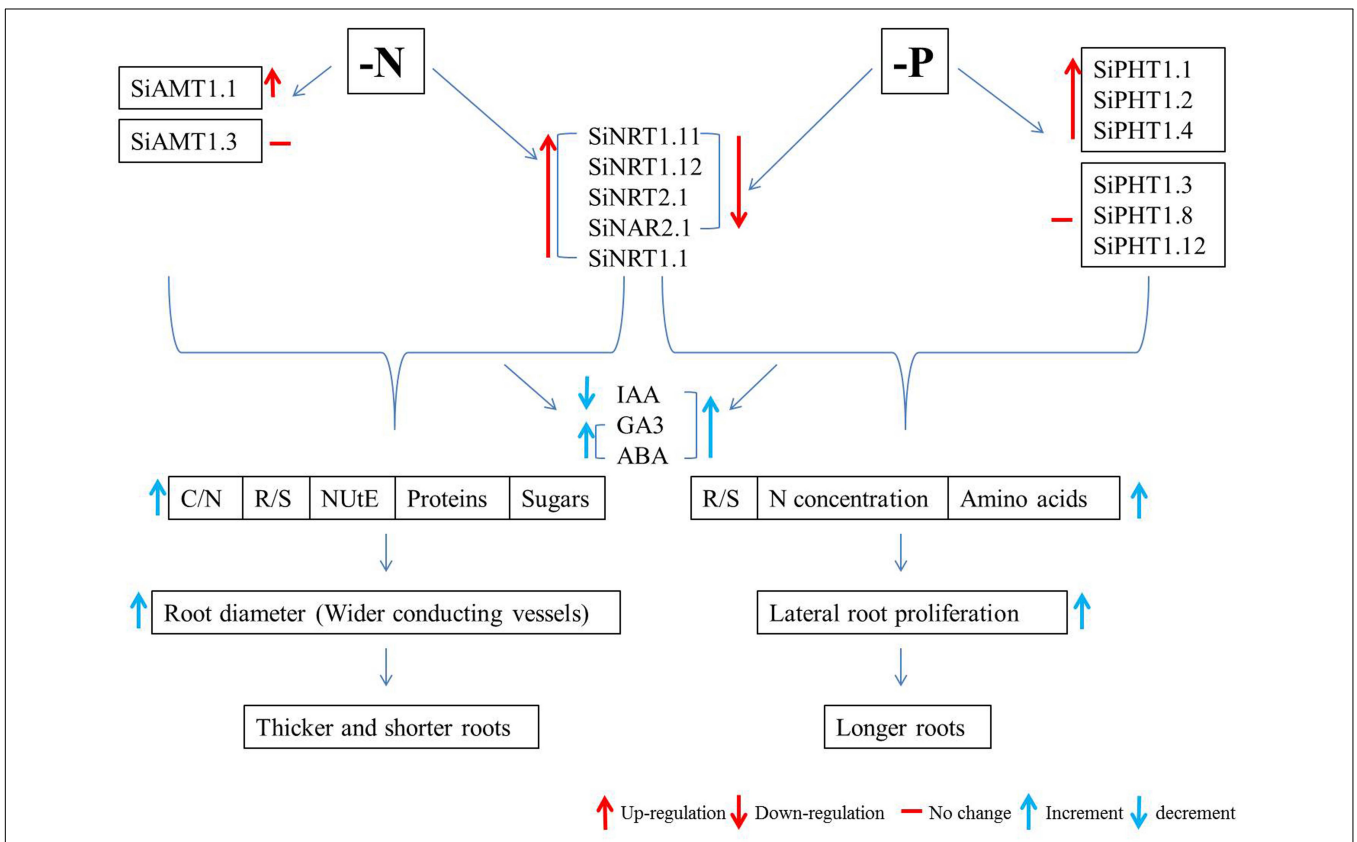

FIGURE 1 | Flow chart of the nitrogen- and phosphorus-limitation responses of foxtail millet. Si, *Sitaria italica*; AMT, ammonium transporter; NRT, nitrate transporter; NAR, nitrate assimilation-related protein; PHT, phosphate transporter; IAA, indole-3-acetic acid; GA3, gibberellic acid; ABA, abscisic acid; C/N, carbon to nitrogen ratio; R/S, root to shoot ratio; NUtE, nitrogen utilization efficiency; N, nitrogen.

metabolites (Bohren et al., 1989). A broad range of substrates like sugars, prostaglandins, chalcones, aliphatic/aromatic aldehydes, and some toxins can be metabolized by AKRs (Narawongsanont et al., 2012). AKRs are also known for their effective detoxification of reactive carbonyls produced during severe oxidative stress. AKR (*MsALR*) proteins in transgenic tobacco plants improve tolerance against methylviologen, heavy metals, osmotic stress, and long periods of oxidative stresses induced by drought (Oberschall et al., 2000), cold (Hegedus et al., 2004), and UV radiation (Hideg et al., 2003). In tobacco plants, heterologous expression of *OsAKR1* shows better tolerance against heat (Turoczy et al., 2011). Overexpression of *Arabidopsis* AKR4C9 in barley enhances freezing tolerance and post-frost regenerative capacity (Eva et al., 2014). Moreover, overexpression of peach AKR1 (*PpAKR1*) in *Arabidopsis* enhances salt tolerance compared to wild type plants (Kanayama et al., 2014). In contrast, *GmAKR1* protein overproduction inhibits nodule development in the hairy roots of soybean (Hur et al., 2009). Malondialdehyde (MDA), a product of lipid peroxidation, is a biomarker of oxidative stresses (Bailly et al., 1996); lower MDA levels indicate better oxidative stress tolerance. *OsAKR1* overexpression in tobacco lowers levels of MDA and methylglyoxal (MG) in leaf tissues under chemical and heat stress treatments (Turoczy et al., 2011). Foxtail millet *AKR1* is a promising stress-responsive gene that modulates and enhances stress tolerance in major crops (Kirankumar et al., 2016). Thus, investigation of the functions of AKR in reactive carbonyl detoxification and the promotion of abiotic stress tolerance in foxtail millet is of interest.

Reactive oxygen species (ROS) are involved in various signal transduction pathways (Apel and Hirt, 2004; Laloi et al., 2004) under stress conditions (Mustilli et al., 2002; Neill et al., 2002). ROS also regulate gene expression under N, P, and potassium deficiency (Shin and Schachtman, 2004; Shin et al., 2005). Superoxide dismutase converts O_2^-, an important component of ROS, into H_2O_2 (Fridovich, 1997). Several classical peroxidases like ascorbate peroxidase (APX), glutathione peroxidases, and catalase (CAT) quench the resulting H_2O_2. APX and glutathione reductase (GR) detoxify H_2O_2 in green leaves (Sofo et al., 2015). They likely act as dehydration stress-responsive components in foxtail millet (Lata et al., 2011b). Maintenance of membrane stability, relative water content, higher levels of APX, CAT, and GR activities, and lower levels of lipid peroxidation and electrolyte provides resistance against the drought stress in foxtail millet (Lata et al., 2011b). Upregulation of phospholipid hydroperoxide glutathione peroxidase (PHGPX) in salt-tolerant foxtail millet lines suggests its role in salt resistance (Sreenivasulu et al., 2004). Aldose reductase is involved in sorbitol biosynthesis and the detoxification of 4-hydroxynon-2-enal (a lipid peroxidation product) in foxtail millet under salt stress; glutathione S-transferase also catalyzes 4-hydroxynon-2-enal detoxification under stress conditions (Veeranagamallaiah et al., 2009). Differentially expressed ESTs and peptides between salt-tolerant and sensitive cultivars (Puranik et al., 2011a), along with other proteins involved in the NaCl stress (Veeranagamallaiah et al., 2008), can be extended to future studies in foxtail millet.

APETALA 2/ethylene responsive element binding factor (AP2/ERF) superfamily members contain a characteristic conserved AP2 domain to bind the core DRE (Dehydration Responsive Element) (5′-A/GCCGAC-3′) *cis*-acting element in the promoter region of target genes (Yamaguchi-Shinozaki and Shinozaki, 1994; Yamaguchi-Shinozaki and Shinozaki, 2006). The single nucleotide polymorphism (SNP) of a dehydration-responsive element binding (DREB) gene is associated with stress tolerance (Lata et al., 2011a). A similar SNP accounts for 27% of variations in stress-induced lipid peroxidation in foxtail millet (Lata and Prasad, 2013). Re-sequencing of foxtail millet may identify vast libraries of SNPs and other markers (Bai et al., 2013; Jia et al., 2013). Small interfering RNAs and non-coding RNAs also have their regulatory roles in drought responses in foxtail millet (Qi et al., 2013). In addition, late embryogenesis-abundant proteins protect higher plants against environmental stresses; *SiLEA14* plays an important role in resisting abiotic damage in foxtail millet (Wang et al., 2014). Its small genome (∼490 Mbp; Bennetzen et al., 2012; Zhang et al., 2012) and a wide array of stress responses make foxtail millet a model cereal crop for stress biology and functional genomics (**Table 1**).

RESPONSES OF FOXTAIL MILLET TO N LIMITATION

Roots are the means by which plants take up nutrients; hence, root architectural modifications become vital to explore N under its low availability. Different crop species respond to external low-N conditions differentially. Legumes, for example, develop root nodules to capture atmospheric N through N-fixation (Postgate, 1998), whereas cereals such as maize enhance their root surface area by means of increasing axial and lateral root length to access N in a heterogeneous environment (Wang et al., 2003; Chun et al., 2005). As mentioned before, plants undergo these morphological and physiological alterations to maximize their N use efficiency (NUE), which can be discussed as either N utilization efficiency (NUtE) or N uptake (acquisition) efficiency (Garnett et al., 2009; Xu et al., 2012; Wang et al., 2019). At one extreme, the carbon to N ratio and biomass accumulation (dry weight; root to shoot ratio) in roots of foxtail millet increase under low N, which suggests that its higher N utilization efficiency contributes to maximize its N use efficiency, whereas on the other extreme, foxtail millet responds to increase N translocation efficiency by root thickening. These adaptive responses of foxtail millet to low N signals along with regulation of N uptake activities through N influx transporters located at the plasma membrane eventually maximize N acquisition efficiency (Nadeem et al., 2018).

Surprisingly, foxtail millet produces a specific root length (SRL) of 46852 cm g^{-1} of root dry weight under low N (Nadeem et al., 2018), which is 10 times that of maize seedlings under similar conditions (Han et al., 2015). In addition to the SRL, the average root diameter of low-N foxtail millet also increases (Nadeem et al., 2018). Resource absorption and transportation are two important resource acquisition processes for roots, with the former being used by cortex and the latter by stele (Guo et al., 2008). The ratio of cortex to stele thickness determines

TABLE 1 | Genes functionally characterized in foxtail millet.

Gene	Functions	References
SET domain genes	Abiotic stress tolerance	Yadav et al., 2016
PHT1 gene family	Phosphate transporters	Ceasar et al., 2014
Argonaute protein 1 encoding gene	Regulation of stress responses	Liu et al., 2016
Abscisic acid stress ripening gene (ASR)	Tolerance to drought and oxidative stresses	Feng et al., 2016
Autophagy-related gene (ATG)	Tolerance to nitrogen starvation and drought stresses	Li et al., 2015
Late embryogenesis abundant protein (LEA)	Tolerance to salt, osmotic, and drought stresses	Wang et al., 2014
ABA-responsive DRE-binding protein (ARDP)	Tolerance to salt and drought stresses	Li et al., 2014
WD-40	Associated with dehydration stress-responsive pathway	Mishra et al., 2012
Acetyl-CoA carboxylase	Resistance to sethoxydim herbicide	Dong et al., 2011
Dehydration-responsive element-binding protein 2 (DREB2)	Dehydration tolerance	Lata et al., 2011a
NAC transcription factor	Salinity tolerance	Puranik et al., 2011b
Si69	Aluminum tolerance	Zhao et al., 2009
Aldose reductase	Associated with salinity stress-responsive pathway	Veeranagamallaiah et al., 2009
Glutamine synthetase Pyrroline-5-carboxylate reductase		Veeranagamallaiah et al., 2007
12-oxophytodienoic acid reductase (OPR1)	Drought tolerance	Zhang et al., 2007
Photosystem II D1protein	Atrazine resistance	Jia et al., 2007
Phospholipid hydroperoxide glutathione peroxidase (*PHGPX*)	Associated with salinity tolerance	Sreenivasulu et al., 2004
Nuclear factor-Y (*SiNF-YA1, SiNFYB8*) genes	Drought and salt tolerance	Feng et al., 2015
Nitrate transporters (*SiNRT*), Ammonium transporters (*SiAMT*)	Nitrate and ammonium uptake and transport	Nadeem et al., 2018
Phosphate transporters (*SiPHP*)	Phosphate transport	Ahmad et al., 2018

the suitability of a plant species for adapting to a certain environment for favorable resource distribution. The increased thickness of foxtail millet roots under low N indicates the anatomical modification of stele, where it can accommodate more conduits like vessels and tracheid for efficient transport of N and metabolites.

Hormones help plants to adapt to environmental cues through the regulation of growth and development (Wolters and Jürgens, 2009; Marsch-Martinez and de Folter, 2016). Indole-3-acetic acid (IAA) regulates primary and lateral root growth (Sabatini et al., 1999; Casimiro et al., 2001), whereas cytokinins (CKs) influence apical root dominance (Aloni et al., 2006). IAA and CK accumulation decreases during root shortening in foxtail millet under low N despite enhanced carbon allocation toward the roots (higher dry mass and C/N ratio). Contrary to IAA and CKs, gibberellic acid (GA3) concentrations increase in the root and shoot of foxtail millet (Nadeem et al., 2018). Accumulation of GA3 antagonistic to IAA and CKs could have contributed to root thickening (increased root diameter) through tissue differentiation and anatomical modifications to roots (Yamaguchi, 2008). Abscisic acid (ABA) is known to be an internal signal of stress responses (Wilkinson and Davies, 2002; Kiba et al., 2011). Higher levels of ABA in N-deprived roots (Nadeem et al., 2018) is rather a stress response of foxtail millet that needs to be further dissected to determine the underlying mechanisms.

Sensing the external nutritional alterations, certain specific proteins act as channels, pumps, or transporters in roots to acquire nutrients from their vicinity and transport them within the root or along the vasculature for long-distance source-to-sink transport (Tegeder and Masclaux-Daubresse, 2018). To transport nitrate (NO_3^-), a nutrient as well as a signaling molecule for plant growth and root system modifications (Vidal and Gutiérrez, 2008; Krouk et al., 2010; Alvarez et al., 2012), plants have evolved a high-affinity transport system (HATS) and low-affinity transport system (LATS) (Crawford and Glass, 1998). *NRT2.1* belongs to the high-affinity nitrate transport system (Li et al., 2007), whereas *NRT1.1* is a sensor as well as a dual-affinity nitrate transporter (transceptor) in *Arabidopsis* (Tsay et al., 1993; Liu and Tsay, 2003). NRT2 transporters interact with nitrate accessory protein *NAR2.1* (NAR2 like-proteins) for nitrate absorption. Upregulation of expressions of *SiNRT1.1*, *SiNRT2.1*, and *SiNAR2.1*, together with root architectural modifications, optimizes N acquisition in foxtail millet, which is confirmed by enhanced ^{15}N influx into roots (Nadeem et al., 2018). Once nitrate is absorbed, the next phase is its redistribution or translocation from root to shoot and from mature expanded leaves to the youngest leaves (Okamoto et al., 2006; Orsel et al., 2006; Tsay et al., 2007; Miller et al., 2009). In this regard, *NRT1.11* and *NRT1.12* mediate xylem to phloem loading and redistribution of nitrate in *Arabidopsis* (*Arabidopsis thaliana*) leaves with normal nitrate provision (Hsu and Tsay, 2013). Foxtail millet seedlings supplied with only 0.02 mM of NH_4NO_3 for 7 days show nitrate redistribution in the shoot through upregulation of *SiNRT1.11* and *SiNRT1.12* expressions, indicating an extraordinary ability to adapt to extreme N limitation. Alongside nitrate uptake, ammonium uptake and transport are controlled by ammonium transporters (AMTs) (Loqué and von Wirén, 2004). *SiAMT1.1* accelerates N acquisition by upregulating its expression (Nadeem et al., 2018).

Interlinked carbon and N metabolism generally give rise to balanced carbohydrates to N-metabolites ratios in plant tissues. However, N limitation leads to higher carbon/N ratios (Sun et al., 2002; Reich et al., 2006; Taub and Wang, 2008). In

foxtail millet, the root and shoot maintain the balance between free amino acids and total soluble sugar concentrations owing to low N concentrations of these tissues under low external N provision. Interestingly, concentrations of total soluble proteins in roots increase, in contrast to those in shoots (Nadeem et al., 2018), indicating the probable role of proteins (enzymes in particular) in the regulation of carbon and N metabolism-related cellular activities at the tissue level.

FOXTAIL MILLET RESPONSES TO Pi STARVATION

Plants have evolved strategies for enhancing their P-uptake capacity either through arbuscular mycorrhizal symbiosis or modification of the root system architecture (Marschner, 1995; Lambers et al., 2008; Cheng et al., 2011). As explained previously, root system modification is the primary adaptive strategy of plants coping with low availability of nutrients. Low mobility of Pi in soils favors shallow root plants (Panigrahy et al., 2009; Péret et al., 2011; Li et al., 2012; Shi et al., 2013). In *Arabidopsis thaliana*, reduced Pi metabolism (Nussaume et al., 2011; Wang et al., 2011), indirect low-P-mediated stress effects (Thibaud et al., 2010), and genetic control of root responses to low P (Svistoonoff et al., 2007; Ticconi et al., 2009) inhibit primary root growth (Abel, 2011; Niu et al., 2013; Giehl et al., 2014). In addition, blue light suppresses elongation of the primary root of petri dish-grown *Arabidopsis* seedlings under Pi deficiency (Zheng et al., 2019). Thus, environmental factors collectively reshape root structure in response to Pi starvation.

Plant responses to Pi starvation could also be genotype-dependent (Reymond et al., 2006). In monocots like rice and barley, low Pi has a less pronounced effect on primary root growth, perhaps due to high P reserves in seeds (Calderón-Vázquez et al., 2011), whereas primary root growth of maize is stimulated under low Pi (Li et al., 2012). In contrast with the primary root inhibition, lateral root formation in plants is enhanced by low Pi (Williamson et al., 2001; Hodge, 2004; Pérez-Torres et al., 2008). Foxtail millet, on the other hand, develops a larger root system in terms of crown root length and lateral root number, length, and density under Pi deficiency (Ahmad et al., 2018), which is in total contrast to what is observed under low N (Nadeem et al., 2018). The enlargement of the root system in response to low Pi and reduction under low N in foxtail millet could be due to the immobile and mobile nature of Pi and nitrate, respectively; longer roots can reach immobile Pi at its location, and shorter roots can intercept mobile nitrate in the microenvironment of the rhizosphere. This root enlargement of foxtail millet couples with hormonal enhancements (auxin and GA3) and increase in root to shoot ratio due to the allocation of carbon to the P-deficient root.

A larger root system functions to enhance Pi acquisition by transporters (Rausch and Bucher, 2002). Pi transporters are mostly conserved across cereal crops (Rakshit and Ganapathy, 2014). Pi limitation stimulates transcription of PHT1 members (Mudge et al., 2002; Rae et al., 2003) and induces *OsPHT1.2* expression in the stele and lateral roots, along with upregulation of *OsPHT1.4*, probably to improve Pi uptake through roots and translocation to the shoot (Ye et al., 2015; Zhang et al., 2015). Substantial upregulation of *SiPHT1.1, SiPHT1.2,* and *SiPHT1.4* expression in root tissues possibly preconditions for enhanced Pi uptake to replenish the internal P-reserves, whereas down-regulation of *SiPHT1.3* expression probably assists with the retention of Pi in the shoot (Ahmad et al., 2018). On the other end, respective down-regulation of expression of *SiNRT2.1* and *SiNAR2.1* (in roots) and that of *SiNRT1.11* and *SiNRT1.12* (in shoots) (Ahmad et al., 2018) helps balance the N/P ratio within permissible limits for proper root and shoot functionality (Aerts and Chapin, 2000). Such correlative interpretation of the expression of *SiPHRs* in relation to Pi uptake and source-sink remobilization under low Pi calls for in-depth mechanistic dissection (Jia et al., 2011; Ceasar et al., 2014). Alternatively, foxtail millet uses internal Pi reserves for higher utilization efficiency (Rose et al., 2011).

Interestingly, the reduction of SPAD values in the foxtail millet shoot is in contrast to differential accumulation of free amino acids (higher in shoot and root) and total soluble proteins (lower in shoot and root) under low Pi provision (Ahmad et al., 2018). These variations in the accumulation of N-metabolites upon low P suggest a potential link between N and P nutrition at the physiological level. Nutrient provision affects biomass allocation within plants (Poorter et al., 2012). N and P are both considered as the limiting factors in plant growth and development; therefore, the N/P ratio plays a critical role in resource distribution (Graham and Mendelssohn, 2016). The uptake of N and P is adjusted by whole-plant signaling to balance N/P ratios between plant tissues (Imsande and Touraine, 1994; Raghotama, 1999; Forde, 2002). To maintain the N/P ratio, foxtail millet reduces N translocation toward the shoot under Pi limitation (Ahmad et al., 2018), similar to the terrestrial plants that adapt to low-N conditions by decreasing Pi uptake (Aerts and Chapin, 2000). P and N signals are indeed integrated by nitrate-inducible GARP-type transcriptional repressor 1 (*NIGT1*) in *Arabidopsis*; PHR1 promotes the expression of NIGT1-clade genes under low P, which in turn down-regulates *NRT2.1* expression to reduce N uptake (Maeda et al., 2018). *NIGT1* expression is stimulated when N availability is high in order to repress N starvation genes (Kiba et al., 2018). *NIGT1* also regulates Pi starvation responses by directly repressing expression of Pi starvation-responsive genes and *NRT2.1* to equilibrate N and P (Maeda et al., 2018). The potential involvement of the *PHR1-NIGT1-NRT2.1* pathway in low P responses of foxtail millet and subsequent readouts needs to be further studied in future.

CONCLUSION

Foxtail millet has been studied for its structural and functional genomics for the purpose of developing genetic and genomic resources and delineating the physiology and molecular biology of stress tolerance, especially drought and salinity stress tolerance. Apart from its adaptation to drought and salinity, foxtail millet

is also an N- and P-efficient crop. In parallel to those in major cereals, studies should be conducted to develop nutrient-efficient and environment friendly cultivars of foxtail millet. Its small genome size, short life cycle and inbreeding nature make foxtail millet a perfect choice for a model crop for studies of a broad range of plant nutritional biology research. This review presents a unique perspective of the adaptation of foxtail millet to low N and low P along with a brief background on various abiotic stress tolerance strategies. It can serve as a base to plan future studies in the field of plant nutritional genomics using foxtail millet as a model crop.

AUTHOR CONTRIBUTIONS

FN, ZA, XD, and XL conceived and wrote the review. FN, MU, RW, XD, and XL revised the manuscript. All authors have approved the final manuscript.

FUNDING

This work was supported by the National Natural Science Foundation of China (31972491 and 31772385).

REFERENCES

Abel, S. (2011). Phosphate sensing in root development. *Curr. Opin. Plant Biol.* 14, 303–309. doi: 10.1016/j.pbi.2011.04.007

Aerts, R., and Chapin, F. S. (2000). The mineral nutrition of wild plants revisited: a re-evaluation of processes and patterns. *Adv. Ecol. Res.* 30, 1–67. doi: 10.1016/S00652504(08)60016-1

Ahmad, Z., Nadeem, F., Wang, R., Diao, X., Han, Y., Wang, X., et al. (2018). A larger root system is coupled with contrasting expression patterns of phosphate and nitrate transporters in foxtail millet [*Setaria italica* (L.) Beauv.] under phosphate limitation. *Front. Plant Sci.* 9:1367. doi: 10.3389/fpls.2018.01367

Aloni, R., Aloni, E., Langhans, M., and Ullrich, C. I. (2006). Role of cytokinin and auxin in shaping root architecture: regulating vascular differentiation, lateral root initiation, root apical dominance and root gravitropism. *Ann. Bot.* 97, 883–893. doi: 10.1093/aob/mcl027

Alvarez, J. M., Vidal, E. A., and Gutiérrez, R. A. (2012). Integration of local and systemic signaling pathways for plant N responses. *Curr. Opin. Plant Biol.* 15, 185–191. doi: 10.1016/j.pbi.2012.03.009

Apel, K., and Hirt, H. (2004). Reactive oxygen species: metabolism, oxidative stress, and signal transduction. *Annu. Rev. Plant Biol.* 55, 373–399. doi: 10.1146/annurev.arplant.55.031903.141701

Bai, H., Cao, Y., Quan, J., Dong, L., Li, Z., Zhu, Y., et al. (2013). Identifying the genome-wide sequence variations and developing new molecular markers for genetics research by resequencing a landrace cultivar of foxtail millet. *PLoS One* 8:e73514. doi: 10.1371/journal.pone.0073514

Bailly, C., Benamar, A., and Corbineau, Y. (1996). Changes in malondialdehyde content and in superoxide dismutase, catalase and glutathione reductase activities in sunflower seeds as related to deterioration during accelerated aging. *Physiol. Plant.* 97, 104–110. doi: 10.1111/j.1399-3054.1996.tb00485.x

Baltensperger, D. D. (1996). "Foxtail and proso millet," in *Progress in New Crops*, ed. J. Janick, (Alexandria, VA: ASHS Press).

Bechtold, U., and Field, B. (2018). Molecular mechanisms controlling plant growth during abiotic stress. *J. Exp. Bot.* 69, 2753–2758. doi: 10.1093/jxb/ery157

Bennetzen, J. L., Schmutz, J., Wang, H., Percifield, R., Hawkins, J., Pontaroli, A. C., et al. (2012). Reference genome sequence of the model plant *Setaria*. *Nat. Biotechnol.* 30, 555–561. doi: 10.1038/nbt.2196

Bohren, K. M., Bullock, B., Wermuth, B., and Gabbay, K. M. (1989). The Aldo-Keto Reductase Superfamily: cDNAs and deduced amino acid sequences of human aldehyde and aldose reductase. *J. Biol. Chem.* 264, 9547–9551.

Boyer, J. S. (1982). Plant productivity and environment. *Science* 218, 443–448. doi: 10.1126/science.218.4571.443

Burger, J., Davis, V., Franklin, J., Zipper, C., Skousen, J., Barton, C., et al. (2009). *Tree-Compatible Ground Covers for Reforestation And Erosion Control. Forest Reclamation Advisory No. 6, Appalachian Regional Reforestation Initiative (ARRI)*. Available at: http://arri.osmre.gov/PDFs/Pubs/FRA_No.6_7-24-09.pdf (accessed October 12, 2019).

Calderón-Vázquez, C., Sawers, R. J., and Herrera-Estrella, L. (2011). Phosphate deprivation in maize: genetics and genomics. *Plant Physiol.* 156, 1067–1077. doi: 10.1104/pp.111.174987

Casimiro, I., Marchant, A., Bhalerao, R. P., Beeckman, T., Dhooge, S., Swarup, R., et al. (2001). Auxin transport promotes *Arabidopsis* lateral root initiation. *Plant Cell* 13, 843–852. doi: 10.1105/tpc.13.4.843

Ceasar, S. A., Hodge, A., Baker, A., and Baldwin, S. A. (2014). Phosphate concentration and arbuscular mycorrhizal colonisation influence the growth, yield and expression of twelve *PHT1* family phosphate transporters in foxtail millet (*Setaria italica*). *PLoS One* 9:e108459. doi: 10.1371/journal.pone.0108459

Cheng, L., Bucciarelli, B., Shen, J., Allan, D. L., and Vance, C. P. (2011). Update on white lupin cluster roots acclimation to phosphorus deficiency. *Plant Physiol.* 156, 1025–1032. doi: 10.1104/pp.111.175174

Chun, L., Chen, F., Zhang, F., and Mi, G. (2005). Root growth, nitrogen uptake and yield formation of hybrid maize with different N efficiency. *Plant Nutr. Fertil. Sci.* 11, 615–619.

Cordell, D., Drangert, J. O., and White, S. (2009). The story of phosphorus: global food security and food for thought. *Glob. Environ. Change.* 19, 292–305. doi: 10.1016/j.gloenvcha.2008.10.009

Cramer, G. R. (2010). Abiotic stress and plant responses from the whole vine to the genes. *Aust. J. Grape Wine Res.* 16, 86–93. doi: 10.1111/j.1755-0238.2009.00058.x

Crawford, N. M., and Glass, A. D. M. (1998). Molecular and physiological aspects of nitrate uptake in plants. *Trends Plant Sci.* 3, 389–395. doi: 10.1016/s1360-1385(98)01311-9

Creamer, N. G., and Baldwin, K. R. (1999). *Summer Cover Crops*. Raleigh, NC: NC State University.

Doebley, J. (2006). Unfallen grains: how ancient farmers turned weeds into crops. *Science* 312, 1318–1319. doi: 10.1126/science.1128836

Dong, Z., Zhao, H., He, J., Huai, V., Lin, H., Zheng, J., et al. (2011). Overexpression of a foxtail millet Acetyl-CoA carboxylase gene in maize increases sethoxydim resistance and oil content. *Afr. J. Biotechnol.* 10, 3986–3995. doi: 10.5897/AJB11.053

Doust, A. N., Kellogg, E. A., Devos, K. M., and Bennetzen, J. L. (2009). Foxtail millet: a sequence-driven grass model system. *Plant Physiol.* 149, 137–141. doi: 10.1104/pp.108.129627

Eulgem, T., Rushton, P. J., Robatzek, S., and Somssich, I. E. (2000). The WRKY superfamily of plant transcription factor. *Trends Plant Sci.* 5, 199–206. doi: 10.1016/s1360-1385(00)01600-9

Eva, C., Zelenyanszki, H., Farkas, R. T., and Tamas, L. (2014). Transgenic barley expressing the *Arabidopsis* AKR4C9 Aldo-Keto Reductase enzyme exhibits enhanced freezing tolerance and regenerative capacity. *S. Afr. J. Bot.* 93, 179–184. doi: 10.1016/j.sajb.2014.04.010

Feng, Z. J., He, G. H., Zheng, W. J., Lu, P. P., Chen, M., Gong, Y. M., et al. (2015). Foxtail millet NF-Y families: genome-wide survey and evolution analyses identified two functional genes important in abiotic stresses. *Front. Plant Sci.* 6:1142. doi: 10.3389/fpls.2015.01142

Feng, Z. J., Xu, Z. S., Sun, J., Li, L. C., Chen, M., Yang, G. X., et al. (2016). Investigation of the ASR family in foxtail millet and the role of *ASR1* in drought/oxidative stress tolerance. *Plant Cell Rep.* 35, 115–128. doi: 10.1007/s00299-015-1873-y

Forde, B. G. (2002). The role of long-distance signalling in plant responses to nitrate and other nutrients. *J. Exp. Bot.* 53, 39–43. doi: 10.1093/jexbot/53.366.39

Fridovich, I. (1997). Superoxide anion radical (O2-), superoxide dismutases, and related matters. *J. Biol. Chem.* 272, 18515–18517. doi: 10.1074/jbc.272.30.18515

Garnett, T., Conn, V., and Kaiser, B. N. (2009). Root based approaches to improving nitrogen use efficiency in plants. *Plant Cell Environ.* 32, 1272–1283. doi: 10.1111/j.1365-3040.2009.02011.x

Giehl, R. F., Gruber, B. D., and von Wirén, N. (2014). It's time to make changes: modulation of root system architecture by nutrient signals. *J. Exp. Bot.* 65, 769–778. doi: 10.1093/jxb/ert421

Giehl, R. F., and von Wirén, N. (2014). Root nutrient foraging. *Plant Physiol.* 166, 509–517. doi: 10.1104/pp.114.245225

Good, A. G., Shrawat, A. K., and Muench, D. G. (2004). Can less yield more? Is reducing nutrient input into the environment compatible with maintaining crop production? *Trends Plant Sci.* 9, 597–605. doi: 10.1016/j.tplants.2004.10.008

Graham, S. A., and Mendelssohn, I. A. (2016). Contrasting effects of nutrient enrichment on below-ground biomass in coastal wetlands. *J. Ecol.* 104, 249–260. doi: 10.1111/1365-2745.12498

Guo, D., Xia, M., Wei, X., Chang, W., Liu, Y., and Wang, Z. (2008). Anatomical traits associated with absorption and mycorrhizal colonization are linked to root branch order in twenty-three Chinese temperate tree species. *New Phytol.* 180, 673–683. doi: 10.1111/j.1469-8137.2008.02573.x

Guo, X., Sun, W., Wei, W., Yang, J., Kang, Y., Wu, J., et al. (2009). Effects of NPK on physiological and biochemical characteristics of winter rape seed in northwest cold and drought region. *Acta Agric. Boreali-Occident. Sin.* 2:027.

Han, J. N., Wang, L. F., Zheng, H. Y., Pan, X. Y., Li, H. Y., Chen, F. J., et al. (2015). ZD958 is a low-nitrogen-efficient maize hybrid at the seedling stage among five maize and two teosinte lines. *Planta* 242, 935–949. doi: 10.1007/s00425-015-2331-3

Hancock Seed (2014). *German Foxtail Millet Seed*. Dade City, FL: Hancock Seed Company.

Hegedus, A., Erdei, S., Janda, T., Toth, E., Horvath, G., and Dudits, D. (2004). Transgenic tobacco plants overproducing alfalfa aldose/aldehyde reductase show higher tolerance to low temperature and cadmium stress. *Plant Sci.* 166, 1329–1333. doi: 10.1016/j.plantsci.2004.01.013

Hermans, C., Hammond, J. P., White, P. J., and Verbruggen, N. (2006). How do plants respond to nutrient shortage by biomass allocation? *Trends Plant Sci.* 11, 610–617. doi: 10.1016/j.tplants.2006.10.007

Hideg, E., Nagy, T., Oberschall, A., Dudits, D., and Vass, I. (2003). Detoxification function of aldose/aldehyde reductase during drought and ultra violet-b (230-320 nm) stresses. *Plant Cell Environ.* 26, 513–522. doi: 10.1046/j.1365-3040.2003.00982.x

Hodge, A. (2004). The plastic plant: root responses to heterogeneous supplies of nutrients. *New Phytol.* 162, 9–24. doi: 10.1111/j.1469-8137.2004.01015.x

Hsu, P. K., and Tsay, Y. F. (2013). Two phloem nitrate transporters, *NRT1.11* and *NRT1.12* are important for redistributing xylem born nitrate to enhance plant growth. *Plant Physiol.* 163, 844–856. doi: 10.1104/pp.113.226563

Hur, Y., Shin, K., Kim, S., Nam, K. H., Lee, M., Chun, J., et al. (2009). Overexpression of GmAKR1 a stress-induced aldo-keto reductase from soybean, retards nodule development. *Mol. Cells* 27, 217–223. doi: 10.1007/s10059-009-0027-x

Imsande, J., and Touraine, B. (1994). N demand and the regulation of nitrate uptake. *Plant Physiol.* 105, 3–7. doi: 10.1104/pp.105.1.3

Jayaraman, A., Puranik, S., Rai, N. K., Vidapu, S., Sahu, P. P., Lata, C., et al. (2008). cDNA-AFLP analysis reveals differential gene expression in response to salt stress in foxtail millet (*Setaria italica* L.). *Mol. Biotechnol.* 40, 241–251. doi: 10.1007/s12033-008-90814

Jia, G., Huang, X., Zhi, H., Zhao, Y., Zhao, Q., Li, W., et al. (2013). A haplotype map of genomic variations and genome-wide association studies of agronomic traits in foxtail millet (*Setaria italica*). *Nat. Genet.* 45, 957–961. doi: 10.1038/ng.2673

Jia, H., Ren, H., Gu, M., Zhao, J., Sun, S., Zhang, X., et al. (2011). The phosphate transporter gene *OsPht1;8* is involved in phosphate homeostasis in rice. *Plant Physiol.* 156, 1164–1175. doi: 10.1104/pp.111.175240

Jia, X., Shi, Y. S., Song, Y. C., Wang, G. Y., Wang, T. Y., and Li, Y. (2007). Development of EST-SSR in foxtail millet (*Setaria italica*). *Genet. Resour. Crop Evol.* 54, 233–236. doi: 10.1007/s10722-006-9139-8

Jones, D. L., and Kielland, K. (2012). Amino acid, peptide and protein mineralization dynamics in a taiga forest soil. *Soil Biol. Biochem.* 55, 60–69. doi: 10.1016/j.soilbio.2012.06.005

Kanayama, Y., Mizutani, R., Yaguchi, S., Hojo, A., Ikeda, H., Nishiyama, M., et al. (2014). Characterization of an uncharacterized aldo-keto reductase gene from peach and its role in abiotic stress tolerance. *Phytochemistry* 104, 30–36. doi: 10.1016/j.phytochem.2014.04.008

Kiba, T., Inaba, J., Kudo, T., Ueda, N., Konishi, M., Mitsuda, N., et al. (2018). Repression of nitrogen starvation responses by members of the arabidopsis GARP-Type transcription factor NIGT1/HRS1 subfamily. *Plant Cell* 30, 925–945. doi: 10.1105/tpc.17.00810

Kiba, T., Kudo, T., Kojima, M., and Sakakibara, H. (2011). Hormonal control of nitrogen acquisition: roles of auxin, abscisic acid, and cytokinin. *J. Exp. Bot.* 62, 1399–1409. doi: 10.1093/jxb/erq410

Kirankumar, T. V., Madhusudhan, K. V., Nareshkumar, A., Kiranmai, K., Lokesh, U., Venkatesh, B., et al. (2016). Expression analysis of Aldo-Keto Reductase 1 (AKR1) in foxtail millet (*Setaria italica* L.) subjected to abiotic stresses. *Am. J. Plant Sci.* 7, 500–509. doi: 10.4236/ajps.2016.73044

Koch, D. W. (2002). *Foxtail Millet-Management for Supplemental and Emergency Forage. University of Wyoming, Cooperative Extension Service, B-1122.3*. Available at: http://www.wyomingextension.org/agpubs/pubs/B1122-3.pdf (accessed October 10, 2019).

Krishnamurthy, L., Upadhyaya, H. D., Gowda, C. L. L., Kashiwagi, J., Purushothaman, R., Singh, S., et al. (2014). Large variation for salinity tolerance in the core collection of foxtail millet (*Setaria italica* (L.) P. Beauv.) germplasm. *Crop Pasture Sci.* 65, 353–361. doi: 10.1071/CP13282

Krouk, G., Crawford, N. M., Coruzzi, G. M., and Tsay, Y. F. (2010). Nitrate signaling: adaptation to fluctuating environments. *Curr. Opin. Plant Biol.* 13, 265–272. doi: 10.1016/j.pbi.2009.12.003

Laloi, C., Apel, K., and Danon, A. (2004). Reactive oxygen signalling: the latest news. *Curr. Opin. Plant Biol.* 7, 323–328. doi: 10.1016/j.pbi.2004.03.005

Lambers, H., Raven, J. A., Shaver, G. R., and Smith, S. E. (2008). Plant nutrient-acquisition strategies change with soil age. *Trends Ecol. Evol.* 23, 95–103. doi: 10.1016/j.tree.2007.10.008

Lata, C., Bhutty, S., Bahadur, R. P., Majee, M., and Prasad, M. (2011a). Association of an SNP in a novel DREB2-like gene SiDREB2 with stress tolerance in foxtail millet [*Setaria italica* (L.)]. *J. Exp. Bot.* 62, 3387–3401. doi: 10.1093/jxb/err016

Lata, C., and Prasad, M. (2013). Validation of an allele-specific marker associated with dehydration stress tolerance in a core set of foxtail millet accessions. *Plant Breed.* 132, 496–499. doi: 10.1111/j.1439-0523.2012.01983.x

Lata, C., Sarita, J. H. A., Dixit, V., Sreenivasulu, N., and Parasad, M. (2011b). Differential antioxidative responses to dehydration-induced oxidative stress in core set of foxtail millet cultivars [*Setaria italica* (L.)]. *Protoplasma* 248, 817–828. doi: 10.1007/s00709-010-0257-y

Li, C., Yue, J., Wu, X., Xu, C., and Yu, J. (2014). ABA-responsive DRE binding protein gene from *Setaria italica*, *SiARDP*, the target gene of *SiAREB*, plays a critical role under drought stress. *J. Exp. Bot.* 65, 5415–5427. doi: 10.1093/jxb/eru302

Li, P., and Brutnell, T. P. (2011). *Setaria viridis* and *Setaria italica*, model genetic systems for the panicoid grasses. *J. Exp. Bot.* 62, 3031–3037. doi: 10.1093/jxb/err096

Li, W., Wang, Y., Okamoto, M., Crawford, N. M., Siddiqi, M. Y., and Glass, A. D. (2007). Dissection of the *AtNRT2.1:AtNRT2.2* inducible high-affinity nitrate transporter gene cluster. *Plant Physiol.* 143, 425–433. doi: 10.1104/pp.106.091223

Li, W. W., Chen, M., Zhong, L., Liu, J. M., Xu, Z. S., Li, L. C., et al. (2015). Overexpression of the autophagy-related gene SiATG8a from foxtail millet (*Setaria italica* L.) confers tolerance to both nitrogen starvation and drought stress in *Arabidopsis*. *Biochem. Biophys. Res. Commun.* 468, 800–806. doi: 10.1016/j.bbrc.2015.11.035

Li, Z., Xu, C., Li, K., Yan, S., Qu, X., and Zhang, J. (2012). Phosphate starvation of maize inhibits lateral root formation and alters gene expression in the lateral root primordium zone. *BMC Plant Biol.* 12:89. doi: 10.1186/1471-2229-12-89

Liu, K. H., and Tsay, Y. F. (2003). Switching between the two action modes of the dual-affinity nitrate transporter CHL1 by phosphorylation. *EMBO J.* 22, 1005–1013. doi: 10.1093/emboj/cdg118

Liu, X., Tang, S., Jia, G., Schnable, J. C., Su, H., Tang, C., et al. (2016). The C-terminal motif of SiAGO1b is required for the regulation of growth, development and stress responses in foxtail millet (*Setaria italica* (L.) P. Beauv). *J. Exp. Bot.* 67, 3237–3249. doi: 10.1093/jxb/erw135

Loqué, D., and von Wirén, N. (2004). Regulatory levels for the transport of ammonium in plant roots. *J. Exp. Bot.* 55, 1293–1305. doi: 10.1093/jxb/erh147

Maeda, Y., Konishi, M., Kiba, T., Sakuraba, Y., Sawaki, N., Kurai, T., et al. (2018). A NIGT1-centred transcriptional cascade regulates nitrate signalling

and incorporates phosphorus starvation signals in *Arabidopsis*. *Nat. Commun.* 9:1376. doi: 10.1038/s41467-018-03832-6

Marsch-Martinez, N., and de Folter, S. (2016). Hormonal control of thedevelopment of the gynoecium. *Curr. Opin. Plant Biol.* 29, 104–114. doi: 10.1016/j.pbi.2015.12.006

Marschner, H. (1995). *Mineral Nutrition of Higher Plants*. San Diego, CA: Academic Press.

Miller, A. J., and Cramer, M. D. (2004). Root nitrogen acquisition and assimilation. *Plant Soil* 27, 1–36. doi: 10.1007/s11104-004-0965-1

Miller, A. J., Shen, Q., and Xu, G. (2009). Freeways in the plant: transporters for N, P and S and their regulation. *Curr. Opin. Plant Biol.* 12, 284–290. doi: 10.1016/j.pbi.2009.04.010

Mishra, A. K., Puranik, S., Bahadur, R. P., and Prasad, M. (2012). The DNAbinding activity of an AP2 protein is involved in transcriptional regulation of a stress-responsive gene, SiWD40, in foxtail millet. *Genomics* 100, 252–263. doi: 10.1016/j.ygeno.2012.06.012

Mittler, R. (2006). Abiotic stress, the field environment and stress combination. *Trends Plant Sci.* 11, 15–19. doi: 10.1016/j.tplants.2005.11.002

Mudge, S. R., Rae, A. L., Diatloff, E., and Smith, F. W. (2002). Expression analysis suggests novel roles for members of the Pht1 family of phosphate transporters in *Arabidopsis*. *Plant J.* 3, 341–353. doi: 10.1046/j.1365-313x.2002.01356.x

Mustilli, A. C., Merlot, S., Vavasseur, A., Fenzi, F., and Giraudat, J. (2002). Arabidopsis OST1 protein kinase mediates the regulation of stomatal aperture by abscisic acid and acts upstream of reactive oxygen species production. *Plant Cell* 14, 3089–3099. doi: 10.1105/tpc.007906

Muthamilarasan, M., Bonthala, V. S., Khandelwal, R., Jaishankar, J., Shweta, S., Nawaz, K., et al. (2015). Global analysis of WRKY transcription factor superfamily in *Setaria* identifies potential candidates involved in abiotic stress signaling. *Front. Plant Sci.* 6:910. doi: 10.3389/fpls.2015.00910

Muthamilarasan, M., Mangu, V. R., Zandkarimi, H., Prasad, M., and Baisakh, N. (2016). Structure, organization and evolution of ADP-ribosylation factors in rice and foxtail millet, and their expression in rice. *Sci. Rep.* 6:24008. doi: 10.1038/srep24008

Nacry, P., Bouguyon, E., and Gojon, A. (2013). Nitrogen acquisition by roots: physiological and developmental mechanisms ensuring plant adaptation to a fluctuating resource. *Plant Soil* 370, 1–29. doi: 10.1007/s11104-013-1645-9

Nadeem, F., Ahmad, Z., Wang, R., Han, J., Shen, Q., Chang, F., et al. (2018). Foxtail Millet [*Setaria italica* (L.) Beauv.] Grown under low nitrogen shows a smaller root system, enhanced biomass accumulation, and nitrate transporter expression. *Front. Plant Sci.* 9:205. doi: 10.3389/fpls.2018.00205

Narawongsanont, R., Kabinpong, S., Auiyawong, B., and Tantitadapitak, C. (2012). Cloning and characterization of AKR4C14, a rice Aldo-Keto Reductase, from Thai jasmine rice. *Protein J.* 31, 35–42. doi: 10.1007/s10930-011-9371-8

Neill, S. J., Desikan, R., Clarke, A., and Hancock, J. T. (2002). Nitric oxide is a novel component of abscisic acid signaling in stomatal guard cells. *Plant Physiol.* 128, 13–16. doi: 10.1104/pp.010707

Niu, Y. F., Chai, R. S., Jin, G. L., Wang, H., Tang, C. X., and Zhang, Y. S. (2013). Responses of root architecture development to low phosphorus availability: a review. *Ann. Bot.* 112, 391–408. doi: 10.1093/aob/mcs285

Nussaume, L., Kanno, S., Javot, H., Marin, E., Pochon, N., Ayadi, A., et al. (2011). Phosphate import in plants: focus on the *PHT1* transporters. *Front. Plant Sci.* 2:83. doi: 10.3389/fpls.2011.00083

Oberschall, A., Deak, M., Torok, K., Sass, L., Vass, I., Kovacs, I., et al. (2000). A novel aldose/aldehyde reductase protects transgenic plants against lipid peroxidation under chemical and drought stress. *Plant J.* 24, 437–446. doi: 10.1046/j.1365-313x.2000.00885.x

Okamoto, M., Kumar, A., Li, W., Wang, Y., Siddiqi, M. Y., Crawford, N. M., et al. (2006). High-affinity nitrate transport in roots of *Arabidopsis* depends on expression of the NAR2-like gene *AtNRT3.1*. *Plant Physiol.* 140, 1036–1046. doi: 10.1104/pp.105.074385

Orsel, M., Chopin, F., Leleu, O., Smith, S. J., Krapp, A., Daniel-Vedele, F., et al. (2006). Characterization of a two-component high-affinity nitrate uptake system in *Arabidopsis*: physiology and protein-protein interaction. *Plant Physiol.* 142, 1304–1317. doi: 10.1104/pp.106.085209

Panigrahy, M., Rao, D. N., and Sarla, N. (2009). Molecular mechanisms in response to phosphate starvation in rice. *Biotechnol. Adv.* 27, 389–397. doi: 10.1016/j.biotechadv.2009.02.006

Péret, B., Clément, M., Nussaume, L., and Desnos, T. (2011). Root developmental adaptation to phosphate starvation: better safe than sorry. *Trends Plant Sci.* 16, 442–450. doi: 10.1016/j.tplants.2011.05.006

Pérez-Torres, C. A., López-Bucio, J., Cruz-Ramírez, A., Ibarra-Laclette, E., Dharmasiri, S., Estelle, M., et al. (2008). Phosphate availability alters lateral root development in *Arabidopsis* by modulating auxin sensitivity via a mechanism involving the TIR1 auxin receptor. *Plant Cell* 20, 3258–3272. doi: 10.1105/tpc.108.058719

Poorter, H., Niklas, K. J., Reich, P. B., Oleksyn, J., Poot, P., and Mommer, L. (2012). Biomass allocation to leaves, stems and roots: meta-analyses of interspecific variation and environmental control. *New Phytol.* 193, 30–50. doi: 10.1111/j.1469-8137.2011.03952.x

Postgate, J. (1998). *Nitrogen Fixation*, 3rd Edn. Cambridge: Cambridge University Press.

Puranik, S., Bahadur, R. P., Srivastava, P. S., and Prasad, M. (2011a). Molecular cloning and characterization of a membrane associated NAC family gene, *SiNAC* from foxtail millet [*Setaria italica* (L.) P. Beauv.]. *Mol. Biotechnol.* 49, 138–150. doi: 10.1007/s12033-011-9385-7

Puranik, S., Jha, S., Srivastava, P. S., Sreenivasulu, N., and Prasad, M. (2011b). Comparative transcriptome analysis of contrasting foxtail millet cultivars in response to short-term salinity stress. *J. Plant Physiol.* 168, 280–287. doi: 10.1016/j.jplph.2010.07.005

Qi, X., Xie, S., Liu, Y., Yi, F., and Yu, J. (2013). Genome-wide annotation of genes and noncoding RNAs of foxtail millet in response to simulated drought stress by deep sequencing. *Plant Mol. Biol.* 83, 459–473. doi: 10.1007/s11103-013-0104-6

Rae, A. L., Cybinski, D. H., Jarmey, J. M., and Smith, F. W. (2003). Characterization of two phosphate transporters from barley: evidence for diverse function and kinetic properties among members of the *Pht1* family. *Plant Mol. Biol.* 53, 27–36. doi: 10.1023/B:PLAN.0000009259.75314.15

Raghotama, K. G. (1999). Phosphate acquisition. *Annu. Rev. Plant Physiol. Plant Mol. Biol.* 50, 665–693. doi: 10.1146/annurev.arplant.50.1.665

Rakshit, S., and Ganapathy, K. N. (2014). "Comparative genomics of cereal crops: status and future prospects," in *Agricultural Bioinformatics*, eds P. B. Kavi Kishor, R. Bandopadhyay, and P. Suravajhala, (New Delhi: Springer), 59–87. doi: 10.1007/978-81-322-1880-7_4

Rausch, C., and Bucher, M. (2002). Molecular mechanisms of phosphate transport in plants. *Planta* 216, 23–37. doi: 10.1007/s00425-002-0921-3

Regad, F., Bardet, C., Tremousaygue, D., Moisan, A., Lescure, B., and Axelos, M. (1993). cDNA cloning and expression of an *Arabidopsis* GTP-binding protein of the ARF family. *FEBS Lett.* 316, 133–136. doi: 10.1016/0014-5793(93)81201-a

Reich, P. B., Hobbie, S. E., Lee, T., Ellsworth, D. S., West, J. B., Tilman, D., et al. (2006). Nitrogen limitation constrains sustainability of ecosystem response to CO_2. *Nature* 440, 922–925. doi: 10.1038/nature04486

Reymond, M., Svistoonoff, S., Loudet, O., Nussaume, L., and Desnos, T. (2006). Identification of QTL controlling root growth response to phosphate starvation in *Arabidopsis thaliana*. *Plant Cell Environ.* 29, 115–125. doi: 10.1111/j.1365-3040.2005.01405.x

Rose, T. J., Rose, M. T., Pariasca-Tanaka, J., Heuer, S., and Wissuwa, M. (2011). The frustration with utilization: why have improvements in internal phosphorus utilization efficiency in crops remained so elusive? *Front. Plant Nutr.* 2:73. doi: 10.3389/fpls.2011.00073

Sabatini, S., Beis, D., Wolkenfelt, H., Murfett, J., Guilfoyle, T., Malamy, J., et al. (1999). An auxin-dependent distal organizer of pattern and polarity in the *Arabidopsis* root. *Cell* 99, 463–472. doi: 10.1016/s0092-8674(00)81535-4

Sanchez, P. A., and Salinas, J. G. (1981). Low input technology for managing oxisol and ultisols in tropical America. *Adv. Agron.* 34, 279–406. doi: 10.1016/S0065-2113(08)60889-5

Schachtman, D. P., Reid, R. J., and Ayling, S. M. (1998). Phosphorus uptake by plants: from soil to cell. *Plant Physiol.* 116, 447–453. doi: 10.1104/pp.116.2.447

Schonbeck, M., and Morse, R. (2006). *Cover Crops for All Seasons: Expanding the Cover Crop Tool Box for Organic Vegetable Producers. Virginia Association for Biological Farming Information Sheet*. Available at: https://www.sare.org/content/download/69536/985534/Cover_crops_for_all_seasons.pdf (accessed November 6, 2019).

Sheahan, C. M. (2014). *Plant Guide for Foxtail Millet (Setaria italica)*. Cape May, NJ: USDA-Natural Resources Conservation Service.

Shi, L., Shi, T., Broadley, M. R., White, P. J., Long, Y., Meng, J., et al. (2013). High-throughput root phenotyping screens identify genetic loci associated with root architectural traits in *Brassica napus* under contrasting phosphate availabilities. *Ann. Bot.* 112, 381–389. doi: 10.1093/aob/mcs245

Shin, R., Berg, R. H., and Schachtman, D. P. (2005). Reactive oxygen species and root hairs in *Arabidopsis* root response to nitrogen, phosphorus and potassium deficiency. *Plant Cell Physiol.* 46, 1350–1357. doi: 10.1093/pcp/pci145

Shin, R., and Schachtman, D. P. (2004). Hydrogen peroxide mediates plant root cell response to nutrient deprivation. *Proc. Natl. Acad. Sci. U.S.A.* 101, 8827–8832. doi: 10.1073/pnas.0401707101

Skirycz, A., and Inze, D. (2010). More from less: plant growth under limited water. *Curr. Opin. Biotechnol.* 21, 197–203. doi: 10.1016/j.copbio.2010.03.002

Sofo, A., Scopa, A., Nuzzaci, M., and Vitti, A. (2015). Ascorbate peroxidase and catalase activities and their genetic regulation in plants subjected to drought and salinity stresses. *Int. J. Mol. Sci.* 16, 13561–13578. doi: 10.3390/ijms160613561

Sreenivasulu, N., Miranda, M., Prakash, H. S., Wobus, U., and Weschke, W. (2004). Transcriptome changes in foxtail millet genotypes at high salinity: identification and characterization of a PHGPX gene pecifically upregulated by NaCl in a salt-tolerant line. *J. Plant Physiol.* 161, 467–477. doi: 10.1078/0176-1617-01112

Stevens, C. J., Lind, E. M., Hautier, Y., Harpole, W. S., Borer, E. T., Hobbie, S., et al. (2015). Anthropogenic nitrogen deposition predicts local grassland primary production worldwide. *Ecology* 96, 1459–1465. doi: 10.1890/14-1902.1

Sudhakar, C., Veeranagamallaiah, G., Nareshkumar, A., Sudhakarbabu, O., Sivakumar, M., Pandurangaiah, M., et al. (2015). Polyamine metabolism influences antioxidant defense mechanism in foxtail millet (*Setaria italica* L.) cultivars with different salinity tolerance. *Plant Cell Rep.* 34, 141–156. doi: 10.1007/s00299-014-1695-3

Sun, J., Gibson, K. M., Kiirats, O., Okita, T. W., and Edwards, G. E. (2002). Interactions of nitrate and CO_2 enrichment on growth, carbohydrates and rubisco in *Arabidopsis* starch mutants. Significance of starch and hexose. *Plant Physiol.* 130, 1573–1583. doi: 10.1104/pp.010058

Sutton, M. A., Oenema, O., Erisman, J. W., Leip, A., van Grinsven, H., and Winiwarter, W. (2011). Too much of a good thing. *Nature* 472, 159–161. doi: 10.1038/472159a

Svistoonoff, S., Creff, A., Reymond, M., Sigoillot-Claude, C., Ricaud, L., Blanchet, A., et al. (2007). Root tip contact with low-phosphate media reprograms plant root architecture. *Nat. Genet.* 39, 792–796. doi: 10.1038/ng2041

Syers, J., Johnston, A., and Curtin, D. (2008). *Efficiency of Soil and Fertilizer Phosphorus Use: Reconciling Changing Concepts of Soil Phosphorus Behaviour With Agronomic Information.* Rome: FAO.

Taub, D. R., and Wang, X. (2008). Why are nitrogen concentrations in plant tissues lower under elevated CO2? A critical examination of the hypotheses. *J. Integr. Plant Biol.* 50, 1365–1374. doi: 10.1111/j.1744-7909

Tegeder, M., and Masclaux-Daubresse, C. (2018). Source and sink mechanisms of nitrogen transport and use. *New Phytol.* 217, 35–53. doi: 10.1111/nph.14876

Thibaud, M. C., Arrighi, J. F., Bayle, V., Chiarenza, S., Creff, A., Bustos, R., et al. (2010). Dissection of local and systemic transcriptional responses to phosphate starvation in *Arabidopsis*. *Plant J.* 64, 775–789. doi: 10.1111/j.1365-313X.2010.04375.x

Ticconi, C. A., Lucero, R. D., Sakhonwasee, S., Adamson, A. W., Creff, A., Nussaume, L., et al. (2009). ER-resident proteins PDR2 and LPR1 mediate the developmental response of root meristems to phosphate availability. *Proc. Natl. Acad. Sci. U.S.A.* 106, 14174–14179. doi: 10.1073/pnas.0901778106

Tilman, D., Reich, P. B., and Knops, J. M. (2006). Biodiversity and ecosystem stability in a decade-long grassland experiment. *Nature* 441, 629–632. doi: 10.1038/nature04742

Tsay, Y. F., Chiu, C. C., Tsai, C. B., Ho, C. H., and Hsu, P. K. (2007). Nitrate transporters and peptide transporters. *FEBS Lett.* 581, 2290–2300. doi: 10.1016/j.febslet.2007.04.047

Tsay, Y. F., Schroeder, J. I., Feldmann, K. A., and Crawford, N. M. (1993). The herbicide sensitivity gene Chl1 of Arabidopsis encodes a nitrate-inducible nitrate transporter. *Cell* 72, 705–713. doi: 10.1016/0092-8674(93)90399-b

Turoczy, Z., Kis, P., Torok, K., Cserhati, M., Lendvai, A., Dudits, D., et al. (2011). Overproduction of a rice Aldo-Keto reductase increases oxidative and heat stress tolerance by malondialdehyde and methylglyoxal detoxification. *Plant Mol. Biol.* 75, 399–412. doi: 10.1007/s11103-011-9735-7

Veeranagamallaiah, G., Chandraobulreddy, P., Jyothsnakumari, G., and Sudhakar, C. (2007). Glutamine synthetase expression and pyrroline-5-carboxylate reductase activity influence proline accumulation in two cultivars of foxtail millet (*Setaria italica* L.) with differential salt sensitivity. *Environ. Exp. Bot.* 60, 239–244. doi: 10.1016/j.envexpbot.2006.10.012

Veeranagamallaiah, G., Jyothsnakumari, G., Thippeswamy, M., Reddy, C. O. P., Surabhi, G. K., Sriranganayakulu, G., et al. (2008). Proteomic analysis of salt stress responses in foxtail millet (*Setaria italica* L. cv. Prasad) seedlings. *Plant Sci.* 175, 631–641. doi: 10.1016/j.plantsci.2008.06.017

Veeranagamallaiah, G., Ranganayakulu, G. S., Thippeswamy, M., Sivakumar, M., Reddy, E. K., Pandurangaiah, M., et al. (2009). Aldose reductase expression contributes in sorbitol accumulation and 4-hydroxynon-2-enal detoxification in two foxtail millet (*Setaria italica* L.) cultivars with different salt stress tolerance. *Plant Growth Regul.* 59, 137–143. doi: 10.1007/s10725-009-9396-6

Verwoert, I., Brown, A., Slabas, A. R., and Stuitje, A. R. (1995). A *Zea mays* GTP-binding protein of the ARF family complements an *Escherichia coli* mutant with a temperature-sensitive malonylcoenzyme A:acyl carrier protein transacylase. *Plant Mol. Biol.* 27, 629–633. doi: 10.1007/bf00019329

Vidal, E. A., and Gutiérrez, R. A. (2008). A systems view of nitrogen nutrient and metabolite responses in Arabidopsis. *Curr. Opin. Plant Biol.* 11, 521–529. doi: 10.1016/j.pbi.2008.07.003

Wang, M., Li, P., Li, C., Pan, Y., Jiang, X., Zhu, D., et al. (2014). *SiLEA14*, a novel atypical LEA protein, confers abiotic stress resistance in foxtail millet. *BMC Plant Biol.* 14:290. doi: 10.1186/s12870-014-0290-7

Wang, M., Pan, Y., Li, C., Liu, C., Zhao, Q., Ao, G. M., et al. (2011). Culturing of immature inflorescences and Agrobacterium-mediated transformation of foxtail millet (*Setaria italica*). *Afr. J. Biotechnol.* 10, 16466–16479. doi: 10.5897/ajb10.2330

Wang, W., Hu, B., Li, A., and Chu, C. (2019). NRT1.1s in plants: functions beyond nitrate transport. *J. Exp. Bot.* doi: 10.1093/jxb/erz554 [Epub ahead of print].

Wang, Y., Mi, G., Chen, F., and Zhang, F. (2003). Genotypic differences in nitrogen uptake by maize inbred lines its relation to root morphology. *Acta Ecol. Sin.* 23, 297–302.

Wang, Y., Tang, H., DeBarry, J. D., Tan, X., Li, J. P., Wang, X. Y., et al. (2012). MCScanX: a toolkit for detection and evolutionary analysis of gene synteny and collinearity. *Nucleic Acids Res.* 40:e49. doi: 10.1093/nar/gkr1293

Werdin-Pfisterer, N. R., Kielland, K., and Boone, R. D. (2012). Buried organic horizons represent amino acid reservoirs in boreal forest soils. *Soil Biol. Biochem.* 55, 122–131. doi: 10.1016/j.soilbio.2012.06.012

Wilkinson, S., and Davies, W. J. (2002). ABA-based chemical signalling: the co-ordination of responses to stress in plants. *Plant Cell Environ.* 25, 195–210. doi: 10.1046/j.0016-8025.2001.00824.x

Williamson, L. C., Ribrioux, S. P., Fitter, A. H., and Leyser, H. M. (2001). Phosphate availability regulates root system architecture in *Arabidopsis*. *Plant Physiol.* 126, 875–882. doi: 10.1104/pp.126.2.875

Wilmoth, J. C., Wang, S., Tiwari, S. B., Joshi, A. D., Hagen, G., Guilfoyle, T. J., et al. (2005). NPH4/ARF7 and ARF19 promote leaf expansion and auxin-induced lateral root formation. *Plant J.* 43, 118–130. doi: 10.1111/j.1365-313X.2005.02432.x

Wolters, H., and Jürgens, G. (2009). Survival of the flexible: hormonal growthcontrol and adaptation in plant development. *Nat. Rev.* 10, 305–317. doi: 10.1038/nrg2558

Xu, G., Fan, X., and Miller, A. J. (2012). Plant nitrogen assimilation and use efficiency. *Ann. Rev. Plant Biol.* 63, 153–182. doi: 10.1146/annurev-arplant-042811-105532

Yadav, C. B., Muthamilarasan, M., Dangi, A., Shweta, S., and Prasad, M. (2016). Comprehensive analysis of SET domain gene family in foxtail millet identifies the putative role of *SiSET14* in abiotic stress tolerance. *Sci. Rep.* 6:32621. doi: 10.1038/srep32621

Yamaguchi, S. (2008). Gibberellin metabolism and its regulation. *Ann. Rev. Plant Biol.* 59, 225–251. doi: 10.1146/annurev.arplant.59.032607.092804

Yamaguchi-Shinozaki, K., and Shinozaki, K. (1994). A novel *cis*-acting element in an *Arabidopsis* gene is involved in responsiveness to drought, low-temperature, or high-salt stress. *Plant Cell* 6, 251–264. doi: 10.1105/tpc.6.2.251

Yamaguchi-Shinozaki, K., and Shinozaki, K. (2006). Transcriptional regulatory networks in cellular responses and tolerance to dehydration and cold stresses. *Annu. Rev. Plant Biol.* 57, 781–803. doi: 10.1146/annurev.arplant.57.032905.105444

Ye, Y., Yuan, J., Chang, X., Yang, M., Zhang, L., Lu, K., et al. (2015). The phosphate transporter gene *OsPht1*; 4 is involved in phosphate homeostasis in rice. *PLoS One* 10:e0126186. doi: 10.1371/journal.pone.0126186

Yuan, J. C., Song, J. H., Ma, H. L., Song, X. Q., Wei, H. P., and Liu, Y. H. (2013). Ectopic expression a maize ADP-ribosylation factor gene in *Arabidopsis*, increase plant size and growth rate. *J. Plant. Biochem. Biotechnol.* 24, 161–166. doi: 10.1007/s13562-013-0248-0

Zhang, F., Sun, Y., Pei, W., Jain, A., Sun, R., Cao, Y., et al. (2015). Involvement of OsPht1;4 in phosphate acquisition and mobilization facilitates embryo development in rice. *Plant J.* 82, 556–569. doi: 10.1111/tpj.12804

Zhang, G., Liu, X., Quan, Z., Cheng, S., Xu, X., Pan, S., et al. (2012). Genome sequence of foxtail millet (*Setaria italica*) provides insights into grass evolution and biofuel potential. *Nat. Biotechnol.* 30, 549–554. doi: 10.1038/nbt.2195

Zhang, J. P., Liu, T. S., Zheng, J., Jin, Z., Zhu, Y., Guo, J. F., et al. (2007). Cloning and characterization of a putative 12-oxophytodienoic acid reductase cDNA induced by osmotic stress in roots of foxtail millet. *DNA Seq.* 18, 138–144. doi: 10.1080/10425170601060764

Zhao, L., Zhao, Q., Ao, G., and Yu, J. (2009). The foxtail millet *Si69* gene is a Wali7 (wheat aluminium-induced protein 7) homologue and may function in aluminium tolerance. *Chin. Sci. Bullet.* 54, 1697–1706. doi: 10.1007/s11434-009-0238-8

Zheng, Z., Wang, Z., Wang, X., and Liu, D. (2019). Blue light-triggered chemical reactions underlie phosphate deficiency-induced inhibition of root elongation of *Arabidopsis* seedlings grown in petri dishes. *Mol. Plant* 12, 1515–1523. doi: 10.1016/j.molp.2019.08.001

Zhu, X. L., Zhang, L., Chen, Q., Wan, J., and Yang, G. F. (2006). Interactions of aryloxyphenoxypropionic acids with sensitive and resistant acetyl-coenzyme a carboxylase by homology modeling and molecular dynamic simulations. *J. Chem. Inf. Model.* 46, 1819–1826. doi: 10.1021/ci0600307

Conflict of Interest: The authors declare that the research was conducted in the absence of any commercial or financial relationships that could be construed as a potential conflict of interest.

frontiers in Plant Science

ORIGINAL RESEARCH
published: 09 April 2020
doi: 10.3389/fpls.2020.00405

Genome-Wide Association Study and Genomic Prediction Elucidate the Distinct Genetic Architecture of Aluminum and Proton Tolerance in *Arabidopsis thaliana*

*Yuki Nakano[1], Kazutaka Kusunoki[1], Owen A. Hoekenga[2], Keisuke Tanaka[3], Satoshi Iuchi[4], Yoichi Sakata[5], Masatomo Kobayashi[4], Yoshiharu Y. Yamamoto[1], Hiroyuki Koyama[1] and Yuriko Kobayashi[1]**

[1] Faculty of Applied Biological Sciences, Gifu University, Gifu, Japan, [2] Cayuga Genetics Consulting Group LLC, Ithaca, NY, United States, [3] NODAI Genome Research Center, Tokyo University of Agriculture, Tokyo, Japan, [4] Experimental Plant Division, RIKEN BioResource Research Center, Tsukuba, Japan, [5] Department of Bioscience, Tokyo University of Agriculture, Tokyo, Japan

OPEN ACCESS

Edited by:
Manny Delhaize, CSIRO Plant Industry, Australia

Reviewed by:
Miguel A. Pineros, Robert W. Holley Center for Agriculture & Health, USDA-ARS, United States
Peter Ryan, Commonwealth Scientific and Industrial Research Organisation (CSIRO), Australia

***Correspondence:**
Yuriko Kobayashi
k_yuriko@gifu-u.ac.jp

Specialty section:
This article was submitted to Plant Abiotic Stress, a section of the journal Frontiers in Plant Science

Received: *16 December 2019*
Accepted: *20 March 2020*
Published: *09 April 2020*

Citation:
Nakano Y, Kusunoki K, Hoekenga OA, Tanaka K, Iuchi S, Sakata Y, Kobayashi M, Yamamoto YY, Koyama H and Kobayashi Y (2020) Genome-Wide Association Study and Genomic Prediction Elucidate the Distinct Genetic Architecture of Aluminum and Proton Tolerance in Arabidopsis thaliana. Front. Plant Sci. 11:405. doi: 10.3389/fpls.2020.00405

Under acid soil conditions, Al stress and proton stress can occur, reducing root growth and function. However, these stressors are distinct, and tolerance to each is governed by multiple physiological processes. To better understand the genes that underlie these coincidental but experimentally separable stresses, a genome-wide association study (GWAS) and genomic prediction (GP) models were created for approximately 200 diverse *Arabidopsis thaliana* accessions. GWAS and genomic prediction identified 140/160 SNPs associated with Al and proton tolerance, respectively, which explained approximately 70% of the variance observed. Reverse genetics of the genes in loci identified novel Al and proton tolerance genes, including *TON1-RECRUITING MOTIF 28* (*AtTRM28*) and *THIOREDOXIN H-TYPE 1* (*AtTRX1*), as well as genes known to be associated with tolerance, such as the Al-activated malate transporter, *AtALMT1*. Additionally, variation in Al tolerance was partially explained by expression level polymorphisms of *AtALMT1* and *AtTRX1* caused by cis-regulatory allelic variation. These results suggest that we successfully identified the loci that regulate Al and proton tolerance. Furthermore, very small numbers of loci were shared by Al and proton tolerance as determined by the GWAS. There were substantial differences between the phenotype predicted by genomic prediction and the observed phenotype for Al tolerance. This suggested that the GWAS-undetectable genetic factors (e.g., rare-allele mutations) contributing to the variation of tolerance were more important for Al tolerance than for proton tolerance. This study provides important new insights into the genetic architecture that produces variation in the tolerance of acid soil.

Keywords: acid soil tolerance, ALMT1, aluminum and proton tolerance, co-expression network analysis, ELP – expression level polymorphism, GP – genomic prediction, GWAS – genome-wide association study, natural variation

INTRODUCTION

Acid soil syndrome is a serious limiting factor for food production worldwide (von Uexküll and Mutert, 1995; Kochian et al., 2004). In acid soil, plant root growth is inhibited by various stressors, such as rhizotoxicities of excess Al, proton, manganese (Mn), and iron (Fe), and deficiencies in the available phosphate (Pi) (Kochian et al., 2004). Plants have adapted to acidic environments by developing a number of stress tolerance mechanisms which can have pleiotropic effects on other traits. For example, organic acid excretion from roots contributes to Al tolerance and efficient P-utilization under acid soil conditions (see review, Wu et al., 2018). In contrast, the expression of Al and proton tolerance genes is co-regulated under the downstream of STOP1 (SENSITIVE TO PROTON RHIZOTOXICITY1) in *Arabidopsis thaliana* (Iuchi et al., 2007). Identification of the molecular mechanisms which underlie tolerance to co-existing stress factors may allow for improved crop yields in acid soils, through the use of biotechnology and molecular breeding.

Al occurs in many chemical forms in the soil but the higher concentration of soluble Al^{3+} cations that are present in acidic soils is a major limitation to many crop species. Al toxicity in the growing root tip is reversible over short periods of time, but over long-term exposure, Al treatment disturb various cellular processes, such as cell wall expansion and membrane transport (Ma, 2007). Molecular physiological studies of these events have identified a number of Al tolerance genes (see review, Kochian et al., 2015), and several Al tolerant transgenic crops have already been developed through the overexpression of Al tolerant genes. Ectopic expression of *ALUMINUM ACTIVATED MALATE TRANSPORTER 1* (*ALMT1*) from wheat (*Triticum aestivum*; Sasaki et al., 2004) in barley (*Hordeum vulgare*) (Delhaize et al., 2004), and of *CITRATE SYNTHASE* of *Arabidopsis* (*Arabidopsis thaliana*) in canola (*Brassica napus*) (Anoop, 2003) conferred Al tolerance. However, proton rhizotoxicity can be more toxic than Al rhizotoxicity in natural acid soils (Kinraide, 2003), and is also a complex polygenic trait which requires many genes to achieve distinct physiological processes (Shavrukov and Hirai, 2016). For example, the maintenance of cellular pH, which is essential for adapting to proton stress (Sawaki et al., 2009; Bissoli et al., 2012; Gujas et al., 2012) and the stabilization of pectin, which is essential for protection against proton toxicity (Koyama et al., 2001), are processes regulated by multiple genes. Identification of proton tolerance mechanisms and their interactions with Al tolerance is important for improving the acid soil tolerance of crops.

In certain plant species such as *Arabidopsis* and tobacco (*Nicotiana tabacum*), both Al tolerance and proton tolerance are mutually regulated by the STOP1 (SENSITIVE TO PROTON RHIZOTOXICITY 1) transcription factor (e.g., AtSTOP1, Iuchi et al., 2007, NtSTOP1, Ohyama et al., 2013). Al tolerance genes such as Al activated organic acid transporters (i.e., ALMT and MATE; see review, Daspute et al., 2017), and proton tolerance genes such as *AKT1*, *HAK5,* and *SULTR3;5* are co-regulated by STOP1 (Sawaki et al., 2009). In addition, activation of STOP1/ALMT1 is also involved in the low-phosphate response in *Arabidopsis*, and has been shown to alter root architecture to induce efficient P-uptake (Balzergue et al., 2017). These findings suggest that Al and proton tolerance are controlled by a common molecular mechanism. However, Al and proton tolerant mechanisms are complex and likely involve unidentified mechanisms. Elucidation of such complex adaptive mechanisms can be investigated using genome-wide approaches in *Arabidopsis* (*Arabidopsis thaliana*), that utilize differences in Al and proton tolerance among accessions.

Studies of the natural phenotypic variation in *Arabidopsis* may provide an opportunity to study interactions among Al and proton tolerance mechanisms, which usually co-exist in naturally acid soil environments (Ikka et al., 2007). A genome-wide association study (GWAS) in *Arabidopsis* is a useful way to clarify complex mechanisms, especially when integrated with other genomics approaches. Although a GWAS may likely yield poor detection of quantitative traits with weak locus effects (Bergelson and Roux, 2010), integration with other genome-wide approaches would help to clarify such effects included in the natural variation. For example, genomic prediction (GP), a genome-wide population genetic method, may allow for the assessment of the cumulative effects of associated loci (Crossa et al., 2010; Desta and Ortiz, 2014). Furthermore, integration of GP and co-expression gene network analysis could further improve the sensitivity and accuracy of the population genetic methods used for GWAS (Kobayashi et al., 2016; Kooke et al., 2016; Butardo et al., 2017). Novel and unidentified Al tolerance genes were detected previously using genome-wide expression level polymorphism [Expression level polymorphism (ELP); Delker and Quint, 2011] analyses, by comparing the transcriptomes of three Al tolerant and Al sensitive accessions (Kusunoki et al., 2017). This identified genes that had not previously been reported to relate to known Al tolerant mechanisms (e.g., Al extrusion and internal Al tolerant mechanisms), for example BINDING PROTEIN 3, that is linked to the quality control of proteins in endoplasmic reticulum. Integration of these approaches is a useful method to investigate the molecular determinants driving Al and proton tolerance mechanisms in plants. In this study, we conducted GWAS for Al and proton tolerance, and identified 140 and 160 loci respectively that explained approximately 70% of the variations estimated by GP. Application of other genome-wide approaches identified distinct Al and proton tolerance mechanisms, which independently segregated under natural conditions.

MATERIALS AND METHODS

Plant Materials

Worldwide *Arabidopsis thaliana* accessions described in the 1001 Genomes Project[1] were derived from the Arabidopsis Biological Resource Center, Nottingham Arabidopsis Stock Centre (NASC; Nottingham, United Kingdom), and RIKEN BioResource Research Center (RIKEN BR; Tsukuba, Japan) (**Supplementary Table S1**). The seed progenies used were obtained via single seed descent from the original seeds. Mutants

[1]http://1001genomes.org/

and T-DNA/transposon insertion lines were obtained from NASC (**Supplementary Table S2**).

Transgenic Col-0 for GUS (β-glucuronidase) reporter assays used to characterize *AtALMT1* promoters were generated using *Agrobacterium tumefaciens* (GV3101)-mediated transformation, using methods described by Clough and Bent (1998). Promoter-GUS was cloned into the binary vector (pBE2113) by overlap-extension PCR (Horton et al., 1989) using the gene-specific primers described in **Supplementary Table S3**.

Plant Growth Conditions and Phenotyping of Al and Proton Tolerance

Al and proton tolerance of accessions was judged by the relative root growth (treatments/control) of hydroponically grown seedlings as described previously (Kobayashi et al., 2007). Approximately 20 seedlings of accessions were grown hydroponically for 5 days in modified MGRL nutrient solution (Fujiwara et al., 1992), which contained 2% MGRL nutrients [other than P and Ca (-P, $CaCl_2$ adjusted to 200 μM)]. The initial pH of the control (modified MGRL; no Al) and Al toxic (modified MGRL plus 5 μM of $AlCl_3$) solutions were adjusted to 5.0, whereas that of the proton toxic (modified MGRL) solution was adjusted to 4.6. All solutions were renewed every two days. Approximately 200 accessions were equally divided into two and grown in each plastic container containing 10 L of culture solution using the method developed by Toda et al. (1999). The growth test at one condition among three conditions was conducted at the same time. Seedlings were placed on solidified agar (1%, w/v) and photographed using a digital camera (Canon EOS kiss X5). The length of the primary roots was then determined using LIA32 software (LIA for Win32[2]). Relative root length (RRL; root length under stressed conditions/root length under control conditions [%]) was calculated for each line using the five longest roots in each condition (average of five biological replicates seedlings, $n = 5$). All growth experiments were conducted under controlled environmental conditions (12 h day/night cycle, 37 μmol m^{-2} s^{-1} at 24°C ± 2°C). After removing accessions with low germination percentages, we obtained the phenotype of 206, 196, and 200 accessions under the control, Al stress, and proton tress conditions respectively. Broad-sense heritability (H_b^2) and CV were calculated following the methods of Ikka et al. (2007).

Estimation of Population Structure

Information for 211,781 SNPs was obtained from various web sites[3,4]; see Cao et al., 2011; Horton et al., 2012) and was used to analyze population structure and for the GWAS.

Population structure among *Arabidopsis* accessions was estimated using an admixture model following Pritchard et al. (2000) with the model-based program STRUCTURE v. 2.3.4[5] and a set of 1000 selected SNPs. Selection of the 1000 SNPs was based on the following criteria: (1) MAF ≥ 10%, (2) no missing calls for all accessions, (3) consisting of two alleles, and (4) having similar intervals. STRUCTURE was used to estimate the number of subpopulations [defined as L(K), where K is the number of ancestor subpopulations inputted] and the Q-matrix (indicating ancestor subpopulation components of each accession by given K) for K = 1 to 15. The burn-in period was set to 50,000, with the Markov Chain Monte Carlo iterations and run length set to five replications of 50,000. The largest possible number of K (i.e., 6), which was used for genome-wide association study (GWAS), was determined by the ΔK method (Evanno et al., 2005) using the formula $L'(K) = L(K) - L(K-1)$, $|L'(K)| = |L'(K+1) - L'(K)|$.

GWAS and Other Genetic Analyses

The GWAS was performed with a compressed linear mixed model using "Q-matrix" + "kinship-matrix" (Yu et al., 2006; Zhang et al., 2010) with the software TASSEL v. 3.0 (Bradbury et al., 2007). The Q-matrix was computed using STRUCTURE, and the kinship-matrix was processed using TASSEL. A total of 175,324 genome-wide SNPs (MAF ≥ 5%, missing call rate ≤ 5%) were used for the GWAS analysis. Genomic prediction (GP) analysis using the glmnet R package (Friedman et al., 2010) was performed to evaluate the cumulative effect of loci linked to the top-ranked SNPs obtained on the basis of *p*-values in the GWAS as previously described (Kobayashi et al., 2016). Using randomly selected SNPs throughout the genome as a reference, the cumulative effects of the linked loci were estimated with 20–300 (each 20 intervals) top-SNPs and defined 140 and 160 top-SNPs as significantly associated SNPs for Al and proton tolerance, respectively. Missing SNPs were imputed using the program BEAGLE (Browning and Browning, 2009). The cumulative effect and predictive accuracies were estimated using 100 replicates of five-fold cross-validation using the coefficient of determination (r^2) and RMSE respectively as indexes.

The local LD (pairwise $r^2 > 0.80$) of each associated SNP was analyzed using other surrounding SNPs within the 10 kb window using the program PLINK v. 1.07[6]; Purcell et al., 2007). Physical positions of the SNPs on the genome, open reading frames (ORF), and untranslated regions (UTR) were obtained from the TAIR 9 database[7]. The genomic DNA region of each gene was defined as the region consisting of a UTR, ORF, and putative promoter (−2 kb from the end of 5′ UTR). Together with the above information, genes located within the LD region of each associated SNP were grouped as the tolerance candidate genes. However, when no LD region was detected in an associated SNP, we chose the closest gene as the candidate associated with the corresponding SNP.

The accessions with unusual phenotype were inferred from the rate of difference in RRL between that observed and that predicted by GP. The difference rate was calculated using the formula $\log_2$ (observed RRL/predicted RRL). The predicted RRLs were calculated using the average of the RRLs of 100 cross-validations with the top 140 and 160 SNPs detected by the GWAS. The unusual accessions were mapped onto a world map

[2]https://www.agr.nagoya-u.ac.jp/~shinkan/LIA32/index-e.html

[3]https://cynin.gmi.oeaw.ac.at/

[4]http://1001genomes.org/index.html

[5]http://pritchardlab.stanford.edu/structure.html

[6]http://pngu.mgh.harvard.edu/purcell/plink/

[7]http://www.arabidopsis.org

using the "Geocoding and Mapping" web tool[8]. The map of soil pH in Europe was obtained from the European Soil Data Centre's (ESDAC) 'Map of Soil pH in Europe' (Land Resources Management Unit, Institute for Environment & Sustainability, European Commission Joint Research Centre, 2010[9].

Reverse Genetics and Co-expression Network Analysis

Al and proton tolerance of T-DNA and mutant lines were judged using the RRL from hydroponically grown seedlings as described in the preceding sections. Co-expression network analyses were conducted using the tool NetworkDrawer implemented in ATTED-II (Obayashi et al., 2018) using co-expression data of "Ath-r" with the 'add many genes' option.

Expression Analysis of Accessions and Expression GWAS

Approximately 100 seedlings of each accession were grown hydroponically for 10 d in control solution (0 μM Al, pH 5.6). Subsequently, the roots were treated with the Al stress solution (10 μM Al, pH 5.0) for 9 h, and the total RNA isolation from the roots and reverse transcription were conducted using Sepasol-RNA I Super G (Nacalai Tesque, Kyoto, Japan) with High-Salt Solution for Precipitation (Plant) (Takara Bio, Japan) and ReverTra Ace qPCR RT Master Mix with gDNA Remover (Toyobo, Osaka, Japan), respectively, following the manufacturer's instructions. Quantitative RT-PCR was performed using the standard curve as previously described by Bustin et al. (2009). *AtSAND* (AT2G28390) was used as an internal control, and the gene expression level of each accession was normalized by that of Col-0 as the control of experimental batches. Sequences of gene-specific primers used for qPCR are shown in the **Supplementary Table S3**. Gene expression level of each accession was defined by mean from three replicates. The *p*-values for the correlation between the SNP alleles (MAF $\geq$ 10%) and gene expression levels were calculated from the expression level of accessions with the tolerant and sensitive allele (from 8 to 17 biological replicates per allele) using the "lm" function in R version 3.3.0[10]. Expression GWAS analysis using gene expression level of approximately 70 accessions was conducted in the program TASSEL v. 3.0 using a generalized linear model (GLM) with the genome-wide SNPs used for the GWAS evaluating RRL.

Sequence Analysis of *AtALMT1* Locus

The *AtALMT1* promoter sequences (-2235 bp from ATG) of *Arabidopsis* accessions were sequenced using direct sequencing for the genomic PCR-amplicons using a BigDye Terminator v. 3.1 Cycle Sequencing Kit (Applied Biosystems), according to the manufacturer's recommended protocol. Genomic PCR for direct sequencing was conducted using TaKaRa Ex Taq (Takara), and clean-up of PCR products was conducted using ExoSap-IT (Affymetrix). Assembly and multiple sequence alignment were carried out using the programs GENETYX v. 11 (Genetyx) and MEGA 6.06 (Tamura et al., 2013). The *AtALMT1* promoter sequences of *Arabidopsis* accessions determined in this study were submitted to the DDBJ database. The DDBJ accession numbers are shown in the **Supplementary Table S8**. The sequences of reference accessions (e.g., Col-0) were obtained from the TAIR 10 database. The haplotypes of the *AtALMT1* promoter were initially estimated from the sequence data of 46 accessions with MAF > 10% and haplotype frequency > 10%. We then determined a series of variants constituting the haplotypes for an additional 25 accessions to estimate the four major haplotypes (**Supplementary Table S4**). The haplotype network of the *AtALMT1* promoter was constructed using the reduced median network method (Bandelt et al., 1995) with the "frequency > 1" criterion in the program NETWORK 5.0[11]. Insertion and deletion sites, including putative transposon element insertions, were handled as a single mutation in the calculation. The accessions with Hap2 type *AtALMT1* promoter were mapped onto a world map as described above.

GUS Staining, Expression Level Analysis

GUS staining of 5-day-old seedlings was performed following Kosugi et al. (1990) following 9 h of exposure to hydroponic solution containing 10 μM $AlCl_3$ at pH 5.0. Expression level analysis of GUS was conducted as described above using *UBQ1* (AT3G52590) as an internal control (three technical replicates in three individual transgenic lines for each construct).

Malate Excretion Analysis

Malate excretion from the *Arabidopsis* roots was analyzed as previously described (Kobayashi et al., 2007). Approximately 10 seedlings were hydroponically pre-grown for 4 d in sterile growth MGRL medium (pH 5.0) in Magenta GA-7 boxes (Sigma-Aldrich). Subsequently, their roots were aseptically transferred to 2% MGRL medium supplemented with 1% sucrose, with or without 10 μM $AlCl_3$ at pH 5.0 in 6-well plates. Root exudates were collected after 9 h, and malate levels were quantified enzymatically using the procedure reported by Hampp et al. (1984). Mean values of three biological replicates in each condition were calculated.

RESULTS

Variation of Al and Proton Tolerance Among *Arabidopsis* Accessions and Subpopulations

The relative root length of seedlings grown in Al (RRL_{Al}; pH 5.0 plus 5 μM Al to minus Al) and proton (RRL_{proton}; pH 4.6 to pH 5.0) hydroponic culture correlates with the tolerance of *Arabidopsis* to Al (Kobayashi et al., 2005) and proton (i.e., proton stress, Kobayashi et al., 2013) rhizotoxicities in acid soils. We scored the indices of 206 accessions of *Arabidopsis thaliana* from the 1001 Genomes Project collection (see

[8]http://ktgis.net/gcode/index.php

[9]https://esdac.jrc.ec.europa.eu/content/soil-ph-europe

[10]http://www.R-project.org/

[11]http://www.fluxus-engineering.com/index.htm

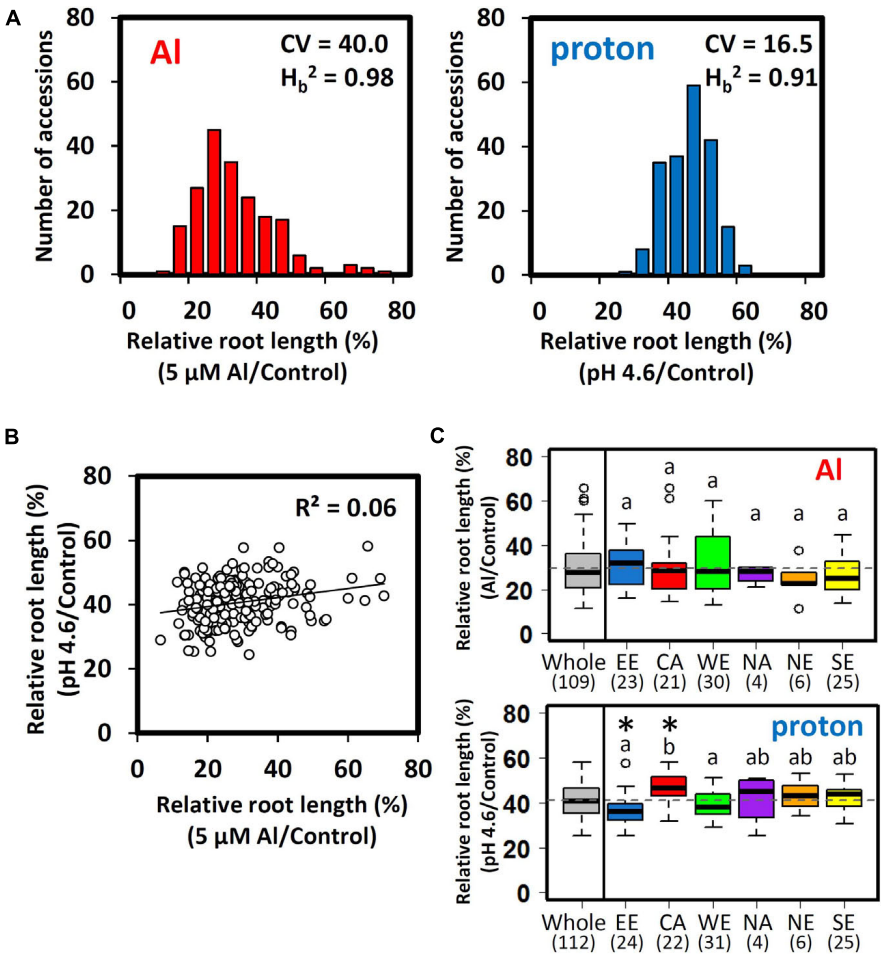

FIGURE 1 | Al and proton tolerance of *Arabidopsis thaliana* accessions. **(A)** Distribution of the relative root lengths (RRLs) of 206 *A. thaliana* accessions under Al and proton stress conditions (CV; coefficient of variation, H_b^2; broad-sense heritability). Seedlings were grown hydroponically for 5 days in either Al (5 µM Al, pH 5.0)/proton (0 µM Al, pH 4.6) solutions or a control solution (0 µM Al, pH 5.0). Five biological replicates of root length were used for calculation of relative root length [RRL; root length under stress conditions/root length under control conditions (%)] (n = 5). **(B)** Correlation between Al and proton tolerance among *A. thaliana* accessions. **(C)** Boxplot of Al and proton tolerance for 112 representative accessions from six ancestral subpopulations inferred from STRUCTURE (EE; Eastern Europe, NA; North America, CA; Central Asia, WE; Western Europe, NE; Northern Europe, SE; Southern Europe). The values under EE-SE represent the number of representative accessions of each subpopulation (**Supplementary Table S1**). Significant outliers from the mean RRL for each subpopulation are indicated by open circles above or below the boxplots. The mean RRL value for the whole population is represented by a dashed line. Asterisks above the boxplots indicate a significant difference from the mean RRL value for the whole population (permutation test, $p < 0.05$). Different letters indicate statistically significant differences in mean RRL value among the six subpopulations (Tukey's HSD test, $p < 0.05$).

Seren et al., 2017), which included subpopulations adapted to multiple geographic locations. Using the STRUCTURE software, we identified six ancestral subpopulations (**Supplementary Figure S1**), which can be grouped by the geographic distribution of accessions, corresponding to six locations [Eastern Europe (EE), North America (NA), Central Asia (CA), Western Europe (WE), Northern Europe (NE), and Southern Europe (SE) (**Supplementary Table S1** and **Supplementary Figure S1**)]. After excluding accessions with a low germination rate ($n \leq 5$), we obtained 196 RRL_{Al} and 200 RRL_{proton}, respectively (**Figure 1A**). While broad-sense heritability estimates were similar ($H_b^2{}_{Al}$ = 0.98, $H_b^2{}_{proton}$ = 0.91), variation in Al tolerance responses was more than twice as large as that for proton tolerance responses, as estimated by the coefficient of variation (CV) of each phenotype (CV_{Al} = 40.0, CV_{proton} = 16.5). However, there were no significant correlations between Al and proton tolerance among the accessions (**Figure 1B**). These results suggested that, for the most part, each trait is differently regulated and segregated among *Arabidopsis* accessions.

Differences in segregation patterns between Al and proton tolerances among subpopulations were compared using 112 accessions (i.e., accessions without typical admixture of subpopulations), which carried more than 70% of the estimated membership of each ancestral subpopulation (**Supplementary Table S1**). There were no significant differences in the mean RRL_{Al} between subpopulations. However, there were significant differences in the mean RRL_{proton} between the CA (proton tolerance) and the EE subpopulations (proton sensitive)

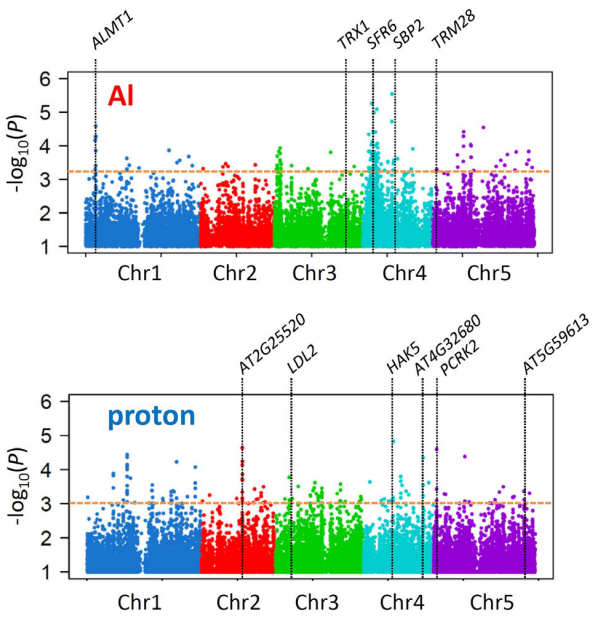

FIGURE 2 | Association mapping for Al and proton tolerance. Manhattan plots for GWA mapping of Al and proton tolerance. Only SNPs with a p-value < 0.1 are shown. The horizontal dashed line indicates the p-value cutoff based on the cumulative effects of the associated SNPs (Al; $p < 6.2 \times 10^{-4}$, proton; 1.1×10^{-3}) respectively. The loci of the genes are shown as a part of genes influenced on the tolerances (**Figure 5**).

(permutation test, $p < 0.05$; **Figure 1C**). Several subpopulations showed larger within-subpopulation variation of RRL_{Al} (WE and EE) and RRL_{proton} (NA). However, these subpopulations showed relatively lower levels of within-subpopulation variation for the other trait. These observations suggested that Al and proton tolerance did not co-segregate between and within the subpopulations. Several accessions were significantly more tolerant or sensitive in comparison to other accessions belonging to the same subpopulation. Only one accession of the EE subpopulation showed unusual proton tolerance (RRL_{proton}), whereas four accessions of the CA and NE subpopulations showed remarkable differences in Al tolerance (RRL_{Al}) when compared to other members of the same subpopulation (**Figure 1C**). This suggests that the unusual phenotype of Al tolerance may occur more frequently than for proton tolerance.

Identification of Effective Loci That Control Al and Proton Tolerance

GWA mapping using linear mixed models in the TASSEL software (Bradbury et al., 2007), utilizing 175,324 genome-wide SNPs (MAF ≥ 5%, missing call rate ≤ 5%), identified several loci controlling each trait. The different shapes of Manhattan plots obtained by GWA mapping suggested that our analyses successfully identified different loci controlling Al and proton tolerance variations (**Figure 2**). Ridge regression analyses of the phenotype (RRL_{Al} and RRL_{proton}) and genotype of accessions (i.e., genomic prediction; GP) were conducted using the top-ranked SNPs (i.e., SNPs with the lowest p-value in GWA mapping; **Figure 2**) to estimate effective SNPs, which in relatively small numbers cumulatively explain large proportions of phenotypes.

Both R^2 curves of the GP, which indicate the proportion of the phenotype explained using a given number of SNPs, peaked before they attained plateau (**Figure 3A**). According to the corresponding number of SNPs that presented the highest R^2 values before plateauing, we assumed that the 140 (Al) and 160 (proton) SNPs would most effectively explain each trait with relatively small numbers. The highest p-values for these SNPs determined by GWA mapping were less than 6.2×10^{-4} for RRL_{Al} and 1.1×10^{-3} for RRL_{proton} (see **Figure 2**), and each set of SNPs explained approximately 75 and 68% of phenotypic variation of each trait, respectively. None of the associated SNPs was detected in both GWA mapping analyses, which reinforces the observation that Al and proton tolerance were unrelated (**Figure 2**). The R^2 of the ridge regression of GP for the top-20 SNPs was greater for Al tolerance (approximately 40%) than for proton tolerance (approximately 20%) (**Figure 3A**). This suggests that a larger proportion of RRL_{Al} is controlled by a relatively small number of loci in comparison to the proportion of RRL_{proton}.

The RMSE (root-mean-square error) in GP evaluates the difference between predicted phenotype and observed phenotype for all accessions. Al tolerance (at 120 SNPs, RMSE = 5.75) had a larger RMSE than proton tolerance (at 140 SNPs = 3.81) which suggests that individual accessions show larger differences between predicted and observed RRLs under Al stressed conditions. To test this, we calculated the "difference rate" [i.e., Log_2(observed RRL/predicted RRL)] of individual accessions under Al and proton toxic conditions (**Figure 3B**). Although most accessions showed small differences (difference rate < |0.5|) between the predicted and observed RRL in both conditions (**Figure 3B**), 12 and four accessions showed markedly different observed RRL from predicted RRL in Al and proton tolerance, respectively (indicated in **Supplementary Table S1**). This observation suggests that rare-allelic mutations, or other genetic events that induce unusual phenotypes, may occur more frequently in Al tolerance than in proton tolerance.

Among the unusual accessions, Voeran-1 showed the largest difference in its RRL_{Al} when compared using GP (Difference rate = -1.35; 6.6% in observed RRL and 16.9% in predicted RRL). The accession showed no Al inducible malate excretion, which was comparable with the *AtALMT1*-knockout (KO) mutant (**Figure 4A**). We confirmed that a mutation introducing a premature STOP codon was present in *AtALMT1* of Voeran-1 by sequencing (**Figure 4B**), which explains why its hypersensitivity to Al stress deviated from the GP.

Identification of Genes Control Al and Proton Tolerance Associated With Effective SNPs

We identified total 453 and 578 candidate gene that were located within the 10 kb region (average linkage disequilibrium [LD] decay of *Arabidopsis*; Kim et al., 2007) flanking the 140 and 160 GWAS-detected SNPs for Al and proton tolerance, respectively.

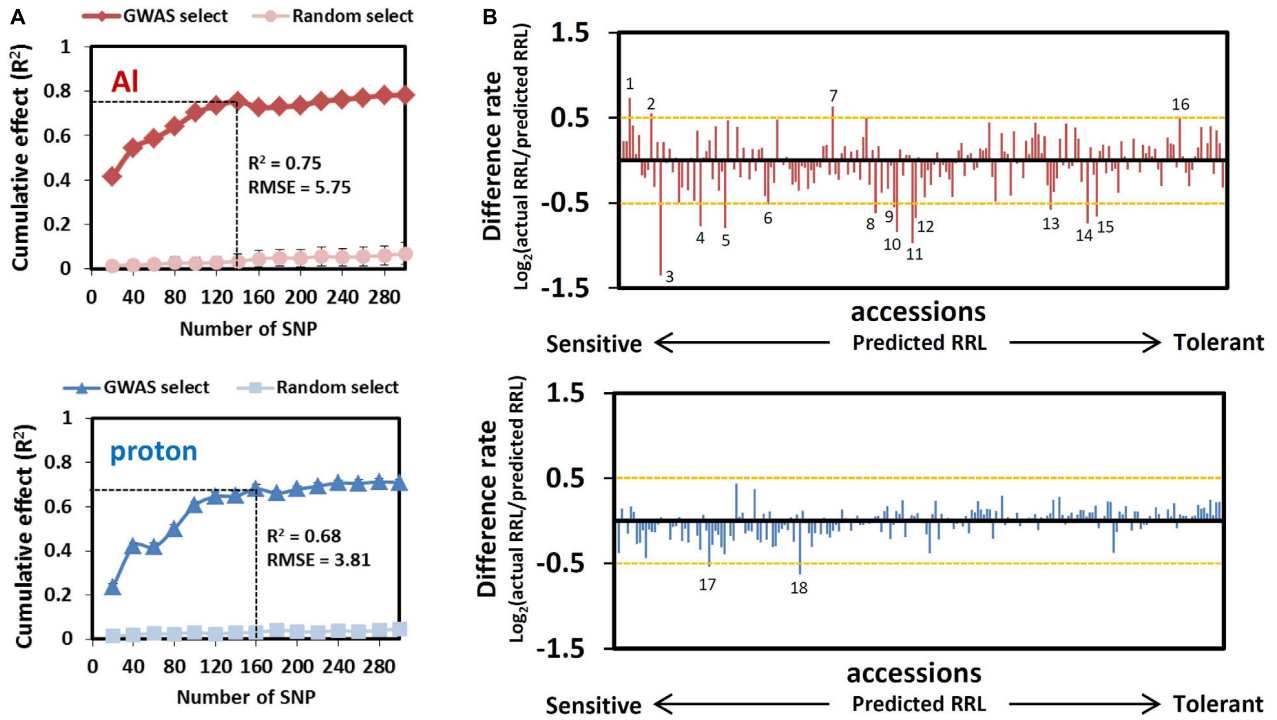

FIGURE 3 | Estimation of the cumulative effect of GWAS detected SNPs by genomic prediction. **(A)** Cumulative effect of 20–300 top-ranked SNPs detected by the GWAS of Al and proton tolerance. Cumulative effects and prediction accuracies were calculated using 100 times 5-fold cross-validations using coefficients of determination (r^2) and root mean squared error (RMSE) as indexes respectively. **(B)** Difference rate of Al and proton tolerance between actual RRL and predicted RRL. The orange horizontal dashed line indicates the cutoff for unusual phenotype (|Difference rate| ≥ 0.5). Numbers on or under bar plot represent the accessions showing an unusual phenotype (1: Lm-2, 2: Tsu-0, 3: Voeran-1, 4: Bil-7, 5: Bak-2, 6: Dra-2, 7: Fei-0, 8: Bolin-1, 9: Lp2-2, 10: Pna-17, 11: Nermut-1, 12: Bch-4, 13: Jablo-1, 14: Pa-3, 15: Ct-1, 16: Shigu-2, 17: Dra-2, 18: Buckhorn Pass).

The genes listed in **Supplementary Tables S5, S6** were investigated for their contribution to the observed phenotypic variation, in order to identify mechanisms underlying the natural variation detected by GWA mapping. The gene list contained some reported tolerance genes such as *AtALMT1*, which has been previously associated with Al tolerance (Hoekenga et al., 2006). However, most genes had never been reported as controlling Al or proton tolerance. The contribution of these unidentified genes were evaluated by reverse-genetics and co-expression gene network analysis.

The genes in the list were first filtered as to whether or not they were in the local linkage disequilibrium (LD) block ($r^2 \geq 0.8$), with the detected SNPs calculated individually (i.e., 168 genes for RRL_{Al} GWA mapping and 187 genes for RRL_{proton} GWA mapping; **Supplementary Tables S5, S6**). Reverse-genetics approaches were applied for all the publicly available mutants of the filtered genes at world-wide *Arabidopsis* bioresource centers (i.e., 44 and 38 genes of the genes detected by Al and proton GWA mapping). Using this approach, we found that 16 and 6 mutants showed significantly altered RRL_{Al} and RRL_{proton} tolerance respectively (Student's t-test, $p < 0.05$) (**Figure 5**).

The most sensitive of these knockouts was the previously studied *AtALMT1* (RRL [/WT] = 0.14), which served as a positive control for our analyses. However, all of the other 16 mutants with reduced tolerance to Al stress were newly identified by this study, these include: *TON1 RECRUITING MOTIF 28* (*AtTRM28*; *At5G03670*) (RRL [/WT] = 0.36), *SENSITIVE TO FREEZING 6* (*AtSFR6*; *AT4G04920*) (RRL [/WT] = 0.53) and *THIOREDOXIN H-TYPE 1* (*AtTRX1*; *AT3G51030*) (RRL [/WT] = 0.64) (**Figure 5**). Mutant analysis for proton tolerance led to decreased stress tolerance far less frequently; in fact, only two of the six knockouts had reduced tolerance to proton stress while the other four were more tolerant. The mutants of *LSD1-LIKE2* (*AtLDL2;* AT3G13682) and *PATTERN-TRIGGERED IMMUNITY COMPROMISED RECEPTOR-LIKE CYTOPLASMIC KINASE 2* (*AtPCRK2;* AT5G03320) were mildly more sensitive to proton stress, while the mutants of *HIGH AFFINITY* K^+ *TRANSPORTER 5* (*AtHAK5*; AT4G13420), three genes encoding drug/metabolite transporter superfamily protein (AT2G25520), ATP synthase (AT5G59613) and transmembrane protein (AT4G32680) were mildly more tolerant to proton stress. These results suggest that we successfully identified several genes that control natural variation of Al and proton tolerance in *Arabidopsis* polygenically.

Co-expression gene network analysis was conducted using the ATTED-II database to identify additional tolerance genes to those found using the reverse genetics approach. Although no networks were formed by proton tolerance genes, we found three co-expression gene networks that contained multiple Al tolerance genes identified

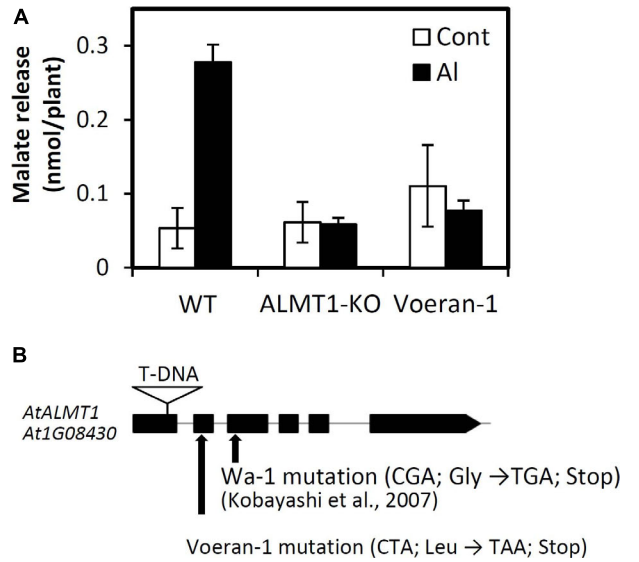

FIGURE 4 | Characterization of Al hypersensitivity in Voeran-1. **(A)** Malate excretion from the root of WT (Col-0), knockout mutant of AtALMT1 and Voeran-1 under control (0 μM Al, pH 5.0) and Al (10 μM Al, pH 5.0) condition for 9 h. Mean values ± SD are shown (average of three biological replicates samples; $n = 3$). **(B)** Position of mutation in *AtALMT1* of Voeran-1 and Wa-1, and T-DNA inserted site of knock out mutant.

by reverse-genetics (**Supplementary Figures S2, S3**). In addition, each network contained several other genes that were linked to the effective SNPs for RRL_{Al} by GP (**Figure 6**). One co-expression network contained *AtALMT1* and AT2G16980. This network was composed of the two Al tolerance genes and 25 co-expression genes including two GWAS-detected genes (*FATTY ALCOHOL:CAFFEOYL-COA CAFFEOYL TRANSFERASE* [*FACT*] and *RGF1 INSENSITIVE 2* [*RGFR2;* AT5G48940]) located within ± 10 kb of the 30th and 41st associated SNPs respectively. Another network was composed of *AtTRM28* and *AtTRX1*, which were demonstrated to have a relatively large contribution to Al tolerance (**Figure 5**), and 14 co-expression genes including one GWAS-detected gene *AUXIN-INDUCED IN ROOT CULTURES 9* (*AIR9*) located within ± 10 kb of the 79th associated SNP. Among the three co-expression networks, two networks contained genes involved in biological processes including "protein processing in endoplasmic reticulum" and "biosynthesis of secondary metabolites." These biological processes are regulated by each network and may have important roles in Al tolerance.

Expression Level Polymorphism of *AtALMT1* and *AtTRX1*

Expression level polymorphism is one of the mechanisms which causes phenotypic variation of Al tolerance among *Arabidopsis* accessions (Kusunoki et al., 2017). Using randomly chosen 25 accessions, we measured the expression level of four GWAS-detected Al tolerance genes, *AtALMT1*, *AtTRM28*, *AtTRX1,* and *AtSFR6*, that showed more than 30% decrease of Al tolerance in the mutant compared to WT as shown in **Figure 5**, and analyzed the correlation between the ELP of tolerance genes and RRL_{Al}-associated SNP (**Figure 7**). We found that expression levels of *AtALMT1* and *AtTRX1* were significantly greater in accessions carrying tolerant allele than in accessions carrying sensitive allele. Both *AtALMT1* and *AtTRX1* are directly linked to top-ranked SNPs, but there was no association between the SNPs and amino acid polymorphisms of either proteins obtained from the 1001 proteomes database (Joshi et al., 2012) (**Supplementary Table S7**). This suggests that protein polymorphism does not play an important role in the variation in Al tolerance caused by these genes. Instead, it suggests that ELP of *AtALMT1* and *AtTRX1* is involved in the mechanism of RRL_{Al} variation.

Expression GWAS (eGWAS) was conducted on both genes to identify possible mechanisms controlling ELP. The eGWAS of *AtTRX1* solely identified a single peak at its own locus and the most significant SNP was the same as that detected using GWAS of RRL_{Al} (Chr.3_18951741, **Figures 8A–C**). This strongly suggests that ELP of *AtTRX1*, caused by cis-polymorphism (e.g., polymorphism in promoter), contributes to generating Al tolerance variation. By contrast, eGWAS of *AtALMT1* linked to the *AtALMT1* promoter region and several other loci, suggesting that a portion of ELP of *AtALMT1* could be explained by the difference in promoter activity, which may be directly regulated by the locus (**Figures 8D–F**). To test this possibility, we conducted haplotype analysis and promoter-*GUS* fusion analysis on *AtALMT1* promoter.

Haplotype analysis of *AtALMT1* promoter was conducted using 71 accessions. This analysis provided several haplotypes, in which there were four major haplotypes (Hap1-Hap4, frequency > 10%) (**Figure 9A** and **Supplementary Table S4**). All 10 accessions with minor alleles of GWAS-detected SNP constituted Hap2, which carried 498 bp insertion corresponding to a transposable element (TE) AT1TE08660 of the ATLANTYS3 family 879 bp upstream of the ORF. Additionally, several SNPs and small indels constituting each haplotype were found (**Figures 9A,B**). To evaluate this model further, we compared the activity of the Hap2 type promoter (Col-0) and a sensitive promoter (Bil-7) using transgenic carrying promoter-*GUS* (**Figure 10**). The part of GUS activity in the root was similar in both lines (**Figure 10A**), however, the *GUS* expression level of the Col-0 promoter-*GUS* line was significantly greater than that of the Bil-7 promoter-*GUS* line (**Figure 10B**). By contrast, deletion of TE showed lower *GUS* expression compared with that of the Col-0 promoter-*GUS* line (**Figure 10B**), indicating that greater expression of Hap2 is, in part, caused by the TE insertion, which is involved in the greater expression level of *AtALMT1* observed in Col-0.

DISCUSSION

Tolerance to Al and proton toxicities are mostly quantitative traits but single major genes can account for a large proportion of the phenotypic variation in many species (e.g., Kobayashi and Koyama, 2002; Hoekenga et al., 2003; Kobayashi et al., 2005; Ikka et al., 2007). In the present study, a GWAS of Al and proton tolerance using the RRLs of *Arabidopsis* accessions

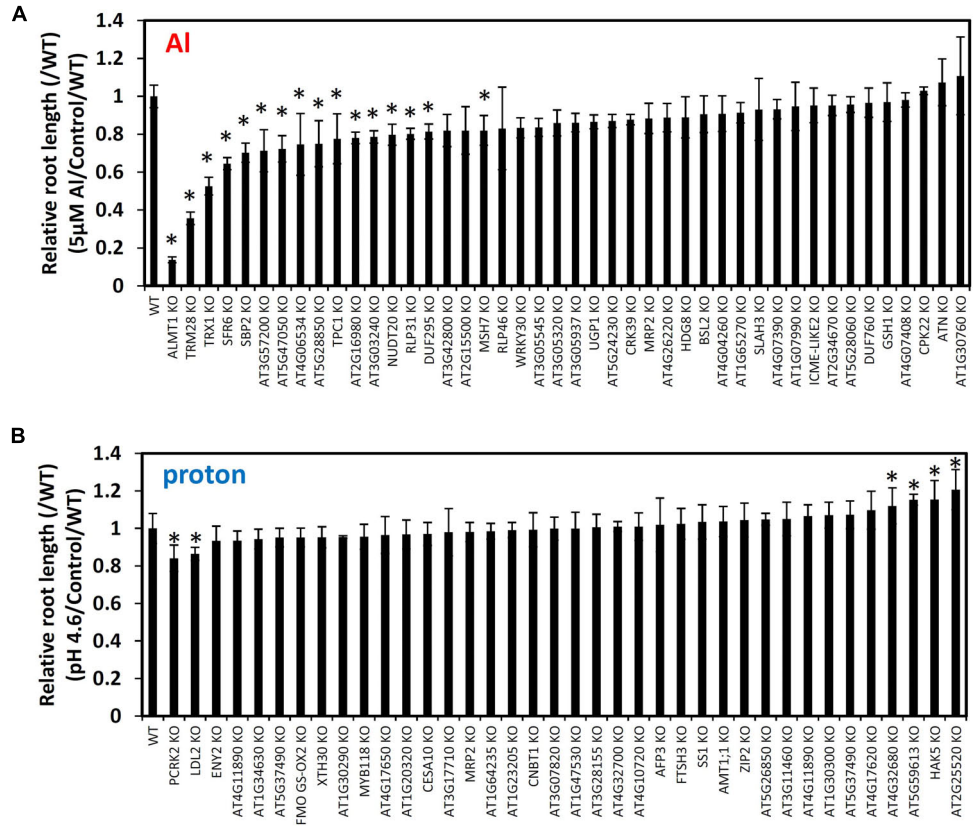

FIGURE 5 | Root growth of mutant lines of GWAS-identified candidate genes for Al **(A)** and proton **(B)** tolerance. Seedlings were grown hydroponically for 5 days in either Al (5 μM Al, pH 5.0)/proton (0 μM Al, pH 4.6) solutions or a control solution (0 μM Al, pH 5.0). Five biological replicates of root length were used for calculation of relative root length (RRL; root length under stress conditions/root length under control conditions). It was divided by the RRL value of WT. Mean values ± SD are shown (n = 5). Asterisks indicate significant differences ($p < 0.05$; Student's t-test) compared to WT.

identified various genes linked to the detected SNPs, which cumulatively explained approximately 70% of the phenotypic variations of each trait, which included some of major genes controlling each trait (**Figure 3A**). The identified genes (168 and 187 genes by RRL_{Al} and RRL_{proton} respectively, **Supplementary Tables S5, S6**) included a number of critical genes (e.g., *AtALMT1* for Al tolerance, Hoekenga et al., 2006) for which dysfunctional mutation could directly alter tolerance (**Figure 5**). GWAS revealed the cumulative effects of multiple genes that controlled these tolerances, which belonged to the distinct biological process of either Al or proton tolerance (**Figure 6** and **Supplementary Figures S2, S3**). These results provide new insights into the complex mechanisms underlying Al and proton tolerance in plants.

A comprehensive reverse genetics approach using the T-DNA mutants of the GWAS-detected genes revealed the importance of STOP1-regulated genes, *AtALMT1* and *HAK5*, for variation in Al tolerance and proton tolerance, respectively (**Figure 5**). *AtALMT1*, which encodes an Al activated malate transporter, is one of the critical Al tolerance genes in *Arabidopsis* (Hoekenga et al., 2006) and was linked to the major QTL of the L*er*/Col (Kobayashi and Koyama, 2002) and L*er*/Cvi population (Kobayashi et al., 2005). The T-DNA KO line of *HAK5*, which encodes a high-affinity K^+ transporter, slightly enhanced proton tolerance (**Figure 5**). In contrast, higher expression of *HAK5* was observed in the proton-sensitive STOP1 mutant compared to WT when under proton stress (Sawaki et al., 2009). This could account for the role of K^+ homeostasis in the protection of cells against proton stress through the maintenance of cytosolic pH (Britto and Kronzucker, 2005; Bissoli et al., 2012).

Our GWAS and GP did not identify the STOP1 locus in either Al or proton stress tolerance (**Supplementary Table S5, S6**). It appears that the gradual adaptation of *Arabidopsis* to acid soils relied on modifications to the genes downstream of this major transcription factor, rather than changes to the transcription factor itself. In contrast, the polymorphism of STOP1-like protein (rice ortholog ART1) was identified as being important for variation in Al tolerance in rice (Arbelaez et al., 2017). This suggests that polymorphisms in STOP1 do not cause the variation in Al and proton tolerance among *Arabidopsis* accessions, where this is not the case in rice. This may be a result of the pleiotropic nature of STOP1-like proteins and the differences in the number of copies in the two species. Rice contains at least five copies of STOP1-like proteins (Yamaji et al., 2009). However, *Arabidopsis* contains only two copies of the genes

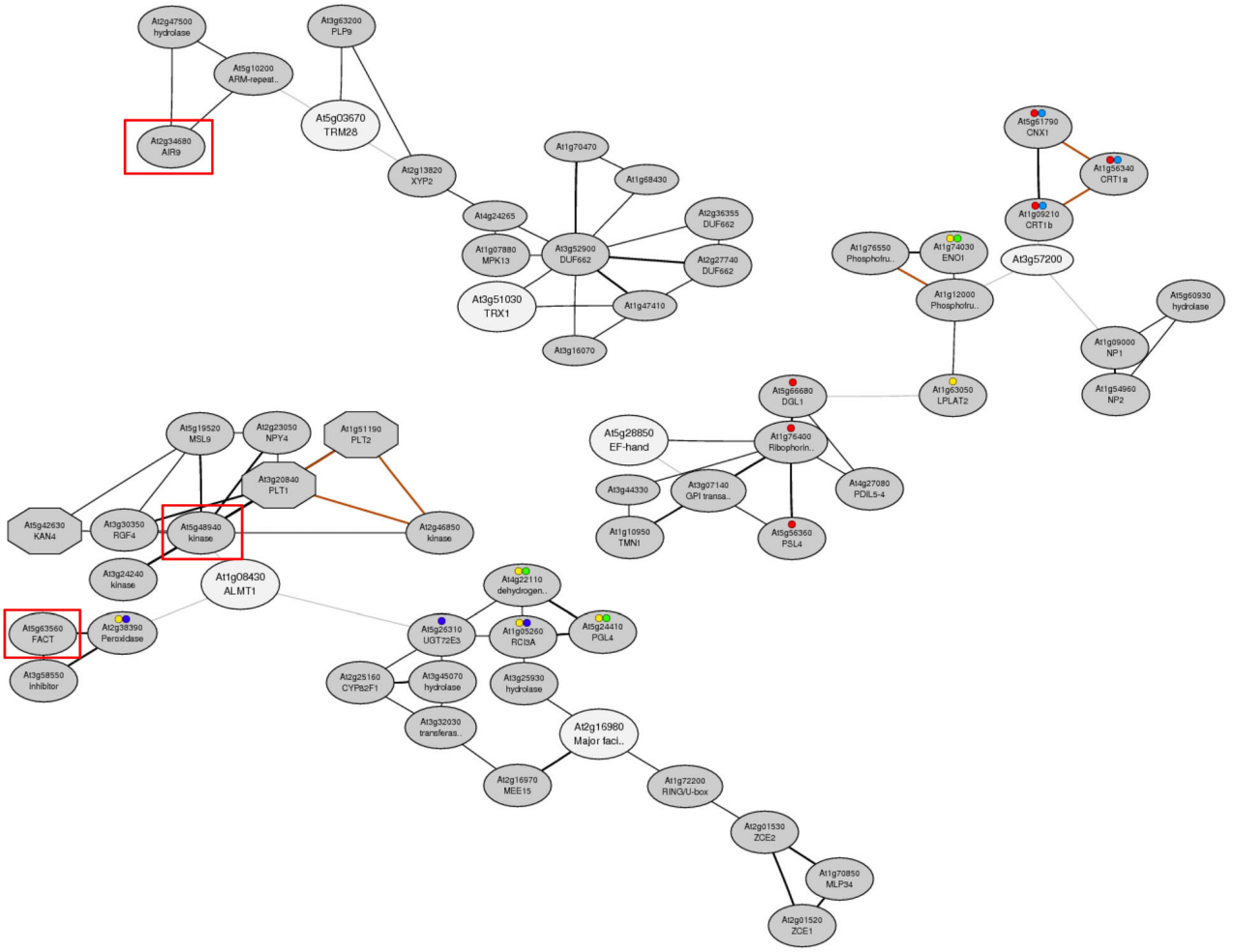

KEGG ID	Title
ath04141	Protein processing in endoplasmic reticulum
ath01110	Biosynthesis of secondary metabolites
ath01130	Biosynthesis of antibiotics
ath04145	Phagosome
ath00940	Phenylpropanoid biosynthesis

FIGURE 6 | Co-expression networks containing the candidate genes for Al tolerance detected by GWAS. The co-expression networks were constructed by using 16 candidate genes that showed altered Al tolerance in the mutant (represented on **Figure 5**) as query genes by ATTED-II. Among all constructed networks (**Supplementary Figure S2**), only the networks that contained more than two candidate genes are shown. White and gray ellipses indicate query genes and added co-expressed genes respectively. Red rectangle indicates the genes located within the 10 kb of GWAS-detected SNP for Al tolerance (**Supplementary Table S5**) respectively. Colored circles indicated the genes involved in enriched biological processes represented on the table.

for STOP1-like proteins (including the STOP1's downstream STOP2; Kobayashi et al., 2014). Recent studies have identified that dysfunction of STOP1 can repress salt and hypoxia tolerance, while enhancing drought tolerance in *Arabidopsis* (Enomoto et al., 2019; Sadhukhan et al., 2019). This suggests that the polymorphism of STOP1 directly interferes with other stress tolerant traits in *Arabidopsis*, but not in rice, as a result of its redundancy. This hypothesis warrants investigation by further studies.

Our approach, namely integration of GWAS and reverse genetics, would fail to identify several critical genes for Al and proton tolerance due to underlying technical limitations. For example, our GWAS did not detect several critical Al tolerance genes of *Arabidopsis*, such as genes for citrate transporting MATE (Liu et al., 2012) and ALS3 (Larsen et al., 2004), and any genes encoding proteins belong to cell-wall metabolism, while several polysaccharides of cell-wall are involved in Al tolerance mechanisms (Yang et al., 2008). It could be

explained by insufficient power of our GWAS conducted with multiple subpopulations to detect the subpopulation specific allele (Korte and Farlow, 2013; Imamura et al., 2016), which may segregate only in some subpopulations. By contrast, the background accession of most T-DNA inserted plants (i.e., Col-0), is one of the most proton sensitive among all accessions (RRL_{proton} = 34.9). It may affect sensitivity of reverse genetic analysis, which evaluate the loss of proton tolerance by the disruption of particular gene. Different approach such as overexpression of GWAS-identified genes in Col-0 would be useful to evaluate the candidate genes for proton tolerance.

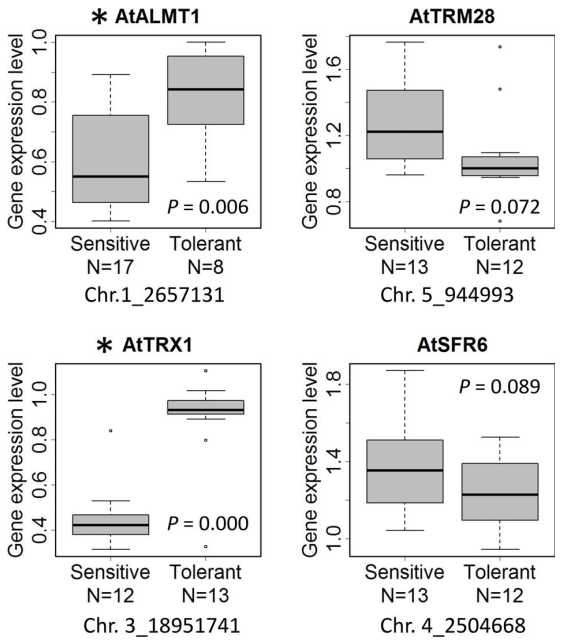

FIGURE 7 | Box plot of expression level of the genes that showed more than 30% decrease of Al tolerance in the mutants (**Figure 5**). The gene expression level of the accessions carrying sensitive and tolerant allele of the most associated SNP linked with the gene in GWAS (**Supplementary Table S5**) are shown. Asterisk indicates a significant difference of expression level between the accessions with tolerant and sensitive alleles ($p < 0.05$). N indicates the number of biological replicates per allele (n = 8–17).

Combining GWAS and genome-wide functional genomics approaches, such as joint genetic and network analysis (Kobayashi et al., 2016; Butardo et al., 2017), is a useful approach to elucidate the polygene-regulated tolerance mechanisms. In this study, co-expression gene network analysis revealed that multiple Al tolerance genes identified by reverse-genetics belonged to the same/small co-expression network (**Figure 6**). The network formed with *AtALMT1* contained another Al tolerance gene and two genes collocated near the top-ranked SNPs of RRL_{Al}. The linked genes contained *RGFR2*, which is directly associated with *AtALMT1* in the co-expression network and is a critical protein kinase for root meristem growth (Shinohara et al., 2016). Another network was formed by AtTRX1 and AtTRM28, which showed severe Al sensitivity through the growth assay of T-DNA insertion mutants next to the *AtALMT1*-KO (**Figure 5**). TRXs play roles in processes that maintain ROS-status and ROS-signaling (Foyer and Noctor, 2005; Navrot et al., 2007; Skelly et al., 2016), while the TRM family proteins are known to regulate polymerization of microtubules, such as the formation of the microtubule array during cell division (Struk and Dhonukshe, 2014; Schaefer et al., 2017). This suggests that AtTRX1 and AtTRM28 may contribute to Al tolerance through the regulation of processes that require microtubules, including cell wall synthesis (Höfte and Voxeur, 2017), which is a typical target biological process by

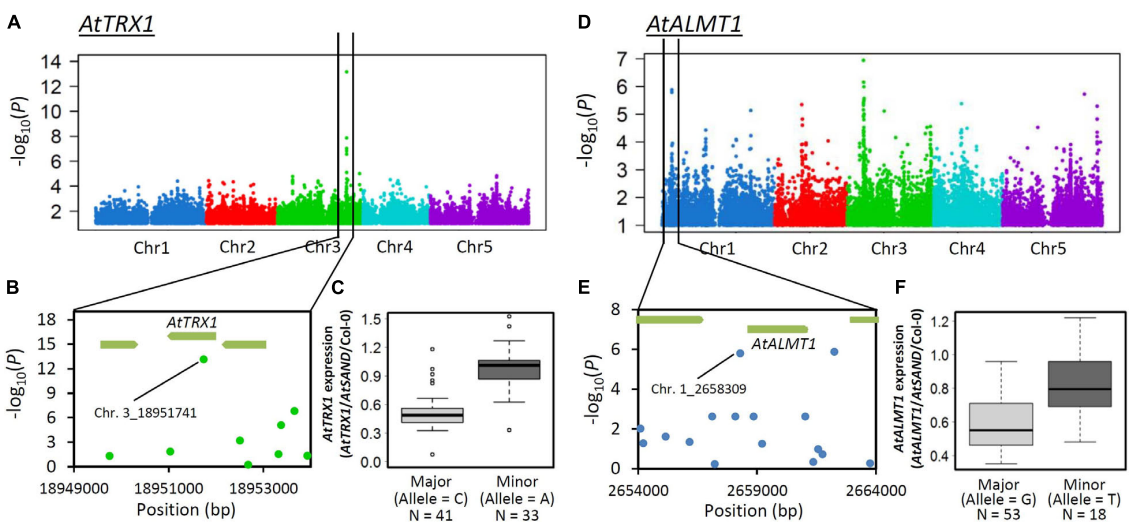

FIGURE 8 | GWA mapping of gene expression level of *AtTRX1* and *AtALMT1*under Al stress. **(A)** Manhattan plots of GWAS of *AtTRX1* expression level. **(B)** Detailed plot of the region of the most associated SNP on Chr.3 in GWAS of *AtTRX1* expression level. **(C)** Box plot of *AtTRX1* expression levels of the most strongly associated SNP (Chr.3_18951741). **(D)** Manhattan plots of GWAS of *AtALMT1* expression levels. **(E)** Detailed plot of the region of higher associated SNP on *AtALMT1* locus in GWAS of *AtALMT1* expression level. **(F)** Box plot of *AtALMT1* expression levels of the higher associated SNP in the *AtALMT1* promoter region (Chr.1_2658309).

A

Haplotype	Distance from ATG											N
	-1963	-1924	-1831	-1824	-1669	-1570	-1485	TE	-789	-701	-491	
Hap1	T	G	T	-	C	G	A	-	A	T	G	16
Hap2	-	C	G	GGGGG	T	C	-	+	-	C	T	10
Hap3	T	G	T	-	C	C	A	-	A	T	T	8
Hap4	T	G	T	-	C	C	A	-	A	T	G	8

B

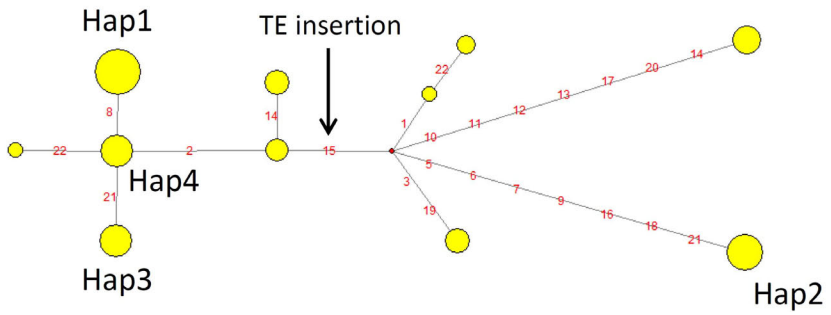

FIGURE 9 | Haplotype analysis of *AtALMT1* promoter. **(A)** Major haplotypes of the *AtALMT1* promoter region observed among 71 *A. thaliana* accessions. The positions indicate distance from the start codon of *AtALMT1*. "-" indicates deletion. The SNPs of -1669 and -701 correspond to the higher associated SNPs (Chr.1_2657131 and Chr.1_2658099) in GWAS of Al tolerance (**Figures 2**, **7**). The SNP of -491 corresponds to the higher associated SNP (Chr.1_2658309) in eGWAS of *AtALMT1* expression level (**Figures 8E,F**). **(B)** Haplotype network of *AtALMT1* promoter. Yellow circles represent each haplotype, and circle sizes represent the number of accessions within the haplotype. Red circles represent the median vector. Red letters indicate the variants, and the black arrow indicates the TE insertion.

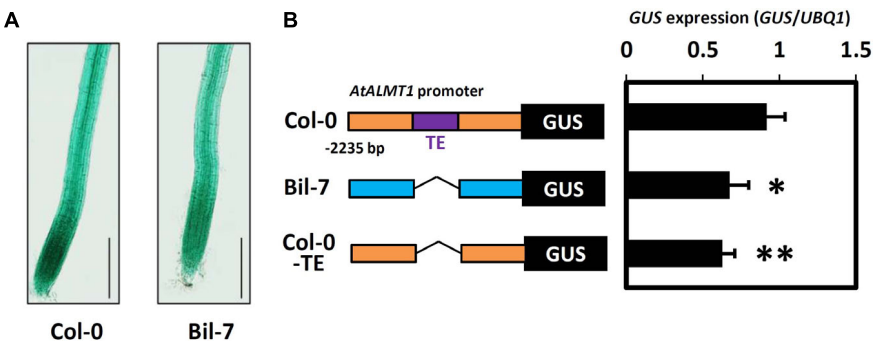

FIGURE 10 | Promoter activity analysis of the *AtALMT1* promoter. **(A)** GUS staining patterns in root of the transgenic plants carrying the *AtALMT1* promoter of Col-0 and Bil-7. Transgenic plants were grown hydroponically for 5-days in a control solution (0 μM Al, pH 5.0) and then exposed to an Al stress solution (10 μM Al, pH 5.0) for 9 h. Bar = 200 μm. **(B)** *GUS* expression levels in the roots of transgenic plants carrying different *AtALMT1* promoters. Col-0 type and Bil-7 type promoters are indicated by orange and blue boxes respectively. TE (498 bp length transposable element insertion at 879 bp upstream from the ATG codon of *AtALMT1*) is indicated by a purple box. *GUS* expression levels were analyzed using real-time quantitative RT-PCR. Approximately 100 seedlings were grown hydroponically for 10 days in a control solution (0 μM Al, pH 5.6) and then treated with an Al stress (10 μM Al, pH 5.0) solution for 9 h. Mean values ± SD are shown (three technical replicates in three individual transgenic lines for each construct). Asterisks indicate significant differences compared with the Col-0 type promoter (Student's *t*-test, $^{**}p < 0.05$, $^{*}p < 0.1$).

Al (Sasaki et al., 1997; Sivaguru et al., 2003). The network also contained a gene linked to the top-ranked SNPs, which encoded one of the microtubule associated proteins (AT2G34680). The other network, which contained four genes annotated as "protein processing in endoplasmic reticulum (ER)," was formed by three genes which were identified by reverse-genetic assay, and one other gene linked to the top-ranked SNPs (**Figures 5**, **6** and **Supplementary Table S5**). This suggests that protein processing in the ER is involved in *Arabidopsis* Al tolerance mechanisms. In fact, a gene encoding the ER-localized protein chaperon (BINDING PROTEIN3) was previously identified as one of the Al tolerant genes in *Arabidopsis* (Kusunoki et al., 2017).

Expression level polymorphism of *AtALMT1* and *AtTRX1* due to cis-regulatory allelic variation was identified as one of the causes of Al tolerance variation detected by GWA mapping. An eGWAS for *AtTRX1* revealed a single and significant linkage of the *AtTRX1* locus, suggesting that greater expression of the gene was mostly determined by mutations in the cis-acting factor, which was also associated with Al tolerance (**Figures 7**, **8A,B**; **Supplementary Table S5**). This variation is similar to the natural

variations in *NIP1;1* that regulate H_2O_2 tolerance by ELP as a result of mutations in the promoter (Sadhukhan et al., 2017). In this study, mutations in the promoter were also identified as an ELP mechanism of *AtALMT1* (**Figures 7**, **8D,E**). The typical pyramiding of historical mutations consists of TE insertion followed by a single nucleotide mutation (**Figures 9A,B**). The insertion of a TE is one of the major mechanisms causing ELP that drives adaptation to new environments (Yang et al., 2013). This accounts for the greater expression levels of major Al tolerance genes occurring in several Al tolerant crop varieties such as barley, wheat, sorghum, and rice (Magalhaes et al., 2007; Fujii et al., 2012; Tovkach et al., 2013; Yokosho et al., 2016; Pereira and Ryan, 2019). In this study, most of the accessions with a Hap2 type *AtALMT1* promoter (higher *AtALMT1* expression type) originated from the Western Europe region where acid soils are dominant (**Supplementary Figure S4**). This suggests that they have adapted to the acid soil common to the region by enhancing their *AtALMT1* expression level. On the other hand, the eGWAS of *AtALMT1* identified complex regulation of *AtALMT1* expression, which has also been identified by previous studies investigating *AtALMT1* expression (e.g., Tokizawa et al., 2015). Further study of the loci detected by eGWAS may uncover the molecular mechanisms which act in this complex system.

Accessions with unusual phenotypes, which were indicated by a large gap between the observed and predicted phenotype using GP, occurred more frequently in Al tolerant accessions (**Figures 1A**, **3B**). By contrast, only few accessions showed unusual phenotypes in proton tolerance (**Figures 1A**, **3B**), supporting our hypothesis that proton tolerance appears to be strongly regulated by polygenes. These differential patterns in the genetic architecture of Al and proton tolerance variation need to be considered when breeding crop varieties tolerant to acid soils. On the other hand, distribution of Al and proton tolerant accessions shows different pattern. Accessions that were unusually tolerant to Al tended to be located in the acid soils regions of Western Europe (**Supplementary Figure S4**). By contrast, accessions that were unusually sensitive to Al were located in the non-acid soil region of Southern Europe included the most Al sensitive accession, Voeran-1, a natural *AtALMT1* loss-of-function mutant, found in Northern Italy (**Supplementary Figure S4**). This suggests that variation in Al tolerance would be beneficial in order to adapt to acid soil conditions. However, the loss of Al tolerance would not have negative effects on survival in a non-acid soil environment. By contrast, there were no such trends in proton tolerance levels of accessions. It may be accounted for the pleiotropic role of proton tolerance, which interfere various other traits such as nutrient acquisition and cell expansion (Shavrukov and Hirai, 2016). This hypothesis warrants investigation by further studies.

DATA AVAILABILITY STATEMENT

All datasets generated for this study are included in the article/**Supplementary Material**.

AUTHOR CONTRIBUTIONS

YN performed most of the experiments and writing. KK, KT, and YS carried out the expression analysis. SI and MK generated the plant materials and assisted with gene sequencing. KK, OH, and YY discussed the study and assisted in the writing and GWA mapping. YK and HK designed the work and supervised, and wrote and edited the manuscript. All authors approved the manuscript.

FUNDING

This research was supported by a cooperative research grant of the Genome Research for Bioresource, NODAI Genome Research Center, Tokyo University of Agriculture, and by JSPS KAKENHI grant numbers 24688009, 15K14676, and 18J11757.

ACKNOWLEDGMENTS

We thank the RIKEN-BRC, ABRC and NASC for providing the *Arabidopsis* seeds. We also thank Hirofumi Yamanaka and Satoru Ohashi of the Gifu University for processing the *Arabidopsis* association panels, the gene list and for growing the *Arabidopsis* accessions during the first stage of this study. We thank Fumie Mori and Atsuko Iuchi of the RIKEN BRC for establishing the *Arabidopsis* transgenic line and for the *AtALMT1* promoter sequencing. We would like to thank Michael A. Gore of Cornell University and Alexander E. Lipka of the University of Illinois for their discussions regarding GWAS during the early stages of this project. We would like to thank Editage (www.editage.com) for English language editing.

SUPPLEMENTARY MATERIAL

The Supplementary Material for this article can be found online at: https://www.frontiersin.org/articles/10.3389/fpls.2020.00405/full#supplementary-material

REFERENCES

Anoop, V. M. (2003). Modulation of citrate metabolism alters aluminum tolerance in yeast and transgenic canola overexpressing a mitochondrial citrate synthase. *Plant Physiol.* 132, 2205–2217. doi: 10.1104/pp.103.023903

Arbelaez, J. D., Maron, L. G., Jobe, T. O., Piñeros, M. A., Famoso, A. N., Rebelo, A. R., et al. (2017). Aluminum resistance transcription factor 1 (ART1) contributes to natural variation in aluminum resistance in diverse genetic backgrounds of rice (*O. sativa*). *Plant Direct* 1:e00014. doi: 10.1002/pld3.14

Balzergue, C., Dartevelle, T., Godon, C., Laugier, E., Meisrimler, C., Teulon, J. M., et al. (2017). Low phosphate activates STOP1-ALMT1 to rapidly inhibit root cell elongation. *Nat. Commun.* 8:15300. doi: 10.1038/ncomms15300

Bandelt, H. J., Forster, P., Sykes, B. C., and Richards, M. B. (1995). Mitochondrial portraits of human populations using median networks. *Genetics* 141, 743–753.

Bergelson, J., and Roux, F. (2010). Towards identifying genes underlying ecologically relevant traits in *Arabidopsis thaliana*. *Nat. Rev. Genet.* 11, 867–879. doi: 10.1038/nrg2896

Bissoli, G., Niñoles, R., Fresquet, S., Palombieri, S., Bueso, E., Rubio, L., et al. (2012). Peptidyl-prolyl cis-trans isomerase ROF2 modulates intracellular pH homeostasis in *Arabidopsis*. *Plant J.* 70, 704–716. doi: 10.1111/j.1365-313X.2012.04921.x

Bradbury, P. J., Zhang, Z., Kroon, D. E., Casstevens, T. M., Ramdoss, Y., and Buckler, E. S. (2007). TASSEL: software for association mapping of complex traits in diverse samples. *Bioinformatics* 23, 2633–2635. doi: 10.1093/bioinformatics/btm308

Britto, D. T., and Kronzucker, H. J. (2005). Nitrogen acquisition, PEP carboxylase, and cellular pH homeostasis: new views on old paradigms. *Plant Cell Environ.* 28, 1396–1409. doi: 10.1111/j.1365-3040.2005.01372.x

Browning, B. L., and Browning, S. R. (2009). A unified approach to genotype imputation and haplotype-phase inference for large data sets of trios and unrelated individuals. *Am. J. Hum. Genet.* 84, 210–223. doi: 10.1016/j.ajhg.2009.01.005

Bustin, S. A., Benes, V., Garson, J. A., Hellemans, J., Huggett, J., Kubista, M., et al. (2009). The MIQE guidelines: minimum information for publication of quantitative real-time PCR experiments. *Clin. Chem.* 55, 611–622. doi: 10.1373/clinchem.2008.112797

Butardo, V. M., Anacleto, R., Parween, S., Samson, I., de Guzman, K., Alhambra, C. M., et al. (2017). Systems genetics identifies a novel regulatory domain of amylose synthesis. *Plant Physiol.* 173, 887–906. doi: 10.1104/pp.16.01248

Cao, J., Schneeberger, K., Ossowski, S., Günther, T., Bender, S., Fitz, J., et al. (2011). Whole-genome sequencing of multiple *Arabidopsis thaliana* populations. *Nat. Genet.* 43, 956–963. doi: 10.1038/ng.911

Clough, S. J., and Bent, A. F. (1998). Floral dip: a simplified method for Agrobacterium-mediated transformation of *Arabidopsis thaliana*. *Plant J.* 16, 735–743. doi: 10.1046/j.1365-313X.1998.00343.x

Crossa, J., Campos, G. D. L., Perez, P., Gianola, D., Burgueno, J., Araus, J. L., et al. (2010). Prediction of genetic values of quantitative traits in plant breeding using pedigree and molecular markers. *Genetics* 186, 713–724. doi: 10.1534/genetics.110.118521

Daspute, A. A., Sadhukhan, A., Tokizawa, M., Kobayashi, Y., Panda, S. K., and Koyama, H. (2017). Transcriptional regulation of aluminum-tolerance genes in higher plants: clarifying the underlying molecular mechanisms. *Front. Plant Sci.* 8:1358. doi: 10.3389/fpls.2017.01358

Delhaize, E., Ryan, P. R., Hebb, D. M., Yamamoto, Y., Sasaki, T., and Matsumoto, H. (2004). Engineering high-level aluminum tolerance in barley with the ALMT1 gene. *Proc. Natl. Acad. Sci. U.S.A.* 101, 15249–15254. doi: 10.1073/pnas.0406258101

Delker, C., and Quint, M. (2011). Expression level polymorphisms: heritable traits shaping natural variation. *Trends Plant Sci.* 16, 481–488. doi: 10.1016/j.tplants.2011.05.009

Desta, Z. A., and Ortiz, R. (2014). Genomic selection: genome-wide prediction in plant improvement. *Trends Plant Sci.* 19, 592–601. doi: 10.1016/j.tplants.2014.05.006

Enomoto, T., Tokizawa, M., Ito, H., Iuchi, S., Kobayashi, M., Yamamoto, Y. Y., et al. (2019). STOP1 regulates the expression of HsfA2 and GDHs that are critical for low-oxygen tolerance in *Arabidopsis*. *J. Exp. Bot.* 70, 3297–3311. doi: 10.1093/jxb/erz124

Evanno, G., Regnaut, S., and Goudet, J. (2005). Detecting the number of clusters of individuals using the software STRUCTURE: a simulation study. *Mol. Ecol.* 14, 2611–2620. doi: 10.1111/j.1365-294X.2005.02553.x

Foyer, C. H., and Noctor, G. (2005). Oxidant and antioxidant signalling in plants: a re-evaluation of the concept of oxidative stress in a physiological context. *Plant Cell Environ.* 28, 1056–1071. doi: 10.1111/j.1365-3040.2005.01327.x

Friedman, J., Hastie, T., and Tibshirani, R. (2010). Regularization paths for generalized linear models via coordinate descent. *J. Stat. Softw.* 33, 1–22. doi: 10.18637/jss.v033.i01

Fujii, M., Yokosho, K., Yamaji, N., Saisho, D., Yamane, M., Takahashi, H., et al. (2012). Acquisition of aluminium tolerance by modification of a single gene in barley. *Nat. Commun.* 3:713. doi: 10.1038/ncomms1726

Fujiwara, T., Hirai, M. Y., Chino, M., Komeda, Y., and Naito, S. (1992). Effects of sulfur nutrition on expression of the soybean seed storage protein genes in transgenic petunia. *Plant Physiol.* 99, 263–268. doi: 10.1104/pp.99.1.263

Gujas, B., Alonso-Blanco, C., and Hardtke, C. S. (2012). Natural *Arabidopsis* brx loss-of-function alleles confer root adaptation to acidic soil. *Curr. Biol.* 22, 1962–1968. doi: 10.1016/j.cub.2012.08.026

Hampp, R., Goller, M., and Füllgraf, H. (1984). Determination of compartmented metabolite pools by a combination of rapid fractionation of oat mesophyll protoplasts and enzymic cycling. *Plant Physiol.* 75, 1017–1021. doi: 10.1104/pp.75.4.1017

Hoekenga, O. A., Maron, L. G., Pineros, M. A., Cancado, G. M. A., Shaff, J., Kobayashi, Y., et al. (2006). AtALMT1, which encodes a malate transporter, is identified as one of several genes critical for aluminum tolerance in *Arabidopsis*. *Proc. Natl. Acad. Sci. U.S.A.* 103, 9738–9743. doi: 10.1073/pnas.0602868103

Hoekenga, O. A., Vision, T. J., Shaff, J. E., Monforte, A. J., Lee, G. P., Howell, S. H., et al. (2003). Identification and characterization of aluminum tolerance loci in *Arabidopsis* (Landsberg erecta x Columbia) by quantitative trait locus mapping. A physiologically simple but genetically complex trait. *Plant Physiol.* 132, 936–948. doi: 10.1104/pp.103.023085

Höfte, H., and Voxeur, A. (2017). Plant cell walls. *Curr. Biol.* 27, R865–R870. doi: 10.1016/j.cub.2017.05.025

Horton, M. W., Hancock, A. M., Huang, Y. S., Toomajian, C., Atwell, S., Auton, A., et al. (2012). Genome-wide patterns of genetic variation in worldwide *Arabidopsis thaliana* accessions from the RegMap panel. *Nat. Genet.* 44, 212–216. doi: 10.1038/ng.1042

Horton, R. M., Hunt, H. D., Ho, S. N., Pullen, J. K., and Pease, L. R. (1989). Engineering hybrid genes without the use of restriction enzymes: gene splicing by overlap extension. *Gene* 77, 61–68. doi: 10.1016/0378-1119(89)90359-4

Ikka, T., Kobayashi, Y., Iuchi, S., Sakurai, N., Shibata, D., Kobayashi, M., et al. (2007). Natural variation of *Arabidopsis thaliana* reveals that aluminum resistance and proton resistance are controlled by different genetic factors. *Theor. Appl. Genet.* 115, 709–719. doi: 10.1007/s00122-007-0602-5

Imamura, M., Takahashi, A., Yamauchi, T., Hara, K., Yasuda, K., Grarup, N., et al. (2016). Genome-wide association studies in the Japanese population identify seven novel loci for type 2 diabetes. *Nat. Commun.* 7:10531. doi: 10.1038/ncomms10531

Iuchi, S., Koyama, H., Iuchi, A., Kobayashi, Y., Kitabayashi, S., Kobayashi, Y., et al. (2007). Zinc finger protein STOP1 is critical for proton tolerance in *Arabidopsis* and coregulates a key gene in aluminum tolerance. *Proc. Natl. Acad. Sci. U.S.A.* 104, 9900–9905. doi: 10.1073/pnas.0700117104

Joshi, H. J., Christiansen, K. M., Fitz, J., Cao, J., Lipzen, A., Martin, J., et al. (2012). 1001 proteomes: a functional proteomics portal for the analysis of *Arabidopsis thaliana* accessions. *Bioinformatics* 28, 1303–1306. doi: 10.1093/bioinformatics/bts133

Kim, S., Plagnol, V., Hu, T. T., Toomajian, C., Clark, R. M., Ossowski, S., et al. (2007). Recombination and linkage disequilibrium in *Arabidopsis thaliana*. *Nat. Genet.* 39, 1151–1155. doi: 10.1038/ng2115

Kinraide, T. B. (2003). Toxicity factors in acidic forest soils: attempts to evaluate separately the toxic effects of excessive Al3+ and H+ and insufficient Ca2+ and Mg2+ upon root elongation. *Eur. J. Soil Sci.* 54, 323–333. doi: 10.1046/j.1365-2389.2003.00538.x

Kobayashi, Y., Furuta, Y., Ohno, T., Hara, T., and Koyama, H. (2005). Quantitative trait loci controlling aluminium tolerance in two accessions of *Arabidopsis thaliana* (Landsberg erecta and Cape Verde Islands). *Plant Cell Environ.* 28, 1516–1524. doi: 10.1111/j.1365-3040.2005.01388.x

Kobayashi, Y., Hoekenga, O. A., Itoh, H., Nakashima, M., Saito, S., Shaff, J. E., et al. (2007). Characterization of AtALMT1 expression in aluminum-inducible malate release and its role for rhizotoxic stress tolerance in *Arabidopsis*. *Plant Physiol.* 145, 843–852. doi: 10.1104/pp.107.102335

Kobayashi, Y., Kobayashi, Y., Watanabe, T., Shaff, J. E., Ohta, H., Kochian, L. V., et al. (2013). Molecular and physiological analysis of Al3+ and H+ rhizotoxicities at moderately acidic conditions. *Plant Physiol.* 163, 180–192. doi: 10.1104/pp.113.222893

Kobayashi, Y., and Koyama, H. (2002). QTL Analysis of Al Tolerance in Recombinant Inbred Lines of *Arabidopsis thaliana*. *Plant Cell Physiol.* 43, 1526–1533. doi: 10.1093/pcp/pcf174

Kobayashi, Y., Ohyama, Y., Kobayashi, Y., Ito, H., Iuchi, S., Fujita, M., et al. (2014). STOP2 activates transcription of several genes for Al- and low pH-Tolerance that are regulated by STOP1 in *Arabidopsis*. *Mol. Plant* 7, 311–322. doi: 10.1093/mp/sst116

Kobayashi, Y., Sadhukhan, A., Tazib, T., Nakano, Y., Kusunoki, K., Kamara, M., et al. (2016). Joint genetic and network analyses identify loci associated with root growth under NaCl stress in *Arabidopsis thaliana*. *Plant. Cell Environ.* 39, 918–934. doi: 10.1111/pce.12691

Kochian, L. V., Hoekenga, O. A., and Pineros, M. A. (2004). How do crop plants tolerate acid soils? Mechanisms of aluminum tolerance and phosphorous efficiency. *Annu. Rev. Plant Biol.* 55, 459–493. doi: 10.1146/annurev.arplant.55.031903.141655

Kochian, L. V., Piñeros, M. A., Liu, J., and Magalhaes, J. V. (2015). Plant adaptation to acid soils: the molecular basis for crop aluminum resistance. *Annu. Rev. Plant Biol.* 66, 571–598. doi: 10.1146/annurev-arplant-043014-114822

Kooke, R., Kruijer, W., Bours, R., Becker, F., Kuhn, A., van de Geest, H., et al. (2016). Genome-wide association mapping and genomic prediction elucidate the genetic architecture of morphological traits in *Arabidopsis*. *Plant Physiol.* 170, 2187–2203. doi: 10.1104/pp.15.00997

Korte, A., and Farlow, A. (2013). The advantages and limitations of trait analysis with GWAS: a review. *Plant Methods* 9:29. doi: 10.1186/1746-4811-9-29

Kosugi, S., Ohashi, Y., Nakajima, K., and Arai, Y. (1990). An improved assay for β-glucuronidase in transformed cells: methanol almost completely suppresses a putative endogenous β-glucuronidase activity. *Plant Sci.* 70, 133–140. doi: 10.1016/0168-9452(90)90042-M

Koyama, H., Toda, T., and Hara, T. (2001). Brief exposure to low-pH stress causes irreversible damage to the growing root in *Arabidopsis thaliana*: pectin–Ca interaction may play an important role in proton rhizotoxicity. *J. Exp. Bot.* 52, 361–368. doi: 10.1093/jexbot/52.355.361

Kusunoki, K., Nakano, Y., Tanaka, K., Sakata, Y., Koyama, H., and Kobayashi, Y. (2017). Transcriptomic variation among six *Arabidopsis thaliana* accessions identified several novel genes controlling aluminium tolerance. *Plant. Cell Environ.* 40, 249–263. doi: 10.1111/pce.12866

Larsen, P. B., Geisler, M. J. B., Jones, C. A., Williams, K. M., and Cancel, J. D. (2004). ALS3 encodes a phloem-localized ABC transporter-like protein that is required for aluminum tolerance in *Arabidopsis*. *Plant J.* 41, 353–363. doi: 10.1111/j.1365-313X.2004.02306.x

Liu, J., Luo, X., Shaff, J., Liang, C., Jia, X., Li, Z., et al. (2012). A promoter-swap strategy between the AtALMT and AtMATE genes increased *Arabidopsis* aluminum resistance and improved carbon-use efficiency for aluminum resistance. *Plant J.* 71, 327–337. doi: 10.1111/j.1365-313X.2012.04994.x

Ma, J. F. (2007). Syndrome of aluminum toxicity and diversity of aluminum resistance in higher plants. *Int. Rev. Cytol.* 264, 225–252. doi: 10.1016/S0074-7696(07)64005-4

Magalhaes, J. V., Liu, J., Guimarães, C. T., Lana, U. G. P., Alves, V. M. C., Wang, Y.-H., et al. (2007). A gene in the multidrug and toxic compound extrusion (MATE) family confers aluminum tolerance in sorghum. *Nat. Genet.* 39, 1156–1161. doi: 10.1038/ng2074

Navrot, N., Rouhier, N., Gelhaye, E., and Jacquot, J. P. (2007). Reactive oxygen species generation and antioxidant systems in plant mitochondria. *Physiol. Plant.* 129, 185–195. doi: 10.1111/j.1399-3054.2006.00777.x

Obayashi, T., Aoki, Y., Tadaka, S., Kagaya, Y., and Kinoshita, K. (2018). ATTED-II in 2018: a plant coexpression database based on investigation of the statistical property of the mutual rank index. *Plant Cell Physiol.* 59:e3. doi: 10.1093/pcp/pcx191

Ohyama, Y., Ito, H., Kobayashi, Y., Ikka, T., Morita, A., Kobayashi, M., et al. (2013). Characterization of AtSTOP1 orthologous genes in tobacco and other plant species. *Plant Physiol.* 162, 1937–1946. doi: 10.1104/pp.113.218958

Pereira, J. F., and Ryan, P. R. (2019). The role of transposable elements in the evolution of aluminium resistance in plants. *J. Exp. Bot.* 70, 41–54. doi: 10.1093/jxb/ery357

Pritchard, J. K., Stephens, M., and Donnelly, P. (2000). Inference of population structure using multilocus genotype data. *Genetics* 155, 945–959.

Purcell, S., Neale, B., Todd-Brown, K., Thomas, L., Ferreira, M. A. R., Bender, D., et al. (2007). PLINK: a tool set for whole-genome association and population-based linkage analyses. *Am. J. Hum. Genet.* 81, 559–575. doi: 10.1086/519795

Sadhukhan, A., Enomoto, T., Kobayashi, Y., Watanabe, T., Iuchi, S., Kobayashi, M., et al. (2019). sensitive to proton rhizotoxicity1 regulates salt and drought tolerance of *Arabidopsis thaliana* through transcriptional regulation of CIPK23. *Plant Cell Physiol.* 60, 2113–2126. doi: 10.1093/pcp/pcz120

Sadhukhan, A., Kobayashi, Y., Nakano, Y., Iuchi, S., Kobayashi, M., Sahoo, L., et al. (2017). Genome-wide association study reveals that the aquaporin NIP1;1 contributes to variation in hydrogen peroxide sensitivity in *Arabidopsis thaliana*. *Mol. Plant* 10, 1082–1094. doi: 10.1016/j.molp.2017.07.003

Sasaki, M., Yamamoto, Y., and Matsumoto, H. (1997). Aluminum inhibits growth and stability of cortical microtubules in wheat (*Triticum aestivum*) roots. *Soil Sci. Plant Nutr.* 43, 469–472. doi: 10.1080/00380768.1997.10414772

Sasaki, T., Yamamoto, Y., Ezaki, B., Katsuhara, M., Ahn, S. J., Ryan, P. R., et al. (2004). A wheat gene encoding an aluminum-activated malate transporter. *Plant J.* 37, 645–653. doi: 10.1111/j.1365-313X.2003.01991.x

Sawaki, Y., Iuchi, S., Kobayashi, Y., Kobayashi, Y., Ikka, T., Sakurai, N., et al. (2009). STOP1 regulates multiple genes that protect *Arabidopsis* from proton and aluminum toxicities. *Plant Physiol.* 150, 281–294. doi: 10.1104/pp.108.134700

Schaefer, E., Belcram, K., Uyttewaal, M., Duroc, Y., Goussot, M., Legland, D., et al. (2017). The preprophase band of microtubules controls the robustness of division orientation in plants. *Science* 356, 186–189. doi: 10.1126/science.aal3016

Seren, Ü, Grimm, D., Fitz, J., Weigel, D., Nordborg, M., Borgwardt, K., et al. (2017). AraPheno: a public database for *Arabidopsis thaliana* phenotypes. *Nucleic Acids Res.* 45, D1054–D1059. doi: 10.1093/nar/gkw986

Shavrukov, Y., and Hirai, Y. (2016). Good and bad protons: genetic aspects of acidity stress responses in plants. *J. Exp. Bot.* 67, 15–30. doi: 10.1093/jxb/erv437

Shinohara, H., Mori, A., Yasue, N., Sumida, K., and Matsubayashi, Y. (2016). Identification of three LRR-RKs involved in perception of root meristem growth factor in *Arabidopsis*. *Proc. Natl. Acad. Sci. U.S.A.* 113, 3897–3902. doi: 10.1073/pnas.1522639113

Sivaguru, M., Ezaki, B., He, Z. H., Tong, H., Osawa, H., Baluska, F., et al. (2003). Aluminum-induced gene expression and protein localization of a cell wall-associated receptor kinase in *Arabidopsis*. *Plant Physiol.* 132, 2256–2266. doi: 10.1104/pp.103.022129.plasma

Skelly, M. J., Frungillo, L., and Spoel, S. H. (2016). Transcriptional regulation by complex interplay between post-translational modifications. *Curr. Opin. Plant Biol.* 33, 126–132. doi: 10.1016/j.pbi.2016.07.004

Struk, S., and Dhonukshe, P. (2014). MAPs: cellular navigators for microtubule array orientations in *Arabidopsis*. *Plant Cell Rep.* 33, 1–21. doi: 10.1007/s00299-013-1486-2

Tamura, K., Stecher, G., Peterson, D., Filipski, A., and Kumar, S. (2013). MEGA6: molecular evolutionary genetics analysis Version 6.0. *Mol. Biol. Evol.* 30, 2725–2729. doi: 10.1093/molbev/mst197

Toda, T., Koyama, H., and Hara, T. (1999). A simple hydroponic culture method for the development of a highly viable root system in *Arabidopsis thaliana*. *Biosci. Biotechnol. Biochem.* 63, 210–212. doi: 10.1271/bbb.63.210

Tokizawa, M., Kobayashi, Y., Saito, T., Kobayashi, M., Iuchi, S., Nomoto, M., et al. (2015). Sensitive to proton rhizotoxicity1, calmodulin binding transcription activator2, and other transcription factors are involved in aluminum-activated malate transporter1 expression. *Plant Physiol.* 167, 991–1003. doi: 10.1104/pp.114.256552

Tovkach, A., Ryan, P. R., Richardson, A. E., Lewis, D. C., Rathjen, T. M., Ramesh, S., et al. (2013). Transposon-mediated alteration of TaMATE1B expression in wheat confers constitutive citrate efflux from root apices. *Plant Physiol.* 161, 880–892. doi: 10.1104/pp.112.207142

von Uexküll, H. R., and Mutert, E. (1995). Global extent, development and economic impact of acid soils. *Plant Soil* 171, 1–15. doi: 10.1007/BF00009558

Wu, L., Kobayashi, Y., Wasaki, J., and Koyama, H. (2018). Organic acid excretion from roots: a plant mechanism for enhancing phosphorus acquisition, enhancing aluminum tolerance, and recruiting beneficial rhizobacteria. *Soil Sci. Plant Nutr.* 64, 697–704. doi: 10.1080/00380768.2018.1537093

Yamaji, N., Huang, C. F., Nagao, S., Yano, M., Sato, Y., Nagamura, Y., et al. (2009). A zinc finger transcription factor ART1 regulates multiple genes implicated in aluminum tolerance in rice. *Plant Cell* 21, 3339–3349. doi: 10.1105/tpc.109.070771

Yang, J. L., Li, Y. Y., Zhang, Y. J., Zhang, S. S., Wu, Y. R., Wu, P., et al. (2008). Cell wall polysaccharides are specifically involved in the exclusion of aluminum from the rice root apex. *Plant Physiol.* 146, 602–611. doi: 10.1104/pp.107.111989

Yang, Q., Li, Z., Li, W., Ku, L., Wang, C., Ye, J., et al. (2013). CACTA-like transposable element in ZmCCT attenuated photoperiod sensitivity and accelerated the postdomestication spread of maize. *Proc. Natl. Acad. Sci. U.S.A.* 110, 16969–16974. doi: 10.1073/pnas.1310949110

Yokosho, K., Yamaji, N., Fujii-Kashino, M., and Ma, J. F. (2016). Retrotransposon-mediated aluminum tolerance through enhanced expression of the citrate transporter OsFRDL4. *Plant Physiol.* 172, 2327–2336. doi: 10.1104/pp.16.01214

Yu, J., Pressoir, G., Briggs, W. H., Bi, I. V., Yamasaki, M., Doebley, J. F., et al. (2006). A unified mixed-model method for association mapping that accounts for multiple levels of relatedness. *Nat. Genet.* 38, 203–208. doi: 10.1038/ng1702

Zhang, Z., Ersoz, E., Lai, C. Q., Todhunter, R. J., Tiwari, H. K., Gore, M. A., et al. (2010). Mixed linear model approach adapted for genome-wide association studies. *Nat. Genet.* 42, 355–360. doi: 10.1038/ng.546

Conflict of Interest: The authors declare that the research was conducted in the absence of any commercial or financial relationships that could be construed as a potential conflict of interest.

frontiers in Plant Science

ORIGINAL RESEARCH
published: 21 April 2020
doi: 10.3389/fpls.2020.00392

Apoplastic Hydrogen Peroxide in the Growth Zone of the Maize Primary Root. Increased Levels Differentially Modulate Root Elongation Under Well-Watered and Water-Stressed Conditions

Priya Voothuluru[1,2†], Pirjo Mäkelä[3], Jinming Zhu[1,2†], Mineo Yamaguchi[1,2], In-Jeong Cho[2,4], Melvin J. Oliver[2,4], John Simmonds[5] and Robert E. Sharp[1,2]*

[1] Division of Plant Sciences, University of Missouri, Columbia, MO, United States, [2] Interdisciplinary Plant Group, University of Missouri, Columbia, MO, United States, [3] Department of Agricultural Sciences, University of Helsinki, Helsinki, Finland, [4] United States Department of Agriculture-Agricultural Research Service, Plant Genetics Research Unit, University of Missouri, Columbia, MO, United States, [5] Agriculture and Agri-Food Canada, Ottawa, ON, Canada

Reactive oxygen species (ROS) can act as signaling molecules involved in the acclimation of plants to various abiotic and biotic stresses. However, it is not clear how the generalized increases in ROS and downstream signaling events that occur in response to stressful conditions are coordinated to modify plant growth and development. Previous studies of maize (*Zea mays* L.) primary root growth under water deficit stress showed that cell elongation is maintained in the apical region of the growth zone but progressively inhibited further from the apex, and that the rate of cell production is also decreased. It was observed that apoplastic ROS, particularly hydrogen peroxide (H_2O_2), increased specifically in the apical region of the growth zone under water stress, resulting at least partly from increased oxalate oxidase activity in this region. To assess the function of the increase in apoplastic H_2O_2 in root growth regulation, transgenic maize lines constitutively expressing a wheat *oxalate oxidase* were utilized in combination with kinematic growth analysis to examine effects of increased apoplastic H_2O_2 on the spatial pattern of cell elongation and on cell production in well-watered and water-stressed roots. Effects of H_2O_2 removal (via scavenger pretreatment) specifically from the apical region of the growth zone were also assessed. The results show that apoplastic H_2O_2 positively modulates cell production and root elongation under well-watered conditions, whereas the normal increase in apoplastic H_2O_2 in water-stressed roots is causally related to down-regulation of cell production and root growth inhibition. The effects on cell production were accompanied by changes in spatial profiles of cell elongation and in the length of the growth zone. However, effects on overall cell elongation, as reflected in final cell lengths, were minor. These results reveal a fundamental role of apoplastic H_2O_2 in regulating cell production and root elongation in both well-watered and water-stressed conditions.

Keywords: cell elongation, cell production, root growth, hydrogen peroxide, kinematics, reactive oxygen species, water stress, *Zea mays*

OPEN ACCESS

Edited by:
Idupulapati Madhusudana Rao, International Center for Tropical Agriculture (CIAT), Colombia

Reviewed by:
Nobuhiro Suzuki, Sophia University, Japan
Isaac Zepeda Jazo, University of the Wetland of the State of Michoacan de Ocampo, Mexico
Riccardo Angelini, Roma Tre University, Italy

***Correspondence:**
Priya Voothuluru
pvoothul@utk.edu

†Present address:
Priya Voothuluru, Center for Renewable Carbon, University of Tennessee Institute of Agriculture, Knoxville, TN, United States
Jinming Zhu, Bayer Crop Science, St. Louis, MO, United States

Specialty section:
This article was submitted to Plant Abiotic Stress, a section of the journal Frontiers in Plant Science

Received: *05 February 2020*
Accepted: *18 March 2020*
Published: *21 April 2020*

Citation:
Voothuluru P, Mäkelä P, Zhu J, Yamaguchi M, Cho I-J, Oliver MJ, Simmonds J and Sharp RE (2020) Apoplastic Hydrogen Peroxide in the Growth Zone of the Maize Primary Root. Increased Levels Differentially Modulate Root Elongation Under Well-Watered and Water-Stressed Conditions. Front. Plant Sci. 11:392. doi: 10.3389/fpls.2020.00392

INTRODUCTION

The growth of plant organs does not occur indiscriminately but is restricted in its distribution to certain regions that are referred to as the growth zones. Within these zones, there is considerable spatial and temporal heterogeneity of cell production and cell expansion rates (Erickson and Silk, 1980). This heterogeneity can occur during the course of development (Beemster and Baskin, 1998) and in response to various environmental conditions (Sharp et al., 1988; Sacks et al., 1997; Muller et al., 1998; Yang et al., 2017), and thereby impacts the structure and function of different plant tissues and organs.

Drought is the major environmental factor reducing plant growth and crop productivity on a global basis (Boyer, 1982; Boyer et al., 2013). Understanding how water-stressed plants regulate growth and development of different organs is vitally important for developing crops with improved drought tolerance (Sharp and Davies, 1989; Gonzalez et al., 2012; Tardieu et al., 2018). Maintenance of root system development is a prominent adaptation of plants to water deficit (Ober and Sharp, 2007), which can enable access to water from deeper soil profiles (Sharp and Davies, 1985; Sponchiado et al., 1989; Kirkegaard et al., 2007). In some circumstances, to reach moist soil, roots must grow through soil that is already dry, and it has been demonstrated that some root types, including the primary root of several species, can continue growing at low soil water potentials that completely inhibit shoot growth (Sharp and Davies, 1979; Westgate and Boyer, 1985; Sharp et al., 1988; Spollen et al., 1993; Yamaguchi et al., 2010).

The physiological mechanisms underlying root growth maintenance at low water potentials have been studied extensively in the primary root of maize (*Zea mays* L.; reviewed in Sharp et al., 2004; Yamaguchi and Sharp, 2010; Ober and Sharp, 2013). Kinematic growth analysis (Erickson and Silk, 1980; Walter et al., 2009) was used to characterize the spatial and temporal patterns of cell expansion within the growth zone (Sharp et al., 1988; Liang et al., 1997). The results demonstrated that cell elongation is differentially responsive to water stress in different regions. Local elongation rates are maintained in the apical region even under conditions of severe water stress (water potential of −1.6 MPa), but are then progressively inhibited as cells are displaced further from the apex, resulting in a shortened growth zone. Interestingly, despite the maintenance of cell elongation in the apical region, which encompasses the meristem, the cell production rate was reported to decrease by 30% or more in maize primary roots growing under water stress (Fraser et al., 1990; Saab et al., 1992; Sacks et al., 1997). It is unclear whether the decrease in cell production reflects a negative effect of water stress or, potentially, a component of root growth adaptation to water-limited conditions (Sacks et al., 1997). Mechanisms regulating the decrease in cell production in water-stressed roots have not been investigated.

In association with the spatially variable response of cell elongation to water stress in the maize primary root, cell wall extension properties are enhanced in the apical region of growth maintenance but reduced in the basal region of growth inhibition (Wu et al., 1996). The increase in extensibility in the apical region helps to maintain cell elongation despite incomplete turgor maintenance (Spollen and Sharp, 1991). Integration of spatial growth analyses with functional genomics revealed that the majority of changes involved region-specific patterns of responses (Zhu et al., 2007; Spollen et al., 2008; Voothuluru et al., 2016). Transcriptome and cell wall proteome analyses showed that gene expression and abundance of proteins involved in generating reactive oxygen species (ROS) increased under water stress, particularly in the apical region (Zhu et al., 2007; Spollen et al., 2008). Subsequent studies confirmed that apoplastic hydrogen peroxide (H_2O_2) increased specifically in the apical region of the growth zone in water-stressed compared with well-watered roots (Voothuluru and Sharp, 2013).

Apoplastic ROS may have cell wall loosening or tightening effects that could be region specific, and may also have other growth regulatory functions (Córdoba-Pedregosa et al., 2003; Foreman et al., 2003; Tyburski et al., 2010). Apoplastic ROS have been implicated in cleaving cell wall polysaccharides to promote wall loosening and cell expansion (Schopfer, 2001; Fry, 2004; Müller et al., 2009). Schopfer (2001) provided evidence that hydroxyl radicals are involved in wall loosening and growth promotion in maize coleoptiles, and inhibition of hydroxyl radical production using various ROS scavengers or inhibitors of ROS-producing enzymes resulted in growth inhibition of maize primary roots (Liszkay et al., 2004) and leaves (Rodriguez et al., 2002) under well-watered conditions. On the other hand, apoplastic ROS could potentially be involved in signaling processes that regulate cell production (Menon and Goswami, 2007; Foyer and Noctor, 2011). An increase in apoplastic ROS production and perception has been implicated in cellular signaling and the regulation of nuclear gene transcription (Padmanabhan and Dinesh-Kumar, 2010; Shapiguzov et al., 2012), and studies in both animal and plant systems suggested that redox balance is critical for cell cycle progression and the maintenance of cell proliferation (Burhans and Heintz, 2009; Tsukagoshi et al., 2010; Yu et al., 2013; Tsukagoshi, 2016). Whether the increase in apoplastic ROS in the apical region of the growth zone of water-stressed roots is involved in regulating wall loosening and/or cell production has not been investigated.

In plants, apoplastic ROS can be generated by different enzymatic and non-enzymatic processes. The NADPH oxidases, located in the plasma membrane, utilize cytosolic NADPH to generate apoplastic superoxide (Foreman et al., 2003; Liszkay et al., 2004). The superoxide could participate in signaling processes in the apoplast or can be converted into H_2O_2 or hydroxyl radicals by action of superoxide dismutases and peroxidases (Liszkay et al., 2004; Dunand et al., 2007). Apoplastic H_2O_2 can also be produced by cell wall-localized enzymes including oxalate oxidases and polyamine oxidases (Davidson et al., 2009; Waszczak et al., 2018) or by the non-enzymatic degradation of apoplastic ascorbate (Green and Fry, 2005). The increase in apoplastic ROS in the growth zone of water-stressed roots likely results, at least partly, from the marked increase in gene expression, protein abundance and activity of oxalate oxidase that occurs in this region (Zhu et al., 2007; Spollen et al., 2008; Voothuluru and Sharp, 2013). Oxalate oxidases catalyze the conversion of oxalate to H_2O_2 and CO_2, and are known

to be cell wall localized (Davidson et al., 2009). In this study, transgenic maize lines constitutively expressing a wheat *oxalate oxidase* (Ramputh et al., 2002; Mao et al., 2007) were utilized in combination with kinematic growth analysis to examine effects of increased oxalate oxidase activity and apoplastic H_2O_2 on the spatial patterns of elongation and on cell production rates in well-watered and water-stressed maize primary roots. The results indicate that apoplastic H_2O_2 positively modulates cell production and root elongation under well-watered conditions, whereas in water-stressed roots, increased apoplastic H_2O_2 is causally related to down-regulation of cell production and root growth inhibition. Although spatial growth patterns were altered, increased H_2O_2 levels had relatively minor effects on overall cell elongation, as reflected in final cell lengths, in roots growing under both well-watered and water-stressed conditions. Potential mechanisms by which apoplastic H_2O_2 may modulate cell production and root elongation are discussed.

MATERIALS AND METHODS

Plant Materials and Growth Conditions

Transgenic maize (*Z. mays* L.) lines that were stably expressing a wheat *oxalate oxidase* gene regulated by a constitutive rice actin promoter were used. The lines were in the CK44 (Transgenic T_8 generation) and B73 (T_5 generation) inbred backgrounds (Ramputh et al., 2002; Mao et al., 2007). Corresponding segregated transgene negative lines were used as controls and are referred to as "wild-type." Experiments focused on the CK44 line, and key findings were repeated with the B73 line.

Seeds were sterilized in 5% NaClO (v/v) for 15 min, rinsed with deionized water for 15 min, imbibed in aerated 1 mM $CaSO_4$ for 24 h, and germinated between sheets of germination paper moistened with 1 mM $CaSO_4$ at 29°C and near-saturation humidity in the dark. Seedlings with primary roots 10–20 mm in length were transplanted against the sides of Plexiglas boxes containing vermiculite (no. 2A, Therm-O-Rock East Inc.) at water potentials of −0.03 MPa (well-watered) or −1.6 MPa (water-stressed), which were obtained by thorough mixing with pre-calibrated amounts of 1 mM $CaSO_4$ (Sharp et al., 1988; Spollen et al., 2000). In some experiments, vermiculite water potentials of −0.3 and −0.8 MPa were also used. Water potentials were measured in each experiment by isopiestic thermocouple psychrometry (Boyer and Knipling, 1965). Seedlings were grown at 29°C and near-saturation humidity in the dark (to minimize further drying of the media) until harvest (Sharp et al., 1988). Primary root elongation rates were determined by periodically marking the position of the root apices on the sides of the boxes. Transplanting, growth measurements and harvesting were performed using a green "safe" light (Saab et al., 1990).

Oxalate Oxidase Activity Staining Assay

In-situ oxalate oxidase activity was detected in apical segments (approximately 12 mm in length; 48 and 72 h after transplanting) or in transverse sections (48 h after transplanting) of primary roots using a solution containing 25 mM succinic acid, 3.5 mM EDTA, 2.5 mM oxalic acid at pH 4, and 0.6 mg mL^{-1} 4-chloro-1-naphthol (Dumas et al., 1995; Voothuluru and Sharp, 2013). Segments were stained for 24 h at 25°C (length measurements showed that the segments did not grow during staining). Transverse sections (14 μm) were obtained using a cryostat microtome (Leica CM 1850) at 1–2, 5–6, and 9.5–10.5 mm from the apex, and stained for 45 min (Caliskan and Cuming, 1998). The segments or sections were then washed several times in deionized water and imaged using a stereomicroscope (Leica MZFLIII). Controls for oxalate oxidase staining were incubated in staining solution without oxalic acid. The oxalate oxidase activity in water-stressed roots was evaluated using non-isoosmotic staining solution, since it was previously shown that using melibiose to lower the water potential (as used in experiments described below) interferes with the assay (Voothuluru and Sharp, 2013).

Oxalate Oxidase Transgene Expression

Primary roots were collected from batches of five to eight seedlings at 36 and 48 h after transplanting. Root tips were sectioned into apical (0–5 mm) and basal (5–12 mm) regions, frozen in liquid nitrogen and stored at −80°C. Samples were ground in liquid nitrogen and RNA was extracted using RNeasy (Qiagen). After cleaning with 0.5 units of DNase (Invitrogen) μg^{-1} total RNA, 5 μg RNA was used to synthesize single-stranded cDNA using one unit of Superscript II Reverse Transcriptase (Invitrogen) and 0.5 μg oligo dT primers. Transgene-specific primers (Forward 5′ CATGGTCGTCTCCTTCAACA and Reverse 3′ CATTTCAGGGAAGGCTCCTA) were designed using Primer3 Software, and 0.2 μg aliquots were used for qRT-PCR with 1 μg cDNA to amplify the wheat *oxalate oxidase* expression. Glyceraldehyde phosphate dehydrogenase was used as a reference gene.

In situ Imaging of Apoplastic ROS

Imaging of apoplastic ROS in the apical region of the primary root was conducted using the fluorescent dye 2′,7′-dichlorodihydrofluorescein (H_2DCF; custom synthesized by Molecular Probes), as described by Zhu et al. (2007). The dye is a derivative of 5-(and-6)-carboxy-2′,7′- H_2DCF diacetate (carboxy-H_2DCFDA, an indicator of intracellular ROS) in which the acetate groups (which allow the molecule to cross the plasma membrane) have been cleaved. Evidence of apoplastic localization of H_2DCF staining in the apical region of well-watered and water-stressed maize primary roots was detailed in Zhu et al. (2007).

Staining was conducted using a protocol to minimize diffusion of the dye and ROS from the apoplast (Zhu et al., 2007). Briefly, roots of the CK44 transgenic and wild-type lines were harvested 48 h after transplanting and placed in a solution containing 1% high- and 1% low-gelling temperature agarose (1:1) in 1 mM $CaSO_4$, which solidified at approximately 30°C, and 30 μM H_2DCF. As the solution cooled, roots were immersed immediately before the onset of solidification. To avoid osmotic shock, for the water-stressed roots the

solution water potential was lowered to −1.6 MPa (the water potential of the vermiculite in which the roots had been growing) using melibiose. Melibiose was used for this purpose because of evidence that it is neither hydrolyzed nor taken up by plant cells (Dracup et al., 1986). After 30 min, agarose blocks containing the root apical 20 mm were removed and H_2DCF fluorescence in epidermal cells was imaged at 1.5–2.0 mm from the apex using two-photon laser-scanning confocal microscopy (Zeiss LSM NLO 510 combined with a Coherent, Chameleon 720–950 nm laser). Seven optical sections (5 μm in thickness) were merged into a single image for each root, and normalized fluorescence intensity (sum of pixel intensities in a defined area divided by pixel number) was quantified using the threshold option of Metamorph software (Molecular Devices Inc.).

Cytosolic ROS

Cytosolic ROS was imaged by staining with the membrane-permeable fluorescent dye carboxy-H_2DCFDA (Molecular Probes). Briefly, roots were harvested 48 h after transplanting, placed in a solution containing 1 mM $CaSO_4$ and 15 μM carboxy-H_2DCFDA, and stained for 30 min. For the water-stressed roots, melibiose was added to lower the solution water potential to −1.6 MPa. The apical 10 mm were then imaged for carboxy-H_2DCFDA fluorescence using a stereomicroscope (Leica MZFLIII) with a GFP filter (excitation 488 nm, emission 515/30 nm). Normalized fluorescence intensity was quantified as described above.

Cell Length and Relative Elongation Rate Profiles

Spatial distributions of relative elongation rate (h^{-1}) were calculated from root elongation rates and cell length profiles (Silk et al., 1989; Yamaguchi et al., 2010). Accurate determination of relative elongation rate profiles from anatomical records requires steady growth and cell length distribution. Root elongation was essentially steady in well-watered and water-stressed roots after 12 and 24 h from transplanting, respectively. However, because the water-stressed roots elongated more slowly, the harvest time was increased from 48 h in well-watered roots to 72 h in water-stressed roots to allow greater time for stabilization of the cell length profile.

Briefly, 25–30 seedlings were transplanted to well-watered or water-stressed conditions, and root elongation rates were measured from 36–48 h to 48–72 h after transplanting, respectively. In each treatment, several roots that were straight and had an elongation rate similar to the mean were selected, and the apical 15 mm were sectioned longitudinally (125 μm in thickness) using a Vibratome (Vibratome 3000 plus), stained with 1 mg mL^{-1} Calcofluor (Sigma-Aldrich) for 15 min to visualize the cell walls, and imaged by confocal microscopy (Yamaguchi et al., 2010). The spatial distribution of cortical cell length for each root was determined from 4 to 12 cells per position (well-watered: 0.5-mm intervals to 4 mm from the apex, then at 1-mm intervals; water-stressed: 0.25-mm intervals to 4 mm from the apex, then at 1-mm intervals) until unchanging mean lengths were obtained.

Spatial distributions of displacement velocity (mm h^{-1}) were calculated using the relationship $L_A/L_F = V_A/V_F$, where L_A is mean cell length at position A, L_F is final cell length (average of the 4–6 most distal measurement positions), V_A is velocity at position A, and V_F is final velocity (equal to the root elongation rate) (Silk et al., 1989). This method cannot accurately calculate displacement velocities in the meristem because cell lengths in this region are determined by both elongation and division. Therefore, displacement velocities were calculated from the distal end of the meristem, approximated as the position where cell lengths reached 2.5 times the length of the shortest cells (Erickson, 1961). Velocity profiles were obtained for individual roots, and sigmoidal (Slogistic 1) curves were fitted using Origin software (OriginLab Corp.) using the function:

$$y = a/[1 + e^{-K(x-xc)}]$$

where x is distance from the root cap junction and a, K, and xc are parameters obtained from the non-linear fit of the curve. The goodness of fit (R^2) for each velocity profile was >0.98. Derivatives of the curves provided relative elongation rate profiles for each root, which were averaged to obtain mean profiles per treatment.

Residence times for cells within the growth zone (beyond the meristem) were obtained according to Dumlao et al. (2015). Briefly, using the analytical function described above, interpolated displacement velocities were calculated at 0.25 mm intervals on an individual root basis. Local displacement times were calculated from the interpolated velocities (local displacement time = 0.25/local velocity) and were then numerically integrated to obtain growth trajectories (position versus time). The relative elongation rate associated with each position was then plotted against time to provide the temporal pattern of relative elongation rate as cells were displaced from the distal end of the meristem to the end of the growth zone.

Cell Production Rate

Rates of cell flux (cells h^{-1}) were calculated by dividing root elongation rates by final cell lengths; under steady conditions, cell flux approximates the cell production rate (Silk et al., 1989). Since cell length profiles in the growth zone were not obtained for the B73 lines, the end of the growth zone was not precisely determined for these roots. Therefore, to ensure that cell lengths were measured in regions where elongation had ceased, final cortical cell lengths were calculated by averaging mean cell lengths from 16 to 24 mm and 11 to 18 mm from the apex in well-watered and water-stressed roots, respectively.

H_2O_2 Scavenger Experiments

Hydrogen peroxide scavenger experiments were conducted using maize inbred line FR697 due to the large number of seeds required combined with limited availability of seeds of the transgenic and wild-type lines. FR697 was previously used to characterize spatial patterns of transcript (Spollen et al., 2008), cell wall protein (Zhu et al., 2007), and apoplastic H_2O_2 (Voothuluru and Sharp, 2013) in well-watered and water-stressed primary roots. Seeds were germinated as described above, and

seedlings with primary roots 5–20 mm in length were pretreated with the H_2O_2 scavenger potassium iodide (KI) (Liszkay et al., 2004; Encina and Fry, 2005). Plexiglas holders (32 cm long, 4 cm wide, three sides of 2 cm in height) were used to cast a 5-mm layer of 1% agarose gel containing 0, 30, or 45 mM KI, and the apical 3 mm of the roots were inserted into the edge of the gel (20 seedlings per holder) for 6 h. Because the roots elongated during the pretreatment, kernels were moved every 2 h such that only the apical 3 mm of the roots remained in the gel. Seedlings were then transplanted into vermiculite at water potentials of −0.03 or −1.6 MPa. Environmental conditions during pretreatment and after transplanting were as described above. In preliminary experiments, the effectiveness of several KI concentrations was examined for effects on root elongation after transplanting to the well-watered and water-stressed treatments. The 30 mM (as also used by Liszkay et al. (2004) in studies of the maize primary root growth zone) and 45 mM pretreatments were selected as being the most effective.

In each treatment, several roots that were straight and had an elongation rate similar to the mean were harvested 36 h after transplanting and used to measure final cell lengths and cell production rates, as described above. The growth zone length in FR697 is approximately 12 and 7 mm under well-watered and water-stressed (−1.6 MPa) conditions, respectively (Sharp et al., 2004). Accordingly, final cell lengths were calculated by averaging mean lengths at 1-mm intervals from 12 to 17 mm from the apex in well-watered roots, and at 2-mm intervals from 9 to 13 mm from the apex in water-stressed roots.

RESULTS

Unless otherwise noted, water stress was imposed by transplanting seedlings into vermiculite at a water potential of −1.6 MPa, as used in previous studies of ROS metabolism in water-stressed maize primary roots (Zhu et al., 2007; Voothuluru and Sharp, 2013).

Spatial Profiles of Oxalate Oxidase Activity in *Oxalate Oxidase* Transgenic and Wild-Type Roots Under Well-Watered and Water-Stressed Conditions

The spatial distribution of oxalate oxidase activity was determined in apical 12-mm segments of the primary root of CK44 wild-type and transgenic lines at 48 h after transplanting to well-watered or water-stressed conditions (**Figure 1A**). In all cases, this segment encompassed the growth zone, which was approximately 9 and 11 mm in length, respectively, in wild-type and transgenic roots in the well-watered treatment, and was shortened to 5 and 4 mm in wild-type and transgenic roots under water-stress (growth zone lengths are presented below). Consistent with previous results in a different genotype (inbred line FR697; Voothuluru and Sharp, 2013), the CK44 wild-type line showed no discernable staining for oxalate oxidase activity at any location in well-watered roots, whereas water-stressed roots exhibited a pronounced increase in activity in the apical 2-mm region immediately behind the root cap junction (**Figure 1A**). The water-stressed wild-type roots also showed an increase in oxalate oxidase activity from approximately 9 to 12 mm from the root apex, which was beyond the growth zone. Roots stained in buffer without oxalic acid showed no staining in either treatment, demonstrating that the staining was specific to oxalate oxidase activity (data not shown). The lack of staining in the no-oxalic acid control for the water-stressed roots was probably attributable to limited sensitivity of the assay, rather than lack of endogenous apoplastic oxalate.

In contrast to the lack of staining for oxalate oxidase activity in well-watered wild-type roots, well-watered roots of the CK44 transgenic line exhibited substantial activity in the apical region, extending to approximately 4 mm from the apex (**Figure 1A**). Faint and stippled staining also occurred throughout the rest of the segment. In the water-stressed treatment, the transgenic roots showed extended apical and basal regions of staining compared to the wild-type roots, such that staining occurred throughout most of the segment (**Figure 1A**). In both the wild-type and transgenic lines, staining patterns obtained at 72 h after transplanting to well-watered and water-stressed conditions were similar to those obtained at 48 h (**Supplementary Figure S1**), indicating that the region-specific patterns of staining were steady rather than transient events.

Spatial patterns of staining for oxalate oxidase activity in the apical segments of the B73 wild-type and transgenic lines under well-watered and water-stressed conditions were similar to those observed in the CK44 lines (**Figure 2**). Well-watered wild-type roots did not exhibit staining at any location, whereas water-stressed wild-type roots showed increased activity in the apical 2-mm region, as well as in the basal region (generally beyond 8 mm from the apex, although with considerable variation in intensity and extent between individual roots). The transgenic line showed increased oxalate oxidase activity in the apical 6-mm region of well-watered roots, and throughout the segment in water-stressed roots.

To ensure that the spatial patterns of staining for oxalate oxidase activity observed in the intact root segments were not attributable to differential penetration of the staining solution into the different regions, transverse sections were made at several distances from the apex of well-watered and water-stressed roots of the CK44 wild-type and transgenic lines, and were stained after sectioning. The results were generally consistent with the staining patterns in the intact segments (**Figure 1B**). In well-watered wild-type roots, sections taken at 1.5, 5.5, and 10 mm from the apex showed minimal oxalate oxidase activity in all tissues, whereas in the water-stressed treatment, the wild-type line showed a substantial increase in activity at 1.5 mm from the apex, and mild and moderate staining, respectively, at 5.5 and 10 mm. It should be noted that at 10 mm from the apex of water-stressed roots, oxalate oxidase activity was transitioning from the region of minimal activity to the region of stronger activity at the basal end of the segments (**Figure 1A**), and thus corresponded to the moderate intensity of staining observed in the transverse section at this location. In all locations, staining was more pronounced in the cortex and epidermis than in the

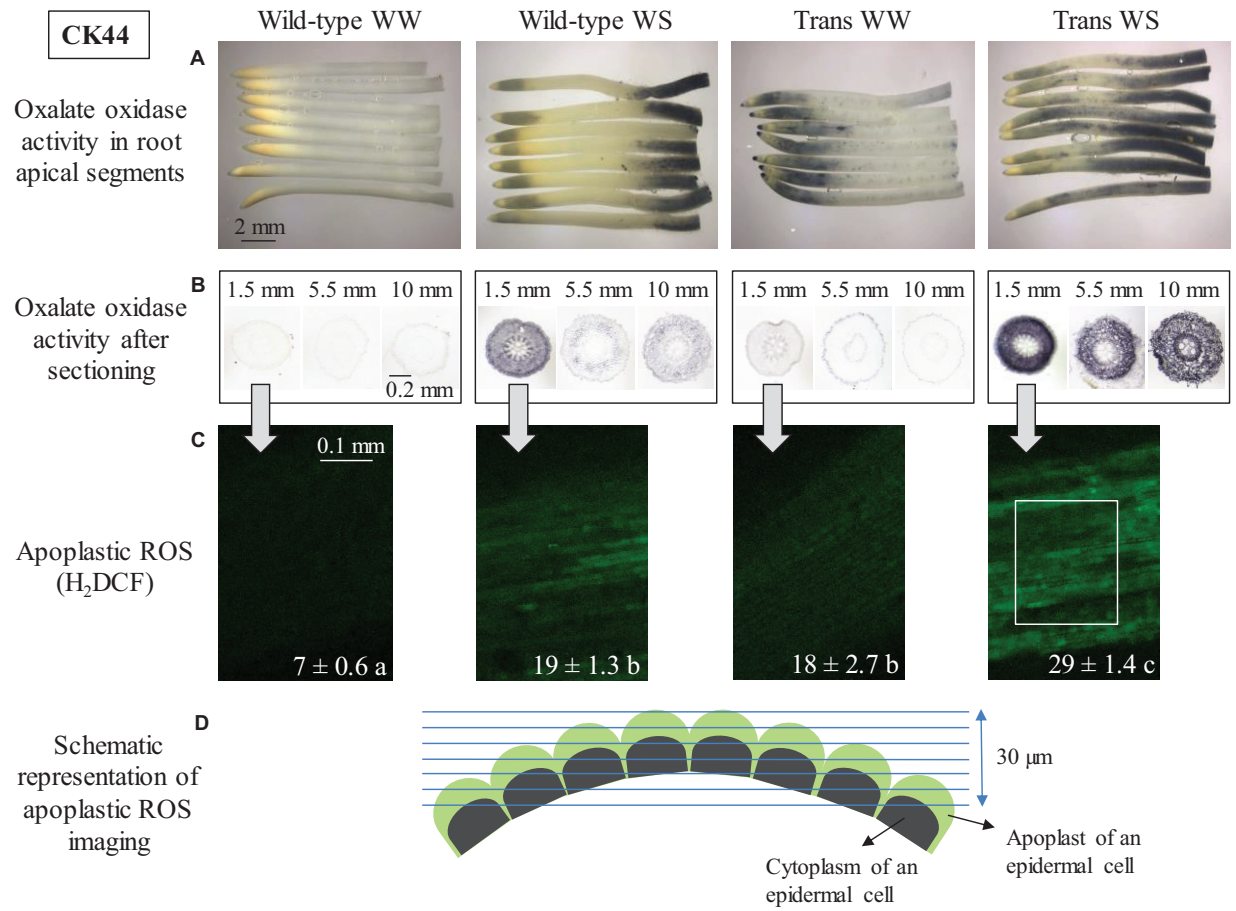

FIGURE 1 | Oxalate oxidase activity and apoplastic ROS in the apical region of the primary root in CK44 *oxalate oxidase* transgenic (Trans) and wild-type lines at 48 h after transplanting to well-watered (WW) or water-stressed (WS; –1.6 MPa) conditions. Oxalate oxidase activity was measured by oxidation of 4-chloro-1-naphthol, seen as dark blue staining, in approximately 12-mm apical segments **(A)** and in 14-µm transverse sections at various distances from the root apex **(B)**. Apoplastic ROS **(C)** was stained using the fluorescent ROS indicator H_2DCF (membrane impermeable); confocal images of the epidermis at 1.5–2.0 mm from the root apex are shown. The images are composed of projections of seven consecutive optical sections (5 µm in thickness) obtained by two-photon confocal microscopy. The numbers on the images indicate normalized pixel intensities (± SE; $n = 3$ roots) of a 0.04 mm^2 area of the root (0.18 mm length, 0.23 mm width), as illustrated in the Trans WS image. Different letters indicate significant differences (*t*-test; $P < 0.05$). All experiments were repeated with similar results, and representative images are shown. Panel **D** shows a schematic representation of apoplastic ROS imaging in the epidermal cell file **(D)**. Green and black semicircles indicate the apoplast and cytoplasm of the epidermal cells, respectively, and blue lines indicate the consecutive optical planes at which fluorescence was captured. The schematic also illustrates the curvature of the root, which necessitated capture of fluorescence in multiple optical planes.

FIGURE 2 | Oxalate oxidase activity measured by oxidation of 4-chloro-1-naphthol, seen as dark blue staining, in approximately 12-mm apical segments of the primary root in the B73 *oxalate oxidase* transgenic (Trans) and wild-type lines at 48 h after transplanting to well-watered (WW) or water-stressed (WS; –1.6 MPa) conditions. The experiments were repeated with similar results and representative images are shown.

stele. In the transgenic line, well-watered roots showed moderate staining in all tissues at 1.5 mm from the apex, and low levels of staining at the other locations. Water-stressed roots of the transgenic line exhibited a pronounced increase in staining in the cortex and epidermis at 1.5 mm from the apex, and also showed substantial staining at both 5.5 and 10 mm.

To assess the relationship of the spatial profiles of oxalate oxidase activity with transgene expression, qRT-PCR experiments were conducted with the CK44 transgenic line at 36 and 48 h after transplanting to well-watered and water-stressed conditions. In well-watered roots, transgene expression was about threefold higher in the apical 0–5 mm region compared with the 5–12 mm region (**Table 1**). In water-stressed roots, similarly, transgene expression was fourfold higher in the 0–5 mm region compared with the 5–12 mm region. Accordingly, the increased oxalate oxidase activity in the apical compared with the basal region of both well-watered and water-stressed transgenic roots could be explained, at least partly, by the greater *oxalate oxidase* transgene expression in the apical region. Interestingly, the results also showed that in both the apical and basal regions of the water-stressed roots, *oxalate oxidase* transgene transcript abundance was 30–50% lower than in well-watered roots.

Apoplastic ROS Levels in *Oxalate Oxidase* Transgenic and Wild-Type Roots Under Well-Watered and Water-Stressed Conditions

It was previously shown that the increase in oxalate oxidase activity in the apical region of the growth zone in water-stressed maize primary roots was associated with a pronounced increase in the level of apoplastic H_2O_2 compared with the well-watered control (Zhu et al., 2007; Voothuluru and Sharp, 2013). Accordingly, the increases in oxalate oxidase activity observed in the apical region of both well-watered and water-stressed roots of the CK44 transgenic line predicted an increase in apoplastic H_2O_2 levels under both conditions. This hypothesis was tested by *in situ* confocal imaging of apoplastic ROS in epidermal cells of the apical region (1.5–2 mm from the apex) using the membrane-impermeable fluorescent indicator dye H_2DCF. Consistent with previous results using this technique (in line FR697; Zhu et al., 2007), the level of apoplastic ROS in water-stressed roots of the wild-type was higher (approximately threefold) than in well-watered roots (**Figure 1C**). Moreover, as anticipated, both well-watered and water-stressed roots of the transgenic line exhibited substantially increased apoplastic ROS levels compared to the wild-type controls. Evidence of apoplastic localization of H_2DCF staining was provided by analysis of the pattern of staining in consecutive focal planes, which showed no evidence of intracellular staining (**Figure 1D** and **Supplementary Video S1**). The variation in apoplastic ROS levels among the different lines and treatments correlated closely with the relative intensity of staining for oxalate oxidase activity (especially with that in the transverse sections; **Figure 1B**). Since the oxalate oxidase protein is specifically involved in production of apoplastic H_2O_2 (Davidson et al., 2009), the observed increases in fluorescence in the apical region of the transgenic line under both well-watered and water-stressed conditions likely reflect increases in apoplastic H_2O_2, although the possible involvement of other ROS cannot be excluded. Levels of apoplastic ROS were not assessed in the basal region of the growth zone because of evidence of membrane permeability to H_2DCF in the epidermal cells of this region (Zhu et al., 2007).

To assess whether the CK44 transgenic line also exhibited increases in cytosolic ROS levels, well-watered and water-stressed roots were stained with the membrane-permeable dye carboxy-H_2DCFDA. Cytosolic ROS levels were not increased in roots of the transgenic compared to the wild-type line in either the well-watered or the water-stressed condition (**Supplementary Figure S2**). Although there was a marginal increase in cytosolic ROS levels in the apical 2.5 mm region of water-stressed compared with well-watered roots in both the transgenic and wild-type lines, the increases were not significant.

Root Elongation in *Oxalate Oxidase* Transgenic Lines Responds Differentially to Well-Watered or Water-Stressed Conditions

Under well-watered conditions, primary root elongation in the CK44 transgenic line was increased compared with the wild-type throughout the experiments (**Figure 3A**). At 48 h after transplanting, the root length of the transgenic was 13% greater than that of the wild-type (111 ± 2 mm versus 98 ± 1 mm; data are means ± SE of four experiments). The increase in root elongation was accompanied by a 17% increase in shoot elongation (shoot lengths were 125 ± 2 mm in the transgenic compared with 107 ± 3 mm in the wild-type). In the water stress treatment, in contrast, root elongation of the transgenic line was consistently reduced compared with the wild-type, such that root length at 72 h after transplanting was 24% less in the transgenic than in the wild-type (44 ± 2 mm versus 58 ± 3 mm; data are means ± SE of three experiments). Shoot growth was completely inhibited in both the wild-type and transgenic lines due to the severity of the water stress treatment (Sharp et al., 1988).

Similar results were obtained with the B73 transgenic and wild-type lines (**Figure 3B**). The transgenic showed a 33% increase in root length at 48 h in the well-watered treatment and a 22% decrease in root length at 72 h in the water stress treatment compared with the wild-type. Root elongation rates were approximately steady after 12 and 24 h from transplanting to the well-watered and water-stressed conditions, respectively,

TABLE 1 | Transgene expression quantification by qRT-PCR.

Treatment	Distance from apex	$2^{-[\Delta][\Delta]Ct}$ values for transgene expression	
		36 h	48 h
Well-watered	0–5 mm	0.73 ± 0.06**	0.64 ± 0.07*
	5–12 mm	0.21 ± 0.02	0.20 ± 0.02
Water-stressed	0–5 mm	0.43 ± 0.01*▲▲	0.45 ± 0.07*
	5–12 mm	0.10 ± 0.04▲	0.12 ± 0.01▲▲

*$2^{-[\Delta][\Delta]Ct}$ values in the apical (0–5 mm from the apex) and basal (5–12 mm from the apex) regions of the primary root in the CK44 oxalate oxidase transgenic line at 36 or 48 h after transplanting to well-watered or water-stressed (−1.6 MPa) conditions. Data are means ± SE of three samples. Asterisks denote significant differences between the 0–5 mm and 5–12 mm regions (t-test; *P < 0.05; **P < 0.01). Triangles denote significant differences between well-watered and water-stressed treatments (t-test; ▲P < 0.1; ▲▲P < 0.05).*

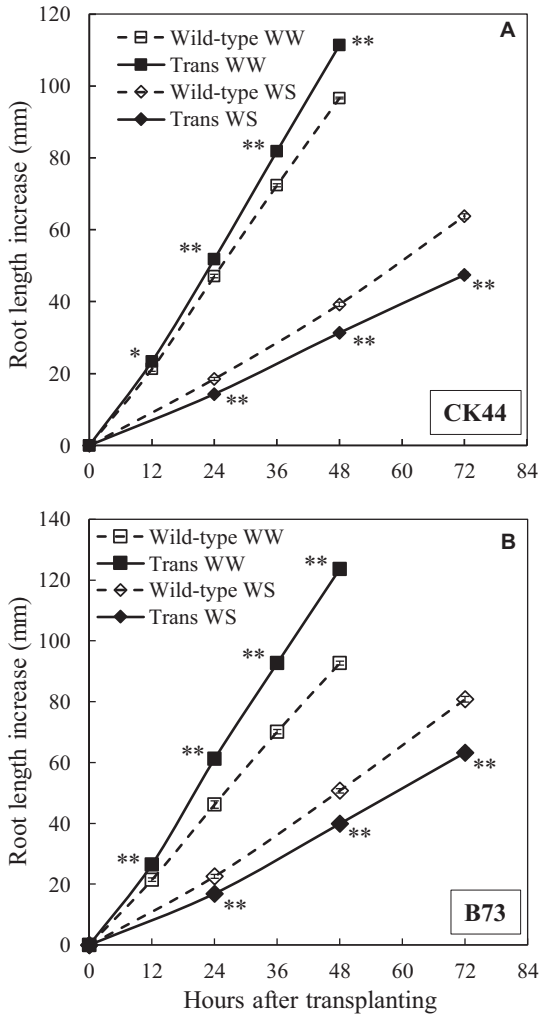

FIGURE 3 | Primary root elongation of CK44 **(A)** and B73 **(B)** *oxalate oxidase* transgenic (Trans) and wild-type lines after transplanting to well-watered (WW) or water-stressed (WS; –1.6 MPa) conditions. Data are means ± SE (n = 10–32). Asterisks denote significant differences between the transgenic and wild-type lines (t-test; $^*P < 0.05$; $^{**}P < 0.01$). The experiment was repeated three (CK44) or two (B73) times with similar results.

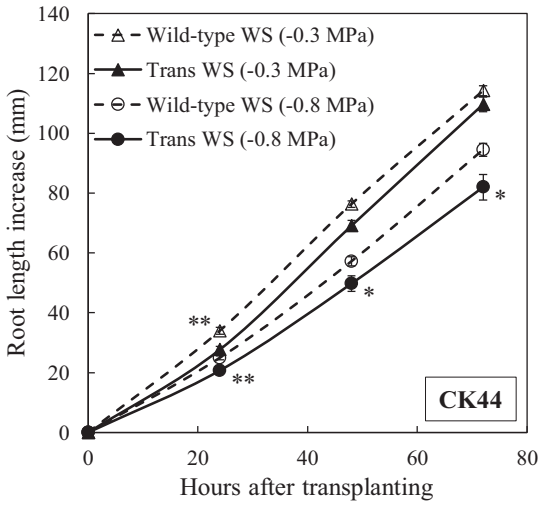

FIGURE 4 | Primary root elongation of CK44 *oxalate oxidase* transgenic and wild-type lines after transplanting to mild (–0.3 MPa) or moderate (–0.8 MPa) water stress conditions. Data are means ± SE (n = 14–20). Asterisks denote significant differences between the transgenic and wild-type lines (t-test; $^*P < 0.05$; $^{**}P < 0.01$).

in both the CK44 and B73 transgenic and wild-type lines (**Supplementary Tables S1, S2**).

The responses of primary root elongation were also evaluated under mild (water potential of −0.3 MPa) and moderate (water potential of −0.8 MPa) water stress levels in the CK44 transgenic and wild-type lines (**Figure 4**). In the mild stress condition, root length was slightly reduced in the transgenic compared with the wild-type line throughout the experiment, although this effect was significant only at the 24 h time point. In the moderate stress treatment, root length was consistently reduced (by 13% at 72 h after transplanting) in the transgenic compared with the wild-type. Taking into account the fact that root elongation in the transgenic line was promoted in the well-watered condition, these results show that inhibition of root elongation under water stress was considerably greater in the transgenic compared with the wild-type line. At 48 h after transplanting, the transgenic line exhibited decreases in root length of 38, 55, and 72% under mild, moderate and severe stress conditions, respectively. In the wild-type, in contrast, root length was inhibited by only 21, 41, and 59%, respectively, in these treatments. Because the transgenic line showed decreased root elongation at all of the water stress levels tested, further experiments were conducted only under the severe water stress (−1.6 MPa) condition.

Taken together, the results shown in **Figures 1–4** indicate that the oxalate oxidase-mediated increase in apoplastic H_2O_2 in the growth zone of the transgenic lines positively and negatively modulated root growth under well-watered and water-stressed conditions, respectively.

Kinematic Analysis of *Oxalate Oxidase* Transgenic and Wild-Type Roots Under Well-Watered and Water-Stressed Conditions

The overall rate of root elongation is determined by the product of cell flux (the rate per cell file at which cells exit the growth zone) and final cell length. Under steady conditions, the cell flux approximates the rate of cell production (the rate per cell file at which cells leave the meristem; Silk et al., 1989). Accordingly, cortical cell length profiles were obtained for the CK44 transgenic and wild-type lines to determine whether the differential effects of enhanced oxalate oxidase activity/increased apoplastic H_2O_2 on root elongation under well-watered and water-stressed conditions were primarily attributable to changes in final cell length and/or cell production, and also to localize any effects on the spatial distribution of relative elongation rate within the growth zone (Sharp et al.1988; Silk et al., 1989).

In the well-watered treatment, despite the fact that the transgenic line exhibited a 25% increase in root elongation rate compared with the wild-type during the period of steady growth before harvest, the final cell length at the end of the growth zone was only 5% greater in the transgenic (**Figure 5A** and **Table 2**). In contrast, the estimated cell production rate was 19% greater in the transgenic line (**Table 2**). The cell length profile also revealed a basal shift in the location at which final cell length was achieved in the transgenic compared with the wild-type (**Figure 5A**), such that the length of the growth zone increased by 22% from 9 mm in the wild-type to 11 mm in the transgenic line, approximately reflecting the increase in root elongation rate. The lengthening of the growth zone was also reflected in the profiles of displacement velocity (**Figure 5C**) and relative elongation rate (**Figure 5E**), which showed that local relative elongation rates were lower in the apical region and higher in the basal region of the transgenic compared to the wild-type. In contrast, the maximum relative elongation rate was not significantly different between the lines (**Figure 5E**).

In the water-stressed treatment, the root elongation rate was decreased by 29% in the transgenic compared with the wild-type, but final cell length was not significantly different between the lines (**Figure 5B** and **Table 2**). In contrast, the estimated cell production rate was decreased by 26% in the transgenic compared with the wild-type line (**Table 2**). Consistent with previous studies (Sharp et al., 1988; Liang et al., 1997), the growth zone was substantially shorter in the water-stressed compared with well-watered roots in both the transgenic and wild-type lines (**Figures 5A,B**). Opposite to the effect in well-watered transgenic roots, however, the profiles of cell length, displacement velocity and relative elongation rate were shifted apically in the transgenic line under water stress, reflecting a further shortening of the growth zone from 5 to 4 mm (**Figures 5B,D,F**). The peak relative elongation rate was slightly decreased in the transgenic compared with the wild-type, although this difference was not significant ($P = 0.17$).

In the B73 transgenic line, effects on cell length and cell production rate under well-watered and water-stressed conditions were consistent with those observed in the CK44 background. In this case, only final cell lengths (**Supplementary Figure S3**) rather than complete cell length profiles were measured. In well-watered roots, the cell production rate in the transgenic was 22% higher than in the wild-type (**Table 3**). In addition, the transgenic line showed a 13% increase in final cell length under the well-watered condition. In the water-stressed roots, in contrast, cell production rate was 17% lower in the transgenic compared with the wild-type (**Table 3**). Final cell lengths were slightly but not significantly ($P = 0.12$) decreased in the transgenic line in the water-stressed condition.

Taking into account that rates of cell production were increased in the well-watered roots, the analysis revealed that cell production was more sensitive to water stress in the transgenic lines compared with the wild-type lines. In the CK44 background, the transgenic showed a 55% decrease in cell production rate in water-stressed compared with well-watered roots, while the wild-type showed only a 28% decrease (**Table 2**). Similarly, in the B73 background, cell production rate was decreased by 41% in the transgenic but by only 12% in the wild-type (**Table 3**). In contrast, the difference in the response of final cell length to water-stress was less pronounced between the transgenic and wild-type lines, being inhibited by 38 and 33% in the CK44 background and by 37 and 24% in the B73 background, respectively.

To analyze whether oxalate oxidase-mediated increases in apoplastic H_2O_2 impacted temporal aspects of cell elongation, time courses of relative elongation rate in the root growth zone of CK44 transgenic and wild-type lines growing under well-watered or water-stressed conditions were calculated (**Figure 6**). The results show that the temporal patterns of relative elongation rate were similar between the lines in both treatments, and moreover, that the total residence time for cells to move from the distal end of the meristem to the end of the growth zone was not significantly different ($P > 0.2$) between the lines and treatments. Thus, cessation of elongation occurred in tissue of approximately the same age regardless of the modifications of growth zone length that occurred in the different treatments.

Apoplastic H_2O_2 Removal Differentially Affects Cell Production and Root Elongation Under Well-Watered and Water-Stressed Conditions

As detailed above, the increases in apoplastic H_2O_2 in the root growth zone in the transgenic lines resulted in differential effects on cell production and root elongation in well-watered (both processes increased) and water-stressed (both processes decreased) roots. Accordingly, these findings suggest that the normal increase in apoplastic H_2O_2 in water-stressed roots may be involved in down-regulation of cell production and root elongation. On the other hand, it is also possible that the additional increase in apoplastic H_2O_2 that occurred in the transgenic lines under water-stress (**Figure 1C**) may have caused excess H_2O_2 levels, leading to a spurious inhibition of cell production and root elongation and obscuring the function of the normal increase in H_2O_2. To distinguish between these alternate possibilities, an additional set of experiments was conducted to examine the effects of removing apoplastic H_2O_2 from the apical region of the growth zone in non-transgenic roots growing under well-watered and water-stressed conditions. Based on the transgenic results, it was hypothesized that H_2O_2 removal would lead to decreased rates of cell production and root elongation under well-watered conditions, and conversely, to increased rates of cell production and root elongation under water stress. The results, as follows, were consistent with this hypothesis.

These experiments were conducted using maize inbred line FR697, which was shown previously to exhibit a pronounced increase in apoplastic H_2O_2 in the apical region of the root growth zone under water-stressed conditions (Voothuluru and Sharp, 2013). To decrease H_2O_2 levels, the roots were pretreated with KI, which has been used in previous studies to scavenge H_2O_2 from cell walls (Nose et al., 1995; Encina and Fry, 2005; Dunand et al., 2007), including from the growth zone of the maize primary root (Liszkay et al., 2004). In order to scavenge H_2O_2 specifically in the apical region of the growth zone, the roots were pretreated by placing the apical 3 mm into agarose

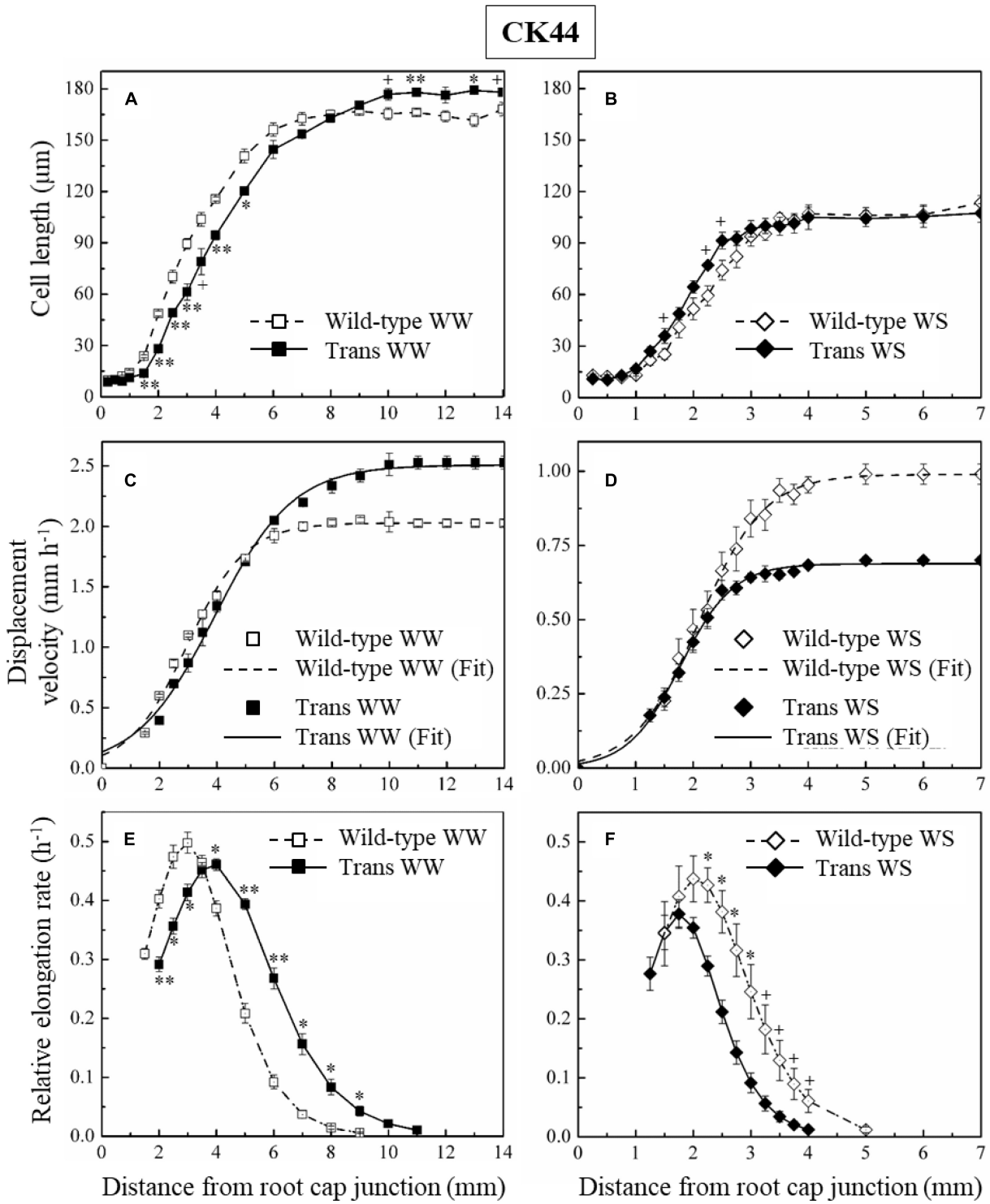

FIGURE 5 | Cortical cell length profiles **(A,B)**, displacement velocity profiles **(C,D)**, and relative elongation rate profiles **(E,F)** as a function of distance from the root cap junction in the primary root of CK44 *oxalate oxidase* transgenic (Trans) and wild-type lines growing under well-watered (WW) or water-stressed (WS; −1.6 MPa) conditions. (In the water-stressed roots, cell lengths were also measured from 8 to 10 mm from the apex, but are not shown for clarity). Derivatives of sigmoidal curves fitted to the displacement velocity profiles of individual roots were used to obtain the mean relative elongation rate profiles. For clarity, only the curves fitting the mean velocity profiles (Fit) are shown, for which the goodness of fit (R^2) was >0.99 in all cases. Roots were harvested 48 h after transplanting to well-watered conditions and 72 h after transplanting to water-stressed conditions; values are means ± SE of three to four roots. Significant differences between the transgenic and wild-type lines are shown for the cell length and relative elongation rate data (*t*-test; $^{+}P < 0.1$; $^{*}P < 0.05$; $^{**}P < 0.01$). The experiments were repeated with similar results.

TABLE 2 | Elongation rate, final cell length, and cell production rate of the primary root in the CK44 *oxalate oxidase* transgenic and wild-type lines at 48 or 72 h after transplanting to well-watered or water-stressed (−1.6 MPa) conditions, respectively.

	CK44, well-watered			CK44, water-stressed		
	Wild-type	Transgenic	Change compared to wild-type (%)	Wild-type	Transgenic	Change compared to wild-type (%)
Root elongation rate (mm h^{-1})	2.03 ± 0.03	2.53 ± 0.05**	25	0.99 ± 0.02	0.70 ± 0.01**	−29
Final cell length (μm)	165 ± 2	173 ± 1*	5	111 ± 5	107 ± 6	−4
Cell production rate (cells h^{-1})	12.3 ± 0.2	14.6 ± 0.3**	19	8.9 ± 0.2	6.6 ± 0.4**	−26

*Elongation rates were calculated for the preceding 12 h (well-watered) or 24 h (water-stressed) periods. Values are means ± SE of three to four roots. Asterisks denote significant differences between the transgenic and wild-type lines (t-test; *P < 0.05; **P < 0.01).*

TABLE 3 | Elongation rate, final cell length, and cell production rate of the primary root in the B73 *oxalate oxidase* transgenic and wild-type lines at 48 or 72 h after transplanting to well-watered or water-stressed (−1.6 MPa) conditions, respectively.

	B73, well-watered			B73, water-stressed		
	Wild-type	Transgenic	Change compared to wild-type (%)	Wild-type	Transgenic	Change compared to wild-type (%)
Root elongation rate (mm h^{-1})	1.86 ± 0.03	2.56 ± 0.04**	38	1.24 ± 0.01	0.96 ± 0.06**	−23
Final cell length (μm)	187 ± 1	210 ± 2**	13	142 ± 2	132 ± 4	−7
Cell production rate (cells h^{-1})	10.0 ± 0.1	12.2 ± 0.2**	22	8.8 ± 0.2	7.2 ± 0.2*	−17

*Elongation rates were calculated for the preceding 12 h (well-watered) or 24 h (water-stressed) periods. Values are means ± SE of three to four roots. Asterisks denote significant differences between the transgenic and wild-type lines (t-test; *P < 0.05; **P < 0.01).*

gel containing either 30 or 45 mM KI for 6 h (**Figure 7A**), and the seedlings were then transplanted as usual to well-watered or water-stressed conditions.

In both well-watered and water-stressed seedlings, effects of the KI pretreatment on root elongation were opposite to the effects of enhanced H_2O_2 that were observed in the transgenic lines. Thus, after transplanting to the well-watered condition, root elongation was substantially inhibited in KI-pretreated roots compared with the untreated control; from 24 to 40 h, elongation rates were decreased by 20 and 28%, respectively, following the 30 and 45 mM pretreatments (**Figure 7B**). Conversely, after transplanting to the water-stressed condition, KI-pretreated roots showed a significant increase in elongation compared with the control; from 24 to 40 h, elongation rates were increased by 12 and 26%, respectively, following the 30 and 45 mM pretreatments. In both the well-watered and water-stressed seedlings, effects of the KI pretreatment on root elongation diminished after 40 h from transplanting (**Figure 7B**).

To evaluate the relative effects of the scavenger pretreatment on final cell length and cell production rate, cortical cell length measurements were made 36 h after transplanting in roots pretreated with 0, 30 mM (well-watered), or 45 mM (water-stressed) KI (**Supplementary Figure S4**); these pretreatments resulted in almost steady root elongation during the preceding 20 h (**Figure 7B**). In well-watered roots, the KI pretreatment caused a 16% decrease in cell production rate whereas final cell length was not significantly decreased (**Table 4**). Conversely, in the water-stressed roots, the KI pretreatment resulted in a 20% increase in cell production rate, which, together with a 15% increase in final cell length, accounted for the 38% increase in root elongation observed in this experiment (**Table 4**).

DISCUSSION

Spatial Variability of Oxalate Oxidase Activity in the Growth Zone of Wild-Type and *Oxalate Oxidase* Transgenic Roots Under Well-Watered and Water-Stressed Conditions

In this study, transgenic maize lines constitutively expressing a wheat *oxalate oxidase* (Ramputh et al., 2002; Mao et al., 2007), in combination with H_2O_2 scavenger experiments and kinematic growth analysis, were used to investigate the involvement of apoplastic H_2O_2 in regulating maize primary root elongation under well-watered and water-stressed conditions. The rationale for the use of the transgenic lines was to provide reliable increases in oxalate oxidase activity and apoplastic H_2O_2 in the root growth zone under both well-watered and water-stressed conditions. Transgene expression was under the control of the rice actin promoter, which is considered to have a constitutive expression pattern (McElroy et al., 1991). Nevertheless, marked spatial variability in the pattern of oxalate oxidase activity was observed in the transgenic as well as the wild-type roots.

In water-stressed wild-type roots (both the CK44 and B73 backgrounds), oxalate oxidase activity increased substantially only in the apical few mm of the growth zone (**Figures 1A,B**, **2**), in agreement with previous findings in inbred line FR697

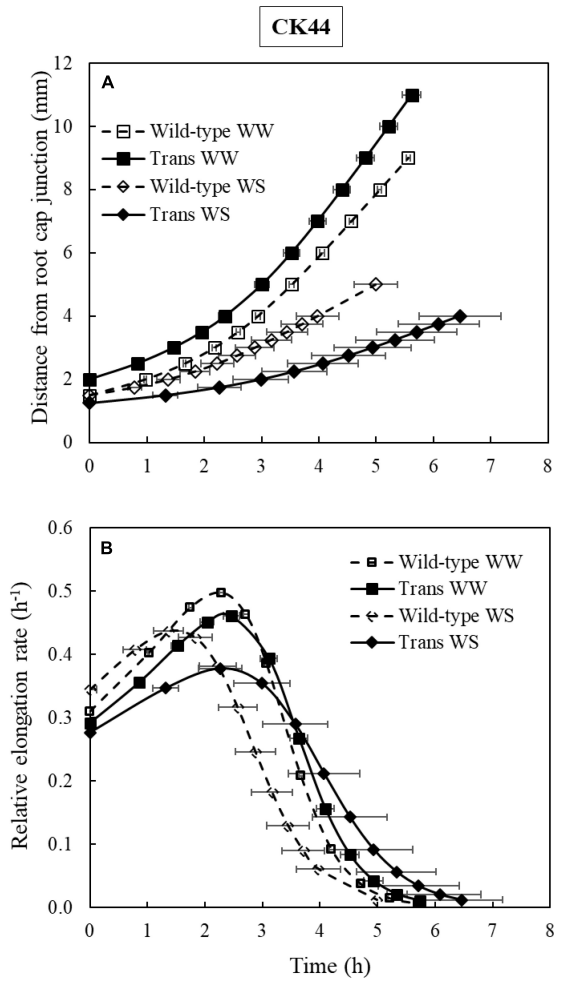

FIGURE 6 | Growth trajectories **(A)** and temporal relative elongation rate profiles **(B)** of the primary root of CK44 *oxalate oxidase* transgenic (Trans) and wild-type lines growing under well-watered (WW) or water-stressed (WS; –1.6 MPa) conditions. Growth trajectories were used to determine the times required for cells to move from the distal end of the meristem to more basal locations, and were obtained by plotting position versus the integrated local displacement time. The relative elongation rate corresponding to a particular position (**Figures 5E,F**) was then plotted against the integrated displacement time to obtain the temporal relative elongation rate profiles **(B)**. The total residence times of cells within the growth zone were not significantly different between the transgenic and wild-type lines in either well-watered or water-stressed comparisons (*t*-test; $P > 0.1$).

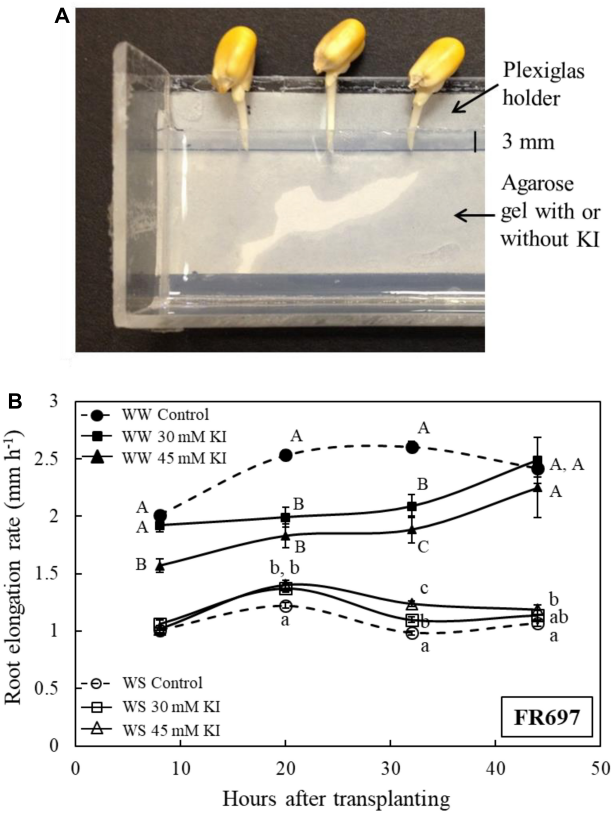

FIGURE 7 | (A) Part of the Plexiglas holder, viewed from above, which was used to pretreat the apical 0–3 mm region of the primary root of line FR697 with the H_2O_2 scavenger KI. The holder contained a 5-mm thick layer of 1% agarose gel, with or without KI, into which the root tip was inserted. Because the roots elongated during the pretreatment, the kernels were moved away from the gel every 2 h such that only the apical 3 mm of the roots were embedded in the gel. After 6 h, the seedlings were transplanted to well-watered or water-stressed conditions. **(B)** Elongation rates of control and KI-pretreated (30 or 45 mM) primary roots after transplanting to well-watered (WW) or water-stressed (WS; –1.6 MPa) conditions. The elongation rates are plotted at the midpoint between marking intervals, which were at 0, 16, 24, 40, and 48 h after transplanting. Data are means ± SE of three independent experiments (n = 15–40 seedlings per treatment in each experiment). Different letters denote significant differences between treatments at specific times within each condition (*t*-test; $P < 0.05$).

(Voothuluru and Sharp, 2013). This region encompassed the meristem, which was shown to extend approximately 2 mm from the apex in well-watered maize primary roots, and to be shortened under water stress (Sacks et al., 1997). The water-stressed roots also showed a pronounced increase in oxalate oxidase activity from approximately 9 to 12 mm from the root apex; however, this region was beyond the growth zone (**Figure 5**), and thus the increase in activity may be involved in cell wall maturation rather than growth regulatory processes (Caliskan and Cuming, 1998; Fry, 2004). Interestingly, the minimal activity in the basal region of the growth zone in water-stressed roots occurred despite increases in gene expression (Spollen et al., 2008) and protein abundance (Zhu et al., 2007) of oxalate oxidases. Further, the disparity in protein abundance and activity cannot be explained by spatially variable apoplastic pH (Fan and Neumann, 2004) or substrate availability, since the assay conditions controlled for these factors (Voothuluru and Sharp, 2013).

In well-watered transgenic roots, pronounced oxalate oxidase activity was observed only in the apical 4 mm (CK44) or 6 mm (B73) regions. Transgene expression was threefold greater in the apical compared to the basal region (**Table 1**), which could at least partly explain the activity profile. In the water-stressed transgenic roots, in contrast, there was a substantial

TABLE 4 | Elongation rate, final cell length, and cell production rate of control and KI-treated primary roots in line FR697 at 36 h after transplanting to well-watered or water-stressed (−1.6 MPa) conditions.

	FR697, well-watered			FR697, water-stressed		
	Control	30 mM KI	Change compared to control (%)	Control	45 mM KI	Change compared to control (%)
Root elongation rate (mm h^{-1})	2.57 ± 0.02	2.07 ± 0.05**	−20	1.00 ± 0.00	1.38 ± 0.00**	38
Final cell length (μm)	190 ± 3	182 ± 8	−4	142 ± 4	164 ± 6**	15
Cell production rate (cells h^{-1})	13.6 ± 0.3	11.5 ± 0.5**	−16	7.1 ± 0.2	8.5 ± 0.4*	20

*Elongation rates were calculated for the preceding 14 h (well-watered) or 8 h (water-stressed) periods. Values are means ± SE of five to six roots. Asterisks denote significant differences between the control and KI-treated roots (t-test; *P < 0.05; **P < 0.01). Roots were pretreated with 30 mM and 45 mM KI for well-watered and water-stressed roots, respectively, since these pretreatments resulted in almost steady root elongation during the preceding 20 h (**Figure 7B**).*

increase in oxalate oxidase activity throughout most of the apical 12 mm, which appeared to reflect more than an additive effect of the normal increase in activity observed in wild-type roots plus the activity attributable to the transgene observed in well-watered transgenic roots (**Figure 1A,B**). Moreover, the increased activity occurred despite the fact that transgene expression was substantially reduced in both the apical and basal regions of water-stressed compared with well-watered roots (**Table 1**). The latter result suggests that the actin promoter may in fact respond to water deficit conditions; however, the factors underlying the spatial pattern and stress-responsiveness of transgene expression are beyond the scope of this study.

Collectively, these results suggest that the spatial patterns of oxalate oxidase activity in both well-watered and water-stressed transgenic roots, as well as in the water-stressed wild-type, likely involved unknown processes of post-translational regulation or metabolic control of enzyme activity. Despite this complexity, the apical region of the growth zone of both well-watered and water-stressed transgenic roots exhibited substantially increased apoplastic H_2O_2 compared with the respective wild-type roots (**Figure 1C**).

Apoplastic H_2O_2 Modulates Root Elongation via Effects on Cell Production and Spatial Profiles of Cell Elongation

The oxalate oxidase transgenic lines showed an increase in root elongation under well-watered conditions and a decrease in root elongation under water-stressed conditions (**Figures 3**, **4**). Kinematic analyses indicated that these differential effects on root elongation involved substantial effects on both cell production rate and the spatial profiles of cell elongation. Cell production rate was positively and negatively modulated under well-watered and water-stressed conditions, respectively, in close proportion to the increases and decreases in root elongation rate (**Tables 2**, **3**). Conversely, scavenging of apoplastic H_2O_2 in the apical region of the growth zone by pretreatment with KI resulted in a decrease of elongation in well-watered roots and an increase of elongation in water-stressed roots (**Figure 7B**), and these responses were also accompanied by substantial effects on cell production rate (**Table 4**). Effects on overall cell elongation, as reflected in final cell lengths, were relatively minor in the transgenic lines and in the scavenger-treated roots under both well-watered and water-stressed conditions (**Tables 2–4**).

In contrast to the minor effects on overall cell elongation, however, spatial profiles of relative elongation rate were markedly affected in the transgenic lines under both well-watered and water-stressed conditions. For example, in well-watered roots, the relative elongation rate at 6 mm from the apex, in the basal region of deceleration, was threefold higher in the transgenic compared to the wild-type, whereas local elongation rates were decreased in the transgenic line in the apical region of acceleration (**Figure 5E**). Conversely, in water-stressed roots, the relative elongation rate at 3 mm from the apex, in the decelerating region of the shortened growth zone in this condition, was decreased by 63% in the transgenic compared to the wild-type (**Figure 5F**).

The causal interrelationship, if any, between the effects on cell production rate and cell elongation profiles is not known. One perspective to interpret these results is provided by spatial models of the regulation of cell elongation, wherein local elongation rates are determined by various positional control mechanisms (for example, gradients of hormones, certain metabolites, etc.) that may or may not be coordinated with effects on cell production (Green, 1976; Silk, 1992; Gonzalez et al., 2012; Yang et al., 2017). In this scenario, the modifications of apoplastic H_2O_2 in the transgenic lines would be interpreted as exerting major effects on local controls of cell elongation, with inhibitory and promotive effects occurring in different regions of the growth zone such that final cell lengths were not markedly altered. For example, local control of cell elongation could have involved effects of apoplastic H_2O_2 on cell wall loosening and tightening processes, and such effects could be region specific (Fry, 1998; Córdoba-Pedregosa et al., 2003; Foreman et al., 2003; Tyburski et al., 2010).

An alternative explanation is provided by the cellular model of organ growth regulation, wherein growth is determined by the number of cells produced in the meristem, each with a pre-specified capacity for elongation. In this view, as discussed by Beemster and Baskin (1998), changes in cell production rate influence the length of the growth zone by determining the number of cells that are undergoing elongation. From this perspective, the substantial effects on local relative elongation rates in the transgenic lines under both the well-watered and water-stressed conditions would be a consequence of the changes in cell production rate, rather than positionally determined controls of cell elongation processes. In other words,

the increased number of cells produced from the meristem in well-watered transgenic roots need more space to expand and, consequentially, result in proportional lengthening of the growth zone, as was observed. Conversely, in the water-stressed transgenic roots, the decreased number of cells produced from the meristem would need less space to expand, resulting in a proportionally shortened growth zone, as also observed.

Spatial elongation patterns can also reflect changes in the temporal regulation of cell elongation. For example, in the well-watered and water-stressed transgenic roots, the cells could have been elongating for an increased or decreased duration of time, respectively, compared with the wild-type controls. However, the constancy of the residence time for cells to move from the end of the meristem to the distal end of the growth zone in the transgenic and wild-type lines under both well-watered and water-stressed conditions (approximately 6 h in all cases; **Figure 6**) indicates that temporal aspects of cell elongation control were not altered, regardless of changes in growth zone length. These results are similar to the findings of Sharp et al. (1988), who reported that the duration of cell elongation in the growth zone of the maize primary root was not impacted by varying levels of water deficit, despite the progressively smaller distances over which elongation occurred as the severity of water stress increased.

Our results cannot readily distinguish between the alternative possibilities of spatial versus cellular control as the basis of the changes in relative elongation rate profiles in the transgenic lines. Moreover, these two processes are not mutually exclusive and could occur concomitantly. However, the closely proportional changes in growth zone length to the changes in cell production rate, as well as the minor changes in overall cell elongation, are consistent with the possibility that regulation of cell production was the primary determinant of the effects of apoplastic H_2O_2 manipulation on root elongation under both well-watered and water-stressed conditions. Clearly, given that the overall rate of root elongation is determined by the product of cell production rate and final cell length, the changes in cell production appeared to play a key role in the effects on root elongation. This interpretation is similar to the findings of several previous studies in which organ growth rates were modified by changes in cell production, including those by Foard and Haber (1961), who demonstrated that reduced cell production by γ-ray irradiation resulted in reduced tissue elongation, by Beemster and Baskin (1998), who reported that developmental acceleration of *Arabidopsis* roots could be explained by increasing rates of cell production, and by Doerner et al. (1996), who demonstrated that overexpression of a cyclin gene in root meristems resulted in increased cell production and root elongation.

How Does Apoplastic H_2O_2 Differentially Modulate Cell Production Under Well-Watered and Water-Stressed Conditions?

Maintenance of cellular redox balance, by regulating the production of ROS or antioxidant metabolites, has been shown to be important for cell cycle progression (Kerk and Feldman, 1995; Menon and Goswami, 2007; Diaz Vivancos et al., 2010a), and there is considerable evidence in both plant and animal systems that changes in cellular ROS levels can positively or negatively impact cell production (Tsukagoshi, 2016). For example, several studies have shown that low levels of exogenous ROS can lead to an increase in cell production, whereas scavenging endogenous ROS resulted in inhibition of cell production (Laurent et al., 2005; Diaz Vivancos et al., 2010b). ROS were also reported to oxidize key proteins involved in the initiation and maintenance of cell division (Menon and Goswami, 2007; Burhans and Heintz, 2009; Diaz Vivancos et al., 2010a). Conversely, there is evidence that changes in ROS metabolism can lead to inhibition of cell production. For example, *Arabidopsis* mutants deficient in the biosynthesis and reduction of glutathione were shown to exhibit cell cycle arrest and defects in meristem maintenance in roots and shoots (Vernoux et al., 2000; Reichheld et al., 2007; Yu et al., 2013). In addition, an indiscriminate increase in ROS levels, as may occur in response to prolonged or severe stress conditions, could lead to DNA damage and uncontrolled inhibition of cell production (Diaz Vivancos et al., 2010b). Interestingly, some studies indicate that the spatial distribution and balance of H_2O_2 and superoxide are important for regulating the transition from cell proliferation to elongation and differentiation in roots (Dunand et al., 2007; Tsukagoshi et al., 2010). Similar to the apical localization of water-stress-induced apoplastic H_2O_2 (Voothuluru and Sharp, 2013), apoplastic superoxide was also shown to occur preferentially in the apical region of the growth zone in both well-watered and osmotically stressed maize primary roots (Liszkay et al., 2004; Bustos et al., 2008). Accordingly, it is possible that differences in ROS balance may have played a role in the differential effects of increased H_2O_2 on cell production observed in well-watered and water-stressed roots in the present study.

Interestingly, together with two putative oxalate oxidases, a superoxide dismutase and an ascorbate peroxidase were also shown to increase in abundance specifically in the apical region of the growth zone of water-stressed maize primary roots in a cell wall proteomic study by Zhu et al. (2007). Therefore, superoxide and ascorbate could also be potential sources of the increase in H_2O_2 in the apical region. Superoxide may also interact with peroxidases to convert H_2O_2 to hydroxyl radicals, and can also reduce Fe^{3+} to Fe^{2+} to sustain the Fenton reaction, thereby increasing hydroxyl radical generation (Liszkay et al., 2004; Dunand et al., 2007). Plasma membrane NADPH oxidase is an important source of apoplastic superoxide (Foreman et al., 2003), and up-regulation of NADPH oxidase by both water stress and ABA treatment was reported in maize leaves (Jiang and Zhang, 2002). However, four NADPH oxidase-related sequences that were included in a transcriptomic analysis were not differentially expressed in the growth zone of water-stressed maize primary roots (Spollen et al., 2008). Collectively, these findings indicate that various processes may be involved in the modulation of apoplastic ROS in the growth zone of water-stressed roots.

However, it is not apparent from these previous studies how the increased levels of apoplastic H_2O_2 in the *oxalate oxidase* transgenic lines under both well-watered and water-stressed conditions may have modulated cell cycle processes

occurring within the nucleus. Since there were no significant increases in cytosolic ROS in the apical region of the growth zone in the transgenic compared with the wild-type line under either condition (**Supplementary Figure S2**), it is unlikely that H_2O_2 itself was traversing the plasma membrane at significantly increased rates. Interestingly, an increase in apoplastic ROS production and perception has been implicated in cellular signaling and the regulation of nuclear gene transcription (Padmanabhan and Dinesh-Kumar, 2010; Foyer and Noctor, 2011; Shapiguzov et al., 2012; Waszczak et al., 2018). In particular, Munné-Bosch et al. (2013) proposed the involvement of a trans-plasma membrane ascorbate-based shuttle system in ROS signaling from the apoplast to the cytosol, and suggested its involvement in plant responses to multiple stressors. It is notable that several components involved in this pathway have been identified in the apical region of the growth zone of maize primary roots growing under both well-watered and water-stressed conditions. For example, Zhu et al. (2007) provided evidence for apoplastic accumulation of ascorbate peroxidase, which oxidizes ascorbate in the presence of H_2O_2, in the apical region of water-stressed roots. Also, plasma membrane proteomic analyses showed an increased abundance of ascorbate-dependent cytochrome b_{561} protein in the apical region of well-watered (Zhang et al., 2013) and water-stressed roots (Voothuluru et al., 2016). This protein can be oxidized by monodehydroascorbate and reduced by ascorbate, and has been implicated in trans-plasma membrane electron transport (Preger et al., 2009). There is also a significant increase in glutathione levels in the apical region of the growth zone of water-stressed roots (Kang, 2019). Whether these proteins and metabolites are involved in apoplastic ROS-mediated signaling and regulation of cell production in well-watered and water-stressed maize primary roots remains to be investigated.

Is the Decrease in Cell Production in Water-Stressed Roots of Adaptive Advantage?

As noted in the Introduction, previous studies of water-stressed maize primary roots have shown that although local elongation rates were maintained in the apical region of the growth zone (Sharp et al., 1988; Liang et al., 1997), rates of cell production were decreased substantially (Fraser et al., 1990; Saab et al., 1992; Sacks et al., 1997). In the present study, similarly, local elongation rates were unaffected by water stress in the apical 2 mm of the growth zone in the CK44 wild-type line (compare **Figures 5E** and **F**), whereas cell production rate was substantially decreased (**Table 2**). These findings illustrate that the responses of cell elongation and proliferation to water stress are not coordinately regulated, and it has been speculated that decreased rates of cell production in roots (Sacks et al., 1997) and leaves (Skirycz et al., 2011; Claeys et al., 2012) may be of adaptive advantage for plants growing under conditions of limited water availability. As emphasized by Sacks et al. (1997), decreased cell production combined with maintenance of local elongation results in a tendency toward longer cells in the apical region of water-stressed compared with well-watered roots. In the present study, this effect was clearly apparent in the CK44 transgenic line; for example, at 2 mm from the apex, cell lengths were approximately 60 and 30 μm in the water-stressed and well-watered roots, respectively (**Figures 5A,B**). This response may facilitate symplastic translocation from the phloem to the meristematic cells because of the smaller number of plasmodesmata that have to be traversed (Bret-Harte and Silk, 1994; Sacks et al., 1997). In addition, decreased cell production contributes to the shortening of the growth zone toward the apex that occurs in water-stressed roots (Sharp et al., 1988), since fewer cells require less space for expansion. This effect is evidenced by the further truncation of the growth zone observed in the CK44 transgenic line compared with the wild-type (compare **Figures 5E** and **F**). This response could also facilitate solute and water transport to the apical region (Wiegers et al., 2009), thereby helping to promote osmotic adjustment and the maintenance of cell expansion (Voetberg and Sharp, 1991; Verslues and Sharp, 1999).

Intriguingly, however, the results of the present study do not provide evidence in support of these hypotheses. In particular, if the decrease in cell production in water-stressed roots provides an advantage for root growth maintenance, then the partial restoration of cell production that occurred in the H_2O_2 scavenger experiments might be expected to have resulted in inhibition of root elongation. This was not the case; instead, root elongation increased in association with the increase in cell production (**Table 4**). Accordingly, the results indicate that the normal decrease in cell production under water stress results in root elongation being more inhibited than would otherwise be the case, and thus the adaptive significance of the response, if any, is not clear.

CONCLUSION

The combined results from the characterization of *oxalate oxidase* transgenic lines and H_2O_2 scavenger experiments present compelling evidence that apoplastic H_2O_2 positively and negatively modified primary root elongation under well-watered and water-stressed conditions, respectively. The effects of increased H_2O_2 on root elongation were attributable to modulation of both cell production rate and changes in the spatial profiles of cell elongation, although only minor changes in overall cell elongation occurred. The results are consistent with the possibility that the effects on cell production were the primary determinant of the effects on root elongation under both well-watered and water-stressed conditions. Future studies will explore the intra-cellular signaling mechanisms involved in apoplastic H_2O_2-mediated differential regulation of cell production under well-watered and water-stressed conditions.

DATA AVAILABILITY STATEMENT

All datasets generated for this study are included in the article/**Supplementary Material**.

AUTHOR CONTRIBUTIONS

PV, PM, JZ, and RS conceived and designed the experiments. JS provided the transgenic lines. PV, JZ, and MY characterized root growth responses and oxalate oxidase activity staining. I-JC and JZ conducted apoplastic ROS assays. PV conducted kinematic analyses and cytosolic ROS assays. PV, I-JC, and MO conducted transgene expression studies. PM and PV conducted H_2O_2 scavenger experiments. PV, MO, and RS drafted the manuscript with revisions from other authors.

FUNDING

This work was supported by the Division of Plant Sciences and Food for the 21st Century Program, University of Missouri, and by a National Science Foundation Plant Genome Research Program grant (IOS-1444448) to RS and MO.

ACKNOWLEDGMENTS

We thank Drs. Wendy Silk (University of California-Davis), Yajun Wu (South Dakota State University), and Ron Mittler (University of Missouri) for helpful consultation and insight. Confocal and bright field microscopy were conducted at the University of Missouri Molecular Cytology Core Facility. Mention of a trademark or proprietary product does not constitute a guarantee or warranty of the product by the United States Department of Agriculture, and does not imply its approval to the exclusion of other products that may also be suitable.

SUPPLEMENTARY MATERIAL

The Supplementary Material for this article can be found online at: https://www.frontiersin.org/articles/10.3389/fpls.2020.00392/full#supplementary-material

REFERENCES

Beemster, G. T., and Baskin, T. I. (1998). Analysis of cell division and elongation underlying the developmental acceleration of root growth in *Arabidopsis thaliana*. *Plant Physiol.* 116, 1515–1526.

Boyer, J. S. (1982). Plant productivity and environment. *Science* 218, 443–448.

Boyer, J. S., Byrne, P., Cassman, K. G., Cooper, M., Delmer, D., Greene, T., et al. (2013). The US drought of 2012 in perspective: a call to action. *Glob. Food Sec.* 2, 139–143.

Boyer, J. S., and Knipling, E. B. (1965). Isopiestic technique for measuring leaf water potentials with a thermocouple psychrometer. *Proc. Natl. Acad. Sci. U.S.A.* 54, 1044–1051.

Bret-Harte, M. S., and Silk, W. K. (1994). Nonvascular, symplasmic diffusion of sucrose cannot satisfy the carbon demands of growth in the primary root tip of *Zea mays* L. *Plant Physiol.* 105, 19–33.

Burhans, W. C., and Heintz, N. H. (2009). The cell cycle is a redox cycle: linking phase-specific targets to cell fate. *Free Radic. Biol. Med.* 47, 1282–1293.

Bustos, D., Lascano, R., Villasuso, A. L., Machado, E., Senn, M. E., Córdoba, A. et al. (2008). Reductions in maize root-tip elongation by salt and osmotic stress do not correlate with apoplastic O_2levels. *Ann. Bot.* 102, 551–559.

Caliskan, M., and Cuming, A. C. (1998). Spatial specificity of H_2O_2-generating oxalate oxidase gene expression during wheat embryo germination. *Plant J.* 15, 165–171.

Claeys, H., Skirycz, A., Maleux, K., and Inzé, D. (2012). DELLA signaling mediates stress-induced cell differentiation in *Arabidopsis* leaves through modulation of anaphase-promoting complex/cyclosome activity. *Plant Physiol.* 159, 739–747.

Córdoba-Pedregosa, M. C., Córdoba, F., Villalba, J. M., and González-Reyes, J. A. (2003). Zonal changes in ascorbate and hydrogen peroxide contents, peroxidase, and ascorbate-related enzyme activities in onion roots. *Plant Physiol.* 131, 697–706.

Davidson, R. M., Reeves, P. A., Manosalva, P. M., and Leach, J. E. (2009). Germins: a diverse protein family important for crop improvement. *Plant Sci.* 117, 499–510.

Diaz Vivancos, P., Dong, Y., Ziegler, K., Markovic, J., Pallardó, F. V., Pellny, T. K., et al. (2010a). Recruitment of glutathione into the nucleus during cell proliferation adjusts whole-cell redox homeostasis in *Arabidopsis thaliana* and lowers the oxidative defence shield. *Plant J.* 64, 825–838.

Diaz Vivancos, P., Wolff, T., Markovic, J., Pallardó, F. V., and Foyer, C. H. (2010b). A nuclear glutathione cycle within the cell cycle. *Biochem. J.* 431, 169–178.

Doerner, P., Jorgensen, J., You, R., Steppuhn, J., and Lamb, C. (1996). Control of root growth and development by cyclin expression. *Nature* 380, 520–523.

Dracup, M., Gibbs, J., and Greenway, H. (1986). Melibiose, a suitable, non-permeating osmoticum for suspension-cultured tobacco cells. *J. Exp. Bot.* 37, 1079–1089.

Dumas, B., Freyssinet, G., and Pallett, K. E. (1995). Tissue-specific expression of germin-like oxalate oxidase during development and fungal infection of barley seedlings. *Plant Physiol.* 107, 1091–1096.

Dumlao, M. R., Ramananarivo, S., Goyal, V., DeJong, J. T., Waller, J., and Silk, W. K. (2015). The role of root development of *Avena fatua* in conferring soil strength. *Am. J. Bot.* 102, 1050–1060.

Dunand, C., Crèvecoeur, M., and Penel, C. (2007). Distribution of superoxide and hydrogen peroxide in *Arabidopsis* root and their influence on root development: possible interaction with peroxidases. *New Phytol.* 174, 332–341.

Encina, A., and Fry, S. C. (2005). Oxidative coupling of a feruloyl-arabinoxylan trisaccharide (FAXX) in the walls of living maize cells requires endogenous hydrogen peroxide and is controlled by a low-M_r apoplastic inhibitor. *Planta* 223, 77–89.

Erickson, R. O. (1961). Probability of division of cells in the epidermis of the *Phleum* root. *Am. J. Bot.* 48, 268–274.

Erickson, R. O., and Silk, W. K. (1980). The kinematics of plant growth. *Sci. Am.* 242, 134–151.

Fan, L., and Neumann, P. M. (2004). The spatially variable inhibition by water deficit of maize root growth correlates with altered profiles of proton flux and cell wall pH. *Plant Physiol.* 135, 2291–2300.

Foard, D. E., and Haber, A. H. (1961). Anatomic studies of gamma radiated wheat growing without cell division. *Am. J. Bot.* 48, 438–446.

Foreman, J., Demidchik, V., Bothwell, J. H., Mylona, P., Miedema, H., Torres, M. A., et al. (2003). Reactive oxygen species produced by NADPH oxidase regulate plant cell growth. *Nature* 422, 442–446.

Foyer, C. H., and Noctor, G. (2011). Ascorbate and glutathione: the heart of the redox hub. *Plant Physiol.* 155, 2–18.

Fraser, T. E., Silk, W. K., and Rost, T. L. (1990). Effects of low water potential on cortical cell length in growing regions of maize roots. *Plant Physiol.* 93, 648–651.

Fry, S. C. (1998). Oxidative scission of plant cell wall polysaccharides by ascorbate-induced hydroxyl radicals. *Biochem. J.* 332, 507–515.

Fry, S. C. (2004). Primary cell wall metabolism: tracking the careers of wall polymers in living plant cells. *New Phytol.* 161, 641–675.

Gonzalez, N., Vanhaeren, H., and Inzé, D. (2012). Leaf size control: complex coordination of cell division and expansion. *Trends Plant Sci.* 17, 332–340.

Green, P. B. (1976). Growth and cell pattern formation on an axis: critique of concepts, terminology and modes of study. *Bot. Gaz.* 137, 187–202.

Green, M. A., and Fry, S. C. (2005). Vitamin C degradation in plant cells via enzymatic hydrolysis of 4-O-oxalyl-L-threonate. *Nature* 433, 83–87.

Jiang, M., and Zhang, J. (2002). Involvement of plasma-membrane NADPH oxidase in abscisic acid- and water-stress-induced antioxidant defense in leaves of maize seedlings. *Planta* 215, 1022–1030.

Kang, J. (2019). *Cotton and Maize Primary Root Growth Responses to Water Deficit: Comparative Physiological and Metabolic Analysis*. Ph.D. dissertation, University of Missouri, Columbia, MO.

Kerk, N. M., and Feldman, L. J. (1995). A biochemical model for the initiation and maintenance of the quiescent center: implications for organization of root meristems. *Development* 121, 2825–2833.

Kirkegaard, J. A., Lilley, J. M., Howe, G. N., and Graham, J. M. (2007). Impact of subsoil water use on wheat yield. *Aust. J. Agric. Res.* 58, 303–315.

Laurent, A., Nicco, C., Chereau, C., Goulvestre, C., Alexandre, J., Alves, A., et al. (2005). Controlling tumor growth by modulating endogenous production of reactive oxygen species. *Cancer Res.* 65, 948–956.

Liang, B. M., Sharp, R. E., and Baskin, T. I. (1997). Regulation of growth anisotropy in well-watered and water-stressed maize roots. I. Spatial distribution of longitudinal, radial and tangential expansion rates. *Plant Physiol.* 115, 101–111.

Liszkay, A., van der Zalm, E., and Schopfer, P. (2004). Production of reactive oxygen intermediates ($O_2^{\bullet -}$, H_2O_2, and $^{\bullet}OH$) by maize roots and their role in wall loosening and elongation growth. *Plant Physiol.* 136, 3114–3123.

Mao, J., Burt, A. J., Ramputh, A. I., Simmonds, J., Cass, L., Hubbard, K., et al. (2007). Diverted secondary metabolism and improved resistance to European corn borer (*Ostrinia nubilalis*) in maize (*Zea mays* L.) transformed with wheat oxalate oxidase. *J. Agric. Food Chem.* 55, 2582–2589.

McElroy, D., Blowers, A. D., Jenes, B., and Wu, R. (1991). Construction of expression vectors based on the rice actin 1 (Act1) 5 region for use in monocot transformation. *Mol. Gen. Genet.* 231, 150–160.

Menon, S. G., and Goswami, P. C. (2007). A redox cycle within the cell cycle: ring in the old with the new. *Oncogene* 26, 1101–1109.

Muller, B., Stosser, M., and Tardieu, F. (1998). Spatial distributions of tissue expansion and cell division rates are related to irradiance and to sugar content in the growing zone of maize roots. *Plant Cell Environ.* 21, 149–158.

Müller, K., Linkeis, A., Vreeburg, R. A. M., Fry, S. C., Krieger-Liszkay, A., and Luebner-Metzger, G. (2009). In vivo cell wall loosening by hydroxyl radicals during cress seed germination and elongation growth. *Plant Physiol.* 150, 1855–1865.

Munné-Bosch, S., Queval, G., and Foyer, C. H. (2013). The impact of global change factors on redox signaling underpinning stress tolerance. *Plant Physiol.* 161, 5–19.

Nose, M., Bernards, M. A., Furlan, M., Zajicek, J., Eberhardt, T. L., and Lewis, N. G. (1995). Towards the specification of consecutive steps in macromolecular lignin assembly. *Phytochemistry* 39, 71–79.

Ober, E. S., and Sharp, R. E. (2007). "Regulation of root growth responses to water deficit," in *Advances in Molecular Breeding toward Drought and Salt Tolerant Crops*, eds M. A. Jenks, P. M. Hasegawa, and S. M. Jain (Dordrecht: Springer), 33–53.

Ober, E. S., and Sharp, R. E. (2013). "Maintaining root growth in drying soil: a review of progress and gaps in understanding," in *Plant Roots: The Hidden Half*, 4th Edn, eds A. Eshel, and T. Beekman (Boca Raton, FL: CRC Press), 1–11.

Padmanabhan, M. S., and Dinesh-Kumar, S. P. (2010). All hands on deck – the role of chloroplasts, endoplasmic reticulum and the nucleus in driving plant innate immunity. *Mol. Plant Microbe Interact.* 23, 1368–1380.

Preger, V., Tango, N., Marchand, C., Lemaire, S. D., Carbonera, D., Valentin, M. D., et al. (2009). Auxin-responsive genes AIR12 code for a new family of plasma membrane b-type cytochromes specific to flowering plants. *Plant Physiol.* 150, 606–620.

Ramputh, A. I., Arnason, J. T., Cass, L., and Simmonds, J. A. (2002). Reduced herbivory of the European corn borer (*Ostrinia nubilalis*) on corn transformed with germin, a wheat oxalate oxidase. *Plant Sci.* 162, 431–440.

Reichheld, J. P., Khafif, M., Riondet, C., Droux, M., Bonnard, G., and Meyer, Y. (2007). Inactivation of thioredoxin reductases reveals a complex interplay between thioredoxin and glutathione pathways in *Arabidopsis* development. *Plant Cell* 19, 1851–1865.

Rodriguez, A. A., Grunberg, K. A., and Taleisnik, E. L. (2002). Reactive oxygen species in the elongation zone of maize leaves are necessary for leaf extension. *Plant Physiol.* 129, 1627–1632.

Saab, I. N., Sharp, R. E., and Pritchard, J. (1992). Effect of inhibition of abscisic acid accumulation on the spatial distribution of elongation in the primary root and mesocotyl of maize at low water potentials. *Plant Physiol.* 99, 26–33.

Saab, I. N., Sharp, R. E., Pritchard, J., and Voetberg, G. S. (1990). Increased endogenous abscisic acid maintains primary root growth and inhibits shoot growth of maize seedlings at low water potentials. *Plant Physiol.* 93, 1329–1336.

Sacks, M. M., Silk, W. K., and Burman, P. (1997). Effects of water stress on cortical cell division within the apical meristem of primary roots of maize. *Plant Physiol.* 114, 519–527.

Schopfer, P. (2001). Hydroxyl radical-induced cell-wall loosening *in vitro* and *in vivo*: implications for the control of elongation growth. *Plant J.* 28, 679–688.

Shapiguzov, A., Vainonen, J. P., Wrzaczek, M., and Kangasjarvi, Y. (2012). ROS-talk – how the apoplast, the chloroplast, and the nucleus get the message through. *Front. Plant Sci.* 3:292. doi: 10.3389/fpls.2012.00292

Sharp, R. E., and Davies, W. J. (1979). Solute regulation and growth by roots and shoots of water-stressed maize plants. *Planta* 146, 319–326.

Sharp, R. E., and Davies, W. J. (1985). Root growth and water uptake by maize plants in drying soil. *J. Exp. Bot.* 36, 1441–1456.

Sharp, R. E., and Davies, W. J. (1989). "Regulation of growth and development of plants growing with a restricted supply of water," in *Plants Under Stress*, eds H. G Jones, T. L. Flowers, and M. B. Jones (Cambridge: Cambridge University. Press), 71–93.

Sharp, R. E., Poroyko, V., Hejlek, L. G., Spollen, W. G., Springer, G. K., Bohnert, H. J., et al. (2004). Root growth maintenance during water deficits: physiology to functional genomics. *J. Exp. Bot.* 55, 2343–2351.

Sharp, R. E., Silk, W. K., and Hsiao, T. C. (1988). Growth of the maize primary root at low water potentials. I. Spatial distribution of expansive growth. *Plant Physiol.* 87, 50–57.

Silk, W. K. (1992). Steady form from changing cells. *Int. J. Plant Sci.* 153, S49–S58.

Silk, W. K., Lord, E. M., and Eckard, K. J. (1989). Growth patterns inferred from anatomical records. *Plant Physiol.* 90, 708–713.

Skirycz, A., Claeys, H., De Bodt, S., Oikawa, A., Shinoda, S., Andriankaja, M., et al. (2011). Pause-and-stop; the effects of osmotic stress on cell proliferation during early leaf development in *Arabidopsis* and a role for ethylene signaling in cell cycle arrest. *Plant Cell* 23, 1876–1888.

Spollen, W. G., and Sharp, R. E. (1991). Spatial distribution of turgor and root growth at low water potentials. *Plant Physiol.* 96, 438–443.

Spollen, W. G., LeNoble, M. E., Samuels, T. D., Bernstein, N., and Sharp, R. E. (2000). ABA accumulation maintains primary root elongation at low water potentials by restricting ethylene production. *Plant Physiol.* 122, 967–976.

Spollen, W. G., Sharp, R. E., Wu, Y., and Saab, I. N. (1993). "Regulation of cell expansion in roots and shoots at low water potentials," in *Water Deficits: Plant Responses from Cell to Community*, eds J. A. C. Smith, and H. Griffiths (Oxford: BIOS Scientific Publishers), 37–52.

Spollen, W. G., Tao, W., Valliyodan, B., Chen, K., Hejlek, L. G., Kim, J. J., et al. (2008). Spatial distribution of transcript changes in the maize primary root elongation zone at low water potential. *BMC Plant Biol.* 8:32. doi: 10.1186/1471-2229-8-32

Sponchiado, B. N., White, J. W., Castillo, J. A., and Jones, P. G. (1989). Root growth of four common bean cultivars in relation to drought tolerance in environments with contrasting soil types. *Exp. Agricult.* 25, 249–257.

Tardieu, F., Simonneau, T., and Muller, T. (2018). The physiological basis of drought tolerance in crop plants: a scenario-dependent probabilistic approach. *Ann. Rev. Plant Biol.* 69, 733–759.

Tsukagoshi, H. (2016). Control of root growth and development by reactive oxygen species. *Curr. Opin. Plant Biol.* 29, 57–63.

Tsukagoshi, H., Busch, W., and Benfey, P. N. (2010). Transcriptional regulation of ROS controls transition from proliferation to differentiation in the root. *Cell* 143, 606–616.

Tyburski, J., Dunajska, K., and Tretyn, A. (2010). A role for redox factors in shaping root architecture under phosphorus deficiency. *Plant Signal. Behav.* 5, 64–66.

Vernoux, T., Wilson, R. C., Seeley, K. A., Reichheld, J.-P., Muroy, S., Brown, S., et al. (2000). The ROOT MERISTEMLESS1/CADMIUM SENSITIVE2 gene defines a glutathione-dependent pathway involved in initiation and maintenance of cell division during postembryonic root development. *Plant Cell* 12, 97–109.

Verslues, P. E., and Sharp, R. E. (1999). Proline accumulation in maize (*Zea mays* L.) primary roots at low water potentials. II. Metabolic source of increased proline deposition in the elongation zone. *Plant Physiol.* 119, 1349–1360.

Voetberg, G. S., and Sharp, R. E. (1991). Growth of the maize primary root at low water potentials. III. Role of increased proline deposition in osmotic adjustment. *Plant Physiol.* 96, 1125–1130.

Voothuluru, P., and Sharp, R. E. (2013). Apoplastic hydrogen peroxide in the growth zone of the maize primary root under water stress. I. Increased levels are specific to the apical region of growth maintenance. *J. Exp. Bot.* 64, 1223–1233.

Voothuluru, P., Anderson, J. C., Sharp, R. E., and Peck, S. C. (2016). Plasma membrane proteomics in the maize primary root growth zone: novel insights into root growth adaptation to water stress. *Plant Cell Environ.* 39, 2043–2054.

Walter, A., Silk, W. K., and Schurr, U. (2009). Environmental effects on spatial and temporal patterns of leaf and root growth. *Ann. Rev. Plant Biol.* 60, 279–304.

Waszczak, C., Carmody, M., and Kangasjarvi, J. (2018). Reactive oxygen species in plant signaling. *Ann. Rev. Plant Biol.* 69, 209–236.

Westgate, M. E., and Boyer, J. S. (1985). Osmotic adjustment and the inhibition of leaf, root, stem and silk growth at low water potentials in maize. *Planta* 164, 540–549.

Wiegers, B. S., Cheer, A. Y., and Silk, W. K. (2009). Modeling the hydraulics of root growth in three dimensions with phloem water sources. *Plant Physiol.* 150, 2092–2103.

Wu, Y., Sharp, R. E., Durachko, D. M., and Cosgrove, D. J. (1996). Growth maintenance of the maize primary root at low water potentials involves increases in cell-wall extension properties, expansin activity, and wall susceptibility to expansins. *Plant Physiol.* 111, 765–772.

Yamaguchi, M., and Sharp, R. E. (2010). Complexity and coordination of root growth at low water potentials: recent advances from transcriptomic and proteomic analyses. *Plant Cell Environ.* 33, 590–603.

Yamaguchi, M., Valliyodan, B., Zhang, J., LeNoble, M. E., Yu, O., Rogers, E. E., et al. (2010). Regulation of growth response to water stress in the soybean primary root. I. Proteomic analysis reveals region-specific regulation of phenylpropanoid metabolism and control of free iron in the elongation zone. *Plant Cell Environ.* 33, 223–243.

Yang, X., Dong, G., Palaniappan, K., Mi, G., and Baskin, T. I. (2017). Temperature-compensated cell production rate and elongation zone length in the root of *Arabidopsis thaliana*. *Plant Cell Environ.* 40, 264–276.

Yu, X., Pasternak, T., Eiblmeier, M., Ditengou, F., Kochersperger, P., Sun, J., et al. (2013). Plastid-localized glutathione reductase2-regulated glutathione redox status is essential for *Arabidopsis* root apical meristem maintenance. *Plant Cell* 25, 4451–4468.

Zhang, Z., Voothuluru, P., Yamaguchi, M., Sharp, R. E., and Peck, S. C. (2013). Developmental distribution of the plasma membrane-enriched proteome in the maize primary root growth zone. *Front. Plant Sci.* 4:33 doi: 10.3389/fpls.2013.00033

Zhu, J., Alvarez, S., Marsh, E. L., LeNoble, M. E., Cho, I. J., Sivaguru, M., et al. (2007). Cell wall proteome in the maize primary root elongation zone. II. Region-specific changes in water soluble and lightly ionically bound proteins under water deficit. *Plant Physiol.* 145, 1533–1548.

Conflict of Interest: The authors declare that the research was conducted in the absence of any personal, commercial or financial relationships that could be construed as a potential conflict of interest.

frontiers in Plant Science

REVIEW
published: 15 May 2020
doi: 10.3389/fpls.2020.00546

Should Root Plasticity Be a Crop Breeding Target?

*Hannah M. Schneider and Jonathan P. Lynch**

Department of Plant Science, The Pennsylvania State University, University Park, PA, United States

Root phenotypic plasticity has been proposed as a target for the development of more productive crops in variable environments. However, the plasticity of root anatomical and architectural responses to environmental cues is highly complex, and the consequences of these responses for plant fitness are poorly understood. We propose that root phenotypic plasticity may be beneficial in natural or low-input systems in which the availability of soil resources is spatiotemporally dynamic. Crop ancestors and landraces were selected with multiple stresses, competition, significant root loss and heterogenous resource distribution which favored plasticity in response to resource availability. However, in high-input agroecosystems, the value of phenotypic plasticity is unclear, since human management has removed many of these constraints to root function. Further research is needed to understand the fitness landscape of plastic responses including understanding the value of plasticity in different environments, environmental signals that induce plastic responses, and the genetic architecture of plasticity before it is widely adopted in breeding programs. Phenotypic plasticity has many potential ecological, and physiological benefits, but its costs and adaptive value in high-input agricultural systems is poorly understood and merits further research.

Keywords: anatomy, architecture, breeding, crop, ideotype, plasticity, root

OPEN ACCESS

Edited by:
Idupulapati Madhusudana Rao, International Center for Tropical Agriculture (CIAT), Colombia

Reviewed by:
Hillel Fromm, Tel Aviv University, Israel
Philip Benfey, Duke University, United States

***Correspondence:**
Jonathan P. Lynch
jpl4@psu.edu

Specialty section:
This article was submitted to Plant Abiotic Stress, a section of the journal Frontiers in Plant Science

Received: *11 February 2020*
Accepted: *09 April 2020*
Published: *15 May 2020*

Citation:
Schneider HM and Lynch JP (2020) Should Root Plasticity Be a Crop Breeding Target? Front. Plant Sci. 11:546. doi: 10.3389/fpls.2020.00546

INTRODUCTION

Unpredictable growth environments, decreasing freshwater availability, altered precipitation patterns, ongoing soil degradation, and the rising cost of nitrogen and phosphorus fertilizer demand the development of crop varieties that are resilient to abiotic stress (Tebaldi and Lobell, 2008; Brisson et al., 2010; Woods et al., 2010; Sandhu et al., 2016; Lynch, 2019). Root phenotypic plasticity is a widespread and important phenomenon for the optimized capture of edaphic resources. An array of biotic and abiotic constraints limit plant productivity, and phenotypic plasticity is an important phenomenon to enable plants to adapt to spatiotemporal changes in their environment. In this article we consider the benefits and tradeoffs of root phenotypic plasticity in the development of more productive annual agricultural crops. Many studies of phenotypic plasticity measure the plastic response of allometric traits (length, volume, or biomass), which display plasticity, but may not be adaptive, as they merely reflect growth itself. Many ecological studies of phenotypic plasticity focus on comparisons of distinct species, which is not as relevant to crop improvement as comparisons of genotypes within a species. We will not attempt to provide a comprehensive review of a large and disparate literature, much of which only has tangential relevance to annual crops, but instead focus on opportunities and costs of plasticity for root anatomical and architectural phenotypes in agroecosystems.

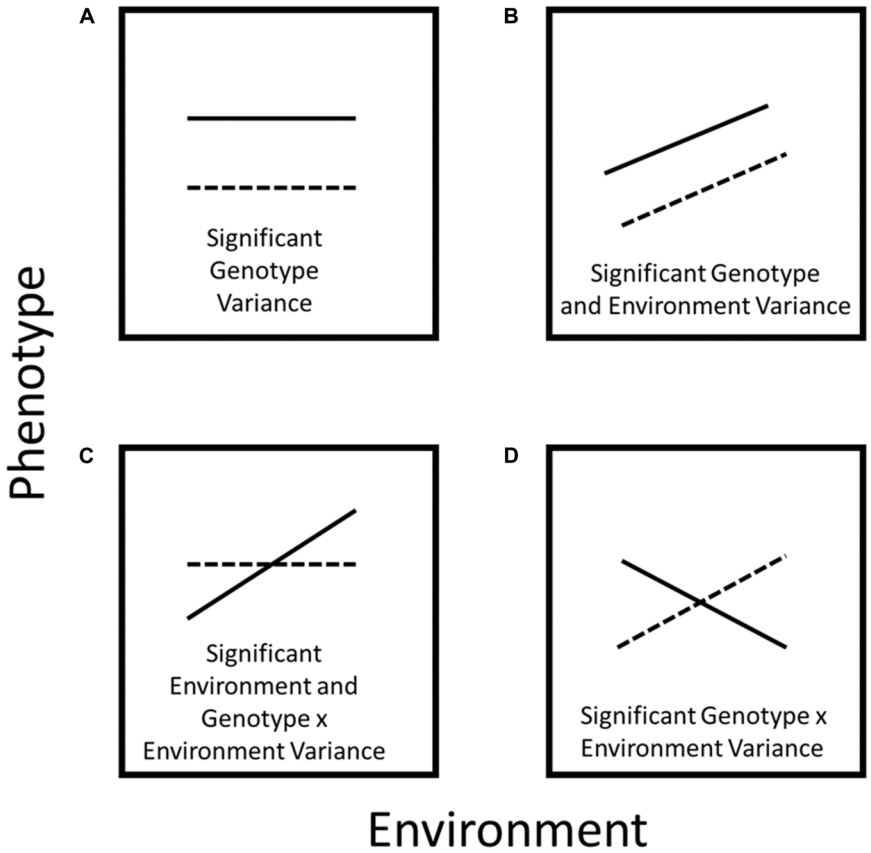

FIGURE 1 | Schematic diagram of plastic responses. In **(A)** the phene value does not change across environments, however, phene expression varies between genotypes. In **(B)** the phene value changes across environments but the reaction norm runs parallel because the response to the environment is the same for both genotypes. In **(C)** one genotype does not exhibit plasticity for a specific phene, while another genotype demonstrates significant environmental plasticity. In **(D)** the reaction norms cross because there is a strong plastic phenotypic response to different environments for both genotypes.

The classic paradigm is that a phenotype (P) is the product of genetics or intrinsic developmental processes (G), environment (E), and the interaction between genetics and the environment (G × E) (Sultan, 2000). Phenotypic plasticity is the ability of an organism to alter its phenotype in response to the environment and may involve changes in physiology, morphology, anatomy, development, or resource allocation (**Figure 1**; Sultan, 2000). Plasticity is not a characteristic of an organism as a whole, but rather is a characteristic of a given phene ("phene" is to "phenotype" as "gene" is to "genotype") (Lynch, 2011; Pieruschka and Poorter, 2012; York et al., 2013) in response to a given environment. A phene state is the outcome of complex synergistic developmental systems, influenced by many genes and gene products, as well as the environment (Miklos and Rubin, 1996; Trewavas and Malho, 1997). Plastic responses can affect the fitness of a genotype and be a response to physical, chemical, and biological processes or resource limitations (Weiner, 2004). The phenotypic spectrum, or an array of possible phenotypes a single genotype can display in a single environment, illustrates that many factors influence the expression of a phenotype. For example, the effects of roots of neighboring plants and priority effects determined by germination time may have large effects on the expression of a phenotype in a single environment (Xie et al., 2019). Phenotypic plasticity may include components of genotype by environment interaction, adaptation, and acclimation.

Biologists have long been aware of plasticity (which is one reason that many experiments are performed in controlled environmental conditions), and for much of the past century phenotypic plasticity has been regarded as "noise" and was thought to obstruct the true or native phenotype of an organism. In a paper entitled "The problem of environment and selection," Falconer argued that environmental effects were a major problem in breeding programs since they interfered with the artificial selection of a trait (Falconer, 1952). However, it is now understood that plasticity is genetically controlled, heritable, and important for the evolution of the species (Bradshaw, 2006). Phenotypic plasticity is now recognized as a significant source of phenotypic variation and diversity and is an important aspect of how organisms develop, function, and evolve (Sultan, 2000).

Phenotypic plasticity may be adaptive, maladaptive, or neutral in regard to fitness. In the heterogenous matrix of soil, many phenes and combinations of phene states may have utility for resource capture and display a wide range of variation,

providing opportunity for plastic responses to evolve. Phenotypic plasticity has utility in enabling a genotype to produce better adapted phenotypes and phenotype-environment combinations across more environments than would be otherwise be possible. However, if no tradeoffs or constraints existed, organisms should be able to exhibit perfect or infinite plasticity by expressing the more adaptive phene or combinations of phenes in every environment with no cost. Costly, but maladaptive or neutral phenotypic responses are expected to go extinct (Dewitt et al., 1998) and we would only expect costly forms of plasticity to persist if they have fitness value.

A plastic response does not imply an adaptive response, although many types of plasticity have important adaptive effects. Adaptive plasticity (positively associated with fitness) and apparent plasticity [lacking adaptive value (e.g., specific types of allometry or stress responses); Correa et al., 2019] are both types of plasticity. Maladaptive plasticity can occur when a plastic response that was adaptive in an evolutionary context is counterproductive in a novel environment. This is especially relevant for crop breeding, since many agroecosystems, especially high-input agroecosystems, differ sharply from ancestral selection environments, as discussed below. By definition, allometric responses to the environment may be considered plastic responses, however, they are often just a function of alterations in plant size (or development), and they may not necessarily be adaptive. For example, maize plants with greater biomass had increased stele cross-sectional area and number of metaxylem vessels, which is not necessarily an adaptive response (Yang et al., 2019). However, changes in allometric partitioning (e.g., changes in root to shoot partitioning) may be adaptive by refocusing plant resources to address resource shortfalls (Bloom et al., 1985). In order to interpret differences in biomass allocation, it is necessary to distinguish these sources of variation. It is difficult to distinguish apparent plasticity from plasticity that may be adaptive.

By definition, edaphic stress reduces plant growth, which is a plastic response but is not necessarily adaptive. For example, reduced grain yield or total root biomass under drought is not an adaptive response, but is a plastic response to stress (Ehdaie et al., 2012) and different growing environments and/or different genotypes may display different rates or types of developmental retardation in response to the same stress. In contrast, the plastic response of genotypes during stress recovery may be adaptive. Phenotypic plasticity encompasses a wide range of environmental responses.

Here we focus on understanding the fitness landscape (i.e., how phenes affect crop performance in an array of environments and phene combinations) of root anatomical and architectural phenotypes in agroecosystems. We discuss the benefits and trade-offs to plasticity and the utility of root plasticity in monocots and dicots, acid soils, high and low input environments, and polycultures. We also review the genetic architecture and potential breeding strategies of root phene plasticity. Additionally, we highlight future research directions for root plasticity to enable a comprehensive understanding of the fitness landscape and integration into breeding programs.

ROOT PHENES ARE IMPORTANT FOR RESOURCE CAPTURE

Root phenes have important roles in soil resource capture, especially in environments with suboptimal water and nutrient availability. Root anatomical and architectural phenes determine the temporal and spatial distribution of root foraging in specific soil domains and hence the capture of mobile and immobile resources (Lynch, 1995, 2013, 2019; Hirel et al., 2007; Lynch and Brown, 2012; Lynch and Wojciechowski, 2015). Mobile soil resources, including nitrate and water, are generally more available in deeper soil domains over time due to crop uptake, evaporation, and leaching throughout the growth season. In contrast, immobile soil nutrients, including phosphorus and potassium, are more available in the topsoil (Lynch and Brown, 2001; Lynch and Wojciechowski, 2015). Plants that are able to acquire edaphic resources at reduced metabolic cost will have increased productivity and performance by permitting greater resource allocation to growth, continued soil resource acquisition, and reproduction (Lynch, 2013, 2015, 2018, 2019). For example, root growth angle influences root depth, and therefore plant performance in nutrient and water stress conditions (Bonser et al., 1996; Uga et al., 2011; Trachsel et al., 2013; York et al., 2013; Dathe et al., 2016) since steep growth angles enable deeper rooting and the capture of mobile nutrients in deep soil domains (Trachsel et al., 2013; Dathe et al., 2016) while shallow growth angles are more beneficial for the capture of immobile resources in the topsoil (Bonser et al., 1996; Lynch and Brown, 2001; Ho et al., 2005; Zhu et al., 2005c).

Root anatomical phenes improve plant growth and performance in edaphic stress by reducing the nutrient and carbon costs of tissue construction and maintenance (Lynch, 2013, 2015, 2018, 2019). Root cortical aerenchyma are air-filled lacunae that result from programmed cell death in root cortical cells (Drew et al., 2000). Air-filled lacunae replace living cortical parenchyma, thereby reducing root segment respiration and nutrient demand (Saengwilai et al., 2014a; Chimungu et al., 2015; Galindo-Castañeda et al., 2018). The reduction in tissue maintenance costs associated with the formation of root cortical aerenchyma enable roots to explore deeper soil domains and improve the capture of water and nitrogen, and thereby improve plant growth and yield in environments with low water and nitrogen availability (Zhu et al., 2010a; Jaramillo et al., 2013; Saengwilai et al., 2014a; Lynch, 2015; Chimungu et al., 2015). Similar to root cortical aerenchyma, a reduction in the number of cortical cell files or an increase in cortical cell size also results in a reduction in tissue maintenance and/or construction costs which enables deeper rooting and improved plant growth in drought environments (Chimungu et al., 2014a,b). In temperate small grains, root cortical senescence enables greater exploration of deeper soil domains and greater plant growth in edaphic stress due to reduced cortical burden (Schneider et al., 2017a,b; Schneider and Lynch, 2018). In common bean, reduced secondary growth resulted in reduced specific root respiration and subsequently greater shoot mass and root length in phosphorus-stress conditions (Strock et al., 2018). Plastic

responses of root phenes may have large implications in the capture of edaphic resources.

In the field, plants may be exposed to successive or multiple, simultaneous stresses. For example, in conditions of terminal drought, seeds are planted in moist soil but the soil progressively dries from the surface due to drainage, evaporation, and plant water uptake, resulting in relatively greater water availability in deeper soil strata and progressively harder topsoils in most agroecosystems (Lynch, 2013; Lynch et al., 2014). Root tissue construction and maintenance demand significant resources, and in bean cumulative tissue maintenance demands may exceed root tissue construction costs after 1 week of growth (Nielsen et al., 1994, 2001). The investment of those carbon and nutrient resources in tissue construction and maintenance early in plant growth limits the opportunity for the construction of additional roots in different soil domains as resource availability changes. For example, if roots proliferate early in the growth season in the moist topsoil, this limits the opportunity for the construction of roots in deeper soil domains where resources are likely to be located later in the growth season. In addition, early root proliferation in topsoil may not have utility in hard, dry soils later in the season. Root deployment therefore implies opportunity costs, especially during multiple successive or simultaneous stresses.

Root architectural and anatomical phenes have important roles in the capture of soil resources in specific environments, for example sustained nitrogen or phosphorus stress (Lynch, 2013, 2018, 2019), however, root phene states can be functionally maladaptive in fluctuating environments or environments with multiple simultaneous stresses (Ho et al., 2005; Poot and Lambers, 2008). For example, shallow growth angles can improve topsoil foraging and improve the capture of phosphorus, but may be functionally maladaptive for the capture of deep resources like water (Ho et al., 2005). In common bean, shallow growth angle and greater number of basal root whorls and hypocotyl-borne roots increase total root length in the topsoil resulting in greater phosphorus acquisition (Rangarajan et al., 2018). However, as the number of axial roots and/or basal root whorl number increase, the resulting carbon limitation leads to a reduced root depth and therefore trade-offs for the capture of deep resources, such as nitrogen (Rangarajan et al., 2018). In monocots, in which axial roots emerge from shoot nodes, shallow roots lack the ability to forage for deep resources, while deep rooting permits the capture of deep resources like nitrogen and water while also being capable of capturing shallow resources, thus creating asymmetric phenotypic trade-offs for the capture of deep and shallow resources (Lynch, 2013). No single phene state is optimal across a range of environments and management practices (Dathe et al., 2016; Tardieu, 2018; Rangarajan et al., 2018).

MANY ROOT PHENES ARE PLASTIC

Plasticity has been observed for a number of root anatomical and architectural phenes (**Figures 2**, **3**). In soybean grown under drought, metaxylem vessel number increased, thereby improving root hydraulic conductivity, while reducing total cortical area which reduced the metabolic cost of accessing water in deep soil domains (Prince et al., 2017). In drought and low phosphorus environments, increased plasticity of root architecture traits correlated with high yield stability in rice (Sandhu et al., 2016). In water stress, plasticity in root length and root cortical aerenchyma formation has been observed in rice and was associated with greater shoot biomass and yield (Niones et al., 2012, 2013). In water stress in wheat and rice, xylem vessel diameter and number and stele diameter were highly plastic (Kadam et al., 2017). Greater phenotypic plasticity in wheat root anatomical traits may be associated with greater stress tolerance compared to rice (Kadam et al., 2017). In common bean, plasticity in secondary root growth influenced root depth and shoot growth in low phosphorus environments (**Figure 4**; Strock et al., 2018). In rice, plasticity in lateral root length and density (Kano et al., 2011; Kano-Nakata et al., 2013), root length density, and total root length (Kano-Nakata et al., 2011; Tran et al., 2014) correlated with greater shoot biomass, water uptake, and photosynthesis in drought. The number of nodal roots in rice (Suralta et al., 2010) and maize (Gao and Lynch, 2016), lateral branching density and length in maize (Zhan et al., 2015), and deep rooting in wheat (Ehdaie et al., 2012; Wasson et al., 2012), millet (Rostamza et al., 2013), rice (Hazman and Brown, 2018), and maize (Nakamoto, 1993) also have displayed plastic responses to water deficit. A plastic response of lateral root proliferation was induced in barley in response to patches of nitrogen (**Figure 5**; Drew et al., 1975) and in maize in response to phosphorus patches (Yano and Kume, 2005). Hydropatterning is a plastic response involving the development of lateral branches, root hairs, and aerenchyma toward available water (Bao et al., 2014). Maize genotypes with plastic root hairs that became longer under low phosphorus had better performance under low phosphorus availability than genotypes with constitutively long root hairs (**Figure 6**; Zhu et al., 2010b). Root anatomical and architectural phenes express a wide range of plastic responses in a wide range of environments. However, it is unclear which plastic responses are adaptive and how phenes interact to create adaptive responses to edaphic stress.

POTENTIAL BENEFITS AND TRADEOFFS OF PHENOTYPIC PLASTICITY

There are many examples of adaptive plasticity of root phenes, including the increased development of root cortical aerenchyma, fewer lateral root branches in water deficit, or deeper distribution of lateral root branches, and it has been proposed that phenotypic plasticity may be the future of crop breeding since it would enable the development of more efficient crops that could adapt to changing environments (Gifford et al., 2013; Hazman and Brown, 2018; Lobet et al., 2019). Adaptive plasticity may promote establishment and persistence in novel environments and allows genotypes to have broader tolerance and greater fitness across environments. It has been proposed that understanding the genetic and mechanistic basis of root phenotypic plasticity will enable the rapid development of more productive crop varieties that will be robust and stable in future climates (Topp, 2016).

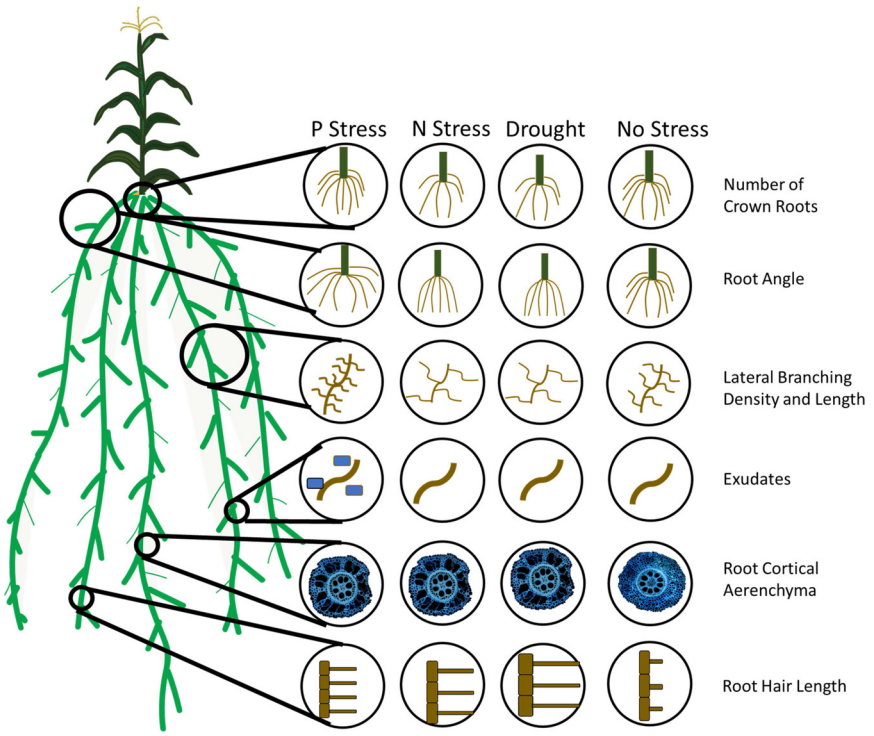

FIGURE 2 | Adaptive root phene plasticity to optimize soil resource capture in edaphic stress. A number of root phenes have been demonstrated to have an adaptive plastic response to edaphic stress. In phosphorus stress, plants with many nodal roots with a steep angle, many short lateral branches, root exudation, root cortical aerenchyma formation, and long, dense root hairs are adaptive or proposed adaptive responses for stress tolerance. In nitrogen and water stress, few crown roots with a steep angle, few long lateral branches, root cortical aerenchyma formation, and long root hairs are adaptive or proposed adaptive responses for stress tolerance.

The adaptation of taxa to sudden environmental changes, like those caused by human disturbance, could also be an advantage of plasticity since these changes generally occur at too rapid of a pace for an evolutionary response, or the development of new crop cultivars through breeding.

However, "perfect" plasticity is unattainable due to an inability to consistently produce the optimum phenotype, fluctuating environmental signals, and/or because phenotypic plasticity comes at a cost (León, 1993; Via and Lande, 2006). A cost of plasticity is when a plastic organism exhibits less fitness while producing the same phene state as a fixed organism. Costs of plasticity have been identified in a variety of systems (Relyea, 2002; Merilä et al., 2004). Maintenance cost of phenotypic plasticity may be incurred if facultative development requires the maintenance or construction of sensory and regulatory machinery that fixed development does not require.

Genetic costs of plasticity also exist. Phenotypic plasticity may manifest because structural genes or their products are directly affected by the external environment (i.e., allelic sensitivity) or because regulatory genes are affected by the environment which in turn affect the expression of structural genes (Via et al., 1995). However, genetic linkage may cause genes associated with plasticity to be linked with genes conferring reduced fitness, plasticity genes may have negative pleiotropic effects on phenes other than the plastic phene, or epistasis may cause the regulatory loci producing the plastic response to modify expression of other genes. With little known about the molecular mechanisms and genetic control of the plastic response, linkage and pleiotropic effects could severely limit the productivity of plastic crop varieties.

In specific environmental scenarios, plasticity may limit plant productivity. For example, if environmental information is not reliable, plastic organisms can produce maladapted phenotypes when environmental cues are incorrectly interpreted, or when correct signals are interpreted about the initial environment, but the environment fluctuates or is highly variable. In many cases, especially with developmental or morphological plasticity, the development of tissues takes time and often there is a lag time between environmental cues and the development of tissues expressing the plastic response. For example, nitrogen, phosphorus, and water are all growth regulators but have different mobilities in soil. Nitrogen and water are mobile and can move faster through the soil profile than plants are able to respond by constructing new tissues or modifying established tissues. Even in the case of phosphorus, an immobile soil resource, changes in phosphate uptake kinetics contribute more to increased phosphorus acquisition than root proliferation in heterogeneous soil environments (Jackson et al., 1990; Caldwell et al., 1992). It also has been suggested that genotypes with fixed development (i.e., non-plastic phenes) may be able to express

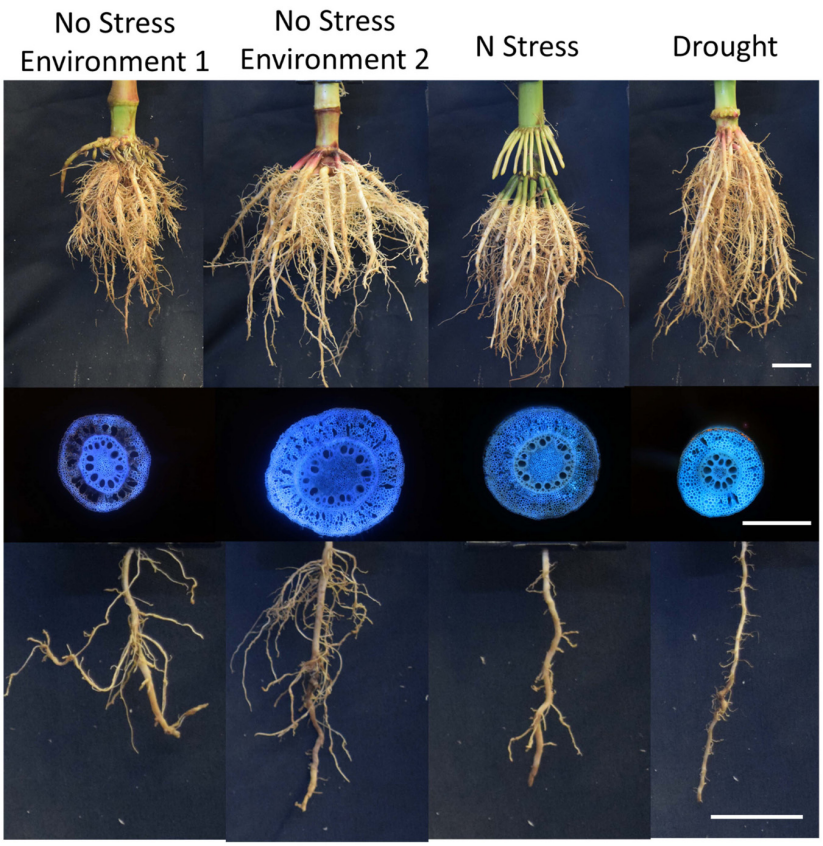

FIGURE 3 | Gentoypes vary in their plastic response to environment, nitrogen stress, and drought. Architectural and anatomical images are presented from a single genotype in response to different environments and edaphic stress conditions. Phenotypic plasticity is shown for root architecture, root anatomy, and lateral branching length and density. Scale bar represents 2 cm (root crown and lateral branch) and 1 mm (anatomy).

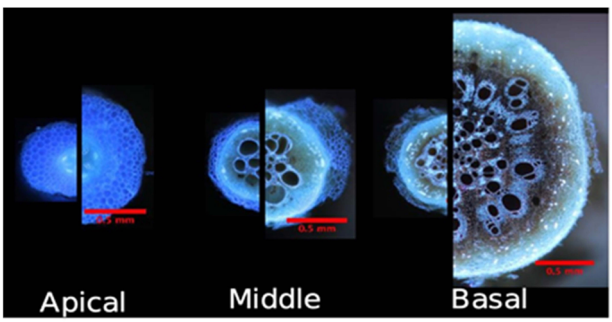

FIGURE 4 | Secondary root growth in common bean (Phaseolus vulgaris) is plastic in response to phosphorus availability. Comparison of basal root anatomy under high P and P stress in greenhouse conditions at 46 DAP. A11 cross-sections are at the same scale. Modified and reproduced with permission from Strock et al. (2018).

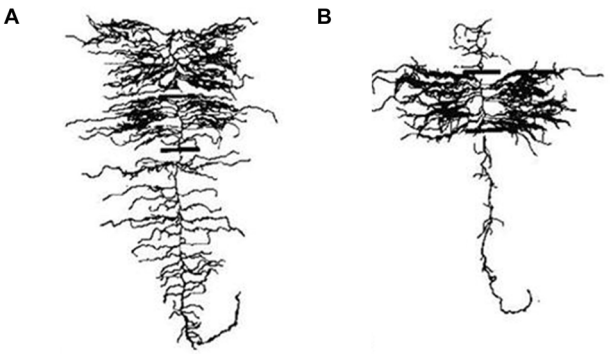

FIGURE 5 | Lateral root proliferation of barley in response to a nutrient patch. **(A)** A plant supplied with a uniform treatment of nitrate has a uniform lateral branching density and length along the axial root. **(B)** A plant supplied with nitrate through a banded treatment displays lateral root proliferation in the banded region. Modified and reproduced with permission from Drew (1975).

more extreme phene states than plastic genotypes since there may be a trade-off between the developmental range that can be expressed across habitats and the magnitude of expression within an environment (Wilson and Yoshimura, 1994; DeWitt, 1998).

Costly, but maladaptive or neutral phenotypic responses are expected to go extinct (Dewitt et al., 1998) and we would only expect costly forms of plasticity to persist if they have fitness

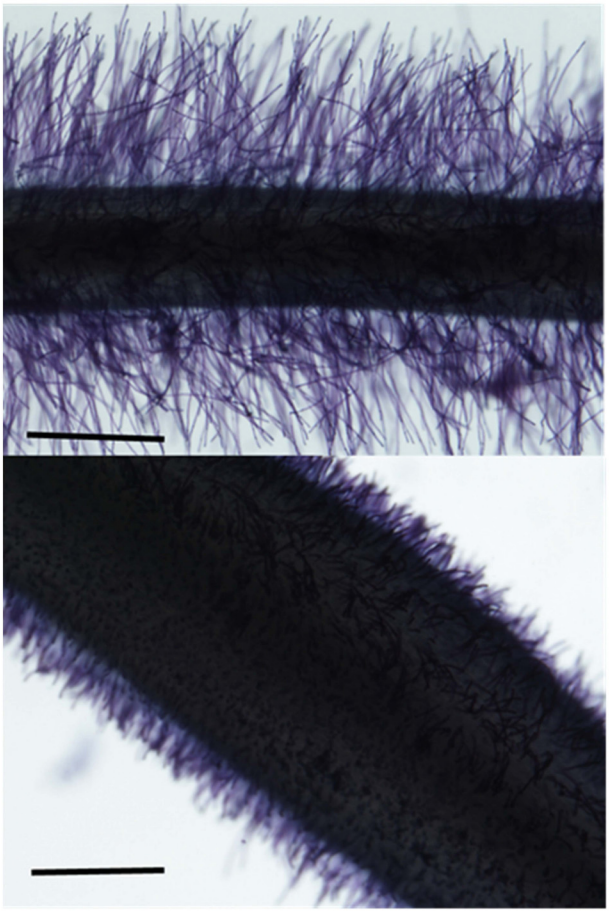

FIGURE 6 | Root hair length is plastic in response to 10W phosphorus environments. Root hairs become longer in low phosphorus environments and are associated with greater shoot biomass. Root hair image courtesy of Anica Massas.

value in some seasons or environments. We speculate that plasticity was a useful mechanism for crop ancestors to grow and develop in novel environments and thrive in unmanaged, unfertilized, and non-irrigated natural ecosystems. In low-input systems, plasticity may be advantageous by exploiting resource patches with increased lateral root proliferation which may confer a competitive advantage (Lynch, 2018). However, in modern agricultural environments with high-inputs, plasticity may come at a greater cost than a benefit. Indirect evidence for this is the observation that during selection of modern temperate maize breeding, regions of the genome contributing to G × E variance and plasticity were not directly or indirectly selected to increase plant productivity and yield stability (Gage et al., 2017).

Short duration plasticity, or physiological plasticity, in variable environments may be advantageous in specific environments, however, plasticity may be maladaptive in high-input environments with intensive fertilization and greater nutrient availability. In high-input environments, constraints for soil resource acquisition and plant growth in stress are mitigated and strategies that evolved in environments with biotic and abiotic stress influencing root function may not have utility in these high-input environments (Lynch, 2018). Root phenotypes that explore deep soil domains, whether plastic or not, enhance the capture of deep resources like water and nitrogen in most agricultural systems, despite the fact that water and nitrogen availability are sometimes greater in surface soils of high-input systems (Manschadi et al., 2006; Gowda et al., 2011; Henry et al., 2011).

If a population is exposed to a novel environment and becomes successful, but becomes restricted to that environment, alleles that contributed to plastic responses in the new environment should trend toward fixation in the absence of gene flow from other populations and therefore their ability to confer plasticity is also reduced (Mitchell-Olds et al., 2007; Anderson et al., 2017; Gage et al., 2017). The utility of phenotypic plasticity in successful and highly productive modern crop varieties in heavily managed high-input environments is limited and not required for the survival or migration of the species.

PLASTICITY IN THE CONTEXT OF TEMPORAL RESOURCE DURATION

The expression of plant phenes as a result of plasticity may be of variable duration and plastic responses may be long- or short-term. Short-term plasticity, is also referred to as physiological plasticity, allows plants to adjust to temporally variable aspects of the environment such as water or nitrogen availability. For example, the expression of aquaporins or nitrate transporters fluctuates as a short-term response to water or nitrogen availability (Feng et al., 2011; Zargar et al., 2017). In contrast, changes due to morphological or developmental plasticity may be of longer duration (Sultan, 2000). For example, the size and number of cortical cells or initial root angle is established near the growing root apex, and potential for change in mature tissues is limited. Phenotypic plasticity that is established early in development, such as root growth angle, may be beneficial in conditions of sustained edaphic stress (e.g., low phosphorus availability), but may be maladaptive in stresses that fluctuate on shorter time scales (e.g., drought, low nitrogen availability) by creating sustained responses to ephemeral conditions (Lynch, 2013). In addition, the timing of development itself, and its response to the environment, may be plastic. Developmental plasticity may be limited to early growth stages, or its timing may vary in different genotypes or species (Pigliucci and Schlichting, 1995). For example, the development of root cortical senescence has the greatest utility in edaphic stress conditions when development occurs relatively early in plant growth, however, genotypic contrasts exist for the rate and timing of its development in root cortical tissues (Schneider et al., 2017b).

In response to heterogeneous soil conditions, root plasticity can also vary spatially. Lateral root branches have been documented in some species and genotypes to proliferate in response to localized patches of nutrient availability (**Figure 5**; Drew, 1975; Zhu and Lynch, 2004). Lateral root proliferation in response to nutrient patches has been proposed as a beneficial

strategy for enhanced nitrogen acquisition (Mi et al., 2010), however, if mobile resources move faster through the soil profile than roots can proliferate, this response may be maladaptive. In some species, plasticity of lateral root branching in response to local nutrient patches may enhance nutrient resource capture in environments with sustained nutrient sources or in conditions of interspecific competition (Robinson et al., 1999). However, this can be detrimental when proliferation in response to local nutrients diverts resources from other soil domains with greater resource availability, particularly deeper soil domains in leaching precipitation regimes later in the growing season (Lynch, 2013, 2018).

UTILITY OF ROOT PLASTICITY VARIES BETWEEN DICOTS AND MONOCOTS

Monocots and dicots have different foraging strategies for edaphic resources. Throughout the growth season, monocots continually produce new roots from stem nodes, and tillers. In contrast, new roots of dicots are predominately lateral roots arising from older root axes. Dicots do have younger hypocotyl-borne roots that emerge throughout the growth season, however, they normally do not comprise a large portion of the root system, which usually consists of relatively few axial roots of larger diameter with a highly developed lateral root system having multiple orders of lateral branching. Monocots may have superior topsoil foraging, as new flushes of roots are continuously pushed down through shallow soils, whereas in dicots many new roots form in deeper soil domains (Lynch, 2013). In addition, in tillering monocot species, an optimum number of tillers should exist to enhance capture of edaphic resources as the number of tillers is directly related to the number of adventitious roots (Hecht et al., 2016). Reduced crown root number improves plant growth with low nitrogen (Saengwilai et al., 2014b) and drought (Gao and Lynch, 2016) by reducing inter- and intra-plant competition for internal and external resources, thereby increasing root depth and acquisition of deep soil resources. However, greater crown root number improves plant growth in low phosphorus soil by reducing axial root elongation and improving topsoil foraging (Sun et al., 2018). We speculate that the number of tillers (and therefore the number of adventitious roots originating from tillers), and its plastic response to plant density and stress, is important for edaphic stress tolerance in monocot species.

There are important differences between the anatomy of monocot and dicot roots. Roots of dicot species radially expand through secondary growth, which has important implications for edaphic stress tolerance. Phosphorus stress reduces secondary growth in *Phaseolus vulgaris* in a genotype-dependent manner, and genotypes with greater reduction of secondary growth had reduced metabolic costs, increased root length, improved phosphorus capture, and increased shoot biomass in low phosphorus soil (**Figure 4**; Strock et al., 2018). In monocots, temperate small grain species develop root cortical senescence (RCS), a type of programmed cell death. Simulation studies suggest that RCS may be an adaptive trait for water and nutrient acquisition. RCS reduces the carbon and nutrient costs of soil exploration by destroying living cortical tissue, thereby reducing carbon and nutrient costs of maintaining a living cortex. The development of RCS may be plastic as limited phosphorus and nitrogen availability accelerate the development of RCS (Schneider et al., 2017a,b). After the development of RCS in monocots or secondary growth in dicots, assimilates that would have been partitioned to the root for maintenance of the cortex may be used for the growth of shoots or new roots, which can increase soil exploration. Monocots and dicots have different foraging and resource acquisition strategies and therefore may have different adaptive plastic responses for soil resource capture.

UTILITY OF ROOT PLASTICITY FOR ACID SOILS

Acid subsoils (generally defined as having a pH < 5) present several challenges to root growth and resource acquisition including aluminum (Al) toxicity, deficiency of phosphorus (P), calcium (Ca), magnesium (Mg) and potassium (K), and possibly manganese (Mn) toxicity. In acid soils, the solubility of Al increases and injury to root apices occurs, therefore reducing root growth, soil exploration, and subsequent resource acquisition.

Commonly, acidic soils are located in humid environments with weathered soils, and acidity increases with soil depth. Plasticity of root phenes that increase topsoil foraging would be beneficial by improving the capture of resources that have greater availability in the topsoil, including P, Ca, Mg, and K (Lynch, 2019), while also avoiding subsoils with greater acidity and Al toxicity (Lynch and Wojciechowski, 2015). The tradeoff of reduced access to deep soil water would probably be less important in humid environments because of greater water availability in shallower soil domains. Topsoil foraging can be improved through a shallower axial root growth angle (Bonser et al., 1996; Liao et al., 2001), greater production of axial roots (Walk et al., 2006; Miguel et al., 2013; Rangarajan et al., 2018; Sun et al., 2018), denser lateral roots (Postma et al., 2014; Jia et al., 2018), and greater root hair length and density (Zhu et al., 2010b; Miguel et al., 2015). Reduced root metabolic cost improves growth in soils with low phosphorus availability. In maize, the formation of root cortical aerenchyma reduces root respiration and the phosphorus cost of maintaining root tissue therefore improving plant growth in low phosphorus (Postma and Lynch, 2011; Galindo-Castañeda et al., 2018). In bean, phosphorus stress inhibits secondary growth of roots which reduces root costs and improves phosphorus capture and plant growth in low phosphorus soils (Strock et al., 2018). Plastic root phenes that improve topsoil foraging may be beneficial for improved capture of phosphorus in acidic soils.

Plasticity in carboxylate exudation may also be an important mechanism for phosphorus uptake in acidic soils. Carboxylate exudation into the rhizosphere solubilizes phosphorus from metal complexes (Ryan et al., 2012). Carboxylates also can precipitate toxic levels of aluminum in the soil (Lambers et al., 2003). Exudation of carboxylates in plant roots is a common phenomenon in many plants including rice (Kirk et al., 1999),

wheat (Ryan et al., 1995), and lupin (Gardner et al., 1983). The exudation of carboxylates including citrate and malate into the rhizosphere can incur a large carbon cost (Lambers et al., 2013). Plasticity in the spatiotemporal control of carboxylate exudation, i.e., exudation triggered by aluminum toxicity and phosphorus stress may permit a reduction in the metabolic burden of the root.

Low Ca availability is a major challenge to root growth in acid subsoils (Foy et al., 1969). Differences in cell wall composition may influence tissue Ca requirements and plants with reduced internal Ca requirement therefore may be more productive in acid soils (Lynch and Wojciechowski, 2015). Cortical cell size, file number, and aerenchyma all influence the amount of cell wall material per root volume and therefore affect tissue Ca requirement. Genotypes with reduced pectin content, which has a reduced demand for Ca, may also reduce the Ca requirement of the root (Marschner, 1995). We propose that plasticity of phenes that reduce tissue Ca requirements, like increased cortical cell size, reduced file number, reduced pectin content, and increased aerenchyma formation may be beneficial in acid soils. Crops with a reduced Ca tissue requirement may be able to continue to explore acidic subsoils, despite reduced Ca availability and Al toxicity.

ROOT PLASTICITY IN THE CONTEXT OF HIGH AND LOW INPUT ENVIRONMENTS

It has been proposed that wild crop ancestors and landraces produce more roots than directly needed for the capture of edaphic resources to compensate for root loss from biotic stress, edaphic stress, and competition for soil resources with neighboring plants (Lynch, 2018). We speculate that plasticity was a useful mechanism for crop ancestors in natural ecosystems. Short duration plasticity, or physiological plasticity, in variable environments may be advantageous in specific environments, however, plasticity may be maladaptive in high-input environments with intensive fertilization, greater nutrient availability, and reduced biotic stress. In high-input agroecosystems, parsimonious, non-plastic root phenotypes including e.g., fewer axial roots, reduced density and length of lateral roots, reduced cortical cell file number, and reduction of cortical parenchyma through formation of aerenchyma and senescence may be beneficial by permitting deeper rooting and the capture of deep resources like water and nitrogen (Lynch, 2018). Plastic responses to increase topsoil foraging in response to shallow localization of water and N early in the growth season may optimize resource capture in natural systems or low-input agroecosystems, characterized by intense belowground competition from neighboring plants. However, in high-input monocultures, where immobile resources like P and K are likely to be non-limiting, non-plastic phenotypes would be advantageous since eventually water and N would be localized at depth regardless of early season patterns, and resources lost to neighboring plants would still contribute to stand-level fitness (i.e., yield) in high density monocultures (Lynch, 2018). We propose that in low-input systems, highly plastic root phenotypes with a variable number of axial and lateral roots, variable root growth angle, variable length and density of root hairs, variable formation of root cortical aerenchyma and cortical cell files, would be beneficial for the capture of heterogeneous soil resources in environments with significant root loss due to biotic factors. However, in high-input systems, a sparser root system with fewer axial roots may be more beneficial, since the negative effects of biotic stress is diminished (Lynch, 2018).

PLASTICITY IN THE CONTEXT OF POLYCULTURES

In many low-input agroecosystems, which traditionally consist of polycultures and generally experience greater weed competition, interplant competition with other species has important implications in plant performance. For example, the maize/bean/squash polyculture used in small-scale subsistence farming has a yield advantage over the average yield of the respective monocultures (Mt. Pleasant and Burt, 2010). Maize, bean, and squash have contrasting root architectures (Postma and Lynch, 2012; Zhang et al., 2014) and differences in root architecture and vertical root distribution result in differences in spatial niches and allows polycultures to be productive when plants are competing for soil resources (Zhang et al., 2014). In these polyculture systems, species co-optimize, and spatial niches allow a yield advantage by reducing competition for edaphic resources. In polyculture or multiline systems, highly plastic root architectural phenes could disrupt complementary spatial niche foraging strategies (Zhang et al., 2014). If these species had highly plastic root architectural phenotypes, this would create more competition for the same soil resources, which would be detrimental. For example, if roots of all species proliferate in response to localized patches of nutrient availability, this creates greater inter-plant and species competition. In this scenario, phenotypic plasticity may not be adaptive, as complementary spatial niches are needed for the success of all species or the population.

PROGENY MAY BE PRIMED FOR A PLASTIC RESPONSE

Plants cannot only respond to environmental signals by adjusting their own phenotypes, but also can influence the phenotypes of their offspring, through changes in the quantity and quality of seed production and the structure and quality of the seed coat and fruit tissues (Sultan, 2000). The phenotype of offspring can be influenced by the parental environment. For example, plants can respond to specific environments by changing the structure of thickness of the seed coat while maintaining the quantity and quality of the embryo and endosperm tissues (Sultan, 1996; Lacey et al., 1997). Genotypes may vary in the extent to which seedling and mature root phenes are affected by parental stress. For example, progeny of some common bean genotypes from drought-stressed parents developed fewer and shorter basal roots with smaller diameters (Lorts et al., 2019). Progeny from some genotypes from phosphorus stress parents

developed fewer shoot-borne roots and had a greater basal root whorl number (Lorts et al., 2019). Progeny of nutrient-deprived plants increase allocation to root biomass compared to progeny of plants with ample nutrients (Wulff and Bazzaz, 1992). Offspring of light-deprived plants reduce root elongation relative to shoot growth compared to progeny of plants grown in high light (Sultan, 2000). In addition, epigenetic processes, including DNA methylation and histone modification, may alter gene expression and therefore may be important drivers in phenotypic plasticity (Chinnusamy and Zhu, 2009; Nicotra et al., 2010). These plastic changes may enable offspring to maintain critical aspects of plant growth and function, even if the initial seedling biomass is reduced by parental stress.

GENETIC ARCHITECTURE OF PLASTICITY AND BREEDING STRATEGIES

Some genetic loci have been associated with root phenes including root stele and xylem vessel diameter in rice (Uga et al., 2008, 2010), xylem vessel phenes in wheat (Sharma et al., 2010), root cortical aerenchyma in *Zea* species (Mano et al., 2006, 2007), areas of cross section, stele, cortex, aerenchyma, and cortical cells, root cortical aerenchyma, cortical cell file number, and length, number, and diameter of nodal roots in maize (Burton et al., 2014a,b). However, genes associated with phene expression are distinct from those associated with plasticity for that expression. Genes associated with plasticity have been identified for root hair length (Zhu et al., 2005a) and lateral root branching and length (Zhu et al., 2005b) in low phosphorus availability in maize, root length density and root dry weight (Sandhu et al., 2016) in rice in response to drought, lateral root branching in rice in response to fluctuating moisture levels (Niones et al., 2015), and wheat and rice root anatomical phenes in response to drought (Kadam et al., 2017). In maize, genes associated with plasticity in response to water deficit and different environments are distinct for cortical phenes, root angle, and lateral branching phenes (Schneider et al., 2020a,b; **Table 1**). Understanding the genetic architecture of plasticity could provide useful breeding targets for crop improvement in specific environments and improve our understanding of phenotypic plasticity. Plasticity is heritable, and this enables selection for or against plasticity in manmade populations (Pigliucci, 2005). Historically, breeding programs have focused on selecting crop varieties based on uniformity and yield stability in specific environments and management practices, and plasticity has often considered to be a breeding obstacle (Basford and Cooper, 1998; Cooper et al., 1999). Large and complex genotype by environment interactions complicate the design and implementation of breeding strategies (Cooper et al., 1999) and breeders often select for a low genotype by environment contribution to enable genotypes to perform predictably in specific environments. Crop breeding has made huge advancements in the development of productive varieties that are stable across diverse conditions and recent studies have suggested that plasticity was not directly or indirectly selected for in the development of modern crop varieties (Gage et al., 2017). It is important to note that maladaptive plasticity in a specific environment may be adaptive in different environments, including future climates. Plasticity that is not currently adaptive can provide sources of variation that may be important for phenotypic evolution or variation for breeding (Lande, 2009).

The genetic architecture of plasticity is highly complex and quantitative. Many genes with small effects control plastic responses and distinct genes control plastic responses of different root phenes and in response to different stresses and environments (Schneider et al., 2020a,b). This can pose a challenge for breeding programs that use conventional tools like single-trait breeding strategies and marker assisted selection, as hundreds of genes would need to be stacked for the development of desirable root ideotypes for specific environments. However, modern breeding methods, like genomic selection enable the selection of multiple loci.

In addition, genes controlling root anatomical and architectural phenes and their plastic responses are probably highly pleiotropic. For example, multiple root anatomical and architectural phenes are regulated by ethylene (Takahashi et al., 2015; Schneider et al., 2018). Ethylene signaling induces root cortical aerenchyma and RCS formation via programmed cell death (Evans, 2003; Schneider et al., 2018) and presumably common signaling pathways (e.g., ethylene) control expression of other root phenes under a range of edaphic stresses [i.e., lateral root formation (Negi et al., 2008)]. For example, the upregulation of an ethylene-related gene may be intended to increase aerenchyma formation for adaptation in drought environments, however, increased ethylene production may also have unintended effects such as reduced axial root elongation which may be maladaptive in these environments. We must fully understand the genetic architecture of phene plasticity as well as the function of phenes and phene aggregates in order to develop adaptive crop cultivars for specific environment.

In breeding programs with capabilities to use genomic selection, selection should include phenes and integrated phenotypes (and their plastic responses), not just selection for yield. Selection for individual phenes has merits compared with brute-force yield selection for edaphic stress (Lynch, 2019). In training sets for genomic selection, consideration must be given to wild germplasm and landraces, since elite germplasm has been developed through selection in high-input environments and often against plasticity. Landraces and wild germplasm presumably express more phenotypic plasticity than uniform, stable elite crop germplasm and could provide unique sources of phenotypic variation.

Phenotypic selection for plasticity may also be a viable strategy for breeding programs, however, selection must occur in specific targeted environments or under specific edaphic stresses. A genotype that displays adaptive plastic responses to water stress may not express an adaptive (or any) plastic responses to other edaphic stresses such as limited nutrient availability. The phenotyping of plasticity should be evaluated for individual phenes, as plasticity in a variety of phenes and phene combinations can result in similar yield or measures of plant performance.

TABLE 1 | Summary of identified genetic loci associated with root plasticity and architecture.

Species	Root trait	Response	References
Soybean	Root length, Number of adventitious roots, Number of root tips	Waterlogging	Ye et al., 2018
Rice	Root diameter, Stele diameter, Cortical diameter, Metaxylem vessel number and diameter, Root length, Specific root length, Root volume, Root surface area	Drought	Kadam et al., 2017
Rice	Lateral root branching	Drought	Niones et al., 2015
Rice	Root length density and root dry weight	Drought	Sandhu et al., 2016
Arabidopsis	Root volume, Weight, Deep root weight	Drought	Li et al., 2017
Arabidopsis	Root length and dry weight	Drought	El-Soda et al., 2015
Maize	Lateral root branching and length	Low Phosphorus	Zhu et al., 2005b
Maize	Root hair length	Low Phosphorus	Zhu et al., 2005a
Maize	Root cortical aerenchyma, Cortical cell size and file number, Metaxylem vessel area, Cortical area, Stele area, Root cross-sectional area	Drought	Schneider et al., 2020a
Maize	Root angle, Lateral root branching length and density, Distance to the first lateral branch	Drought	Schneider et al., 2020b

Several genes have been identified in many different species for a number of anatomical and architectural phenes.

The adaptive value of plasticity in breeding programs is limited by distinct genetically controlled plasticity responses to different environmental conditions. Breeders may need to target a specific plastic response of a specific phene or set of phenes to a specific abiotic or biotic stress or environment, rather than just breed for a variety that highly expresses phenotypic plasticity. Genotypes that have a plastic response to water deficit are not the same set of genotypes with a plastic response to different environments (i.e., G × E) (Schneider et al., 2020a,b). Breeding efforts to develop varieties that are plastic to a wide range of environments and stresses, may be maladaptive in environments with multiple stresses or stresses that fluctuate on short time scales or that vary throughout the growth season. The development of new crop varieties can take decades, and the utility of phene states in the current target environment may change in future environments and climates. Since each plastic response to an environmental cue has distinct genetics, use of plasticity as a selection criterion is challenging for breeders who must target each plastic response to a specific environment or stress.

FUTURE RESEARCH DIRECTIONS

Should root plasticity be a breeding target? The answer is complex. The fitness landscape of root phenotypic plasticity is dependent on specific agroecologies and management practices, and the genetic control of plasticity is in general highly quantitative and is dependent on many loci having small effects. To better understand and interpret plasticity, first we need a comprehensive understanding of the utility of individual phenes. Numerous studies evaluate plasticity of specific root length, root biomass, or yield. However, specific root length may depend on the expression of many individual phenes including the formation of root cortical aerenchyma, cortical cell file number, and stele area. Previous studies have demonstrated that phenotypic plasticity is phene-specific, not necessarily genotype-specific (Schneider et al., 2020a,b) so it is important to measure individual phenes as opposed to phene aggregates. When plasticity of a phene aggregate, or combinations of multiple elemental phenes, is measured, it may reflect a plastic response of one or multiple phenes. In addition, when phene aggregates are measured, phenotypic plasticity may be masked by different responses of elemental phenes. For example, the diameter of the root may not exhibit plasticity, but the stele size, cortical cell file number, or size of cortical cells may have changed their phenotype. Many combinations of elemental phenes have the potential to produce the same expression of combinations of phenes.

Contrary to earlier neo-Darwinian views of plasticity as trivial "noise," plasticity is now considered to be an important source of phenotypic variation. Root systems consist of multiple phenes, each under distinct genetic control, that interact with each other and the environment to determine fitness. The fitness landscape of root phenes and their plastic responses that vary among genotypes, species, and environment is poorly understood. Plants are not equipped with unlimited phenotypic plasticity, which suggests that there are constraints to its expression (Schlichting, 1986).

Several recent studies have focused on the utility of specific phenes in edaphic stress (Trachsel et al., 2013; Chimungu et al., 2014a,b; Saengwilai et al., 2014a,b; Schneider et al., 2017a; Strock et al., 2018), however, the utility of many other root phenes in edaphic stress remains to be explored. In addition, recent studies have explored interactions between root phenes which may be synergistic or antagonistic in nature (Miguel et al., 2015; Rangarajan et al., 2018). For example, in dicots tradeoffs exist between shallow and deep soil foraging (Ho et al., 2005). Recent studies suggest that plasticity is phene-specific and a single genotype may produce an adaptive plastic response for one phene and maladaptive plastic response for a different phene on the same plant (Schneider et al., 2020a).

Presumably, genes controlling adaptive phenotypic plasticity would have to be stacked in breeding programs to create a suite of adaptive synergistic phenes. Understanding the utility of root phenes and their interactions will have important implications in understanding adaptive or maladaptive plasticity under specific edaphic stresses. In many cases, more detailed and refined phenotyping methods are needed to be able to characterize and phenotype phene states, rather than phene aggregates. In many knockout collections, the annotation of "no visible phenotype" is common and is partly due to the lack of capacity for the plant science community to analyze subtle and complex elemental phenes. Field phenotyping is a bottleneck in crop breeding programs and high-throughput, industrial-scale phenotyping often does not allow for the identification and understanding of subtle, complex phene states. In the context of plant roots, there are many combinations of phenes that affect fitness of a plant in a specific environment. In order to interpret the adaptive value, utility of phenotypic plasticity, and consider plasticity in breeding programs we must first understand the fitness landscape of individual phenes and phene combinations.

To understand patterns of plasticity, we need to better understand and monitor local environments and changes in the environment. Subtle changes in the environment, such as localized nutrient patches, may induce a phenotypic response and if the environment is not carefully monitored, it makes interpretation of the plastic responses challenging (Schneider et al., 2020a). Field environments are often heterogeneous and difficult to monitor and replicate. *In silico* approaches enable the evaluation of many environment and phenotype combinations including those that do not exist in nature (Dunbabin et al., 2013). The use of modern *in silico* approaches will be necessary to understand the complex interactions of the root fitness landscape that are not possible empirically.

Growth differences between controlled and field environments are often overlooked. Planting density, light, temperature, and other growing conditions have large effects on plant growth and are often dramatically different in the field compared to controlled environments and phenotypic correlations between lab and field data are often poor (Poorter et al., 2016). Controlled environments and growing systems do not represent the heterogeneous matrix of the soil and therefore are difficult to use to discover true plant responses. There is a clear need to employ abiotic conditions that are overall more similar to those which the plants experience in the field (e.g., more natural soils, appropriate planting densities, light intensity). Many previous studies on phenotypic plasticity have focused on environmental responses in straightforward traits including biomass and root-shoot ratios (Bradshaw and Hardwick, 1989) and numerous studies have observed plastic or genotype by environment responses of below- and above-ground plant phenes (Robinson et al., 1999; Gage et al., 2017; Rabbi et al., 2017). Now that we have a basic understanding of plasticity, we can move to understanding more complex and subtle aspects of phenotypic plasticity. Single-factor experiments have been important in understanding plastic responses, however, more realistic environmental complexity is needed in studies (e.g., multiple, simultaneous dynamic stresses). For example, understanding plastic responses to multiple constraints is important. Very few studies have tested plastic responses to multiple simultaneous abiotic and biotic stresses.

Short-term or dynamic plasticity is an important but poorly understood component of plasticity that includes the rate of phenotypic response or patterns of development. Plasticity of short duration may be important in maintaining fitness, particularly in fluctuating environments. Dynamic plasticity is challenging to measure, as it requires phenes to be measured over time in many individuals in different environments. Common phenotyping tools require destructive harvests at fixed times or at fixed growth stages and are slow and costly. However, this is critical to understanding plasticity, as the determination of whether plasticity is adaptive or maladaptive depends strongly on its temporal expression.

The extent of variation in expression of plasticity still remains to be explored in many root phenes. Phenotypic plasticity may be an important source of genetic variation to be exploited for the development of crop varieties for future environments. However, breeding for genotypes with plastic responses will be complicated by their complex genetic architecture, genetic and metabolic costs of plasticity, and potential maladaptive responses in many environments.

We propose that some of the main ideas discussed here regarding root phenotypic plasticity are applicable to shoot phenotypic plasticity. In high-input environments, shoot architecture and anatomy is optimized for enhanced plant performance. Similar to root plasticity, we speculate that in high-input environments, shoot plasticity may not be advantageous, since human management has removed many constraints to shoot function. However, shoot phenotypic plasticity ideotypes, benefits, and trade-offs in many ways are not equivalent to root plasticity as soil resources are spatially and temporally dynamic and much more complex than above-ground environments. Like root phenes, we must fully understand the fitness landscape of shoot phenotypic plasticity before its integration into breeding programs.

To harness the power and knowledge of genomic information and agricultural application of plasticity, we need to be able to comprehensively link genetic information to "real world" phenotypes in "real world" environments. We need to measure the adaptive significance of patterns in plasticity and understand the complex pathways that lead from environmental cues to a plastic response. The fitness landscape of plasticity is highly complex, yet poorly understood and merits further research to understand the utility of plasticity for edaphic stress tolerance. The study of phenotypic plasticity involves many disciplines including ecology, physiology, development morphology, genetics, *in silico* biology and evolution and offers many research opportunities to understand links among these areas.

AUTHOR CONTRIBUTIONS

JL conceived the idea. JL and HS contributed to the writing of this manuscript.

FUNDING

This work was supported by USDOE ARPA-E Award Number DE-AR0000821.

ACKNOWLEDGMENTS

We thank Kathleen Brown, Meredith Hanlon, and Christopher Strock for helpful comments.

REFERENCES

Anderson, J., Lee, C.-R., Rushworth, C., Colautti, R., and Mitchell-Olds, T. (2017). Genetic trade-offs and conditional neutrality contribute to local adaptation. *PLoS ONE* 32:e0178059. doi: 10.1371/journal.pone.0178059

Bao, Y., Aggarwal, P., Robbins, N. E., Sturrock, C. J., Thompson, M. C., Tan, H. Q., et al. (2014). Plant roots use a patterning mechanism to position lateral root branches toward available water. *Proc. Natl. Acad. Sci. U.S.A.* 111, 9319–9324. doi: 10.1073/pnas.1400966111

Basford, K. E., and Cooper, M. (1998). Genotype x environment interactions and some considerations of their implications for wheat breeding in Australia. *Aust. J. Agric. Res.* 49, 153–174.

Bloom, A. J., Chapin, F. S., and Mooney, H. A. (1985). Resource limitation in plants-an economic analogy. *Annu. Rev. Ecol. Syst.* 16, 363–392.

Bonser, A., Lynch, J., and Snapp, S. (1996). Effect of phosphorus deficiency on growth angle of basal roots in Phaseolus vulgaris. *New Phytol.* 132, 281–288.

Bradshaw, A. (2006). Unraveling phenotypic plasticity – Why should we bother? *New Phytol.* 170, 644–648.

Bradshaw, A., and Hardwick, K. (1989). Evolution and stress—genotypic and phenotypic components. *Biol. J. Linn. Soc.* 37, 137–155. doi: 10.1111/j.1095-8312.1989.tb02099.x

Brisson, N., Gate, P., Gouache, D., Charmet, G., Oury, F. X., and Huard, F. (2010). Why are wheat yields stagnating in Europe? A comprehensive data analysis for France. *F. Crop. Res.* 119, 201–212. doi: 10.1016/j.fcr.2010.07.012

Burton, A. L., Johnson, J., Foerster, J., Hanlon, M. T., Kaeppler, S. M., Lynch, J. P., et al. (2014a). QTL mapping and phenotypic variation of root anatomical traits in maize (*Zea mays* L.). *Theor. Appl. Genet.* 128, 93–106. doi: 10.1007/s00122-014-2414-8

Burton, A. L., Johnson, J. M., Foerster, J. M., Hirsch, C. N., Buell, C. R., Kaeppler, S. M., et al. (2014b). QTL mapping and phenotypic variation for root architectural traits in maize (*Zea mays* L.). *Theor. Appl. Genet.* 127, 2293–2311. doi: 10.1007/s00122-014-2353-4

Caldwell, M. M., Dudley, L. M., and Lilieholm, B. (1992). Soil solution phosphate, root uptake kinetics and nutrient acquisition: implications for a patchy soil environment. *Oecologia* 89, 305–309. doi: 10.1007/BF00317406

Chimungu, J., Brown, K., and Lynch, J. (2014a). Large root cortical cell size improves drought tolerance in maize. *Plant Physiol.* 166, 2166–2178. doi: 10.1104/pp.114.250449

Chimungu, J. G., Brown, K. M., and Lynch, J. P. (2014b). Reduced root cortical cell file number improves drought tolerance in maize. *Plant Physiol.* 166, 1943–1955. doi: 10.1104/pp.114.249037

Chimungu, J. G., Maliro, M. F. A., Nalivata, P. C., Kanyama-Phiri, G., Brown, K. M., and Lynch, J. P. (2015). Utility of root cortical aerenchyma under water limited conditions in tropical maize (*Zea mays* L.). *F. Crop. Res.* 171, 86–98. doi: 10.1016/j.fcr.2014.10.009

Chinnusamy, V., and Zhu, J. K. (2009). Epigenetic regulation of stress responses in plants. *Curr. Opin. Plant Biol.* 12, 133–139. doi: 10.1016/j.pbi.2008.12.006

Cooper, M., Rajatasereekul, S., Somrith, B., Sriwisut, S., Immark, S., Boonwite, C., et al. (1999). Rainfed lowland rice breeding strategies for Northeast Thailand II. Comparison of intrastation and interstation selection. *F. Crop. Res.* 64, 153–176. doi: 10.1016/S0378-4290(99)00057-X

Correa, J., Postma, J. A., Watt, M., and Wojciechowski, T. (2019). Root system architectural plasticity and soil compaction: a review. *J. Exp. Bot.* 70, 6019–6034. doi: 10.1093/jxb/erz383

Dathe, A., Postma, J., Postma-Blaauw, M., and Lynch, J. (2016). Impact of axial root growth angles on nitrogen acquisition in maize depends on environmental conditions. *Ann. Bot.* 118, 401–414. doi: 10.1093/aob/mcw112

DeWitt, T. (1998). Costs and limits of phenotypic plasticity: tests with predator-induced morphology and life history in a freshwater snail. *J. Evol. Biol.* 11, 465–480. doi: 10.1046/j.1420-9101.1998.11040465.x

Dewitt, T. J., Sih, A., and Wilson, D. S. (1998). Costs and limits of phenotypic plasticity. *Tree* 13, 77–81.

Drew, M. (1975). Comparison of the effects of a localized supply of phosphate, nitrate, ammonium and potassium on the growth of the seminal root system, and the shoot, in barley. *New Phytol.* 75, 479–490.

Drew, M. C., He, C. J., and Morgan, P. W. (2000). Programmed cell death and aerenchyma formation in roots. *Trends Plant Sci.* 5, 123–127. doi: 10.1016/S1360-1385(00)01570-3

Drew, M. C., Saker, L. R., and Ashley, T. W. (1975). Nutrient supply and the growth of the seminal root system in barley. *J. Exp. Bot.* 24, 1189–1202. doi: 10.1093/jxb/24.6.1189

Dunbabin, V. M., Postma, J. A., Schnepf, A., Pagès, L., Javaux, M., Wu, L., et al. (2013). Modelling root-soil interactions using three-dimensional models of root growth, architecture and function. *Plant Soil* 372, 93–124. doi: 10.1007/s11104-013-1769-y

Ehdaie, B., Layne, A. P., and Waines, J. G. (2012). Root system plasticity to drought influences grain yield in bread wheat. *Euphytica* 186, 219–232. doi: 10.1007/s10681-011-0585-9

El-Soda, M., Kruijer, W., Malosetti, M., Koornneef, M., and Aarts, M. G. M. (2015). Quantitative trait loci and candidate genes underlying genotype by environment interaction in the response of *Arabidopsis thaliana* to drought. *Plant Cell Environ.* 38, 585–599. doi: 10.1111/pce.12418

Evans, D. E. (2003). Aerenchyma formation. *New Phytol.* 161, 35–49.

Falconer, D. S. (1952). The problem of environment. *Am. Nat.* 86, 293–298.

Feng, H., Yan, M., Fan, X., Li, B., Shen, Q., Miller, A. J., et al. (2011). Spatial expression and regulation of rice high-affinity nitrate transporters by nitrogen and carbon status. *J. Exp. Bot.* 62, 2319–2332. doi: 10.1093/jxb/erq403

Foy, C. D., Fleming, A. L., and Armiger, W. H. (1969). Aluminum tolerance of soybean varieties in relation to calcium nutrition. *Agron. J.* 61, 505. doi: 10.2134/agronj1969.00021962006100040007x

Gage, J. L., Jarquin, D., Romay, C., Lorenz, A., Buckler, E. S., Kaeppler, S., et al. (2017). The effect of artificial selection on phenotypic plasticity in maize. *Nat. Commun.* 8, 1–11. doi: 10.1038/s41467-017-01450-2

Galindo-Castañeda, T., Brown, K. M., and Lynch, J. P. (2018). Reduced root cortical burden improves growth and grain yield under low phosphorus availability in maize. *Plant Cell Environ.* 7, 1579–1592. doi: 10.1111/pce.13197

Gao, Y., and Lynch, J. P. (2016). Reduced crown root number improves water acquisition under water deficit stress in maize (*Zea mays* L.). *J. Exp. Bot.* 67, 4545–4587. doi: 10.1093/jxb/erw243

Gardner, W. K., Barber, D. A., and Parbery, D. G. (1983). The acquisition of phosphorus by Lupinus albus L. – III. The probable mechanism by which phosphorus movement in the soil/root interface is enhanced. *Plant Soil* 70, 107–124. doi: 10.1007/BF02374754

Gifford, M. L., Banta, J. A., Katari, M. S., Hulsmans, J., Chen, L., Ristova, D., et al. (2013). Plasticity regulators modulate specific root traits in discrete nitrogen environments. *PLoS Genet.* 9:e1003760. doi: 10.1371/journal.pgen.1003760

Gowda, V. R. P., Henry, A., Yamauchi, A., Shashidhar, H. E., and Serraj, R. (2011). Root biology and genetic improvement for drought avoidance in rice. *F. Crop. Res.* 122, 1–13. doi: 10.1016/j.fcr.2011.03.001

Hazman, M., and Brown, K. M. (2018). Progressive drought alters architectural and anatomical traits of rice roots. *Rice* 11:62. doi: 10.1186/s12284-018-0252-z

Hecht, V. L., Temperton, V. M., Nagel, K. A., Rascher, U., and Postma, J. A. (2016). Sowing density: a neglected factor fundamentally affecting root distribution and biomass allocation of field grown spring barley (Hordeum Vulgare L.). *Front. Plant Sci.* 7:944. doi: 10.3389/fpls.2016.00944

Henry, A., Gowda, V. R. P., Torres, R. O., Mcnally, K. L., and Serraj, R. (2011). Variation in root system architecture and drought response in rice (Oryza sativa): phenotyping of the OryzaSNP panel in rainfed lowland fields. *F. Crop. Res.* 120, 205–214. doi: 10.1016/j.fcr.2010.10.003

Hirel, B., Le Gouis, J., Ney, B., and Gallais, A. (2007). The challenge of improving nitrogen use efficiency in crop plants: towards a more central role for genetic

variability and quantitative genetics within integrated approaches. *J. Exp. Bot.* 58, 2369–2387. doi: 10.1093/jxb/erm097

Ho, M. D., Rosas, J. C., Brown, K. M., and Lynch, J. P. (2005). Root architectural tradeoffs for water and phosphorus acquisition. *Funct. Plant Biol.* 32, 737–748. doi: 10.1071/FP05043

Jackson, R. B., Manwaring, J. H., and Caldwell, M. M. (1990). Rapid physiological adjustment of roots to localized soil enrichment. *Nature* 344, 58–60. doi: 10.1038/344058a0

Jaramillo, R. E., Nord, E. A., Chimungu, J. G., Brown, K. M., and Lynch, J. P. (2013). Root cortical burden influences drought tolerance in maize. *Ann. Bot.* 112, 429–437. doi: 10.1093/aob/mct069

Jia, X., Liu, P., and Lynch, J. P. (2018). Greater lateral root branching density in maize improves phosphorus acquisition from low phosphorus soil. *J. Exp. Bot.* 69, 4961–4790. doi: 10.1093/jxb/ery252

Kadam, N. N., Tamilselvan, A., Lawas, L. M. F. M. F., Quinones, C., Bahuguna, R. N., Thomson, M. J., et al. (2017). Genetic control of plasticity in root morphology and anatomy of rice in response to water-deficit. *Plant Physiol.* 174, 2302–2315. doi: 10.1104/pp.17.00500

Kano, M., Inukai, Y., Kitano, H., and Yamauchi, A. (2011). Root plasticity as the key root trait for adaptation to various intensities of drought stress in rice. *Plant Soil* 342, 117–128. doi: 10.1007/s11104-010-0675-9

Kano-Nakata, M., Gowda, V. R. P., Henry, A., Serraj, R., Inukai, Y., Fujita, D., et al. (2013). Functional roles of the plasticity of root system development in biomass production and water uptake under rainfed lowland conditions. *F. Crop. Res.* 144, 288–296. doi: 10.1016/j.fcr.2013.01.024

Kano-Nakata, M., Inukai, Y., Wade, L. J., Siopongco, J. D., and Yamauchi, A. (2011). Root development, water uptake, and shoot dry matter production under water deficit conditions in two CSSLs of rice: functional roles of root plasticity. *Plant Prod. Sci.* 14, 307–317. doi: 10.1626/pps.14.307

Kirk, G. J. D., Santos, E. E., and Santos, M. B. (1999). Phosphate solubilization by organic anion excretion from rice growing in aerobic soil: rates of excretion and decomposition, effects on rhizosphere pH and effects on phosphate solubility and uptake. *New Phytol.* 142, 185–200. doi: 10.1046/j.1469-8137.1999.00400.x

Lacey, E. P., Smith, S., and Case, A. L. (1997). Parental effects on seed mass: seed coat but not embryo/endosperm effects. *Am. J. Bot.* 84, 1617–1620. doi: 10.2307/2446624

Lambers, H., Clements, J. C., and Nelson, M. N. (2013). How a phosphorus-acquisition strategy based on carboxylate exudation powers the success and agronomic potential of lupines (Lupinus. Fabaceae). *Am. J. Bot.* 100, 263–288. doi: 10.3732/ajb.1200474

Lambers, H., Juniper, D., Cawthray, G. R., Veneklaas, E. J., and Martínez-Ferri, E. (2003). The pattern of carboxylate exudation in *Banksia grandis* (Proteaceae) is affected by the form of phosphate added to the soil. *Plant Soil* 238, 111–122.

Lande, R. (2009). Adaptation to an extraordinary environment by evolution of phenotypic plasticity and genetic assimilation. *J. Evol. Biol.* 22, 1435–1446. doi: 10.1111/j.1420-9101.2009.01754.x

León, J. A. (1993). "Plasticity in fluctuating environments," in *Adaptation in Stochastic Environments*, eds J. Yoshimura and C. W. Clark (Berlin: Springer).

Li, X., Guo, Z., Lv, Y., Cen, X., Ding, X., Wu, H., et al. (2017). Genetic control of the root system in rice under normal and drought stress conditions by genome-wide association study. *PLoS Genet.* 13:1–24. doi: 10.1371/journal.pgen.1006889

Liao, H., Rubio, G., Yan, X., Cao, A., Brown, K. M., and Lynch, J. P. (2001). Effect of phosphorus availability on basal root shallowness in common bean. *Plant Soil* 232, 69–79.

Lobet, G., Paez-Garcia, A., Schneider, H., Junker, A., Atkinson, J. A., and Tracy, S. (2019). Demystifying roots: a need for clarification and extended concepts in root phenotyping. *Plant Sci.* 282, 11–13. doi: 10.1016/j.plantsci.2018.09.015

Lorts, C., Lynch, J. P., and Brown, K. M. (2019). Parental effects and provisioning under drought and low phosphorus stress in common bean. *Food Energy Secur.* 9:e192. doi: 10.1002/fes3.192

Lynch, J. (2013). Steep, cheap and deep: an ideotype to optimize water and N acquisition by maize root systems. *Ann. Bot.* 112, 347–357. doi: 10.1093/aob/mcs293

Lynch, J., and Brown, K. (2001). Topsoil foraging – An architectural adaptation of plants to low phosphorus availability. *Plant Soil* 237, 225–237.

Lynch, J. P. (1995). Root architecture and plant productivity. *Plant Physiol.* 109, 7–13.

Lynch, J. P. (2011). Root phenes for enhanced soil exploration and phosphorus acquisition: tools for future crops. *Plant Physiol.* 156, 1041–1049. doi: 10.1104/pp.111.175414

Lynch, J. P. (2015). Root phenes that reduce the metabolic costs of soil exploration: opportunities for 21st century agriculture. *Plant Cell Environ.* 38, 1775–1784. doi: 10.1111/pce.12451

Lynch, J. P. (2018). Rightsizing root phenotypes for drought resistance. *J. Exp. Bot.* 69, 3279–3292.

Lynch, J. P. (2019). Root phenotypes for improved nutrient capture: an underexploited opportunity for global agriculture. *New Phytol.* 223, 548–564. doi: 10.1111/nph.15738

Lynch, J. P., and Brown, K. M. (2012). New roots for agriculture: exploiting the root phenome. *Philos. Trans. R. Soc. Ser. B* 367, 1598–1604. doi: 10.1098/rstb.2011.0243

Lynch, J. P., Chimungu, J. G., and Brown, K. M. (2014). Root anatomical phenes associated with water acquisition from drying soil: targets for crop improvement. *J. Exp. Bot.* 65, 6155–6166. doi: 10.1093/jxb/eru162

Lynch, J. P., and Wojciechowski, T. (2015). Opportunities and challenges in the subsoil: pathways to deeper rooted crops. *J. Exp. Bot.* 66, 2199–2210. doi: 10.1093/jxb/eru508

Mano, Y., Omori, F., Takamizo, T., Kindiger, B., Bird, R. M. K., and Loaisiga, C. H. (2006). Variation for root aerenchyma formation in flooded and non-flooded maize and teosinte seedlings. *Plant Soil* 281, 269–279. doi: 10.1007/s11104-005-4268-y

Mano, Y., Omori, F., Takamizo, T., Kindiger, B., Bird, R. M., Loaisiga, C. H., and Takahashi, H. (2007). QTL mapping of root aerenchyma formation in seedlings of a maize × rare teosinte "*Zea nicaraguensis*" cross. *Plant Soil* 295, 103–113. doi: 10.1007/s11104-007-9266-9

Manschadi, A. M., Christopher, J., deVoil, P., and Hammer, G. L. (2006). The role of root architectural traits in adaptation of wheat to water-limited environments. *Funct. Plant Biol.* 33, 823. doi: 10.1071/FP06055

Marschner, H. (1995). *Mineral Nutrition of Higher Plants*, 2nd Edn. San Diego, CA: Academic.

Merilä, J., Laurila, A., and Lindgren, B. (2004). Variation in the degree and costs of adaptive phenotypic plasticity among Rana temporaria populations. *J. Evol. Biol.* 17, 1132–1140. doi: 10.1111/j.1420-9101.2004.00744.x

Mi, G. H., Chen, F. J., Wu, Q. P., Lai, N. W., Yuan, L. X., and Zhang, F. S. (2010). Ideotype root architecture for efficient nitrogen acquisition by maize in intensive cropping systems. *Sci. China Life Sci.* 53, 1369–1373. doi: 10.1007/s11427-010-4097-y

Miguel, M., Widrig, A., Vieira, R., Brown, K., and Lynch, J. (2013). Basal root whorl number: a modulator of phosphorus acquisition in common bean (*Phaseolus vulgaris*). *Ann. Bot.* 112, 973–982. doi: 10.1093/aob/mct164

Miguel, M. A., Postma, J. A., and Lynch, J. (2015). Phene synergism between root hair length and basal root growth angle for phosphorus acquisition. *Plant Physiol.* 167, 1430–1439. doi: 10.1104/pp.15.00145

Miklos, G. L. G., and Rubin, G. M. (1996). The role of the genome project in determining gene function: insights from model organisms. *Cell* 86, 521–529. doi: 10.1016/S0092-8674(00)80126-9

Mitchell-Olds, T., Willis, J. H., and Goldstein, D. B. (2007). Which evolutionary processes influence natural genetic variation for phenotypic traits? *Nat. Rev. Genet.* 8, 845–856. doi: 10.1038/nrg2207

Mt. Pleasant, J., and Burt, R. F. (2010). Estimating productivity of traditional iroquoian cropping systems from field experiments and historical literature. *J. Ethnobiol.* 30, 52–79. doi: 10.2993/0278-0771-30.1.52

Nakamoto, T. (1993). Effect of soil water content on the gravitropic behavior of nodal roots in maize. *Plant Soil* 152, 261–267. doi: 10.1007/BF00029096

Negi, S., Ivanchenko, M. G., and Muday, G. K. (2008). Ethylene regulates lateral root formation and auxin transport in Arabidopsis thaliana. *Plant J.* 55, 175–187. doi: 10.1111/j.1365-313X.2008.03495.x

Nicotra, A. B., Atkin, O. K., Bonser, S. P., Davidson, A. M., Finnegan, E. J., Mathesius, U., et al. (2010). Plant phenotypic plasticity in a changing climate. *Trends Plant Sci.* 15, 684–692. doi: 10.1016/j.tplants.2010.09.008

Nielsen, K. L., Eshel, A., and Lynch, J. P. (2001). The effect of phosphorus availability on the carbon economy of contrasting common bean (*Phaseolus vulgaris* L.) genotypes. *J. Exp. Bot.* 52, 329–339. doi: 10.1093/jxb/52.355.329

Nielsen, K. L., Lynch, J. P., Jablokow, A. G., and Curtis, P. S. (1994). Carbon cost of root systems: an architectural approach. *Plant Soil* 165, 161–169. doi: 10.1007/BF00009972

Niones, J. M., Inukai, Y., Suralta, R. R., and Yamauchi, A. (2015). QTL associated with lateral root plasticity in response to soil moisture fluctuation stress in rice. *Plant Soil* 391, 63–75. doi: 10.1007/s11104-015-2404-x

Niones, J. M., Suralta, R. R., Inukai, Y., and Yamauchi, A. (2012). Field evaluation on functional roles of root plastic responses on dry matter production and grain yield of rice under cycles of transient soil moisture stresses using chromosome segment substitution lines. *Plant Soil* 359, 107–120. doi: 10.1007/s11104-012-1178-7

Niones, J. M., Suralta, R. R., Inukai, Y., and Yamauchi, A. (2013). Roles of root aerenchyma development and its associated QTL in dry matter production under transient moisture stress in rice. *Plant Prod. Sci.* 16, 205–216. doi: 10.1626/pps.16.205

Pieruschka, R., and Poorter, H. (2012). Phenotyping plants: genes, phenes and machines. *Funct. Plant Biol.* 39, 813–820. doi: 10.1071/FPv39n11-IN

Pigliucci, M. (2005). Evolution of phenotypic plasticity: where are we going now? *Trends Ecol. Evol.* 20, 481–486. doi: 10.1016/j.tree.2005.06.001

Pigliucci, M., and Schlichting, C. (1995). Ontogenetic reaction norms in Lobelia siphilitica (*Lobeliaceae*): response to shading. *Ecology* 76, 2134–2144.

Poorter, H., Fiorani, F., Pieruschka, R., Putten, W. H., Van Der, Kleyer, M., et al. (2016). Pampered inside, pestered outside? Differences and similarities between plants growing in controlled conditions and in the field. *New Phytol.* 122, 838–855.

Poot, P., and Lambers, H. (2008). Shallow-soil endemics: adaptive advantages and constraints of a specialized root-system morphology. *New Phytol.* 178, 371–381. doi: 10.1111/j.1469-8137.2007.02370.x

Postma, J. A., Dathe, A., and Lynch, J. (2014). The optimal lateral root branching density for maize depends on nitrogen and phosphorus availability. *Plant Physiol.* 166, 590–602. doi: 10.1104/pp.113.233916

Postma, J. A., and Lynch, J. P. (2011). Theoretical evidence for the functional benefit of root cortical aerenchyma in soils with low phosphorus availability. *Ann. Bot.* 107, 829–841. doi: 10.1093/aob/mcq199

Postma, J. A., and Lynch, J. P. (2012). Complementarity in root architecture for nutrient uptake in ancient maize/bean and maize/bean/squash polycultures. *Ann. Bot.* 110, 521–534. doi: 10.1093/aob/mcs082

Prince, S. J., Murphy, M., Mutava, R. N., Durnell, L. A., Valliyodan, B., Grover Shannon, J., et al. (2017). Root xylem plasticity to improve water use and yield in water-stressed soybean. *J. Exp. Bot.* 66, 2027–2036. doi: 10.1093/jxb/erw472

Rabbi, S. M. F., Guppy, C. N., Tighe, M. K., Flavel, R. J., and Young, I. M. (2017). Root architectural responses of wheat cultivars to localised phosphorus application are phenotypically similar. *J. Plant Nutr. Soil Sci.* 180, 169–177. doi: 10.1002/jpln.201600503

Rangarajan, H., Postma, J. A., and Lynch, J. (2018). Co-optimisation of axial root phenotypes for nitrogen and phosphorus acquisition in common bean. *Ann. Bot.* 122, 485–499. doi: 10.1093/aob/mcy092

Relyea, R. (2002). Costs of phenotypic plasticity. *Am. Nat.* 159, 272–282. doi: 10.2307/3079078

Robinson, D., Hodge, A., Gri, B. S., and Fitter, A. H. (1999). Plant root proliferation in nitrogen-rich patches confers competitive advantage. *Proc. R. Soc. Lond.* 266, 431–435.

Rostamza, M., Richards, R. A., and Watt, M. (2013). Response of millet and sorghum to a varying water supply around the primary and nodal roots. *Ann. Bot.* 112, 439–446. doi: 10.1093/aob/mct099

Ryan, M. H., Tibbett, M., Edmonds-Tibbett, T., Suriyagoda, L. D. B., Lambers, H., Cawthray, G. R., et al. (2012). Carbon trading for phosphorus gain: the balance between rhizosphere carboxylates and arbuscular mycorrhizal symbiosis in plant phosphorus acquisition. *Plant Cell Environ.* 35, 2170–2180. doi: 10.1111/j.1365-3040.2012.02547.x

Ryan, P. R., Delhaize, E., and Randall, P. J. (1995). Characterisation of Al-stimulated efflux of malate from the apices of Al-tolerant wheat roots. *Planta* 196, 103–110. doi: 10.1007/BF00193223

Saengwilai, P., Nord, E. A., Chimungu, J. G., Brown, K. M., and Lynch, J. P. (2014a). Root cortical aerenchyma enhances nitrogen acquisition from low-nitrogen soils in maize. *Plant Physiol.* 166, 726–735. doi: 10.1104/pp.114.241711

Saengwilai, P., Tian, X., and Lynch, J. P. (2014b). Low crown root number enhances nitrogen acquisition from low-nitrogen soils in maize. *Plant Physiol.* 166, 581–589. doi: 10.1104/pp.113.232603

Sandhu, N., Raman, K. A., Torres, R. O., Audebert, A., Dardou, A., Kumar, A., et al. (2016). Rice root architectural plasticity traits and genetic regions for adaptability to variable cultivation and stress conditions. *Plant Physiol.* 171, 2562–2576. doi: 10.1104/pp.16.00705

Schlichting, C. D. (1986). The evolution of phenotypic plasticity in plants. *Annu. Rev. Ecol. Syst.* 17, 667–693.

Schneider, H., Klein, S., Hanlon, M., Brown, K., Kaeppler, S., and Lynch, J. (2020a). Genetic control of root anatomical plasticity in maize. *Plant Genome* e20003. doi: 10.1002/tpg2.20003

Schneider, H., Klein, S., Hanlon, M., Nord, E., Kaeppler, S., Brown, K., et al. (2020b). Genetic control of root architectural plasticity in maize. *J. Exp. Bot.* eraa084. doi: 10.1093/jxb/eraa084

Schneider, H. M., and Lynch, J. P. (2018). Functional implications of root cortical senescence for soil resource capture. *Plant Soil* 423, 13–26. doi: 10.1007/s11104-017-3533-1

Schneider, H. M., Postma, J. A., Wojciechowski, T., Kuppe, C., and Lynch, J. (2017a). Root cortical senescence improves barley growth under suboptimal availability of nitrogen, phosphorus, and potassium. *Plany Physiol.* 174, 2333–2347.

Schneider, H. M., Wojciechowski, T., Postma, J. A., Brown, K. M., Lücke, A., Zeisler, V., et al. (2017b). Root cortical senescence decreases root respiration, nutrient content and radial water and nutrient transport in barley. *Plant Cell Environ.* 40, 1392–1408. doi: 10.1111/pce.12933

Schneider, H. M., Wojciechowski, T., Postma, J. A., Brown, K. M., and Lynch, J. P. (2018). Ethylene modulates root cortical senescence in barley. *Ann. Bot.* 28, 95–105. doi: 10.1093/aob/mcy059

Sharma, S., Demason, D. A., Ehdaie, B., Lukaszewski, A. J., and Waines, J. G. (2010). Dosage effect of the short arm of chromosome 1 of rye on root morphology and anatomy in bread wheat. *J. Exp. Bot.* 61, 2623–2633. doi: 10.1093/jxb/erq097

Strock, C. F., Morrow de la Riva, L., and Lynch, J. (2018). Reduction in root secondary growth as a strategy for phosphorus acquisition. *Plant Physiol.* 176, 691–703. doi: 10.1104/pp.17.01583

Sultan, S. (1996). Phenotypic plasticity for offspring traits in Polygonum Persicaria. *Ecol. Monogr.* 77, 1791–1807.

Sultan, S. E. (2000). Phenotypic plasticity for plant development, function and life history. *Trends Plant Sci.* 5, 537–542. doi: 10.1016/S1360-1385(00)01797-0

Sun, B., Gao, Y., and Lynch, J. (2018). Large crown root number improves topsoil foraging and phosphorus acquisition. *Plant Physiol.* 177, 90–104. doi: 10.1104/pp.18.00234

Suralta, R. R., Inukai, Y., and Yamauchi, A. (2010). Dry matter production in relation to root plastic development, oxygen transport, and water uptake of rice under transient soil moisture stresses. *Plant Soil* 332, 87–104. doi: 10.1007/s11104-009-0275-8

Takahashi, H., Yamauchi, T., Rajhi, I., Nishizawa, N. K., and Nakazono, M. (2015). Transcript profiles in cortical cells of maize primary root during ethylene-induced lysigenous aerenchyma formation under aerobic conditions. *Ann. Bot.* 115, 879–894. doi: 10.1093/aob/mcv018

Tardieu, F. (2018). Any trait or trait-related allele can confer drought tolerance: just design the right drought scenario. *J. Exp. Bot.* 63, 25–31. doi: 10.1093/jxb/err269

Tebaldi, C., and Lobell, D. B. (2008). Towards probabilistic projections of climate change impacts on global crop yields. *Geophys. Res. Lett.* 41, 1–14. doi: 10.1029/2008GL033423

Topp, C. N. (2016). Hope in change: the role of root plasticity in crop yield stability. *Plant Physiol.* 172, 5–6. doi: 10.1104/pp.16.01257

Trachsel, S., Kaeppler, S. M., Brown, K. M., and Lynch, J. P. (2013). Maize root growth angles become steeper under low N conditions. *F. Crop. Res.* 140, 18–31. doi: 10.1016/j.fcr.2012.09.010

Tran, T. T., Kano-Nakata, M., Suralta, R. R., Menge, D., Mitsuya, S., Inukai, Y., et al. (2014). Root plasticity and its functional roles were triggered by water deficit but not by the resulting changes in the forms of soil N in rice. *Plant Soil* 386, 65–76. doi: 10.1007/s11104-014-2240-4

Trewavas, A. J., and Malho, R. (1997). Signal perception and transduction: the origin of the phenotype. *Plant Cell* 9, 1181–1195. doi: 10.1105/tpc.9.7.1181

Uga, Y., Okuno, K. and Yano, M. (2008). QTLs underlying natural variation in stele and xylem structures of rice root. 58, 7–14. doi: 10.1270/jsbbs.58.7

Uga, Y., Okuno, K. and Yano, M. (2010). Fine mapping of *Sta1*, a quantitative trait locus determining stele transversal area, on rice chromosome 9. *Mol. Breeding* 26, 533–538. doi: 10.1007/s11032-010-9450-0

Uga, Y., Okuno, K., and Yano, M. (2011). Dro1, a major QTL involved in deep rooting of rice under upland field conditions. *J. Exp. Bot.* 62, 2485–2494. doi: 10.1093/jxb/erq429

Via, S., Gomulkiewicz, R., De Jong, G., Scheiner, S., Schlichting, C., and Van Tienderen, P. (1995). Adaptive phenotypic plasticity: consensus and controversy. *Tree* 10, 212–217. doi: 10.1016/S0169-5347(00)89061-8

Via, S., and Lande, R. (2006). Genotype-environment interaction and the evolution of phenotypic plasticity. *Evolution (N. Y).* 39:505. doi: 10.2307/2408649

Walk, T. C., Jaramillo, R., and Lynch, J. P. (2006). Architectural tradeoffs between adventitious and basal roots for phosphorus acquisition. *Plant Soil* 279, 347–366. doi: 10.1007/s11104-005-0389-6

Wasson, A. P., Richards, R. A., Chatrath, R., Misra, S. C., Prasad, S. V. S., Rebetzke, G. J., et al. (2012). Traits and selection strategies to improve root systems and water uptake in water-limited wheat crops. *J. Exp. Bot.* 63, 3485–3498. doi: 10.1093/jxb/ers111

Weiner, J. (2004). Allocation, plasticity, and allometry in plants. *Perspect. Plant Ecol. Evol. Syst.* 6, 207–215.

Wilson, D. S., and Yoshimura, J. (1994). On the coexistence of specialists and generalists. *Am. Nat.* 144, 692–707.

Woods, J., Williams, A., Hughes, J. K., Black, M., and Murphy, R. (2010). Energy and the food system. *Philos. Trans. R. Soc. B Biol. Sci.* 365, 2991–3006. doi: 10.1098/rstb.2010.0172

Wulff, R., and Bazzaz, F. (1992). Effect of the parental nutrient regime on growth of the progeny in *Abutilon theophrasti* (Malvaceae). *Am. J. Bot.* 79, 1102–1107.

Xie, L., Burridge, J., Klepp, N., Chutoe, C., Miller, J., Saengwilai, P., et al. (2019). "The phenotypic spectrum: identifying whole root architecture types in genotypes of common bean (Phaseolus vulgaris L.)," in *Poster at CROPS 2019*, Huntsville, AL.

Yang, J. T., Schneider, H. M., Brown, K. M., and Lynch, J. P. (2019). Genotypic variation and nitrogen stress effects on root anatomy in maize are node specific. *J. Exp. Bot.* 70, 5311–5325. doi: 10.1093/jxb/erz293

Yano, K., and Kume, T. (2005). Root morphological plasticity for heterogeneous phosphorus supply in *Zea mays* L. *Plant Prod. Sci.* 8, 427–432. doi: 10.1626/pps.8.427

Ye, H., Song, L., Chen, H., Valliyodan, B., Cheng, P., Ali, L., et al. (2018). A major natural genetic variation associated with root system architecture and plasticity improves waterlogging tolerance and yield in soybean. *Plant Cell Environ.* 41, 2169–2182. doi: 10.1111/pce.13190

York, L. M., Nord, E. A., and Lynch, J. P. (2013). Integration of root phenes for soil resource acquisition. *Front. Plant Sci.* 4:355. doi: 10.3389/fpls.2013.00355

Zargar, S. M., Nagar, P., Deshmukh, R., Nazir, M., Wani, A. A., Masoodi, K. Z., et al. (2017). Aquaporins as potential drought tolerance inducing proteins: toward instigating stress tolerance. *J. Proteomics.* 169, 233–238. doi: 10.1016/j.jprot.2017.04.010

Zhan, A., Schneider, H., and Lynch, J. P. (2015). Reduced lateral root branching density improves drought tolerance in maize. *Plant Physiol.* 168, 1603–1615. doi: 10.1104/pp.15.00187

Zhang, C., Postma, J. A., York, L. M., and Lynch, J. P. (2014). Root foraging elicits niche complementarity-dependent yield advantage in the ancient "three sisters" (maize/bean/squash) polyculture. *Ann. Bot.* 114, 1719–1733. doi: 10.1093/aob/mcu191

Zhu, J., Brown, K. M., and Lynch, J. P. (2010a). Root cortical aerenchyma improves the drought tolerance of maize (*Zea mays* L.). *Plant. Cell Environ.* 33, 740–749. doi: 10.1111/j.1365-3040.2009.02099.x

Zhu, J., Zhang, C., and Lynch, J. P. (2010b). The utility of phenotypic plasticity of root hair length for phosphorus acquisition. *Funct. Plant Biol.* 37, 313–322. doi: 10.1071/FP09197

Zhu, J., Kaeppler, S. M., and Lynch, J. P. (2005a). Mapping of QTL controlling root hair length in maize (*Zea mays* L.) under phosphorus deficiency. *Plant Soil* 270, 299–310. doi: 10.1007/s11104-004-1697-y

Zhu, J., Kaeppler, S. M., and Lynch, J. P. (2005b). Mapping of QTLs for lateral root branching and length in maize (*Zea mays* L.) under differential phosphorus supply. *Theor. Appl. Genet.* 111, 688–695. doi: 10.1007/s00122-005-2051-3

Zhu, J., Kaeppler, S. M., and Lynch, J. P. (2005c). Topsoil foraging and phosphorus acquisition efficiency in maize (*Zea mays*). *Funct. Plant Biol.* 32, 749–762. doi: 10.1071/FP05005

Zhu, J., and Lynch, J. P. (2004). The contribution of lateral rooting to phosphorus acquisition efficiency in maize (*Zea mays*) seedlings. *Funct. Plant Biol.* 31, 949–958. doi: 10.1071/FP04046

Conflict of Interest: The authors declare that the research was conducted in the absence of any commercial or financial relationships that could be construed as a potential conflict of interest.

frontiers in Plant Science

ORIGINAL RESEARCH
published: 11 June 2020
doi: 10.3389/fpls.2020.00815

Overexpression of the *NMig1* Gene Encoding a NudC Domain Protein Enhances Root Growth and Abiotic Stress Tolerance in *Arabidopsis thaliana*

Valentin Velinov[1], Irina Vaseva[1], Grigor Zehirov[1], Miroslava Zhiponova[2], Mariana Georgieva[1], Nick Vangheluwe[3,4], Tom Beeckman[3,4] and Valya Vassileva[1]**

[1] Department of Molecular Biology and Genetics, Institute of Plant Physiology and Genetics, Bulgarian Academy of Sciences, Sofia, Bulgaria, [2] Department of Plant Physiology, Faculty of Biology, Sofia University "St. Kliment Ohridski", Sofia, Bulgaria, [3] Department of Plant Biotechnology and Bioinformatics, Ghent University, Ghent, Belgium, [4] VIB-UGent Center for Plant Systems Biology, Ghent, Belgium

OPEN ACCESS

Edited by:
Manny Delhaize, Plant Industry (CSIRO), Australia

Reviewed by:
Men-Chi Chang, National Taiwan University, Taiwan
Vijay Pratap Singh, University of Allahabad, India

***Correspondence:**
Tom Beeckman
tobee@psb.ugent.be
Valya Vassileva
valyavassileva@bio21.bas.bg

Specialty section:
This article was submitted to Plant Abiotic Stress, a section of the journal Frontiers in Plant Science

Received: *15 February 2020*
Accepted: *20 May 2020*
Published: *11 June 2020*

Citation:
Velinov V, Vaseva I, Zehirov G, Zhiponova M, Georgieva M, Vangheluwe N, Beeckman T and Vassileva V (2020) Overexpression of the NMig1 Gene Encoding a NudC Domain Protein Enhances Root Growth and Abiotic Stress Tolerance in Arabidopsis thaliana. Front. Plant Sci. 11:815. doi: 10.3389/fpls.2020.00815

The family of NudC proteins has representatives in all eukaryotes and plays essential evolutionarily conserved roles in many aspects of organismal development and stress response, including nuclear migration, cell division, folding and stabilization of other proteins. This study investigates an undescribed *Arabidopsis* homolog of the *Aspergillus nidulans NudC* gene, named *NMig1* (for *Nuclear Migration 1*), which shares high sequence similarity to other plant and mammalian *NudC*-like genes. Expression of *NMig1* was highly upregulated in response to several abiotic stress factors, such as heat shock, drought and high salinity. Constitutive overexpression of *NMig1* led to enhanced root growth and lateral root development under optimal and stress conditions. Exposure to abiotic stress resulted in relatively weaker inhibition of root length and branching in *NMig1*-overexpressing plants, compared to the wild-type Col-0. The expression level of antioxidant enzyme-encoding genes and other stress-associated genes was considerably induced in the transgenic plants. The increased expression of the major antioxidant enzymes and greater antioxidant potential correlated well with the lower levels of reactive oxygen species (ROS) and lower lipid peroxidation. In addition, the overexpression of *NMig1* was associated with strong upregulation of genes encoding heat shock proteins and abiotic stress-associated genes. Therefore, our data demonstrate that the *NudC* homolog *NMig1* could be considered as a potentially important target gene for further use, including breeding more resilient crops with improved root architecture under abiotic stress.

Keywords: *NudC* gene, *NMig1*, abiotic stress, reactive oxygen species, heat shock proteins, *Arabidopsis thaliana*

INTRODUCTION

Nuclear distribution C (*NudC*) genes encode proteins with high structural and functional conservation from yeast to human (Osmani et al., 1990; Fu et al., 2016). *NudC* has been identified in the filamentous fungus *Aspergillus nidulans* as an essential gene required for the microtubule-dependent migration of cell nuclei and for normal colony growth (Osmani et al., 1990;

Chiu et al., 1997). NudC proteins play roles in diverse cellular processes, including cell division, cell cycle progression, neuronal migration, dynein-dependent functions (Aumais et al., 2003; Zhou et al., 2003; Fu et al., 2016). Homologs of NudC from mammals, Drosophila, *Caenorhabditis elegans* and *Arabidopsis thaliana* complement *nudC3* mutation in *A. nidulans*, and result in the normal movement of nuclei and colony growth (Cunniff et al., 1997; Morris et al., 1997; Dawe et al., 2001). These observations suggest that some functions of NudC are evolutionarily and functionally conserved in different eukaryotic organisms.

The levels of NudC mRNA and protein correlate with the proliferative activity in different cell types and tissues. The human NudC homolog is highly expressed in proliferating cells (Gocke et al., 2000) and participates in spindle formation during mitosis (Zhang et al., 2002). Depletion of NudC leads to the occurrence of multiple spindles during metaphase and induces lagging chromosomes during anaphase (Zhou et al., 2003). Either depletion or overexpression of NudC components induces cytokinesis defects in mammalian cells (Aumais et al., 2003; Zhou et al., 2003). NudC is also intimately involved in the regulation of actin dynamics by stabilizing cofilin 1, a key regulator of actin polymerization and depolymerization (Zhang et al., 2016).

The NudC homologs possess a core CS domain (a domain shared by CHORD-containing proteins and SGT1) that occurs preferably in proteins with chaperone or co-chaperone activities (Lee et al., 2004; Zheng et al., 2011). The CS domain in the NudC family has a molecular architecture similar to small heat shock chaperones, such as p23 and HSP20/alpha-crystallin proteins (Garcia-Ranea et al., 2002). One of the most important functions of p23 and HSP20 is to simultaneously interact with HSP90 and specific client proteins (Lee et al., 2004; Botër et al., 2007). The CS domain is considered as a binding module for HSP90, implying that CS domain-containing proteins are involved in recruiting heat shock proteins (HSPs) to multiprotein complexes (Lee et al., 2004). Experimental evidences support both the HSP90 co-chaperone and intrinsic chaperone functions of the NudC family. For instance, the microtubule-associated *C. elegans* NudC homolog, NUD-1, has shown chaperone activity *in vitro*, inhibiting heat-induced aggregation and precipitation of citrate synthase and luciferase (Faircloth et al., 2009). Human NudC stabilizes Lis1 (lissencephaly protein 1) through HSP90-mediated pathways and exhibits intrinsic chaperone activity *in vitro* preventing aggregation of citrate synthase (Yang et al., 2010; Zhu et al., 2010). There have been only few studies aimed at exploring the functions of NudC proteins in plants (Jurkuta et al., 2009; Perez et al., 2009; Ishibashi et al., 2012; Silverblatt-Buser et al., 2018; Liu et al., 2019). In *A. thaliana*, a gene named *BOBBER1* (*BOB1*), encodes a small 34.5 kDa protein that interacts genetically with two 26S proteasome subunits and maintains a functional proteostasis network enabling proper plant development (Silverblatt-Buser et al., 2018). A partial loss-of-function mutation in *BOB1* results in numerous developmental defects, including obstructed root growth (Perez et al., 2009). BOB1 displays features typical for canonical small heat shock proteins (sHSPs), such as *in vitro* chaperone activity, heat stress induction and the availability of an α-crystallin-like NudC domain (Haslbeck et al., 2005; Perez et al., 2009). At high temperatures, BOB1 colocalizes with HSP17.6 and incorporates into heat shock granules that are formed mainly in the cytoplasm of heat-exposed plant cells (Kirschner et al., 2000; Miroshnichenko et al., 2005). It has been demonstrated that heat exposure of a partial loss-of-function mutant *bob1-3* during germination and at seedling stage leads to reduced thermotolerance, compared to wild-type seeds. This defect can be complemented by a functional *BOB1* transgene, confirming that the phenotype is a result of the reduced BOB1 function (Perez et al., 2009).

In search of regulators of root development, we identified a previously undescribed *Arabidopsis* homolog of the *Aspergillus NudC* gene, named *NMig1* (for *Nuclear Migration 1*), which shares structural similarity to other plant and mammalian *NudC-like* members. Since *NMig1* is a *BOB1* homolog and given the presence of the CS domain, we hypothesized the putative role of *NMig1* in root development and modulation of plant defense systems under stress. Accordingly, we generated *Arabidopsis* plants overexpressing *NMig1* and compared their root phenotypic features and responses to abiotic stress conditions (heat shock, drought, and high salinity) with those in the wild-type plants. Evaluation of the antioxidant status, accumulation of reactive oxygen species (ROS) and lipid peroxidation, as well as analysis of the expression levels of stress-related genes were undertaken. The results obtained strongly suggest a potential regulatory function of *NMig1* in root development and tolerance to abiotic stress.

MATERIALS AND METHODS

Bioinformatics Analysis

The *NMig1* (*At5g58740*) sequence was used as a query to search for *NMig1* homologs from the NCBI database through BLAST analysis. The amino acid sequence of *NMig1* and some of its homologs were aligned using Clustal Omega (Pundir et al., 2016), and the alignment image was generated using BoxShade version 3.21 (K. Hofmann, Koeln, Germany and M. Baron, Surrey, United Kingdom). The accession numbers are as follows: Q8VXX3, NP_200682.1 (*Arabidopsis thaliana*); Q9LV09, NP_200152.1 (*A. thaliana*); Q9STN7, NP_194518.1 (*A. thaliana*); NP_001357629 (*Zea mays*); XP_002467510.1 (*Sorghum bicolor*); XP_015617572.1 (*Oryza sativa*); XP_003579589.1 (*Brachypodium distachyon*); NP_001236519.1 (*Glycine max*); XP_002525640.1 (*Ricinus communis*); XP_002274773.1 (*Vitis vinifera*), and CAL37614 (*Homo sapiens*). The conserved motifs and domain structure of NMig1 protein were analyzed using InterPro scan program[1] (**Supplementary Figure S1**).

Generation of Constructs and Transformation of *Arabidopsis thaliana*

The recombinant plasmids were obtained through the GATEWAY™ recombination cloning technology (Invitrogen Life Technologies). The Entry Clones were generated by inserting

[1] https://www.ebi.ac.uk/interpro/

the coding sequence of *NMig1* into the pDONR221 donor vector, then the Entry Clones were recombined into the destination vectors pK7WG2 or pK7FWG2 [with C-terminal translational green fluorescent protein (GFP) fusion] under the control of *CaMV 35S* promoter and *neomycin phosphotransferase II* (*nptII*) gene for plant selection (Karimi et al., 2007). The generated *35S:NMig1* and *35S:NMig1-GFP* constructs were introduced into *Agrobacterium tumefaciens* strain C58C1 (pMP90), harboring the helper plasmid *pSoup*. The positive clones were selected on agar solidified YEB nutrient medium supplemented with 100 mg l^{-1} rifampicin, 100 mg l^{-1} spectinomycin and 50 mg l^{-1} gentamicin, and subsequently transformed into wild-type Col-0 plants by the floral-dip method (Clough and Bent, 1998). The primary transformants (T_0) were selected on 50 mg l^{-1} kanamycin and their progeny genotyped with gene specific and *nptII* gene primers. The positive transformants were further tested by kanamycin selection and five representative transgenic lines (L1 – L5) were generated. All analyses were carried out with homozygous T_3 seedlings.

Plant Material and Growth Conditions

Arabidopsis thaliana seeds were surface sterilized, stratified for 2 days in the dark at 4°C, and grown on half-strength Murashige and Skoog (1/2MS) (Murashige and Skoog, 1962) medium (pH 5.7) solidified with 1.0% agar at 22°C. To evaluate the root phenotypes of wild-type and transgenic (T_3 generation) plants, approximately 30–35 seeds from each independent transgenic line and controls were plated at least in triplicate and cultivated in a growth chamber under a 16-h light/8-h dark cycle and a light intensity of ∼150 μmol m^{-2} s^{-1}. For all phenotypic analyses, plants were vertically grown on square plates (Greiner Labortechnik) for 10 days unless otherwise stated. For comparison of the root phenotype of transgenic and wild-type plants, *NMig1*-overexpressing lines were co-cultivated with the wild-type plants on the same agar plates divided into two equal parts. Each plate contained seedlings of one individual transgenic line and Col-0. To analyze responses to abiotic stress, 5-day-old seedlings were transferred to plates containing solid 1/2MS medium supplemented with or without 150 mM sorbitol or 150 mM NaCl and scanned every day. Heat stress was applied by exposure of 8-day-old seedlings to 42°C for 1 h and subsequently transferred into a growth chamber for 2 additional days of growth under optimal conditions. Untreated wild-type and transgenic plants were used as controls and these were grown at the same time as the individuals subjected to the stress treatments.

Morphological Characterization of Roots

Plates were scanned every day with an Epson Perfection V850 Pro scanner. Root length was quantified using the image processing software ImageJ 1.48 (National Institutes of Health, Bethesda, MD, United States), and the visible lateral roots were counted and calculated per seedling. Non-emerged lateral root primordia were quantified on the roots of 10-day-old seedlings after root clearing (Malamy and Benfey, 1997). The stress-induced inhibition of primary root growth, formation of lateral root primordia and emerging lateral roots was calculated in percentages for each genotype as a difference between growth and branching under control and stress conditions. The density of lateral root formation events was quantified by dividing the total number of emerged lateral roots plus lateral root primordia by the primary root length, and expressed as lateral root formation events per cm of primary root. In each experiment, the root system of at least 30 plants was examined under an Olympus BX51 upright microscope with a differential interference contrast (DIC) and XC50 digital microscope camera.

Confocal Microscopy and Image Analysis

Fluorescent images were acquired on an inverted laser scanning confocal microscope Zeiss LSM 710 using the ZEN software package (Carl Zeiss, Germany) after excitation by a 488 nm argon laser and detected using the bandpass 505–530 nm emission filter setting. Autofluorescence of photosynthetic pigments was observed after excitation with a 543 nm helium-neon (He-Ne) laser and detected using the bandpass 560–615 nm emission filter. The root apical meristem was imaged on an Andor Dragonfly spinning disk confocal system equipped with the Fusion software (Andor Technologies, Inc.) and iXon897 EMCCD camera at 488 nm laser excitation. Confocal images were processed with ImageJ1.52r or the CellTool software[2] (Danovski et al., 2018).

Determination of Free Radical Scavenging Activity and Antioxidant Status

Fresh plant material (200 mg) was frozen in liquid nitrogen, grinded to fine powder in TissueLyser LT (QIAGEN) and mixed with 500 μl ice-cold 80% ethanol. The samples were centrifuged at 10 000 rpm for 30 min at 4°C and the supernatants were used for determination of antiradical activity by 2,2′-diphenyl-1-picrylhydrazyl (DPPH) Radical Scavenging assay, according to Brand-Williams et al. (1995), and antioxidant capacity by Ferric Reducing Antioxidant Power (FRAP) assay, as decribed by Benzie and Strain (1999).

The antiradical activity of the plant extract (40 μl) was measured by mixing it with DPPH solution (960 μl) in methanol (6.10^{-5}M). The absorbance of the reaction solution at 515 nm was determined after 30 min of incubation at room temperature in the dark. The rate of antiradical activity was calculated by Trolox standard curve and the results were represented as μmol Trolox g^{-1} FW.

The antioxidant capacity assay is based on the reduction of ferric tripyridyl-s-triazine (Fe^{3+}-TPTZ) complex to the blue colored ferrous (Fe^{2+}) form by the antioxidants present in the plant extract. Briefly, 50 μl of the supernatant was mixed with 1.5 ml of freshly prepared FRAP reagent (0.3 M acetate buffer, 0.01 M TPTZ in 0.04 M HCl and 0.02 M $FeCl_3.6H_2O$ in 10:1:1 proportion) and 150 μl distilled water. The optical density was spectrophotometrically determined after 15 min at 593 nm. Antioxidant capacity was expressed as μmol FRAP g^{-1} FW.

[2] dnarepair.bas.bg/software/CellTool

Measurement of Lipid Peroxidation and Hydrogen Peroxide Content

Fresh plant material (200 mg) was frozen in liquid nitrogen, grinded to fine powder in TissueLyser LT (QIAGEN) and mixed with 0.1% trichloroacetic acid (w/v) (TCA). The samples were centrifuged at 10 000 rpm for 30 min at 4°C and the supernatant was used for determination of lipid peroxidation and H_2O_2 content.

Lipid peroxidation was determined by the thiobarbituric (TBA) method, which quantifies the amount of malondialdehyde (MDA) as the end product of the lipid peroxidation (Hodges et al., 1999). Reaction mixture contained 500 μl supernatant, 500 μl 0.1 M phosphate buffer (pH 7.3) ant 1 ml TBA (0.5% w/v). The samples were placed in a boiling water bath for 45 min. After cooling on ice, the sample absorbance was read at 440, 532, and 600 nm. The MDA extinction coefficient (ε = 155 mM^{-1} cm^{-1}) was used for calculations of MDA concentration and expressed as nmol g^{-1} FW.

Hydrogen peroxide (H_2O_2) content was determined according to Wolff (1994). One ml of 0.1% TCA extract was mixed with 1.9 ml reagent (composed by 100 μM xylenol orange, 250 μM ammonium ferrous sulphate, and 100 mM sorbitol in 25 mM H_2SO_4). The absorbance of the reactions was evaluated spectrophotometrically at 560 nm after 30 min incubation at room temperature and H_2O_2 extinction coefficient used for the calculations was $\varepsilon = 2.24 \times 10^5$ M^{-1} cm^{-1}.

In situ ROS Assays

In situ detection of reactive oxygen species (ROS) accumulation was performed by nitroblue tetrazolium (NBT) and diaminobenzidine (DAB) staining methods, according to Kumar et al. (2014) with slight modifications, as described in Nguyen et al. (2017). For tissue-specific detection of the superoxide anion (O^{2-}) abundance, 6-day-old *A. thaliana* plants grown on 1/2MS, were stained in freshly prepared 0.05% NBT (w/v) in 50 mM sodium phosphate buffer (pH 7.4) for 30 min, covered with aluminum foil and incubated on a lab shaker (80 rpm) at room temperature. To detect H_2O_2 content, the seedlings were stained for 1 h in 1 mg ml^{-1} DAB dissolved in 10 mM Na_2HPO_4 (freshly prepared). After the incubation in NBT and DAB solutions, the seedlings were transferred into bleaching solution (ethanol: acetic acid: glycerol in ratio 3:1:1) and kept at 4°C overnight. The analyzes of the samples were performed on the following day on an Olympus BX51 upright microscope coupled to an XC50 digital microscope camera.

RNA Extraction and Gene Expression Analysis

Total RNA was extracted using the Trizol reagent (Invitrogen), followed by clean-up with RNeasy Mini Kit (Qiagen), including DNase I (Qiagen) treatment, according to the manufacturer's protocols. The quantity and quality of RNA samples were evaluated with Thermo Fisher Scientific NanoDrop 1000 Spectrophotometer. Complementary DNA (cDNA) was synthesized from 1 mg of total RNA with the iScript cDNA Synthesis Kit (Bio-Rad), according to the manufacturer's instructions. The quantitative PCR analysis was carried out in a BioRad CFX96 real time C1000 thermal cycler with SsoFast EvaGreen supermix (BioRad) or in a LightCycler 480 system (Roche Diagnostics) with the SYBR Green I Master kit (Roche Diagnostics), according to the manufacturer's instructions. Conventional PCR analysis was performed with the same cDNA templates in a PCR Eppendorf Mastercycler (Eppendorf, Germany). Primer pairs were designed with Beacon Designer 4.0 (Premier Biosoft International) or Primer 3.0 (Untergasser et al., 2012). Efficiency curves were generated for each primer set and amplification efficiency between 98 and 102% was considered acceptable for a quantitative gene expression analysis (Raymaekers et al., 2009). Expression levels were normalized to those of *EF1α* and *CDKA1;1*. The average Cycle threshold (Ct) values of the reference genes *EF1α* and *CDKA1;1* were calculated using three untreated biological replicates. Delta Ct (ΔCt) values were obtained by subtracting from the average reference Ct values the individual Ct values of each treated and untreated sample within a specific gene dataset. The relative quantity (RQ = 2^ΔCt) and the normalization factor [NF = RQ (*EF1α* + *CDKA1;1*)] were used to calculate the normalized expression of the genes of interest. In semi-quantitative analyses, *EF1α* was used as a reference gene. Each individual sample was analyzed in triplicate. The list of specific primer sets for the monitored genes is provided in **Supplementary Table S1**.

Statistical Analysis

All values reported in this study are the means of at least three independent experiments with three replicates, unless otherwise stated. Mean data from all plants on a single plate were used to generate a single replicate. The significance of the results and statistical differences were analyzed using Statgraphics Plus 5.1 software (Statistical Graphics, Warrenton, VA, United States). The data were evaluated by multifactor analysis of variance and expressed as mean ± standard error (SE). A *p*-value equal to or lower than 0.05 was considered statistically significant.

Accession Numbers

The Arabidopsis Information Resource (TAIR) locus identifiers for the genes mentioned in this study are *At5g58740* for *NMig1*, *At5g53400* for *BOB1*, *At4g27890* for *BOB2*, *At3g53990* for *USP17*, *At4g27320* for *USP21*, *At1g08830* for *SOD1*, *At1g20630* for *CAT1*, *At4g35090* for *CAT2*, *At1g07890* for *APX1*, *At2g33210* for *HSP60*, *At4g24190* for *HSP90*, *At1g74310* for *HSP101*, *At5g52310* for *RD29A*, *At2g01980* for *SOS1*, *At1g07940* for *EF1a*, and *At3g48750* for *CDKA1;1*.

RESULTS

NMig1 Is a Small HSP With NudC Domain

Proteins belonging to the NudC family contain a highly conserved NudC domain of approximately 140 amino acids that share significant sequence similarity in different species (**Supplementary Figure S1**). The *A. thaliana NMig1* (locus *At5g58740*) gene is located in chromosome 5 (Chr5: 23725675-23727628), and consists of five exons and four introns. The

deduced protein sequence (accession number AED97093.1) is annotated in the databases as a "HSP20-like chaperones superfamily protein." The coding sequence of *NMig1* is 477 bp in length and encodes a protein of 158 amino acids with a molecular mass of 18.2 kDa (pI 5.77) (Aramemnon database; Schwacke et al., 2003).

According to the *Arabidopsis* developmental and root maps in the eFP Browser (electronic Fluorescent Pictograph[3]), *NMig1* is expressed in an organ specific manner (**Supplementary Figure S2**). The developmental map showed that the highest expression level (expression potential) in the leaves, stem, flowers, pollen and seeds was about 510 absolute signal value (a.s.v.) (**Supplementary Figure S2A**). In the root, the *NMig1* expression potential reached about 2766 a.s.v. depending on the growth conditions. At tissue resolution within the root, the highest level of *NMig1* expression was found in the lateral root cap and columella cells (**Supplementary Figure S2B**).

In the *A. thaliana* genome, besides *NMig1*, two additional genes encode proteins with NudC domain, *BOB1* (*At5g53400*) and *BOB2* (*At4g27890*) (**Supplementary Figure S1**; Jurkuta et al., 2009; Perez et al., 2009). BOB1 and BOB2 show weak sequence similarity to NMig1. BOB1 displays 42.1% similarity, 27.3% identity, gaps 48.6% and overlap in 40 amino acids when compared to NMig1. BOB2 has 41.4% similarity, 30.7% identity, gaps 47% and overlap in 42 amino acids [The European Bioinformatics Institute, Pairwise Sequence Alignment, accession numbers: AAO23639.1 (BOB1), AEE85405.1 (BOB2)].

In addition, protein sequence analysis revealed the presence of a CS (CHORD-containing proteins and SGT1) domain (PF04969) that is typical for proteins functioning as independent sHSPs or co-chaperones of other HSPs (Zheng et al., 2011). The CS domain encompasses almost all of NMig1 protein and consists of approximately 100 amino acids. Comparison of NudC family members in different species displayed conservation of CS domain sequences across monocots and dicots, and also human (**Supplementary Figure S1**).

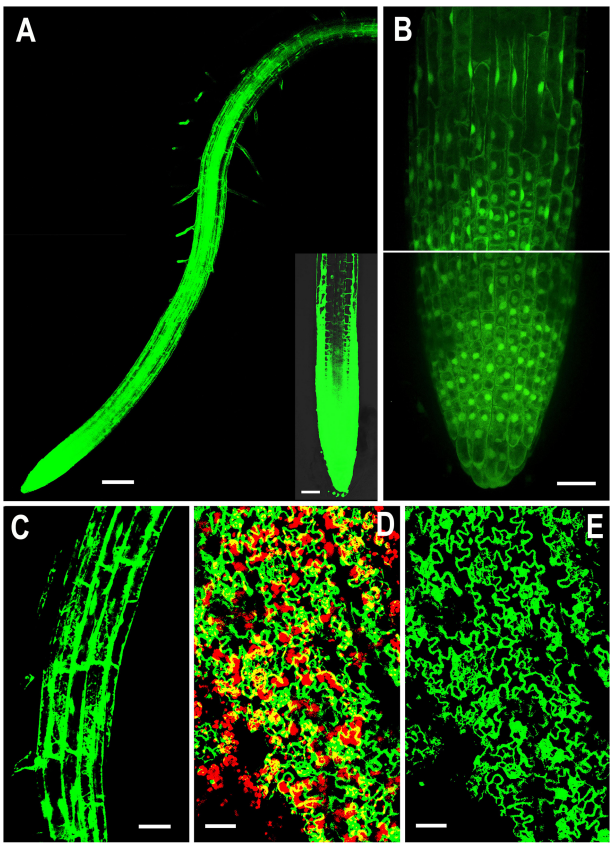

FIGURE 1 | Representative confocal images showing localization of overexpressed *NMig1* gene in the root and leaf tissues of 6-day-old *Arabidopsis thaliana*. Expression pattern of *35S:NMig1-GFP* in: **(A)** primary root, **(B)** primary root meristem, **(C)** cells from root elongation zone, **(D)** and **(E)** leaf epidermal cells and chlorophyll autofluorescence (red). Scale bars: **(A)** 100 μm; **(B)**, **(D)** and **(E)** 20 μm; **(C)** 50 μm.

Expression Patterns and Root System Architecture of *NMig1* Overexpressors

To investigate the biological functions of *NMig1*, we constructed five transgenic lines (L1, L2, L3, L4, and L5) that stably expressed *NMig1* under the control of *CaMV 35S* promoter. In lines L4 and L5, the *NMig1* gene was fused upstream of a reporter gene encoding the green fluorescent protein (GFP) (**Figure 1**). Quantification of *NMig1* expression in the generated homozygous lines revealed strong upregulation of *NMig1* transcripts, which increased between 35- and 50-fold compared to the wild-type values (**Figure 2**). Based on the obtained results, the lines with the highest *NMig1* expression levels (L2, L3 for *35S:NMig1* and L5 for *35S:NMig1-GFP*), were chosen for further phenotypic analyses and assessment of abiotic stress response.

Examination of the transgenic lines harboring the *35S:NMig1-GFP* construct demonstrated very strong expression in the primary roots, as the most intense signal was seen in the root apical meristem (**Figure 1A**). At the cellular level, high strength of the GFP signal was detected in the cytoplasm, in the nuclei, excluding the nucleolus (**Figure 1B**), as well as in the membrane and endomembrane systems (**Figure 1C**). Confocal imaging also showed intense GFP signal in the leaf epidermis, which was particularly strong in stomatal guard cells (**Figures 1D,E**). Overlap of *NMig1-GFP* and red chlorophyll autofluorescence in the leaf chloroplasts could be seen as yellow patches (**Figure 1D**).

After 10 days of growth, a detailed phenotypic analysis was carried out to compare root growth and branching in the lines with ectopic expression of *NMig1* and the wild-type plants (**Figures 3A–D**). Under favorable growth conditions, all transgenic lines, overexpressing *NMig1*, displayed significantly greater primary root length (between 18 and 28%), as compared to the wild-type Col-0 (**Figure 3C**). The number of lateral roots was also enhanced, as the increase ranged between 33 and 50% in the different transgenic lines. To assess whether this increase was caused by enhanced lateral root initiation events, we additionally quantified the number of non-emerged lateral root primordia in the roots of *NMig1* overexpressors and the wild-type Col-0

[3]http://bar.utoronto.ca/efp/cgi-bin/efpWeb.cgi

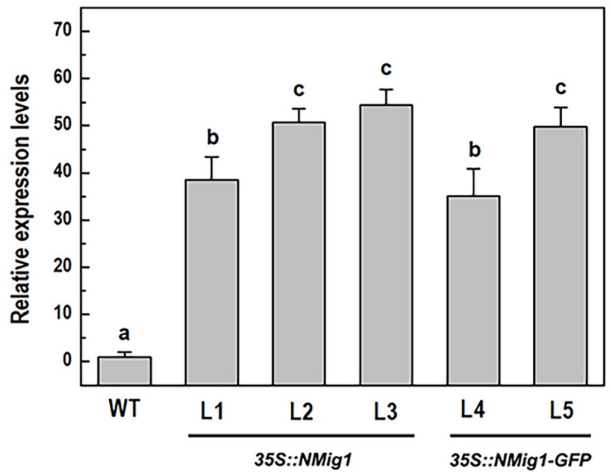

FIGURE 2 | Expression analysis of the *NMig1* gene in 10-day-old wild-type seedlings and homozygous transgenic lines overexpressing *NMig1* (L1-L5). Expression levels were normalized to those of *EF1a* and *CDKA1;1*, as described in Materials and Methods. Data represents the mean values ± SE from at least three biological replicates. Different lowercase letters indicate statistically significant difference ($p \leq 0.05$).

(**Figure 3D**). The results showed an increased number of lateral root primordia (between 24 and 66%) in transgenic lines, as compared to the controls. Calculation of the density of all events associated with lateral root development that include emerged lateral roots and developing non-emerged primordia estimated as a function of primary root length, revealed 26% greater density of the formative events in L2 and L5, compared to the wild-type Col-0. In L3, despite that the number of all events associated with lateral root development increased about 30%, the calculated density did not show statistically significant difference from the control (**Figure 3D**).

Differential Expression of *NMig1* Under Exposure to Abiotic Stress

Given the presence of the CS domain, which has structural homology to the HSP90 co-chaperone p23 (Botër et al., 2007), we checked the possibility of involvement of NMig1 in abiotic stress responses. To study this experimentally, we quantified the *NMig1* transcript abundance after exposure of the wild-type Col-0 plants to heat shock, drought or high salinity (**Figure 4**). Expression of *NMig1* was significantly upregulated by all the applied stress treatments between 1.5- and 2.5-fold, compared to the control (**Figure 4A**). The degree of the *NMig1* stress induction was compared with that of two genes encoding universal stress proteins (USPs), *USP17* and *USP21*. The USPs are involved in a wide range of stress responses, and in general, their overexpression enhances stress tolerance and alleviates the oxidative damage through the activation of oxidative stress-responsive genes and the removal of intracellular ROS (Chi et al., 2019). Both *USP* genes studied were upregulated by the

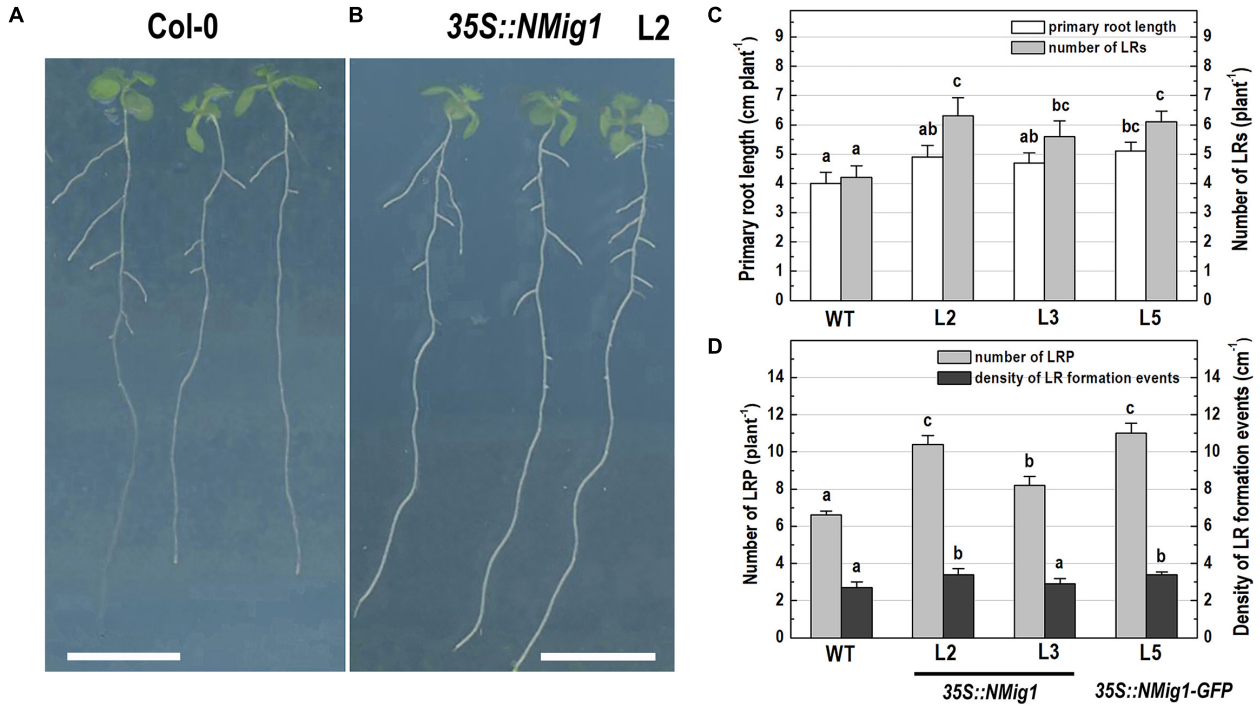

FIGURE 3 | Primary root length and lateral root development of 10-day-old wild-type Col-0 seedlings **(A),** and transgenic lines overexpressing *NMig1* (L2, L3, and L5) **(B)** under optimal growth conditions: **(C)** average length of the primary root and number of lateral roots; **(D)** number of lateral root primordia and density of lateral root formation events. Different lowercase letters indicate statistically significant difference ($p \leq 0.05$). Scale bar = 1.0 cm.

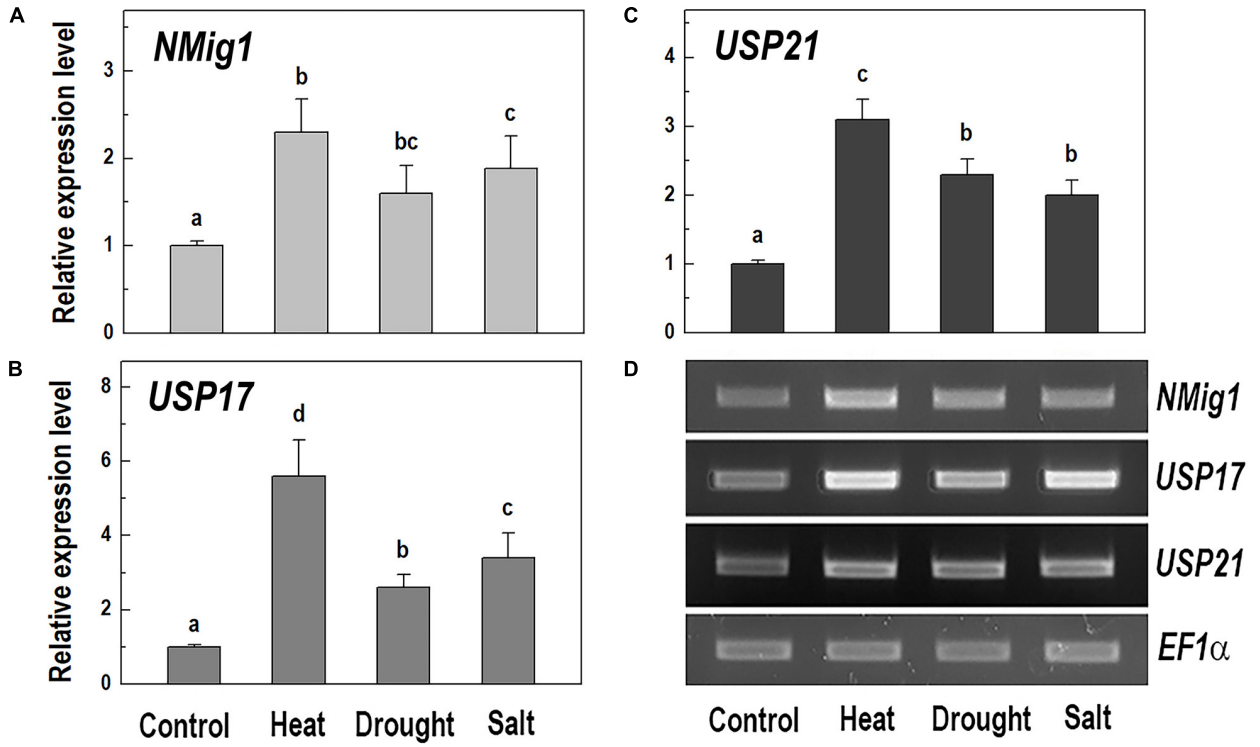

FIGURE 4 | Quantitative RT-PCR **(A–C)** and semi-quantitative RT-PCR analysis **(D)** of the expression levels of *NMig1* **(A)**, and the universal stress proteins *USP17* **(B)**, and *USP21* **(C)** in 10-day-old wild-type seedlings subjected to heat shock, drought and high salinity. Expression levels were normalized to those of *EF1a* and *CDKA1;1*, as described in Materials and Methods. For semi-quantitative RT-PCR analysis *EF1α* was used as a reference gene. Data represents the mean values ± SE from at least three biological replicates. Different lowercase letters indicate statistically significant difference ($p \leq 0.05$).

applied stress treatments (**Figures 4B–D**) with increases of 2.6- to 5.6-fold for *USP17* and 2.0- to 3.1-fold for *USP21*, compared to those of untreated controls. Thus, the stress-induced expression changes of *NMig1* were of similar magnitude and direction to those found for the studied USPs. The transcript abundance of the reference gene *EF1α* did not change under different experimental conditions (**Figure 4D**).

Overexpression of *NMig1* Promotes Root Growth and Branching Under Abiotic Stress

The response of transgenic plants to abiotic stress factors was analyzed in *NMig1* overexpressors and the wild-type Col-0 grown under the above-mentioned stress conditions, heat stress, drought and high salinity (**Figure 5**). Evaluation of the root system morphology when compared showed that all *NMig1*-overexpressing lines were more tolerant toward the tested abiotic factors since the stress-mediated reduction of root growth and branching was significantly lower, compared to the wild-type Col-0 (**Figures 5A,B** and **Supplementary Figures S3A–L**), as visualized by presenting the relative inhibition of the primary root growth and branching under each stress treatment within the tested genotypes (**Figures 5A,B**). The most obvious beneficial effect of the *NMig1* overexpression was seen for the number of lateral root primordia (**Figure 5C**) and density of all branching events under heat stress and salinity (**Figure 5D**). The heat- and salt-mediated reductions in these parameters were significantly lower in *NMig1*-overexpressing lines, compared to Col-0. Exposure to heat stress resulted in more than 20% inhibition in the density of all initiation and formative events associated with lateral root development in Col-0, whereas in the overexpressors L2 and L3, this parameter was inhibited by only about 6% (**Figure 5D**). Similarly, the inhibitory effect of drought and salinity on the density of all lateral root initiation events was at least twice lower in L2 and L3 than that observed in the wild-type.

NMig1 Overexpression Improves Free Radical Scavenging Activity and Antioxidant Status

To further elucidate the abiotic stress responses of the transgenic plants, the effect of *NMig1* overexpression on the antioxidant status was monitored using two antioxidant assays, DPPH (**Figure 6A**) and FRAP (**Figure 6B**). Both analyses displayed that antioxidant status did not differ in unstressed transgenic and wild-type plants. The DPPH radical scavenging activity was increased by the overexpression of *NMig1* under all applied stress factors (**Figure 6A**). The assessment of antioxidant activity also showed higher stress-induced levels in the transgenic lines, as compared to the wild-type Col-0. Thus, both antioxidant assays

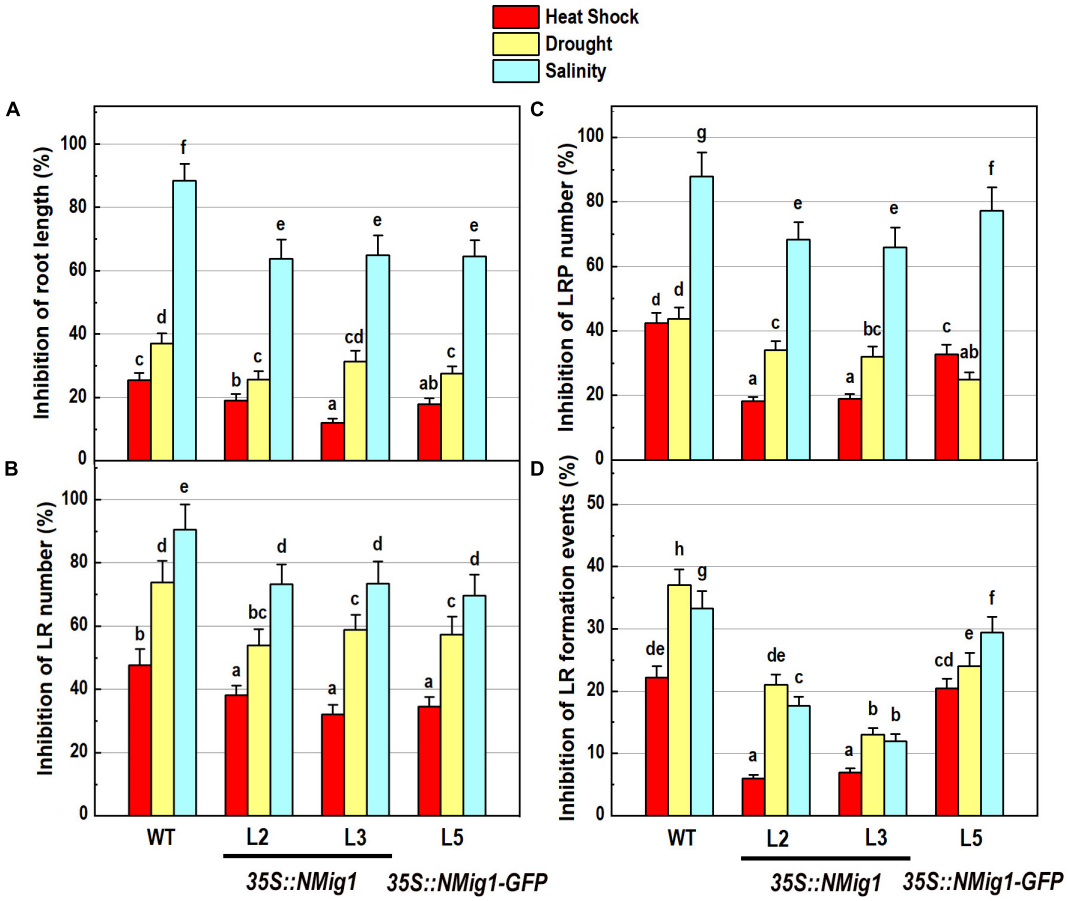

FIGURE 5 | Inhibitory effect of various abiotic stress factors (heat shock, drought and salinity) on primary root length and lateral root development of 10-day-old wild-type seedlings and transgenic lines overexpressing *NMig1* (L2, L3, and L5): **(A)** inhibition of the primary root length, **(B)** inhibition of the number of lateral roots, **(C)** inhibition of the number of lateral root primordia, and **(D)** inhibition of the density of lateral root formation events. Different lowercase letters indicate statistically significant difference ($p \leq 0.05$).

showed similar trends of change manifested by lower values in the stress-treated wild-type seedlings and higher values in the transgenic lines (**Figures 6A,B**).

Hydrogen peroxide is one of the most common and early produced ROS in stress-treated plants and comparison of H_2O_2 content in *NMig1*-overexpressing and Col-0 plants displayed considerably reduced H_2O_2 production in the transgenic lines (**Figure 6C**). The most obvious difference between *NMig1*-overexpressors and Col-0 plants was observed under heat stress. Exposure of Col-0 to heat shock led to more than 2-fold higher H_2O_2 accumulation, compared to transgenic plants. Under salinity stress, the content of $O2^{\bullet-}$ H_2O_2 greatly increased in both the wild-type Col-0 and *NMig1* overexpressors. However, this increase was less pronounced in the transgenic than in the wild-type seedlings.

Since ROS usually induce the peroxidation of membrane lipids, a quantitative assay was carried out to compare the level of lipid peroxidation, determined by the amount of MDA (**Figure 6D**). At control conditions, no significant difference in MDA content was detected between the *NMig1*-overexpressing and wild-type plants. However, the applied abiotic stresses induced greater accumulation of MDA in Col-0, as compared to that in *NMig1* overexpressors. Exposure to high salinity increased about 4.0-fold the content of MDA in Col-0 and less than 2.0-fold in the transgenic lines, compared to the respective controls. Similarly, under heat shock and drought *NMig1* overexpressors accumulated lower levels of MDA, compared to the wild-type Col-0.

In addition, to evaluate the effect of *NMig1* overexpression on the stress-induced production of reactive oxygen species (ROS) in plant roots, the formation of superoxide anion ($O2^{\bullet-}$) and hydrogen peroxide (H_2O_2) was monitored using NBT (**Figure 7**) and DAB staining (**Figure 8**), respectively. Under benign growth conditions, both staining procedures showed that the $O2^{\bullet-}$ and H_2O_2 levels in transgenic and wild-type plants exhibited no differences (**Figures 7A,E**, **8A,E**). Abiotic stresses, however, led to a higher accumulation of $O2^{\bullet-}$ and H_2O_2 in Col-0, where in the plant roots strong blue (**Figures 7B–D**) and brown (**Figures 8B–D**) staining was visualized. The most obvious difference between the *NMig1*-overexpressing

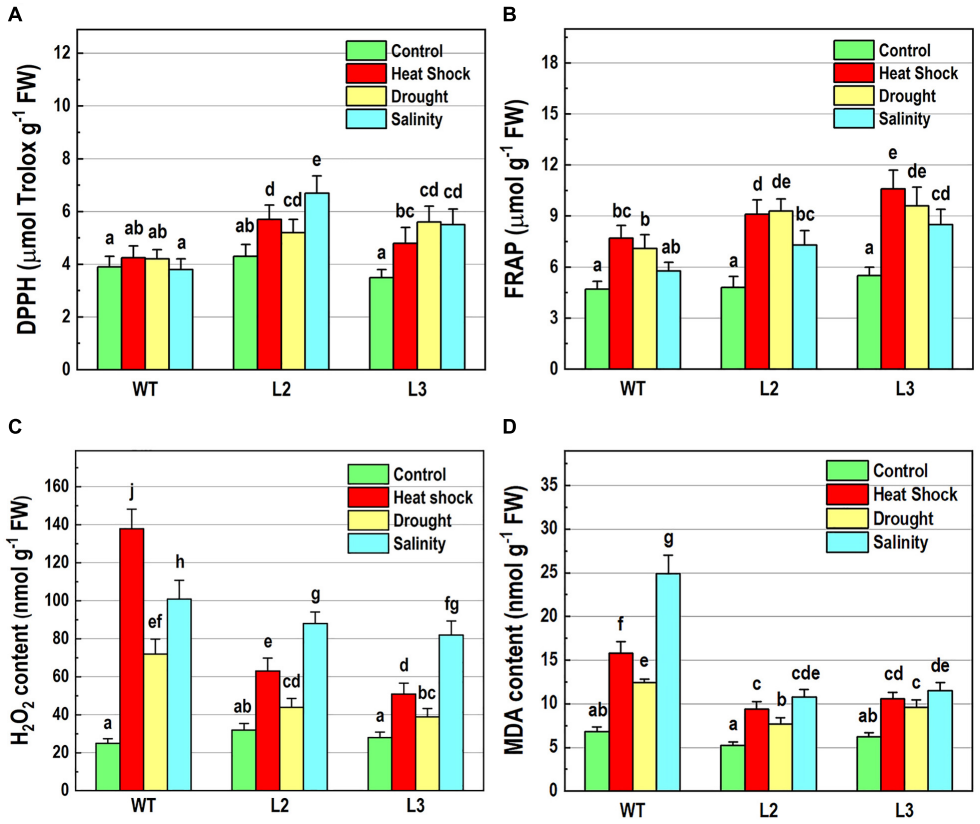

FIGURE 6 | Determination of antioxidant-related parameters in 10-day-old wild-type seedlings and transgenic lines overexpressing *NMig1* (L2 and L3) after exposure to heat shock, drought and high salinity: **(A)** free radical scavenging activity, **(B)** antioxidant capacity, **(C)** hydrogen peroxide (H_2O_2) content, and **(D)** malondialdehyde (MDA) level. Different lowercase letters indicate statistically significant difference ($p \leq 0.05$).

plants and the wild-type Col-0 was detected under heat stress (**Figures 7B,F**, **8B,F**). The accumulation of $O2^{\bullet-}$ in the heat-treated roots of Col-0 was very strong (**Figure 7B**), whereas in the *NMig1* overexpressors, the NBT staining intensity was compatible to the control level (**Figure 7F**). Exposure to drought and salinity also showed distinct staining patterns in Col-0 (**Figures 7C,D**, **8C,D**) and in the transgenic plants (**Figures 7G,H**, **8G,H**), but the difference in $O2^{\bullet-}$ and H_2O_2 contents between treated and untreated seedlings was considerably lower.

Overexpression of *NMig1* Changed the Expression of Stress-Related Genes

To explore the molecular mechanisms behind ROS detoxification under stress conditions, mediated by *NMig1* overexpression, we compared the expression levels of several genes encoding major enzymes involved in antioxidant defense (**Figure 9**) and other stress-related maker genes (**Figure 10**) in the transgenic plants and the wild-type Col-0. Very low expression of the genes *SOD1*, *CAT1*, *CAT2*, and *APX1*, encoding the ROS scavenging enzymes superoxide dismutase 1, catalase 1, catalase 2 and ascorbate peroxidase 1, respectively, was detected in the control plants (**Figures 9A–D**). The quantitative expression analysis revealed profound stress-induced upregulation of these genes in both the wild-type and *NMig1* overexpressors. More specifically, exposure of wild-type plants to heat shock, drought and salinity, increased the level of *SOD1* transcripts by 3.3-, 13-, and 14.8-fold, respectively, compared to untreated controls (**Figure 9A**). The expression levels of *CAT1* and *CAT2* also showed differential responses depending of the stress type (**Figures 9B,C**). In both the wild-type and *NMig1* overexpressors, *CAT1* was maximally induced by drought and salt stress (**Figure 9B**), while *CAT2* had the highest expression levels (more than 30-fold upregulation) under heat shock in the transgenic lines (**Figure 9C**). Similar expression pattern was observed for *APX1* after the plant exposure to heat shock, where the *APX1* expression increased by 12.5-fold in the wild-type but reached more than 25.0-fold in L2 and L3 (**Figure 9D**). When challenged with drought and salinity, the transgenic lines also showed higher accumulation of *APX1* transcripts, but the relative increase in the gene expression was lower, as compared to the control.

Additionally, the applied stress factors led to upregulation of genes encoding heat shock proteins, *HSP60*, *HSP90*, and *HSP101* (**Figures 10A–C**), and the abiotic stress-responsive genes *RD29A* and *SOS1* (**Figures 10D,E**). Exposure to stress of the wild-type plants resulted in an increase of all studied genes, however, this increase was much lower than that observed in the transgenic

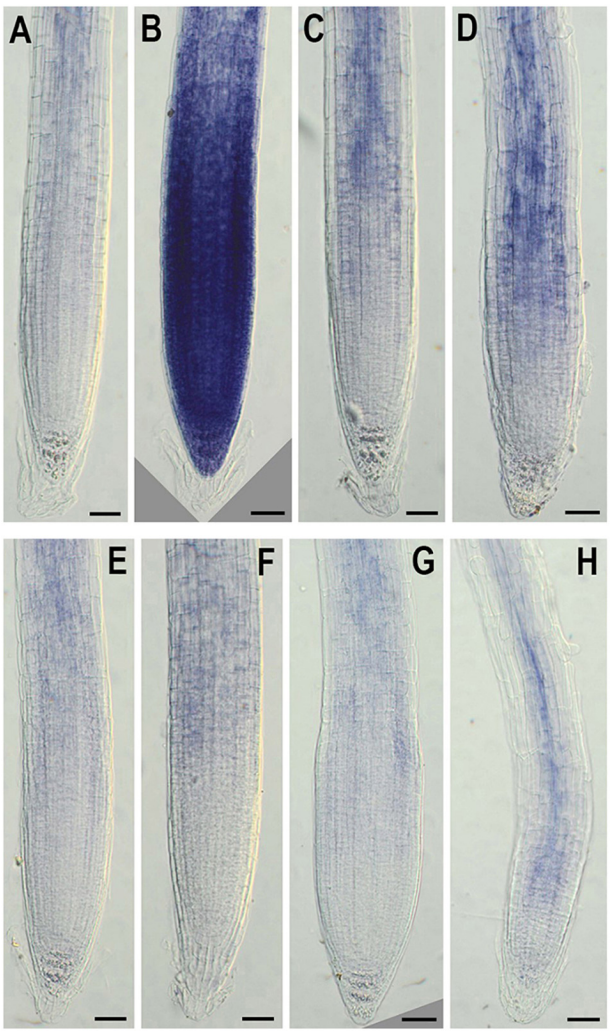

FIGURE 7 | *In situ* detection of $O2^{\bullet-}$ by nitroblue tetrazolium (NBT) staining in 6-day-old wild-type **(A–D)** and *NMig1*-overexpressing **(E–H)** seedlings under optimal growth conditions **(A,E)**, and after exposure to heat shock **(B,F)**, drought **(C,G)** and high salinity **(D,H)**. Representative images from three independent experiments are shown. Scale bars = 50 μm.

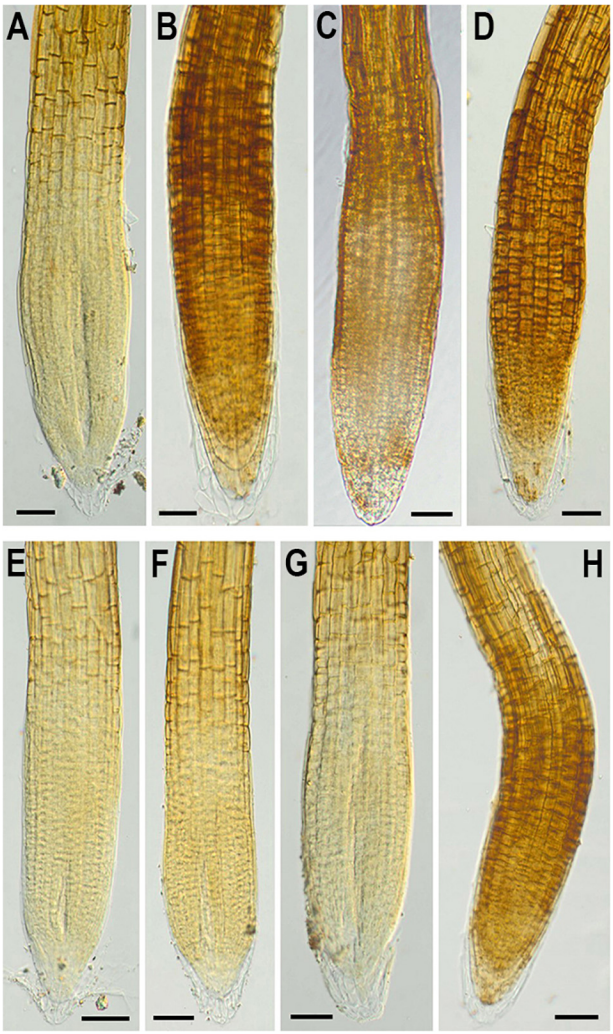

FIGURE 8 | *In situ* detection of H_2O_2 by 3,3-diaminobenzidine (DAB) staining in 6-day-old wild-type **(A–D)** and *NMig1*-overexpressing **(E–H)** seedlings under optimal growth conditions **(A,E)**, and after exposure to heat shock **(B,F)**, drought **(C,G)**, and high salinity **(D,H)**. Representative images from three independent experiments are shown. Scale bars = 50 μm.

lines (**Figures 10A–E**). In *NMig1*-overexpressing plants, the heat stress induced greater accumulation of *HSP60* and *HSP101* transcripts, between 3.3-fold and 28.5-fold, compared to the transcript abundance in the same lines under benign growth conditions (**Figures 10A,C**). Sorbitol-mediated drought stress and high salinity led to an increase in the expression of *HSP60*, *RD29A* and *SOS1* between 3.3-fold and 7.25-fold, compared to the expression levels detected under optimal conditions.

DISCUSSION

In the present study, we identified a heretofore uncharacterized *Arabidopsis* gene, designated *NMig1* (for *Nuclear Migration 1*), which encodes NudC domain-containing protein. Overexpression of *NMig1* resulted in increased primary root growth and formation of more lateral branches, demonstrating that the studied root traits positively correlated with the higher level of *NMig1*. Consistent with these findings are the developmental defects including obstructed root growth due to a partial loss-of-function mutation in the NudC protein BOB1 (Perez et al., 2009). The stimulating effect on lateral root formation was nearly twice stronger than that on primary root growth. These results led us to further explore how overexpression of *NMig1* contributes to remodeling of root system architecture. Quantification of all branching events in the transgenic and the wild-type Col-0 plants indicated increased density of both emerging lateral roots and developing non-emerged primordia. Hence, NMig1 exerts a dual function in *Arabidopsis* root development,

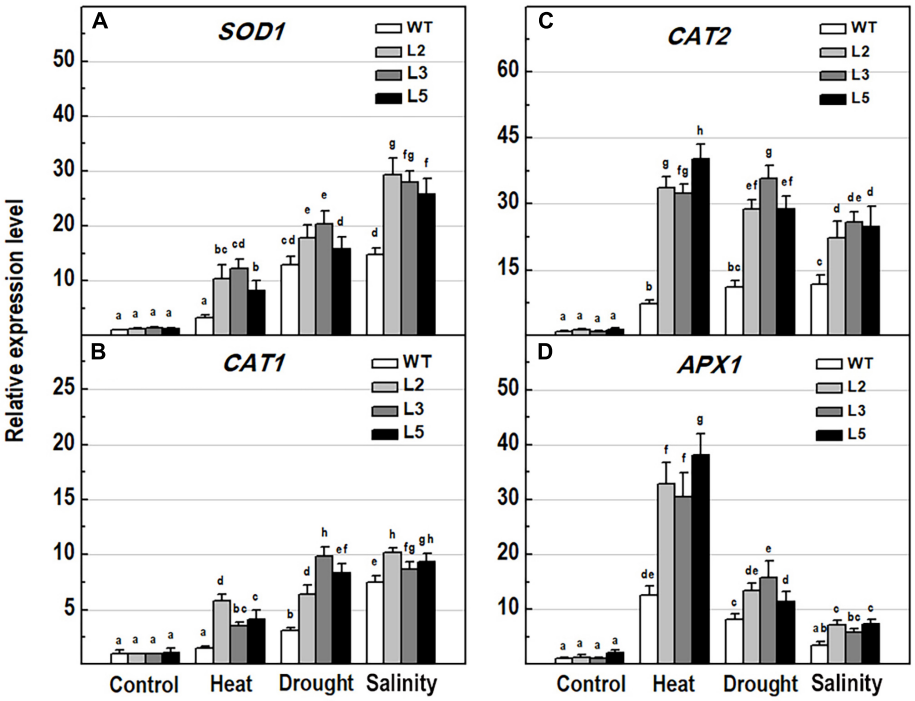

FIGURE 9 | Analysis of the expression levels of major antioxidant genes in 10-day-old wild-type seedlings and transgenic lines overexpressing *NMig1* (L2, L3, and L5) after exposure to heat shock, drought and high salinity: **(A)** *SOD1*, **(B)** *CAT1*, **(C)** *CAT2*, and (**D**) *APX1*. Expression levels were normalized to those of *EF1a* and *CDKA1;1*, as described in section "Materials and Methods." Data represents the mean values ± SE from at least three biological replicates. Different lowercase letters indicate statistically significant difference ($p \leq 0.05$).

increasing lateral root initiation events and promoting lateral root emergence.

Generally, plants can adjust their root system in correlation with variable environmental conditions and it is very likely that every change in root architecture may contribute to plant performance under stress (Rellán-Álvarez et al., 2016; Motte and Beeckman, 2019). Overexpression of *NMig1* positively affected root growth and branching under heat shock, drought and salinity stress manifested by longer primary roots and more lateral branches in the transgenic plants compared to the wild-type Col-0. These beneficial root traits suggest that high expression levels of *NMig1* could at least partially counteract the inhibitory effect of different environmental extremes. In agreement with this observation is the transcriptional activation of *NMig1* upon exposure of the wild-type Col-0 to different stress factors. The level of *NMig1* induction by stress was compared to that of the genes encoding the universal stress proteins *USP17* and *USP21*. The USPs exhibit a redox-dependent chaperone function and are involved in plant protection from abiotic stress (Jung et al., 2015; Bhuria et al., 2016). The magnitude and profile of the stress-induced expression of both *USP* genes were similar to those of *NMig1*, which indicate that molecular adjustment of *Arabidopsis* to stress requires transcriptional activation of these three genes at comparable levels.

A common plant response to internal and external stimuli is the generation of ROS that can potentially lead to oxidative injury of cell components (You and Chan, 2015). Plant cells control the levels of ROS by balancing ROS generation and scavenging through antioxidant enzymes and molecules, such as superoxide dismutase, catalase, peroxidase and other antioxidants that protect cells from oxidative damage (Mittler, 2017). Under benign conditions, ROS are efficiently reduced by non-enzymatic and enzymatic antioxidant components, whereas under stress the production of ROS surpasses the capacity of the antioxidant defense systems to remove them, which causes oxidative stress (Vanderauwera et al., 2005). In our experiments, the expression of four genes, *SOD1*, *CAT1*, *CAT2*, and *APX1*, encoding major antioxidant enzymes was induced by the applied stress factors with especially high expression rates in the transgenic lines. This suggests that overexpression of *NMig1* largely upregulated antioxidant defense components in transgenic plants providing better protection against ROS damages. The overexpression of *NMig1* was also associated with greater total antioxidant activity and ROS scavenging potential, assessed by DPPH and FRAP assays. These observations correlate well with the reduced H_2O_2 levels in the stress-treated transgenic plants when compared with the wild-type Col-0. Additional histochemical detection of the accumulation of $O2^{\bullet-}$ and hydrogen peroxide (H_2O_2) specifically in the roots of the transgenic and wild-type seedlings also displayed a greater stress-induced staining in the wild-type Col-0, which was utmost under heat stress. In transgenic plants, a visible increase in staining intensities was not documented, in particular after the heat treatment. In addition, the degree of lipid peroxidation, a generally used marker for oxidative stress,

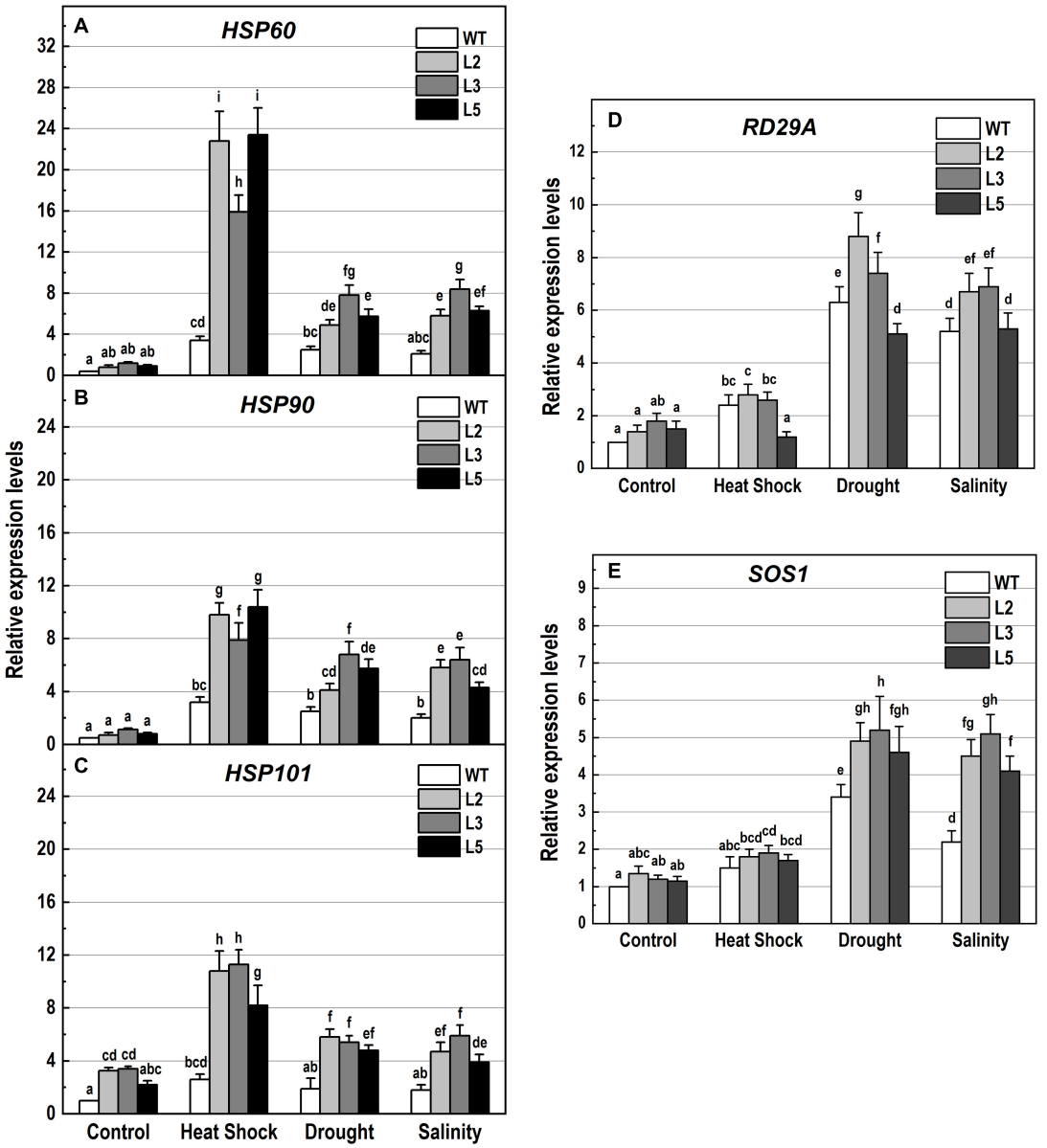

FIGURE 10 | Analysis of the expression levels of genes encoding the heat shock proteins *HSP60*, *HSP90* and *HSP101*, and the stress-responsive genes *RD29A* and *SOS1* in 10-day-old wild-type seedlings and transgenic lines overexpressing *NMig1* (L2, L3, and L5) after exposure to heat shock, drought and high salinity: **(A)** *HSP60*, **(B)** *HSP90*, **(C)** *HSP101*, **(D)** *RD29A*, and **(E)** *SOS1*. Expression levels were normalized to those of *EF1a* and *CDKA1;1*, as described in section "Materials and Methods." Data represents the mean values ± SE from at least three biological replicates. Different lowercase letters indicate statistically significant difference ($p \leq 0.05$).

quantified by the level of MDA concentration (Yadav et al., 2016) was considerably reduced in the transgenics compared to the wild-type.

Taken together, these results suggest that under stress conditions, different components of antioxidant defense system were mobilized by the overexpression of *NMig1*, which led to a decrease in ROS accumulation and reduction of oxidative damage in the transgenic plants. Hence, *NMig1* overexpressors possess a more efficient antioxidant system compared to the wild-type plants. Since the level of antioxidants in plant tissues is closely related to plant stress tolerance (Xing et al., 2007; Sofo et al., 2015), we can suggest that overexpression of *NMig1* confers tolerance to multiple abiotic stresses through optimization of antioxidant defense system (Zhang et al., 2013; Yong et al., 2017).

Furthermore, since *NMig1* encodes a HSP20-like chaperone superfamily protein, it could be expected that its overexpression is associated with increased accumulation of other HSPs. In general, various HSPs are coordinately expressed and operate in chaperone networks (Haslbeck et al., 2005; Waters, 2013). Many

studies have shown a correlation between HSP induction and plant adaptation to stress (Jacob et al., 2017). We quantified the transcript levels of *HSP60*, *HSP90* and the well-known stress responsive gene *HSP101* (Queitsch et al., 2000) in the transgenic plants and Col-0 under abiotic stress. Although some expression differences depending on the nature of the stress imposed were detected, all tested HSPs followed a similar expression pattern, featuring substantial increase in *NMig1* overexpressors and lower detected levels in Col-0. Based on these results, we suggest that the *NMig1*-mediated induction of the studied *HSPs* could represent another mechanism contributing to abiotic stress tolerance in Arabidopsis. However, the exact molecular link between the HSP accumulation and protective role of *NMig1*-induced expression under various stress conditions still needs to be studied and defined.

It should be also noted that the impact of *NMig1* overexpression in promoting plant tolerance varied depending on the nature of the stress imposed. Exposure to heat shock coincided with the highest expression of the studied HSPs. Drought and high salinity led to a stronger induction of the stress-related marker genes *RD29A* and *SOS1* (Shi et al., 2000; Magwanga et al., 2019). This observation could be associated with the specific stress response mechanisms triggered by each particular stress factor and the involvement of *NMig1* in the concrete molecular relays. Nevertheless, overexpression of *NMig1* positively regulated the accumulation of defense gene transcripts, such as *HSPs*, *RD29A*, and *SOS1*, which is consistent with the higher stress tolerance of the transgenic plants.

In conclusion, the present work has provided novel insights into the involvement of plant NudC proteins in *Arabidopsis* root growth and in plant protection against abiotic stress factors. The proposed functions of NMig1 and the insufficient information on the precise biological roles of plant NudC proteins are challenging aspects that require further investigation.

DATA AVAILABILITY STATEMENT

The datasets generated for this study are available on request to the corresponding author.

AUTHOR CONTRIBUTIONS

VVa and TB designed the experiments and wrote the manuscript. VVe, IV, GZ, MZ, MG, NV, and VVa conducted the experiments and analyzed the data. All the authors read and approved the final manuscript.

FUNDING

This research was financially supported by the Bulgarian National Science Fund (BNSF), Grant No. DN11/8/15.12.2017. The first steps of this work have been carried out under the joint research project between the Research Foundation – Flanders (FWO), Belgium and the Bulgarian Academy of Sciences, Grant No. VS.035.10N.

SUPPLEMENTARY MATERIAL

The Supplementary Material for this article can be found online at: https://www.frontiersin.org/articles/10.3389/fpls.2020.00815/full#supplementary-material

REFERENCES

Aumais, J. P., Williams, S. N., Luo, W., Nishino, M., Caldwell, K. A., Caldwell, G. A., et al. (2003). Role for NudC, a dynein-associated nuclear movement protein, in mitosis and cytokinesis. *J. Cell Sci.* 116, 1991–2003. doi: 10.1242/jcs.00412

Benzie, I. F. F., and Strain, J.-J. (1999). Ferric reducing antioxidant power assay: direct measure of total antioxidant activity of biological fluids and modified version of simultaneous measurement of total antioxidant power and ascorbic acid concentration. *Methods Enzymol.* 299, 15–27. doi: 10.1016/s0076-6879(99)99005-5

Bhuria, M., Goel, P., Kumar, S., and Singh, A. K. (2016). The promoter of AtUSP is co-regulated by phytohormones and abiotic stresses in *Arabidopsis thaliana*. *Front. Plant Sci.* 7:1957. doi: 10.3389/fpls.2016.01957

Botër, M., Amigues, B., Peart, J., Breuer, C., Kadota, Y., Casais, C., et al. (2007). Structural and functional analysis of SGT1 reveals that its interaction with HSP90 is required for the accumulation of Rx, an R protein involved in plant immunity. *Plant Cell* 19, 3791–3804. doi: 10.1105/tpc.107.050427

Brand-Williams, W., Cuvelier, M. E., and Berset, C. (1995). Use of a free radical method to evaluate antioxidant activity. *LWT Food Sci. Technol.* 28, 25–30. doi: 10.1016/S0023-6438(95)80008-5

Chi, Y. H., Koo, S. S., Oh, H. T., Lee, E. S., Park, J. H., Phan, K. A. T., et al. (2019). The physiological functions of universal stress proteins and their molecular mechanism to protect plants from environmental stresses. *Front. Plant Sci.* 10:750. doi: 10.3389/fpls.2019.00750

Chiu, Y., Xiang, X., Dawe, A. L., and Morris, N. R. (1997). Deletion of *nudC*, a nuclear migration gene of *Aspergillus nidulans*, causes morphological and cell wall abnormalities and is lethal. *Mol. Biol. Cell* 8, 1735–1749. doi: 10.1091/mbc.8.9.1735

Clough, S. J., and Bent, A. F. (1998). Floral dip: a simplified method for Agrobacterium-mediated transformation of *Arabidopsis thaliana*. *Plant J.* 16, 735–743. doi: 10.1046/j.1365-313x.1998.00343.x

Cunniff, J., Chiu, Y. H., Morris, N. R., and Warrior, R. (1997). Characterization of *DnudC*, the *Drosophila* homolog of an Aspergillus gene that functions in nuclear motility. *Mech. Dev.* 66, 55–68. doi: 10.1016/S0925-4773(97)00085-3

Danovski, G., Dyankova, T., and Stoynov, S. (2018). CellTool: an open source software combining bio-image analysis and mathematical modelling. *bioRxiv* [Preprint]. doi: 10.1101/454256

Dawe, A. L., Caldwell, K. A., Harris, P. M., Morris, N. R., and Caldwell, G. A. (2001). Evolutionarily conserved nuclear migration genes required for early embryonic development in *Caenorhabditis elegans*. *Dev. Genes Evol.* 211, 434–441. doi: 10.1007/s004270100176

Faircloth, L. M., Churchill, P. F., Caldwell, G. A., and Caldwell, K. A. (2009). The microtubule-associated protein, NUD-1, exhibits chaperone activity in vitro. *Cell Stress Chaperones* 14, 95–103. doi: 10.1007/s12192-008-0061-1

Fu, Q., Wang, W., Zhou, T., and Yang, Y. (2016). Emerging roles of NudC family: from molecular regulation to clinical implications. *Sci. China Life Sci.* 59, 455–462. doi: 10.1007/s11427-016-5029-2

Garcia-Ranea, J. A., Mirey, G., Camonis, J., and Valencia, A. (2002). p23 and HSP20/alpha-crystallin proteins define a conserved sequence domain present in other eukaryotic protein families. *FEBS Lett.* 529, 162–167. doi: 10.1016/S0014-5793(02)03321-5

Gocke, C. D., Osmani, S. A., and Miller, B. A. (2000). The human homologue of the *Aspergillus* nuclear migration gene *nudC* is preferentially expressed in

dividing cells and ciliated epithelia. *Histochem. Cell Biol.* 114, 293–301. doi: 10.1007/s004180000197

Haslbeck, M., Franzmann, T., Weinfurtner, D., and Buchner, J. (2005). Some like it hot: the structure and function of small heat-shock proteins. *Nat. Struct. Mol. Biol.* 12, 842–846. doi: 10.1038/nsmb993

Hodges, D. M., DeLong, J. M., Forney, C. F., and Prange, R. K. (1999). Improving the thiobarbituric acid-reactive-substances assay for estimating lipid peroxidation in plant tissues containing anthocyanin and other interfering compounds. *Planta* 207, 604–611. doi: 10.1007/s004250050524

Ishibashi, N., Kanamaru, K., Ueno, Y., Kojima, S., Kobayashi, T., Machida, C., et al. (2012). ASYMMETRIC-LEAVES2 and an ortholog of eukaryotic NudC domain proteins repress expression of *AUXIN-RESPONSE-FACTOR* and class 1 *KNOX* homeobox genes for development of flat symmetric leaves in *Arabidopsis*. *Biol. Open* 1, 197–207. doi: 10.1242/bio.2012406

Jacob, P., Hirt, H., and Bendahmane, A. (2017). The heat-shock protein/chaperone network and multiple stress resistance. *Plant Biotech. J.* 15, 405–414. doi: 10.1111/pbi.12659

Jung, Y. J., Melencion, S. M. B., Lee, E. S., Park, J. H., Alinapon, C. V., Oh, H. T., et al. (2015). Universal stress protein exhibits a redox-dependent chaperone function in *Arabidopsis* and enhances plant tolerance to heat shock and oxidative stress. *Front. Plant Sci.* 6:1141. doi: 10.3389/fpls.2015.01141

Jurkuta, R. J., Kaplinsky, N. J., Spindel, J. E., and Barton, M. K. (2009). Partitioning the apical domain of the *Arabidopsis* embryo requires the BOBBER1 NudC domain protein. *Plant Cell* 21, 1957–1971. doi: 10.1105/tpc.108.065284

Karimi, M., Bleys, A., Vanderhaeghen, R., and Hilson, P. (2007). Building blocks for plant gene assembly. *Plant Physiol.* 145, 1183–1191. doi: 10.1104/pp.107.110411

Kirschner, M., Winkelhaus, S., Thierfelder, J. M., and Nover, L. (2000). Transient expression and heat-stress-induced co-aggregation of endogenous and heterologous small heat-stress proteins in tobacco protoplasts. *Plant J.* 24, 397–411. doi: 10.1046/j.1365-313x.2000.00887.x

Kumar, D., Yusuf, M. A., Singh, P., Sardar, M., and Sarin, N. B. (2014). Histochemical detection of superoxide and H2O2 accumulation in *Brassica juncea* seedlings. *Bio Protocol* 4:e1108.

Lee, Y. T., Jacob, J., Michowski, W., Nowotny, M., Kuznicki, J., and Chazin, W. J. (2004). Human Sgt1 binds HSP90 through the CHORD-Sgt1 domain and not the tetratricopeptide repeat domain. *J. Biol. Chem.* 279, 16511–16517. doi: 10.1074/jbc.M400215200

Liu, S., Wang, J., Jiang, S., Wang, H., Gao, Y., Zhang, H., et al. (2019). Tomato SlSAP3, a member of the stress-associated protein family, is a positive regulator of immunity against *Pseudomonas syringae* pv. *tomato DC*3000. *Mol. Plant Pathol.* 20, 815–830. doi: 10.1111/mpp.12793

Magwanga, R. O., Kirungu, J. N., Lu, P., Yang, X., Dong, Q., Cai, X., et al. (2019). Genome wide identification of the trihelix transcription factors and overexpression of *Gh_A05G2067* (*GT-2*), a novel gene contributing to increased drought and salt stresses tolerance in cotton. *Physiol. Plant.* 167, 447–464. doi: 10.1111/ppl.12920

Malamy, J. E., and Benfey, P. N. (1997). Organization and cell differentiation in lateral roots of *Arabidopsis thaliana*. *Development* 124, 33–44.

Miroshnichenko, S., Tripp, J., Nieden, U., Neumann, D., Conrad, U., and Manteuffel, R. (2005). Immunomodulation of function of small heat shock proteins prevents their assembly into heat stress granules and results in cell death at sublethal temperatures. *Plant J.* 41, 269–281. doi: 10.1111/j.1365-313X.2004.02290.x

Mittler, R. (2017). ROS are good. *Trends Plant Sci.* 22, 11–19. doi: 10.1016/j.tplants.2016.08.002

Morris, S. M., Anaya, P., Xiang, X., Morris, N. R., May, G. S., and Yu-Lee, L. (1997). A prolactin-inducible T cell gene product is structurally similar to the *Aspergillus nidulans* nuclear movement protein NUDC. *Mol. Endocrinol.* 11, 229–236. doi: 10.1210/mend.11.2.9892

Motte, H., and Beeckman, T. (2019). The evolution of root branching: increasing the level of plasticity. *J. Exp. Bot.* 70, 785–793. doi: 10.1093/jxb/ery409

Murashige, T., and Skoog, F. (1962). A revised medium for rapid growth and bio assays with tobacco tissue cultures. *Physiol. Plant.* 15, 473–497. doi: 10.1111/j.1399-3054.1962.tb08052.x

Nguyen, H. M., Sako, K., Matsui, A., Suzuki, Y., Mostofa, M. G., Ha, C. V., et al. (2017). Ethanol enhances high-salinity stress tolerance by detoxifying reactive oxygen species in *Arabidopsis thaliana* and rice. *Front. Plant Sci.* 8:1001. doi: 10.3389/fpls.2017.01001

Osmani, A. H., Osmani, S. A., and Morris, N. R. (1990). The molecular cloning and identification of a gene product specifically required for nuclear movement in *Aspergillus nidulans*. *J. Cell. Biol.* 111, 543–555. doi: 10.1083/jcb.111.2.543

Perez, D. E., Hoyer, J. S., Johnson, A. I., Moody, Z. R., Lopez, J., and Kaplinsky, N. J. (2009). BOBBER1 is a noncanonical *Arabidopsis* small heat shock protein required for both development and thermotolerance. *Plant Physiol.* 151, 241–252. doi: 10.1104/pp.109.142125

Pundir, S., Martin, M. J., and O'Donovan, C. (2016). UniProt tools. *Curr. Protoc. Bioinformatics* 53, 1–29. doi: 10.1002/0471250953.bi0129s53

Queitsch, C., Hong, S. W., Vierling, E., and Lindquist, S. (2000). Heat shock protein 101 plays a crucial role in thermotolerance in *Arabidopsis*. *Plant Cell* 12, 479–492. doi: 10.1105/tpc.12.4.479

Raymaekers, M., Smets, R., Maes, B., and Cartuyvels, R. (2009). Checklist for optimization and validation of real-time PCR assays. *J. Clin. Lab. Anal.* 23, 145–151. doi: 10.1002/jcla.20307

Rellán-Álvarez, R., Lobet, G., and Dinneny, J. R. (2016). Environmental control of root system biology. *Annu. Rev. Plant Biol.* 67, 619–642. doi: 10.1146/annurev-arplant-043015-111848

Schwacke, R., Schneider, A., Van Der Graaff, E., Fischer, K., Catoni, E., Desimone, M., et al. (2003). ARAMEMNON, a novel database for Arabidopsis integral membrane proteins. *Plant Physiol.* 131, 16–26. doi: 10.1104/pp.011577

Shi, H., Ishitani, M., Kim, C., and Zhu, J. K. (2000). The *Arabidopsis thaliana* salt tolerance gene *SOS1* encodes a putative Na+/H+ antiporter. *Proc. Natl. Acad. Sci. U.S.A.* 97, 6896–6901. doi: 10.1073/pnas.120170197

Silverblatt-Buser, E. W., Frick, M. A., Rabeler, C., and Kaplinsky, N. J. (2018). Genetic interactions between BOB1 and multiple 26S proteasome subunits suggest a role for proteostasis in regulating *Arabidopsis* development. *G3* 8, 1379–1390. doi: 10.1534/g3.118.300496

Sofo, A., Scopa, A., Nuzzaci, M., and Vitti, A. (2015). Ascorbate peroxidase and catalase activities and their genetic regulation in plants subjected to drought and salinity stresses. *ıInt. J. Mol. Sci.* 16, 13561–13578. doi: 10.3390/ijms160613561

Untergasser, A., Cutcutache, I., Koressaar, T., Ye, J., Faircloth, B. C., Remm, M., et al. (2012). Primer3-new capabilities and interfaces. *Nucleic Acids Res.* 40:e115. doi: 10.1093/nar/gks596

Vanderauwera, S., Vandenbroucke, K., Inzé, A., van de Cotte, B., Mühlenbock, P., De Rycke, R., et al. (2005). AtWRKY15 perturbation abolishes the mitochondrial stress response that steers osmotic stress tolerance in *Arabidopsis*. *Proc. Natl. Acad. Sci. U.S.A.* 109, 20113–20118. doi: 10.1073/pnas.1217516109

Waters, E. R. (2013). The evolution, function, structure, and expression of the plant sHSPs. *J. Exp. Bot.* 64, 391–403. doi: 10.1093/jxb/ers355

Wolff, S. P. (1994). Ferrous ion oxidation in presence of ferric ion indicator xylenol orange for measurement of hydroperoxides. *Methods Enzymol.* 233, 182–189. doi: 10.1016/S0076-6879(94)33021-2

Xing, Y., Jia, W. S., and Zhang, J. H. (2007). AtMEK1 mediates stress-induced gene expression of *CAT1* catalase by triggering H2O2 production in *Arabidopsis*. *J. Exp. Bot.* 58, 2969–2981. doi: 10.1093/jxb/erm144

Yadav, V., Arif, N., Singh, S., Srivastava, P. K., Sharma, S., Tripathi, D. K., et al. (2016). Exogenous mineral regulation under heavy metal stress: advances and prospects. *Biochem. Pharmacol.* 5:220. doi: 10.4172/2167-0501.1000220

Yang, Y., Yan, X., Cai, Y., Lu, Y., Si, J., and Zhou, T. (2010). NudC-like protein 2 regulates the LIS1/dynein pathway by stabilizing LIS1 with Hsp90. *Proc. Natl. Acad. Sci. U.S.A.* 107, 3499–3504. doi: 10.1073/pnas.0914307107

Yong, B., Wang, X., Xu, P., Zheng, H., Fei, X., Hong, Z., et al. (2017). Isolation and abiotic stress resistance analyses of a catalase gene from *Ipomoea batatas* (L.) Lam. *BioMed Res. Internat* 2017, 1–10. doi: 10.1155/2017/6847532

You, J., and Chan, Z. (2015). ROS regulation during abiotic stress responses in crop plants. *Front. Plant Sci.* 6:1092. doi: 10.3389/fpls.2015.01092

Zhang, C., Zhang, W., Lu, Y., Yan, X., Yan, X., Zhu, X., et al. (2016). NudC regulates actin dynamics and ciliogenesis by stabilizing cofilin 1. *Cell Res.* 26, 239–253. doi: 10.1038/cr.2015.152

Zhang, M.-Y., Huang, N.-N., Clawson, G. A., Osmani, S. A., Pan, W., Xin, P., et al. (2002). Involvement of the fungal nuclear migration gene NudC human

homolog in cell proliferation and mitotic spindle formation. *Exp. Cell Res.* 273, 73–84. doi: 10.1006/excr.2001.5414

Zhang, Z., Zhang, Q., Wu, J., Zheng, X., Zheng, S., Sun, X., et al. (2013). Gene knockout study reveals that cytosolic ascorbate peroxidase 2 (OsAPX2) plays a critical role in growth and reproduction in rice under drought, salt and cold stresses. *PLoS One* 8:e57472. doi: 10.1371/journal.pone.0057472

Zheng, M., Cierpicki, T., Burdette, A. J., Utepbergenov, D., Janczyk, P. Ł, Derewenda, U., et al. (2011). Structural features and chaperone activity of the NudC protein family. *J. Mol. Biol.* 409, 722–741. doi: 10.1016/j.jmb.2011.04.018

Zhou, T., Aumais, J. P., Liu, X., Yu-Lee, L. Y., and Erikson, R. L. (2003). A role for Plk1 phosphorylation of NudC in cytokinesis. *Dev. Cell* 5, 127–138. doi: 10.1016/S1534-5807(03)00186-2

Zhu, X. J., Liu, X., Jin, Q., Cai, Y., Yang, Y., and Zhou, T. (2010). The L279P mutation of nuclear distribution gene C (NudC) influences its chaperone activity and lissencephaly protein 1 (LIS1) stability. *J. Biol. Chem.* 285, 29903–29910. doi: 10.1074/jbc.M110.105494

Conflict of Interest: The authors declare that the research was conducted in the absence of any commercial or financial relationships that could be construed as a potential conflict of interest.

frontiers in Plant Science

ORIGINAL RESEARCH
published: 24 June 2020
doi: 10.3389/fpls.2020.00661

Characterization of Purple Acid Phosphatase Family and Functional Analysis of *GmPAP7a/7b* Involved in Extracellular ATP Utilization in Soybean

Shengnan Zhu[1†], Minhui Chen[1†], Cuiyue Liang[1], Yingbin Xue[2], Shuling Lin[1] and Jiang Tian[1]*

[1] State Key Laboratory for Conservation and Utilization of Subtropical Agro-Bioresources, Root Biology Center, South China Agricultural University, Guangzhou, China, [2] Department of Resources and Environmental Sciences, College of Chemistry and Environment, Guangdong Ocean University, Zhanjiang, China

OPEN ACCESS

Edited by:
Zhichang Chen,
Fujian Agriculture and Forestry University, China

Reviewed by:
Weifeng Xu,
Fujian Agriculture and Forestry University, China
Chuang Wang,
Huazhong Agricultural University, China

***Correspondence:**
Jiang Tian
jtian@scau.edu.cn

[†] These authors have contributed equally to this work

Specialty section:
This article was submitted to Plant Abiotic Stress, a section of the journal Frontiers in Plant Science

Received: 17 March 2020
Accepted: 28 April 2020
Published: 24 June 2020

Citation:
Zhu S, Chen M, Liang C, Xue Y, Lin S and Tian J (2020) Characterization of Purple Acid Phosphatase Family and Functional Analysis of GmPAP7a/7b Involved in Extracellular ATP Utilization in Soybean. Front. Plant Sci. 11:661. doi: 10.3389/fpls.2020.00661

Low phosphate (Pi) availability limits crop growth and yield in acid soils. Although root-associated acid phosphatases (APases) play an important role in extracellular organic phosphorus (P) utilization, they remain poorly studied in soybean (*Glycine max*), an important legume crop. In this study, dynamic changes in intracellular (leaf and root) and root-associated APase activities were investigated under both Pi-sufficient and Pi-deficient conditions. Moreover, genome-wide identification of members of the *purple acid phosphatase* (*PAP*) family and their expression patterns in response to Pi starvation were analyzed in soybean. The functions of both *GmPAP7a* and *GmPAP7b*, whose expression is up regulated by Pi starvation, were subsequently characterized. Phosphate starvation resulted in significant increases in intracellular APase activities in the leaves after 4 days, and in root intracellular and associated APase activities after 1 day, but constant increases were observed only for root intracellular and associated APase activities during day 5–16 of P deficiency in soybean. Moreover, a total of 38 *GmPAP* members were identified in the soybean genome. The transcripts of 19 *GmPAP* members in the leaves and 17 in the roots were upregulated at 16 days of P deficiency despite the lack of a response for any *GmPAP* members to Pi starvation at 2 days. Pi starvation upregulated *GmPAP7a* and *GmPAP7b*, and they were subsequently selected for further analysis. Both GmPAP7a and GmPAP7b exhibited relatively high activities against adenosine triphosphate (ATP) *in vitro*. Furthermore, overexpressing *GmPAP7a* and *GmPAP7b* in soybean hairy roots significantly increased root-associated APase activities and thus facilitated extracellular ATP utilization. Taken together, these results suggest that GmPAP7a and GmPAP7b might contribute to root-associated APase activities, thus having a function in extracellular ATP utilization in soybean.

Keywords: phosphorus deficiency, soybean, root-associated APase, purple acid phosphatase, ATP utilization

Abbreviations: APase, acid phosphatase; P, phosphorus; PAP, purple acid phosphatase; Pi, phosphate; qRT-PCR, quantitative real-time polymerase chain reaction.

INTRODUCTION

Phosphorus (P), an important macronutrient, is involved in many biochemical and metabolic processes in plants, such as photosynthesis, nucleotide synthesis, membrane remodeling, and protein modification (Liang et al., 2010; Zhang et al., 2014; Ham et al., 2018). However, a large proportion of P exists in immobile forms (i.e., organic P esters and inorganic complexes) and is thus unavailable for plant utilization in most soils, especially in acid soils (Chiou and Lin, 2011; Tian et al., 2012b; Plaxton and Lambers, 2015). Therefore, Pi fertilizer application is required to meet the Pi requirements for crop production. However, excess application of Pi fertilizer causes serious environmental eutrophication (Conley et al., 2009; Veneklaas et al., 2012; Abel, 2017; Wang and Liu, 2018). Thus, breeding cultivars with high P efficiency and optimizing field P management practices are necessary to maintain sustainable agricultural development (Tian et al., 2012b; Abel, 2017). It has been well documented that plants have evolved complex adaptation strategies to increase Pi foraging and recycling, such as altering root morphology and architecture, increasing organic acid and PAP exudation, and enhancing root–microbe interactions (Chiou and Lin, 2011; Liang et al., 2014; Ham et al., 2018; Jung et al., 2018).

In terms of adaptive strategies, plant PAPs are believed to play a vital role in Pi mobilization (Tran et al., 2010a; Plaxton and Lambers, 2015; Tian and Liao, 2015; Wang and Liu, 2018). It is generally observed that plant PAPs harbor a binuclear metal center binding either Fe (III)-Zn (II) or Fe (III)-Mn (II) ions and comprise five conserved motif blocks (DXG/GDXXY/GNH(D/E)/VXXH/GHXH) (Tran et al., 2010a; Tian and Liao, 2015). With the aid of genome sequence availability for plant species, a variety of PAPs have been identified and annotated. For example, there are 29 annotated PAP members in Arabidopsis (*Arabidopsis thaliana*), 26 in rice (*Oryza sativa*), 33 in maize (*Zea mays*), 25 in chickpea (*Cicer arietinum*), and 25 in physic nut (*Jatropha curcas*) (Li et al., 2002; Zhang et al., 2010; Gonzalez-Munoz et al., 2015; Bhadouria et al., 2017; Venkidasamy et al., 2019). Plant PAPs are widely divided into two major groups on the basis of PAP mass and structure: low molecular-mass monomeric PAPs, with a mass of approximately 35 kD, and high molecular-mass oligomeric PAPs, with a subunit mass of approximately 55 kD (Olczak et al., 2003; Tran et al., 2010a; Plaxton and Lambers, 2015; Tian and Liao, 2015).

It has been documented that P deficiency enhances the expression levels of most plant *PAPs*. For example, in rice, 10 out of 26 *PAP* members (*OsPAP1a*, *1d*, *3b*, *9b*, *10a*, *10c*, *20b*, *21b*, *23*, and *27a*) are upregulated in the roots under P-deficient conditions (Zhang et al., 2010). Similarly, Pi starvation enhanced transcripts of *PAP* members are also observed in 11 of 33 *PAP* members in maize, at least 20 of 25 *PAP* members in physic nut, 11 of 29 *PAP* members in Arabidopsis, 23 of 35 *PAP* members in soybean (*Glycine max*), and 12 of 25 *PAP* members in chickpea (Del Pozo et al., 1999; Haran et al., 2000; Li C. C. et al., 2012; Wang et al., 2014; Gonzalez-Munoz et al., 2015; Bhadouria et al., 2017; Venkidasamy et al., 2019). Therefore, it is suggested that increased transcription levels of *PAPs* could contribute to significant increases in intracellular and extracellular APase activities in plant species, such as Arabidopsis, wheat (*Triticum aestivum*), soybean, and tomato (*Lycopersicon esculentum*) (Del Pozo et al., 1999; Li et al., 2002; Kaida et al., 2003; Zimmermann et al., 2004; Liang et al., 2010; Chiou and Lin, 2011).

Recently, accumulating evidence has suggested that most PAP members participate in extracellular organic P utilization, including adenosine triphosphate (ATP), deoxynucleotide triphosphate (dNTPs), and phytate-P (Tran et al., 2010a; Plaxton and Lambers, 2015; Tian and Liao, 2015; Wang and Liu, 2018). A pioneer study on PAP function in extracellular ATP utilization has been conducted in common bean (*Phaseolus vulgaris*) in which overexpression of Pi starvation-enhanced *PvPAP3* resulted in significant increases of fresh weight and P content in bean hairy roots cultured in media supplemented with ATP as the sole P source (Liang et al., 2010). Similar functions have also been observed for other *PAP* members, such as *OsPAP10a*, *OsPAP21b*, *OsPAP26*, and *OsPAP10c* in rice (Tian et al., 2012a; Lu et al., 2016; Gao et al., 2017; Mehra et al., 2017). In addition to extracellular ATP utilization, plant PAP members have also been suggested to participate in extracellular dNTP utilization, including *PvPAP1*/*3* from common bean, *SgPAP7*/*10*/*26* from stylo (*Stylosanthes* spp.) and *GmPAP1-like* from soybean (Liang et al., 2012; Liu et al., 2016; Wu et al., 2018). Recently, some PAP members exhibiting phytase activity have been suggested to mediate extracellular phytate utilization, including *SgPAP23* from stylo, *OsPHY1* from rice, *MtPHY1* from Medicago (*Medicago truncatula*), and *GmPAP4* and *GmPAP14* from soybean (Ma et al., 2009; Li R. J. et al., 2012; Kong et al., 2014, 2018; Liu et al., 2018), suggesting diverse functions of *PAP* members in P scavenging and recycling in plants.

Soybean is an important legume crop species and an important oil and high-protein food or forage crop species worldwide (Conner et al., 2004; Herridge et al., 2008). In the face of low Pi availability conditions, soybean has evolved strategies to maintain Pi homeostasis, including the formation of a shallower root system, increased organic acid exudation and APase activities, and the formation of symbiotic associations with arbuscular mycorrhizal (AM) fungi (Tian et al., 2003; Zhao et al., 2004; Liao et al., 2006; Liu et al., 2008; Wang et al., 2010; Li et al., 2019). Furthermore, a functional analysis of several Pi starvation-responsive genes, such as *GmEXPB2*, *GmPHR25*, *GmPT5*/*7,* and *GmSPX1*/*3,* has highlighted molecular mechanisms underlying soybean adaptation to Pi starvation (Li et al., 2014, 2015; Yao Z. et al., 2014; Xue et al., 2017; Chen et al., 2018). However, the dynamic changes in intracellular and root-associated APase activities in soybean in response to Pi starvation, and the functions of GmPAP in extracellular ATP utilization remain unclear. Therefore, in this study, dynamic changes of intracellular (leaves and roots) and root-associated APase activities were investigated under both Pi-sufficient and Pi-deficient conditions. Moreover, genome-wide identification of members of the PAP family, and their expression patterns in response to Pi starvation were analyzed in soybean. Furthermore, the functions of the Pi starvation responsive *GmPAP7a* and *GmPAP7b* genes are suggested to participate in extracellular ATP utilization in soybean.

MATERIALS AND METHODS

Plant Materials and Growth Conditions

The soybean genotype YC03-3 was used in this study. To analyze dynamic changes in APase activities at two P levels, soybean seeds were surface-sterilized and rolled in absorbent papers, which are soaked with one-fourth strength nutrient solution as described previously (Liang et al., 2010). After 5 days of germination, uniform seedlings were transferred to a nutrient solution comprising the following components (in μM): 1500 KNO_3, 1200 $Ca(NO_3)_2$, 400 NH_4NO_3, 25 $MgCl_2$, 500 $MgSO_4$, 300 K_2SO_4, 0.3 $(NH_4)_2SO_4$, 1.5 $MnSO_4$, 0.5 $CuSO_4$, 1.5 $ZnSO_4$, 0.16 $(NH_4)_6Mo_7O_{24}$, 2.5 NaB_4O_7, 40 Fe-Na-EDTA, and 5 (−P) or 250 (+P) KH_2PO_4, as previously described (Wu et al., 2018). The nutrient solution was aerated hourly and refreshed weekly. Moreover, the pH value of the nutrient solution was adjusted to 5.8 every 2 days. The fresh weight of the soybean shoots and roots was determined daily within 7 days after P treatments were applied, and at 10, 13, and 16 days after P treatments were applied. Moreover, the roots were harvested to determine total P concentration, intracellular and root-associated APase activities. Primary leaves were also harvested to determine total P concentration and intracellular APase activities except at 0 and after 1 days of P treatment. To assay the temporal expression patterns of *GmPAP* members in response to Pi starvation, the primary leaves and roots after 2 days and 16 days of P treatments were also separately harvested for further analysis. All experiments had four biological replicates.

Total P Concentration and APase Activity Analysis

The total P concentration was measured as described previously (Murphy and Riley, 1963; Xue et al., 2017; Mo et al., 2019). Briefly, approximately 0.1 g of dry samples was ground and digested using H_2SO_4-H_2O_2 reagent. Afterward, the mixtures were reacted with ammonium molybdate reagent and measured 30 min later at 700 nm.

To determine intracellular APase activities, the reaction product hydrolyzed by APase, ρ-nitrophenol (ρ-NP), was measured at an absorbance of 405 nm as described previously (Liang et al., 2010; Liu et al., 2016; Wu et al., 2018). Briefly, approximately 0.1 g of leaves and roots was ground and homogenized with 1.2 mL 0.1 M Tris–HCl (pH 8.0), and then the mixtures were centrifuged at 12,000 *g* for 30 min. After centrifugation, the supernatants were mixed with 1.8 mL of 45 mM Na-acetate buffer (pH 5.0) consisting of 1 mM ρ-nitrophenyl phosphate (ρ-NPP) as the substrate at 37°C for 15 min. After adding 1 M NaOH, the released ρ-NP was measured spectrophotometrically at 405 nm. The protein content in the supernatants was quantified using the Coomassie brilliant blue method (Bradford, 1976). Intracellular APase activities were expressed as the amount of ρ-NP produced per minute per milligram protein.

To analyze root-associated APase activities, seedlings grown in a nutrient solution containing 250 μM (+P) or 5 μM (−P) KH_2PO_4 were rinsed in a 0.2 M $CaCl_2$ solution once and deionized water three times. After that, the whole roots of seedlings subjected to 0–7 days of P treatments and detached partial lateral roots of seedlings at 10–16 days of P treatment were transferred separately into tubes containing 40 mL of reaction buffer containing 45 mM Na-acetate buffer (pH 5.0) and 1 mM ρ-NPP. The reactions were incubated at 25°C for 2 h to allow the reactions to occur, and they were then terminated by the addition of 1 M NaOH. The absorbance of the reaction mixtures was separately measured at 405 nm (Liu et al., 2016). Moreover, the fresh weight of the roots was also determined. Root-associated APase activities were calculated as the amount of released ρ-NP per minute per gram of fresh roots.

To visualize root-associated APase activities, the roots were incubated in solid Murashige and Skoog (MS) media containing the substrate 5-bromo-4-chloro-3-indolyl-phosphate (BCIP) (Sigma-Aldrich, United States) as described previously (Wang et al., 2014). Briefly, the detached roots were placed on solid MS media containing 0.03% agar and then covered with solid MS media containing 0.06% agar and 0.1% (w/v) BCIP. After incubation at 28°C for 2 h, the cleavages of BCIP showed a bright blue color, which was imaged by a single-lens reflex camera (Canon, Japan). Each experiment was conducted for at least four biological replicates.

Bioinformatic and Phylogenetic Tree Analysis of PAPs

For bioinformatic analysis, the sequences of PAP members from soybean were extracted from the NCBI[1] and Phytozome[2] databases. After multiple sequence alignment using ClustalX and conserved domain (metallophos domain) searches using the SMART tool[3] (Bhadouria et al., 2017), GmPAP members were identified and named on the basis of their homology with corresponding PAP members in Arabidopsis. Detailed information about the GmPAP members, including their protein mass, number of amino acids, subcellular localization, and N-glycosylation site prediction, was retrieved separately from servers, including the ExPASy[4], TargetP 1.1[5] and NetNGlyc 1.0 server[6] as described previously (Bhadouria et al., 2017; Xue et al., 2017; Yin et al., 2019). Moreover, a group of PAP members with known functions from other species, such as common bean, rice, maize, Arabidopsis, lupinus (*Lupinus luteus*), sweet potato (*Ipomoea batatas*), wheat, tobacco (*Nicotiana tabacum*), barely (*Hordeum vulgare*), stylo, Medicago, white lupin (*Lupinus albus*), potato (*Solanum tuberosum*), and chickpea, were retrieved from the NCBI database (Kaida et al., 2003; Li and Wang, 2003; Ma et al., 2009; Dionisio et al., 2011; Li C. C. et al., 2012;

[1]https://www.ncbi.nlm.nih.gov/pubmed
[2]https://phytozome.jgi.doe.gov/pz/portal.html
[3]http://smart.embl-heidelberg.de/smart/set_mode.cgi?NORMAL=1
[4]https://web.expasy.org/protparam/
[5]http://www.cbs.dtu.dk/services/TargetP-1.1/index.php
[6]http://www.cbs.dtu.dk/services/NetNGlyc/

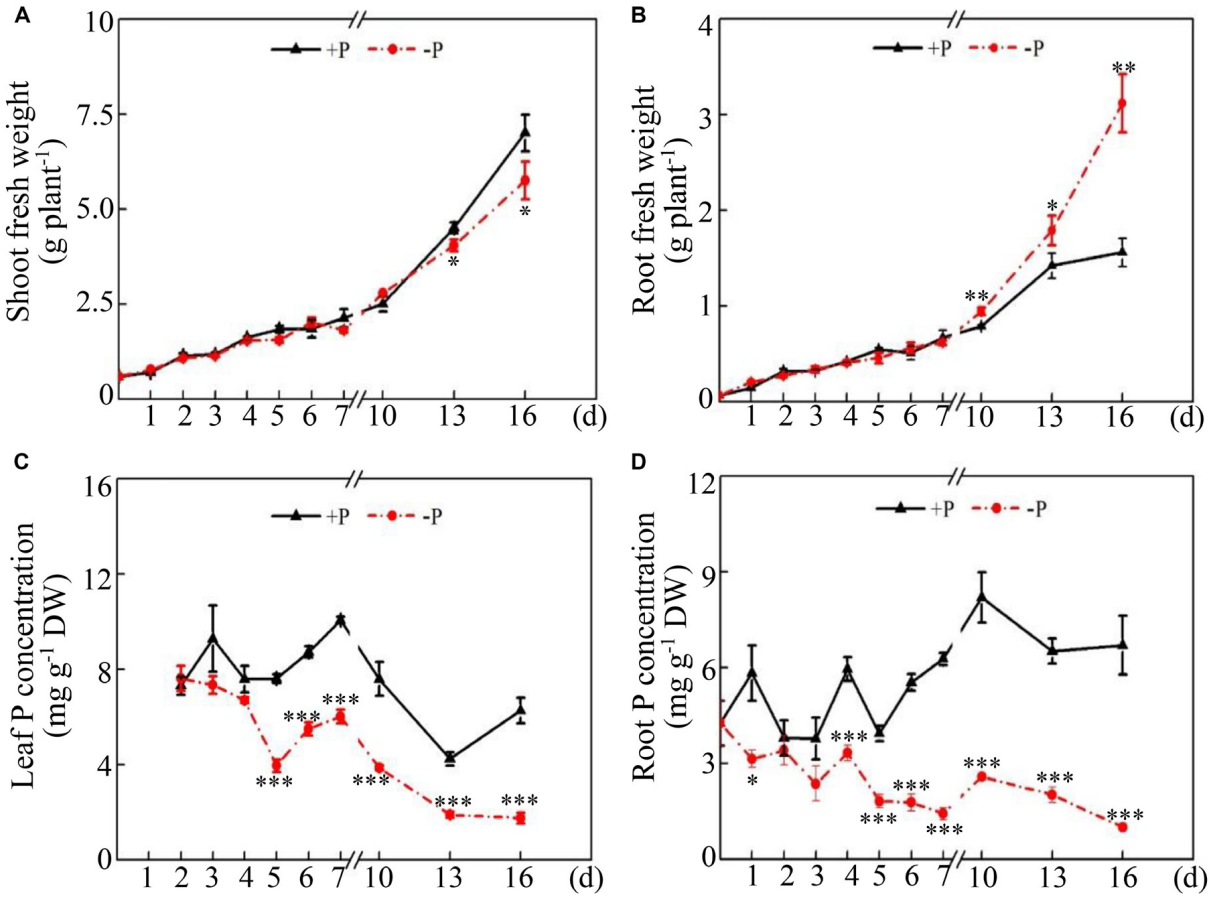

FIGURE 1 | Dynamic changes in soybean growth and P concentration at two P levels. **(A)** Shoot fresh weight. **(B)** Root fresh weight. **(C)** Leaf P concentration. **(D)** Root P concentration. Soybean seedlings were grown in nutrient solution supplemented with 5 μM (–P) or 250 μM (+P) KH_2PO_4. Fresh weight and P concentration were dynamically measured. The data are the means of four replicates with standard errors. The asterisks indicate significant differences between the –P and +P treatments according to Student's *t*-test: $^*P < 0.05$; ** $0.001 < P < 0.01$; $^{***}P < 0.001$.

Madsen et al., 2013; Bhadouria et al., 2017; Liu et al., 2018). A phylogenetic tree was constructed using MEGA 5.01 with 1000 bootstrap values using the neighbor-joining method as described previously (Xue et al., 2017).

RNA Extraction and Quantitative RT-PCR Analysis

Total RNA was extracted and purified as described previously (Xue et al., 2018). To eliminate genomic DNA contamination, the total RNA was further treated with RNase-free DNase I (Invitrogen, United States), and the purity was evaluated via A260/A280 ratios by using a Nanodrop spectrophotometer (Thermo, United States). Approximately 1 μg of RNA was reversely transcribed using MMLV-reverse transcriptase (Promega, United States) following the manufacturer's protocols. Synthesized first-strand cDNA was used for SYBR Green-monitored quantitative RT-PCR (qRT-PCR) analysis on a Rotor-Gene 3,000 real-time PCR system (Corbett Research, Australia). The primers used for *GmPAP* members and the housekeeping gene *GmEF1-α* (*Glyma.17G186600*) are detailed in the **Supplementary Table S1**. Relative transcript levels of soybean *GmPAP* members were also presented using a heatmap generated by TBtools software.

Subcellular Localization and Histochemical Localization of *GmPAP7a/7b*

The full-length *GmPAP7a/7b* coding sequence without a stop codon was separately amplified using the gene specific primers *GmPAP7a/7b-GFP-F/R* (**Supplementary Table S1**) and then cloned into a *pEGAD* vector to generate *35S:GmPAP7a/7b-GFP* fusion constructs. The constructs fusion with GFP and the plasma membrane marker *AtPIP2A*-mCherry were co-transformed into tobacco epidermal cells as described previously (Liu et al., 2016). The fluorescent signals were observed via a Zeiss LSM7 Duo confocal microscope (Zeiss, Germany) at 488 nm for GFP and 568 nm for mCherry (Liu et al., 2018). Fluorescent images were further processed using Zen2011 software (Carl Zeiss Microscopy, Germany). A 3.0 kb upstream sequence of *GmPAP7a/7b* from the start

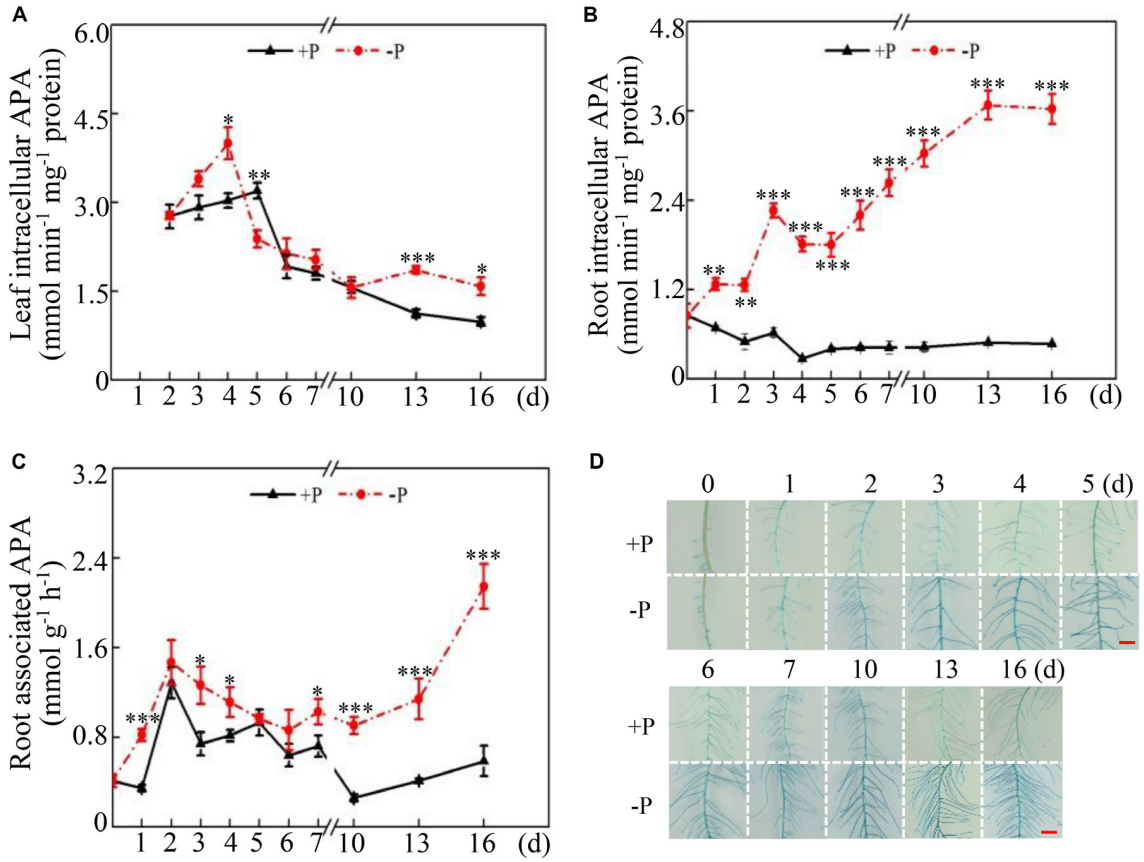

FIGURE 2 | Dynamic changes in intracellular and root-associated APase activities in soybean. **(A)** Leaf intracellular APase activities. **(B)** Root intracellular APase activities. **(C)** Root-associated APase activities. **(D)** Root-associated APase activities detected by BCIP staining. Soybean seedlings were grown in nutrient solution supplemented with 5 μM (–P) or 250 μM (+P) KH_2PO_4. Intracellular and associated APase activities were dynamically measured. Data are means of four replicates with standard errors. Asterisks indicate significant differences between the –P and +P treatments by according to Student's *t*-test: $^*P < 0.05$; ** $0.001 < P < 0.01$; $^{***}P < 0.001$. The bars = 1 cm.

of codon was amplified using primers *GmPAP7a/7b-GUS-F/R* (**Supplementary Table S1**) and then inserted into a *pTF102* plasmid containing β-*glucuronidase* (*GUS*). The plasmids were subsequently transformed into soybean hairy roots for analysis of their histochemical localization. Transgenic soybean hairy roots were cultivated in MS media supplied with 1250 μM (+P) or 5 μM KH_2PO_4 (−P) for 1 week and then incubated in GUS staining solution (0.1 M Na_2HPO_4/NaH_2PO_4 buffer, pH 7.0, 1 mM X-Gluc) for 8 h at 37°C as described previously (Jefferson et al., 1987). After GUS staining, the root samples were separately observed under a light microscope (Leica, Germany).

Purification and Biochemical Characterization of *GmPAP7a/7b*

The entire coding sequences of both *GmPAP7a* and *GmPAP7b* were separately cloned into a *pGEX-6P-3* vector (GE Healthcare, United States) constructs fusion to a GST tag using an in-fusion cloning kit (TAKARA, United States) with primers *GmPAP7a/7b-GST-F/R* (**Supplementary Table S1**). The expression constructs were introduced into *Escherichia coli* (*E. coli*) strain BL21. Recombinant proteins were extracted using BeaverBeads™ GSH magnetic beads (Beaver Nano, China) and recognized by immunoblot analysis using anti-GST antibodies as described previously (Liu et al., 2018). Purified proteins were used to analyze their enzymatic properties. The effects of different pH values (ranging from 3.0 to 9.0) on GmPAP7a/7b activities were estimated separately by the addition of 5 mM ρ-NPP to the reaction buffers for 15 min at 37°C as described previously (Liu et al., 2018). The reaction buffer included 45 mM of glycine-HCl buffer (pH 3.0–4.5), Na-acetate buffer (pH 5.0–5.5), Tris–HCl 2-(N-morpholino)-ethanesulfonic acid (MES) buffer (pH 6.0–7.0), and Tris–HCl buffer (pH 7.5–9.0). Moreover, the effects of different temperatures (over a range of 20–80°C) on the enzymatic activities were also measured in 45 mM Na-acetate buffer (pH 5.0) with 5 mM ρ-NPP used as a substrate. The relative activities of GmPAP7a/7b were calculated as the percentages of their activities out of the highest activities under different pH values or temperatures. Moreover, a broad range of substrates were added to 45 mM Na-acetate buffer (pH 5.0) to test their substrate specificities, including the following (at concentrations of 5 mM): phytate-P, ATP, adenosine diphosphate (ADP),

TABLE 1 | General information of *GmPAP* members in soybean.

Name	Locus	Chromosomal location	Length of ORF (bp)	Number of amino acids (aa)	Protein size (kD)	Subcellular location	N-glycosylation sites
GmPAP1a	Glyma.02G117000.1	2	1926	642	72	–	5
GmPAP18a	Glyma.02G290100.1	2	1365	454	51	S	1
GmPAP22a	Glyma.03G194100.1	3	1476	491	55	C	2
GmPAP20a	Glyma.03G194200.1	3	1293	432	48	S	3
GmPAP27c	Glyma.04G195600.1	4	1560	519	59	M	0
GmPAP27a	Glyma.05G047900.1	5	1875	524	70	S	5
GmPAP7d	Glyma.05G138300.1	5	933	310	35	S	0
GmPAP7a	Glyma.05G138400.1	5	1008	335	37	S	2
GmPAP17d	Glyma.05G247800.1	5	1065	354	40	S	1
GmPAP17a	Glyma.05G247900.1	5	996	331	37	S	1
GmPAP12a	Glyma.06G028100.1	6	1135	444	51	–	5
GmPAP12b	Glyma.06G028200.1	6	1425	474	54	S	4
GmPAP27b	Glyma.06G170300.1	6	1872	623	70	S	5
GmPAP17b	Glyma.08G056400.1	8	987	328	37	S	1
GmPAP7e	Glyma.08G093300.1	8	969	322	36	S	2
GmPAP7c	Glyma.08G093500.1	8	999	332	38	S	1
GmPAP7b	Glyma.08G093600.1	8	1008	335	38	S	1
GmPAP1b	Glyma.08G291600.1	8	1856	616	69	S	3
GmPAP18b	Glyma.08G314800.1	8	1410	469	53	–	1
GmPAP15a	Glyma.08G351000.1	8	1644	547	62	S	4
GmPAP27d	Glyma.09G225000.1	9	1923	640	71	S	5
GmPAP10a	Glyma.09G229200.1	9.	1395	464	53	S	5
GmPAP22b	Glyma.10G071000.1	10	1266	421	48	S	3
GmPAP15b	Glyma.11G255700.1	11	1398	466	52	M	7
GmPAP10b	Glyma.12G007500.1	12	1395	464	53	S	5
GmPAP27e	Glyma.12G012000.1	12	1980	659	73	S	6
GmPAP10c	Glyma.12G221100.1	12	1410	469	54	S	4
GmPAP26a	Glyma.13G161900.1	13	1428	475	54	S	2
GmPAP10d	Glyma.13G280500.1	13	1416	471	54	S	4
GmPAP18c	Glyma.14G024700.1	14	1383	460	52	S	1
GmPAP26b	Glyma.17G109400.1	17	1539	512	59	M	4
GmPAP15c	Glyma.18G001300.1	18	1719	572	56	S	6
GmPAP1c	Glyma.18G132500.1	18	1851	616	69	S	3
GmPAP23	Glyma.19G026600.1	19	1764	587	65	S	5
GmPAP22c	Glyma.19G193900.1	19	1473	490	55	C	1
GmPAP20b	Glyma.19G194000.1	19	1290	429	48	S	1
GmPAP17c	Glyma.20G011900.1	20	984	327	37	S	3
GmPAP9	Glyma.20G026800.1	20	1989	662	74	S	6

For predicted subcellular location, "S", "C", "M", and "–" mean secretory, chloroplast, mitochondrial, and any other location, respectively.

adenosine monophosphate (AMP), glucose-6-phosphate (G-6-P), glycerol-2-phosphate (G-2-P), guanosine monophosphate (GMP), inosine monophosphate (IMP), phospho-threonine (P-Thr), phospho-serine (P-Ser), and ρ-NPP. The relative activities were shown as the amount of Pi released from different substrates against the Pi released from ρ-NPP as the substrate. To determine the effects of different metal ions on GmPAP7a/7b activities, a total of nine different metal ions were applied at a final concentration of 5 mM: Mg^{2+}, Fe^{2+}, Al^{3+}, Mn^{2+}, Zn^{2+}, Cu^{2+}, Ba^{2+}, Ca^{2+}, and Co^{2+}. The metal ions and GmPAP7a/7b proteins were separately incubated in reaction mixtures which consisted of 45 mM Na-acetate buffer (pH 5.0) and 5 mM ρ-NPP to analyze their activities. The relative activities were expressed as the activities with different metal ions divided by the activities without the addition of metal ions. Furthermore, the V_{max} and K_m values of GmPAP7a/7b toward ATP substrate were determined using a Lineweaver–Burk double reciprocal plot at different ATP concentrations. The units were expressed as the amount of Pi released per minute per milligram protein. All the data are shown as the means of three independent experiments.

Functional Analysis of *GmPAP7a/7b* in Soybean Hairy Roots

The open reading frame of *GmPAP7a/7b* was separately amplified using specific primers (*GmPAP7a/7b-OX-F/R*) and subsequently cloned into a *pTF101s* binary vector. This enables glufosinate ammonium selection for positive transformants. *Agrobacterium*

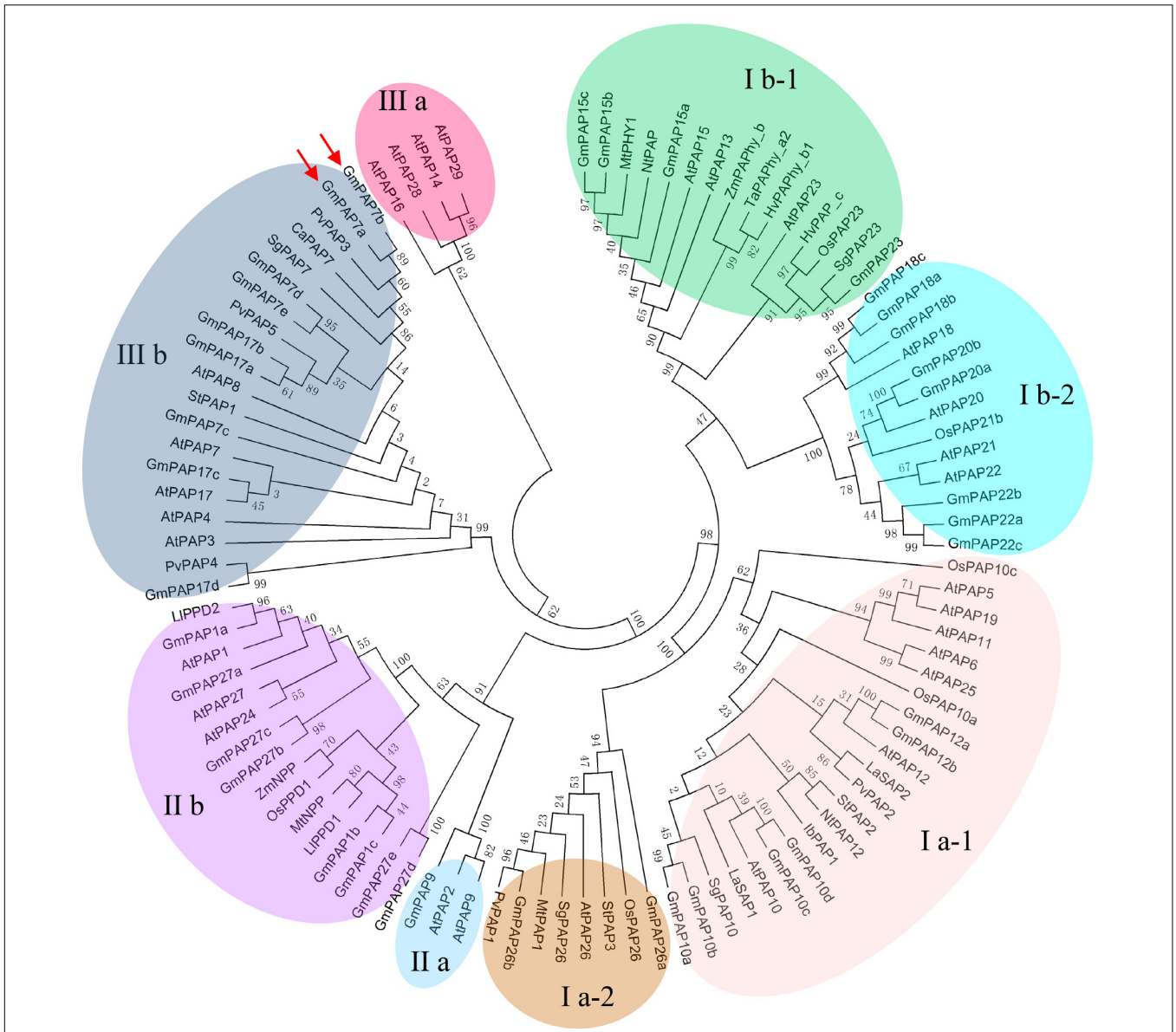

FIGURE 3 | Phylogenetic analysis of PAPs in different plant species. The first two letters of each PAP indicate the abbreviated species name. At: *Arabidopsis thaliana*, Gm: *Glycine max*, Pv: *Phaseolus vulgaris*, Os: *Oryza sativa*, Zm: *Zea mays*, Ll: *Lupinus luteus*, Ta: *Triticum aestivum*, Nt: *Nicotiana tabacum*, Hv: *Hordeum vulgare*, Sg: *Stylosanthes guianensis*, Mt: *Medicago truncatula*, La: *Lupinus albus*, St: *Solanum tuberosum*, Ib: *Ipomoea batatas*, Ca: *Cicer arietinum*. The phylogenetic tree was constructed by MEGA 5.01 program using the neighbor-joining method, with 1000 bootstrap replicates. The bootstrap values are indicated for major branches as percentages. GmPAP7a and GmPAP7b are indicated by red arrows.

rhizogenes-mediated soybean hairy root transformation was performed as described previously (Wu et al., 2018). Briefly, YC03-3 seeds were surface sterilized and germinated on half-strength MS media for 4 days. The cotyledons were wounded and then transferred to MS media containing 100–200 μg L^{-1} glufosinate ammonium and 500 μg mL^{-1} carbenicillin disodium. After 14–20 days of growth, 18 independent transgenic lines, including nine overexpression lines and nine empty controls (verified by qRT-PCR), were selected for ATP utilization analysis as described previously (Liang et al., 2010). Briefly, approximately 0.1 g of transgenic soybean hairy roots was transferred to new solid MS media containing 0.4 mM ATP (Sigma-Aldrich, United States) or 6.25 μM KH_2PO_4 (−P), separately. After the root grew for 14 days, intercellular and root-associated APase activities, root fresh weight, and total P content were measured.

Statistical Analyses

Data analyses and standard error calculations were statistically performed using Microsoft Excel 2016 (Microsoft Company, United States), and *t*-tests were performed with the SPSS program (v21.0; SPSS Institute, United States).

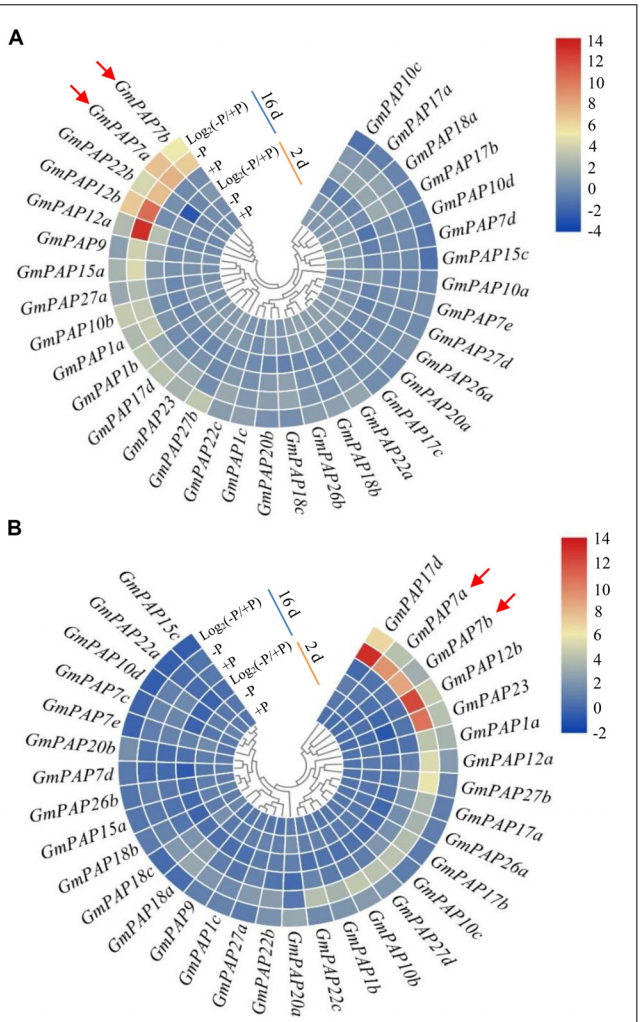

FIGURE 4 | Heatmap analysis of the expression patterns of *GmPAP* members in leaves and roots in response to P deficiency. **(A)** Leaves. **(B)** Roots. Soybean seedlings were grown in nutrient solution supplemented with 5 μM (–P) or 250 μM (+P) KH_2PO_4. The leaves and roots were harvested for qRT-PCR analysis after 2 and 16 days of P treatment. Log_2(–P/+P) represents the binary logarithm of the fold changes of the relative expression of *GmPAP* members under Pi-deficient and Pi-sufficient conditions. The data are the means of four replicates. *GmPAP7a* and *GmPAP7b* are indicated by red arrows.

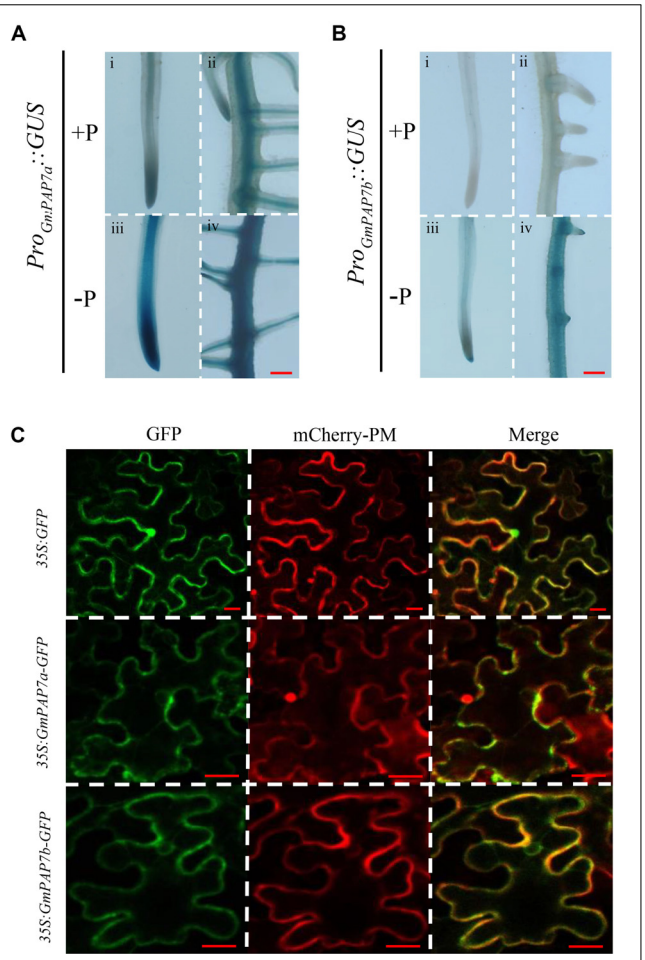

FIGURE 5 | Histochemical and subcellular localization of *GmPAP7a/7b*. **(A)** GUS staining of transgenic soybean hairy roots harboring the *GmPAP7a* promoter (i–iv). **(B)** GUS staining of transgenic soybean hairy roots harboring the *GmPAP7b* promoter (i–iv). Transgenic soybean hairy roots were grown on MS media supplemented with 1250 (+P) μM or 5 μM (–P) KH_2PO_4 for 7 days, and then incubated with GUS staining for further analysis. Bars = 50 μm. **(C)** Subcellular localization of GmPAP7a and GmPAP7b. Transient expression of empty vector control (*35S:GFP*) or *35S:GmPAP7a/7b-GFP* constructs in tobacco leaf epidermal cells. Both GFP and mCherry-PM fluorescence were observed using confocal microscopy. mCherry-PM indicated the plasma membrane *AtPIP2A*-mCherry marker. Bars = 20 μm.

RESULTS

Dynamic Effects of Pi Starvation on Soybean Biomass and P Concentration

To investigate the effects of low Pi availability on soybean growth, the fresh weight of soybean shoots and roots and the total P concentration in both the leaves and roots were determined on different days after two P treatments. Although both shoot and root fresh weight increased during the period of the two P treatments, Pi availability exhibited different effects on dynamic changes in shoot and root fresh weight (**Figures 1A,B**). For shoot fresh weight, there was no difference between the +P and −P treatments during the early period of P treatments (i.e., 0–10 days), but shoot fresh weight under −P conditions was 10% and 17% less than that under +P conditions at 13 days and 16 days, respectively (**Figure 1A**), suggesting that Pi starvation significantly inhibited shoot growth after 13 days of P treatment. However, root fresh weight increased in response to Pi starvation at 10 days and reached the highest at 16 days, which was 99% more than that under +P conditions (**Figure 1B**), suggesting that Pi starvation enhanced soybean root growth. In contrast, significant decreases in total P concentration were observed in both the leaves and roots in response to Pi starvation, as reflected by the 48.1% decrease in the leaves at 5 days and the 46.1% decrease in the roots at 1 day (**Figures 1C,D**). Furthermore, the

ratios of leaf P concentration at low P levels to that at high P levels were approximately 0.9 at 4 days and 0.3 at 16 days, but the ratios in the roots were 0.6 at 4 days and 0.2 at 16 days (**Figures 1C,D**). This suggests that Pi homeostasis in roots seems more susceptible to Pi availability than that in the leaves.

Phosphate Starvation Increases APase Activities in the Leaves and Roots

Dynamic changes in intracellular and root-associated APase activities were further investigated in both leaves and roots at two P levels. Distinct changes in APase activities were observed between leaves and roots under two P conditions. In the leaves, intracellular APase activities reached their highest levels at 4 and 5 days under low- and high-P conditions, respectively, followed by significant decreases with increased duration of P treatment (**Figure 2A**). Furthermore, leaf intracellular APase activities at low P levels were significantly higher than those at high P levels at 4, 13, and 16 days (**Figure 2A**), strongly suggesting that low Pi availability significantly affected intracellular APase activities in the leaves. Unlike changes in leaf intracellular APase activities, root intracellular APase activities were significantly enhanced at 1 day and increased by approximately 7-fold at 16 days in response to by Pi starvation (**Figure 2B**). Furthermore, root intracellular APase activities were gradually enhanced with increased duration of Pi starvation, but they remained unchanged after 5 days of high P treatment (**Figure 2B**). Although changes of root-associated APase activities exhibited a similar trend between the two P levels, Pi starvation led to more increases of root-associated APase activities after 10 days of P treatment (**Figure 2C**). Especially at 16 days, root-associated APase activities at low P levels were approximately 4-fold higher than those at high P levels (**Figure 2C**). When BCIP served as the substrate, root-associated APase activities were also visualized. A more intense blue color was detected on root surface under low-P conditions than that under high-P conditions, especially at 10, 13, and 16 days (**Figure 2C**), strongly suggesting that Pi starvation enhanced root-associated APase activities in soybean.

Bioinformatic and Phylogenetic Analyses

When sequence homology alignment and conserved PAP domain analysis were used, compared to the 35 GmPAP members identified previously (Li C. C. et al., 2012), five new GmPAP members were identified, and two GmPAP members were not found in the updated soybean genome database. Therefore, a total of 38 GmPAP members were annotated and named in terms of sequence homology with corresponding AtPAP members by using multiple alignments and phylogenetic analysis. The general information of *GmPAP* members, including chromosomal location, length of coding sequence (CDS), and protein mass, is summarized in **Table 1**. The *GmPAP* members were found to be localized on different chromosomes (**Table 1**). The protein mass of the GmPAP family varied from 35 kD (GmPAP7d) to 74 kD (GmPAP9), and the full length of the CDS and number of amino acids varied from 933 to 1,989 bp, and from 310 to 662 aa, respectively (**Table 1**). Most GmPAP members were predicted to be involved in the secretory pathway. However, GmPAP22a and GmPAP22c were localized in the chloroplasts; GmPAP26b, GmPAP15b, and GmPAP27c in the mitochondria; and GmPAP1a, GmPAP12a, and GmPAP18b in other subcellular organelles (**Table 1**). Moreover, all GmPAP members except GmPAP27c and GmPAP7d were predicted to be modified by glycans (**Table 1**).

An unrooted phylogenetic tree was constructed by MEGA 5.01 using the neighbor-joining method; PAPs were identified in various plant species, including common bean, rice, Arabidopsis, sweet potato, soybean, maize, lupinus, wheat, tobacco, barely, stylo, Medicago, white lupin, potato, and chickpea (**Figure 3**). It was observed that all plant PAPs could be mainly divided into three main groups comprising eight subgroups, all of which encompassed GmPAP members except subgroup III a (**Figure 3**). The molecular weights of the plant PAPs in group I and group II were approximately 55 kD and 75 kD, respectively, which were higher than those in the group III, of which the PAPs had a molecular weight of approximately 35 kD (**Table 1** and **Figure 3**). Twenty out of 38 GmPAP members were assigned to group I. Notably, nine GmPAP members (GmPAP1a, 1b, 1c, 9, 27a, 27b, 27c, 27d, and 27e) were clustered into group II, and nine GmPAP members (GmPAP7a, 7b, 7c, 7d, 7e, 17a, 17b, 17c, and 17d) belonged to subgroup III b (**Figure 3**). Furthermore, GmPAP7a and GmPAP7b were close to PvPAP3 in common bean (**Figure 3**), which was reported to be involved in extracellular ATP utilization.

Transcripts of *GmPAPs* in Response to Pi Starvation

Relative expression levels of *GmPAP* members in the leaves and roots were analyzed at 2 and 16 days at two P levels through qRT-PCR analysis. Transcripts of all *GmPAP* members were detectable at both P levels, except for those of four members in the leaves (i.e., *GmPAP27c*, *GmPAP27e*, *GmPAP7c,* and *GmPAP15b*) and for those of five in the roots (i.e., *GmPAP10a*, *GmPAP15b*, *GmPAP17c*, *GmPAP27c,* and *GmPAP27e*) (**Figure 4** and **Supplementary Table S2**). At 2 days of P treatment, transcripts of the detected *GmPAP* members were not influenced by Pi availability in either the leaves or the roots (**Figure 4** and **Supplementary Table S2**), suggesting that *GmPAP* members exhibited no response to early Pi starvation in soybean. However, at 16 days of P treatments, the transcript levels of nineteen genes (*GmPAP1a*, *1b*, *1c*, *7a*, *7b*, *9*, *10b*, *12a*, *12b*, *15a*, *17d*, *18b*, *22a*, *22b*, *22c*, *23*, *26b*, *27a*, and *27b*) were enhanced by more than 1-fold in the leaves of plants under Pi-deficient conditions compared with those under Pi-sufficient conditions (**Figure 4A** and **Supplementary Table S2**). Furthermore, five *GmPAP* members (*GmPAP7a*, *GmPAP7b*, *GmPAP12a*, *GmPAP12b,* and *GmPAP22b*) exhibited the highest expression levels in the leaves at low P level and clustered together (**Figure 4A** and **Supplementary Table S2**). In the roots, transcripts of 17 *GmPAP* members (*GmPAP1a*, *1b*, *1c*, *7a*, *7b*, *10b*, *10c*, *12a*, *12b*, *17b*, *17d*, *20a*, *22b*, *26a*, *23*, *27b,* and *27d*) were found to be significantly upregulated under Pi-deficient conditions (**Figure 4B** and **Supplementary Table S2**). Furthermore, five *GmPAP* members (*GmPAP7a*, *GmPAP7b*,

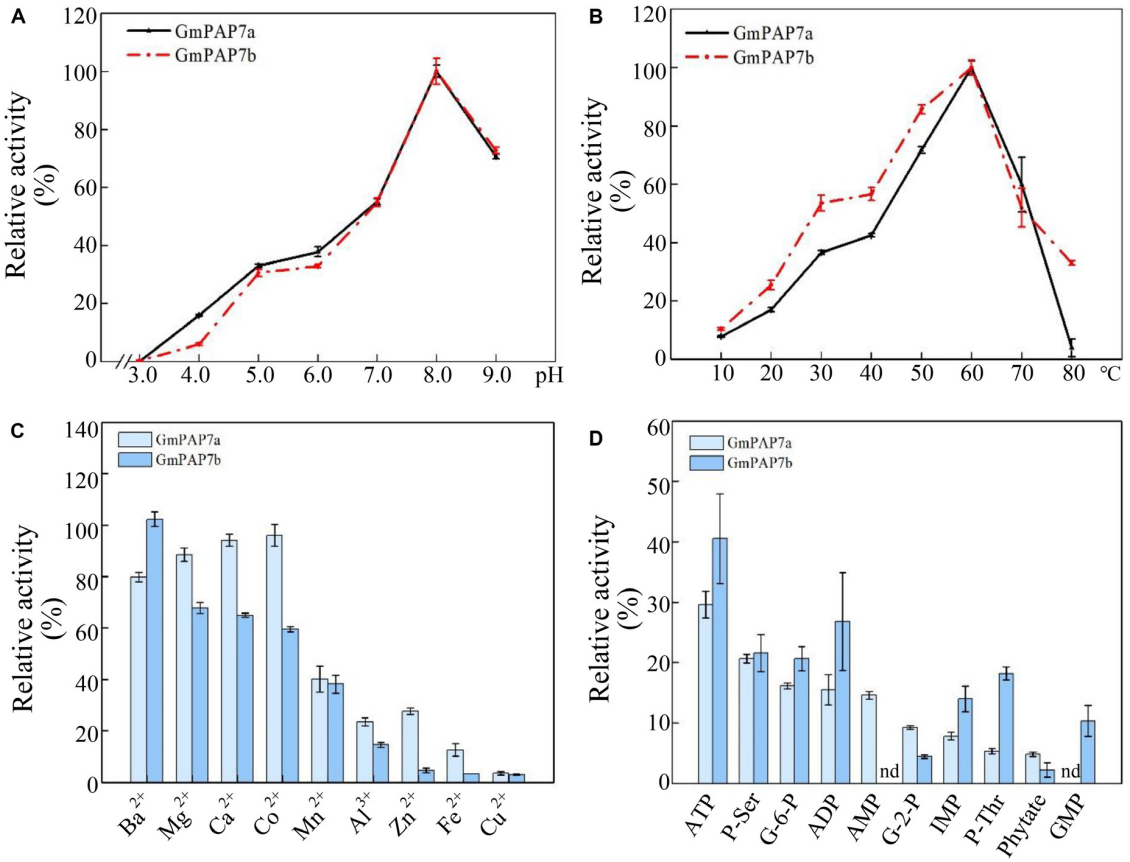

FIGURE 6 | Enzymatic properties of GmPAP7a and GmPAP7b. **(A)** Effects of pH on the relative activities of GmPAP7a and GmPAP7b. **(B)** Effects of temperature on the relative activities of GmPAP7a and GmPAP7b. **(C)** Effects of metal ions on the relative activities of GmPAP7a and GmPAP7b. **(D)** Relative activities of GmPAP7a and GmPAP7b against different substrates. The data are the means of three replicates with standard errors. nd indicates that no activity was detected.

GmPAP12b, *GmPAP17d,* and *GmPAP23*) exhibited the highest expression levels in the roots at low P level (**Figure 4B** and **Supplementary Table S2**). Overall, the expression levels of 12 *GmPAP* members (*GmPAP1a*, *1b*, *1c*, *7a*, *7b*, *10b*, *12a*, *12b*, *17d*, *22b*, *23*, and *27b*) were observed to be commonly increased in response to Pi starvation in both the leaves and roots, and this was especially the case for *GmPAP7a*, *GmPAP7b*, and *GmPAP12b* (**Figure 4** and **Supplementary Table S2**).

Tissue Expression Patterns and Subcellular Localization of *GmPAP7a/7b*

To further determine the tissue-specific expression patterns of *GmPAP7a/7b* in response to Pi starvation, $Pro_{GmPAP7a}$*:GUS* and $Pro_{GmPAP7b}$*:GUS* constructs were separately generated and introduced into soybean hairy roots subjected to P deficiency. Pi starvation led to higher GUS activity in both transgenic soybean hairy roots (**Figures 5A,B**), suggesting that Pi starvation could enhance *GmPAP7a/7b* transcript levels in the roots. Furthermore, under high P conditions, GUS activity was detected in both the root tips and steles of soybean hairy roots transformed with $Pro_{GmPAP7a}$*:GUS* and only in the stele for $Pro_{GmPAP7b}$*:GUS* (**Figures 5A,B**), suggesting that different tissue expression patterns might be present between *GmPAP7a* and *GmPAP7b* in roots under high P conditions. However, under low P conditions, GUS activity was separately detected in the whole roots transformed with two constructs (**Figures 5A,B**), suggesting that *GmPAP7a* and *GmPAP7b* exhibited similar expression patterns in roots at low P level.

To investigate their subcellular localization, *GmPAP7a* and *GmPAP7b* were separately fused to *GFP* and transiently over-expressed in tobacco leaves. The GFP signals of both *35S:GmPAP7a-GFP* and *35S:GmPAP7b-GFP* were detected mainly in the plasma membrane and cytoplasm (**Figure 5C**). However, the GFP signals of the control (*35S:GFP*) were detected throughout whole cells, including the plasma membrane, cytoplasm, and nucleus (**Figure 5C**). The results suggested that both GmPAP7a and GmPAP7b were located predominantly in the plasma membrane and cytoplasm (**Figure 5C**).

Biochemical Characterization of *GmPAP7a/7b*

To determine the enzymatic properties of GmPAP7a/7b, recombinant proteins GmPAP7a-GST and GmPAP7b-GST were

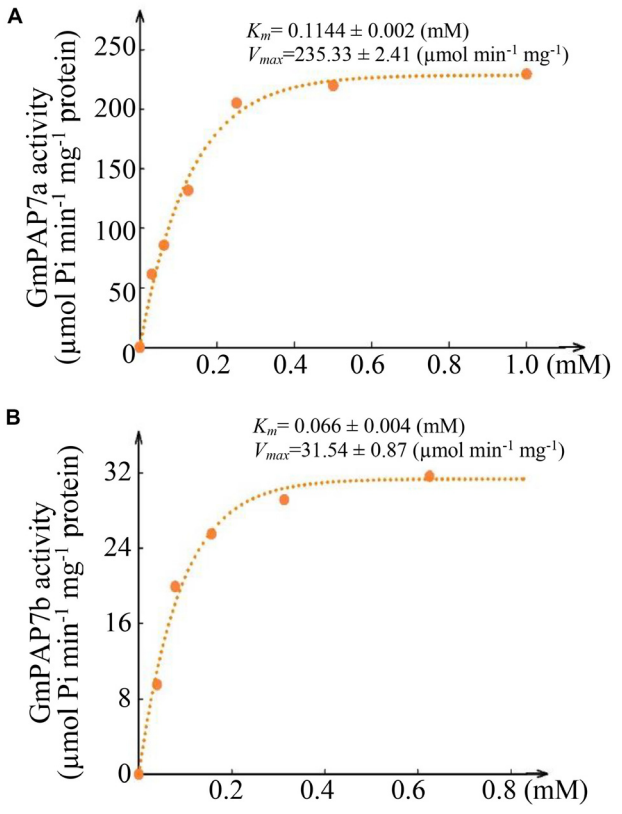

FIGURE 7 | Kinetic parameters of GmPAP7a and GmPAP7b against ATP. **(A)** Kinetic parameter of GmPAP7a. **(B)** Kinetic parameter of GmPAP7b. The K_m and V_{max} of GmPAP7a and GmPAP7b were calculated from Lineweaver–Burke plots of enzyme activities at different concentrations of ATP. The data are the means of three replicates.

separately expressed and successfully purified from *E. coli* lysates (**Supplementary Figure S1**). The optimum pH and temperature for GmPAP7a/7b catalytic reactions were analyzed *in vitro* using ρ-NPP as the substrate, and it was observed that both GmPAP7a and GmPAP7b exhibited similar properties for optimum pH and temperature, as reflected by the maximum relative activities that were separately observed at pH 8.0 and 60°C (**Figures 6A,B**). However, GmPAP7a activities seem more sensitive to high temperature than GmPAP7b because the relative activities of GmPAP7a and GmPAP7b were 2% and 30% at 80°C, respectively (**Figure 6B**). In addition, the effects of metal ions on the activities of GmPAP7a and GmPAP7b were separately investigated (**Figure 6C**). The relative activities of both GmPAP7a and GmPAP7b were reduced by more than 50% by application of Mn^{2+}, Al^{3+}, Zn^{2+}, Fe^{2+}, and Cu^{2+}, especially Cu^{2+}, which inhibited their relative activities by 90% (**Figure 6C**). However, significant inhibition of relative activities was observed only for GmPAP7b and not for GmPAP7a, when Mg^{2+}, Co^{2+} or Ca^{2+} was applied (**Figure 6C**).

In a test of substrate specificity, the relative activities of both GmPAP7a and GmPAP7b were highest against ATP, followed by phosphate-serine for GmPAP7a and ADP for GmPAP7b (**Figure 6D**). Furthermore, activities against AMP were observed only for GmPAP7a, not for GmPAP7b. Similarly, activities against GMP were observed only for GmPAP7b and not for GmPAP7a (**Figure 6D**). When ATP served as the substrate, kinetic analyses showed that K_m and V_{max} values were 0.11 mM and 235.3 μmol min^{-1} mg^{-1} protein for GmPAP7a and 0.066 mM and 31.5 μmol min^{-1} mg^{-1} protein for GmPAP7b, respectively (**Figure 7**), suggesting that the catalytic properties differ between GmPAP7a and GmPAP7b.

Overexpressing *GmPAP7a/7b* Enhanced Exogenous ATP Utilization

To investigate the functions of *GmPAP7a* and *GmPAP7b* in exogenous ATP utilization, transgenic soybean hairy roots overexpressing *GmPAP7a* or *GmPAP7b* were generated (**Figure 8**). The increased expression levels of *GmPAP7a* or *GmPAP7b* in transgenic hairy root lines (*OX-GmPAP7a/7b*) were verified through qRT-PCR analysis, as reflected by more than 11-fold increases compared to those of the control (CK) lines (**Supplementary Figure S2a**). Moreover, overexpression of *GmPAP7a* and *GmPAP7b* led to significant increases in intracellular APase activities (**Supplementary Figure S2b**) and root-associated APase activities under P-deficient conditions and ATP application (**Figure 8**). Furthermore, the fresh weight and the total P content were approximately 50% and 28% higher, respectively, in the soybean hairy root lines with *GmPAP7a* or *GmPAP7b* overexpression than in the control lines with ATP application, while no difference was observed in the −P treatments (**Figure 8**), strongly suggesting that GmPAP7a and GmPAP7b might participate in extracellular ATP utilization in soybean.

DISCUSSION

Phosphorus is an essential macronutrient participating in many biochemical and metabolic processes (Liang et al., 2010; Zhang et al., 2014; Ham et al., 2018). Low Pi availability imposes serious limitations on crop growth and production (Vance et al., 2003; Zhang et al., 2014; Dissanayaka et al., 2018). It is generally observed that P deficiency alters root system to increase the root surface area and exploitable soil volume for Pi uptake (Pérez-Torres et al., 2008; Lambers et al., 2011; Lynch, 2011). In this study, enhanced soybean root growth was also observed in soybean in response to Pi starvation, as reflected by increased soybean root fresh weight after 10 days of Pi starvation (**Figure 1**), strongly suggesting that significant changes in the soybean root system occur under P-deficient conditions.

In addition to changes in root morphology and architecture, Pi starvation also results in increases in intracellular and extracellular APase activities in plants (Zimmermann et al., 2004; Plaxton and Lambers, 2015; Tian and Liao, 2015; Wang and Liu, 2018). Furthermore, accumulating evidence has suggested that

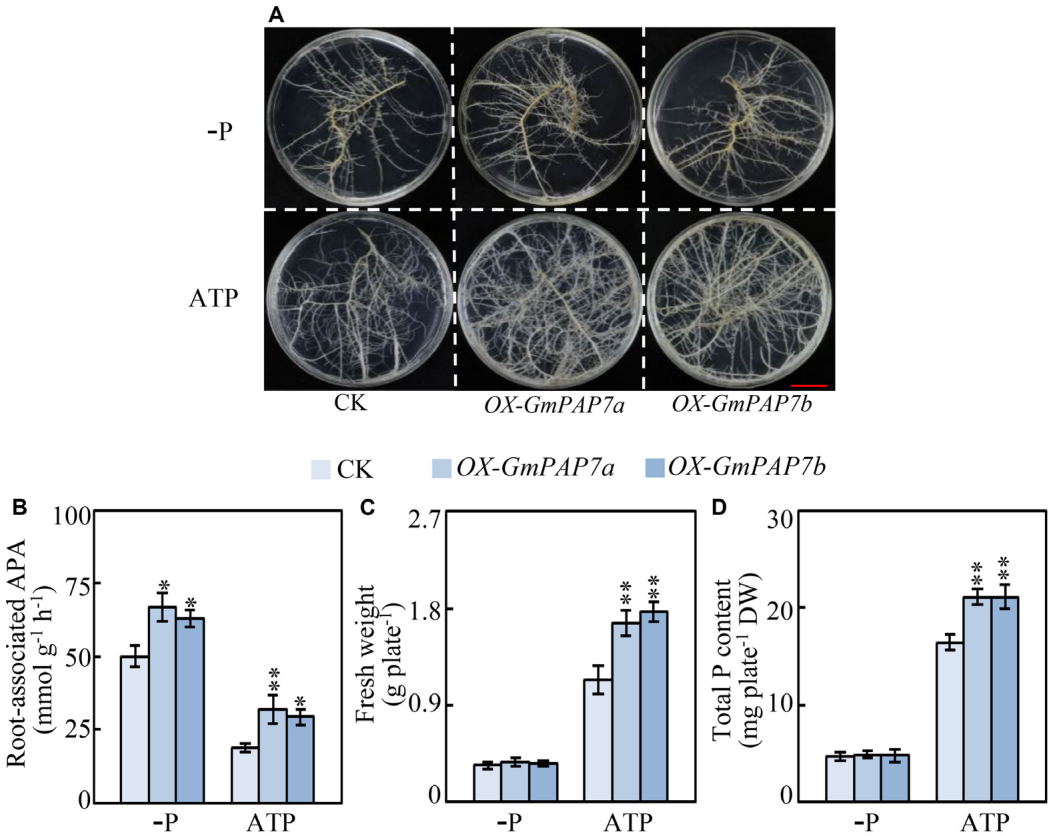

FIGURE 8 | Effects of *GmPAP7a* and *GmPAP7b* overexpression on APase activities, total P content and fresh weight of transgenic soybean hairy roots. **(A)** Image of transgenic hairy roots supplied with different P sources. Bars = 1 cm. **(B)** Root-associated APase activities. **(C)** Fresh weight of transgenic soybean hairy roots. **(D)** Total P content in transgenic soybean hairy roots. Transgenic soybean hairy roots were grown for 14 days on MS media supplemented with 6.25 μM KH_2PO_4 (–P) or 0.4 mM ATP as the sole P source. Fresh weight and total P content were separately measured. CK represents transgenic hairy root lines transformed with an empty vector. *OX-GmPAP7a* and *OX-GmPAP7b* indicate transgenic hairy root lines overexpressing *GmPAP7a* and *GmPAP7b*, respectively. The data are the means of nine replicates with standard errors. The asterisks indicate significant differences between the overexpression and CK lines according to Student's *t*-test: $^*P < 0.05$, $^{**}P < 0.01$.

increases in APase activities are mainly due to an enhanced *PAP* transcripts under low P conditions in plants, such as *PvPAP3* in bean, *AtPAP10*/*12* in Arabidopsis, *OsPAP10a* and *OsPAP21b* in rice (Liang et al., 2010; Tran et al., 2010b; Wang et al., 2011; Tian et al., 2012a; Mehra et al., 2017). In this study, root intracellular and associated APase activities were significantly enhanced by Pi starvation at 16 days (**Figure 2**), accompanied by significantly increased transcripts of 17 *GmPAP* members in the roots (**Figure 4B** and **Supplementary Table S2**), strongly suggesting that increased transcripts of *GmPAP* members could lead to enhanced APase activities in soybean. However, increases of root intracellular APase activities were also detected after 2 days of Pi starvation, while the transcript abundance of no *GmPAP* member changed in response to Pi starvation in either the leaves or roots (**Figures 2**, **4**), suggesting that there must be other molecular mechanisms underlying APase activity regulation in addition to controlling the transcript levels of *GmPAP* members. In soybean, 36 out of 38 GmPAP members were predicted to exhibit more than one glycosylation site (**Table 1**). Moreover, it has been suggested that the enzymatic properties of plant PAPs could be impacted by their glycosylation (Navazio et al., 2002; Olczak and Olczak, 2007; Tran et al., 2010b). Therefore, it is plausible that glycosylation modification of GmPAP members may play a role in regulating APase activities in response to 2 days of Pi starvation, which merits further analysis.

With the aid of genome sequence availability in various plant species, increased transcripts of *PAP* members in response to Pi starvation have been found in plant species, such as Arabidopsis, rice, maize, and chickpea (Zhang et al., 2010; Wang et al., 2014; Gonzalez-Munoz et al., 2015; Bhadouria et al., 2017). Similarly, the expression levels of 19 and 17 *GmPAP* members increased in response to Pi starvation in the leaves and roots, respectively (**Figure 4** and **Supplementary Table S2**), suggesting that increased *PAP* transcription is a common response to Pi starvation in plants. Moreover, a group of plant *PAP* members have been suggested to be downstream genes of *PHR1* (or its homologs), which is the central regulator in the P signaling network; these *PAPs* include *AtPAP17* in Arabidopsis, 10 *OsPAP* members in rice, and *PvPAP3* in bean (Rubio et al., 2001; Bari et al., 2006; Zhang et al., 2010; Yao Z. F. et al., 2014).

These findings suggest that *GmPAP* members might also be regulated by *PHR1* or its homologs in soybean. Consistently, *GmPAP14* (i.e., *GmPAP7e*) and *GmPAP21* (i.e., *GmPAP22b*) have been suggested to be downstream genes of *GmPHR25* because *GmPHR25* overexpression leads to increased transcript levels in roots of *GmPHR25* overexpression composite plants (Xue et al., 2017). However, the regulatory mechanisms of other Pi starvation-responsive *GmPAP* members remain unclear.

Root-associated PAPs are well known to play a role in the utilization of extracellular organic P sources, such as ATP, phytate-P and dNTPs (Liang et al., 2010, 2012; Wang et al., 2011, 2014; Robinson et al., 2012; Liu et al., 2016, 2018; Lu et al., 2016; Gao et al., 2017; Mehra et al., 2017; Wu et al., 2018). For example, AtPAP10/12/26 are suggested to participate in the utilization of extracellular DNA and ADP in Arabidopsis (Wang et al., 2011, 2014). However, the functions of PvPAP3 in bean and OsPAP10a/21b/26/10c in rice are suggested to mediate extracellular ATP utilization (Liang et al., 2010; Tian et al., 2012a; Lu et al., 2016; Gao et al., 2017; Mehra et al., 2017). In this study, phylogenetic tree analysis revealed that PvPAP3, GmPAP7a, and GmPAP7b belonged to group III b (**Figure 3**), suggesting they might have similar functions in plants. Moreover, both GmPAP7a and GmPAP7b exhibited relatively high activities against ATP *in vitro* (**Figure 6D**) and localized to the plasma membrane and cytoplasm (**Figure 5C**), which was similar to that occurred for PvPAP3 (Liang et al., 2010). Furthermore, the fresh weight and total P content in soybean hairy roots with *GmPAP7a* and *GmPAP7b* overexpression were significantly higher than those of control lines with ATP application (**Figure 8**), strongly suggesting that GmPAP7a and GmPAP7b could utilize extracellular ATP. Interestingly, pH optima of GmPAP7a and GmPAP7b activity was 8.0 *in vitro* (**Figure 6A**). Similarly, pH optima of several plant PAP activity was found to be above 7.0 despite how the pH optima of activity for most plant PAPs is generally below 7.0 (Tran et al., 2010a; Plaxton and Lambers, 2015; Tian and Liao, 2015; Wang and Liu, 2018). For example, pH optima of PvPAP3 against ρ-NPP and KbPAP against ATP was 7.0 or above (Cashikar et al., 1997; Liang et al., 2010). Therefore, these results suggest that some plant PAPs might have functions as an alkaline phosphatase, which merits further study.

Remobilization of internal phosphorylated metabolites (e.g., phosphorylated carbon) is generally considered to be an adaptive strategy plants in responses to Pi starvation (Chiou and Lin, 2011; Tian et al., 2012b; Plaxton and Lambers, 2015; Abel, 2017). Consistently, decreased accumulation of phosphorylated compounds was widely observed in plants under Pi-deficient conditions (Chiou and Lin, 2011; Tian et al., 2012b; Plaxton and Lambers, 2015; Mo et al., 2019). Given that plant PAPs exhibit activity against a set of phosphorylated metabolites, it is suggested that internal plant PAP might play a role in metabolic processes of internal phosphorylated metabolites (Tian et al., 2012b; Plaxton and Lambers, 2015). In this study, since transcript levels of both *GmPAP7a* and *GmPAP7b* were also significantly upregulated in leaves after 16 d of P deficiency, it is plausible that GmPAP7a and GmPAP7b might participate in the recycling of internal phosphorylated metabolites in leaves.

In summary, a total of 38 GmPAP members were identified in the soybean genome. However, the transcript levels of 19 and 17 *GmPAP* members were upregulated by 16 days of P deficiency in the leaves and roots, respectively. Among them, both GmPAP7a and GmPAP7b had the highest activities against ATP *in vitro*. Furthermore, overexpressing *GmPAP7a* and *GmPAP7b* resulted in significant increases in root-associated APase activities and total P content in soybean hairy roots when ATP was supplied as the sole P source. Taken together, these results suggest that Pi starvation responsive *GmPAP7a* and *GmPAP7b* may mediate root-associated APase activities and thus control extracellular ATP utilization in soybean in response to P deficiency.

DATA AVAILABILITY STATEMENT

All datasets generated for this study are included in the article/**Supplementary Material**.

AUTHOR CONTRIBUTIONS

JT and CL conceived and designed the experiments. SZ, MC, and SL performed the experiments. JT, CL, SZ, MC, and YX analyzed the data. JT, CL, SZ, and YX wrote the manuscript. All authors have read and approved the final manuscript.

FUNDING

This work was supported by the Major Program of Guangdong Basic and Applied Research (2019B030302006), the National Natural Science Foundation of China (31872164 and 31672220), the Integrated Demonstration of Key techniques for the Industrial Development of Featured Crops in Rocky Desertification Areas of Yunnan-Guangxi-Guizhou Provinces (SMH2019-2021), the Guangdong Natural Science Funds for Distinguished Young Scholars (2015A030306034), the Key R&D Program of Guangdong Province (2019B020219003), and the Research Team Project of the Natural Science Foundation of Guangdong Province (2016A030312009).

SUPPLEMENTARY MATERIAL

The Supplementary Material for this article can be found online at: https://www.frontiersin.org/articles/10.3389/fpls.2020.00661/full#supplementary-material

FIGURE S1 | Analysis of the expression and purification of recombinant GmPAP7a-GST and GmPAP7b-GST proteins.

FIGURE S2 | Analysis of *GmPAP7a/7b* transcription and intracellular APase activities in transgenic overexpression soybean hairy roots.

TABLE S1 | Primers used for qRT-PCR or vector construction.

TABLE S2 | Relative expression levels of *GmPAP* members.

REFERENCES

Abel, S. (2017). Phosphate scouting by root tips. *Curr. Opin. Biotechnol.* 39, 168–177. doi: 10.1016/j.pbi.2017.04.016

Bari, R., Datt, P. B., Stitt, M., and Scheible, W. R. (2006). PHO2, microRNA399, and PHR1 define a phosphate-signaling pathway in plants. *Plant Physiol.* 141, 988–999.

Bhadouria, J., Singh, A. P., Mehra, P., Verma, L., Srivastawa, R., Swarup, K., et al. (2017). Identification of purple acid phosphatases in chickpea and potential roles of CaPAP7 in seed phytate accumulation. *Sci. Rep.* 7:11012. doi: 10.1038/s41598-017-11490-9

Bradford, M. M. (1976). A rapid and sensitive method for the quantitation of microgram quantities of protein utilizing the principle of protein-dye binding. *Anal. Biochem.* 72, 248–254. doi: 10.1016/0003-2697(76)90527-3

Cashikar, A. G., Kumaresan, R., and Rao, N. M. (1997). Biochemical characterization and subcellular localization of the red kidney bean purple acid phosphatase. *Plant Physiol.* 114, 907–915. doi: 10.1104/pp.114.3.907

Chen, L. Y., Qin, L., Zhou, L., Li, X. X., Chen, Z. J., Sun, L., et al. (2018). A nodule-localized phosphate transporter GmPT7 plays an important role in enhancing symbiotic N2 fixation and yield in soybean. *New Phytol.* 221, 2013–2025. doi: 10.1111/nph.15541

Chiou, T. J., and Lin, S. I. (2011). Signaling network in sensing phosphate availability in plants. *Annu. Rev. Plant Biol.* 62, 185–206. doi: 10.1146/annurev-arplant-042110-103849

Conley, D. J., Paerl, H. W., Howarth, R. W., Boesch, D. F., Seitzinger, S. P., Havens, K. E., et al. (2009). Controlling eutrophication: nitrogen and phosphorus. *Science* 323, 1014–1015. doi: 10.1126/science.1167755

Conner, T., Paschal, E. H., Barbero, A., and Johnson, E. (2004). The challenges and potential for future agronomic traits in soybeans. *Agbio. Forum.* 7, 47–50.

Del Pozo, J. C., Allona, I., Rubio, V., Leyva, A., De la Pena, A., Aragoncillo, C., et al. (1999). A type 5 acid phosphatase gene from Arabidopsis thaliana is induced by phosphate starvation and by some other types of phosphate mobilizing/oxidative stress conditions. *Plant J.* 19, 579–589. doi: 10.1046/j.1365-313x.1999.00562.x

Dionisio, G., Madsen, C. K., Holm, P. B., Welinder, K. G., Jorgensen, M., Stoger, E., et al. (2011). Cloning and characterization of purple acid phosphatase phytases from wheat, barley, maize, and rice. *Plant Physiol.* 156, 1087–1100. doi: 10.1104/pp.110.164756

Dissanayaka, D. M. S. B., Nishida, S., Tawaraya, K., and Wasaki, J. (2018). Organ-specific allocation pattern of acquired phosphorus and dry matter in two rice genotypes with contrasting tolerance to phosphorus deficiency. *J. Plant Nutr. Soil Sci.* 64, 1–9. doi: 10.1080/00380768.2018.1436941

Gao, W. W., Lu, L. H., Qiu, W. M., Wang, C., and Shou, H. X. (2017). OsPAP26 encodes a major purple acid phosphatase and regulates phosphate remobilization in rice. *Plant Cell Physiol.* 58, 885–892. doi: 10.1093/pcp/pcx041

Gonzalez-Munoz, E., Avendano-vazquez, A. Q., Chavez-Montes, R. A., de Folter, S., Andres-Hernandez, L., Abreu-Goodger, L. C., et al. (2015). The maize (*Zea mays* ssp. Mays var B73) genome encodes 33 members of the purple acid phosphatases family. *Front. Plant Sci.* 6:341. doi: 10.3389/fpls.2015.00341

Ham, B. K., Chen, J. Y., Yan, Y., and William, J. L. (2018). Insights into plant phosphate sensing and signaling. *Curr. Opin. Biotechnol.* 49, 1–9.

Haran, S., Logendra, S., Seskar, M., Bratanova, M., and Raskin, I. (2000). Characterization of Arabidopsis acid phosphatase promoter and regulation of acid phosphatase expression. *Plant Physiol.* 124, 615–626. doi: 10.2307/4279464

Herridge, D. F., Peoples, M. B., and Boddey, R. M. (2008). Global inputs of biological nitrogen fixation in agricultural systems. *Plant Soil* 311, 1–18. doi: 10.1104/pp.126.4.1598

Jefferson, R. A., Kavanagh, T. A., and Bevan, M. W. (1987). GUS fusions: β-glucuronidase as a sensitive and versatile gene fusion marker in higher plants. *EMBO J.* 6, 3901–3907.

Jung, J. Y., Riled, M. K., Hothorn, M., and Poirier, Y. (2018). Control of plant phosphate homeostasis by inositol pyrophosphatase and the SPX domain. *Curr. Opin. Biotechnol.* 49, 156–162.

Kaida, R., Sage-Ono, K., Kamada, H., Okuyama, H., Syono, K., and Kaneko, T. S. (2003). Isolation and characterization of four cell wall purple acid phosphatase genes from tobacco cells. *Biochim. Biophys. Acta* 1625, 134–140. doi: 10.1016/S0167-4781(02)00599-7

Kong, Y. B., Li, X. H., Ma, J., Li, W. L., Yan, G. J., and Zhang, C. Y. (2014). GmPAP4, a novel purple acid phosphatase gene isolated from soybean (Glycine max), enhanced extracellular phytate utilization in Arabidopsis thaliana. *Plant Cell Rep.* 33, 655–667. doi: 10.1007/s00299-014-1588-5

Kong, Y. B., Li, X. H., Wang, B., Li, W. L., Du, H., and Zhang, C. Y. (2018). The soybean purple acid phosphatase GmPAP14 predominantly enhances external phytate utilization in plants. *Front. Plant Sci.* 9:292. doi: 10.3389/fpls.2018.00292

Lambers, H., Finnegan, P. M., Laliberté, E., Pearse, S. J., Ryan, M. H., Shane, M. W., et al. (2011). Phosphorus nutrition of proteaceae in severely phosphorus-impoverished soils: are there lessons to be learned for future crops? *Plant Physiol.* 156, 1058–1066. doi: 10.1104/pp.111.174318

Li, C. C., Gui, S. H., Yang, T., Walk, T., Wang, X. R., and Liao, H. (2012). Identification of soybean purple acid phosphatase genes and their expression responses to phosphorus availability and symbiosis. *Ann. Bot.* 109, 275–285. doi: 10.1093/aob/mcr246

Li, C. C., Zhou, J., Wang, X. R., and Liao, H. (2019). A purple acid phosphatase, GmPAP33, participates in arbuscule degeneration during arbuscular mycorrhizal symbiosis in soybean. *Plant Cell Envir.* 42, 2015–2027. doi: 10.1111/pce.13530

Li, D. P., and Wang, D. W. (2003). cDNA cloning and in vitro expressions of three putative purple acid phosphatase genes from *Arabidopsis*. *J. Nat. Sci.* 26, 3–29. doi: 10.1023/A:1022289509702

Li, D. P., Zhu, H. F., Liu, K. F., Liu, X., Leggewie, G., and Udvardi, M. (2002). Purple acid phosphatases of Arabidopsis thaliana. *J. Biol. Chem.* 31, 27772–27781. doi: 10.1074/jbc.M204183200

Li, R. J., Lu, W. J., Guo, C. J., Li, X. J., Gu, J. T., and Xiao, K. (2012). Molecular characterization and functional analysis of OsPHY1, a purple acid phosphatase (PAP)-type phytase gene in rice (*Oryza sativa* L.). *J. Integr. Plant Biol.* 11, 1217–1226.

Li, X. H., Wang, Y. J., Wu, B., Kong, Y. B., Li, W. L., Chang, W. S., et al. (2014). GmPHR1, a novel homolog of the AtPHR1 transcription factor, plays a role in plant tolerance to phosphate starvation. *J. Integr. Agric.* 13, 2584–2593. doi: 10.1016/S2095-3119(14)60775-9

Li, X. X., Zhao, J., Tan, Z. Y., Zeng, R. S., and Liao, H. (2015). GmEXPB2, a cell wall β-expansin, affects soybean nodulation through modifying root architecture and promoting nodule formation and development. *Plant Physiol.* 169, 2640–2653. doi: 10.1104/pp.15.01029

Liang, C. Y., Sun, L. L., Yao, Z. F., Liao, H., and Tian, J. (2012). Comparative analysis of PvPAP gene family and their functions in response to phosphorus deficiency in common bean. *PLoS One* 7:e38106. doi: 10.1371/journal.pone.0038106

Liang, C. Y., Tian, J., Lam, H. M., Lim, B. L., Yan, X., and Liao, H. (2010). Biochemical and molecular characterization of PvPAP3, a novel purple acid phosphatase isolated from common bean enhancing extracellular ATP utilization. *Plant Physiol.* 152, 854–865. doi: 10.1104/pp.109.147918

Liang, C. Y., Wang, J. X., Zhao, J., Tian, J., and Liao, H. (2014). Control of phosphate homeostasis through gene regulation in crops. *Curr. Opin. Plant Biol.* 21, 59–66. doi: 10.1016/j.pbi.2014.06.009

Liao, H., Wan, H. Y., Shaff, J., Wang, X. R., Yan, X. L., and Kochian, L. V. (2006). Phosphorus and aluminum interactions in soybean in relation to aluminum tolerance. Exudation of specific organic acids from different regions of the intact root system. *Plant Physiol.* 141, 674–684. doi: 10.1104/pp.105.076497

Liu, L., Liao, H., Wang, X. R., and Yan, X. L. (2008). Regulation effect of soil P availability on mycorrhizal infection in relation to root architecture and P efficiency of Glycine max. *Chinese J. Appl. Ecol.* 19, 564–568.

Liu, P. D., Cai, Z. F., Chen, Z. J., Mo, X. H., and Ding, X. P. (2018). A root-associated purple acid phosphatase, SgPAP23, mediates extracellular phytate-P utilization in *Stylosanthes guianensis*. *Plant Cell Environ.* 41, 2821–2834. doi: 10.1111/pce.13412

Liu, P. D., Xue, Y. B., Chen, Z. J., Liu, G. D., and Tian, J. (2016). Characterization of purple acid phosphatases involved in extracellular dNTP utilization in Stylosanthes. *J. Exp. Bot.* 67, 4141–4154. doi: 10.1093/jxb/erw190

Lu, L. H., Qiu, W. M., Gao, W. W., Tyerman, S. D., Shou, H. X., and Wang, C. (2016). OsPAP10c, a novel secreted acid phosphatase in rice, plays an important role in the utilization of external organic phosphorus. *Plant Cell Environ.* 39, 2247–2259. doi: 10.1111/pce.12794

Lynch, J. P. (2011). Root phenes for enhanced soil exploration and phosphorus acquisition: tools for future crops. *Plant Physiol.* 156, 1041–1049. doi: 10.2307/41435018

Ma, X. F., Wright, E., Ge, Y. X., Bell, J., Xi, Y. J., and Bouton, J. H. (2009). Improving phosphorus acquisition of white clover (*Trifolium repens* L.) by transgenic expression of plant-derived phytase and acid phosphatase genes. *Plant Sci.* 176, 479–488. doi: 10.1016/j.plantsci.2009.01.001

Madsen, C. K., Dionisio, G., Holme, I. B., Holm, P. B., and Henrik, B. P. (2013). High mature grain phytase activity in the Triticeae has evolved by duplication followed by neofunctionalization of the purple acid phosphatase phytase (PAPhy) gene. *J. Exp. Bot.* 64, 3111–3123. doi: 10.1093/jxb/ert116

Mehra, P., Pandey, B. K., and Giri, J. (2017). Improvement in phosphate acquisition and utilization by a secretory purple acid phosphatase (OsPAP21b) in rice. *Plant Biotech. J.* 15, 1054–1067. doi: 10.1111/pbi.12699

Mo, X. H., Zhang, M. K., Liang, C. Y., Cai, L. Y., and Tian, J. (2019). Integration of metabolome and transcriptome analyses highlights soybean roots responding to phosphorus deficiency by modulating phosphorylated metabolite processes. *Plant Physiol. Biochem.* 139, 697–706. doi: 10.1016/j.plaphy.2019.04.033

Murphy, J., and Riley, J. (1963). A modified single solution method for the determination of phosphate in natural waters. *Anal. Chim. Acta* 27, 31–35. doi: 10.1016/S0003-2670(00)88444-5

Navazio, L., Miuzzo, M., Royle, L., Baldan, B., Varotto, S., Merry, A. H., et al. (2002). Monitoring endoplasmic reticulum-to-Golgi traffic of a plant calreticulin by protein glycosylation analysis. *Biochemistry* 41, 14141–14149. doi: 10.1021/bi0204701

Olczak, M., Morawiecka, B., and Watorek, W. (2003). Plant purple acid phosphatases–genes, structures and biological function. *Acta. Biochim. Pol.* 50, 1245–1256. doi: 10.1016/S1381-1177(02)00143-1

Olczak, M., and Olczak, T. (2007). N-glycosylationsites of plant purple acid phosphatases important for protein expression and secretion in insect cells. *Arch. Biochem. Biophys.* 461, 247–254. doi: 10.1016/j.abb.2007.02.005

Pérez-Torres, C. A., López-Bucio, J., Cruz-Ramírez, A., Ibarra-Laclette, E., Dharmasiri, S., Estelle, M., et al. (2008). Phosphate availability alters lateral root development in Arabidopsis by modulating auxin sensitivity via a mechanism involving the TIR1 auxin receptor. *Plant Cell* 20, 3258–3272. doi: 10.1105/tpc.108.058719

Plaxton, W. C., and Lambers, H. (2015). "Phosphorus: back to the roots," in *Annual. Plant Reviews, Volume 48: Phosphorus Metabolism in Plants*, eds W. C. Plaxton, and H. Lambers, (Hoboken, NJ: WileyBlackwell), 3–22.

Robinson, W. D., Park, J., Tran, H. T., Del Vecchio, H. A., Ying, S., Zins, J. L., et al. (2012). The secreted purple acid phosphatases isozymes AtPAP12 and AtPAP26 play a pivotal role in extracellular phosphate-scavenging by Arabidopsis thaliana. *J. Exp. Bot.* 63, 6531–6542. doi: 10.1093/jxb/ers309

Rubio, V., Linhares, F., Solano, R., Martin, A. C., Lglesias, J., and Leyva, A. (2001). A conserved MYB transcription factor involved in phosphate starvation signaling both in vascular plants and in unicellular algae. *Gene Dev.* 15, 2122–2133. doi: 10.1101/gad.204401

Tian, J., and Liao, H. (2015). "The role of intracellular and secreted purple acid phosphatases in plant phosphorus scavenging and recycling," in *Annual. Plant Reviews, Volume 48, Phosphorus Metabolism in Plants*, eds W. C. Plaxton, and H. Lambers, (Hoboken, NJ: WileyBlackwell), 265–287.

Tian, J., Liao, H., Wang, X. R., and Yan, X. L. (2003). Phosphorus starvation-induced expression of leaf acid phosphatase isoforms in soybean. *Acta Bot. Sin.* 45, 1037–1042.

Tian, J., Wang, C., Zhang, Q., He, X. W., Whelan, J., and Shou, H. X. (2012a). Overexpression of OsPAP10a, a root-associated acid phosphatase, increased extracellular organic phosphorus utilization in rice. *J. Integr. Plant Biol.* 54, 631–639. doi: 10.1111/j.1744-7909.2012.01143.x

Tian, J., Wang, X. R., Tong, Y., Chen, X., and Liao, H. (2012b). Bioengineering and management for efficient phosphorus utilization in crops and pastures. *Curr. Opin. Biotechnol.* 23, 866–871. doi: 10.1016/j.copbio.2012.03.002

Tran, H. T., Hurley, B. A., and Plaxton, W. C. (2010a). Feeding hungry plants: the role of purple acid phosphatases in phosphate nutrition. *Plant Sci.* 179, 14–27. doi: 10.1016/j.plantsci.2010.04.005

Tran, H. T., Qian, W. Q., Hurley, B. A., She, Y. M., Wang, D. W., and Plaxton, W. C. (2010b). Biochemical and molecular characterization of AtPAP12 and AtPAP26: the predominant purple acid phosphatase isozymes secreted by phosphate-starved *Arabidopsis thaliana*. *Plant Cell Envir.* 33, 1789–1803. doi: 10.1111/j.1365-3040.2010.02184.x

Vance, C. P., Uhde-Stone, C., and Allan, D. L. (2003). Phosphorus acquisition and use: critical adaptations by plants for securing a nonrenewable resource. *New Phytol.* 157, 423–447. doi: 10.1046/j.1469-8137.2003.00695.x

Veneklaas, E. J., Lambers, H., Bragg, J., Finnegan, P. M., Lovelock, C. E., Plaxton, W. C., et al. (2012). Opportunities for improving phosphorus-use efficiency in crop plants. *New Phytol.* 195, 306–320. doi: 10.1111/j.1469-8137.2012.04190.x

Venkidasamy, B., Selvaraj, D., and Ramalingam, S. (2019). Genome-wide analysis of purple acid phosphatase (PAP) family proteins in *Jatropha curcas* L. *Int. J. Biol. Macromol.* 123, 648–656.

Wang, L., Li, Z., Qian, W., Guo, W., Gao, X., Huang, L., et al. (2011). The Arabidopsis purple acid phosphatase AtPAP10 is predominantly associated with the root surface and plays an important role in plant tolerance to phosphate limitation. *Plant Physiol.* 157, 1283–1299. doi: 10.1104/pp.111.183723

Wang, L., and Liu, D. (2018). Functions and regulation of phosphate starvation-induced secreted acid phosphatases in higher plants. *Plant Sci.* 271, 108–116. doi: 10.1016/j.plantsci.2018.03.013

Wang, L. S., Lu, S., Zhang, Y., Li, Z., Du, X., and Liu, D. (2014). Comparative genetic analysis of Arabidopsis purple acid phosphatases AtPAP10, AtPAP12, and AtPAP26 provides new insights into their roles in plant adaptation to phosphate deprivation. *J. Integr. Plant Biol.* 56, 299–314. doi: 10.1111/jipb.12184

Wang, X. R., Shen, J. B., and Liao, H. (2010). Acquisition or utilization, which is more critical for enhancing phosphorus efficiency in modern crops? *Plant Sci.* 179, 302–306. doi: 10.1016/j.plantsci.2010.06.007

Wu, W. W., Lin, Y., Liu, P. D., Chen, Q. Q., Tian, J., and Liang, C. Y. (2018). Association of extracellular dNTP utilization with a GmPAP1-like protein identified in cell wall proteomic analysis of soybean roots. *J. Exp. Bot.* 69, 603–617. doi: 10.1093/jxb/erx441

Xue, Y. B., Xiao, B. X., Zhu, S. N., Mo, X. H., Liang, C. Y., Tian, J., et al. (2017). GmPHR25, a GmPHR member upregulated by phosphate starvation, controls phosphate homeostasis in soybean. *J. Exp. Bot.* 68, 4951–4967. doi: 10.1093/jxb/erx292

Xue, Y. B., Zhuang, Q. L., Zhu, S. N., Xiao, B. X., Liang, C. Y., Liao, H., et al. (2018). Genome wide transcriptome analysis reveals complex regulatory mechanisms underlying phosphate homeostasis in soybean nodules. *Int. J. Mol. Sci.* 19, 2924–2947. doi: 10.3390/ijms19102924

Yao, Z., Tian, J., and Liao, H. (2014). Comparative characterization of GmSPX members reveals that GmSPX3 is involved in phosphate homeostasis in soybean. *Ann. Bot.* 114, 477–488. doi: 10.1093/aob/mcu147

Yao, Z. F., Liang, C. Y., Zhang, Q., Chen, Z. J., Xiao, B. X., Tian, J., et al. (2014). PvSPX1 is an important component in the phosphorus signaling network of common bean regulating root growth and phosphorus homeostasis. *J. Exp. Bot.* 65, 3299–3310. doi: 10.1093/jxb/eru183

Yin, C. Y., Wang, F., Fan, H. Q., Fang, Y. M., and Li, W. F. (2019). Identification of tea plant purple acid phosphatase genes and their expression responses to excess iron. *Int. J. Mol. Sci.* 20:1954. doi: 10.3390/ijms20081954

Zhang, Q., Wang, C., Tian, J., Li, K., and Shou, H. (2010). Identification of rice purple acid phosphatases related to phosphate starvation signalling. *Plant Biol.* 13, 7–15. doi: 10.1111/j.1438-8677.2010.00346.x

Zhang, Z. L., Liao, H., and William, J. L. (2014). Molecular mechanisms underlying phosphate sensing, signaling, and adaptation in plants. *J. Integr. Plant Biol.* 56, 192–220. doi: 10.1111/jipb.12163

Zhao, J., Fu, J. B., Liao, H., He, Y., Nian, H., Hu, Y. M., et al. (2004). Characterization of root architecture in an applied core collection for phosphorus efficiency of soybean germplasm. *Chinese Sci. Bull.* 49, 1611–1620. doi: 10.1360/04wc0142

Zimmermann, P., Regierer, B., Kossmann, J., Frossard, E., Amrhein, N., and Bucher, M. (2004). Differential expression of three purple acid phosphatases from potato. *Plant Biol.* 6, 519–528. doi: 10.1055/s-2004-821091

Conflict of Interest: The authors declare that the research was conducted in the absence of any commercial or financial relationships that could be construed as a potential conflict of interest.

frontiers in Plant Science

ORIGINAL RESEARCH
published: 25 June 2020
doi: 10.3389/fpls.2020.00949

New Rootsnap Sensor Reveals the Ameliorating Effect of Biochar on *In Situ* Root Growth Dynamics of Maize in Sandy Soil

Fauziatu Ahmed[1,2]*, *Emmanuel Arthur*[2], *Hui Liu*[3] *and Mathias Neumann Andersen*[2]

[1] Regional Office for Africa, Food and Agriculture Organization of the United Nations, Accra, Ghana, [2] Department of Agroecology, Faculty of Technical Sciences, Aarhus University, Tjele, Denmark, [3] Department of Crop Production Ecology, Swedish University of Agricultural Sciences, Uppsala, Sweden

OPEN ACCESS

Edited by:
Idupulapati Madhusudana Rao, International Center for Tropical Agriculture (CIAT), Colombia

Reviewed by:
Arnd Jürgen Kuhn, Institut für Bio- und Geowissenschaften (IBG), Germany
Michael Gomez Selvaraj, Consultative Group on International Agricultural Research (CGIAR), United States

***Correspondence:**
Fauziatu Ahmed
fauziatu_ahmed@yahoo.com

Specialty section:
This article was submitted to Plant Abiotic Stress, a section of the journal Frontiers in Plant Science

Received: *17 February 2020*
Accepted: *10 June 2020*
Published: *25 June 2020*

Citation:
Ahmed F, Arthur E, Liu H and Andersen MN (2020) New Rootsnap Sensor Reveals the Ameliorating Effect of Biochar on In Situ Root Growth Dynamics of Maize in Sandy Soil. Front. Plant Sci. 11:949. doi: 10.3389/fpls.2020.00949

We investigated if subsoil constraints to root development imposed by coarse sand were affected by drought and biochar application over two seasons. Biochar was applied to the subsoil of pots at 20–50 cm depth in concentrations of 0%, 1%, 2%, and 3% (B0, B1, B2, and B3). Maize was grown in the same pots 1 week and 12 months after biochar application. The maize plants were fully irrigated until flowering; thereafter, half of them were subjected to drought. A new method for observing root growth dynamics and root length density *in situ*, the Rootsnap sensor system, was developed. The sensors were installed at 50 cm depth just below the layer of biochar-amended subsoil. Using data from a smaller experiment with grass, the calculated root length densities from the sensors were compared with data from scanning of manually washed roots. In year 2, we investigated the effect of aged biochar on root growth using only the root wash and scanning method. The Rootsnap sensor revealed that the arrival time of the first root in B3 at the 50 cm depth averaged 47 days after planting, which was significantly earlier than in B0, by 9 days. The tendency for faster root proliferation in biochar-amended subsoil indicates that biochar reduced subsoil mechanical impedance and allowed roots to gain faster access to deep soil layers. A linear regression comparing root length density obtained from the Rootsnap sensor with the scanning method yielded an r^2 of 0.50. Our analysis using the scanning method further showed that under drought stress, maize roots responded with reduced root diameter and increased root length density at 50–70 cm depth in the first and second year, respectively. The trend under full irrigation was less clear, with significant decrease in root length density for B1 and B2 in year 2. Overall, reduction in subsoil mechanical impedance observed as early arrival of roots to the subsoil may prevent or delay the onset of drought and reduce leaching of nutrients in biochar-amended soil with positive implications for agricultural productivity.

Keywords: maize root, straw biochar, subsoil, *in situ* root method, drought stress

INTRODUCTION

The plant root is a principal water absorbing organ, that plays a crucial role in the development of plants, especially when water is limited (Upchurch and Ritchie, 1983). Under drought conditions, dehydrating roots synthesize abscisic acid (ABA), which is transported to the shoot to signal the level of drying in the soil (Zhang and Davies, 1989). This results in the partial closure of stomata to prevent water loss (Zhang and Outlaw, 2001) and consequently decrease photosynthesis, often to a smaller degree, thus enhancing water use efficiency (Liu et al., 2005). In maize, the accumulation of ABA results in the maintenance of root elongation and inhibition of shoot elongation at low water potentials (Saab et al., 1990). This is an example—out of many—of how abiotic stress influences root system architecture (Koevoets et al., 2016) as well as shoot growth.

Quantification of plant root geometry, in particular parameters such as root length, root length density or root diameter, is pivotal to understand many plant physiological functions (Pierret et al., 2013) and responses under stress conditions. Most plant studies have, however, focussed on aboveground parameters because root studies are quite cumbersome and labour intensive. Over the years, several methods have been developed and used for root assessment such as soil coring, trench wall and root mapping techniques, core break, minirhizotron, pinboard, excavation, and washing methods (Smit et al., 2000). In samples obtained from soil coring, roots can be washed free of soil and analyzed with software such as the WinRHIZO (Regent Instruments Inc., Canada) after scanning or the length can be estimated with the Newman (1966) counting method. Alternatively, the core-break method may be employed by breaking the retrieved soil core at the depth of interest (Bohm, 1979). Roots visible from the broken cross-section are counted with the naked eye and the root intensity calculated using the cross-sectional area of the soil core. If perpendicular sides are counted, it is possible to calculate root length densities directly (Chopart and Siband, 1999). The trench wall and pinboard techniques, utilize exposed roots from an evacuated plane, the former involves plotting root ends to a transparent sheets and the latter, a board containing nails arranged in a grid that is washed to expose roots (Smit et al., 2000). All the methods mentioned above with the exception of the minirhizotrons are destructive, which poses a challenge or makes it impossible to observe root development over time.

Sandy soils are characterised by low water holding capacity and excessive drainage below the root zone (Andry et al., 2009) and therefore considered marginal for agricultural production especially in dry areas. Nevertheless, many hundred thousands of hectares of this soil type formed by glacial river deposits is under cultivation in north-western Europe (Andersen and Aremu, 1991; Andersen et al., 1992; Ahmed et al., 2018). In coarse sand, lack of soil structure, low moisture content, greater bulk density and low organic content tend to increase the mechanical impedance to root growth (Bruun et al., 2012; Wernerehl and Givnish, 2015). Over the past few years, there have been efforts to enhance productivity of sandy soils by applying biochar, a carbon rich product which is produced by heating biomass to above 250°C in the absence of or with limited oxygen (Lehmann and Joseph, 2015). Several studies have reported improvement in soil water content and root development, decrease in bulk density, pore volume, and nitrate leaching (Abel et al., 2013; Bruun et al., 2014; Abiven et al., 2015; Haider et al., 2017) of sandy soils amended with biochar. Literature describing biochar's influence on maize growth have mostly reported on aboveground biomass (Major et al., 2010; Uzoma et al., 2011; Zhang et al., 2012; Sänger et al., 2017) with only few studies on roots. In tropical sandy soil, Abiven et al. (2015) reported an enhancement of maize root traits such as biomass and surface area with corncob biochar application. In temperate soil, some studies (Prendergast-Miller et al., 2011; Bruun et al., 2014; Ventura et al., 2014; Hansen et al., 2016) have reported effects of biochar on root development; however, studies on maize roots in temperate soils are limited. Although use of fresh biochar dominates research, biochar's effects may vary over time due the oxidation of carboxylic groups on the edges of the aromatic backbone (Glaser et al., 2000) and gradually change soil properties. Hence, its effect on roots may vary as biochar ages in the soil.

In this paper, we investigated the effect of wheat straw biochar on maize subsoil root development and response under drought conditions using a new method for observing roots *in situ* and dynamic changes in root density distribution. The details on how to assemble the Rootsnap sensor, aimed at providing an accurate and cost-effective way of analysing roots growth dynamics are discussed. We assessed whether root length density estimates from the Rootsnap sensor are comparable with conventional methods of soil sampling, separation of roots from soil by washing and measuring root length. Lastly, we investigated the effect of biochar on root development under full irrigation and drought with fresh and aged biochar amendment of the subsoil.

MATERIALS AND METHOD

Rootsnap Sensor

The Rootsnap sensor consists of an imaging device (**Figures 1A, B**) for taking pictures and videos, a frame component (**Figures 1C, D**) and the root-counting component (**Figures 1E, F**). The imaging device is a waterproof standard endoscope (Shenzhen FDL Technology co, PRC) with an image capture resolution of 640 × 480. The lens (**Figure 1A**) is surrounded by six white LED lights, which provide light controlled by an adjustable light switch. The device is powered through the USB of a computer or external USB by a cable, which can be either 2, 5, or 10 m (**Figure 1B**). The view angle of the camera is 66°. The camera and its housing case have a diameter of approximately 7 mm. The frame comprises of a plastic funnel and anti-glare glass (Hengshi Aohong International, PRC). The funnel's conical mouth is 6 cm in diameter at its widest point; the stem is 5.5 cm long and 0.8 cm in diameter. The funnel holds the endoscope and the other components together. It also holds silica gel, which protect the lens from condensation. The anti-glare glass is 4.5 cm in diameter and it functions to prevent roots from

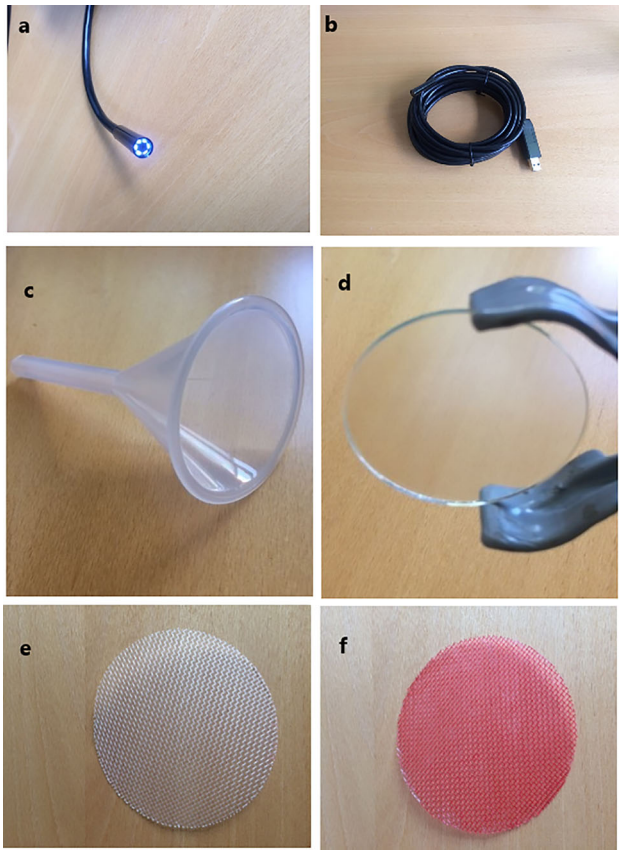

FIGURE 1 | Rootsnap sensor components. **(A)** Imaging device showing the lens with diameter of 7 mm; **(B)** entire endoscope with cable and usb connector; **(C)** frame component showing the funnel with diameter of 6.0 cm; **(D)** antiglare glass with diameter of 4.5 cm; **(E)** white nylon mesh with diameter of 6.5 cm; **(F)** red coloured nylon mesh.

growing directly on the lens. The root-counting component is a nylon wire mesh (Shanghai bolting cloth manufacturing, PRC) of diameter 9 cm with openings of 743 micron. Roots intersecting with the mesh in the plane of observation were counted for determining the root length density. The nylon mesh, which comes originally in white, **Figure 1E** was coloured red **Figure 1F** to enhance contrast.

Assembling the Rootsnap Sensor

The tip of the endoscope camera was coated carefully with epoxy rapid glue to avoid glue sticking on the lens. It was then placed in the funnel through the stem and allowed to set for an hour. The stem of the funnel fitted with the endoscope was filled with a neutral silicon sealant and allowed to set for 3 days. A clamp was used to hold the set up together and glue was applied to the sides of the funnel about 1 cm from the rim. The anti-glare glass was placed in the funnel and allowed to set for a day. The wire mesh was placed on the rim of the funnel and melted silicon was applied to attach the mesh to plastic funnel. The excess mesh was trimmed after the silicon had solidified. The assembled root sensor is presented in **Figure 2**.

Experimental Set Up

Maize Experiment

The study was conducted at Research Centre Foulum of Aarhus University (AU-Foulum), Denmark. The research was part of an experiment reported by Ahmed et al. (2018), who described the setup and results on aboveground growth and physiology of maize. Sand-textured soil was sampled from the Jyndevad research station at depths of 0–25 cm and 25–100 cm to represent topsoil and subsoil, respectively. Further information on the soil textural composition can be found in Ahmadi et al. (2010). The pots that were used had diameter of 36 cm and height of 70 cm. Prior to filling the pots, the inside was coated with subsoil mixed with water insoluble wallpaper glue (Bostik Hernia Vaadrumslim) as done by Bruun et al. (2014) to prevent preferential root growth along the sides of the pot. The preparation of the pots started with placing two Rootsnap sensors in the pots with their USB-cable passing through an opening in the side of the pot. The cable with the USB-connector part of the sensor was connected to a USB hub. The part with the lens was inside, and initially placed on the top edge (opening) of the pot. Prior to filling the pots, samples of soil and biochar were both oven dried to measure the water content. This was used to determine the desired dry weight based proportions, which were then mixed together for 5 min in a mechanical mixer. The soil was packed to a bulk density of 1.2 g/cm^3 and 1.3 g/cm^3 in the topsoil and subsoil sections, respectively. Packing was done by pressing the soil down with fingers to marks placed every 10 cm inside the pots followed by surplus irrigation and allowing the soil to settle. A diagram of the pot setup is presented in **Figure 3A**. After filling the 50–70 cm of the pots with subsoil, the USB-connector end of the cable was then pulled to position the sensors at the 50 cm depth. One was facing vertical and the other facing sideways as shown in **Figure 3B**. To prevent soil from

FIGURE 2 | Assembled Rootsnap sensor.

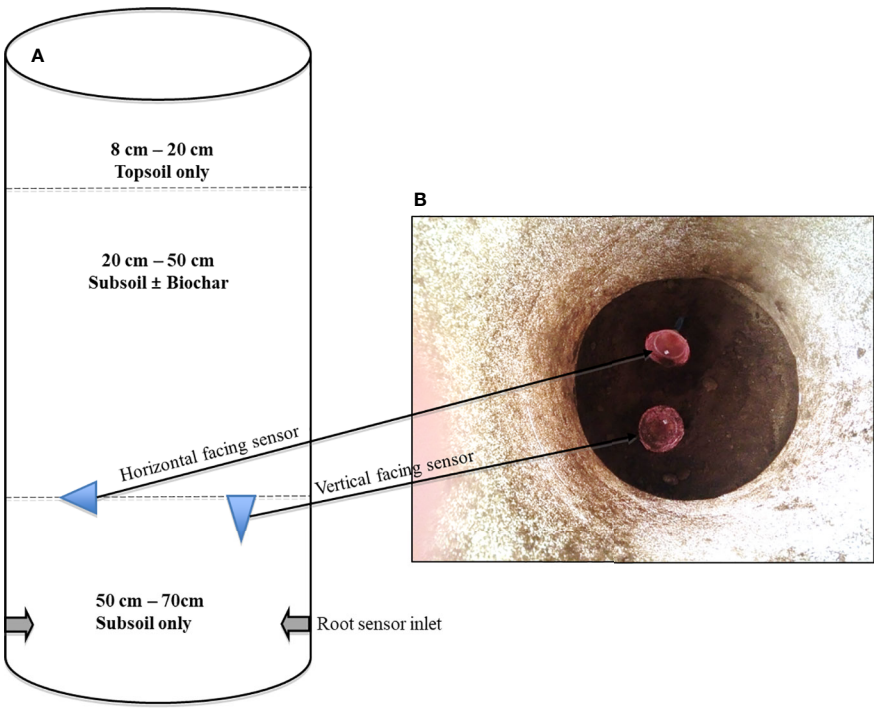

FIGURE 3 | Diagram of the pot set-up **(A)** and illustration of the sensors positions at 50 cm **(B)**.

subsequent layers to go through the mesh, a thin layer of water-soluble wallpaper glue was brushed on the surface of the vertical sensor. Thereafter sandy subsoil (± biochar) was filled in the 20–50 cm depth by slowly placing soil and then pressing gently with the fingers to avoid soil going through the mesh of the vertical sensor. This procedure may successfully be replaced—where convenient—by placing thin plastic foil over the mesh, and this foil is then later removed by carefully pulling it out. Finally, the topmost layer in all pots was filled with sandy topsoil at the depth of 8–20 cm in the pots.

The treatments thus comprised biochar applied at concentrations of 0, 1, 2, and 3% (B0–B3) and irrigation at two levels. Wheat straw biochar used for the experiment was produced by slow pyrolysis at a temperature of 600°C (Frich A/S, Denmark). Biochar properties are shown in Ahmed et al. (2018). The plants were initially irrigated each time the water deficit exceeded 25% of the available water content. At tasselling, pots of each biochar treatment were assigned to one of two groups. In one of the groups, irrigation was continued as described (FI) while the second group of pots was subjected to two drying cycles (D). This resulted in a total of 64 pots (eight replicates per treatment) of which 32 pots had the Rootsnap sensors (64 in total) installed. The treatment combinations are shown in **Table 1**.

Maize was sown on 7th May 2015 and 20th April 2016 in the first and second year, respectively. In both years, three seeds were planted, and then thinned to one plant per pot after emergence. The growing conditions in the greenhouse was a maximum day temperature of 28°C and a night temperature of 10°C with no artificial lightening. The plants were harvested at 104 days after planting (DAP) in 2015 and 111 DAP in 2016. The 32 pots with Rootsnap sensors installed were destructively sampled for bulk density and root length density analysis in 2015. Samples for root determination were taken between 45–50 cm soil layer. The remaining 32 pots without sensors were kept for the second year experiment and destructively sampled at the end of year 2 experiment.

TABLE 1 | Treatment combinations.

Biochar concentration (%)	Irrigation Level	Designation
0	Full	B0FI
0	Drought	B0D
1	Full	B1FI
1	Drought	B1D
2	Full	B2FI
2	Drought	B2D
3	Full	B3FI
3	Drought	B3D

Grass Experiment

A supplementary grass experiment was conducted at the same location as the maize experiment from 4th November to 6th December 2015 with 14 pots of dimensions, 21 cm height and 26 cm in diameter. There were no treatments in this experiment. The Rootsnap sensors were installed at 5–10 cm depth in pots filled with sandy loam soil. Grass turf consisting of a mixture of ryegrass (*Lolium perenne* L.) and red fescue (*Festuca rubra* L.) was transplanted to the surface of the soil. The grass was

subjected to the same growth conditions as the maize. Irrigation to field capacity was carried out every 3 days.

Measurements

Data From Rootsnap Sensor

The Rootsnap sensors were connected to a computer *via* a USB hub. A timer was used to designate times for root images to be taken automatically with a streamer software on a Linux operating system. Images were taken six times per day. When it was time for image capture, the timer switched on electricity for 15 min. During that period, the cameras took a few rounds of images and then the system shut down—including the camera light—until the next scheduled session.

The arrival time of roots at the 50 cm depth was used to determine the ease of movement of roots through the biochar amended subsoil. This was apparent from the root images taken late in the season by capturing the date and time a root had made its way through the above soil layers and the root tip just penetrated the mesh of the sensors. Images were collected into time-lapse videos to give a general overview of the dynamics of root development for the entire experimental period.

The number of roots intersecting with the mesh (n) was counted and the time of each intersect noted. The number of root per square cm (N) was determined by dividing the root count by the area of the field of view (12 cm^2). For the vertical facing camera, this was labelled N_V and for the horizontal facing camera N_H.

The average of root intersects per cm^2 for the two cameras were calculated as:

$$N_A = \frac{N_V + N_H}{2} \quad (1)$$

Anisotropy (A) accounts for the non-uniform directional distribution of roots, which specifically is related to root gravitropism (e.g., Xiao and Zhang, 2020) and more generally results from both morphogenetic and environmental factors interacting during the development of the root systems (Smit et al., 2000). The extent of this phenomenon was calculated using Eq. 2 (Van Noordwijk, 1987; Chopart and Siband, 1999):

$$A = ABS\frac{\left(1 - \frac{N_V}{N_H}\right)}{\left(2 \times \frac{N_V}{N_H} + 1\right)} \quad (2)$$

The root length density (L_V, cm cm^{-3}) was then calculated according to Chopart and Siband (1999) using Eq. 3.

$$L_V = 2 \times N_A\left(0.5 \times A^2 + 1\right) \quad (3)$$

The results of the root length density of maize and grass obtained from the Rootsnap sensor was compared to results obtained from scanning manually washed roots.

Soil Samples

In 2015, the 32 pots of maize containing the Rootsnap sensors were excavated after harvest for sampling. Soil samples for determination of bulk density and soil water content were extracted using sampling cores of 100 cm^3. Thereafter, loose soil-root samples of c. 1 kg were taken with a sharp shovel from depths of 20–50 cm and 50–70 cm. In 2016, the remaining 32 pots were excavated and soil-root samples were extracted only from the 50–70 cm layer. For the grass experiment, samples were taken from the 5–10 cm depth. The samples were weighed and stored in a freezer at -18 °C until roots were extracted. Soil bulk density and the volumetric water content of the soil was obtained by weighing 100 cm^3 samples obtained by the core method, before and after oven drying the samples at 105°C.

Root Extraction and Scanning

The frozen soil samples were allowed to thaw in a 10°C room overnight prior to root washing. Samples were divided with a sample divider and the amount to be washed was weighed. The soil-root sample was mixed with water and stirred in a bucket until the soil was fully dispersed. The supernatant was decanted into a 0.5 mm sieve stacked on top of the 0.25 mm sieve. This was repeated several times until there were no more visible roots floating in the bucket. The content of the 0.5 mm sieve was transferred to a white photo tray leaving the sediment. Debris and biochar particles were removed using tweezers. White live roots were separated from dead ones. Roots that were dark and sank to the bottom were assumed dead and probably derived from previous crops. The same was repeated with the content of 0.25 mm sieve. All live roots were mixed with 3% acetic acid and poured into bags for freezing. Prior to scanning, roots were thawed and stained using a neutral red solution comprising of 0.5 g "neutral red" dissolved in 100 ml 96% ethanol and 900 ml distilled water. The roots were soaked in the staining solution for 24 h while stored in a refrigerator at 5°C. The surplus colour was removed by rinsing with demineralized water before scanning. The resolution of the scanner was set to 600 dpi. After scanning, the analysis of the image was done with the WinRHIZO software (Regent Instruments Inc., Canada). The analysis of the root length was done by excluding the two lowest diameter classes of $0<L \leq 0.05$ mm and $0.05<L \leq 0.10$ mm, which were considered to be mycorrhiza. The root length was divided by the volume of soil to obtain the root length density. The average diameter of roots at the 50–70 cm depth of maize plants was calculated by summing up the product of the root length in each class and the average diameter of that class and dividing by total root length.

Newman Counting

To analyse the effect of biochar on RLD in the subsoil biochar layer in 2015, root samples from the 20–50 cm depth were analysed using the Newman (1966) counting method for the control (B0) and the highest biochar concentration (B3) under both FI and D. The reason for using this procedure was that these samples were too cumbersome to clean sufficiently for scanning and subsequent image analysis. Ten maize root samples, which had been washed and analysed using the scanning method were re-analysed using the counting method. The washed roots were poured into a 0.25 mm sieve and placed in a tray with water forming a thin film over the mesh. Then the roots were carefully

spread to make an even distribution over the area of the sieve. With a binocular microscope, the number of intersections between roots and a horizontal hairline placed in the microscope's eyepiece were counted. The root length, R was determined using Eq. 4, Newman (1966).

$$R = \frac{\pi NA}{2H} \quad 4$$

Where N is the number of intersections, A is the area of the sieve, H is the total length of the lines provided by the hairline of the microscope.

Statistical Analysis

Statistical analysis was conducted with SigmaPlot 11 (Systat Software, San Jose, CA). One and two way Analysis of Variance (ANOVA) was used to analyse the effect of biochar and irrigation. The Holm-Sidak posthoc test was used to compare treatments. P values of less or equal to 0.05 was taken to indicate statistical difference.

RESULTS

Images and Videos From the Rootsnap Sensor

The newly developed Rootsnap sensor was successfully used to automatically capture images of maize and grass roots while they were growing in soil. The images were stored on a computer and were made accessible remotely *via* internet connection. Examples of images obtained from the root sensor are shown in **Figures 4A, B** for maize and grass, respectively. Some of the root videos from the maize and grass experiment can be viewed by scanning the QR codes **Figures 4C, D** (QR codes reader can be downloaded online for both IOS and android mobile and PC devices). The pictures obtained were processed manually by looking through the sequence. Each time a new root tip penetrated the mesh of a sensor, the position and time was noted in an Excel sheet, which mimicked the mesh. An example of this is shown in **Figure 5**.

Effect of Biochar on Root Penetration to Subsoil Layer

Biochar tended to ease the downward growth of roots in coarse sandy soil as opposed to the control, which restricted root penetration. The arrival time of the first root in B3 was significantly ($P \leq 0.006$) earlier than for B0 and B1 treatments (**Figure 6**). A similar observation was made for the mean arrival time of the second root ($P \leq 0.016$). The delay of first control (B0) root to arrive at the 50 cm layer by up to 9 days may have implications for crop growth in terms of access to water especially during drought.

Comparison of Methods With Root Length Density Estimates

One of the advantages of the Rootsnap sensor is that it can be used to determine changes in root length density dynamically over time. The root length density over time in the subsoil tended to follow the S-shape of a typical growth curve increasing with time (**Figure 7**). This was due to spurts of lateral roots observed in the sideways facing Rootsnap sensor in **Figure 5**. Compared to the scanning method, root length density obtained from the Rootsnap sensor method by using Eq. (3) was significantly correlated with the scanning method ($y = 0.4663x+0.0932$, $r^2 = 0.50$, $p = 0.01$) as shown in **Figure 8**.

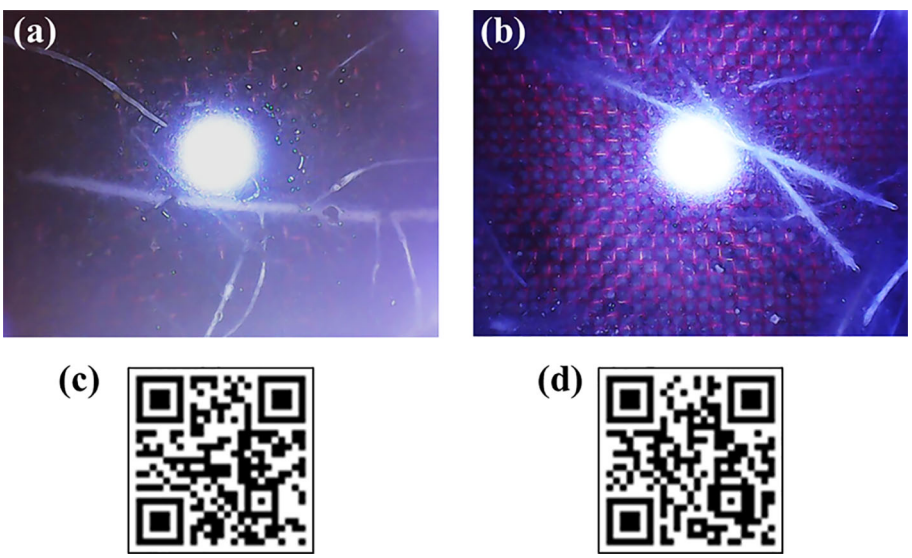

FIGURE 4 | Root images of maize **(A)** and grass **(B)**, and QR codes for root videos of maize **(C)** and grass **(D)**. The openings in red nylon wire mesh shown in a and b are 0.743 mm.

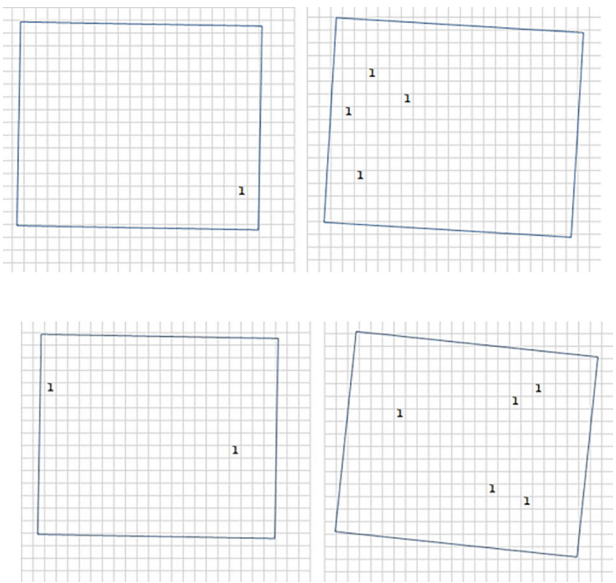

FIGURE 5 | Root distribution in field of view of the Rootsnap sensors for control (B0; top) and biochar 3% (B3; bottom). For counting and registering the position of the roots, an Excel sheet mimicking the nylon mesh (see **Figures 4A, B**) was created. The number and position of roots intersecting with the mesh was counted and the time of each penetration of the mesh by a root tip was noted.

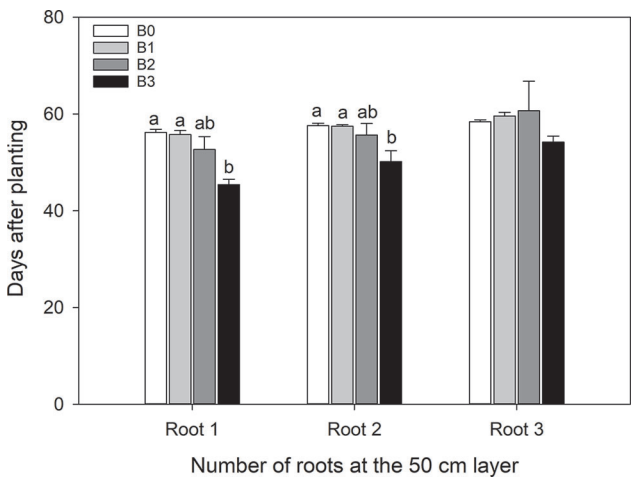

FIGURE 6 | Day of arrival of first, second and third root to the 50 cm depth after passing the subsoil layer with different biochar levels. Values are averaged over irrigation treatments. Error bars indicate standard errors of the mean (n=5(B0), 3(B1), 3(B2), 5(B3)). Different letters indicate significant difference. Letters are not shown when there is no significant difference.

Effect of Biochar on Root Traits

The root length density at the 20–50 cm depth at harvest time of maize in 2015, i.e. at maturity, estimated by the Newman

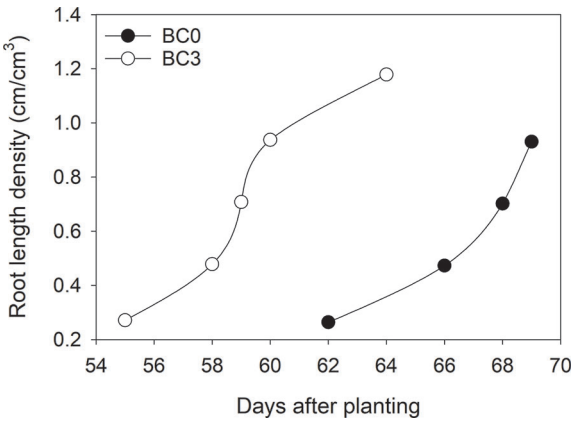

FIGURE 7 | Root length density over time for control (B0) and biochar 3% (B3) averaged over irrigation treatments.

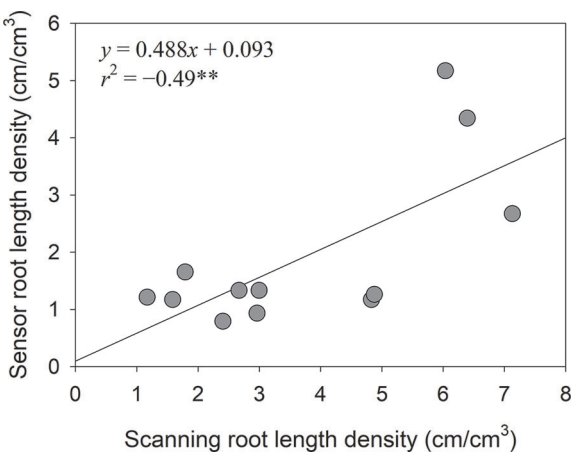

FIGURE 8 | Linear regression of scanning method vs Rootsnap sensor method.

counting method is presented in **Table 2**. Only B0 and B3 were analysed at this depth due to the presence of biochar complicating the analysis of roots. Our results indicate that B3 tended to decrease L_V in both irrigation schemes although not significantly. Also, no interaction among irrigation level and biochar levels was detected. At the 50–70 cm depth (**Table 3**), biochar treatments, with the exception of B2, tended to decrease L_V compared with the control. On the contrary, there was a slight increment with B2. Again, these differences were not significant. The results of 2015 at 50–70 cm depth were compared only between biochar levels due to inadequate number of replicates in the B2 treatment under full irrigation.

In 2016, biochar application tended to decrease L_V at 50–70 cm depth at maturity under both irrigation schemes (**Table 4**). With the exception of B3, all treatments tended to have higher L_V

TABLE 2 | Root length density for B0 and B3 in the 20-50 cm layer in 2015 determined by the Newman method.

Treatment	B0D	B3D	B0FI	B3FI
Root length density (cm/cm^3) at 20-50 cm	4.38 ± 0.70	3.4 ± 0.44	4.02 ± 0.40	3.66 ± 0.90

Mean values ± standard error (n = 4). Letters not shown when there is no significant difference.

TABLE 3 | Root length density and average diameter at 50–70 cm in 2015.

Treatment	B0	B1	B2	B3
Root length density (cm/cm^3)	2.52 ± 0.20	1.73 ± 0.20	2.75 ± 0.64	2.09 ± 0.29
Average diameter (mm)	0.19 c	0.20 ± bc	0.21 ab	0.22a

Mean values ± standard error (n = 7(B0), 7(B1), 3(B2), 6(B3)).Mean values with no letters in common are significantly different (P < 0.05). Letters not shown when there is no significant difference.

under drought than fully irrigated conditions. Under drought, the trend was that of lower L_V with increasing biochar level though there was no significant difference between B0D, B1D and B2D. In contrast B3D was significantly lower (P=0.002) than B0D. Under FI, the direction was less clear with B0FI and B3FI being significantly ($P \leq 0.042$) higher than B1FI and B2FI. A comparison between the 2 years showed the same trend of lower L_V with biochar application when comparing B3 with B0 (compare **Table 3** with **Table 4**) and as well in general appreciably lower L_V in 2016 at maturity. The average root diameter in 2015 in the 50–70 cm soil depth (**Table 3**) showed an increase with increasing biochar concentration. The root diameter in B3 (0.22 mm) and B2 (0.21 mm) were significantly greater ($P \leq 0.027$) than B0 (0.19 mm). In 2016 the picture was, however, opposite with all biochar treatments having significantly (P=0.003) lower root diameter than the B0 (**Table 4**) under drought, whereas there was no significant effect of biochar level under full irrigation. In B0, full irrigation resulted in significantly lower root diameter than under drought while the root diameter in the biochar treatments did not differ between full irrigation and drought.

DISCUSSION

Images and Video From the Rootsnap Sensor

The root sensor is an easily assembled tool that was used to take maize and grass root images *in situ*. The streamer software on Linux operating system allows automatically capturing and storing of images, which can be accessed remotely. The sensor system seems to have broad applicability also for installation in natural soil, where it might be installed into the side of an excavated wall profile.

Effect of Biochar on Root Penetration to Subsoil Layer

The average penetration rate of maize roots has been reported to be 2.4–2.5 cm/day (Hsiao et al., 2009). In sandy loam soils, Bengough & Mullins (1988) cited in Bengough and Mullins (1990) found that maize root elongation was reduced by compaction and mechanical impedance to between 50% and 90% of that of control plants grown in loose sieved soils. This shows that maize root penetration is very sensitive to soil physical conditions. In this study, the first root of the control plant at 50 cm depth arrived at day 56 after planting, giving a root penetration rate of approximately 0.8 cm/day, and thus indicating the large extent of mechanical resistance to root penetration plants experienced in these coarse sandy soils. In general, high soil bulk density and water stress increases penetration resistance and slow root elongation (Lampurlanés and Cantero-Martinez, 2003; Bengough et al., 2011). Studies (Abel et al., 2013; Basso et al., 2013) have shown that biochar amendment to sandy soils decreases bulk density and increase water holding capacity. In Danish coarse sand, Bruun et al. (2014) assumed that the addition of biochar might reduce mechanical resistance due to the reduction in subsoil bulk density. A finding that is consistent with our measurement of bulk density, which indicate significant decrease of bulk density at the 20–50 cm layer with increasing biochar application rate (**Table 5**). Further to this, using observations from the Rootsnap sensor, we were able to demonstrate that biochar decreased penetration resistance as evidenced by the shorter time (**Figure 5**) spend by roots to arrive at the 50 cm depth in the B3 treatment compared to the control. The treatment with

TABLE 4 | Root length density and average diameter at 50–70 cm for different biochar treatments in 2016.

Treatment	B0D	B1D	B2D	B3D	B0FI	B1FI	B2FI	B3FI
Root length density (cm/cm^3)	0.96 ± 0.30a	0.58 ± 0.09ab	0.58 ± 0.10ab	0.36 ± 0.02b	0.82 ± 0.02a	0.53 ± 0.02b	0.52 ± 0.03b	0.71 ± 0.05a
Average diameter (mm)	0.22 a	0.21 b	0.20 b	0.21 b	0.20	0.20	0.20	0.21

Mean values ± standard error (n = 4). SE not shown whenless than 0.01.Mean values with no letters in common are significantly different (P < 0.05). Letters not shown when there is no significant difference.

TABLE 5 | Bulk density measured in 2015.

Bulk density (g/cm^3)	B0	B1	B2	B3
20–50 cm	1.38 ± 0.01a	1.27 ± 0.01b	1.21 ± 0.01c	1.16 ± 0.01d
50–70 cm	1.36 ± 0.02a	1.29 ± 0.02b	1.23 ± 0.02b	1.17± 0.03c

Mean values ± standard error (n = 4). Mean values with no letters in common are significantly different (P < 0.05). Letters not shown when there is no significant difference.

the highest biochar concentration, B3, showed the lowest bulk density and had the fastest emergence time, suggesting that biochar reduced mechanical resistance in coarse sandy soil. Other factors may however have contributed to this finding. The biochar used contained 2.6% K and thus supplied a large amount of this macronutrient to the plant. Andersen et al. (1992) found that increasing supply of K to barley under field conditions significantly increased the root length density in the subsoil of the same soil type. A meta-analysis by Xiang et al. (2017) found that biochar addition in general increases root biomass, length and surface area in annual crops, consistent with the findings of Abiven et al. (2015) in maize grown in the field. In chickpea Egamberdieva et al. (2019) likewise found increased root mass, but only for hydrothermal biochar amendment and not for a conventionally pyrolysed biochar. As soil dries at the surface, water may be available deeper in the profile (Comas et al., 2013) hence the arrival in the deeper layer may result in better adaptation of biochar plants under drought conditions. Ahmed et al. (2018) found indications of this, as sap flow measurements showed transpiration to be higher in biochar amended plants than in unamended, although soil water content was similar during the second drying cycle of 2015.

Rootsnap Root Length Density Estimates

Overall, L_V was under-estimated by the Rootsnap sensor method although it yielded a positive, significant and linear correlation with the scanning method. It should thus be possible to calibrate the method to yield unbiased estimates. Root counting with the Rootsnap sensor resembles the core break method, where a usually vertical soil core is broken to expose a horizontal cross section and roots are counted on both surfaces. This is based on the principle that the same root cannot be exposed on both sides after breakage (Smit et al., 2000). If roots are assumed to grow isotropically (i.e. equally in all directions), anisotropy (A) in Eq. (2) is equal to zero and Eq. (3) simplifies to $L_V = 2N_A$. However, it has often been found that the proportionality factor is higher than 2 (e.g. Andersen et al., 2013), which thus may be taken as an indication of anisotropic growth. Although our method was designed to take such phenomena into account, the horizontally facing Rootsnap sensor (**Figure 4**) may itself have obstructed roots from reaching it. This seems likely as the backside of the sensor cannot be penetrated by roots and thus will induce a "shadowing" effect, which likely decreased the number of root tips reaching the mesh on the horizontally facing sensor. Due to gravitopism it seems more likely that the correct number of root tips will be counted by the vertically facing sensor.

Different techniques of root length density estimation produce highly variable results and more often than not, are difficult to compare (Pierret et al., 2005). Disparities in results obtained from comparing different root methods have been reported by some studies (Majdi et al., 1992; Wahlström et al., 2015). In their experiment with maize roots Majdi et al. (1992) showed a significant correlation (r = 0.78) between the minirhizotron and the line intercept method for estimating root length density. In contrast, they found no correlation between L_V obtained from minirhizotron and washed root analysed using computer image processing. They attributed the higher estimates in L_V by the line intercept method to probable overestimation of actual number of intercepts and lower estimates from the computer processing to discarding of smaller root fragments. Wahlström et al. (2015) demonstrated that L_V estimates of three methods were in general only weekly correlated except for root washing and scanning versus core break for fodder radish (r^2 = 0.77) and core break versus minirhizotron for winter wheat (r^2 = 0.26). The higher estimate by minirhizotron method was attributed to preferential growth along the access tubes.

The overestimation by line intercept and minirhizotron methods presented in the previous paragraph highlights the fact that each method has its own shortcomings. It is important to be aware of the shortcomings of each method and select them based on the root parameters of interest. Our new method yields a significant positive correlation with the scanning method, which shows a potential for determining L_V *in situ*. In addition, it presents the opportunity to study natural positions and arrangement of roots i.e. clumping phenomena, which are lost in the root washing method (Judd et al., 2015). Using Eq. (3) in the isotropic case, it is apparent that the sensor area of 12 cm^2 means that 6 root detections will give an L_V equal to 1 cm cm^{-3}, which constitute an already high root density for subsoils. Accordingly, sensor estimates of low L_V values inherently have a high coefficient of variation. This variation could be reduced by increasing the Rootsnap sensor area, depending on the feasibility of installing more voluminous sensors in a particular application. Nevertheless, the Rootsnap sensor seems unsurpassed for detection of first arrivals of roots to a certain depth avoiding the problems that seems inherent to e.g. the minirhizotron method.

Effect of Biochar on Subsoil Root Length Density and Diameter

A comparison of L_V between the 2 years for all treatments showed lower values in 2016 compared to 2015. This could be due to weather conditions which also resulted in lower aboveground biomass reported by Ahmed et al. (2018). There was no significant difference in L_V at 20–50 cm for B0 and B3 under both irrigation schemes in 2015. In addition, there was no

significant effect of biochar at the 50–70 cm depth in 2015. The trend in 2016 at the 50–70 cm layer under drought was that of a decrease in L_V with increasing biochar level. This could be due to maize root adaptation to drought, which results in the maintenance of root elongation and inhibition of shoot elongation (Saab et al., 1990) in order to maintain an adequate water supply. Thus, the significantly lower RLD in B3 probably indicates that it was the least water stressed. The lack of a clear-cut trend under full irrigation is similar to that observed by Bruun et al. (2014), who reported increases in root density at 40–80 cm depth with 1% and 2% straw biochar. In contrast, application at 4% resulted in decreased density. As soil dries, matric potential becomes more negative and soil strength increases (Bengough et al., 2011). With the tendency of biochar to decrease soil mechanical resistance and increase soil water content, roots under FI may not require adaptation mechanisms such as larger diameter to penetrate the soil, nor more roots to exploit available water. This may explain the lack of significant difference in root diameter under FI and the lower root length densities in the biochar treatments compared with the control.

In drought stressed maize grown in vermiculite, roots showed an increase in length but decrease in diameter (Sharp et al., 1988). In the first year, B2 and B3 significantly increased root diameter compared to B0. The significantly lower diameter in B0 suggests that they experienced the most drought stress. The diameter of roots has also been shown to increase with mechanical resistance (Bengough and Mullins, 1990). Although the soil used here is coarse sand, we do not expect any differences in the mechanical resistance between the control and the biochar treatments at the 50–70 cm depth, as there was no biochar application in this layer. Therefore, we suspect that the decrease in diameter especially for B0 in year 1 was a response to drought. In year 2, however, the soil had been in the pots for a year and frequent irrigation may have caused biochar particles from the 20–50 cm layer to leach into the 50–70 cm layer. As a result, mechanical resistance may have been lesser in the biochar treatments compared with control. Studies on root elongation of cotton as a function of soil strength and soil water content showed root elongation was more sensitive to soil strength than water content (Taylor and Ratliff, 1969 cited in Ball et al., 1994). We therefore speculate that significantly higher diameter in B0D compared to the biochar treatment may be due of higher mechanical resistance.

There is very limited studies on the effect of biochar ageing on root development. The closest comparable study is by Prendergast-Miller et al. (2014), who experimented with fresh and artificially weathered miscanthus and willow biochar. Their results showed a tendency for spring barley roots in weathered biochar-amended soils to have less branched roots than the control and fresh biochar treatments, although this was not significant. Our determination of L_V did not show any change in trends with biochar ageing as B0 tended to have higher L_V than biochar treatment in both years. However the negative root geotropism in B3 reported by Ahmed et al. (2018) in year 1 was not found in year 2.

CONCLUSIONS

The newly developed Rootsnap sensor presents an easily assembled, cost effective means of monitoring roots *in situ*. The new method was shown to provide estimates of root length density that had a significant positive correlation to the conventional root wash and scanning method. Moreover, temporal changes could be followed and thus e.g. provide important input to dynamic simulation models in which root length density is often a key variable and difficult to obtain. Images obtained from the new method demonstrated that biochar did reduce mechanical resistance in coarse sandy subsoils. The early arrival of roots to the 50 cm depth of up to 9 days before the control, indicate that they may gain access to water available in deeper soil layers that may prevent or delay onset of drought stress. Indeed this phenomena was indicated by sap flow measurements on the maize stems (Ahmed et al., 2018). Maize root respond to drought stress with increased root length density and thinner diameters. This is evidenced by increased root diameter for biochar treatments in the first year and decreased root length density in the second year. There is, however, the need for field studies under both full irrigated and drought conditions. From a methodological perspective, more experiments with the Rootsnap sensor with different crops at different depths and under field conditions are needed to further improve the technique.

DATA AVAILABILITY STATEMENT

The datasets generated for this study are available on request to the corresponding author.

AUTHOR CONTRIBUTIONS

FA: The lead in the planning, experimental set up and writing of the manuscript. EA: Involved in the planning, experimental set up and writing of the manuscript. HL: Involved in the analysis of root samples and reviewing of the manuscript. MA: Involved in the planning, experimental set up and writing of the manuscript.

ACKNOWLEDGMENTS

This research was funded by Ministry of Foreign Affairs of Denmark through the project "Green Cohesive Agricultural Resource Management, WEBSOC", *DFC project no: 13-01AU*. We thank Frichs A/S, Denmark for providing straw biochar through the cooperation with Lars Elsgaard, AU. We are grateful to Dennis Christensen for setting up the computer system to automatically capture root images. The assistance of Helle Baadsgaard Sørensen and Jens Bonderup Kjeldsen during the experiment is appreciated. We also acknowledge the assistance of Alfred Magehema, Thomas N. Bwana, and Ghasem Haghayegi in collecting soil and root samples.

REFERENCES

Abel, S., Peters, A., Trinks, S., Schonsky, H., Facklam, M., and Wessolek, G. (2013). Impact of biochar and hydrochar addition on water retention and water repellency of sandy soil. *Geoderma* 202–203, 183–191. doi: 10.1016/j.geoderma.2013.03.003

Abiven, S., Hund, A., Martinsen, V., and Cornelissen, G. (2015). Biochar amendment increases maize root surface areas and branching: a shovelomics study in Zambia. *Plant Soil* 395, 45–55. doi: 10.1007/s11104-015-2533-2

Ahmadi, S. H., Andersen, M. N., Plauborg, F., Poulsen, R. T., Jensen, C. R., Sepaskhah, A. R., et al. (2010). Effects of irrigation strategies and soils on field-grown potatoes: Gas exchange and xylem [ABA]. *Agric. Water Manage.* 97, 1486–1494. doi: 10.1016/j.agwat.2010.05.002

Ahmed, F., Arthur, E., Plauborg, F., Razzaghi, F., Korup, K., and Andersen, M. N. (2018). Biochar amendment of fluvio-glacial temperate sandy subsoil: effects on maize water uptake, growth and physiology. *J. Agron. Crop Sci.* 204, 123–136. doi: 10.1111/jac.12252

Andersen, M. N., and Aremu, J. A. (1991). Drought sensitivity, root development and osmotic adjustment in field grown peas. *Irrig. Sci.* 12, 45–51. doi: 10.1007/BF00190708

Andersen, M. N., Jensen, C. R., and Lösch, R. (1992). The interaction effects of potassium and drought in field-grown barley. I. Yield, water-use efficiency and growth. *Acta Agric. Scand. Section B Soil Plant Sci.* 42, 34–44. doi: 10.1080/09064719209410197

Andersen, M. N., Munkholm, L. J., and Nielsen, L. A. (2013). Soil compaction limits root development, radiation-use efficiency and yield of three winter wheat (*Triticum aestivum L.*) cultivars. *Acta Agric. Scand. Section B Soil Plant Sci.* 63, 409–419. doi: 10.1080/09064710.2013.789125

Andry, H., Yamamoto, T., Irie, T., Moritani, S., Inoue, M., and Fujiyama, H. (2009). Water retention, hydraulic conductivity of hydrophilic polymers in sandy soil as affected by temperature and water quality. *J. Hydrol.* 373, 177–183. doi: 10.1016/j.jhydrol.2009.04.020

Ball, R. A., Oosterhuis, D. M., and Mauromoustakos, A. (1994). Growth dynamics of the cotton plant during water-deficit stress. *Agron. J.* 86, 788–795. doi: 10.2134/agronj1994.00021962008600050008x

Basso, A. S., Miguez, F. E., Laird, D. A., Horton, R., and Westgate, M. (2013). Assessing potential of biochar for increasing water-holding capacity of sandy soils. *GCB Bioenergy* 5, 132–143. doi: 10.1111/gcbb.12026

Bengough, A. G., and Mullins, C. E. (1990). Mechanical impedance to root growth: a review of experimental techniques and root growth responses. *Eur. J. Soil Sci.* 41, 341–358. doi: 10.1111/j.1365-2389.1990.tb00070.x

Bengough, A. G., McKenzie, B., Hallett, P., and Valentine, T. (2011). Root elongation, water stress, and mechanical impedance: a review of limiting stresses and beneficial root tip traits. *J. Exp. Bot.* 62, 59–68. doi: 10.1093/jxb/erq350

Bohm, W. (1979). *Methods of studying root systems* (Berlin: Springer).

Bruun, E. W., Ambus, P., Egsgaard, H., and Hauggaard-Nielsen, H. (2012). Effects of slow and fast pyrolysis biochar on soil C and N turnover dynamics. *Soil Biol. Biochem.* 46, 73–79. doi: 10.1016/j.soilbio.2011.11.019

Bruun, E. W., Petersen, C. T., Hansen, E., Holm, J. K., and Hauggaard-Nielsen, H. (2014). Biochar amendment to coarse sandy subsoil improves root growth and increases water retention. *Soil Use Manage.* 30, 109–118. doi: 10.1111/sum.12102

Chopart, J.-L., and Siband, P. (1999). Development and validation of a model to describe root length density of maize from root counts on soil profiles. *Plant Soil* 214, 61–74. doi: 10.1023/A:1004658918388

Comas, L. H., Becker, S. R., Von Mark, V. C., Byrne, P. F., and Dierig, D. A. (2013). Root traits contributing to plant productivity under drought. *Front. Plant Sci.* 4, 442. doi: 10.3389/fpls.2013.00442

Egamberdieva, D., Li, L., Ma, H., Wirth, S., and Bellingrath-Kimura, S. D. (2019). Soil amendment with different maize biochars improves chickpea growth under different moisture levels by improving symbiotic performance with mesorhizobium ciceri and soil biochemical properties to varying degrees. *Front. Microbiol.* 10, 2423. doi: 10.3389/fmicb.2019.02423

Glaser, B., Balashov, E., Haumaier, L., Guggenberger, G., and Zech, W. (2000). Black carbon in density fractions of anthropogenic soils of the Brazilian Amazon region. *Organic Geochem.* 31, 669–678. doi: 10.1016/S0146-6380(00)00044-9

Haider, G., Steffens, D., Moser, G., Müller, C., and Kammann, C. I. (2017). Biochar reduced nitrate leaching and improved soil moisture content without yield improvements in a four-year field study. *Agric. Ecosyst. Environ.* 237, 80–94. doi: 10.1016/j.agee.2016.12.019

Hansen, V., Hauggaard-Nielsen, H., Petersen, C. T., Mikkelsen, T. N., and Müller-Stöver, D. (2016). Effects of gasification biochar on plant-available water capacity and plant growth in two contrasting soil types. *Soil Till. Res.* 161, 1–9. doi: 10.1016/j.still.2016.03.002

Hsiao, T. C., Heng, L., Steduto, P., Rojas-Lara, B., Raes, D., and Fereres, E. (2009). AquaCrop—the FAO crop model to simulate yield response to water: III. Parameterization and testing for maize. *Agron. J.* 101, 448–459. doi: 10.2134/agronj2008.0218s

Judd, L. A., Jackson, B. E., and Fonteno, W. C. (2015). Advancements in root growth measurement technologies and observation capabilities for container-grown plants. *Plants* 4, 369–392. doi: 10.3390/plants4030369

Koevoets, I. T., Venema, J. H., Elzenga, J. T. M., and Testerink, C. (2016). Roots withstanding their environment: exploiting root system architecture responses to abiotic stress to improve crop tolerance. *Front. Plant Sci.* 7, 1335. doi: 10.3389/fpls.2016.01335

Lampurlanés, J., and Cantero-Martinez, C. (2003). Soil bulk density and penetration resistance under different tillage and crop management systems and their relationship with barley root growth. *Agron. J.* 95, 526–536. doi: 10.2134/agronj2003.5260

Lehmann, J., and Joseph, S. (2015). *"Biochar for environmental management: science, technology and implementation,"* (New York: Routledge).

Liu, F., Jensen, C. R., Shahanzari, A., Andersen, M. N., and Jacobsen, S. E. (2005). ABA regulated stomatal control and photosynthetic water use efficiency of potato (*Solanum tuberosum L.*) during progressive soil drying. *Plant Sci.* 168, 831–836. doi: 10.1016/j.plantsci.2004.10.016

Majdi, H., Smucker, A. M., and Persson, H. (1992). A comparison between minirhizotron and monolith sampling methods for measuring root growth of maize (*Zea mays L.*). *Plant Soil* 147, 127–134. doi: 10.1007/BF00009378

Major, J., Rondon, M., Molina, D., Riha, S. J., and Lehmann, J. (2010). Maize yield and nutrition during 4 years after biochar application to a Colombian savanna oxisol. *Plant Soil* 333, 117–128. doi: 10.1007/s11104-010-0327-0

Newman, E. (1966). A method of estimating the total length of root in a sample. *J. Appl. Ecol.* 3, 139–145. doi: 10.2307/2401670

Pierret, A., Moran, C. J., and Doussan, C. (2005). Conventional detection methodology is limiting our ability to understand the roles and functions of fine roots. *New Phytol.* 166, 967–980. doi: 10.1111/j.1469-8137.2005.01389.x

Pierret, A., Gonkhamdee, S., Jourdan, C., and Maeght, J. L. (2013). IJ_Rhizo: an open-source software to measure scanned images of root samples. *Plant Soil* 373, 531–539. doi: 10.1007/s11104-013-1795-9

Prendergast-Miller, M. T., Duvall, M., and Sohi, S. P. (2011). Localisation of nitrate in the rhizosphere of biochar-amended soils. *Soil Biol. Biochem.* 43, 2243–2246. doi: 10.1016/j.soilbio.2011.07.019

Prendergast-Miller, M. T., Duvall, M., and Sohi, S. P. (2014). Biochar-root interactions are mediated by biochar nutrient content and impacts on soil nutrient availability. *Eur. J. Soil Sci.* 65, 173–185. doi: 10.1111/ejss.12079

Sänger, A., Reibe, K., Mumme, J., Kaupenjohann, M., Ellmer, F., Roß, C.-L., et al. (2017). Biochar application to sandy soil: effects of different biochars and N fertilization on crop yields in a 3-year field experiment. *Arch. Agron. Soil Sci.* 63, 213–229. doi: 10.1080/03650340.2016.1223289

Saab, I. N., Sharp, R. E., Pritchard, J., and Voetberg, G. S. (1990). Increased endogenous abscisic acid maintains primary root growth and inhibits shoot growth of maize seedlings at low water potentials. *Plant Physiol.* 93, 1329–1336. doi: 10.1104/pp.93.4.1329

Sharp, R. E., Silk, W. K., and Hsiao, T. C. (1988). Growth of the maize primary root at low water potentials I. Spatial distribution of expansive growth. *Plant Physiol.* 87, 50–57. doi: 10.1104/pp.87.1.50

Smit, A. L., Bengough, A. G., Engels, C., van Noordwijk, M., Pellerin, S., and van de Geijn, S. (2000). *"Root methods: a handbook,"* (Heidelberg: Springer Science and Business Media).

Taylor, H. M., and Ratliff, L. F. (1969). Root elongation rates of cotton and peanuts as a function of soil strength and soil water content. *Soil Sci.* 108, 113–119. doi: 10.1097/00010694-196908000-00006

Upchurch, D. R., and Ritchie, J. T. (1983). Root Observations Using A Video Recording System In Mini-Rhizotrons1. *Agron. J.* 75, 1009–1015. doi: 10.2134/agronj1983.00021962007500060033x

Uzoma, K., Inoue, M., Andry, H., Fujimaki, H., Zahoor, A., and Nishihara, E. (2011). Effect of cow manure biochar on maize productivity under sandy soil condition. *Soil Use Manage.* 27, 205–212. doi: 10.1111/j.1475-2743.2011.00340.x

Van Noordwijk, M. (1987). "Methods for quantification of root distribution pattern and root dynamics in the field," in *20th Colloq. Int. Potash Institute, Bern* (Berne: Int. Potash Inst. Publishers), 247–265.

Ventura, M., Zhang, C., Baldi, E., Fornasier, F., Sorrenti, G., Panzacchi, P., et al. (2014). Effect of biochar addition on soil respiration partitioning and root dynamics in an apple orchard. *Eur. J. Soil Sci.* 65, 186–195. doi: 10.1111/ejss.12095

Wahlström, E. M., Hansen, E. M., Mandel, A., Garbout, A., Kristensen, H. L., and Munkholm, L. J. (2015). Root development of fodder radish and winter wheat before winter in relation to uptake of nitrogen. *Eur. J. Agron.* 71, 1–9. doi: 10.1016/j.eja.2015.07.002

Wernerehl, R. W., and Givnish, T. J. (2015). Relative roles of soil moisture, nutrient supply, depth, and mechanical impedance in determining composition and structure of Wisconsin prairies. *PloS One* 10, e0137963. doi: 10.1371/journal.pone.0137963

Xiang, Y., Deng, Q., Duan, H., and Guo, Y. (2017). Effects of biochar application on root traits; a meta-analysis. *Global Change Biol. Bioenergy* 9, 1563–1572. doi: 10.1111/gcbb.12449

Xiao, G., and Zhang, Y. (2020). Adaptive growth: Shaping auxin-mediated root system architecture. *Trends Plant Sci.* 25, 121–123. doi: 10.1016/j.tplants.2019.12.001

Zhang, J., and Davies, W. (1989). Abscisic acid produced in dehydrating roots may enable the plant to measure the water status of the soil. *Plant Cell Environ.* 12, 73–81. doi: 10.1111/j.1365-3040.1989.tb01918.x

Zhang, S., and Outlaw, W. (2001). Abscisic acid introduced into the transpiration stream accumulates in the guard-cell apoplast and causes stomatal closure. *Plant Cell Environ.* 24, 1045–1054. doi: 10.1046/j.1365-3040.2001.00755.x

Zhang, A., Liu, Y., Pan, G., Hussain, Q., Li, L., Zheng, J., et al. (2012). Effect of biochar amendment on maize yield and greenhouse gas emissions from a soil organic carbon poor calcareous loamy soil from Central China Plain. *Plant Soil* 351, 263–275. doi: 10.1007/s11104-011-0957-x

Conflict of Interest: The authors declare that the research was conducted in the absence of any commercial or financial relationships that could be construed as a potential conflict of interest.

frontiers in Plant Science

ORIGINAL RESEARCH
published: 29 September 2020
doi: 10.3389/fpls.2020.01200

Dissection of Root Transcriptional Responses to Low pH, Aluminum Toxicity and Iron Excess Under Pi-Limiting Conditions in Arabidopsis Wild-Type and *stop1* Seedlings

Jonathan Odilón Ojeda-Rivera[1], *Araceli Oropeza-Aburto*[1] *and Luis Herrera-Estrella*[1,2*]

[1] *Laboratorio Nacional de Genómica para la Biodiversidad (UGA) del Centro de Investigación y de Estudios Avanzados del IPN, Irapuato, México,* [2] *Plant and Soil Science Department, Institute of Genomics for Crop Abiotic Stress Tolerance, Texas Tech University, Lubbock, TX, United States*

OPEN ACCESS

Edited by:
Idupulapati Madhusudana Rao, International Center for Tropical Agriculture (CIAT), Colombia

Reviewed by:
Hiroyuki Koyama, Gifu University, Japan
Laurent Nussaume, Commissariat à l'Energie Atomique et aux Energies Alternatives (CEA), France

***Correspondence:**
Luis Herrera-Estrella
lherrerae@cinvestav.mx;
luis.herrera-estrella@ttu.edu

Specialty section:
This article was submitted to Plant Abiotic Stress, a section of the journal Frontiers in Plant Science

Received: *18 March 2020*
Accepted: *23 July 2020*
Published: *29 September 2020*

Citation:
Ojeda-Rivera JO, Oropeza-Aburto A and Herrera-Estrella L (2020) Dissection of Root Transcriptional Responses to Low pH, Aluminum Toxicity and Iron Excess Under Pi-Limiting Conditions in Arabidopsis Wild-Type and stop1 Seedlings. Front. Plant Sci. 11:01200. doi: 10.3389/fpls.2020.01200

Acidic soils constrain plant growth and development in natural and agricultural ecosystems because of the combination of multiple stress factors including high levels of Fe^{3+}, toxic levels of Al^{3+}, low phosphate (Pi) availability and proton rhizotoxicity. The transcription factor SENSITIVE TO PROTON RHIZOTOXICITY (STOP1) has been reported to underlie root adaptation to low pH, Al^{3+} toxicity and low Pi availability by activating the expression of genes involved in organic acid exudation, regulation of pH homeostasis, Al^{3+} detoxification and root architecture remodeling in *Arabidopsis thaliana*. However, the mechanisms by which STOP1 integrates these environmental signals to trigger adaptive responses to variable conditions in acidic soils remain to be unraveled. It is unknown whether STOP1 activates the expression of a single set of genes that enables root adaptation to acidic soils or multiple gene sets depending on the combination of different types of stress present in acidic soils. Previous transcriptomic studies of *stop1* mutants and wild-type plants analyzed the effect of individual types of stress prevalent in acidic soils. An integrative study of the transcriptional regulation pathways that are activated by STOP1 under the combination of major stresses common in acidic soils is lacking. Using RNA-seq, we performed a transcriptional dissection of wild-type and *stop1* root responses, individually or in combination, to toxic levels of Al^{3+}, low Pi availability, low pH and Fe excess. We show that the level of STOP1 is post-transcriptionally and coordinately upregulated in the roots of seedlings exposed to single or combined stress factors. The accumulation of STOP1 correlates with the transcriptional activation of stress-specific and common gene sets that are activated in the roots of wild-type seedlings but not in *stop1*. Our data indicate that perception of low Pi availability, low pH, Fe excess and Al toxicity converges at two levels *via* STOP1 signaling: post-translationally

through the regulation of STOP1 turnover, and transcriptionally, *via* the activation of STOP1-dependent gene expression that enables the root to better adapt to abiotic stress factors present in acidic soils.

Keywords: root, transcriptome, acid soil, aluminum, iron, gene regulation, phosphate, combinatorial regulation

INTRODUCTION

Acidic soils prevalent in tropical and subtropical areas of the planet represent up to 40% of the world's arable land and constrain plant development and productivity in both natural and agricultural ecosystems (von Uexküll and Mutert, 1995). At a pH value of 5.5 or below, acidic pH compromises plant development because of a combination of two major stresses: lower nutrient availability, predominantly low phosphate (Pi) availability, and an increased availability of toxic cations, H^+, Al^{3+} and Fe^{3+}, which are detrimental for root development (Kochian et al., 2004; Kobayashi et al., 2013; Das et al., 2017). Given the agronomic relevance of acidic soils, research groups around the globe have focused on the characterization of the genetic, biochemical, physiological and morphological responses that allow plants to better adapt to acidic soils (see Magalhaes et al., 2018 for review).

Several studies in the model plant *Arabidopsis thaliana* have highlighted the role of the Cys_2-His_2-type zinc finger transcription factor SENSITIVE TO PROTON RHIZOTOXICITY 1 (STOP1) in protecting the root from the conditions present in acidic soils. When *stop1* mutants were first isolated, it was discovered that these mutant seedlings were hypersensitive to both H^+ and Al^{3+} rhizotoxicities (Iuchi et al., 2007). STOP1 confers root tolerance to Al toxicity by promoting malate exudation by upregulating the expression of the malate efflux transporter ALUMINUM ACTIVATED MALATE TRANSPORTER 1 (ALMT1). Malate excreted by ALMT1 chelates Al^{3+} ions and prevents its entry into the cell (Hoekenga et al., 2006; Iuchi et al., 2007), thus conferring Al tolerance to the root. Organic acid exudation is, in fact, the best understood Al-exclusion mechanism in plants, and is present in several plant species (Kochian et al., 2015). Further research demonstrated that STOP1 also regulates the expression of several genes involved in ion homeostasis and metabolic pathways that also contribute to Al tolerance such as the citrate transporter *MULTIDRUG AND TOXIC EXTRUSION (MATE1)* and the *ALUMINUM SENSITIVE3* (*ALS3)* a gene that codes for an ABC-like transporter protein and whose mutant (*als3*) is also hypersensitive to Al toxicity (Larsen et al., 2005; Liu et al., 2009; Sawaki et al., 2009).

Besides proton and Al toxicity, another limiting factor for plant growth in in acidic soils is low Pi availability. Under acidic conditions, Pi is rapidly fixed by Al and Fe cations making it unavailable for plant uptake. The responses of plants to low Pi availability have been studied thoroughly (for review see López-Arredondo et al., 2014) and include systemic responses to optimize internal Pi homeostasis and morphological adaptations of the root system to enhance Pi scavenging from upper soil layers where Pi tends to accumulate. Root morphological adaptations in Arabidopsis include an increase in the density and size of root hairs, an increase in lateral root number and the inhibition of primary root growth (Péret et al., 2011). Two recent genetic screenings of EMS-mutagenized seedlings identified a role for STOP1 in the inhibition of root growth in response to low Pi availability (Balzergue et al., 2017; Mora-Macías et al., 2017). These reports proposed that STOP1 activates *ALMT1* transcription under Pi-limiting conditions, leading to the adjustment of primary root growth through the activation of a reactive oxygen species (ROS) signaling pathway, triggered by the malate-dependent accumulation of Fe in the apoplast (for review see Abel, 2017). These reports suggest that organic acid exudation serves a triple role in acidic soils by preventing toxic Al from entering the cell, performing anion displacement to release Pi for plant uptake and enabling root modifications to more efficiently explore the topsoil. Further studies on the subject demonstrated a role for two other Al-tolerance related proteins, ALS3 and SENSITIVE TO ALUMINUM RHIZOTOXICITY (STAR1), in root developmental responses by modifying iron homeostasis in Arabidopsis (Dong et al., 2017). STOP1 regulates the expression of both *ALMT1* and *ALS3*, highlighting STOP1 as a major regulatory hub of responses to the conditions present in acidic soils including low Pi, high Fe availability and Al toxicity.

Given the multifunctional role of STOP1 under acidic soil conditions, a question that arises is: How is the activity of the transcription factor regulated in response to multiple stress factors? Earliest evidence suggested that, because the transcription levels of *STOP1* do not significantly change in response to low pH or Al exposure, STOP1 was post-transcriptionally activated (Sawaki et al., 2009). A recent report on STOP1 regulation corroborated that the transcription factor is regulated at the posttranslational level *via* protein accumulation/stabilization under low Pi and low pH conditions when Fe and Al are present in the medium (Godon et al., 2019). Furthermore, it was demonstrated that STOP1 abundance is regulated by the ubiquitin-proteasome-mediated degradation pathway *via* a member of the F-box E3-type ubiquitin ligase protein family, REGULATION OF ALMT1 EXPRESSION (RAE1). This F-box protein directly binds STOP1 and lack of a functional RAE1 leads to higher levels of STOP1, with the concomitant upregulation of *ALMT1* (Zhang et al., 2019). Because STOP1 regulates *RAE1* expression, authors concluded that STOP1 autoregulates its turnover by upregulating *RAE1* expression and, therefore, there must be another interacting partner that triggers an initial accumulation of STOP1. A dissection of how STOP1-targets are regulated in response to single and combinatorial stress conditions may provide insights into the mechanism(s) that modulate STOP1 activity.

Because of the overlap in the processes that are activated in response to the different stress conditions present in acidic soils, it remains unclear which responses are either shared by or specific to each type of stress. Extensive transcriptional profiling of the response to low Pi availability (Misson et al., 2005; Thibaud et al., 2010; Hoehenwarter et al., 2016; Mora-Macías et al., 2017), Al^{3+} toxicity (Sawaki et al., 2009; Kusunoki et al., 2017) and low pH (Sawaki et al., 2009; Lager et al., 2010) has been performed, however, a combinatorial study that dissects the specificity of the responses is lacking. Analysis of *stop1* global transcriptional changes in response to combinatorial stress conditions could provide insights into the STOP1-dependent regulation of genes because it would elucidate whether STOP1 activates the expression of the same gene set or specific gene sets in response to low Pi, low pH or combined Al^{3+} and Fe^{3+} stress conditions. Transcriptional profiling of *stop1* mutants could also provide insights into STOP1 dependent and independent mechanisms underlying tolerance to proton and metal toxicity. A transcriptomic characterization of *stop1* mutants in response to some of the individual stresses prevalent in acidic soils was previously reported (Sawaki et al., 2009), nonetheless, in this previous study microarray technology was used, which has limited dynamic range when compared to modern RNA-sequencing technology.

In this study, we perform a dissection of the transcriptional responses that are activated by the roots of wild-type and *stop1* Arabidopsis seedlings when exposed to factors that affect plant growth in acidic soils, namely, low Pi availability, low pH, Fe excess and Al toxicity, using RNA-sequencing technology. Our data suggest that a large portion of the transcriptional response is shared by multiple stress conditions, nonetheless, there are specific subsets of genes that are activated only in response to specific stress conditions. We also report that the expression of some STOP1-target genes correlates with the accumulation of STOP1 in the nucleus, whereas others do not follow this trend. We provide this dataset to the community with the intention of moving the field forward by accelerating the identification of new candidate genes that regulate root tolerance to acidic soil conditions.

MATERIALS AND METHODS

Plant Material

Arabidopsis thaliana (Col-0 ecotype; CS70000) seeds were used as the wild-type genotype in this study. *stop1-ko* T-DNA line SALK_114108 was used as the *stop1* (Col-0 ecotype background) mutant genotype.

Gene Cloning and Plant Transformation

The *STOP1* gene (AT1G34370) was cloned using the Golden Gate (GG) Strategy (Engler and Marillonnet, 2014) to produce a scar-free translational fusion to mCherry, as depicted in **Supplementary Figure 1**. We cloned the *STOP1* promoter (proSTOP1; 2085 bp upstream of the 5' Untranslated Region (UTR) of the *STOP1* gene), the 5'UTR (556 bp), 3'UTR (128 bp) sites and the *STOP1-CDS* sequence (1497 bp) into L0 vectors from the GG Plant Toolkit (Engler et al., 2014). Then we performed the L1 synthesis reaction as instructed in Engler and Marillonnet (2014) and added the *mCherry* gene previously cloned in L0 vector that comes readily available in the GG Plant Toolkit, to produce the final synthesis of the C-terminal fusion of mCherry and STOP1 with the STOP1 promoter sequence and native UTR sites (proSTOP1::5'UTR::STOP1~mCherry::3'UTR referred as proSTOP1::STOP1::mCherry in this text for simplicity). proSTOP1::STOP1::mCherry was cloned into an L2 GG binary vector that we introduced into *Agrobacterium tumefaciens* by electroporation. Agrobacterium tumefaciens containing proSTOP1::STOP1::mCherry was used to transform of *stop1* plants using the floral dip method as described in Martinez-Trujillo et al., 2004. Out of 10 transgenic lines that complemented the *stop1* mutant phenotype (under low Pi and low pH conditions) two single locus, homozygous proSTOP1::STOP1~mCherry, lines without any apparent abnormal phenotypes, were selected for further characterization. Primers used to clone the *STOP1* L0 modules are the following: *proSTOP1* (forward (fw): 5'-ttgaagacaaggag gatttcgcgaatccgaat-3'; reverse (rv): '-ttgaagacaaagtaggggtgctct ccactttc -3'), 5'UTR (fw: 5'-ttgaagacaatactaaagctaataaacatgagccc-3'; rv: 5'-ttgaagacaacatttttttagttcaagatcttgtttttc-3'), *STOP1-CDS* (fw: 5'-ttgaagacaaaatggaaactgaagccgatttgtg -3'; rv: 5'- ttgaagacaac gaagcaatgcctttgagactagtatc -3') and 3'-UTR (fw:5'-ttgaagacaagctt ggcattgccatatatatgataag-3'; rv:5'-ttgaagacaaagcgaagaaccaat ctttctgctattc-3').

Complementation Test

For complementation experiments (**Figure 1** and **Supplementary Figure 1**) we surface sterilized seeds and sowed them in 1% agar and 10% Murashige and Skoog Medium as described in López-Bucio et al. (2002). Low Pi medium (-Pi) was prepared with a concentration of 0 mM KH_2PO_4 and high Pi (+Pi) medium was prepared using 1 mM KH_2PO_4; sucrose concentration was 1% and MES at a 3.5 mM concentration to buffer pH Medium. MES optimum buffer range is 5.5 - 6.7, however, we added MES to keep pH below 5.5 which is already toxic to plants and is suitable for testing Al toxicity (Kobayashi et al., 2013). Medium was prepared at high Pi or low Pi concentration with pH adjusted to pH 5 or pH 6 as indicated in the text and figures. Wild-type plants (used as control) and *stop1* seedlings were grown for 10 days after germination (dag) in a Percival chamber at 22°C, under 16/8 h photoperiod with >200 $\mu mol \cdot m^2 \cdot s^1$ photon flux density.

Preparation of Root RNA-Seq Libraries

For the preparation of RNA-seq libraries, plant seedlings were germinated in high Pi medium at pH 5.7 as described in the previous section and 5 days after germination seedlings were transferred to the specified treatments under hydroponic conditions (no agar was added to the medium; 4 mL of each specific medium were added to 6-well cell culture Corning plates) specified in **Figure 1C** during 16 h (Percival chamber at 22°C, 8/8 h photoperiod with >200 $\mu mol \cdot m^2 \cdot s^1$ luminous intensity). Base medium for the preparations of specific treatments was the same as described in complementation

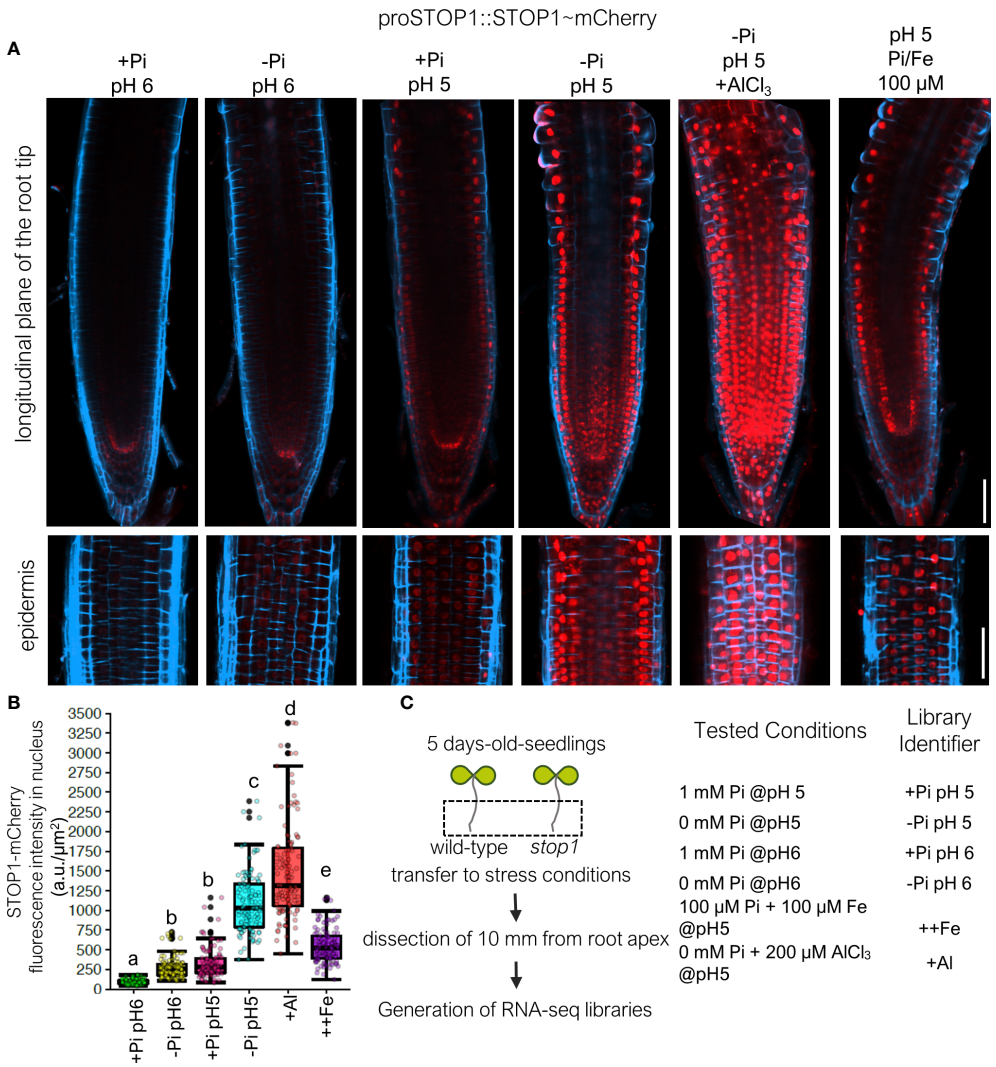

FIGURE 1 | STOP1 accumulation as a molecular marker to direct RNA-seq profiling of acidic pH, low Pi, Al toxicity and Fe toxicity conditions. **(A)** Transgenic *stop1* seedlings expressing proSTOP1::STOP1~mCherry (line #1) were grown 5 days-after-germination (dag) and then transferred to the indicated medium conditions during 16h, at this time STOP1-mCherry signal (Red Channel) was observed using confocal microscopy. The cell-wall was stained using a modified DAPI-staining (see Materials and Methods). Upper panels depict a longitudinal plane of the root apex; lower panels depict epidermis layer of the root apex. Scale bar equals 50 µM. **(B)** Quantification of STOP1-mCherry signal in the nucleus of epidermal cells under the tested conditions in 2 biological replicates using 2 independent transgenic *stop1* seedlings expressing proSTOP1::STOP1~mCherry with 3 technical replicates. A total of n=112 nuclei per condition were measured. Statistical groups are represented by letters and were determined using a Tukey HSD test (P-val <.05). **(C)** RNA-seq profiling experimental strategy and design.

studies with the exception that agar was not added to the medium. For the case of +Al-treatment, Aluminum was added as $AlCl_3$ at a concentration of 200 µM. For the case of ++Fe (Fe excess) treatment Fe was added in as $FeSO_4$ to a final concentration of 100 µM and KH_2PO_4 was added to achieve a final concentration of a 100 µM Pi. Given the lack of agreement between exposure times in the literature (Sawaki et al., 2009; Lager et al., 2010; Zhang et al., 2019) which ranged from 1-24 h of exposure to stress treatment we decided to use 16h to ensure that STOP1 was active. It is possible that 16h exposure to low pH, Al and Fe treatments induced ROS production and some degree of cellular damage because of the relatively long exposure to the stress, however, our treatment was within the time of exposure that has been tested previously which is generally within the 24h range (Sawaki et al., 2009; Zhang et al., 2019). In fact, Arabidopsis seedlings can survive for up to 7 days in low pH medium with an aluminum concentration in the 200-500 µM range (Hoekenga et al., 2006; Illéš et al., 2006). Because we also observed differential STOP1-mCherry accumulation in the root in response to tested treatments (**Figure 1**), we concluded that our exposure time (16h) was adequate for transcriptional profiling. After the 16 h treatments, frozen root tip powder was obtained from root tip sections of approximately 10 mm in length from approximately 150 individuals per treatment. Total

RNA was isolated using TRIzol (Invitrogen) from frozen root powder obtained from two independent biological replicates for each treatment reagent. Strand-specific mRNA-seq libraries were generated using the TrueSeq Illumina protocol and sequenced using the Illumina platform (paired-end reads, 150 base pairs; HiSeq2500). We calculated free Fe-availability in the medium using the chemical speciation software GEOCHEM-EZ (Shaff et al., 2010).

Confocal Microscopy and Fluorescence Signal Quantification

Roots were harvested and mounted after the specified treatments in **Figure 1**. Root cell-wall was stained using a modified DAPI staining. DAPI staining solution was prepared at this time at 0.1 μg/μL in the respective liquid culture medium of the tested conditions (see **Figure 1C**). The roots of proSTOP1::STOP1~mCherry seedlings were mounted on the DAPI-staining solution followed by incubation for 5 min and then imaged with a Zeiss LSM800 upright confocal microscope using a 405 nm Laser line (for DAPI) and a 561 nm Laser line (for mCherry). Fluorescence signal quantification was performed using FIJI software [version 2.0; (Schindelin et al., 2012)] using a protocol by Luke Hammond available on GitHub https://github.com/mfitzp/theolb/blob/master/imaging/measuring-cell-fluorescence-using-imagej.rst; scale was calibrated to pixels/μm and mean fluorescence intensity/μm value was used.

Determination of Number of Replicates per Sample for Bioinformatic Analysis

Biological variation is an important parameter to consider in RNA-seq protocols, hence the need to perform biological replication. To determine whether the level of biological replication in our RNA-seq analysis was adequate, we performed an analysis of the biological coefficient of variation (BCV), defined in edgeR (Robinson et al., 2010) as a parameter to account for variation between biological replicate libraries. According to the edgeR manual (http://bioconductor.org/packages/release/bioc/vignettes/edgeR/inst/doc/edgeRUsersGuide.pdf), a reasonable BCV value is less than 0.4 for a well-controlled experiment with adequate biological replication. Using edgeR, we determined that the BCV value of the biological replicates in our study is 0.1612 (**Supplementary Figure 4**), which is acceptable within edgeR standards and provides a statistical framework for determining significant differential expression between contrasting treatments. To test the levels of astringency that we were using, we decided to use a suggested methodology in the edgeR manual that is useful when there is no biological replication and that consists in selecting "housekeeping" genes, genes that do not variate in response to the tested treatments and have a relatively high level of expression, and calculate the BCV of these genes assuming a similar set of libraries as replicates. In this case, we assumed all wild-type and all *stop1* libraries, respectively, as replicates resulting in 12 replicates per genotype. The BCV of 100 housekeeping genes selected from our data set (included in **Supplementary Table 1**) resulted in a BCV value of 0.06767, less than 2 times the actual BCV of the study, indicating that our approach was at least two times more astringent than the housekeeping approach. This result corroborated that we could proceed with our analysis of differential expression with statistical certainty and that two replicates per sample was an adequate number for the purpose of the analysis reported in this work.

Bioinformatic Analysis of RNA-Seq Data

We performed quality assessment of the resulting reads from the Illumina platform using FastQC (version 0.11.9; https://www.bioinformatics.babraham.ac.uk/projects/fastqc/) and processed sequencing libraries using Trimmomatic (version 0.39; (Bolger et al., 2014)) to remove adapter read sequences. Paired-end reads were aligned to the Arabidopsis genome (TAIR10; Release 46) using HISAT2 (version 2.1.0; (Kim et al., 2015)). Raw counts of read alignment per gene/locus were calculated using HTSeq (version 0.11.2; (Anders et al., 2015)). Differential expression analysis was carried out in R using edgeR package (version 3.28.0; (Robinson et al., 2010)) available from Bioconductor site (http://bioconductor.org/). Gene expression is represented by the normalized raw counts per gene (edgeR's counts per million reads (cpm)). Cpm are obtained as raw counts per gene and normalized by library size. Heatmaps and graphs of the behavior of expression were represented using the z-score ((expression value in cpm – mean cpm across all the conditions tested)/standard deviation of gene expression in cpm across all the conditions tested). Pairwise comparisons were performed using edgeR's glmLRT function, resulting changes were represented using the log2 of fold change (logFC). Venn analysis was performed in R using UpSet package (version 1.4; (Lex et al., 2014)). Gene Ontology (GO) analysis was carried out using the Classification Superviewer from the Bio-Analytic Resource for Plant Biology at http://bar.utoronto.ca/ntools/cgi-bin/ntools_classification_superviewer.cgi (Provart and Zhu, 2003), a summary of the output is presented in **Figure 4**, complete GO analysis with GO identifiers is included in **Supplementary Table 1**.

RESULTS

STOP1 Accumulation as a Molecular Marker to Direct RNA-Seq Profiling

Since STOP1 has been reported to accumulate in the nucleus of epidermal root cells in response to several stress factors present in acid soils (Godon et al., 2019), we decided to test whether the accumulation of STOP1 could be used as a marker to determine the level of stress and/or transcriptional responses of the Arabidopsis root to different factors. With this aim, we generated a translational fusion of STOP1 to a fluorescent protein (mCherry) to use STOP1 accumulation as a stress marker to guide transcriptomic profiling (**Figure 1**). To confirm that the STOP1-mCherry fusion was functional in a biological context, we transformed a *stop1* mutant (Col-0 ecotype) with a construct that expresses a STOP1-mCherry fusion protein under the control of the endogenous *STOP1* promoter (proSTOP1::STOP1~mCherry; **Supplementary Figure 1A**) and tested for complementation. We isolated two

independent transgenic lines with single locus insertion in which STOP1-mCherry was detected in the nucleus of root cells (**Figure 1A**; **Supplementary Figure 1D**) and that complemented the *stop1* mutant phenotype under low pH and low Pi with no apparent phenotypes other than a slight, but statistically significant, root hypersensitivity to low Pi (**Supplementary Figures 1B, C**). Because the proSTOP1::STOP1~mCherry construct was able to complement the *stop1* mutant phenotype under low pH and low Pi conditions, respectively, and because we observed differential accumulation of STOP1~mCherry in response to low Pi and low pH as has been previously reported for STOP1 (Balzergue et al., 2017; Godon et al., 2019) we concluded that the STOP1~mCherry fusion is functional in a biological context. Then, we decided to monitor STOP1-mCherry accumulation in the roots of seedlings exposed for 16h to low Pi conditions (0 mM Pi, pH 6), low pH conditions (1 mM Pi, pH 5), low pH and low Pi conditions (0 mM Pi, pH 5), Al toxicity (0 mM Pi, 200 μM $AlCl_3$, pH 5) and Fe excess (100 μM Pi, 100 μM Fe, pH 5) and compared it to that observed under control conditions (1 mM Pi, pH 6). We observed that STOP1 accumulates differentially in the root tip (**Figure 1A** upper panel), in response to all the conditions tested and that these differences were most evident in epidermal cells (**Figure 1A**, lower panel). STOP1 accumulated in response to individual low pH and low Pi treatments, nonetheless, the effect was potentiated up to 4 orders of magnitude when both treatments are combined (**Figure 1B**). As expected, maximum accumulation of STOP1 was observed in Al-treatment which has a combination of stress treatments including low Pi, low pH and Al presence (**Figures 1A, B**). To simulate increased Fe availability conditions similar to those that happen in acidic soils, at pH 5 we increased Fe supply 10 times and decreased Pi supply 10 times (100 μM supply of Pi and Fe) relative to control conditions (1 mM Pi, 10 μM Fe). We observed that Fe excess triggered accumulation of STOP1 at high levels, however, not as high as those observed for seedlings exposed to low Pi at pH 5 or Al-treatment (**Figure 1B**). This result may indicate that Al has a stronger effect than Fe on the accumulation of STOP1, however, we cannot rule out a low Pi effect on the accumulation of STOP1 in the Al treatment because the Pi concentrations in those treatments was lower than in the Fe treatment (0 μM Pi in Al treatment; 100 μM Pi in Fe excess treatment). We determined that the observed differences in STOP1 accumulation were statistically significant by quantifying the intensity of the STOP1-mCherry signal in the nucleus of epidermal cells from root tips exposed to low Pi, low pH, Al and Fe excess at low pH (**Figure 1B**). It was recently reported that a relative increase of Fe in low Pi media triggers STOP1 accumulation under low pH conditions (Godon et al., 2019). Our data agrees with this report, because we also observed that STOP1 accumulation increases under low pH and elevated Fe levels in the medium. However, our data suggests that low Pi at low pH alone has a greater effect than that of Fe-excess in the accumulation of STOP1, therefore, Pi availability has a more determinant effect on STOP1 accumulation than Fe-excess. We cannot rule out that this effect is due to a modification of the Pi/Fe ratio and that a Fe-threshold in the medium may be sufficient for STOP1 accumulation. This last possibility is unlikely because in the low Pi media the Fe concentration is 10 μM, with a calculated free Fe availability of 50.5% (see Materials and Methods), which is much lower than the Fe concentration (100 μM) and calculated free Fe availability (86.97%) of the Fe-excess treatment.

Since we observed nuclear accumulation of STOP1 under all our proposed treatments (**Figure 1B**), we decided to perform RNA-seq profiling in the roots of wild-type (Col-0 ecotype) and *stop1* seedlings (Col-0 ecotype) that were exposed to low pH, low Pi, Al and Fe-excess treatments which simulate the conditions present in acidic soils *in vitro* (**Figure 1C**).

Multiple Subsets of Genes Are Differentially Regulated in Response to Low Pi, Low pH, Al-Exposure and Fe-Excess

For RNA-Seq analysis, seedlings were exposed for 16h to low Pi conditions (0 mM Pi, pH 6), low pH conditions (1 mM Pi, pH 5), low pH and low Pi conditions (0 mM Pi, pH 5), Al toxicity (0 mM Pi, 200 μM $AlCl_3$, pH 5) and Fe excess (100 μM Pi, 100 μM Fe, pH 5) and RNA was extracted from root tissue. We selected this time point because it was previously reported that the majority of STOP1-dependent genes are not activated at early time points, shorter than 8h, in response to low pH stress (Lager et al., 2010). Strand-specific RNA-Seq libraries for two independent biological replicates for each treatment were prepared using polyA+ RNA and sequenced using an Illumina HiSeq platform. A summary of the reads obtained for each library and alignment percentage is presented in **Supplementary Table 1**. Once RNA-sequencing was performed we decided to perform pairwise comparisons of the treatments (-Pi_pH6, +Pi_pH5, -Pi_pH5, +Al, ++Fe) with respect to control conditions (+Pi_pH6) to determine the genes that are differentially expressed (false discovery rate <.05) in response to each treatment (**Figure 2**, **Supplementary Table 1**). We determined that 51 and 27 genes were upregulated and downregulated, respectively, in response to -Pi_pH6; 64 and 44 genes were upregulated and downregulated, respectively, in response to +Pi_pH5 treatment; 183 and 299 were upregulated and downregulated, respectively, in response to -Pi_pH5 treatment; 1003 and 1023 were upregulated and downregulated, respectively, in response to +Al treatment and, lastly, 2479 and 1745 were upregulated and downregulated, respectively, in response to ++Fe treatment. These data indicate that ++Fe treatment induces changes in the expression of the greatest number of genes followed by +Al, -Pi_pH5, +Pi_pH5 and -Pi_pH6 treatments in descending order. As the increase in STOP1 in the high Fe treatment was lower than the treatment with -Pi_pH5 and +Al, this fact suggests that a large portion of the transcriptional effect of high Fe treatment is independent of STOP1 and probably mediated by other transcription factors and signaling pathways.

We then decided to perform a dissection of the genes whose upregulation is shared or specific to each treatment (**Figure 2**). Using a Venn analysis approach, we determined 17 intersections between the upregulated genes among the five tested treatments, 8 of the intersections are larger than 10 genes and 3 share more than 50 in common genes (**Figure 2A**), indicating that there is a considerable portion of the transcriptomic response shared

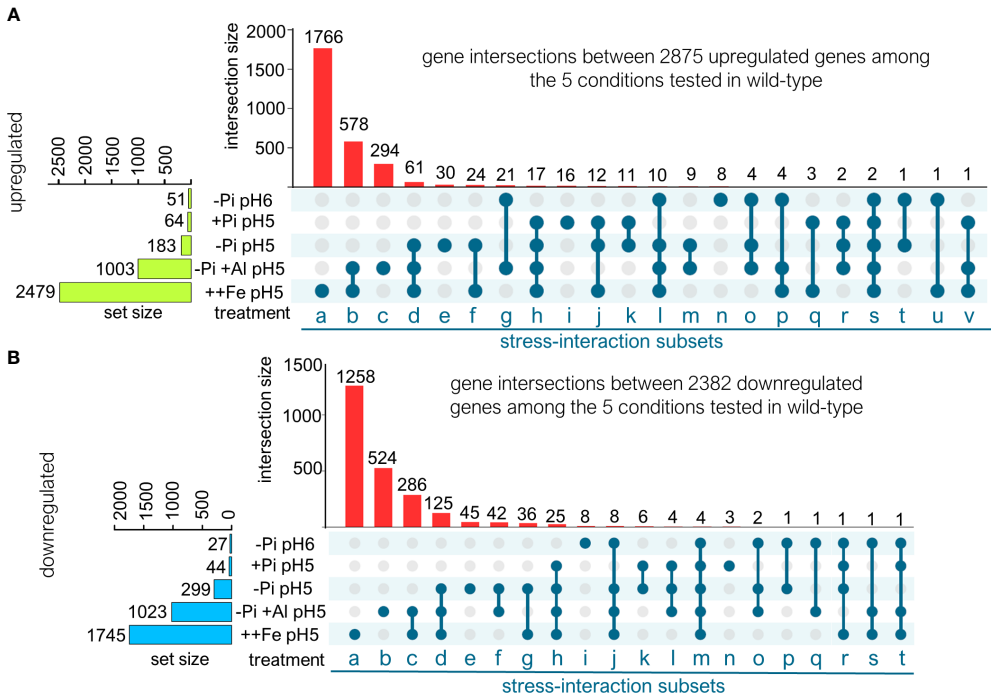

FIGURE 2 | Transcriptomic dissection of upregulated and downregulated gene expression in response to low pH, low Pi, Al and Fe excess. **(A)** Venn analysis of genes that are differentially upregulated (FDR <.05) under the conditions tested in wild-type (using wild-type pH 6 high-Pi as baseline). Venn diagram is represented in UpSet plot style (see Materials and Methods). Resulting intersection subsets are named using letters. **(B)** Venn analysis of genes that are differentially downregulated (FDR <.05) under the conditions tested in wild-type (using wild-type pH 6 high-Pi as baseline). Venn diagram is represented in UpSet plot style (see Materials and Methods). Resulting subsets are named using letters.

between two or more treatments. To further sustain this last conclusion, we calculated the percentages of specificity of upregulated genes for each treatment by dividing the number of genes that are not shared with other treatments by the number of genes that are upregulated by that treatment. The percentages of specificity are listed as follows: -Pi_pH6 (15.6%), +Pi_pH5 (25%), -Pi_pH5 (16.3%), +Al (29.3%) and + +Fe (71.2%). The percentages of specificity of each response indicate that, in low Pi, low pH and Al exposure treatments, over 70% of the transcriptional upregulation is shared by the three conditions. In the case of Fe-excess treatment, which induces the expression of the largest set of genes, 70% of upregulated genes are not shared with the other treatments and seem to be part of a specific response to elevated concentrations of Fe.

We continued our dissection of transcriptional responses by performing Venn analysis of intersections between downregulated genes. We found that the downregulation of genes in response to the tested treatments has less intersections between treatments. Fifteen intersection gene subsets were identified, which is two less than in the upregulation response (**Figure 2B**). At first, this number could indicate that downregulated genes are less stress-specific than upregulated ones. However, the number of specific genes that are downregulated indicates that this might not be the case because the percentages of specificity, calculated by dividing the number of genes downregulated in response to the treatment that are not shared with other treatments by the total number of genes downregulated by the treatment, are as follows: -Pi_pH6 (29.6%), +Pi_pH5 (6.8%), -Pi_pH5 (15%), +Al (51.2%) and ++Fe (72.1%). Overall, it seems that the downregulation of expression is more treatment-specific for -Pi_pH6, +Al and ++Fe. The finding that there are less interaction subsets and more specificity responses indicates that one or more downregulated interaction subsets are larger than the intersection subsets of upregulated genes. This is the case of the downregulated "subset d" which doubles its size (125 genes) with respect to upregulated genes (61 genes) and contains genes whose expression is coordinately regulated under low Pi, +Al, ++Fe at pH 5 conditions. This indicates that the root downregulates a common set of genes, larger than the one it upregulates, when exposed to low Pi, low pH, Al-exposure and Fe-excess. The complete dissection with gene identifiers for downregulated and upregulated responses is included in **Supplementary Table 1**.

STOP1 Has a Major Influence on the Transcriptomic Landscape in Response to Low Pi, Low pH, and Al-Exposure

Once we dissected the transcriptomic responses in the wild-type, we sought to analyze the effect of the *stop1* mutation on the regulation of transcription in response to the tested conditions (**Figure 3**). To gain further insights into the transcriptomic

landscape of the upregulated response for each treatment, we generated heatmaps of the intersection subsets of more than 10 genes for both WT and *stop1* genotypes (**Figure 3**). Overall, we found that the response in *stop1* as compared to the wild-type, was mixed: 1) genes whose expression is downregulated in *stop1* with respect to the WT, which was visibly the major trend across all subsets (activated in the WT but not in *stop1*) and 2) genes whose expression is upregulated in *stop1* with respect to wild-type (**Figures 3A, B**). The finding that the expression of genes that belong to both stress-specific and shared subsets is downregulated in *stop1* seedlings (**Figures 3A, B**) is of major relevance because it indicates that the increased expression of these genes depends not only on the accumulation of STOP1 but also of other factors that are only activated by stress specific signaling pathways. Genes that are induced under all stress treatments and expression levels of which are dependent on the level of STOP1 accumulation, probably only require STOP1 to activate their transcription. In the case of genes that are stress-specific, the accumulation of STOP1 is insufficient to trigger expression, therefore, either other transcription factors activated by the specific stress are required to activate the expression of target genes or different post-translationally modified versions of STOP1 might exist that can differentially bind to the promoter sequence of the target genes in a stress-specific or more general manner.

The second major effect of the *stop1* mutation on the transcriptomic landscape in response to the tested treatments was the upregulation of genes with respect to wild-type, or in other words, an enhanced induction of genes in the roots of *stop1* seedlings in response to the tested stress conditions. This type of response was most evident in the case of subsets "b" and "c" which contain genes that are upregulated specifically by +Al treatment in which the expression of some genes is visibly more activated in *stop1* than in wild-type (**Figure 3A**). We reasoned that this type of transcriptional response could be qualified as a hypersensitive transcriptional response of *stop1* to Al-toxicity. It

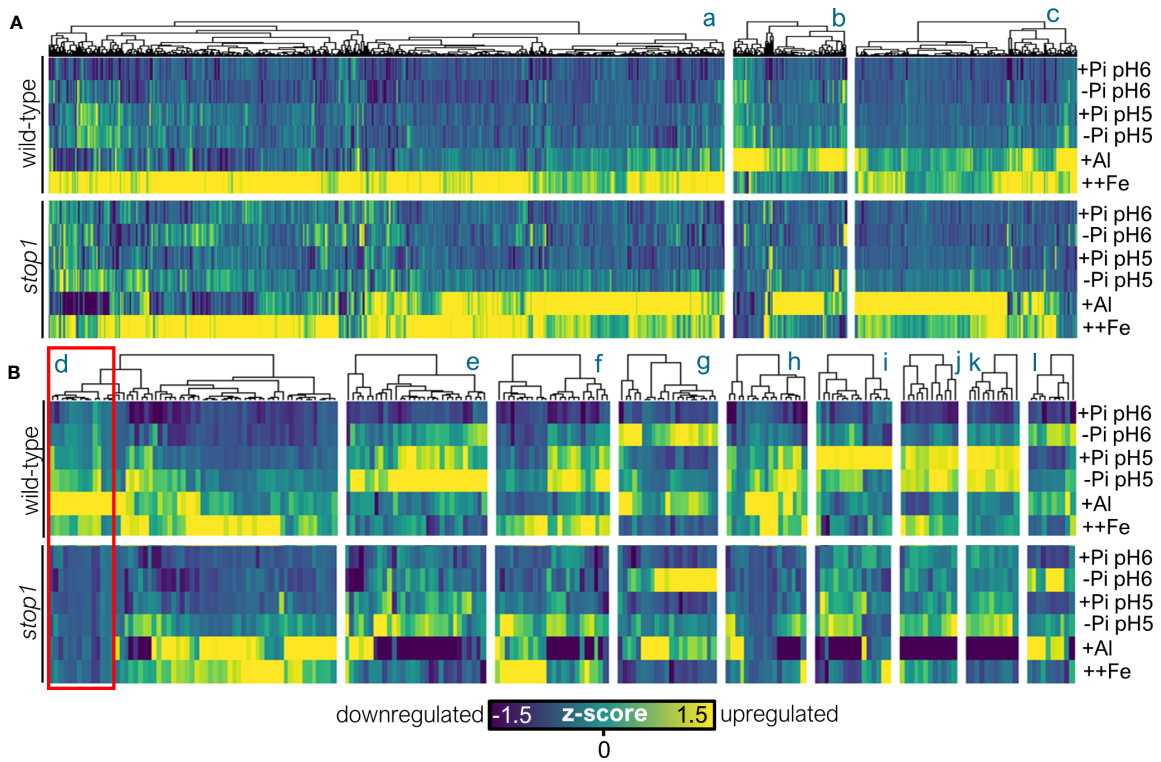

FIGURE 3 | STOP1 has a major effect on the transcriptome landscape in response to low Pi, low pH and Al exposure conditions. **(A)** Upper panel: heatmap of normalized gene expression (z-score) in the roots of wild-type seedlings exposed to the indicated treatment. Differentially upregulated genes (FDR <.05) from upregulated subsets a-c (obtained from **Figure 2**) are presented and clustered using the Pearson method. Lower panel: heatmap of normalized gene expression (z-score) in the roots of *stop1* seedlings exposed to the indicated treatment. Differentially upregulated genes (FDR <.05) from upregulated subsets a-c (obtained from **Figure 2**) are presented and clustered using the Pearson method. The subsets a-c were obtained from the Venn analysis presented in **Figure 2A**, these are the stress-interaction or stress-specific subsets of genes upregulated in response to the tested treatments and have the same letter identifiers as in **Figure 2A**. **(B)** Upper panel: heatmap of normalized gene expression (z-score) in the roots of wild-type seedlings exposed to the indicated treatment. Differentially upregulated genes (FDR <.05) from upregulated subsets d-l (from **Figure 2**) are presented and clustered using the Pearson method. Lower panel: heatmap of normalized gene expression (z-score) in the roots of *stop1* seedlings exposed to the indicated treatment. Differentially upregulated genes (FDR <.05) from upregulated subsets d-l (obtained from **Figure 2**) are presented and clustered using the Pearson method. The subsets d-l were obtained from the Venn analysis presented in **Figure 2A**, these are the stress-interaction or stress-specific subsets of genes upregulated in response to the tested treatments and have the same letter identifiers as in **Figure 2A**.

is most likely that, under the Al treatment conditions that we tested, malate-independent mechanisms to ameliorate Al toxicity were activated in *stop1* mutants because they are defective in malate excretion. In the case of subset "a" which is specific to ++Fe treatment, the transcriptional response was similar in *stop1* and the WT, indicating that STOP1 does not play a specific role in the regulation of transcriptional responses specific to ++Fe excess.

To investigate a possible hypersensitive transcriptional response to +Al treatment in *stop1*, we determined the number of differentially expressed genes in the roots of *stop1* exposed +Al with respect to control conditions (+Pi_pH6, WT). We found that in *stop1* 3431 genes were upregulated and 3680 downregulated, accounting for 3.5 times more differentially expressed genes in the *stop1* mutant than the WT. Then, we compared upregulated genes in STOP1 and the WT (**Supplementary Figure 2**). We observed that 758 genes are upregulated in both WT and *stop1*, whereas 246 genes are upregulated only in the WT and 2673 genes are upregulated only in *stop1* (**Supplementary Figure 2**).

To further understand the hypersensitive transcriptional response of *stop1* to Al-treatment we evaluated the two plant Al-tolerance responses that have been previously described: Al-exclusion, which focuses on preventing Al-entrance to the cell, and Al-detoxification, which focuses on detoxifying the cell once Al has crossed inside the plasma membrane (Kochian et al., 2015). We hypothesized that the hypersensitive transcriptional response to Al-treatment that is triggered in *stop1* mutants occurs because these mutants are defective in Al-exclusion which then leads to a hyper-activation of Al-detoxification. As expected, the expression of *ALMT1, MATE1, PGIP1, ALS3* that participate in preventing the entry of Al into root cell is only activated in wild-type and not in *stop1*. This was not a surprise because these genes have been previously reported to be downregulated in *stop1* mutants (Sawaki et al., 2009). We then analyzed the list of genes that are activated in response to +Al-treatment in *stop1* but not in WT and found genes coding for glutathione-S-transferases (*AT1G69920, AT1G10370, AT2G02380, AT2G47730*) which have been proposed to be involved in detoxifying Al-generated ROS (Daspute et al., 2017), a gene that codes for the tonoplast transporter *ALUMINUM SENSITIVE 1* (*ALS1; AT5G39040*) that contributes to Al-detoxification by sequestrating Al into the vacuole (Larsen et al., 2007; Huang et al., 2012) and *MONODEHYDROASCORBATE REDUCTASE* (*MDAR1; AT3G52880)* a gene whose product is related with hydrogen peroxide detoxification (Daspute et al., 2017). These results further support the hypothesis that Al-detoxification is induced in the root when Al-exclusion is defective or insufficient to prevent the entry of Al into the root.

We observed that the transcriptional response to ++Fe treatment in *stop1* was the least affected of all the conditions tested (**Figure 2**), but also that a portion of Fe-responsive genes were hyper-activated in the roots of Al-treated *stop1* seedlings. This indicates that there are detoxification mechanisms that contribute to both Al and Fe tolerance and are more active when STOP1 is missing most likely because Al- and Fe-exclusion mechanisms are defective in *stop1*. By using hierarchical clusterization, we determined the set of Fe-responsive genes that are hyper-activated in the roots of Al-treated *stop1* seedlings (**Supplementary Table 1**). Among these genes, we found several genes related to metal and oxidative stress detoxification including *ASCORBATE PEROXIDASE 1 (APX1)* whose mutants are defective in H_2O_2-scavenging and in which cytosolic protein oxidation occurs (Davletova et al., 2005), and several genes coding for glutathione-S-transferases (*GST8, GST25, GST29, GSTL3)* that have been related with detoxification of Al-induced ROS (Daspute et al., 2017) and *DEHYDROASCORBATE REDUCTASE 2 (DHAR2)* a gene that is related with the modulation of cellular redox states under oxidative stress conditions (Noshi et al., 2017). Because Fe-excess and Al-toxicity can occur simultaneously in acidic soils and both metals are potent elicitors of oxidative stress, these genes represent interesting candidates that contribute to the detoxification of ROS in response to Fe/Al-induced oxidative stress. The full list of genes is included in **Supplementary Table 1**.

Genes Encoding Proteins With Kinase Activity, Detoxification, Transport, Phosphate Starvation Response, and Cell Wall Related Processes Are Upregulated in Response to Low Pi, Low pH, and Al Treatment

Because low pH, low Pi and Al responses were the most transcriptionally affected in the roots of *stop1*, we sought to determine the genes that are activated in the wild-type in response to low Pi, low Pi and Al, to analyze their gene expression pattern in wild-type and *stop1* backgrounds and then perform a Gene Ontology (GO) enrichment analysis. With this aim, we first clustered gene subsets from our previous transcriptomic dissection by their specific response to low Pi, low pH or Al treatment. We named these subsets the *Aluminum response*, the *low pH response* and the *low Pi response* (**Figure 4**). In the case of the low pH response we analyzed the genes that respond to pH 5 across all treatments (subsets h + i + j + k + q + r), for the low Pi response we analyzed the genes that respond to low Pi across all treatments (subsets e + l + n + o + t) and for Aluminum response we analyzed the genes that respond to Al or to Al and Fe treatment (subsets b + c). We then carried out the GO enrichment analysis of the biological processes, molecular function and cellular components associated with the encoded proteins of the genes that belong to each transcriptional response subset. We present a summary of functional categories (**Figures 4A–C**) that were activated for each response, grouped by biological process, molecular function and cellular component, the complete GO analysis including category names and identifiers (**Supplementary Table 1**). Furthermore, to get a notion of the changes in expression of the genes involved in such response in *stop1* vs WT, we generated graphs of the behavior of expression of each gene under each specific condition for the two tested genotypes and fitted a trend-line of the overall behavior of gene expression (**Figures 4A–C**).

For the case of the response to acidic pH (**Figure 4B**) we found enriched categories in biological processes related to cell organization and biogenesis, transport and response to stress, GO enriched categories for this gene set included [GO:0048768] root hair cell tip growth, [GO:0042545] cell wall modification, [GO:0006810] transport and [GO:0006979] response to oxidative stress. Molecular functions related to transporter activity and kinase activity were also enriched in the set of genes that are responsive to acidic pH. Moreover, the genes that code for enzymes whose products are targeted to the cell wall and extracellular space were the most enriched cellular components in the low pH response. The gene expression graphic and trendline show that the response to low pH is severely downregulated in *stop1* mutants across all the treatments tested (**Figure 4B**). These data highlight a role for the genes that code for cell wall proteins, kinases and transport related processes in root acclimation to acidic conditions.

The GO analysis of the Aluminum response (**Figure 4A**) indicates that, overall, biological processes related to stress responses are activated in the root in response to Aluminum stress conditions, including categories like responses to hydrogen peroxide [GO:0042542], salt stress [GO:0009651] and oxidative stress [GO:0006979]. In the specific case of the response to hydrogen peroxide we found two genes coding for transcription factors that belong to the family of *HEAT SHOCK FACTOR (HSF)*, namely, *HSFA1E* and *HSFA3*. The HSF-family of transcription factors has been related to the response to a myriad of abiotic stresses including heat, drought, hypoxia and oxidative stress (Guo et al., 2016). The expression of *HSFA1E* has been reported to be upregulated in response to H_2O_2 treatment and a quadruple mutant of *HSFA1A/B/D/E* was reported to be more sensitive to H_2O_2 treatment than the wild-type (Liu et al., 2011) confirming a role of this subfamily of transcription factors in the response to hydrogen peroxide. In the case of *HSFA3*, it was demonstrated that overexpression of its transcriptional activator DREB2C (Chen et al., 2010), a transcription factor involved in the response to drought, upregulates *HSFA3* expression and confers tolerance oxidative stress (Hwang et al., 2012). Interestingly, we observed that *DREB2C* expression was also upregulated in response to Al treatment (**Supplementary Table 1**), suggesting an overlap in drought-activated responses and Al^{3+} stress. It is likely that these changes occur because both stresses lead to oxidative stress inside the cell. The *HSF* family of transcription factors activate the expression of *HEAT SHOCK PROTEINS* (*HSP)* which act as chaperones that regulate the folding, localization, accumulation and aggregation of proteins during stress conditions, including oxidative stress (Al-Whaibi, 2011). We found that 4 *HSP* genes (*HSP21, HSP70, AT1G52560, AT2G29500)* which also belong to the hydrogen peroxide response were upregulated in response to Al^{3+} treatment. It is likely that Heat Shock (HS) related proteins protect the cell from oxidative stress during Al toxicity, however, further experimentation with HSFs and HSPs is required to better understand the role of HS related proteins in the tolerance to Al^{3+} stress.

In the case of molecular processes activated in the Aluminum response gene set (**Figure 4A**), we found that the transcript levels of several proteins with kinase activity are increased by Al stress. The upregulation of genes that code for kinases agrees with previous works reporting the involvement of protein phosphorylation in the response of plants to Al^{3+} stress (Osawa and Matsumoto, 2001; Panda and Achary, 2014; Ligaba-Osena et al., 2017). Among the multiple genes coding for kinases enriched in the Aluminum response we found *PROLINE RICH LIKE EXTENSION KINASE 4* (*PERK4*) whose mutant, *perk4*, has reduced sensitivity to abscisic acid (ABA) including reduced inhibition of root growth in response to ABA treatment (Bai et al., 2009). *perk4* mutants have lower cytosolic concentration of Ca^{2+} which causes defects in Ca^{2+}-mediated ABA signaling (Bai et al., 2009). Interestingly, we also found that the expression of another Ca^{2+}-signaling kinase *CBL-INTERACTING KINASE 17* (*CIPK17)* was induced in response to Al. *CIPK17* has been reported to participate in a signaling module that controls Ca^{2+} influx and regulates ABA-signaling during stomatal closure (Song et al., 2018). Moreover, the expression of *CALCINEURIN B-LIKE PROTEIN 1 (CBL1)* was also induced in response to Al, *cbl1* mutants have increased sensitivity to Al^{3+} toxicity and have downregulated expression of *CIPK17* (Ligaba-Osena et al., 2017). CBL1-CIPK17 have been reported to interact *in vivo* (Kolukisaoglu et al., 2004). Our results agree with previous findings that *CBL1* has a role in the activation of Al-tolerance and suggest a role for Ca^{2+}-signaling, ABA-signaling and CBL1-CIPK17 signaling in the Al^{3+}-toxicity response. Interestingly, Ca^{2+}-signaling has also been reported to be involved in the early response to low pH (Lager et al., 2010). Further experimentation is required to more clearly understand the role of these signaling processes in the root tolerance to Al-stress.

The most enriched biological processes in the response to low Pi (**Figure 4C**) were transport and cellular response to phosphate starvation, including GO categories like [GO:0055085] transmembrane transport and [GO:0016036] cellular response to phosphate starvation. Transporter activity, hydrolase activity and DNA/RNA binding were the most enriched molecular functions. With respect to the cellular components, the plasma membrane was the most enriched organelle in the response to low Pi. Most of the low Pi-specific response is downregulated in the roots of *stop1* seedlings (**Figure 4C**). An interesting observation is that Fe excess cannot trigger the expression of Pi-responsive genes suggesting that Fe is not the trigger for the root responses to low Pi. To corroborate this, we analyzed the expression changes in response to the tested treatments of four genes that are well known to be induced by low Pi, *SPX DOMAIN GENE 1 (SPX1), PHOSPHATE TRANSPORTER 1;4, (PHT1;4) PHOSPHOLIPASE D ZETA 2 (PLDZ2), GLYCEROPHOSPHODIESTER PHOSPHODIESTERASE (GDPD1)* and *SULFOQUINOVOSYLDIACYLGLYCEROL 1 (SQD1)* (**Supplementary Figure 3**). The analysis showed that the expression of these 4 genes was only upregulated by low Pi conditions at both pH 6 and pH 5 and that ++Fe treatment was unable to upregulate their expression to the same extent of Pi-limiting conditions. These results agree with a previous report in which it was demonstrated that Fe does not trigger *SPX1* expression under low Pi conditions (Godon et al., 2019).

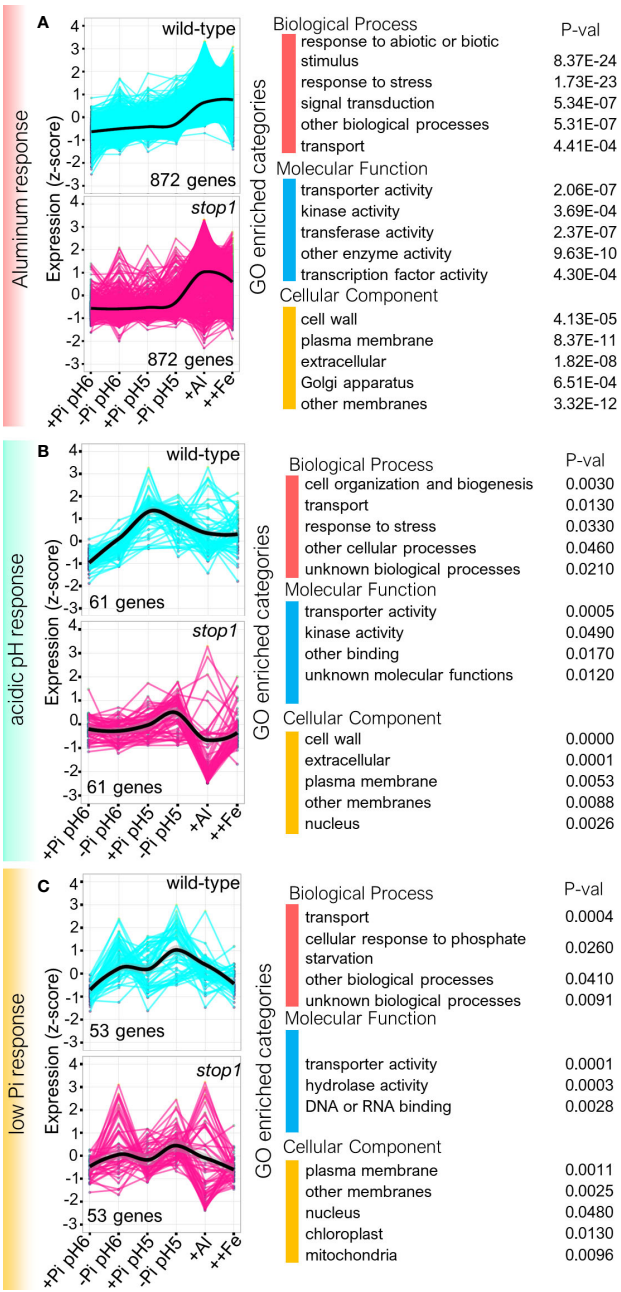

FIGURE 4 | Expression profiling and Gene ontology (GO) analysis of the transcriptionally upregulated processes in the roots of wild-type and *stop1* seedlings in response to low Pi, low pH and Al. **(A)** GO profiling of genes whose expression is significantly induced in wild-type (FDR < 0.05) in response to Al or to Al and Fe treatment (subsets b + c from **Figure 2A**) this gene set is referred to in the text and the figure as the *Aluminum response*. Left: Normalized expression profiles (z-score; y-axis) of *Aluminum response* genes in the roots of wild-type and *stop1* seedlings in response to the tested treatments (x-axis). Right: Summary of GO analysis performed using the Classification SuperViewer with Bootstrap (see Materials and Methods). For the complete analysis including GO categories for each of the classes presented and gene identifiers see **Supplementary Table 1**. **(B)** GO profiling of genes whose expression is significantly induced in wild-type (FDR < 0.05) in response to pH 5 across all treatments (subsets h + i + j + k + q + r from **Figure 2A**), this gene set is referred to as the *acidic pH response*. Left: Normalized expression profiles of *acidic pH response* genes (z-score; y-axis) in the roots of wild-type and *stop1* seedlings in response to the tested treatments (x-axis). Right: Summary of GO analysis performed using the Classification SuperViewer with Bootstrap (see Materials and Methods). For the complete analysis including GO categories for each of the classes presented and gene identifiers see **Supplementary Table 1**. **(C)** GO profiling of genes whose expression is induced in low Pi across all treatments (subsets e + l + n + o + t from **Figure 2A**), this gene set is referred to in the text as *low Pi response*. Left: Normalized gene expression profiles of *low Pi response* (z-score; y-axis) in the roots of wild-type and *stop1* seedlings in response to the tested treatments (x-axis). Right: Summary of GO analysis performed using the Classification SuperViewer with Bootstrap (see Materials and Methods). Significantly enriched GO processes have a P-value <0.05. For the complete analysis including GO categories and gene identifiers see **Supplementary Table 1**.

STOP1 Activates a Specific Set of Targets in Response to Low pH, Low Pi, and Al-Exposure

Using DNA affinity purification sequencing technique (DAP-seq), a recent study reported a set of 1280 genes defined as STOP1-targets, because STOP1 binds their regulatory (promoter/cis) sequence (O'Malley et al., 2016). To determine which DEGs identified for the different treatments use in this study are direct targets of STOP1, we integrated the DAP-Seq data into our analysis (**Figure 5**). Out of 1280 STOP1-targets defined by DAP-Seq, 294 have differential expression in response to at least one of the conditions tested in our study. We then generated a heatmap to visually inspect the differences between the wild-type and *stop1* genotypes (**Figure 5A**). A subset of 76 co-expressed genes, marked in red in **Figure 5A**, showed upregulation in response to the tested treatments in the WT but not in *stop1* (**Figure 5A**). The effect of the *stop1* mutation in the expression of these genes is more evident when observed in a graph of expression vs treatment (**Figure 5B**). Moreover, the level of expression of these genes correlates with the increase in STOP1 accumulation (**Figure 1B**). Overall, these data suggest that this specific subset is integrated by genes that are direct targets of STOP1 whose expression is proportional to STOP1-accumulation. As the expression of these genes is upregulated by STOP1 in response to low Pi, low pH and Al-exposure, these genes apparently only require the accumulation of STOP1 and do not require of other factors stress-specific factors. Further support of this notion came from the fact that genes, such as *ALMT1, ALS3, STOP2, PGIP1, GDH1/2* (Iuchi et al., 2007; Sawaki et al., 2009) and *RAE1* (Zhang et al., 2019), for which experimental evidence shows that STOP1 binds to their promoter sequences are included in this subset. In the specific case of *ALMT1* and *RAE1*, it has been demonstrated both *in vitro* and *in vivo* that STOP1 binds to their promoter region (Tokizawa et al., 2015; Balzergue et al., 2017; Zhang et al., 2019).

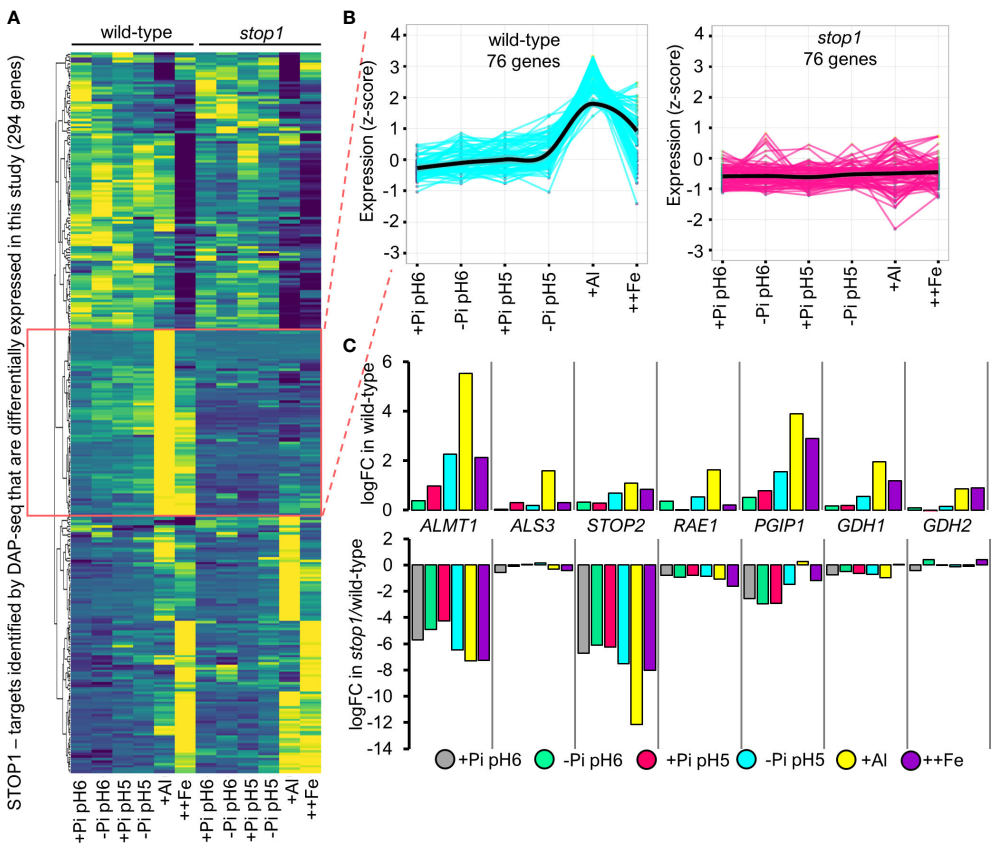

FIGURE 5 | STOP1 triggers the expression of a specific set of its targets that correlate with its accumulation and are important for root tolerance in response to abiotic stress factors prevalent in acidic soils. **(A)** Heatmap of normalized gene expression (z-score) of 294 STOP1-target genes that are differentially expressed under any of the tested treatments (FDR <.05) identified by DNA Purification Affinity (O'Malley et al., 2016). Pearson clusterization was used to cluster genes with similar expression profiles, 5 gene subsets were obtained and the subset of 76 genes that correlate with STOP1 accumulation is highlighted. Gene identifiers and description of the 5 resulting subsets of STOP1-targets is included in **Supplementary Table 1**. **(B)** Normalized gene expression profiles (z-score; y-axis) of the subset of 76 STOP1-targets highlighted in **(A)** of wild-type and *stop1* seedlings in response to the tested treatments (x-axis). **(C)** Changes in the expression in log2 of fold change (logFC) of STOP1-targets in response to the indicated treatments with respect to the expression in control conditions (+Pi_pH6 treatment in wild-type). A table with the logFC of the 294 STOP1-targets is included in **Supplementary Table 1**.

The finding of STOP1-targets whose expression does not correlate with STOP1-accumulation suggests that some STOP1-targets require the presence of other transcription factors or interacting proteins to be activated. Two additional possible explanations for the finding of STOP1-targets that do not correlate with STOP1-acummulation is that STOP1 activates these additional targets in other tissues or in response to other types of stress that STOP1 responds to, including hypoxia and salt stress (Enomoto et al., 2019; Sadhukhan et al., 2019). However, because STOP1 regulation appears to be mainly post-translational (Godon et al., 2019; Zhang et al., 2019), differential activation of gene expression may also happen through a differential interaction with other transcription factors or regulating protein interactors. A fourth possible explanation is that some of these STOP1-targets are activated early in response to the treatments that we tested, and we were not able to detect them at the time that we harvested the tissue (16h) but in that case their expression would be mainly determined by the early presence of a transcription factor other than STOP1. Full list of STOP1-targets that are differentially expressed in our dataset is included in **Supplementary Table 1**.

DISCUSSION

Transcriptional Profiling Provided Insights in the Regulation of Gene Expression in Response to Abiotic Stress Factors Prevalent in Acidic Soils

Acidic soils represent a challenge for modern agriculture, especially for developing countries of the tropical and subtropical areas of the world (von Uexküll and Mutert, 1995). In this work, we report a dissection of root transcriptional responses to the conditions present in acidic soil conditions, namely acidic pH, low Pi availability, Aluminum toxicity and Fe excess. We described an interesting subset of genes (**Figure 2**; subset d) for which expression is differentially regulated by all the factors that affect plant growth and development in acidic soils (low Pi, low pH, Al-toxicity and Fe-excess). This subset of genes includes genes previously demonstrated to play an important role in adaptation to low Pi, low pH and Al-tolerance such as *ALMT1* and *STOP2* (Kobayashi et al., 2014; Balzergue et al., 2017; Mora-Macías et al., 2017), but we also identified other novel genes for which induction is shared by all treatments and may serve as new marker genes for further studies of roots adaptation to acid soils. The fact that among this subset of shared genes, downregulated genes are twice more than upregulated genes (subset d; upregulated 61 genes, downregulated 125) suggests that the root might turn down the same cellular processes when it is exposed to any of the conditions present in acidic soils, whereas upregulated genes appear to be more stress-specific.

We observed that the transcriptional response to ++Fe treatment in *stop1* was the least affected of all the conditions tested (**Figure 2**), but also that a portion of Fe-responsive genes were hyper-activated in the roots of Al-treated *stop1* seedlings. This indicates that detoxification mechanisms that contribute to both Al and Fe tolerance are activated by mechanisms that are independent of STOP1. Nonetheless, our results demonstrate that *stop1* mutants are a suitable model to study the transcriptional activation of mechanisms related to Al-detoxification, and in some extent Fe-detoxification, because they are defective in organic-acid mediated exclusion of metals like Al and Fe. Genes that belong to the Al-detoxification set that are only activated in *stop1* represent interesting candidates to over-express to optimize Al-detoxification in plants. This last statement makes sense as Fe-excess and Al-toxicity are stresses that can occur together in acidic soils and both metals are potent elicitors of oxidative stress.

Analysis of GO enrichment in the sets of genes that are activated in response to low pH conditions (**Figure 4A**), revealed that genes that code for enzymes that are related to the modification of the cell wall are enriched in this gene set. Our results indicate that several genes related to pectin modification, a structural carbohydrate present in the root cell wall, including pectin methylesterase inhibitor genes (see **Supplementary Table 1**), are induced under low pH and Al^{3+} stress. Pectin methylesterase activity was positively correlated with sensitivity to Al^{3+} treatment in rice (Yang et al., 2013), suggesting that the induction of pectin methylesterase inhibitor genes might be a tolerance mechanism to Al^{3+} toxicity in plants. Furthermore, we found that the *POLYGALACTURONASE INHIBITING PROTEIN 1* (*PGIP1*) gene is downregulated in *stop1* mutants which corroborated a previous report (Sawaki et al., 2009) showing that expression of *PGIP1* is downregulated in *stop1* and is involved in remodeling the cell-wall under low pH conditions by stabilizing the pectin network. This was later demonstrated in a report by Kobayashi et al. (2014) that showed that *pgip1* knock-out mutants have less cell wall stability and are more susceptible to root damage than the wild-type in response to low pH treatment. The previously mentioned reports indicate that cell wall stabilization, and specifically the modification of the pectin network, is involved in the tolerance to H^+ and Al^{3+}rhizotoxicities. Therefore, the study of cell-wall dynamics in response to H^+ and Al^{3+} toxicities could provide valuable insights into the tolerance mechanisms of plants to conditions prevalent in acidic soils. Our analysis provides interesting candidate genes to continue the characterization of the role of cell-wall modifying enzymes and cell-wall carbohydrate dynamics in the root tolerance to H^+ and Al^{3+} rhizotoxicities.

RNA-Seq Provided Insights Into the Regulation Mechanism of STOP1

We guided our transcriptomic dissection using the turnover of the major transcriptional regulator of acid soil stress responses in Arabidopsis: STOP1. Our results indicate that low Pi, low pH, Fe excess and Al-exposure coordinately trigger STOP1-acummulation (**Figure 1**). Since we did not find *STOP1* to be differentially expressed in any of the treatments used in this study, our evidence supports the notion that STOP1 is regulated mainly at the posttranslational level. Previous research suggested that STOP1 is post-transcriptionally upregulated (Iuchi et al., 2008; Balzergue et al., 2017; Mora-Macías et al., 2017; Godon et al., 2019; Zhang et al., 2019) in response to stress conditions. Our data indicate that acidic stress signaling converges at two levels *via* STOP1 signaling: post-translationally through the regulation of STOP1 turnover and

transcriptionally, *via* the activation of STOP1-dependent gene expression. A recent report corroborated post-translational regulation of STOP1 *via* the ubiquitin-proteasome pathway through interaction with F-box protein RAE1, establishing a feedback regulation loop of STOP1 turnover. A recent genetic dissection of responses to low Pi proposed that ALS3 functions upstream of STOP1 (Godon et al., 2019) because STOP1 over accumulates in *als3*. However, our results indicate that *ALS3* is regulated by STOP1. *ALS3* is within the group of STOP1-targets and its expression is upregulated in response to +Al-treatment in the wild-type but not in *stop1* (**Figure 5C**). In fact, it was previously reported that the expression of *ALS3* is controlled by STOP1 (Sawaki et al., 2009). Therefore, evidence indicates that RAE1 and ALS3 modulate the levels of STOP1 at the posttranslational level. Because STOP1 controls the expression of *RAE1* and *ALS3* at the transcriptional level, this suggests that at least two negative regulation feedback loops control STOP1 turnover in response to abiotic stress factors. It must be pointed out that, even though these two negative regulation feedback loops that control STOP1 turnover and are under STOP1 control have been identified, the initial activator of the STOP1-acummulation spike in response to stress conditions remains unknown.

Pleiotropy can be defined as the effect of one gene on multiple phenotypes. Multiple lines of evidence indicate that STOP1 has a an important role in response to multiple stresses including low pH, Al-toxicity, low Pi, hypoxia, salt-stress and drought tolerance (Iuchi et al., 2007; Balzergue et al., 2017; Mora-Macías et al., 2017; Enomoto et al., 2019; Sadhukhan et al., 2019). Therefore, mutations in STOP1 have a pleiotropic effect on the developmental and molecular responses to different abiotic stresses. The STOP1 pleiotropy can be explained in part because its target genes have important roles in response to multiple stresses (Magalhaes et al., 2018). This is the case of *ALMT1*, a STOP1-target that is essential for malate excretion, that plays a role in Al-exclusion (Hoekenga et al., 2006) and modification of root growth in response to low Pi conditions (Balzergue et al., 2017; Mora-Macías et al., 2017) and of *ALS3* that plays roles in Al-tolerance (Larsen et al., 2005) and modification of root growth in response to low Pi conditions (Dong et al., 2017). It has also been reported that STOP1 activates the expression of *GDH1/2* in response to hypoxia (Enomoto et al., 2019) and low pH conditions (Sawaki et al., 2009), which activates the GABA-shunt that regulates cellular H+ levels and prevents acidosis of the cytosol (Bouché and Fromm, 2004) in acidic and hypoxic environments. Given the pleiotropic role of STOP1, two main questions arise with respect to its activation mechanism: Does it respond to a single common signal, like a metabolite, ROS, or Ca^{2+} fluxes, or are there specific STOP1-regulation mechanisms for each type of stress? Given that STOP1-regulation appears to be mainly at the post-transcriptional level, it is most likely that STOP1 activity as a transcriptional regulator is modulated by interacting proteins under each type of stress. Nevertheless, further research regarding STOP1-regulation is required to answer these questions.

Using a dataset from a recent report on the global characterization of protein-cis-interactions, named the cistrome of Arabidopsis (O'Malley et al., 2016), we identified the set of STOP1-targets whose expression depends on STOP1-accumulation (**Figure 5**). We detected 76 genes whose expression is dependent on the level of STOP1 accumulation, including *RAE1* and *ALMT1*. However, we also found a large portion of the STOP1 identified targets by O'Malley et al. (2016) whose expression is not altered in *stop1*. Two possible scenarios could explain the latter: 1) STOP1 requires other transcription factors to be able to bind to the cognate binding site or to interact with the basal transcriptional machinery to activate transcription and 2) STOP1 is subjected to multiple posttranslational modifications that alter its affinity for different promoter sequences, like protein phosphorylation or sumoylation. Since STOP1 has orthologs in other species (Ohyama et al., 2013), the list of STOP1 target genes might provide new candidate genes to increase tolerance to acid soils. Further physiological and genetic engineering experiments are an exciting perspective that derives from the presented dataset.

DATA AVAILABILITY STATEMENT

RNA-Sequencing data reported in this article has been deposited in the Gene Expression Omnibus under the accession no. GSE148457 (https://www.ncbi.nlm.nih.gov/geo/query/acc.cgi?acc=GSE148457).

AUTHOR CONTRIBUTIONS

JOO-R and LH-E designed research. JOO-R and AO-A performed experiments. LH-E contributed reagents and analytic tools. JOO-R and LH-E analyzed data and JOO-R and LH-E wrote the paper.

FUNDING

This work was supported in part by grants from the Basic Science program from CONACyT (Grant 00126261), the Governor University Research Initiative program (05-2018) from the State of Texas and by a Senior Scholar grant from Howard Hughes Medical Institute (grant 55005946) to LH-E.

ACKNOWLEDGMENTS

We would like to thank Rubén Rellán Álvarez for his advice on gene cloning. JOO-R is indebted to Consejo Nacional de Ciencia y Tecnología (CONACyT) for a PhD fellowship.

SUPPLEMENTARY MATERIAL

The Supplementary Material for this article can be found online at: https://www.frontiersin.org/articles/10.3389/fpls.2020.01200/full#supplementary-material

REFERENCES

Abel, S. (2017). Phosphate scouting by root tips. *Curr. Opin. Plant Biol.* 39, 168–177. doi: 10.1016/j.pbi.2017.04.016

Al-Whaibi, M. H. (2011). Plant heat-shock proteins: A mini review. *J. King Saud. Univ. - Sci.* 23, 139–150. doi: 10.1016/j.jksus.2010.06.022

Anders, S., Pyl, P. T., and Huber, W. (2015). Genome analysis HTSeq-a Python framework to work with high-throughput sequencing data. *Bioinformatics* 31, 166–169. doi: 10.1093/bioinformatics/btu638

Bai, L., Zhang, G., Zhou, Y., Zhang, Z., Wang, W., Du, Y., et al. (2009). Plasma membrane-associated proline-rich extensin-like receptor kinase 4, a novel regulator of Ca2+ signalling, is required for abscisic acid responses in Arabidopsis thaliana. *Plant J.* 60, 314–327. doi: 10.1111/j.1365-313X.2009.03956.x

Balzergue, C., Dartevelle, T., Godon, C., Laugier, E., Meisrimler, C., Teulon, J.-M., et al. (2017). Low phosphate activates STOP1-ALMT1 to rapidly inhibit root cell elongation. *Nat. Commun.* 8:15300. doi: 10.1038/ncomms15300

Bolger, A. M., Lohse, M., and Usadel, B. (2014). Genome analysis Trimmomatic: a flexible trimmer for Illumina sequence data. *Bioinformatics* 30, 2114–2120. doi: 10.1093/bioinformatics/btu170

Bouché, N., and Fromm, H. (2004). GABA in plants: Just a metabolite? *Trends Plant Sci.* 9, 110–115. doi: 10.1016/j.tplants.2004.01.006

Chen, H., Hwang, J. E., Lim, C. J., Kim, D. Y., Lee, S. Y., and Lim, C. O. (2010). Arabidopsis DREB2C functions as a transcriptional activator of HsfA3 during the heat stress response. *Biochem. Biophys. Res. Commun.* 401, 238–244. doi: 10.1016/j.bbrc.2010.09.038

Das, S., Tyagi, W., Rai, M., and Yumnam, J. S. (2017). Understanding Fe2+ toxicity and P deficiency tolerance in rice for enhancing productivity under acidic soils. *Biotechnol. Genet. Eng. Rev.* 33, 97–117. doi: 10.1080/02648725.2017.1370888

Daspute, A. A., Sadhukhan, A., Tokizawa, M., Kobayashi, Y., Panda, S. K., and Koyama, H. (2017). Transcriptional regulation of aluminum-tolerance genes in higher plants: Clarifying the underlying molecular mechanisms. *Front. Plant Sci.* 8, 1358. doi: 10.3389/fpls.2017.01358

Davletova, S., Rizhsky, L., Liang, H., Shengqiang, Z., Oliver, D. J., Coutu, J., et al. (2005). Cytosolic ascorbate peroxidase 1 is a central component of the reactive oxygen gene network of Arabidopsis. *Plant Cell* 17, 268–281. doi: 10.1105/tpc.104.026971

Dong, J., Piñeros, M. A., Li, X., Yang, H., Liu, Y., Murphy, A. S., et al. (2017). An Arabidopsis ABC Transporter Mediates Phosphate Deficiency-Induced Remodeling of Root Architecture by Modulating Iron Homeostasis in Roots. *Mol. Plant* 10, 244–259. doi: 10.1016/j.molp.2016.11.001

Engler, C., and Marillonnet, S. (2014). Golden Gate cloning. *Methods Mol. Biol.* 1116, 119–131. doi: 10.1007/978-1-62703-764-8_9

Engler, C., Youles, M., Gruetzner, R., Ehnert, T. M., Werner, S., Jones, J. D. G., et al. (2014). A Golden Gate modular cloning toolbox for plants. *ACS Synth. Biol.* 3, 839–843. doi: 10.1021/sb4001504

Enomoto, T., Tokizawa, M., Ito, H., Iuchi, S., Kobayashi, M., Yamamoto, Y. Y., et al. (2019). STOP1 regulates the expression of HsfA2 and GDHs that are critical for low-oxygen tolerance in Arabidopsis. *J. Exp. Bot.* 70, 3297–3311. doi: 10.1093/jxb/erz124

Godon, C., Mercier, C., Wang, X., David, P., Richaud, P., Nussaume, L., et al. (2019). Under phosphate starvation conditions, Fe and Al trigger accumulation of the transcription factor STOP1 in the nucleus of Arabidopsis root cells. *Plant J.* 99, 937–949. doi: 10.1111/tpj.14374

Guo, M., Liu, J. H., Ma, X., Luo, D. X., Gong, Z. H., and Lu, M. H. (2016). The plant heat stress transcription factors (HSFS): Structure, regulation, and function in response to abiotic stresses. *Front. Plant Sci.* 7, 114. doi: 10.3389/fpls.2016.00114

Hoehenwarter, W., Mönchgesang, S., Neumann, S., Majovsky, P., Abel, S., and Müller, J. (2016). Comparative expression profiling reveals a role of the root apoplast in local phosphate response. *BMC Plant Biol.* 16. doi: 10.1186/s12870-016-0790-8

Hoekenga, O. A., Maron, L. G., Piñeros, M. A., Cançado, G. M. A., Shaff, J., Kobayashi, Y., et al. (2006). AtALMT1, which encodes a malate transporter, is identified as one of several genes critical for aluminum tolerance in Arabidopsis. *Proc. Natl. Acad. Sci. U. S. A.* 103, 9738–9743. doi: 10.1073/pnas.0602868103

Huang, C. F., Yamaji, N., Chen, Z., and Ma, J. F. (2012). A tonoplast-localized half-size ABC transporter is required for internal detoxification of aluminum in rice. *Plant J.* 69, 857–867. doi: 10.1111/j.1365-313X.2011.04837.x

Hwang, J. E., Lim, C. J., Chen, H., Je, J., Song, C., and Lim, C. O. (2012). Overexpression of Arabidopsis Dehydration-Responsive Element-Binding Protein 2C Confers Tolerance to Oxidative Stress. *Mol. Cells* 33, 135–140. doi: 10.1007/s10059-012-2188-2

Illéš, P., Schlicht, M., Pavlovkin, J., Lichtscheidl, I., Baluška, F., and Ovečka, M. (2006). Aluminium toxicity in plants: internalization of aluminium into cells of the transition zone in Arabidopsis root apices related to changes in plasma membrane potential, endosomal behaviour, and nitric oxide production. *J. Exp. Bot.* 57, 4201–4213. doi: 10.1093/jxb/erl197

Iuchi, S., Koyama, H., Iuchi, A., Kobayashi, Y., Kitabayashi, S., Kobayashi, Y., et al. (2007). Zinc finger protein STOP1 is critical for proton tolerance in Arabidopsis and coregulates a key gene in aluminum tolerance. *Proc. Natl. Acad. Sci. U. S. A.* 104, 9900–9905. doi: 10.1073/pnas.0700117104

Iuchi, S., Kobayashi, Y., Koyama, H., and Kobayashi, M. (2008). STOP1, a Cys2/His2 type zinc-finger protein, plays critical role in acid soil tolerance in Arabidopsis. *Plant Signal. Behav.* 3, 128–130. doi: 10.4161/psb.3.2.5037

Kim, D., Langmead, B., and Salzberg, S. L. (2015). HISAT: A fast spliced aligner with low memory requirements. *Nat. Methods* 12, 357–360. doi: 10.1038/nmeth.3317

Kobayashi, Y., Kobayashi, Y., Watanabe, T., Shaff, J. E., Ohta, H., Kochian, L. V., et al. (2013). Molecular and physiological analysis of Al3+ and H+ rhizotoxicities at moderately acidic conditions. *Plant Physiol.* 163, 180–192. doi: 10.1104/pp.113.222893

Kobayashi, Y., Ohyama, Y., Kobayashi, Y., Ito, H., Iuchi, S., Fujita, M., et al. (2014). STOP2 activates transcription of several genes for Al- and low pH-tolerance that are regulated by STOP1 in arabidopsis. *Mol. Plant* 7, 311–322. doi: 10.1093/mp/sst116

Kochian, L. V., Hoekenga, O. A., and Piñeros, M. A. (2004). How do crop plants tolerate acid soils? Mechanisms of aluminum tolerance and phosphorous efficiency. *Annu. Rev. Plant Biol.* 55, 459–493. doi: 10.1146/annurev.arplant.55.031903.141655

Kochian, L. V., Piñeros, M. A., Liu, J., and Magalhaes, J. V. (2015). Plant Adaptation to Acid Soils: The Molecular Basis for Crop Aluminum Resistance. *Annu. Rev. Plant Biol.* 66, 571–598. doi: 10.1146/annurev-arplant-043014-114822

Kolukisaoglu, Ü., Weinl, S., Blazevic, D., Batistic, O., and Kudla, J. (2004). Calcium Sensors and Their Interacting Protein Kinases: Genomics of the Arabidopsis and Rice CBL-CIPK Signaling Networks. *Plant Physiol.* 134, 43–58. doi: 10.1104/pp.103.033068

Kusunoki, K., Nakano, Y., Tanaka, K., Sakata, Y., Koyama, H., and Kobayashi, Y. (2017). Transcriptomic variation among six Arabidopsis thaliana accessions identified several novel genes controlling aluminium tolerance. *Plant Cell Environ.* 40, 249–263. doi: 10.1111/pce.12866

Lager, I., Andréasson, O., Dunbar, T. L., Andreasson, E., Escobar, M. A., and Rasmusson, A. G. (2010). Changes in external pH rapidly alter plant gene expression and modulate auxin and elicitor responses. *Plant Cell Environ.* 33, 1513–1528. doi: 10.1111/j.1365-3040.2010.02161.x

Larsen, P. B., Geisler, M. J. B., Jones, C. A., Williams, K. M., and Cancel, J. D. (2005). ALS3 encodes a phloem-localized ABC transporter-like protein that is required for aluminum tolerance in Arabidopsis. *Plant J.* 41, 353–363. doi: 10.1111/j.1365-313X.2004.02306.x

Larsen, P. B., Cancel, J., Rounds, M., and Ochoa, V. (2007). Arabidopsis ALS1 encodes a root tip and stele localized half type ABC transporter required for root growth in an aluminum toxic environment. *Planta* 225, 1447–1458. doi: 10.1007/s00425-006-0452-4

Lex, A., Gehlenborg, N., Strobelt, H., Vuillemot, R., and Pfister, H. (2014). UpSet: Visualization of intersecting sets. *IEEE Trans. Vis. Comput. Graph.* 20, 1983–1992. doi: 10.1109/TVCG.2014.2346248

Ligaba-Osena, A., Fei, Z., Liu, J., Xu, Y., Shaff, J., Lee, S. C., et al. (2017). Loss-of-function mutation of the calcium sensor CBL1 increases aluminum sensitivity in Arabidopsis. *New Phytol.* 214, 830–841. doi: 10.1111/nph.14420

Liu, J., Magalhaes, J. V., Shaff, J., and Kochian, L. V. (2009). Aluminum-activated citrate and malate transporters from the MATE and ALMT families function independently to confer Arabidopsis aluminum tolerance. *Plant J.* 57, 389–399. doi: 10.1111/j.1365-313X.2008.03696.x

Liu, H. C., Liao, H. T., and Charng, Y. Y. (2011). The role of class A1 heat shock factors (HSFA1s) in response to heat and other stresses in Arabidopsis. *Plant Cell Environ.* 34, 738–751. doi: 10.1111/j.1365-3040.2011.02278.x

López-Arredondo, D. L., Leyva-González, M. A., González-Morales, S.II, López-Bucio, J., and Herrera-Estrella, L. (2014). Phosphate Nutrition: Improving

Low-Phosphate Tolerance in Crops. *Annu. Rev. Plant Biol.* 65, 95–123. doi: 10.1146/annurev-arplant-050213-035949

López-Bucio, J., Hernández-Abreu, E., Sánchez-Calderón, L., Nieto-Jacobo, M. F., Simpson, J., and Herrera-Estrella, L. (2002). Phosphate availability alters architecture and causes changes in hormone sensitivity in the Arabidopsis root system. *Plant Physiol.* 129, 244–256. doi: 10.1104/pp.010934

Magalhaes, J. V., Piñeros, M. A., Maciel, L. S., and Kochian, L. V. (2018). Emerging pleiotropic mechanisms underlying aluminum resistance and phosphorus acquisition on acidic soils. *Front. Plant Sci.* 9:1420. doi: 10.3389/fpls.2018.01420

Martinez-Trujillo, M., Limones-Briones, V., Cabrera-Ponce, J. L., and Herrera-Estrella, L. (2004). Improving transformation efficiency of Arabidopsis thaliana by modifying the floral dip method. *Plant Mol. Biol. Rep.* 22, 63–70. doi: 10.1007/BF02773350

Misson, J., Raghothama, K. G., Jain, A., Jouhet, J., Block, M. A., Bligny, R., et al. (2005). A genome-wide transcriptional analysis using Arabidopsis thaliana Affymetrix gene chips determined plant responses to phosphate deprivation. *Proc. Natl. Acad. Sci. U. S. A.* 102, 11934–11939. doi: 10.1073/pnas.0505266102

Mora-Macías, J., Ojeda-Rivera, J. O., Gutiérrez-Alanís, D., Yong-Villalobos, L., Oropeza-Aburto, A., Raya-González, J., et al. (2017). Malate-dependent Fe accumulation is a critical checkpoint in the root developmental response to low phosphate. *Proc. Natl. Acad. Sci. U. S. A.* 114, E3563–E3572. doi: 10.1073/pnas.1701952114

Noshi, M., Yamada, H., Hatanaka, R., Tanabe, N., Tamoi, M., and Shigeoka, S. (2017). Arabidopsis dehydroascorbate reductase 1 and 2 modulate redox states of ascorbate-glutathione cycle in the cytosol in response to photooxidative stress. *Biosci. Biotechnol. Biochem.* 81, 523–533. doi: 10.1080/09168451.2016.1256759

Ohyama, Y., Ito, H., Kobayashi, Y., Ikka, T., Morita, A., Kobayashi, M., et al. (2013). Characterization of AtSTOP1 orthologous genes in Tobacco and other plant species. *Plant Physiol.* 162, 1937–1946. doi: 10.1104/pp.113.218958

O'Malley, R. C., Huang, S. S. C., Song, L., Lewsey, M. G., Bartlett, A., Nery, J. R., et al. (2016). Cistrome and Epicistrome Features Shape the Regulatory DNA Landscape. *Cell* 165, 1280–1292. doi: 10.1016/j.cell.2016.04.038

Osawa, H., and Matsumoto, H. (2001). Possible involvement of protein phosphorylation in aluminum-responsive malate efflux from wheat root apex. *Plant Physiol.* 126, 411–420. doi: 10.1104/pp.126.1.411

Panda, B. B., and Achary, V. M. M. (2014). Mitogen-activated protein kinase signal transduction and DNA repair network are involved in aluminum-induced DNA damage and adaptive response in root cells of Allium cepa L. *Front. Plant Sci.* 5, 256. doi: 10.3389/fpls.2014.00256

Péret, B., Clément, M., Nussaume, L., and Desnos, T. (2011). Root developmental adaptation to phosphate starvation: Better safe than sorry. *Trends Plant Sci.* 16, 442–450. doi: 10.1016/j.tplants.2011.05.006

Provart, N., and Zhu, T. (2003). A Browser-based Functional Classification SuperViewer for Arabidopsis Genomics. *Curr. Comput. Mol. Biol.* 203, 271–272.

Robinson, M. D., Mccarthy, D. J., and Smyth, G. K. (2010). edgeR: a Bioconductor package for differential expression analysis of digital gene expression data. *Bioinforma. Appl. Note* 26, 139–140. doi: 10.1093/bioinformatics/btp616

Sadhukhan, A., Enomoto, T., Kobayashi, Y., Watanabe, T., Iuchi, S., Kobayashi, M., et al. (2019). Sensitive to Proton Rhizotoxicity1 Regulates Salt and Drought Tolerance of Arabidopsis thaliana through Transcriptional Regulation of CIPK23. *Plant Cell Physiol.* 60, 2113–2126. doi: 10.1093/PCP/PCZ120

Sawaki, Y., Iuchi, S., Kobayashi, Y., Kobayashi, Y., Ikka, T., Sakurai, N., et al. (2009). Stop1 regulates multiple genes that protect arabidopsis from proton and aluminum toxicities. *Plant Physiol.* 150, 281–294. doi: 10.1104/pp.108.134700

Schindelin, J., Arganda-Carreras, I., Frise, E., Kaynig, V., Longair, M., Pietzsch, T., et al. (2012). Fiji: An open-source platform for biological-image analysis. *Nat. Methods* 9, 676–682. doi: 10.1038/nmeth.2019

Shaff, J. E., Schultz, B. A., Craft, E. J., Clark, R. T., and Kochian, L. V. (2010). GEOCHEM-EZ: A chemical speciation program with greater power and flexibility. *Plant Soil* 330, 207–214. doi: 10.1007/s11104-009-0193-9

Song, S. J., Feng, Q. N., Li, C. L., Li, E., Liu, Q., Kang, H., et al. (2018). A tonoplast-associated calcium-signaling module dampens ABA signaling during stomatal movement. *Plant Physiol.* 177, 1666–1678. doi: 10.1104/pp.18.00377

Thibaud, M. C., Arrighi, J. F., Bayle, V., Chiarenza, S., Creff, A., Bustos, R., et al. (2010). Dissection of local and systemic transcriptional responses to phosphate starvation in Arabidopsis. *Plant J.* 64, 775–789. doi: 10.1111/j.1365-313X.2010.04375.x

Tokizawa, M., Kobayashi, Y., Saito, T., Kobayashi, M., Iuchi, S., Nomoto, M., et al. (2015). Sensitive to proton Rhizotoxicity1, calmodulin binding transcription activator2, and other transcription factors are involved in Aluminum-Activated Malate transporter1 expression. *Plant Physiol.* 167, 991–1003. doi: 10.1104/pp.114.256552

von Uexküll, H. R., and Mutert, E. (1995). Global extent, development and economic impact of acid soils. *Plant Soil* 171, 1–15. doi: 10.1007/BF00009558

Yang, X. Y., Zeng, Z. H., Yan, J. Y., Fan, W., Bian, H. W., Zhu, M. Y., et al. (2013). Association of specific pectin methylesterases with Al-induced root elongation inhibition in rice. *Physiol. Plant* 148, 502–511. doi: 10.1111/ppl.12005

Zhang, Y., Zhang, J., Guo, J., Zhou, F., Singh, S., Xu, X., et al. (2019). F-box protein RAE1 regulates the stability of the aluminum-resistance transcription factor STOP1 in Arabidopsis. *Proc. Natl. Acad. Sci. U. S. A.* 116, 319–327. doi: 10.1073/pnas.1814426116

Conflict of Interest: The authors declare that the research was conducted in the absence of any commercial or financial relationships that could be construed as a potential conflict of interest.

frontiers in Plant Science

ORIGINAL RESEARCH
published: 23 October 2020
doi: 10.3389/fpls.2020.569687

Remodeling of Root Growth Under Combined Arsenic and Hypoxia Stress Is Linked to Nutrient Deprivation

Vijay Kumar[1,2†], Lara Vogelsang[1†], Romy R. Schmidt[3†], Shanti S. Sharma[4], Thorsten Seidel[1†] and Karl-Josef Dietz[1†]*

[1] Department of Biochemistry and Physiology of Plants, Faculty of Biology, University of Bielefeld, Bielefeld, Germany, [2] Department of Biosciences, Himachal Pradesh University, Shimla, India, [3] Department of Plant Biotechnology, Faculty of Biology, University of Bielefeld, Bielefeld, Germany, [4] Department of Botany, School of Life Sciences, Sikkim University, Gangtok, India

OPEN ACCESS

Edited by:
Manny Delhaize,
CSIRO Plant Industry, Australia

Reviewed by:
Luis Cardenas,
National Autonomous University of Mexico, Mexico
Irene García,
Institute of Plant Biochemistry and Photosynthesis (IBVF), Spain
Ann Cuypers,
Hasselt University, Belgium

***Correspondence:**
Karl-Josef Dietz
karl-josef.dietz@uni-bielefeld.de

†ORCID:
Vijay Kumar
orcid.org/0000-0002-7771-4269
Lara Vogelsang
orcid.org/0000-0002-5310-1708
Romy R. Schmidt
orcid.org/0000-0002-3395-0673
Thorsten Seidel
orcid.org/0000-0003-4423-3001
Karl-Josef Dietz
orcid.org/0000-0003-0311-2182

Specialty section:
This article was submitted to Plant Abiotic Stress, a section of the journal Frontiers in Plant Science

Received: 04 June 2020
Accepted: 06 October 2020
Published: 23 October 2020

Citation:
Kumar V, Vogelsang L, Schmidt RR, Sharma SS, Seidel T and Dietz K-J (2020) Remodeling of Root Growth Under Combined Arsenic and Hypoxia Stress Is Linked to Nutrient Deprivation. Front. Plant Sci. 11:569687. doi: 10.3389/fpls.2020.569687

Root architecture responds to environmental stress. Stress-induced metabolic and nutritional changes affect the endogenous root development program. Transcriptional and translational changes realize the switch between stem cell proliferation and cell differentiation, lateral root or root hair formation and root functionality for stress acclimation. The current work explores the effects of stress combination of arsenic toxicity (As) and hypoxia (Hpx) on root development in *Arabidopsis thaliana*. As revealed previously, combined As and Hpx treatment leads to severe nutritional disorder evident from deregulation of root transcriptome and plant mineral contents. Both As and Hpx were identified to pose stress-specific constraints on root development that lead to unique root growth phenotype under their combination. Besides inhibition of root apical meristem (RAM) activity under all stresses, As induced lateral root growth while root hair density and lengths were strongly increased by Hpx and HpxAs-treatments.

A dual stimulation of phosphate (Pi)-starvation response was observed for HpxAs-treated plant roots; however, the response under HpxAs aligned more with Hpx than As. Transcriptional evidence along with biochemical data suggests involvement of *PHOSPHATE STARVATION RESPONSE 1*; *PHR1*-dependent systemic signaling. Pi metabolism-related transcripts in close association with cellular iron homeostasis modulate root development under HpxAs. Early redox potential changes in meristematic cells, differential ROS accumulation in root hair zone cell layers and strong deregulation of NADPH oxidases, NADPH-dependent oxidoreductases and peroxidases signify a role of redox and ROS signaling in root architecture remodeling under HpxAs. Differential aquaporin expression suggests transmembrane ROS transport to regulate root hair induction and growth. Reorganization of energy metabolism through NO-dependent alternate oxidase, lactate fermentation, and phosphofructokinase seems crucial under HpxAs. TOR and SnRK-signaling network components were potentially involved in

control of sustainable utilization of available energy reserves for root hair growth under combined stress as well as recovery on reaeration. Findings are discussed in context of combined stress-induced signaling in regulation of root development in contrast to As and Hpx alone.

Keywords: root hairs, meristem, phosphate, iron, hypoxia, arsenic, redox, ROS

INTRODUCTION

Root development is a dynamic and highly regulated process (Scheres et al., 2002; Hodge et al., 2009; Petricka et al., 2012). The developmental plasticity of root systems allows plants to establish a sustainable organ tailored to the prevailing environmental conditions. The simple root architecture in seedlings changes to an elaborate post-embryonic root development program in maturing plants. However, fine-tuning of the plant root architecture is required upon stress exposure at any life stage. Molecular understanding of root development and underlying gene regulatory networks presently evolves using genomic and molecular biological approaches. Several transcription factors under control of nutrients, redox and reactive oxygen species (ROS) or hormones have been identified (Shin and Schachtman, 2004; Hodge et al., 2009; Ruiz Herrera et al., 2015).

Root growth plasticity is largely determined by temporal fluctuations in the balance between cell division and cell differentiation (Perilli et al., 2012; Sozzani and Iyer-Pascuzzi, 2014). While cell division in the meristems is mostly regulated by auxins, the differentiation-promoting cytokinin (CK) can inhibit cell division through *ARR1* transcription factor (Moubayidin et al., 2010). *ARR1* activates a negative regulator of *PIN* (auxin transport facilitators) i.e., *SHY2*. ROS participate in controlling the process (Tsukagoshi et al., 2010; Yang et al., 2018). Further, modification of stem cell growth through programmed cell death occurs under severe water stress (Cao and Li, 2010).

Environmental stimuli like nutrient deprivation, salt or water stress modulate the growth phenotype of primary roots, lateral roots as well as root hairs (RHs) (Müller and Schmidt, 2004; De Tullio et al., 2010; Liu et al., 2015; Satbhai et al., 2015). RHs are well-studied structures particularly in seedlings as a model for exploring the genetic control of cell division and differentiation, spatiotemporal onset of regulatory mechanisms and epigenetic influence on development processes (Grierson and Schiefelbein, 2002; Grierson et al., 2014). Their structural simplicity makes them ideal for mechanistic understanding of development (Grierson et al., 2014; Salazar-Henao et al., 2016). Different aspects of RH development are thoroughly scrutinized for regulatory mechanisms especially under nutrient deprivation, e.g., epidermal cell differentiation into trichoblast (RH- or H-cell) and non-trichoblast (N-cells), RH initiation and tip growth, cell wall modifications as facilitators of tip growth and ectopic RH growth (Müller and Schmidt, 2004; Shin et al., 2005; Bruex et al., 2012; Kwon et al., 2015; Shibata and Sugimoto, 2019).

Besides widely studied phosphate- (Pi) and Fe-starvation, interference between N- and K-uptake and N-assimilation has also been recognized as important factors in RH development (Müller and Schmidt, 2004; Salazar-Henao and Schmidt, 2016; Huang et al., 2020). Recent studies described functions of ethylene in RH development among other growth regulatory hormones (Katsumi et al., 2000; Cho and Lee, 2013; Neumann, 2016; Huang et al., 2020). Complex gene regulatory networks determine the response to nutrient deprivation especially for Pi and Fe (Cui S. et al., 2018). However, their functional specificity and relative importance in an event of co-occurrence of multiple nutrient deprivations or other environmental factors remain elusive, especially in adult plants.

Identification of mechanisms underlying plant responses to naturally co-occurring multiple stresses requires experiments where plants are exposed to these stress combinations (Suzuki et al., 2014). The responses and mechanisms governing acclimation to combinatorial stresses often differ from regulatory pathways involved in single stress acclimation (Rasmussen et al., 2013; Suzuki et al., 2014). Unique transcriptomic, proteomic, and metabolic changes are evident in plants exposed to combined stresses (Pandey et al., 2015; Suzuki et al., 2016).

Metabolic and molecular responses of Arabidopsis to a naturally prevalent combination of arsenic (As) and hypoxia (Hpx) were recently described by Kumar et al. (2019). Arsenic contamination is a major problem linked worldwide to either groundwater or irrigation of rice cultivated in affected areas (Naujokas et al., 2013). Numerous agricultural fields and groundwater reservoirs in South East Asia, Europe or North America are highly contaminated with As (Medunić et al., 2020). Remediation of contaminated sites using hyperaccumulator plants and generation of As-tolerant but non-accumulating crops, particularly in edible parts, is the need of hour (Kofroňová et al., 2018). However, co-occurring environmental factors aggravate As toxicity, tolerance and accumulation in crop plants and impede growth potential of As-hyperaccumulators. For example, flooding is required during the early stages of rice cultivation.

The use of As-containing groundwater aggravates pollution in the contaminated areas. Indeed, the As-enriched micro-ecosystem represents a complex environment involving several inherently interacting factors, e.g., low soil pH (increased CO_2), pH-induced As(V) reduction to As(III), and especially Hpx for root growth. Not only Hpx, but subsequent re-oxygenation, when soil dries up, acts as another stress factor. These combined factors likely interfere with As uptake, accumulation including grain deposition and toxicity in rice. A combination of As and Hpx imposes distinct influence on plants due to unique and overlapping features of these stressors. For example, a significant part of the characteristic signaling pattern under As and Hpx is mediated by ROS (Pucciariello et al., 2012; Islam et al., 2015), while both simultaneously affect the cellular energy metabolism (Bailey-Serres and Voesenek, 2008, 2010).

Application of HpxAs stress to *Arabidopsis thaliana* generated unique responses at physiological, transcriptomic, and metabolic level apart from certain overlapping changes (Kumar et al., 2019). Besides characterizing primary stress effects in the roots, it was possible to analyze the dynamics of rapid root-to-shoot communication (Kumar et al., 2019). The most challenging scenario that developed under HpxAs was strong deregulation of nutrient homeostasis. It is known that both stresses affect nutrient uptake (Blokhina and Fagerstedt, 2010; Zhao et al., 2010); however, under HpxAs, plants were challenged to acclimate to As under Hpx-induced inhibition of energy metabolism.

Root growth was severely inhibited during combined stress treatment; however, growth recovery was evident on reaeration (Kumar et al., 2019). In fact, the combined stressed plants showed a lag in root growth recovery compared to individual treatments. Besides a unique and strong downregulation of many transcripts (>500), about 300 other transcripts increased in expression specifically under As and Hpx combination (Kumar et al., 2019). All these observations indicated existence of an energy efficient way to balance root stem cell division and differentiation in a way to best utilize the available resources for coping with nutrient deprivation and to facilitate sequestration of As for stress acclimation.

The present study scrutinizes the root growth phenotype under combinatorial exposure to As and Hpx. Meta-analysis of root growth-related genes specific for combined stress led to the identification of transcriptional adjustments indicative for the remodeling of root architecture to achieve Hpx and As adaptation. Particularly, transcripts involved in root meristem proliferation and cell differentiation displayed pronounced changes. The root phenotype suggested a strong stimulation of epidermal cell differentiation into RHs. Biochemical measurements and transcriptomic data indicate a major role of redox regulation in observed changes in root architecture, while treatment-dependent decrease in epidermal and cortical cell viability was identified as an acclimation tradeoff.

MATERIALS AND METHODS

Plant Growth and Stress Application

Arabidopsis thaliana (Col-0; WT) plants were grown hydroponically as described previously (Kumar et al., 2019). In brief, the plants were grown on 0.25 strength Hoagland nutrient medium (1.25 mM KNO_3, 0.5 mM $NH_4H_2PO_4$, 0.75 mM $MgSO_4$, 1.50 mM $Ca(NO_3)_2$, micronutrients, 14.5 μM Fe-EDTA, 500 μM MES (pH 5.25) for 32 days (10/14 h day/night; 100 μmol photons m^{-2} s^{-1} at 22/19°C (day/night, 50% relative humidity). The nutrient medium was constantly aerated (ambient air 21% O_2) and renewed weekly. For stress application, plant roots after 32 days culture were exposed to 250 μM As(V; Na_2HAsO_4), Hpx or HpxAs. For Hpx, the nutrient medium was pre-flushed with air from a nitrogen generator for 48 h (99.6% N_2 and 0.4% O_2) to achieve average O_2 concentration of 86 ± 4.3 nmol ml^{-1} compared to 262 ± 6.8 nmol ml^{-1} for control and As (mean ± SE, n = 15 experiments). This ensured an immediate hypoxic stress. The nitrogen flushing was continued during the treatment period of 7 days, while control plants and those exposed to As alone were aerated as before (21% O_2). The oxygen content remained stable over the 7 days treatment period. For reaeration, the hypoxic media was replaced with normally aerated one, however presence of As was continued in HpxAs. It is important to add that the shoots remained in air under ambient light conditions throughout. Plant roots (whole) were harvested after respective treatment and re-aeration time points in liquid nitrogen. The stored (−80°C) plant material was used for biochemical assays. Plant shoot and roots were also measured for their fresh weight after 7 d of treatment.

Microarray and Quantitative Transcript Analysis

The raw microarray data analyzed in this study can be accessed from NCBI GEO[1] and was published first by Kumar et al. (2019). They detailed the method for RNA extraction, DNA hybridization, qRT-PCR and data analysis. In brief, plant roots (whole) were pulverized in liquid nitrogen and RNA was extracted to be used for microarray-based transcriptome analysis as well as for quantitative analysis of transcript amounts using qRT-PCR. Quantity and quality of the RNA were tested with the NanoDrop ND-1000 spectrophotometer and by gel electrophoresis (Aranda et al., 2012). RNA quality for microarray hybridization (Affymetrix Arabidopsis Gene 1.0 ST arrays) was again tested prior to hybridization using the Agilent 2100 bioanalyzer system. All samples had RNA integrity numbers ≥ 9. Hybridization was done by KFB, Center of Excellence for Fluorescent Bioanalytics (Regensburg, Germany; www.kfb-regensburg.de). The summarized probe set signals in log2 scale were calculated by using the RMA algorithm (Irizarry et al., 2003) with the Affymetrix Gene Chip Expression Console v1.4 Software. The transcriptome data was initially filtered for transcripts belonging to the three major GO-related terms i.e., "Root and Root Hair Development," "Phosphate Starvation Response," and "Fe-Homeostasis" and showing linear fold change of $-2 \geq fc \geq 2$ for at least one treatment. The identified transcripts were further sub-categorized into those directly related to RH development, root growth-related hormonal signals, root meristem maintenance, cell wall modification, hypoxia or As-dependent phosphate starvation response, Fe-homeostasis, NO-generation, and ROS producing and scavenging enzymes required for root growth regulation. Further, the transcripts in these sub-categories were filtered for false discovery rate (FDR ≤ 5%) adjusted p-value ≤ 0.05 for treatment effect. In the next and last filtering step, those FDR-filtered transcripts which showed a unique expression under HpxAs or had relevance to HpxAs-induced root growth phenotype were converted in suitable heat maps or histograms, while complete lists appear in supplements. Brief description of transcript changes, under As, Hpx and HpxAs-treatments, which relates to cell wall modification and lipid metabolism has been given in supplements by Kumar et al. (2019).

It is pertinent to add that the validity of microarray data has been tested through qRT-PCR for multiple arsenic and

[1]https://www.ncbi.nlm.nih.gov/geo/query/acc.cgi?acc=GSE119327

hypoxia-stress markers as well as through their recovery after e.g., removal of hypoxia by Kumar et al. (2019). Further, qRT-PCR analysis for additional hypoxia markers and their stress recovery has been done in this study and data presented in **Supplementary Figure 2B**. For qRT-PCR, RNA samples were processed to generate cDNA. Transcripts were quantified on MyiQ qPCR cycler (BIO-RAD) using KAPA SYBR qPCR master mix and target specific primers (**Supplementary Table 5**). PCR efficiency and transcript quantification calculation were based on analysis using LinRegPCR 11.0 software (Ramakers et al., 2003; Ruijter et al., 2009). Gene expression was normalized by calculating the normalization factor from the geometric mean of actin (*ACT2*) and tubulin (*TUB5*) expression as described (Vandesompele et al., 2002).

Root Growth Phenotype and Confocal Imaging

Root Hair Phenotype

A quantitative measure of treatment effects on root growth in terms of total accumulated fresh weight is presented in **Figures 1A,B**. However, to identify the regions of new biomass accumulation (taproot, lateral roots, or root hairs) and comparative extent of growth during the 7 d treatment period, a qualitative measurement of root growth was done for two independent experiments. At the start of treatment period, the plant roots were dipped in well stirred active charcoal suspension for 5 min and rinsed with water (Schat and Ten Bookum, 1992). This charcoal staining allows highly effective analysis of root growth during treatment period without interfering with nutrient uptake (Schat and Ten Bookum, 1992). After 7 d, the growth phenotype was recorded, and the roots were freshly stained with active charcoal before start of reaeration (**Figure 1A**). Further, we took a closer look at RH growth under a Leica MZ6 modular stereomicroscope with 4x zoom and an artificial light source. RH zone (65–80 areas) from multiple plants per treatment belonging to two independent experiments were photographed and compared for RH length and density. Representative images are presented in **Figure 1**. The RH images were also recorded after treatment of charcoal-stained roots.

Cell-Viability Analysis

Viability of different cell layers in the RH zone was tested with the fluorescent dye SYTOX Green (Truernit and Haseloff, 2008). SYTOX fluorescent dye only penetrates non-viable cells (permeable plasma membranes) wherein interaction with DNA increases their fluorescence >500 fold, reducing the background appreciably (Truernit and Haseloff, 2008). The confocal imaging (LSM 780, Carl Zeiss, Germany) was carried out on the 7th day of treatment. Intact plant roots were immersed with SYTOX green (250 nM dilution from 5 mM stock in DMSO) for 7 min followed by thorough washing with water. SYTOX green in the labeled roots was excited using the argon multiline laser (488 nm, 25 mW) with corresponding main beam splitter and the emission recorded between 500–550 nm (emission max. 523 nm). At 10X magnification (Zeiss Plan-Apochromat 10x/0.45 M27) with a pixel dwell time of 1.2–2.2 μs and a data depth of 12 bits per pixel, 15–20 images were recorded per treatment and experiment. Imaging was carried out within 30 min of staining, when the signal intensity was maximum. Images were evaluated with the ZEN software for fluorescence intensities. The signal-to-noise ratio was optimized for the treatment with maximal fluorescence intensity and the gain (master) and pinhole values were kept constant throughout the treatments. Fluorescence intensity values for the selected excitation channel were collected separately from three different regions of interests (epidermal/cortical cell layers) within the imaged RH zone avoiding saturated areas. The collected data are presented in form of box plots as well as fold differences among treatments.

Fluorescence Analysis for Reactive Oxygen Species (ROS)

In plant growth and development, ROS generation drives processes like cell wall synthesis and root tip growth. However, a strict control over the intensity of ROS generation is important to protect cells from their deleterious effects. For *in vivo* ROS staining, 2', 7'-dichlorodihydrofluorescein diacetate (H_2DCFDA) was used (Eruslanov and Kusmartsev, 2010). H_2DCFDA converts to the highly fluorescent 2', 7'-dichlorofluorescein (DCF) upon cleavage of the acetate groups by esterases and subsequent oxidation. Intact roots after 7 d of treatment were dipped in DCFDA (5 μM from 10 mM stock in DMSO) for 5 min and then washed with water. The argon multiline laser (488 nm, 25 mW) was used for H_2DCFDA excitation, while emission was collected between 500–550 nm (emission max. 517–527 nm). Representative images are given in **Supplementary Figure 4**.

Biochemical Analysis

Ferric Chelate Reductase Activity

The activity of ferric chelate reductase was measured in whole roots using a spectrophotometric measurement of purple-colored Fe(II)-ferrozine complex (Emre and Koiwa, 2013). The whole plant roots after 7 d of treatment were dark incubated in Fe(III)-EDTA solution (0.1 mM) containing ferrozine ([3-(2-pyridyl)-5, 6-diphenyl-1, 2, 4-triazine sulfonate]; 0.3 mM) for 45 min. The activity proceeds at room temperature in a 2 ml tube with occasional inversion to assure that root surface stays in touch with solution. After incubation, the roots were rinsed several times in the same solution, and liquid droplets were removed. Absorption of the formed purple complex was quantified at 562 nm against the assay reagent. The calculation of the enzyme activity was based on the molar extinction coefficient of the complex (28.6 mM^{-1} cm^{-1}) and pre-recorded fresh weight of roots.

Activities of Hypoxia-Responsive Enzymes of Energy Metabolism

Hypoxic growth conditions inhibit normal energy metabolism and induce fermentation. Committed enzymes are pyruvate decarboxylase (PDC), alcohol dehydrogenase (ADH) and lactic dehydrogenase (LDH). PDC activity was measured as conversion of pyruvate to acetaldehyde in presence of its cofactors thiamine pyrophosphate, Mg^{2+} and enzyme ADH (Mithran et al., 2014). The extraction buffer comprised of Na-Pi buffer (50 mM, pH 7.0) supplemented with $MgCl_2$ (5 mM), EDTA (5 mM) and thiamine pyrophosphate (TPP, 500 μM). Further, phenylmethylsulphonyl

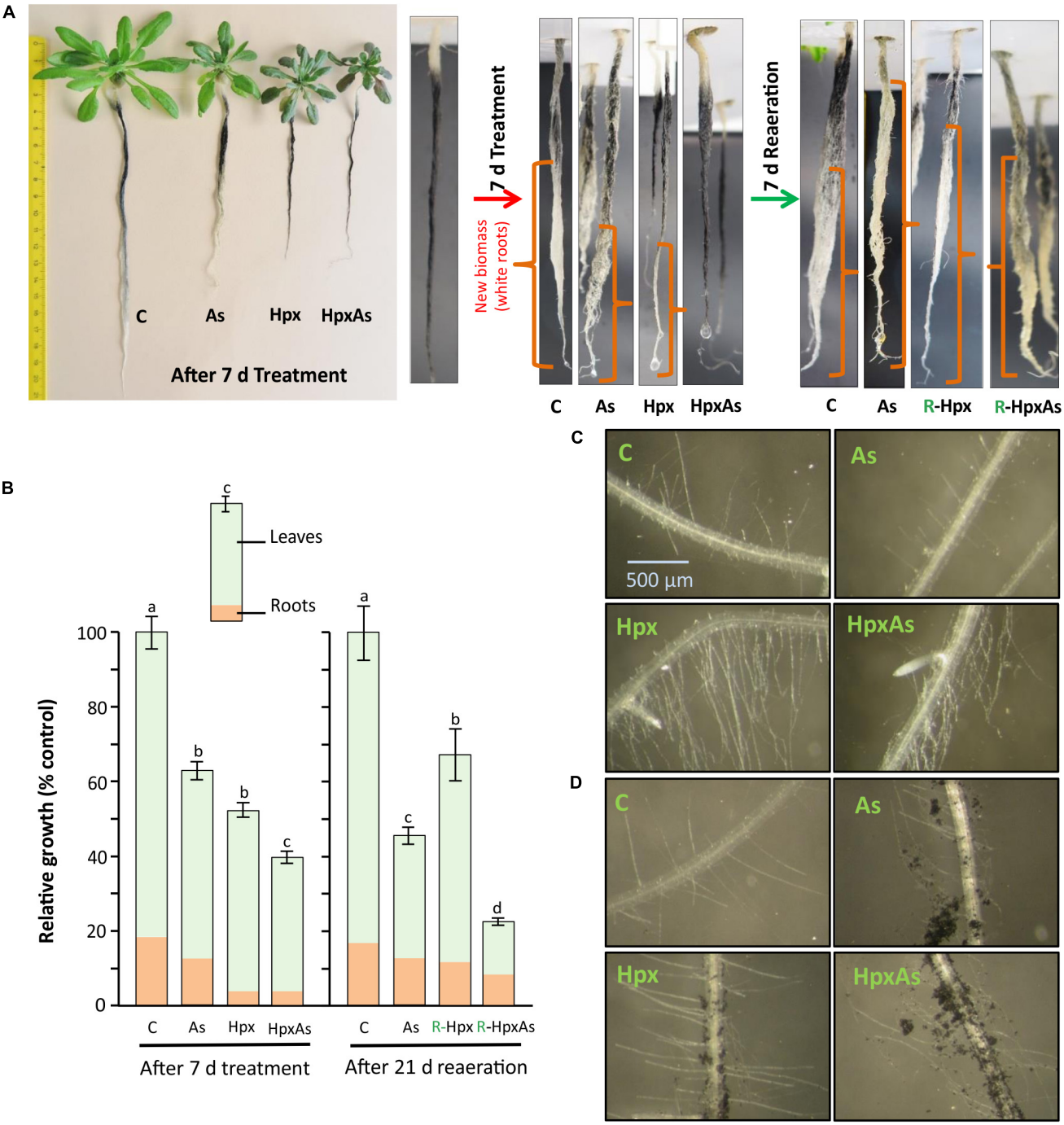

FIGURE 1 | Root and root hair phenotype of plants exposed to arsenic (As), hypoxia (Hpx) and their combination (HpxAs). *A. thaliana* plants were grown for 32 days in hydroculture and then exposed to As (V; 250 µM), Hpx or their combination (HpxAs) for 7 days. **(A)** Plant images (left panel) after 7 days of treatment for comparison of treatment effects on root and shoot growth. Just before the start of treatment and start of reaeration, plant roots were stained with active charcoal. The strong surface adherence of charcoal particles allows assessment of fresh root growth during treatment and reaeration, which appear white. Close-up images of roots (middle) highlight newly formed root biomass after 7 days treatment. In these close-up images roots are not in scale for comparison of total root length however can be compared qualitatively for extent of growth (in different root zones) among different treatments (white color). Also shown are images of stained roots (right) that were reaerated for 7 days after treatment (supplemented with aerated nutrient media; supplemented with As(V) in case of HpxAs-treatment). **(B)** Data on relative total biomass accumulation (shoot and root visible) after 7 days of treatment (means ± SE, $n = 40$; 3 independent experiments; Tukey's test, $p < 0.05$) and long reaeration (21 days) (means ± SE, $n = 12$; Tukey's test, $p < 0.05$). Further, images of the RH zone under different treatments without **(C)** or with **(D)** charcoal staining after 7 days treatment.

fluoride (PMSF, 100 μM), dithiothreitol (DTT, 1 mM) and leupeptin (5 μM) were added to increase protein stability. Approx. 30 mg of root tissue was used for enzymes extraction with 70 μl of extraction buffer. The extraction was done using Precellys® homogenizer (6,800 rpm, 3 cycles of 20 s with 30 s pause in between). The homogenized material was centrifuged at 15,000 × *g* (4°C) for 15 min. The assay mixture (117 μl) contained 95–100 μl MES (50 mM, pH 6.0), 2 μl NADH (670 μM), 5 μl ADH (1.2 U/ml), 5–10 μl of root extract and 5 μl sodium pyruvate (6 mM). Baseline was adjusted after adding ADH, while addition of pyruvate started the reaction. The activity was measured as decrease in NADH absorption at 340 nm for 3 min. Specific activity was calculated based on molar extinction coefficient of NADH (6.22 mM^{-1} cm^{-1}) and protein content in enzyme extracts. Protein content for all the enzyme assays was quantified using Bradford method (Bradford, 1976).

Extraction for ADH and LDH activity tests was performed in 100 mM Tris–HCl (pH 7.7) buffer with EDTA (5 mM), and freshly added DTT (1 mM), cysteine (10 mM), PMSF (100 μM), and 5 μM leupeptin. Enzyme extraction procedure was like PDC except ∼40 mg tissue was extracted with 100 μl buffer. ADH was measured in the direction acetaldehyde to ethanol (Huang et al., 2002). The final assay mixture (115 μl) comprised of 100–107 μl Tris–HCl (100 mM, pH 8.5) with 2 μl NADH (670 μM), 5 μl acetaldehyde and 2.5–10 μl enzyme extract. Baseline was adjusted after addition of acetaldehyde. The reaction was started by addition of enzyme extract and absorption was monitored for 3 min at 340 nm for decrease in NADH amount. LDH activity was measured in the direction pyruvate to lactate (Hanson and Jacobsen, 1984). In addition, 4-bromopyrazole was used to inhibit endogenous ADH. The assay mixture (124.5 μl) comprised 100 mM Tris–HCl (pH 8.0), 2 μl NADH (670 μM), 2.5 μl 4-bromopyrazole (3 M), 10 μl enzyme extract and 10 μl pyruvate (6 mM). The baseline was recorded after addition of extract, while addition of pyruvate started the reaction. Absorbance change of NADH was monitored at 340 nm. NADH molar extinction coefficient was used for calculating specific activity for both ADH and LDH.

XTT Reductase Activity

NADPH-oxidases (RBOH; respiratory burst oxidase homolog) form superoxide radicals. Their activity was measured in crude membrane extracts using NADPH-driven and superoxide-dependent reduction of XTT [2,3-bis(2-methoxy-4-nitro-5-sulfophennyl)-2H-tetrazoilum-5-carboxanilide sodium salt] using a modified method (Hao et al., 2006; Potocký et al., 2012). The crude extraction of the plasma membrane proteins needed two different buffers i.e., (a) extraction buffer (EB) containing Tris–HCl (50 mM, pH 8.0), sucrose (250 mM), and EDTA (80 mM) and freshly added PMSF (100 μM), and (b) resuspension buffer (RB) comprising MOPS (50 mM, pH 7.2) supplemented with 250 mM sucrose and PMSF (100 μM). In the first step of extraction, ∼30 mg root tissue was added with 70 μl of EB and homogenized in Precellys® homogenizer (2 times 3 cycles of 6,800 rpm, 20 s each with 30 s pause every time). The homogenate was centrifuged at 16,000 × *g*, 15 min (4°C). The supernatant was discarded, and the pellet washed with 1 ml of EB. The tube was inverted to resuspend the soluble proteins. After a second centrifugation (16,000 × *g*, 15 min, 4°C), the pellet was resuspended in 50 μl RB. The vortexed suspension was transferred with a blunt end pipette tip to a 1.5 ml tube and was incubated at 30°C for 15 min. After centrifugation (16,000 × *g*, 5 min, 4°C), the crude PM extract was ready in the supernatant and was used for activity analysis. The assay mixture had 60 μl of Tris–HCl (50 mM, pH 7.5), 10 μl XTT (5 mM in DMSO), 10 μl NADPH (2 mM), and 10 μl of protein. The NADPH specificity of the reaction was tested by excluding NADPH from the reaction which completely stopped XTT reduction. Superoxide dismutase (SOD) served as specific inhibitor of the XTT reduction by quenching superoxide. The activity was recorded for 5 min. The supernatant from the first centrifugation (soluble cell lysate) was also used in order to determine the extent of XTT reduction in soluble cell lysate. The protein content estimation for the crude extract did not work with the Bradford assay, so the activities are presented on fresh weight bases. The calculation of XTT reduction or NADPH oxidase activity were based on ε = 21600 M^{-1} cm^{-1} for XTT at 470 nm (Able et al., 1998).

Activities of Antioxidant Enzymes

Enzyme extraction was done in 300 μl of HEPES buffer (100 mM, pH 7.6, freshly added with 100 μM PMSF) for 30–50 mg of root tissue. The homogenization in Precellys® homogenizer was performed 2 times, 3 cycles of 6,800 rpm, 20 s each with a pause of 30 s. The homogenate was centrifuged at 10,000 × *g* for 10 min (4°C). Ascorbate peroxidase (APX) activity was measured immediately after extraction. Assay mixture (115 μl) for APX activity comprised 83 μl HEPES (50 mM, pH 7.6), 7 μl ascorbate (ASC, 5 mM), 10 μl enzyme extract and reaction started by adding 15 μl H_2O_2 (400 μM final concentration). Decrease in ASC absorbance was measured for 3 min at 290 nm. Activity calculations were based on ε_{ASC} = 2.8 mM^{-1} cm^{-1}. The same enzyme extract was used for guaiacol peroxidase (PER) activity. In this reaction the peroxidase oxidizes guaiacol and activity can be recorded as absorbance change at 470 nm (Amako et al., 1994). In a reaction volume of 223 μl, 200 μl K-Pi buffer (100 mM, pH 6.8), 10 μl guaiacol (0.5% in H_2O), 3 μl extract and 10 μl H_2O_2 (12 mM stock) were added. Addition of H_2O_2 started the reaction and the change in absorbance was measured for 5 min. Activity was calculated per unit protein using ε = 22.6 mM^{-1} cm^{-1} for oxidized guaiacol.

Catalase activity was measured in the same extract polarographically using a Clark-type O_2 electrode (Goldstein, 1968). The reaction mixture contained 890 μl of HEPES buffer (100 mM, pH 7.6) along with 100 μl of H_2O_2 (100 mM). The reaction was started by addition of 10 μl of enzyme extract and rate of evolution of oxygen was recorded for 5 min.

Plant Cell Sap Osmolarity

For determination of osmolarity of cell sap, tissue sap was squeezed out from fresh root and leaf tissue (50–100 mg) using micro pestle. The extract was centrifuged (16,000 × *g*, 10 min) and supernatant diluted suitably to be measured for osmolarity on automatic semi-micro osmometer (A0800, Knauer). The

osmometer was calibrated before measurements with 0 and 400 mosmol/l NaCl solutions.

Residual inorganic phosphate (Pi) after 7 d of treatment was measured in the nutrient media using malachite green-based quantification (Baykov et al., 1988). The reagents used were (a) malachite green (1 mM) with polyvinyl alcohol (0.16%) in H_2SO_4 (6 mM) and (b) ammonium molybdate (50 mM) in H_2SO_4 (3.4 M). The reagents were mixed freshly before measurement in a ratio of 1:0.5 (a: b). The measurements were carried out in a plate reader with 198 μl reagent mix and 2 μl sample. Absorbance was measured at 620 nm after thoroughly mixing the contents in each well. In parallel the assay was also calibrated with a Pi-concentration series (0–5 μM; $NH_4H_2PO_4$).

Statistical Analysis

Data are presented as means with standard error. Statistical analysis (one-way analysis of variance; ANOVA followed by Tukey's *post hoc* test) was performed to evaluate significant differences among means using IBM SPSS Statistics for Windows, version 20 (IBM Corp., Armonk, NY, United States). Significantly different means ($p < 0.05$) are marked with different letters while missing letters indicate lack of significance. The statistical analysis for the microarray data was performed as part of complete transcriptome analysis by Transcriptome Analysis Console version 3.1 (Affymetrix).

RESULTS

Several studies report that As stress alters the plant redox state and nutrient availability (Carbonell-Barrachina et al., 1997; Srivastava et al., 2005; Zhao et al., 2010; Duan et al., 2013). Similarly, it is known that Hpx along with generating challenges for energy metabolism and redox homeostasis also alters nutrient uptake (Dat et al., 2004; Bailey-Serres and Voesenek, 2008; Blokhina and Fagerstedt, 2010). Further, HpxAs combined stress induced a profound deregulation of nutrient homeostasis (Kumar et al., 2019). The results presented here identify nutrient deregulation-associated signaling patterns in relation to root growth.

Root Growth

Arabidopsis plants grown hydroponically for 32 days were exposed to As, Hpx and their combination (HpxAs) for 7 days. It has been shown that total root biomass accumulation was affected by these treatments (**Figures 1A,B**). Especially for Hpx and HpxAs, biomass accumulation was significantly reduced (**Figures 1A,B**). To estimate the extent and pattern of new root growth during the treatment period, plant roots were also stained with active charcoal. The images presented in **Figure 1A** reveal the differential pattern of root growth among different treatments. Compared to control plants, main root growth was inhibited to a certain extent in As and lateral roots were generated. Root growth inhibition seemed complete under both Hpx and HpxAs. Plant roots under Hpx showed a slight enlargement of the tap root tip, although growth was severely inhibited. No such root tip growth was visible for plants under HpxAs. Charcoal staining was also carried out after 7 d treatment before start of reaeration and plant roots were again photographed after one week of reaeration in order to judge the severity of applied stresses and plant potential for recovery from Hpx. It became clear from these observations that the root growth inhibition could recover after reoxygenation of the nutrient media (**Figure 1A**). However, total biomass accumulation and growth recovery as recorded after 3 weeks of reaeration were slower for HpxAs than in the single Hpx treatment (**Figure 1B**).

Roots were investigated for RH growth qualitatively (**Figures 1C,D**). RHs increase root surface area and play important roles in increasing nutrient uptake and maintaining osmotic balance. Comparative imaging of the RH zones revealed a strong stimulation of RH growth in Hpx- and HpxAs-treated plants. Although, it was clear from previous data related to root fresh weight and charcoal staining that root growth showed close to complete inhibition under Hpx and HpxAs, it is revealed here that RH growth was not only sustained, but stimulated compared to As and control. This pattern of root growth inhibition and RH stimulation was also evident in charcoal-stained roots (**Figure 1D**). Control plants emerged a certain number of RHs in the newly developed RH zone, while the RH zone of treated roots displayed adsorbed charcoal as an evidence of reduced root growth. Also, a higher density and elongation of RHs in Hpx and HpxAs was observed. The stimulated RH growth could be an adaptive strategy to keep up nutrient uptake to sustain plant growth under these stresses.

Transcriptional Regulation of Root Architecture

To identify mechanistic players possibly involved in the altered root phenotype, root transcriptome data were queried for genes related to root development and their stress responses. A total of 281 genes were filtered for a linear fold change of $-2 \geq fc_{linear} \geq 2$ (**Supplementary Table 1**). The identified genes were grouped into four major categories as shown in **Figures 2A–D**. Among the identified transcripts, categories "root hair growth regulation" "hormonal signaling," and "root meristem and growth maintenance" represented roughly 30% each of total identified genes, while the rest of the around 10% belonged to "cell wall modifications." Sets of 11 to 16 transcripts were selected and presented in four heat maps (**Figure 2**) based on further filtering with FDR $p \leq 0.05$ for the expression change and their response or relevance to HpxAs-treatment.

HpxAs-treated plants showed a strong inhibition of root growth with a simultaneous stimulation of RH density and tip growth. It is significant that besides 86 genes, which were categorized to be causally related to RH growth, several transcripts in other categories were also involved with RH signaling, epidermal cell differentiation or RH tip growth via rapid cell wall formation. A sizable proportion of the differentially regulated root development-related transcripts was associated with RH differentiation, RH growth and its regulation. Significantly, of the 220 genes from above showing a change of $-2 \geq fc_{linear} \geq 2$ for HpxAs, the majority (180) consisted of those

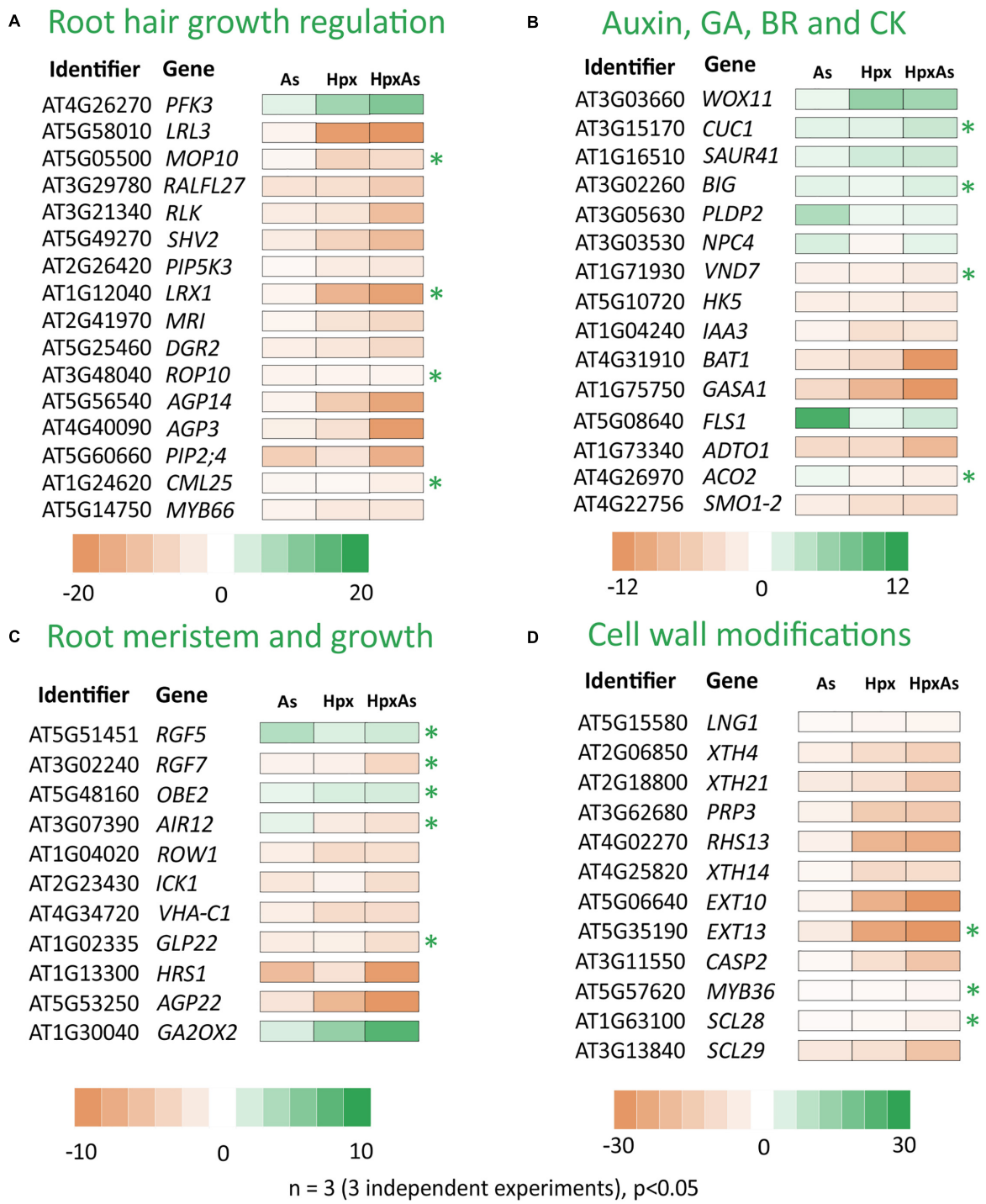

FIGURE 2 | As-, Hpx-, and HpxAs-dependent changes in transcripts linked to root growth and related signaling. Heat maps present root transcriptome data from HpxAs-treatment experiments (GEO-NCBI accession number GSE119327) (Kumar et al., 2019). The transcripts were compared for changed expression under As, Hpx and HpxAs treatment. Four functional categories of genes are presented namely those related to **(A)** RH growth regulation and epidermal cell differentiation, **(B)** biosynthesis and signaling of hormones involved directly in different aspects of root development especially linked to auxins, gibberellic acid (GA), brassinosteroids (BR) and cytokinin (CK), **(C)** control of root meristem activity and total root growth, and **(D)** cell wall growth or modification crucial in RH or lateral root development. The transcripts were initially selected with the GO term "Root development" using the criterion $-2 \geq fc_{linear} \geq 2$ and later sub-categorized. Among transcripts with a significant response (FDR $p \leq 0.05$) to the treatments, heat maps present those with unique response to HpxAs or those with relevance to observed HpxAs-stress effects on root development. Transcripts with unique response to HpxAs ($-2 \geq fc_{linear} \geq 2$ for HpxAs, FDR $p \leq 0.05$ and either response below this threshold for As, Hpx or response statistically not-significant) are marked with an asterisk. **Supplementary Table 1** gives the complete gene list with relative expression under different treatments.

with decreased expression. Complete lists of all these selected genes are given in **Supplementary Table 1**.

Many transcripts in the "root hair growth regulation" category (**Figure 2A**) with decreased expression importantly function in negative regulation of RH elongation like plasma membrane intrinsic protein 2;4 (*PIP2;4*) and calmodulin like 25 (*CML25). PIP2;4* which encodes an H_2O_2-conducting transmembrane aquaporin (Dynowski et al., 2008) decreased 15.2-times for HpxAs compared to control, a response significantly different from As (−9.17), and Hpx (not significant) treatments. Similarly, expression of *CML25* decreased 2.92-times for HpxAs, a unique response compared to other treatments, where no change in expression was recorded. The Rac-like GTP-binding protein ROP10 is active in cell wall hardening on the sides of elongating RH that in turn generates a force to propel the growing RH tip (Hirano et al., 2018). Its transcript amount decreased 2.02-times under HpxAs, while no response was observed for As and Hpx. ROP10 facilitates phosphatidylinositol-4-phosphate 5-kinase 3, PIP5K3 function in RH growth (Hirano et al., 2018). Importantly, 6-phosphofructokinase 3 (*PFK3*), involved in epidermal cell fate determination i.e., H- and N-cell differentiation, increased strongly for HpxAs (12.39-fold) and Hpx (9.15-fold); magnitude of increase being lower for As (2.99) (**Figure 2A**). In addition, the root and hypocotyl epidermal cell fate determining protein *WERWOLF1* or *MYB66*, another negative regulator of RH cell growth (Wang et al., 2019), showed stronger decrease for Hpx (−4.1) and HpxAs (−4.55) compared to As (−2.26).

Slightly different response patterns arose for hormonal signaling-related transcripts compared to the other three categories (**Figure 2B**). More than 35% of the total 64 genes that responded to HpxAs were increased in expression; however, still higher number of genes showed reduced expression. Among those with increased expression, *WUSCHEL* related homeobox 11 or *WOX11* and *CUP-SHAPED COTYLEDON1* or *CUC1* are important in auxin-mediated plasticity of root architecture and lateral root formation, respectively (Baesso et al., 2018). *WOX11* expression increased strongly under both Hpx (6.2-fold) and HpxAs (5.46-fold) while no change was detected for As. On the other hand, *CUC1* showed HpxAs-specific increase (3.18-fold), while no change in expression was observed for As and Hpx. No change in expression was observed for two functionally antagonistic genes namely, phospholipase D P2 (*PLDP2*) and the phosphoesterase *NPC4* under Hpx and HpxAs while both increased in expression by 4.67- and 2.33-fold, respectively under As-treatment. Both genes are targeted by auxin signaling and regulate RH density and elongation under nutrient deprivation, especially phosphate (Su et al., 2018).

Among the genes in category "root meristem and growth," the highlight of the HpxAs-specific response are three root growth factors, i.e., *RGF5*, *RGF7,* and *OBERON* 2 (*OBE2)*, involved in maintenance of root stem cell niche and root meristem identity (**Figure 2C**). *RGF5* increased significantly under HpxAs (2.35-fold), while *RGF7* decreased in expression by 3.8-times. The change in expression was either not significant or no change was observed for As and Hpx. Further, *OBE2* increased specifically in HpxAs (2.11-fold), while no change in expression was observed for As and Hpx-treatments. Further, auxin-induced gene in root cultures *i.e.*, *AIR12*, another gene involved in lateral root morphogenesis, decreased specifically under HpxAs (−2.82). The negative regulator of root meristem cell number *GA2OX2* (gibberellin 2-beta-dioxigenase) transcript increased strongly under Hpx (5.23-fold) and HpxAs (8.26-fold), potentially limiting root meristem cell number (**Figure 2C**; Li et al., 2017). Another crucial gene in this category *i.e.*, *REPRESSOR OF WUSCHEL1* (*ROW1*), regulates the identity of quiescent center cell layers by limiting expression of the *WUSCHEL*-related gene *WOX5* (Zhang et al., 2015). Quite interestingly, its expression was reduced 3.39- and 3.01-times under Hpx and HpxAs-treatments, respectively (**Figure 2C**). This might explain, in a large part, the suppression of root growth observed due to these treatments (**Figures 1A,B**).

A major portion of cell wall modification-related transcripts showed a strong decrease in expression especially under HpxAs (**Figure 2D**). For example, several RH cell specific extensin family members like *EXT10* and *EXT13* as well as the casparian strip membrane domain protein like *CASP2* showed strongly decreased transcript amounts under HpxAs which was 75. 25-, 61-, and 16.63-times, respectively (**Figure 2D**). The expression of these genes was also lower under Hpx and As, however, the extent of decrease was smaller. Expression of the transcription factor *MYB36* which regulates transcription of CASPs in control of differentiation of endodermis, was specifically reduced under HpxAs (−2.65). *SCL28*, encoding a scarecrow-like protein potentially involved in radial root growth regulation, also showed HpxAs-specific 4.25-times decrease in expression. Several other cell wall biogenesis-related genes showed stronger response to HpxAs (**Figure 2D**).

Phosphate Starvation Response

In plants, As(V) interferes with phosphate uptake, assimilation, transport and diverse phosphate-dependent processes like protein activation/deactivation by phosphorylation, membrane properties through phospholipids, and ATP-synthesis (Catarecha et al., 2007; Abercrombie et al., 2008). Similarly, hypoxia interferes with phosphate starvation response through deregulation of related transcripts that in turn affects the root growth regulation (Klecker et al., 2014; Neumann, 2016). Due to this overlap, plants facing HpxAs stress should be severely challenged in maintaining phosphate homeostasis. Phosphate starvation-related transcripts were assessed in HpxAs-treated plants (**Figures 3A,B**) and compared to Hpx- and As-responses. The analysis mainly included the differentially regulated transcripts related to phosphate homeostasis (uptake, transport, and assimilation), galactolipid (glycolipids) and sulfolipid biosynthesis, phosphatidylinositol metabolism and signaling, and sucrose metabolism. A subset of transcripts related to lipid and phosphatidylinositol metabolism is appropriately summarized in **Supplementary Figure 1** and **Supplementary Table 3**. Likewise, the phosphate deficiency-regulated genes with direct involvement in root and RH growth are depicted in **Figures 2A–D** and **Supplementary Table 1** and certain others related to Fe metabolism appear in a subsequent section (**Figure 5B**, **Supplementary Table 4**).

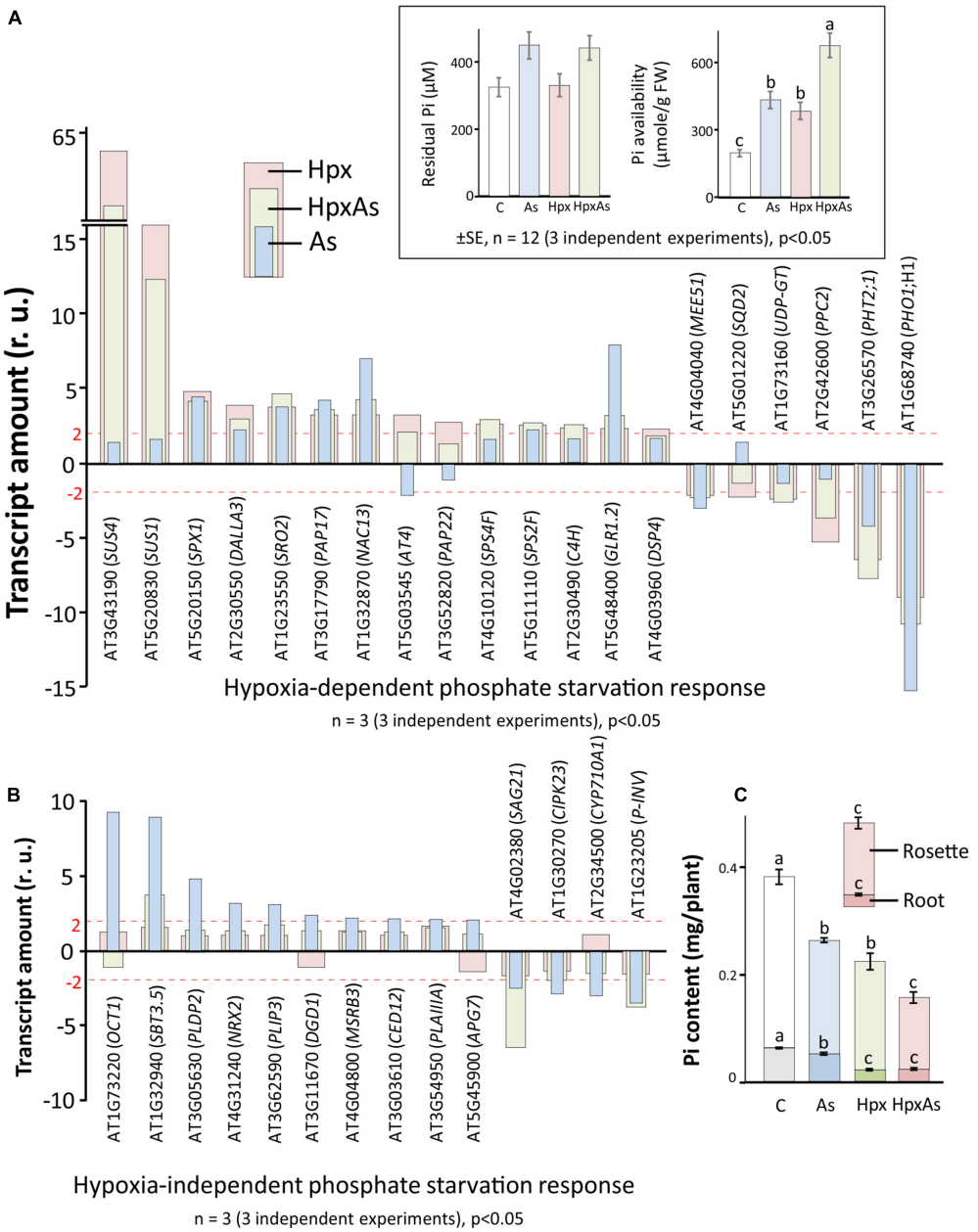

FIGURE 3 | As-, Hpx-, and HpxAs-induced phosphate starvation response in roots. Phosphate starvation-related transcripts were first screened for significant changes ($-2 \geq fc_{linear} \geq 2$, FDR $p \leq 0.05$) and subsequently for specificity of their response to hypoxia. Phosphate starvation response comprises genes not only related to uptake, transport, and assimilation of inorganic phosphate, but also those involved in galactolipid and sulfolipid biosynthesis, as well as phospholipid metabolism. The genes were categorized into those that showed **(A)** significant changes under Hpx-exposure and **(B)** no-response to Hpx, but significant response to As. The inset depicts the residual Pi in the nutrient media after 7 days of treatment given along with calculated Pi-availability per gram tissue based on the total biomass accumulated per pot at the end of treatment. The complete list with relative expression values for phosphate starvation-related genes are given in **Supplementary Table 2**. In addition, heat map and a complete list of additional transcripts related to lipid signaling and phosphatidylinositol metabolism which are not part of **Figures 2**, **3** are given in **Supplementary Figure 1** and **Supplementary Table 3**. **(C)** Phosphate content measured using LC-MS/MS (Kumar et al., 2019) is presented. Data is calculated per plant using accumulated dry weight under different treatments (respective Pi-content in root and rosette is also visible) (means ± SE, $n = 4$; 4 independent experiments; Tukey's test, $p < 0.05$).

The dual stimulation of phosphate starvation response under HpxAs likely necessitates the adoption of an appropriate energy-efficient state to maintain phosphate homeostasis and enable stress acclimation. Thus, the expression of filtered (relevant) transcripts under HpxAs was compared to that induced by As and Hpx alone. Both Hpx and As induced a phosphate starvation response, with a reasonable overlap between As- and Hpx-induced gene expression. Based on their

response, transcripts could be divided into two categories: 20 transcripts were Hpx-responsive (**Figure 3A**), whereas 14 others were unresponsive to Hpx, but responded to As (**Figure 3B**). In general, the HpxAs-response exhibited a strong overlap and resembled more with Hpx than with As. For example, among 20 genes depicted in **Figure 3A**, 15 showed a similar increase or decrease for Hpx and HpxAs, while for 14 genes presented in **Figure 3B**, only 4 showed similarity of expression for As and HpxAs. Among these 4 transcripts, levels of *SBT3.5,* coding for the subtilase 3.5 protein, increased 3.8-fold under HpxAs which was much lower than that for As (8.82). Also, in case of *SAG21* transcripts, encoding an MAPK cascade-associated protein, HpxAs-induced reduction in expression (−6.49-times) was stronger than that for As (−2.42). Among the 20 genes undergoing change of expression under Hpx, 10 genes also responded to As (**Figure 3A**). In summary, it is significant that 15 out of 35 As- and Hpx-induced phosphate starvation-related transcripts did not change under HpxAs compared to control. Key genes among these were phospholipase (*DALLA3*), sulfoquinovosyl transferase (*SQD2*), phosphoenolpyruvate carboxylase (*PPC2*), and digalactosyldiacylglycerol synthase (*DGD1*).

Pi-starvation response is determined by external Pi-availability and internal plant Pi-status. Residual plant Pi-content in the hydroculture nutrient media was measured spectrophotometrically. This was apparently similar for all treatments. However, calculated per unit plant fresh weight, availability of Pi increased substantially under all stresses, most strongly for HpxAs, due to growth inhibition (inset, **Figure 3A**). On the other hand, estimated internal Pi-content showed a sharp decline for different treatments and was significantly lower for HpxAs leaves than all other treatments (**Figure 3C**). Pi-contents also lowered in roots for HpxAs but were only significantly different from control and As-treatments, while they were similar for Hpx and HpxAs-treatment (**Figure 3C**).

Cell Viability Analysis in the Root Hair Zone

Root hair imaging and transcriptomic analysis revealed enhanced RH growth to be an important response to HpxAs involving multiple signaling pathways. RH phenotype is determined by multiple crucial steps including epidermal cell differentiation, RH initiation and unidirectional tip growth. Cell viability analysis reveals the physiological status of RHs and underlying epidermal and cortical cells. This could be performed by employing fluorescent probes in a sensitive and non-invasive manner with minimum inadvertent cell damage. The contrast in fluorescence intensity shows a strong loss of cell viability in RH zone (mostly epidermal and cortical cells) of plants treated with Hpx and HpxAs (**Figure 4A**). A quantitative analysis of several recorded images of fluorescently labeled roots indicated a stronger fluorescence intensity in HpxAs compared to Hpx (**Figure 4B**). Normalized to the control, we observed a 4.14-fold higher loss of viability in HpxAs plants compared to 2.13- and 1.13-fold for Hpx and As, respectively (**Figure 4C**). However, due to variation, the difference between Hpx and HpxAs was insignificant.

Iron Assimilation (and NO Signaling)

Stimulatory influence of Pi- and Fe-starvation on RH growth is well studied in the context of regulatory networks. Plants possess two main Fe-acquisition strategies. The first employs the release of specific chelators into the rhizosphere whereas the second uses membrane-spanning enzymes for reduction of rhizospheric Fe^{3+} to Fe^{2+} that is subsequently taken up through Fe(II)-high affinity transporters. Ferric chelate reductases (FCR) are sensitive to changes in cellular Fe-demand and rhizospheric Fe availability. FCR activity was measured spectrophotometrically in intact plant roots to reveal the treatment-specific differences. After 7 d of treatment, As induced a 4.35-fold increase in FCR activity compared to 3.31- and 1.76-fold increase for Hpx and HpxAs, respectively (**Figure 5A**). The As-induced increase in FCR subsided within 24 h of replenishing the nutrient media (**Figure 5A**).

To further investigate the perturbation of Fe metabolism in response to As and Hpx, applied individually and in combination, transcriptomes were filtered for transcripts related to Fe-homeostasis. Two heat maps in **Figure 5B** only show transcript expression for genes regulating Fe-homeostasis in relation to root development and their relevance to HpxAs (for complete list see **Supplementary Table 4**). Among the 77 identified transcripts (67 related to Fe-homeostasis, 10 to NO generation), 56 responded to HpxAs, where about 50% showed increased expression. Like FCR activity, *FERRIC REDUCTION OXIDASE2; FRO2* increased in expression 2.71-fold under As-treatment, while the response was insignificant under the other two conditions (**Figure 5B**). Another evidence for induction of Fe-uptake mechanism under As came from a 2.05-fold increase in *IRT2* responsible for Fe(II) uptake downstream to FCR, while no significant change was observed for other treatments. Interestingly, *FRO1*, coding for another FCR gene, decreased specifically under HpxAs (−2). *BHLH100*, another key regulator involved in post-translational regulation of FIT (master regulator of Fe-homeostasis) under JA-signaling (Cui Y. et al., 2018), increased 20.6-fold in HpxAs. *NRAMP4*, involved in Fe-mobilization, increased specifically under HpxAs (2.67-fold) (**Figure 5B**). Several treatment-responsive transcripts were related to heme binding, nitrate assimilation, and NO-generation (**Figure 5B**, **Supplementary Table 4**). NO interferes with Fe-homeostasis and root development (García et al., 2011). Most notable is the Hpx- (3.1-fold) and HpxAs- (2.05-fold) induced increase in the expression of *NR2,* which codes for nitrate reductase and functions as NO synthase.

Arsenic Interference With Hypoxia Response in Root Stress Adaptation

Under hypoxia, plants carry out lactate and ethanol fermentation to generate low amounts of ATP, but more crucially to regenerate NAD^+. Thus, plant adaptation and growth under hypoxia rely on these subsidiary energy pathways. Enzymes involved in fermentation are transcriptionally upregulated under hypoxia (Kosmacz et al., 2015). It was reported that presence of As affects the hypoxia-induced increase in transcription of fermentation-related genes like pyruvate

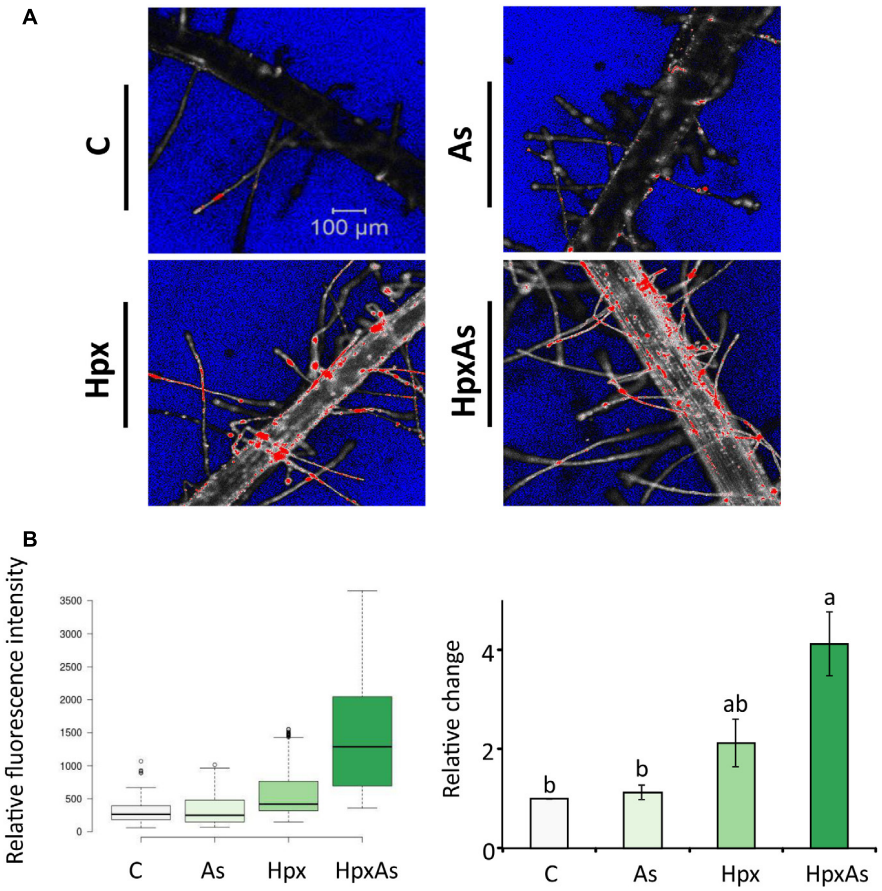

FIGURE 4 | *In vivo* fluorescence analysis for cell non-viability in the root hair zone of As-, Hpx-, and HpxAs-treated Arabidopsis roots. SYTOX green fluorescent probe was used to label non-viable root cells in the RH zone. The roots were exposed to different stresses for 7 days, labeled with SYTOX for 7 min on the last day of treatment and imaged under the confocal laser scanning microscope (LSM780, Zeiss). Fluorescent dye was excited using an argon laser (488 nm) and emission recorded in the range of 500–550 nm. **(A)** The micrographs display the fluorescence of SYTOX green (emission maximum at 523 nm) representing non-viable cells in the RH zone among different applied stresses after 7 days of treatment. The micrographs present fluorescence data in grayscale with added range indicators (Blue; background, Red; fluorescence oversaturated regions) **(B)** Recorded fluorescence intensities were compared for the stresses and are presented as box plot (shiny.chemgrid.org/boxplotr) (left). Center lines show the medians; box limits indicate the 25th and 75th percentiles as determined by R software; whiskers extend 1.5-times the interquartile range from the 25th and 75th percentiles; not connected data points represent outliers. Histogram on the right shows relative changes in SYTOX fluorescence intensity for the treatments compared to control. The data are means ± SE, $n = 3$ (data collected from 3 independent experiments over 250–260 individual RH areas from multiple plants; Tukey's test, $p < 0.05$). For quantitative fluorescence analysis, saturated areas of the micrographs were excluded.

decarboxylase (PDC) and alcohol dehydrogenase (ADH) under HpxAs (Kumar et al., 2019). Therefore, the changes in *PDC2*, *ADH1* and *LDH1* were compared with the activities of PDC, ADH and lactate dehydrogenase (LDH). Increase in *PDC2*, *ADH1* and *LDH1* expression was smaller under HpxAs as compared to Hpx-treatment (**Figure 6A**). *ADH1* also increased by As alone. Microarray data and their qRT-PCR confirmation are given for several other typical Hpx-response markers (**Figure 6A**, **Supplementary Figures 2A,B**). Further, the effects of As in HpxAs, on the recovery of these hypoxia markers was also evaluated after reaeration (**Supplementary Figure 2B**).

Enzyme activity measurements proved the interference of As with Hpx responses (**Figure 6B**). For example, increase in PDC activity was significantly lower under HpxAs as compared to that under Hpx alone. It increased 24- and 16.9-fold under Hpx and HpxAs, respectively. A similar trend was observed for ADH, with a 75.0- and 49.2-fold increase in activity under Hpx and HpxAs-treatment, respectively; however, they were not statistically different. Arsenic did not alter the activity of both enzymes (**Figure 6B**). In contrast to PDC and ADH, LDH activity increased similarly in response to HpxAs (4.38-fold) and Hpx (4-fold). Arsenic also increased LDH activity (82%) but the increase was not statistically significant (**Figure 6B**). The enzyme activity data indicate a preferred upregulation of lactic acid fermentation pathways under HpxAs.

Redox Regulation of Root Growth

ROS and the associated redox regulatory network are crucial in the control of root meristem activity and growth of roots and RHs (Shin et al., 2005; De Tullio et al., 2010). Several transcripts were identified in the GO-related terms "Root

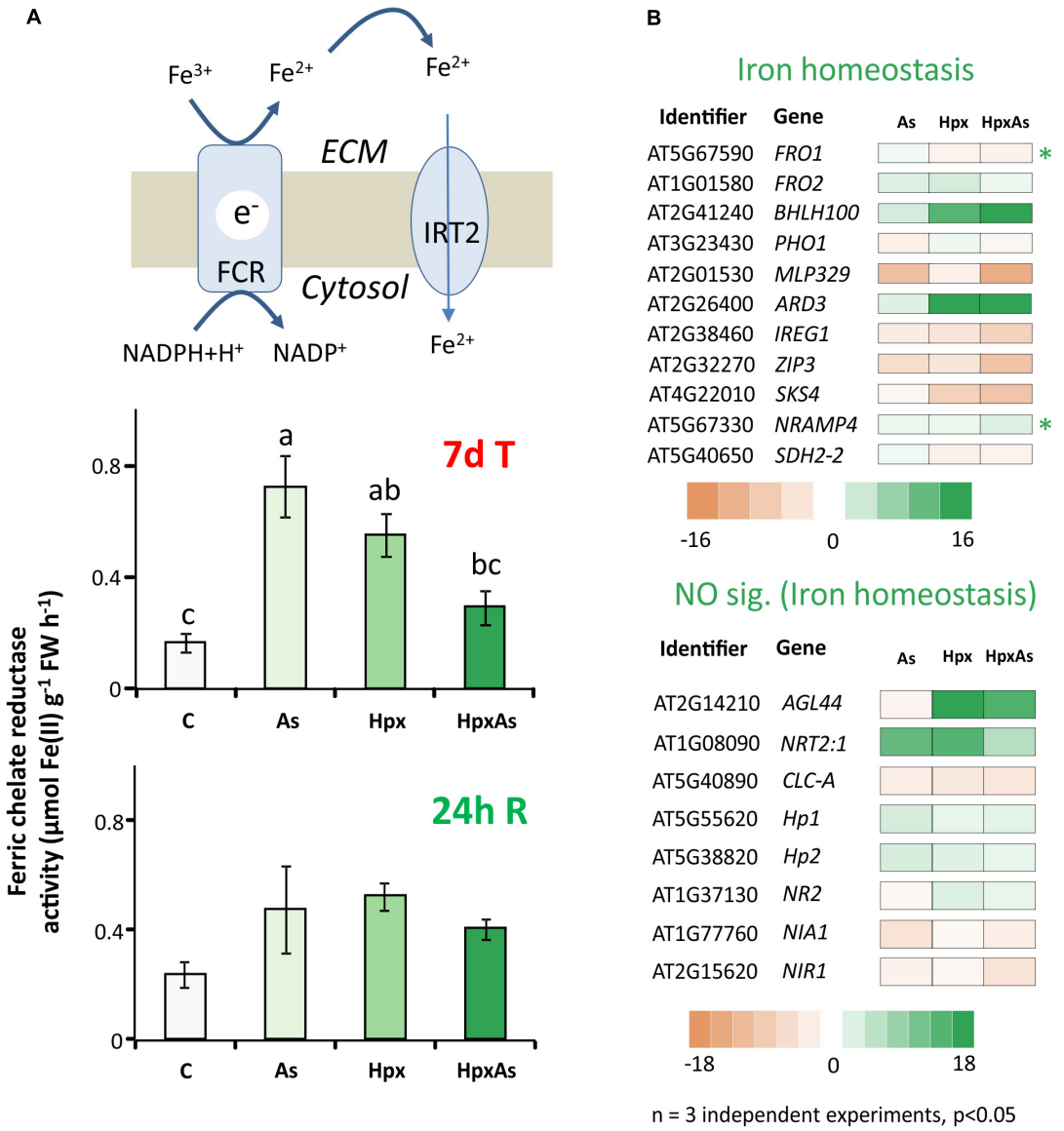

FIGURE 5 | Perturbation of Fe-uptake and assimilation as evident from transcriptomic and biochemical analyses. **(A)** Ferric chelate reductase activity was measured in intact Arabidopsis roots using ferrozine based complexation of Fe(II). The obtained data were compared among different treatments after 7 days of treatment and after additional 24 h of reaeration. The data are means ± SE, n = 5, (5 individual plants, 2 independent experiments, Tukey's test, $p < 0.05$). **(B)** Stress-induced significant changes ($-2 \geq fc_{linear} \geq 2$, FDR $p \leq 0.05$) in Fe-homeostasis-related transcript amounts are presented in heat maps. The heat maps are categorized based on core Fe- uptake-, assimilation- and metabolism-related genes and those involved in NO generation. They all have a putative role in Fe-homeostasis and root development regulation. Transcripts with unique response to HpxAs ($-2 \geq fc_{linear} \geq 2$ for HpxAs, FDR $p \leq 0.05$ and either response below this threshold for As, Hpx or response statistically not-significant) are marked with an asterisk. The complete gene lists with transcript amounts under different treatments for Fe and NO are given in **Supplementary Table 4**.

and Root Hair Development" and "Fe-homeostasis" and were further classified into members of cytochrome P450 family (CYP450s) and peroxidases (**Figures 7A,B**, **Supplementary Table 6**). A large set of these gene products were extracellular and function in redox regulation of cell wall synthesis, hormonal signaling, and diverse stress responses. Among the identified 109 CYP450 family transcripts, 61 responded significantly to HpxAs, with 85% showing a down-regulation (**Figure 7A**, **Supplementary Table 6**). On the other hand, among 30 identified redox regulatory genes, 25 showed significant response under HpxAs-stress and all were down-regulated (**Figure 7A**, **Supplemenatry Table 6**).

Many members of the CYP450 family have NADPH-dependent functions and participate in synthesis of brassinosteroid(s) (BR), glucosinolates, camalexin and sterols. C-22 sterols play a crucial role in cell membrane polarity and hence RH initiation and tip growth axis determination (Ovečka et al., 2010). For example, *CYP710A2* and *A3* decreased

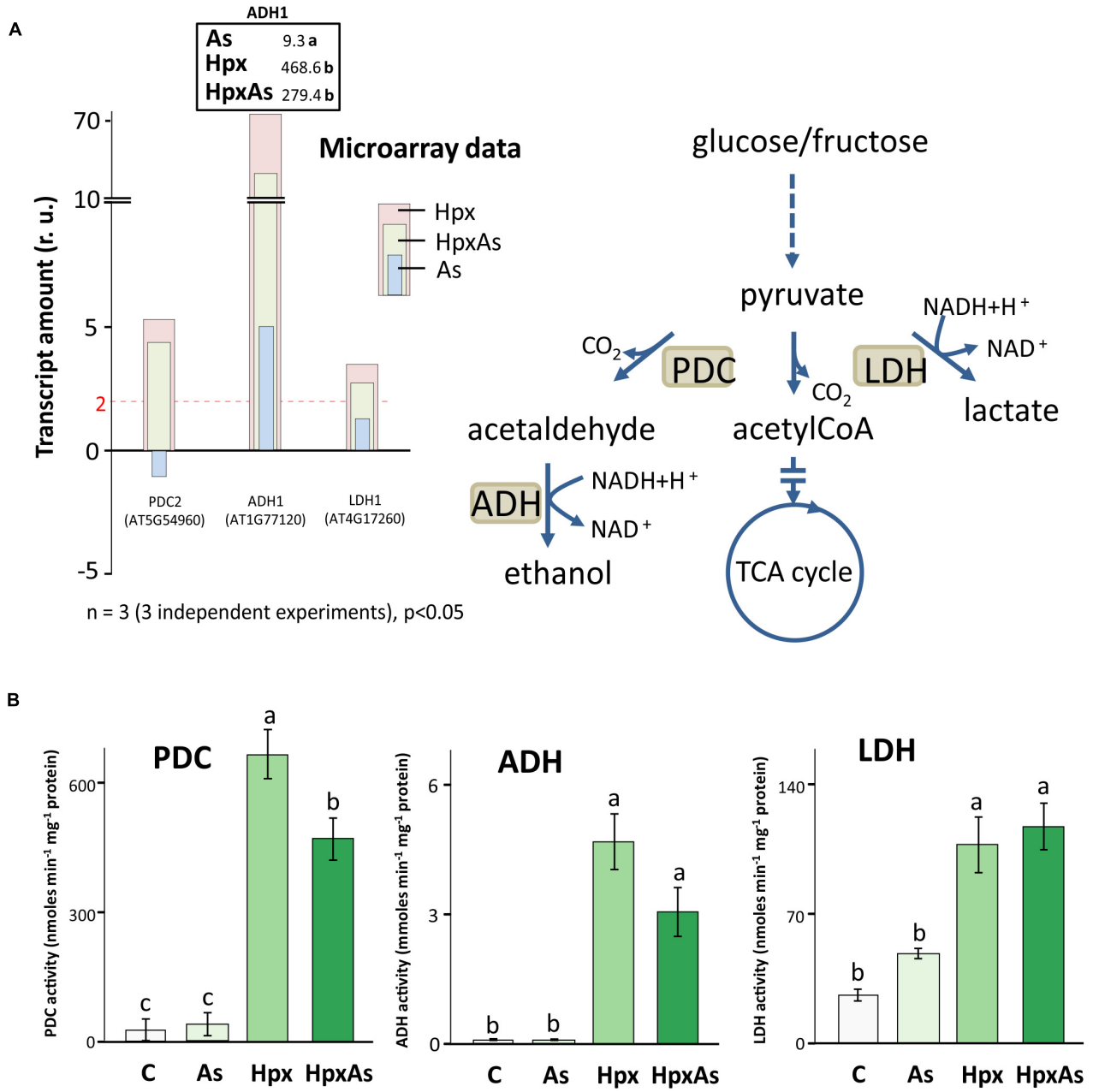

FIGURE 6 | Changes in gene expression and enzyme activity of energy metabolism-related enzymes under HpxAs compared to As and Hpx. Pyruvate decarboxylase (PDC), alcohol dehydrogenase (ADH) and lactate dehydrogenase (LDH) are crucial enzymes under anoxic conditions in ATP generation and regeneration of NAD^+ when the respiratory electron transport is inhibited. **(A)** The histogram presents relative transcript amounts of *PDC2*, *ADH1,* and *LDH1* genes after 7 days of stress application as compared to control. qRT-PCR confirmation of this transcript accumulation under given stresses is given for *ADH1* on top of *ADH1* bar as fold change numbers, while for several other related Hpx marker genes data are presented in **Supplementary Figure 2**. Primer sequences for the qRT-PCR data are given in **Supplementary Table 5**. **(B)** Enzyme activities for PDC, ADH, and LDH were measured spectrophotometrically in root extracts. Data display specific activity as means ± SE, $n = 6$ (3 independent experiments, Tukey's test, $p < 0.05$).

strongly under HpxAs; while the reduction for *CYP710A2* was 4.65-times, *CYP710A3* decreased 18.4-times (**Figure 7A**). No significant change was observed under Hpx or As alone. Further, the amount of *CYP83A1*, involved in auxin homeostasis, was also reduced (−81.3) under HpxAs. The same decreased under As (−5.13) and Hpx (−3.35), however, with a significantly lower magnitude. Among other redox regulatory genes, *UPBEAT1 or UPB1*, another bHLH transcription factor, was reduced in expression for Hpx and HpxAs-exposure by 4.16- and 5.55-times, respectively. It is of significance that *UPB1* plays a crucial role in root meristem development through regulation of ROS accumulation in between the zones of cell proliferation and

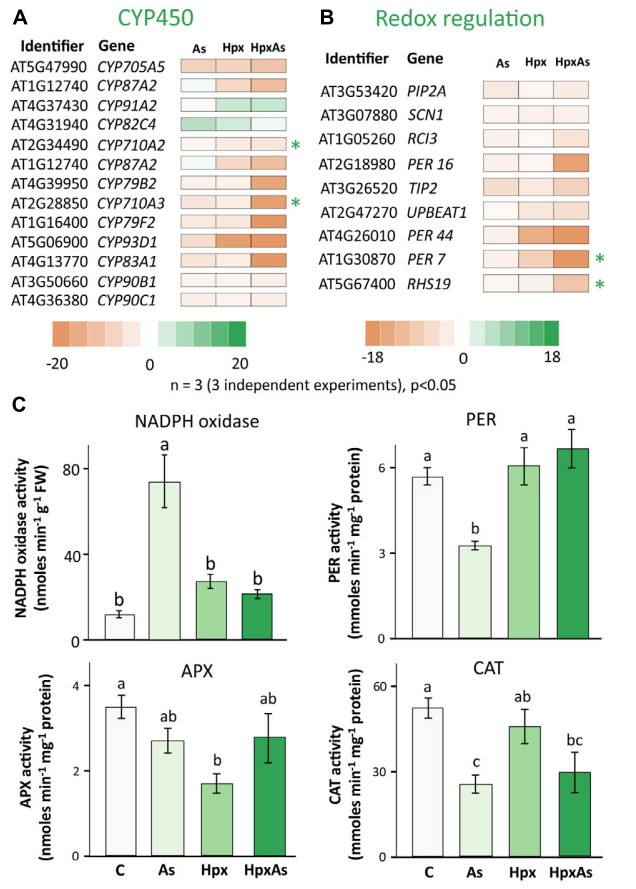

FIGURE 7 | Biochemical and transcriptomic analysis of redox signaling-related regulators of root and root hair growth. **(A)** Cytochrome P450s (CYPs) gene family comprises heme-containing proteins involved in diverse cell metabolic processes, including redox regulation of growth and development. Transcript accumulation as influenced by As, Hpx, and HpxAs is presented in the heat map for different cytochrome P450s. The genes were initially identified in the search for GO-related terms "Root development" and "Fe-homeostasis." Included transcripts showed a significant change in expression ($-2 \geq fc_{linear} \geq 2$, FDR $p \leq 0.05$) and are assumed to be relevant for the HpxAs-induced root growth phenotype. **(B)** Redox regulatory transcripts involved in root development, other than CYP450s presented above, were selected for their significant response ($-2 \geq fc_{linear} \geq 2$, FDR $p \leq 0.05$) and are presented in heat map. Transcripts with unique response to HpxAs ($-2 \geq fc_{linear} \geq 2$ for HpxAs, FDR $p \leq 0.05$ and either response below this threshold for As, Hpx or response statistically not-significant) are marked with an asterisk. The complete lists for all selected CYP450s and other redox regulatory genes are provided in **Supplementary Table 6**. **(C)** NADPH dependent XTT reductase activity was measured in crude membrane extracts to analyze stress effects on NADPH oxidases. The extract was also tested for its superoxide specificity by using SOD randomly for certain samples to demonstrate inhibition of XTT reduction (data not shown). Guaiacol peroxidase (PER), ascorbate peroxidase (APX), and catalase (CAT) were measured for their enzyme activity in root extracts. All enzyme activity data are means ± SE, $n = 6$ (3 independent experiments). Micrographs showing ROS generation in different cell layers in the RH zone, based on 2', 7'-dichlorodihydrofluorescein diacetate (H_2DCFDA) fluorescence are given in **Supplementary Figure 4**.

elongation, thus could impede the onset of differentiation on reduced expression (Tsukagoshi et al., 2010; Li et al., 2019).

The root hair cell-specific peroxidases *PER7* and *PER73* (*RHS19*) showed strongly decreased expression (24.8- and 9.98-times, respectively) under HpxAs (**Figure 7A**). Expression of both did not change significantly under Hpx and As treatments. ROS accumulated in epidermal and cortical cells of the RH zone under Hpx and, more strongly, HpxAs (**Supplementary Figure 4**). The peroxidase *PER16* was less expressed in HpxAs (−16.32), where the extent of reduction was several folds higher than that under As (−2.45). Transcript amounts of the central regulator of RH initiation SCN1 decreased under Hpx (−2.5) and HpxAs (−2.39), with no change for As (**Figure 7A**). SCN1 functions through regulation of trichoblast-specific NADPH oxidase *(RBOH-C)* (Arenas-Alfonseca et al., 2018).

Therefore, NADPH-oxidase activity was measured in crude root membrane extracts (**Figure 7C**). For comparison, XTT-reductase activity was also measured in the soluble supernatant (**Supplementary Figure 3**) and showed the robust nature of NADPH oxidase activity data as the pattern is quite different in two measurements. More importantly no significant treatment-specific difference was observed for the soluble fraction. NADPH oxidase activity tended to be higher for Hpx (2.30-fold) and HpxAs (1.81-fold) but was not statistically significant (**Figure 7C**). In contrast, the increase in activity was substantial (6.26-fold) for As-treatment (**Figure 7C**). Further, activities of different peroxidases showed variable treatment-specific patterns of change, indicating their specific role(s) under different stress regimes. APX activity dropped significantly (50%) under Hpx but decreased only marginally under As and HpxAs (**Figure 7C**). In case of guaiacol peroxidases, activity decreased (−42%) due to As, and increased marginally due to Hpx (7%) and HpxAs (17%). Catalase activity was significantly lower (51%) only under As treatment (**Figure 7C**). Treatment and compartment specificity of function for these enzymes is evident from the above observations.

DISCUSSION

Suppression of Root Growth With Concomitant Stimulation of Root Hair Development

Stress exposure of hydroponically grown Arabidopsis plants allowed distinguishing root-specific responses to HpxAs-stress combination vis-à-vis the individual treatments. Root exposure to HpxAs induced nearly complete inhibition of root growth that recovered upon reaeration (**Figures 1A,B**; Kumar et al., 2019). Lateral root suppression under oxygen depletion has been reported recently (Shukla et al., 2019; Pedersen et al., 2020). Root growth suppression due to HpxAs and Hpx typically coincided with a strong stimulation of RH growth (**Figures 1C,D**). Induction of RH growth serves as an effective strategy to salvage deregulated nutrient uptake by increasing the total root surface area and in turn absorption capability (Gahoonia and Nielsen, 1998; Müller and Schmidt, 2004; Cui S. et al., 2018). A perturbed cellular osmotic balance may also be one of the reasons for RH growth induction (**Supplementary Figure 5**).

Arsenic interferes with phosphate-uptake and phosphate-dependent cellular processes (Zhao et al., 2010), and also with homeostasis of both macro- (S) and micronutrients (Fe, Zn or Mn) (Rai et al., 2011; Duan et al., 2013; Lee et al., 2013). Hypoxia similarly deregulates nutrient assimilation (Dat et al., 2004; Blokhina and Fagerstedt, 2010). Thus, it is plausible that the transient inhibition of root growth and induction of RH differentiation in response to HpxAs reflect the operation of a regulatory mechanism to sustain nutrient uptake at minimum energy cost and prevent excess As-uptake.

Of the HpxAs-specific genes, about 20% were associated with root and RH growth regulation (**Figure 8A**; Kumar et al., 2019). After FDR-*p* value adjustment, additional genes were identified to show unique response to HpxAs, which belonged to the regulatory network of root growth (**Figures 2**, **5**, **7**). Interestingly, the transcriptional response to HpxAs was aligned more with that to Hpx rather than As. In general, the fine-tuning of stress acclimation under HpxAs involved a higher proportion of deregulated genes with reduced expression. Delayed root growth recovery from HpxAs upon reaeration may indicate the effect of this expressional deregulation.

Interaction of Nutrient Homeostasis Networks

Phosphate Starvation

Phosphate starvation triggers adjustment of RAM activity and enhanced formation of lateral roots and RHs (Abel, 2011). Thibaud et al. (2010) proposed that external Pi controls 70% of the genes with function particularly in the local response, while internal Pi contents modulate the systemic Pi-starvation response. HpxAs is challenging since As inhibits high affinity phosphate transporters and hypoxia affects shoot Pi-content

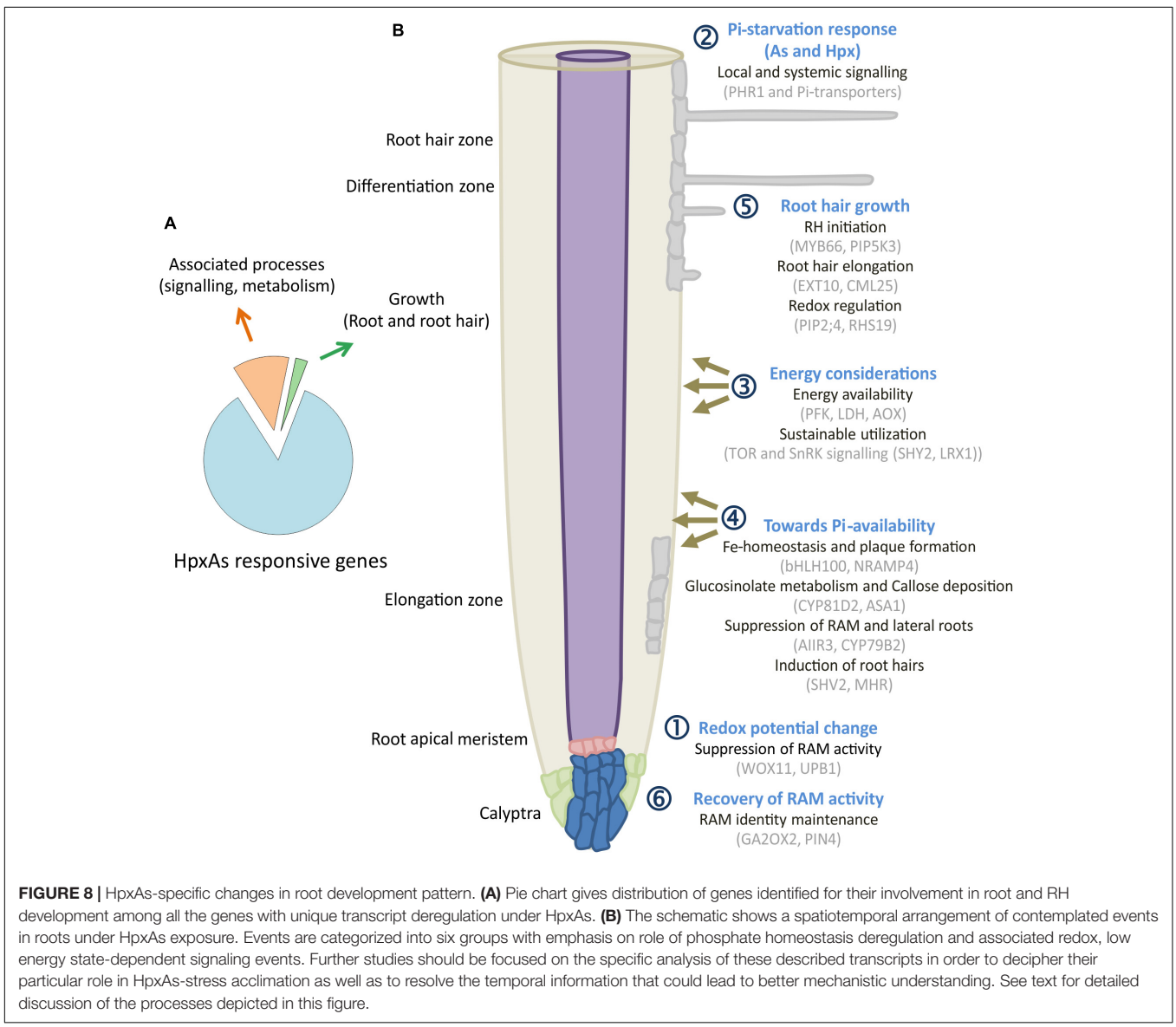

FIGURE 8 | HpxAs-specific changes in root development pattern. **(A)** Pie chart gives distribution of genes identified for their involvement in root and RH development among all the genes with unique transcript deregulation under HpxAs. **(B)** The schematic shows a spatiotemporal arrangement of contemplated events in roots under HpxAs exposure. Events are categorized into six groups with emphasis on role of phosphate homeostasis deregulation and associated redox, low energy state-dependent signaling events. Further studies should be focused on the specific analysis of these described transcripts in order to decipher their particular role in HpxAs-stress acclimation as well as to resolve the temporal information that could lead to better mechanistic understanding. See text for detailed discussion of the processes depicted in this figure.

and/or metabolism (Zhao et al., 2009; Klecker et al., 2014; Kumar et al., 2019). As the external Pi availability was apparently not constrained for HpxAs-treated plants, Hpx-induced phosphate starvation response seems to be regulated systemically. As such, the Pi-starvation response seems to influence internal Pi-redistribution majorly, more than Pi-uptake with significantly different Pi-content for HpxAs in leaves compared to other treatments (**Figure 3C**). The interpretation is supported by the observation that most of the Pi starvation-related, Hpx-deregulated transcripts function in systemic signaling (Thibaud et al., 2010). Klecker et al. (2014) identified a similar response in hypoxic shoots of seedlings that was regulated by *PHR1* in a light-dependent manner.

Phosphate starvation induces membrane lipid reorganization to replace a major portion of phospholipids with phosphate-free galacto- and sulfolipids (Cruz-Ramírez et al., 2006; Nakamura et al., 2009). A lipid profile of Arabidopsis leaves and roots under HpxAs could shed more light on the consequences of this transcriptional change. Observed phenotypic differences, i.e., As-induced lateral root growth and Hpx-induced RH development might potentially be governed by the contrasting intensity of Pi-starvation response (**Figure 1**). Additional contribution of other regulatory pathways might be necessary. The gene network downstream to *PHR1* affects iron uptake and accumulation, sulfate fluxes, anthocyanin synthesis, photosynthesis, sucrose synthases, cell division, and plant growth (Steyn et al., 2002; Rouached et al., 2011; Nilsson et al., 2012; Müller et al., 2015). Perturbation of S-fluxes might directly affect the As sequestration, thereby, increasing its toxicity (Seth et al., 2012), while changes in Fe-homeostasis could influence root meristem activity and root architecture (Müller et al., 2015).

Fe-Homeostasis and Interaction With NO

Müller et al. (2015) described callose formation and iron accumulation in primary roots as a mechanism to block cell communication among stem cells by inhibition of root growth and stimulation of lateral roots as well as RHs. Such a response is regulated by Pi-starvation (Abel, 2011; Müller et al., 2015). Under phosphate starvation plants also tend to accumulate iron plaques on the root surface in order to concentrate nutrients in adsorbed form (Tripathi et al., 2014). This is evident from the brownish color of roots under As and HpxAs (**Figure 1A**; Park et al., 2016; Awasthi et al., 2017). As(V) shows high adsorption efficiency on iron plaques (Lee et al., 2013). ROS facilitate Fe(II) oxidation to Fe(III), and this process is stimulated both under Pi-starvation and in presence of As(V) (Liu et al., 2004; Awasthi et al., 2017), resulting in accumulation of iron oxide on root surface. The rapid oxidation of Fe(II), could lead to enhanced FCR activity under As-exposure to restore the Fe(II) availability (**Figure 5A**).

The situation in HpxAs plants is more complex. A strong and selective deregulation of genes involved in callose deposition, indole glucosinolate biosynthesis and catabolism indicates phosphate starvation-induced callose and iron deposition under different treatments (**Figure 5**, **Supplementary Tables 4,7**) (Müller et al., 2015; Bell, 2018). This might result in the induced lateral growth phenotype in As. Further, selective increase of transcripts involved in glucosinolate biosynthesis and callose deposition (e.g., *CYP91A2*; Hpx, HpxAs, *AGL44*; Hpx, HpxAs, *CYP81D8*; HpxAs, and *ASA1*; HpxAs) coupled with a parallel decrease in abundance of transcripts associated with auxin signaling, root system development, and lateral growth (e.g., *AIR3*; Hpx, HpxAs and *CYP79B2*; HpxAs) might largely explain the observed RH elongation under Hpx and HpxAs (**Figures 2**, **5**, **Supplementary Table 7**) (Francisco et al., 2016).

In addition, a strong reduction in expression of glucosinolate catabolic enzymes i.e., *TTG4*, *TTG5* (Hpx, HpxAs) and *NSP1*, *NSP4* (all) would cause a glucosinolate build-up (**Supplementary Table 7**). Glucosinolates function in root growth regulation through facilitation of cell wall callose deposition and hormonal metabolism (Francisco et al., 2016; Bell, 2018). Contrasting FCR expression and activity response in HpxAs plants compared to As-alone could be explained by strongly increased expression of *bHLH100* transcription factor, a negative regulator of Fe-uptake under Fe-starvation (Cui Y. et al., 2018). The strong deregulation of Fe-starvation transcripts seems to have internal homeostatic and redistribution function, as no bifurcation of RH tips was observed under HpxAs, which is otherwise a distinctive Fe-starvation response (**Figures 1**, **4**, **Supplementary Figure 4**) (Müller and Schmidt, 2004).

Redox Regulation of Root and Root Hair Growth Under HpxAs

Redox cues are central regulatory components in shaping the root system development (De Tullio et al., 2010; Tsukagoshi, 2016; Mhamdi and Van Breusegem, 2018). HpxAs exposure induced a significant redox potential shift toward oxidized cytosol in the quiescent center and surrounding cell layers within the first 4 h of the start of treatment (Kumar et al., 2019). The shift under HpxAs differed from that in As and Hpx and diverged further during the 7 d treatment (Kumar et al., 2019). This redox potential shift might constitute the first trigger for the changing root development program. After 7 d of treatment, expression of several genes involved in stem cell niche maintenance, control of stem cell proliferation and differentiation and RH initiation and growth were specifically modulated under HpxAs (**Figures 2**, **7**).

Three components of the redox regulatory network seem crucial for root development and stress acclimation under HpxAs namely, (a) activation of NADPH oxidases and ROS generation, (b) maintenance of balance between ROS generation and quenching and (c) downstream perturbations by ROS accumulation and redox potential changes (e.g., altered heme and Fe-S cluster synthesis, deregulation of secondary metabolic enzymes of family CYP450s, hormone metabolism). Among the NADPH oxidases (Mittler et al., 2004), *RBOHA* and *RBOHD* increased in all treatments and *RBOHB* only in Hpx (Kumar et al., 2019). *FRO4*, another NADPH oxidase-like transcript, decreased under all treatments. Effects on *FRO4* were stronger in HpxAs than in Hpx and As (Kumar et al., 2019). Measured NADPH oxidase activity, in total root membrane extract, increased significantly due to As (**Figure 7C**). Involvement of NADPH oxidases in As-induced oxidative damage and growth reduction has been reported (Gupta et al., 2013). The increased NADPH oxidase activity might be responsible for induction of

lateral root growth under As-treatment through RAM inhibition (Orman-Ligeza et al., 2016).

NADPH oxidase activity under Hpx and HpxAs was only marginally higher than that in the control. Under these stress conditions, NADPH oxidase may play different roles due to perceived changes in oxygen amounts (Lalucque and Silar, 2003; Schmidt et al., 2018). NADPH oxidases has been implicated in ROS accumulation and redox signaling under hypoxia (Wang W. et al., 2018). ROS accumulation was higher in the epidermis and cortex than in the endodermis and pericycle of RH zone under Hpx and HpxAs in contrast to As and control (**Supplementary Figure 4**). NADPH oxidases play important functions in RH growth and in RAM activity (Kim et al., 2019). Analyses of plants expressing redox sensors like roGFP2 in conjunction with NADPH oxidase inhibitors might provide insight into the NADPH involvement in RH development under HpxAs (Foreman et al., 2003; Gutscher et al., 2008; Lukyanov and Belousov, 2014).

Besides membrane-associated NADPH oxidases, several other heme-based enzymes like peroxidases and oxidoreductase of the CYP450 family function in generation, interconversion, and quenching of ROS. The HpxAs-specific downregulation of many of the CYP450 transcripts and peroxidases could be a part of cellular redox fine tuning. Measurement of the APX, guaiacol PER, and CAT activities in total soluble root protein extracts suggested them to be differentially involved in response to the applied stressor(s) (**Figure 7C**). HpxAs imposed a substantial decline in cell viability in the cortical and epidermal cell layers in the RH zone. Stress-dependent ROS accumulation could lead to lipid peroxidation and damage to plasma membrane (Farmer and Mueller, 2013). However, considering the specific roles of ROS in facilitating tip growth of RHs (Mangano et al., 2017; Wang S.S. et al., 2018), the observed loss of cell viability could also be induced by programmed cell death (PCD), thus having a regulatory relevance (Petrov et al., 2015).

Lower transcript amounts of *MARIS* under Hpx and HpxAs could explain the viability differences, at least for the epidermal cells, as MARIS is a RH membrane protein and positive regulator of membrane integrity (Boisson-Dernier et al., 2015). It is intriguing that *UBP1*, which regulates peroxidase activity and ROS accumulation in the zone between cell proliferation and cell elongation, decreased in expression. The gene product is a negative regulator of cell division (Li et al., 2019), however, its involvement in the development of HpxAs-root phenotype is not clear. Analysis of expression kinetics and protein activity change could be expected to provide important clues. The altered glutathione availability and redox potential (Kumar et al., 2019) might perturb heme and Fe-S cluster synthesis (Hider and Kong, 2013). Downstream changes in activity of heme-containing proteins would considerably impact the redox signaling cascades (Ryter and Tyrrell, 2000; Hider and Kong, 2013).

Transcripts Associated With Remodeling of Root Architecture Under HpxAs

A significant number of deregulated transcripts were related to root growth inhibition, stem cell maintenance for recovery (Hpx and HpxAs), lateral root growth/inhibition (As/HpxAs, respectively), stimulation of RH density and elongation (Hpx and HpxAs). **Figure 8B** depicts a spatiotemporal scheme of envisaged events occurring in roots under combined stress exposure leading to observed remodeling of root architecture. The figures also compile some of the transcripts associated with the six consecutive steps. Subgroups in each category are provided with exemplary sets of proteins which are expected to control root development under HpxAs and during subsequent reaeration. Early redox changes served as primary stress sensory event leading to initial suppression of root apical meristem (RAM) proliferation.

Subsequent dual induction of Pi-starvation response in stressed Arabidopsis further suppressed RAM activity during 7 d treatment. Further, energy considerations led plants to suppression of lateral root growth but induced root hair growth for sustainable nutrient uptake. Redox- and ROS-dependent regulation seems to act primarily in root hair growth and could also be responsible for loss of epidermal and cortical cell viability. Due to increased transcription of genes coding for meristematic cell maintenance-related proteins, plants were able to recover primary root growth to a certain extent. However, a strong downregulation of transcription for a larger set of genes seems to result in lag in recovery for HpxAs-treated plants compared to Hpx (**Figure 1B**). Three categories of transcripts appear crucial for signaling and plant adaptation to HpxAs.

Stem Cell Management

The majority of these genes participate in auxin signaling, and others carry out cytokinin- (CK) and gibberellic acid- (GA) mediated function. Wuschel-related homeobox genes *WOX11* and *WOX5*, work in successive steps of root founder cell establishment and root primordium development in adventitious rooting (Hu and Xu, 2016). However, the synchronous increase of *WOX11* and decrease of gene expression for *WOX5* regulatory protein *ROW1* under Hpx and HpxAs might be important in maintaining developmental plasticity. Similarly, another stem cell proliferation and differentiation regulator *UBP1* revealed reduced transcription which will favor proliferation along with overlapping increase (*SAUR41*, *GA2OX2*) and decrease (*PIN4*, *VHA-c1*) of other transcripts involved in stem cell maintenance and root development. The result of these changes i.e., increased abundance of root hairs despite root growth inhibition and subsequent growth recovery with a lag under HpxAs could be a fine balance of their activity. In addition, reduced expression of root meristem growth factor *RGF7* under HpxAs might be a crucial factor in growth arrest. Finally, reduced expression of mitogen activated protein kinase kinase *MKK6* under Hpx and HpxAs could participate in inhibition of lateral root growth (Zeng et al., 2011).

Energy Constraints and Stress Acclimation

Energy constraint is an important issue dealt by the HpxAs-treated plants, where plant metabolism and growth need to

optimally adapt to low oxygen availability along with investment in As detoxification measures. A strong overlap in transcriptomic response to Hpx and HpxAs is consistent with the same. Although further research is needed to elucidate the specific mechanism(s) of stress acclimation, following three observations related to energy metabolism are intriguing.

(a) Increased expression of *NR2* (Hpx, HpxAs) under hypoxic conditions has been linked to AOX activity that drives mitochondrial ATP generation (Vishwakarma et al., 2018). AOX has a distinct role of stimulating the hemoglobin (Hb)-NO cycle to improve energy status under hypoxic conditions. It needs to be added here that *Hb1* gene expression was significantly lower under HpxAs than Hpx, leading possibly to a bigger energy deficit (**Supplementary Figure 2**).

(b) The phosphofructokinase (PFK)-catalyzed reaction is a tightly regulated committing step of glycolysis. In hypoxic conditions, PPi-dependent PFK is preferred over ATP-dependent PFKs (Bailey-Serres and Voesenek, 2008). Here, transcripts for the ATP-dependent PFK3 increased strongly under Hpx (9.15) and HpxAs (12.39); and its physiological significance needs to be understood (**Figure 2A**, **Supplementary Table 1**). It is known that expression of *PFK3* along other kinases is stimulated by histone deacetylase (HDA18) and that they are involved in epidermal cell fate determination (Liu et al., 2013). Enzyme assays suggest lactic acid fermentation to be a preferred fermentation pathway under HpxAs, while the activity of PDC and most likely that of ADH was lower under HpxAs than Hpx alone (**Figure 6**; Bailey-Serres and Voesenek, 2008).

(c) TOR and SnRK form a central hub in intracellular and extracellular nutrient and energy sensing involved in optimal resource utilization and sustainable growth (Robaglia et al., 2012; Jamsheer et al., 2019). Observed deregulation under HpxAs concerned the following factors with diverse functions: SHY2 is a negative regulator of root growth linking auxin, CK and BR regulation of root meristem. LRX1 interferes with cell wall and RH morphogenesis and is regulated by MAML-4. MLO15 participates in cargo delivery to the plasma membrane during tip growth. RSL4 controls several RH genes. DGR2 interferes with ABA-ROP10 signaling and root morphogenesis. CAP1 controls Ca^{+} gradients for RH tip growth (Weiste et al., 2017; Schoenaers et al., 2018; Schaufelberger et al., 2019; Van Leene et al., 2019; Li et al., 2020; Zhu et al., 2020). All these signaling components downstream of TOR and SnRK signaling may control RH growth under Hpx and HpxAs.

Epidermal Cell Differentiation and Root Hair Development

Besides transcripts described above, several RH morphogenesis (*SHV2*, *MHR1*, *2*, *3*, *6*) and RH-specific (*RHS3*, *10*, *12*, *15*, *16*) genes were deregulated under Hpx and HpxAs, in contrast to As, indicating an active and precise control of RH morphogenesis. Their gene products regulate different aspects of RH tip growth like cellular streaming, plasma membrane composition or cell wall growth. For example, transcripts of negative regulator of RH elongation, *PIP2;4*, decreased under HpxAs. PIP2;4 is proposed to function as H_2O_2-conducting aquaporin and may considerably contribute to the observed phenotype (**Figures 1**, **4** and **Supplementary Figure 4**) (Dynowski et al., 2008). Also, higher RH density phenotype in HpxAs and Hpx may depend on decreased expression of *MYB66* or *WERWOLF1*, a master regulator in determination of epidermal cell fate (Song et al., 2011; Wang et al., 2019).

CONCLUSION

The present study observed a nutrient-deprivation induced and redox-regulated root architecture remodeling under HpxAs. Multiple transcripts involved in root development were identified to be specifically deregulated under HpxAs and potentially responsible for observed root hair growth phenotype. Observed Pi-starvation response and downstream changes in Fe-homeostasis for HpxAs-treated plants highlight an intriguing overlap between As and Hpx. Accumulation of ROS in different cell layers, biochemical analyses and cell viability measurements in RH zone indicated a crucial role of redox regulation in root development under HpxAs. Further research should focus on correlation between redox transients, stem cell activity and cell differentiation. Interestingly in HpxAs-treated plants, a significant part of the deregulated root hair growth-related transcriptome belonged to TOR and SnRK-signaling network. Further analysis for functional specificity of these transcripts under HpxAs could reveal regulatory pathway involved in sustaining growth and acclimation response.

DATA AVAILABILITY STATEMENT

The datasets analyzed for this study can be found in the NCBI-GEO (https://www.ncbi.nlm.nih.gov/geo/query/acc.cgi?acc=GSE119327) (Kumar et al., 2019).

AUTHOR CONTRIBUTIONS

VK, TS, SSS, and K-JD planned the study. VK, LV, and TS carried out the experimental work. VK, TS, SSS, K-JD, and RRS interpreted data and discussed the results. VK and K-JD wrote the manuscript and all authors proofread the manuscript.

FUNDING

VK was supported by the DAAD scholarship (Bonn, Germany; Binationally supervised Ph.D. program). We acknowledge the financial support of the German Research Foundation (DFG) and the Open Access Publication Fund of Bielefeld University for the manuscript processing charge.

ACKNOWLEDGMENTS

The authors are acknowledge laboratory assistance provided by Martina Holt and are thankful for helpful suggestions by Daniel Maynard. VK also acknowledges the financial support provided by Department of Biochemistry and Physiology of Plants, Faculty of Biology, Bielefeld University.

SUPPLEMENTARY MATERIAL

The Supplementary Material for this article can be found online at: https://www.frontiersin.org/articles/10.3389/fpls.2020.569687/full#supplementary-material

Supplementary Figure 1 | Heat map for comparison of stress-induced changes in transcript amounts for genes associated with lipid biosynthesis and signaling as well as phosphatidylinositol metabolism.

Supplementary Figure 2 | Quantitative RT-PCR analysis results for transcript amounts of hypoxia markers.

Supplementary Figure 3 | XTT reductase activity in soluble protein extract.

Supplementary Figure 4 | Images from DCFDA fluorescence-based analysis of ROS generation in Arabidopsis roots under As, Hpx and HpxAs.

Supplementary Figure 5 | Plant cell sap osmolarity in differentially treated plant roots and leaves.

Supplementary Table 1 | Lists of all transcripts related to root and root growth regulation and signaling as influenced by As, Hpx and HpxAs.

Supplementary Table 2 | Deregulation of phosphate starvation-related transcripts under applied stresses.

Supplementary Table 3 | Lipid biosynthesis and signaling- and phosphatidylinositol metabolism-related transcripts with stress-induced changes in transcript amounts.

Supplementary Table 4 | Lists of genes related to Fe-homeostasis and NO formation in regulation of Fe-homeostasis and stress effects.

Supplementary Table 5 | Lists of primers used for qRT-PCR quantification of hypoxia marker genes.

Supplementary Table 6 | As-, Hpx- and HpxAs-induced significant transcriptional deregulation for cytochrome P450 genes associated with redox regulation of root growth.

Supplementary Table 7 | Transcript deregulation for genes related to glucosinolate metabolism.

REFERENCES

Abel, S. (2011). Phosphate sensing in root development. *Curr. Opin. Plant Biol.* 14, 303–309. doi: 10.1016/j.pbi.2011.04.007

Abercrombie, J. M., Halfhill, M. D., Ranjan, P., Rao, M. R., Saxton, A. M., Yuan, J. S., et al. (2008). Transcriptional responses of *Arabidopsis thaliana* plants to As (V) stress. *BMC Plant Biol.* 8:87. doi: 10.1186/1471-2229-8-87

Able, A. J., Guest, D. I., and Sutherland, M. W. (1998). Use of a new tetrazolium-based assay to study the production of superoxide radicals by tobacco cell cultures challenged with avirulent zoospores of *Phytophthora parasitica* varnicotianae. *Plant Physiol.* 117, 491–499. doi: 10.1104/pp.117.2.491

Amako, K., Chen, G.-X., and Asada, K. (1994). Separate assays specific for ascorbate peroxidase and guaiacol peroxidase and for the chloroplastic and cytosolic isozymes of ascorbate peroxidase in plants. *Plant Cell Physiol.* 35, 497–504.

Aranda, P. S., LaJoie, D. M., and Jorcyk, C. L. (2012). Bleach gel: a simple agarose gel for analyzing RNA quality. *Electrophoresis* 33, 366–369. doi: 10.1002/elps.201100335

Arenas-Alfonseca, L., Gotor, C., Romero, L. C., and García, I. (2018). ß-Cyanoalanine synthase action in root hair elongation is exerted at early steps of the root hair elongation pathway and is independent of direct cyanide inactivation of NADPH oxidase. *Plant Cell Physiol.* 59, 1072–1083. doi: 10.1093/pcp/pcy047

Awasthi, S., Chauhan, R., Srivastava, S., and Tripathi, R. D. (2017). The journey of arsenic from soil to grain in rice. *Front. Plant Sci.* 8:1007. doi: 10.3389/fpls.2017.01007

Baesso, B., Chiatante, D., Terzaghi, M., Zenga, D., Nieminen, K., Mahonen, A. P., et al. (2018). Transcription factors PRE 3 and WOX 11 are involved in the formation of new lateral roots from secondary growth taproot in *A. thaliana*. *Plant Biol.* 20, 426–432. doi: 10.1111/plb.12711

Bailey-Serres, J., and Voesenek, L. (2008). Flooding stress: acclimations and genetic diversity. *Annu. Rev. Plant Biol.* 59, 313–339. doi: 10.1146/annurev.arplant.59.032607.092752

Bailey-Serres, J., and Voesenek, L. A. (2010). Life in the balance: a signaling network controlling survival of flooding. *Curr. Opin. Plant Biol.* 13, 489–494. doi: 10.1016/j.pbi.2010.08.002

Baykov, A. A., Evtushenko, O. A., and Avaeva, S. M. (1988). A malachite green procedure for orthophosphate determination and its use in alkaline phosphatase-based enzyme immunoassay. *Anal. Biochem.* 171, 266–270. doi: 10.1016/0003-2697(88)90484-8

Bell, L. (2018). The biosynthesis of glucosinolates: insights, inconsistencies, and unknowns. *Annu. Plant Rev. Online* 2, 1–31.

Blokhina, O., and Fagerstedt, K. V. (2010). Oxidative metabolism, ROS and NO under oxygen deprivation. *Plant Physiol. Biochem.* 48, 359–373. doi: 10.1016/j.plaphy.2010.01.007

Boisson-Dernier, A., Franck, C. M., Lituiev, D. S., and Grossniklaus, U. (2015). Receptor-like cytoplasmic kinase MARIS functions downstream of CrRLK1L-dependent signaling during tip growth. *Proc. Natl. Acad. Sci. U.S.A.* 112, 12211–12216. doi: 10.1073/pnas.1512375112

Bradford, M. M. (1976). A rapid and sensitive method for the quantitation of microgram quantities of protein utilizing the principle of protein-dye binding. *Anal. Biochem.* 72, 248–254. doi: 10.1016/0003-2697(76)90527-3

Bruex, A., Kainkaryam, R. M., Wieckowski, Y., Kang, Y. H., Bernhardt, C., Xia, Y., et al. (2012). A gene regulatory network for root epidermis cell differentiation in *Arabidopsis*. *PLoS Genet.* 8:e1002446. doi: 10.1371/journal.pgen.1002446

Cao, M., and Li, X. (2010). Die for living better: plants modify root system architecture through inducing PCD in root meristem under severe water stress. *Plant Signal. Behav.* 5, 1645–1646. doi: 10.4161/psb.5.12.13811

Carbonell-Barrachina, A. A., Burló-Carbonell, F., and Mataix-Beneyto, J. (1997). Effect of sodium arsenite and sodium chloride on bean plant nutrition (macronutrients). *J. Plant Nutr.* 20, 1617–1633. doi: 10.1080/01904169709365361

Catarecha, P., Segura, M. D., Franco-Zorrilla, J. M., García-Ponce, B., Lanza, M., Solano, R., et al. (2007). A mutant of the *Arabidopsis* phosphate transporter PHT1; 1 displays enhanced arsenic accumulation. *Plant Cell* 19, 1123–1133. doi: 10.1105/tpc.106.041871

Cho, H.-T., and Lee, R. (2013). Auxin, the organizer of the hormonal/environmental signals for root hair growth. *Front. Plant Sci.* 4:448. doi: 10.3389/fpls.2013.00448

Cruz-Ramírez, A., Oropeza-Aburto, A., Razo-Hernández, F., Ramírez-Chávez, E., and Herrera-Estrella, L. (2006). Phospholipase DZ2 plays an important role in extraplastidic galactolipid biosynthesis and phosphate recycling in *Arabidopsis* roots. *Proc. Natl. Acad. Sci. U.S.A.* 103, 6765–6770. doi: 10.1073/pnas.0600863103

Cui, S., Suzaki, T., Tominaga-Wada, R., and Yoshida, S. (2018). Regulation and functional diversification of root hairs. *Semin. Cell Dev. Biol.* 83, 115–122. doi: 10.1016/j.semcdb.2017.10.003

Cui, Y., Chen, C.-L., Cui, M., Zhou, W.-J., Wu, H.-L., and Ling, H.-Q. (2018). Four IVa bHLH transcription factors are novel interactors of FIT and mediate JA inhibition of iron uptake in *Arabidopsis*. *Mol. Plant* 11, 1166–1183. doi: 10.1016/j.molp.2018.06.005

Dat, J. F., Capelli, N., Folzer, H., Bourgeade, P., and Badot, P.-M. (2004). Sensing and signalling during plant flooding. *Plant Physiol. Biochem.* 42, 273–282. doi: 10.1016/j.plaphy.2004.02.003

De Tullio, M. C., Jiang, K., and Feldman, L. J. (2010). Redox regulation of root apical meristem organization: connecting root development to its environment. *Plant Physiol. Biochem.* 48, 328–336. doi: 10.1016/j.plaphy.2009.11.005

Duan, G., Liu, W., Chen, X., Hu, Y., and Zhu, Y. (2013). Association of arsenic with nutrient elements in rice plants. *Metallomics* 5, 784–792. doi: 10.1039/c3mt20277a

Dynowski, M., Schaaf, G., Loque, D., Moran, O., and Ludewig, U. (2008). Plant plasma membrane water channels conduct the signalling molecule H2O2. *Biochem. J.* 414, 53–61. doi: 10.1042/BJ20080287

Emre, A., and Koiwa, H. (2013). Determination of ferric chelate reductase activity in the *Arabidopsis thaliana* root. *Bio Protoc.* 3:e843. doi: 10.21769/BioProtoc.843

Eruslanov, E., and Kusmartsev, S. (2010). "Identification of ROS using oxidized DCFDA and flow-cytometry," in *Advanced Protocols in Oxidative Stress II*, ed. D. Armstrong (Totowa, NJ: Humana Press), 57–72. doi: 10.1007/978-1-60761-411-1_4

Farmer, E. E., and Mueller, M. J. (2013). ROS-mediated lipid peroxidation and RES-activated signaling. *Annu. Rev. Plant Biol.* 64, 429–450. doi: 10.1146/annurev-arplant-050312

Foreman, J., Demidchik, V., Bothwell, J. H. F., Mylona, P., Miedema, H., Torres, M. A., et al. (2003). Reactive oxygen species produced by NADPH oxidase regulate plant cell growth. *Nature* 422, 442–446. doi: 10.1038/nature01485

Francisco, M., Joseph, B., Caligagan, H., Li, B., Corwin, J. A., Lin, C., et al. (2016). Genome wide association mapping in *Arabidopsis thaliana* identifies novel genes involved in linking allyl glucosinolate to altered biomass and defense. *Front. Plant Sci.* 7:1010. doi: 10.3389/fpls.2016.01010

Gahoonia, T. S., and Nielsen, N. E. (1998). Direct evidence on participation of root hairs in phosphorus (^{32}P) uptake from soil. *Plant Soil* 198, 147–152. doi: 10.1023/A:1004346412006

García, M. J., Suárez, V., Romera, F. J., Alcántara, E., and Pérez-Vicente, R. (2011). A new model involving ethylene, nitric oxide and Fe to explain the regulation of Fe-acquisition genes in Strategy I plants. *Plant Physiol. Biochem.* 49, 537–544. doi: 10.1016/j.plaphy.2011.01.019

Goldstein, D. B. (1968). A method for assay of catalase with the oxygen cathode. *Anal. Biochem.* 24, 431–437. doi: 10.1016/0003-2697(68)90148-6

Grierson, C., Nielsen, E., Ketelaarc, T., and Schiefelbein, J. (2014). Root hairs. *Arabidopsis Book* 12:e0172. doi: doi.org/10.1199/tab.0172

Grierson, C., and Schiefelbein, J. (2002). Root hairs. *Arabidopsis Book* 1:e0060. doi: 10.1199/tab.0060

Gupta, D. K., Inouhe, M., Rodríguez-Serrano, M., Romero-Puertas, M. C., and Sandalio, L. M. (2013). Oxidative stress and arsenic toxicity: role of NADPH oxidases. *Chemosphere* 90, 1987–1996. doi: 10.1016/j.chemosphere.2012.10.066

Gutscher, M., Pauleau, A.-L., Marty, L., Brach, T., Wabnitz, G. H., Samstag, Y., et al. (2008). Real-time imaging of the intracellular glutathione redox potential. *Nat. Methods* 5:553. doi: 10.1038/nmeth.1212

Hanson, A. D., and Jacobsen, J. V. (1984). Control of lactate dehydrogenase, lactate glycolysis, and α-amylase by O_2 deficit in barley aleurone layers. *Plant Physiol.* 75, 566–572. doi: 10.1104/pp.75.3.566

Hao, F., Wang, X., and Chen, J. (2006). Involvement of plasma-membrane NADPH oxidase in nickel-induced oxidative stress in roots of wheat seedlings. *Plant Sci.* 170, 151–158. doi: 10.1016/j.plantsci.2005.08.014

Hider, R. C., and Kong, X. (2013). Iron speciation in the cytosol: an overview. *Dalton Trans.* 42, 3220–3229. doi: 10.1039/C2DT32149A

Hirano, T., Konno, H., Takeda, S., Dolan, L., Kato, M., Aoyama, T., et al. (2018). PtdIns (3, 5) P 2 mediates root hair shank hardening in *Arabidopsis*. *Nat. Plants* 4, 888–897. doi: 10.1038/s41477-018-0277-8

Hodge, A., Berta, G., Doussan, C., Merchan, F., and Crespi, M. (2009). Plant root growth, architecture and function. *Plant Soil* 321, 153–187. doi: 10.1007/s11104-009-9929-9

Hu, X., and Xu, L. (2016). Transcription factors WOX11/12 directly activate WOX5/7 to promote root primordia initiation and organogenesis. *Plant Physiol.* 172, 2363–2373. doi: 10.1104/pp.16.01067

Huang, L., Jiang, Q., Wu, J., An, L., Zhou, Z., Wong, C., et al. (2020). Zinc finger protein 5 (ZFP5) associates with ethylene signaling to regulate the phosphate and potassium deficiency-induced root hair development in *Arabidopsis*. *Plant Mol. Biol.* 102, 143–158. doi: 10.1007/s11103-019-00937-4

Huang, Y., Picha, D. H., and Kilili, A. W. (2002). Atmospheric oxygen level influences alcohol dehydrogenase and pyruvate decarboxylase activities in sweetpotato roots. *J. Plant Physiol.* 159, 129–136. doi: 10.1078/0176-1617-00693

Irizarry, R. A., Hobbs, B., Collin, F., Beazer-Barclay, Y. D., Antonellis, K. J., Scherf, U., et al. (2003). Exploration, normalization, and summaries of high density oligonucleotide array probe level data. *Biostatistics* 4, 249–264. doi: 10.1093/biostatistics/4.2.249

Islam, E., Khan, M. T., and Irem, S. (2015). Biochemical mechanisms of signaling: perspectives in plants under arsenic stress. *Ecotoxicol. Environ. Saf.* 114, 126–133. doi: 10.1016/j.ecoenv.2015.01.017

Jamsheer, K. M., Jindal, S., and Laxmi, A. (2019). Evolution of TOR–SnRK dynamics in green plants and its integration with phytohormone signaling networks. *J. Exp. Bot.* 70, 2239–2259. doi: 10.1093/jxb/erz107

Katsumi, M., Izumo, M., and Ridge, R. W. (2000). "Hormonal control of root hair growth and development," in *Root Hairs: Cell and Molecular Biology*, eds R. W. Ridge and A. M. C. Emons (Tokyo: Springer Japan), 101–114. doi: 10.1007/978-4-431-68370-4_7

Kim, E.-J., Kim, Y.-J., Hong, W.-J., Lee, C., Jeon, J.-S., and Jung, K.-H. (2019). Genome-wide analysis of root hair preferred RBOH genes suggests that three RBOH genes are associated with auxin-mediated root hair development in rice. *J. Plant Biol.* 62, 229–238. doi: 10.1007/s12374-019-0006

Klecker, M., Gasch, P., Peisker, H., Dörmann, P., Schlicke, H., Grimm, B., et al. (2014). A shoot-specific hypoxic response of *Arabidopsis* sheds light on the role of the phosphate-responsive transcription factor PHOSPHATE STARVATION RESPONSE1. *Plant Physiol.* 165, 774–790. doi: 10.1104/pp.114.237990

Kofroňová, M., Mašková, P., and Lipavská, H. (2018). Two facets of world arsenic problem solution: crop poisoning restriction and enforcement of phytoremediation. *Planta* 248, 19–35. doi: 10.1007/s00425-018-2906-x

Kosmacz, M., Parlanti, S., Schwarzländer, M., Kragler, F., Licausi, F., and Van Dongen, J. T. (2015). The stability and nuclear localization of the transcription factor RAP 2.*12* are dynamically regulated by oxygen concentration. *Plant Cell Environ.* 38, 1094–1103. doi: 10.1111/pce.12493

Kumar, V., Vogelsang, L., Seidel, T., Schmidt, R., Weber, M., Reichelt, M., et al. (2019). Interference between arsenic-induced toxicity and hypoxia. *Plant Cell Environ.* 42, 574–590. doi: 10.1111/pce.13441

Kwon, T., Sparks, J. A., Nakashima, J., Allen, S. N., Tang, Y., and Blancaflor, E. B. (2015). Transcriptional response of Arabidopsis seedlings during spaceflight reveals peroxidase and cell wall remodeling genes associated with root hair development. *Am. J. Bot.* 102, 21–35. doi: 10.3732/ajb.1400458

Lalucque, H., and Silar, P. (2003). NADPH oxidase: an enzyme for multicellularity? *Trends Microbiol.* 11, 9–12. doi: 10.1016/S0966-842X(02)00007

Lee, C.-H., Hsieh, Y.-C., Lin, T.-H., and Lee, D.-Y. (2013). Iron plaque formation and its effect on arsenic uptake by different genotypes of paddy rice. *Plant Soil* 363, 231–241. doi: 10.1007/s11104-012-1308-2

Li, H., Torres-Garcia, J., Latrasse, D., Benhamed, M., Schilderink, S., Zhou, W., et al. (2017). Plant-specific histone deacetylases HDT1/2 regulate *GIBBERELLIN 2-OXIDASE2* expression to control *Arabidopsis* root meristem cell number. *Plant Cell* 29, 2183–2196. doi: 10.1105/tpc.17.00366

Li, T., Kang, X., Lei, W., Yao, X., Zou, L., Zhang, D., et al. (2020). SHY2 as a node in the regulation of root meristem development by auxin, brassinosteroids, and cytokinin. *J. Integr. Plant Biol.* 62, 1500–1517. doi: 10.1111/jipb.12931

Li, T., Yang, S., Kang, X., Lei, W., Qiao, K., Zhang, D., et al. (2019). The bHLH transcription factor gene AtUPB1 regulates growth by mediating cell cycle progression in *Arabidopsis*. *Biochem. Biophys. Res. Commun.* 518, 565–572. doi: 10.1016/j.bbrc.2019.08.088

Liu, C., Li, L.-C., Chen, W.-Q., Chen, X., Xu, Z.-H., and Bai, S.-N. (2013). HDA18 affects cell fate in *Arabidopsis* root epidermis via histone acetylation at four kinase genes. *Plant Cell* 25, 257–269. doi: 10.1105/tpc.112.107045

Liu, W., Li, R.-J., Han, T.-T., Cai, W., Fu, Z.-W., and Lu, Y.-T. (2015). Salt stress reduces root meristem size by nitric oxide-mediated modulation of auxin accumulation and signaling in *Arabidopsis*. *Plant Physiol.* 168, 343–356. doi: 10.1104/pp.15.00030

Liu, W. J., Zhu, Y. G., Smith, F., and Smith, S. (2004). Do phosphorus nutrition and iron plaque alter arsenate (As) uptake by rice seedlings in hydroponic culture? *New Phytol.* 162, 481–488. doi: 10.1111/j.1469-8137.2004.01035.x

Lukyanov, K. A., and Belousov, V. V. (2014). Genetically encoded fluorescent redox sensors. *Biochim. Biophys. Acta* 1840, 745–756. doi: 10.1016/j.bbagen.2013.05.030

Mangano, S., Denita-Juarez, S. P., Choi, H.-S., Marzol, E., Hwang, Y., Ranocha, P., et al. (2017). Molecular link between auxin and ROS-mediated polar growth. *Proc. Natl. Acad. Sci. U.S.A.* 114:5289. doi: 10.1073/pnas.1701536114

Medunić, G., Fiket, Ž, and Ivanić, M. (2020). "Arsenic contamination status in Europe, Australia, and other parts of the world," in *Arsenic in Drinking Water and Food*, ed. S. Srivastava (Singapore: Springer Singapore), 183–233. doi: 10.1007/978-981-13-8587-2_6

Mhamdi, A., and Van Breusegem, F. (2018). Reactive oxygen species in plant development. *Development* 145:dev164376. doi: 10.1242/dev.164376

Mithran, M., Paparelli, E., Novi, G., Perata, P., and Loreti, E. (2014). Analysis of the role of the pyruvate decarboxylase gene family in *Arabidopsis thaliana* under low-oxygen conditions. *Plant Biol.* 16, 28–34.

Mittler, R., Vanderauwera, S., Gollery, M., and Van Breusegem, F. (2004). Reactive oxygen gene network of plants. *Trends Plant Sci.* 9, 490–498. doi: 10.1111/plb.12005

Moubayidin, L., Perilli, S., Ioio, R. D., Di Mambro, R., Costantino, P., and Sabatini, S. (2010). The rate of cell differentiation controls the *Arabidopsis* root meristem growth phase. *Curr. Biol.* 20, 1138–1143. doi: 10.1016/j.cub.2010.05.035

Müller, J., Toev, T., Heisters, M., Teller, J., Moore, K. L., Hause, G., et al. (2015). Iron-dependent callose deposition adjusts root meristem maintenance to phosphate availability. *Dev. Cell* 33, 216–230. doi: 10.1016/j.devcel.2015.02.007

Müller, M., and Schmidt, W. (2004). Environmentally induced plasticity of root hair development in *Arabidopsis*. *Plant Physiol.* 134, 409–419. doi: 10.1104/pp.103.029066

Nakamura, Y., Koizumi, R., Shui, G., Shimojima, M., Wenk, M. R., Ito, T., et al. (2009). *Arabidopsis* lipins mediate eukaryotic pathway of lipid metabolism and cope critically with phosphate starvation. *Proc. Natl. Acad. Sci. U.S.A.* 106, 20978–20983. doi: 10.1073/pnas.0907173106

Naujokas, M. F., Anderson, B., Ahsan, H., Aposhian, H. V., Graziano, J. H., Thompson, C., et al. (2013). The broad scope of health effects from chronic arsenic exposure: update on a worldwide public health problem. *Environ. Health Perspect.* 121, 295–302. doi: 10.1289/ehp.1205875

Neumann, G. (2016). The role of ethylene in plant adaptations for phosphate acquisition in soils–a review. *Front. Plant Sci.* 6:1224. doi: 10.3389/fpls.2015.01224

Nilsson, L., Lundmark, M., Jensen, P. E., and Nielsen, T. H. (2012). The *Arabidopsis* transcription factor PHR1 is essential for adaptation to high light and retaining functional photosynthesis during phosphate starvation. *Physiol. Plant.* 144, 35–47. doi: 10.1111/j.1399-3054.2011.01520.x

Orman-Ligeza, B., Parizot, B., de Rycke, R., Fernandez, A., Himschoot, E., Van Breusegem, F., et al. (2016). RBOH-mediated ROS production facilitates lateral root emergence in *Arabidopsis*. *Development* 143:3328. doi: 10.1242/dev.136465

Ovečka, M., Berson, T., Beck, M., Derksen, J., Šamaj, J., Baluška, F., et al. (2010). Structural sterols are involved in both the initiation and tip growth of root hairs in *Arabidopsis thaliana*. *Plant Cell* 22, 2999–3019. doi: 10.1105/tpc.109.069880

Pandey, P., Ramegowda, V., and Senthil-Kumar, M. (2015). Shared and unique responses of plants to multiple individual stresses and stress combinations: physiological and molecular mechanisms. *Front. Plant Sci.* 6:723. doi: 10.3389/fpls.2015.00723

Park, J. H., Han, Y.-S., Seong, H. J., Ahn, J. S., and Nam, I.-H. (2016). Arsenic uptake and speciation in *Arabidopsis thaliana* under hydroponic conditions. *Chemosphere* 154, 283–288. doi: 10.1016/j.chemosphere.2016.03.126

Pedersen, O., Sauter, M., Colmer, T. D., and Nakazono, M. (2020). Regulation of root adaptive anatomical and morphological traits during low soil oxygen. *New Phytol.* 1–7. doi: 10.1111/nph.16375

Perilli, S., Di Mambro, R., and Sabatini, S. (2012). Growth and development of the root apical meristem. *Curr. Opin. Plant Biol.* 15, 17–23. doi: 10.1016/j.pbi.2011.10.006

Petricka, J. J., Winter, C. M., and Benfey, P. N. (2012). Control of *Arabidopsis* root development. *Annu. Rev. Plant Biol.* 63, 563–590. doi: 10.1146/annurev-arplant-042811-105501

Petrov, V., Hille, J., Mueller-Roeber, B., and Gechev, T. S. (2015). ROS-mediated abiotic stress-induced programmed cell death in plants. *Front. Plant Sci.* 6:69. doi: 10.3389/fpls.2015.00069

Potocký, M., Pejchar, P., Gutkowska, M., Jiménez-Quesada, M. J., Potocká, A., de Dios Alché, J., et al. (2012). NADPH oxidase activity in pollen tubes is affected by calcium ions, signaling phospholipids and Rac/Rop GTPases. *J. Plant Physiol* 169, 1654–1663. doi: 10.1016/j.jplph.2012.05.014

Pucciariello, C., Banti, V., and Perata, P. (2012). ROS signaling as common element in low oxygen and heat stresses. *Reactive Oxygen Nitrogen Carbonyl Sulf. Species Plants* 59, 3–10. doi: 10.1016/j.plaphy.2012.02.016

Rai, A., Tripathi, P., Dwivedi, S., Dubey, S., Shri, M., Kumar, S., et al. (2011). Arsenic tolerances in rice (Oryza sativa) have a predominant role in transcriptional regulation of a set of genes including sulphur assimilation pathway and antioxidant system. *Chemosphere* 82, 986–995. doi: 10.1016/j.chemosphere.2010.10.070

Ramakers, C., Ruijter, J. M., Deprez, R. H. L., and Moorman, A. F. (2003). Assumption-free analysis of quantitative real-time polymerase chain reaction (PCR) data. *Neurosci. Lett.* 339, 62–66. doi: 10.1016/S0304-3940(02)01423-4

Rasmussen, S., Barah, P., Suarez-Rodriguez, M. C., Bressendorff, S., Friis, P., Costantino, P., et al. (2013). Transcriptome responses to combinations of stresses in *Arabidopsis*. *Plant Physiol.* 161, 1783–1794. doi: 10.1104/pp.112.210773

Robaglia, C., Thomas, M., and Meyer, C. (2012). Sensing nutrient and energy status by SnRK1 and TOR kinases. *Curr. Opin. Plant Biol.* 15, 301–307. doi: 10.1016/j.pbi.2012.01.012

Rouached, H., Secco, D., Arpat, B., and Poirier, Y. (2011). The transcription factor PHR1 plays a key role in the regulation of sulfate shoot-to-root flux upon phosphate starvation in *Arabidopsis*. *BMC Plant Biol.* 11:19. doi: 10.1186/1471-2229-11-19

Ruijter, J. M., Ramakers, C., Hoogaars, W. M. H., Karlen, Y., Bakker, O., Van den Hoff, M. J. B., et al. (2009). Amplification efficiency: linking baseline and bias in the analysis of quantitative PCR data. *Nucleic Acids Res.* 37:e45. doi: 10.1093/nar/gkp045

Ruiz Herrera, L. F., Shane, M. W., and López-Bucio, J. (2015). Nutritional regulation of root development. *Wiley Interdiscip. Rev. Dev. Biol.* 4, 431–443. doi: 10.1002/wdev.183

Ryter, S. W., and Tyrrell, R. M. (2000). The heme synthesis and degradation pathways: role in oxidant sensitivity: heme oxygenase has both pro- and antioxidant properties. *Free Radical Biol. Med.* 28, 289–309. doi: 10.1016/S0891-5849(99)00223-3

Salazar-Henao, J. E., and Schmidt, W. (2016). An inventory of nutrient-responsive genes in *Arabidopsis* root hairs. *Front. Plant Sci.* 7:237. doi: 10.3389/fpls.2016.00237

Salazar-Henao, J. E., Vélez-Bermúdez, I. C., and Schmidt, W. (2016). The regulation and plasticity of root hair patterning and morphogenesis. *Development* 143, 1848–1858. doi: 10.1242/dev.132845

Satbhai, S. B., Ristova, D., and Busch, W. (2015). Underground tuning: quantitative regulation of root growth. *J. Exp. Bot.* 66, 1099–1112. doi: 10.1093/jxb/eru529

Schat, H., and Ten Bookum, W. M. (1992). Genetic control of copper tolerance in *Silene vulgaris*. *Heredity* 68, 219–229. doi: 10.1038/hdy.1992.35

Schaufelberger, M., Galbier, F., Herger, A., de Brito Francisco, R., Roffler, S., Clement, G., et al. (2019). Mutations in the *Arabidopsis* ROL17/isopropylmalate synthase 1 locus alter amino acid content, modify the TOR network, and suppress the root hair cell development mutant lrx1. *J. Exp. Bot.* 70, 2313–2323. doi: 10.1093/jxb/ery463

Scheres, B., Benfey, P., and Dolan, L. (2002). Root development. *Arabidopsis Book* 1:e0101. doi: 10.1199/tab.0101

Schmidt, R. R., Weits, D. A., Feulner, C. F. J., and van Dongen, J. T. (2018). Oxygen sensing and integrative stress signaling in plants. *Plant Physiol.* 176, 1131–1142. doi: 10.1104/pp.17.01394

Schoenaers, S., Balcerowicz, D., Breen, G., Hill, K., Zdanio, M., Mouille, G., et al. (2018). The auxin-regulated CrRLK1L kinase ERULUS controls cell wall composition during root hair tip growth. *Curr. Biol.* 28, 722–732. doi: 10.1016/j.cub.2018.01.050

Seth, C. S., Remans, T., Keunen, E., Jozefczak, M., Gielen, H., Opdenakker, K., et al. (2012). Phytoextraction of toxic metals: a central role for glutathione. *Plant Cell Environ.* 35, 334–346. doi: 10.1111/j.1365-3040.2011.02338.x

Shibata, M., and Sugimoto, K. (2019). A gene regulatory network for root hair development. *J. Plant Res.* 132, 301–309. doi: 10.1007/s10265-019-01100-2

Shin, R., Berg, R. H., and Schachtman, D. P. (2005). Reactive oxygen species and root hairs in *Arabidopsis* root response to nitrogen, phosphorus and potassium deficiency. *Plant Cell Physiol.* 46, 1350–1357. doi: 10.1093/pcp/pci145

Shin, R., and Schachtman, D. P. (2004). Hydrogen peroxide mediates plant root cell response to nutrient deprivation. *Proc. Natl. Acad. Sci. U.S.A.* 101, 8827–8832. doi: 10.1073/pnas.0401707101

Shukla, V., Lombardi, L., Iacopino, S., Pencik, A., Novak, O., Perata, P., et al. (2019). Endogenous hypoxia in lateral root primordia controls root architecture by antagonizing auxin signaling in *Arabidopsis*. *Mol. Plant* 12, 538–551. doi: 10.1016/j.molp.2019.01.007

Song, S.-K., Ryu, K. H., Kang, Y. H., Song, J. H., Cho, Y.-H., Yoo, S.-D., et al. (2011). Cell fate in the *Arabidopsis* root epidermis is determined by competition between WEREWOLF and CAPRICE. *Plant Physiol.* 157, 1196–1208. doi: 10.1104/pp.111.185785

Sozzani, R., and Iyer-Pascuzzi, A. (2014). Postembryonic control of root meristem growth and development. *Curr. Opin. Plant Biol.* 17, 7–12. doi: 10.1016/j.pbi.2013.10.005

Srivastava, M., Ma, L. Q., Singh, N., and Singh, S. (2005). Antioxidant responses of hyper-accumulator and sensitive fern species to arsenic. *J. Exp. Bot.* 56, 1335–1342. doi: 10.1093/jxb/eri134

Steyn, W. J., Wand, S. J. E., Holcroft, D. M., and Jacobs, G. (2002). Anthocyanins in vegetative tissues: a proposed unified function in photoprotection. *New Phytol.* 155, 349–361. doi: 10.1046/j.1469-8137.2002.00482.x

Su, Y., Li, M., Guo, L., and Wang, X. (2018). Different effects of phospholipase Dζ2 and non-specific phospholipase C4 on lipid remodeling and root hair growth in *Arabidopsis* response to phosphate deficiency. *Plant J.* 94, 315–326. doi: 10.1111/tpj.13858

Suzuki, N., Bassil, E., Hamilton, J. S., Inupakutika, M. A., Zandalinas, S. I., Tripathy, D., et al. (2016). ABA is required for plant acclimation to a combination of salt and heat stress. *PLoS One* 11:e0147625. doi: 10.1371/journal.pone.0147625

Suzuki, N., Rivero, R. M., Shulaev, V., Blumwald, E., and Mittler, R. (2014). Abiotic and biotic stress combinations. *New Phytol.* 203, 32–43. doi: 10.1111/nph.12797

Thibaud, M.-C., Arrighi, J.-F., Bayle, V., Chiarenza, S., Creff, A., Bustos, R., et al. (2010). Dissection of local and systemic transcriptional responses to phosphate starvation in *Arabidopsis*. *Plant J.* 64, 775–789. doi: 10.1111/j.1365-313X.2010.04375.x

Tripathi, R. D., Tripathi, P., Dwivedi, S., Kumar, A., Mishra, A., Chauhan, P. S., et al. (2014). Roles for root iron plaque in sequestration and uptake of heavy metals and metalloids in aquatic and wetland plants. *Metallomics* 6, 1789–1800. doi: 10.1039/C4MT00111G

Truernit, E., and Haseloff, J. (2008). A simple way to identify non-viable cells within living plant tissue using confocal microscopy. *Plant Methods* 4:15. doi: 10.1186/1746-4811-4-15

Tsukagoshi, H. (2016). Control of root growth and development by reactive oxygen species. *Curr. Opin. Plant Biol.* 29, 57–63. doi: 10.1016/j.pbi.2015.10.012

Tsukagoshi, H., Busch, W., and Benfey, P. N. (2010). Transcriptional regulation of ROS controls transition from proliferation to differentiation in the root. *Cell* 143, 606–616. doi: 10.1016/j.cell.2010.10.020

Van Leene, J., Han, C., Gadeyne, A., Eeckhout, D., Matthijs, C., Cannoot, B., et al. (2019). Capturing the phosphorylation and protein interaction landscape of the plant TOR kinase. *Nat. Plants* 5, 316–327. doi: 10.1038/s41477-019-0378-z

Vandesompele, J., De Preter, K., Pattyn, F., Poppe, B., Van Roy, N., De Paepe, A., et al. (2002). Accurate normalization of real-time quantitative RT-PCR data by geometric averaging of multiple internal control genes. *Genome Biol.* 3, 1–12. doi: 10.1186/gb-2002-3-7-research0034

Vishwakarma, A., Kumari, A., Mur, L. A., and Gupta, K. J. (2018). A discrete role for alternative oxidase under hypoxia to increase nitric oxide and drive energy production. *Free Radical Biol. Med.* 122, 40–51. doi: 10.1016/j.freeradbiomed.2018.03.045

Wang, S. S., Zhu, X. N., Lin, J. X., Zheng, W. J., Zhang, B. T., Zhou, J. Q., et al. (2018). OsNOX3, encoding a NADPH oxidase, regulates root hair initiation and elongation in rice. *Biol. Plant* 62, 732–740. doi: 10.1007/s10535-018-0814

Wang, W., Chen, D., Zhang, X., Liu, D., Cheng, Y., and Shen, F. (2018). Role of plant respiratory burst oxidase homologs in stress responses. *Free Radic. Res.* 52, 826–839. doi: 10.1080/10715762.2018.1473572

Wang, W., Ryu, K. H., Barron, C., and Schiefelbein, J. (2019). Root epidermal cell patterning is modulated by a critical residue in the WEREWOLF transcription factor. *Plant Physiol.* 181, 1239–1256. doi: 10.1104/pp.19.00458

Weiste, C., Pedrotti, L., Selvanayagam, J., Muralidhara, P., Fröschel, C., Novák, O., et al. (2017). The *Arabidopsis* bZIP11 transcription factor links low-energy signalling to auxin-mediated control of primary root growth. *PLoS Genet.* 13:e1006607. doi: 10.1371/journal.pgen.1006607

Yang, S., Yu, Q., Zhang, Y., Jia, Y., Wan, S., Kong, X., et al. (2018). ROS: the fine-tuner of plant stem cell fate. *Trends Plant Sci.* 23, 850–853. doi: 10.1016/j.tplants.2018.07.010

Zeng, Q., Sritubtim, S., and Ellis, B. E. (2011). AtMKK6 and AtMPK13 are required for lateral root formation in *Arabidopsis*. *Plant Signal. Behav.* 6, 1436–1439. doi: 10.4161/psb.6.10.17089

Zhang, Y., Jiao, Y., Liu, Z., and Zhu, Y.-X. (2015). ROW1 maintains quiescent centre identity by confining WOX5 expression to specific cells. *Nat. Commun.* 6, 1–8. doi: 10.1038/ncomms7003

Zhao, F. J., Ma, J. F., Meharg, A. A., and McGrath, S. P. (2009). Arsenic uptake and metabolism in plants. *New Phytol.* 181, 777–794. doi: 10.1111/j.1469-8137.2008.02716.x

Zhao, F.-J., McGrath, S. P., and Meharg, A. A. (2010). Arsenic as a food chain contaminant: mechanisms of plant uptake and metabolism and mitigation strategies. *Annu. Rev. Plant Biol.* 61, 535–559. doi: 10.1146/annurev-arplant-042809-112152

Zhu, S., Martínez Pacheco, J., Estevez, J. M., and Yu, F. (2020). Autocrine regulation of root hair size by the RALF-FERONIA-RSL4 signaling pathway. *New Phytol.* 227, 45–49. doi: 10.1111/nph.16497

Conflict of Interest: The authors declare that the research was conducted in the absence of any commercial or financial relationships that could be construed as a potential conflict of interest.

frontiers in Plant Science

ORIGINAL RESEARCH
published: 29 October 2020
doi: 10.3389/fpls.2020.584167

The Ankyrin-Repeat Gene *GmANK114* Confers Drought and Salt Tolerance in *Arabidopsis* and Soybean

Juan-Ying Zhao[1,2†], Zhi-Wei Lu[2†‡], Yue Sun[2,3], Zheng-Wu Fang[3], Jun Chen[2], Yong-Bin Zhou[2], Ming Chen[2], You-Zhi Ma[2], Zhao-Shi Xu[2] and Dong-Hong Min[1]**

[1] College of Agronomy, Northwest A&F University/State Key Laboratory of Crop Stress Biology for Arid Areas, Yangling, China, [2] Institute of Crop Science, Chinese Academy of Agricultural Sciences (CAAS)/National Key Facility for Crop Gene Resources and Genetic Improvement, Key Laboratory of Biology and Genetic Improvement of Triticeae Crops, Ministry of Agriculture, Beijing, China, [3] College of Agriculture, Yangtze University, Jingzhou, China

Ankyrin repeat (ANK) proteins are essential in cell growth, development, and response to hormones and environmental stresses. In the present study, 226 *ANK* genes were identified and classified into nine subfamilies according to conserved domains in the soybean genome (*Glycine max* L.). Among them, the *GmANK114* was highly induced by drought, salt, and abscisic acid. The *GmANK114* encodes a protein that belongs to the ANK-RF subfamily containing a RING finger (RF) domain in addition to the ankyrin repeats. Heterologous overexpression of *GmANK114* in transgenic *Arabidopsis* improved the germination rate under drought and salt treatments compared to wild-type. Homologous overexpression of *GmANK114* improved the survival rate under drought and salt stresses in transgenic soybean hairy roots. In response to drought or salt stress, *GmANK114* overexpression in soybean hairy root showed higher proline and lower malondialdehyde contents, and lower H_2O_2 and O^{2-} contents compared control plants. Besides, *GmANK114* activated transcription of several abiotic stress-related genes, including *WRKY13*, *NAC11*, *DREB2*, *MYB84*, and *bZIP44* under drought and salt stresses in soybean. These results provide new insights for functional analysis of soybean ANK proteins and will be helpful for further understanding how ANK proteins in plants adapt to abiotic stress.

Keywords: ankyrin repeat protein, genome-wide analysis, responsive mechanism, drought and salt tolerance, soybean

OPEN ACCESS

Edited by:
Zhi Chang Chen, Fujian Agriculture and Forestry University, China

Reviewed by:
Dezhi Wu, Zhejiang University, China
Umesh K. Reddy, West Virginia State University, United States

****Correspondence:***
Zhao-Shi Xu
xuzhaoshi@caas.cn
Dong-Hong Min
mdh2493@126.com

[†] These authors have contributed equally to this work

[‡] Present address:
Zhi-Wei Lu, Zhanjiang City Key Laboratory for Tropical Crops Genetic Improvement, South Subtropical Crops Institute, Chinese Academy of Tropical Agricultural Sciences, Zhanjiang, China

Specialty section:
This article was submitted to Plant Abiotic Stress, a section of the journal Frontiers in Plant Science

Received: *16 July 2020*
Accepted: *06 October 2020*
Published: *29 October 2020*

Citation:
Zhao J-Y, Lu Z-W, Sun Y, Fang Z-W, Chen J, Zhou Y-B, Chen M, Ma Y-Z, Xu Z-S and Min D-H (2020) The Ankyrin-Repeat Gene GmANK114 Confers Drought and Salt Tolerance in Arabidopsis and Soybean. Front. Plant Sci. 11:584167. doi: 10.3389/fpls.2020.584167

INTRODUCTION

In recent years, various abiotic stresses, especially drought and salt, became more and more frequent with global climate change. Abiotic stresses change the physiological traits and metabolism of plants, affect the growth and development processes, and eventually lead to decreased yield and quality of crops (Veatch-Blohm, 2007; Hasanuzzaman et al., 2012). To adapt to the changing environments, plants induce the expression of stress-related genes by receiving external signals and undergoing a series of complex signal transduction pathways and diverse response mechanisms,

thereby reducing the damage of abiotic stresses on their growth and development (Chen and Murata, 2011; Wang et al., 2015; Zhu, 2016; Qi et al., 2018; Yang and Guo, 2018).

The ankyrin repeat (ANK) proteins, with at least four consecutive ANK motifs (Michaely and Bennett, 1992; Mosavi et al., 2004), are distributed in diverse organisms ranging from viruses to plants (Sedgwick and Smerdon, 1999), and are very crucial in different functions, including cell cycle regulation, transcriptional regulation, cytoskeleton interaction, and signal transduction. In humans and animals, ANK proteins are directly involved in the development of cancer. The human *VBARP* is thought to be involved with cellular apoptosis (anti-apoptotic) and cell survival pathways (Miles et al., 2005).

Similarly, plant ANK proteins were involved in various important biological processes. AKR, the first reported ANK protein with five ankyrin repeats in *Arabidopsis*, played a regulatory role in cell differentiation and development (Zhang et al., 1992). EMB506, similar to AKR with five ankyrin repeats, is an essential chloroplast protein for normal development of *Arabidopsis* embryos (Albert et al., 1999). Subsequently, the EMB506 was proved interact with the AKR protein and caused to lose its function, thereby resulted in an embryo-defective phenotype. It was demonstrated that *EMB506* and *AKR* are involved in crucially and tightly controlled events in plastid differentiation linked to cell differentiation, morphogenesis, and organogenesis during the plant life cycle (Garcion et al., 2006). AtACD6, a regulator and an effector of salicylic acid (SA) signaling, is a dose-dependent activator of the defense responses against virulent bacteria and can activate SA-dependent cell death (Lu et al., 2003, 2005). The interaction of the tobacco ANK protein NEIP2 with ethylene receptor NTHK1 improved plant growth and performance under salt and oxidative stresses (Cao et al., 2015).

In previous studies, ANK proteins were divided into multiple subfamilies according to the conserved domains (Becerra et al., 2004). The ANK-RF subgroup proteins contain the RING finger (RF) domain, which was first identified in the *Really Interesting New Gene* (Freemont et al., 1991). The RF domain, belonging to the zinc finger domain protein family, could bind to RNA, protein or lipid substrates (Elenbaas et al., 1996). A large number of RF-containing proteins have an E3 ligase role in ubiquitination reactions (Stone et al., 2005; Berrocal-Lobo et al., 2010) and the C3HC4 motif of RF domain is essential for conferring E3 ligase activity (Lorick et al., 1999). Rice XA21-binding protein 3 (XB3), an ANK-RF E3 ubiquitin ligase, is a substrate for the XA21 kinase and interacts with the XA21 kinase domain for full accumulation of the XA21 protein and for *XA21*-mediated immunity. Therefore, XB3 contributes to the stability of XA21 and is required for full accumulation of the XA21 protein in *XA21*-mediated rice immunity (Wang et al., 2006).

ANK-RF proteins functions in various biological processes in plant growth and development. The *Arabidopsis* ANK-RF protein AtXBAT32, an ubiquitin ligase, positively affected ethylene biosynthesis by degradation of the ethylene biosynthetic enzyme1-aminocyclopropane-1-carboxylate synthase 7 (Lyzenga et al., 2012), resulting in regulation of lateral root initiation (Nodzon et al., 2004; Prasad et al., 2010). Another ANK-RF protein AtXBAT35 participated in ubiquitin-mediated protein degradation, and played an important role in negatively regulating ethylene-mediated apical hook curvature in *Arabidopsis* (Carvalho et al., 2012). The overexpression of *LIANK*, a lily ANK-RF protein, resulted in pollen tube growing abnormally and its silencing impaired pollen germination and tube growth (Huang et al., 2006).

Recently, ANK-RF subfamily genes were proven to play diverse roles in the stress responses. A RING zinc finger ankyrin protein gene *AdZFP1* was isolated from drought-tolerant *Artemisia desertorum* and the transcript level of *AdZFP1* was strongly induced by drought, salt, cold, heat, and exogenous abscisic acid (ABA) treatments. Besides, overexpression of the *AdZFP1* gene enhanced drought tolerance in transgenic tobacco (Yang et al., 2008). The pepper ANK-RF gene *CaKR1* participates in various biotic and abiotic stresses, such as NaCl, cold, SA, ethylene, and pathogens infection. Overexpression of *CaKR1* enhances resistance to salt and oxidative stresses in tomato (Seong et al., 2007a). The potato ANK-RF gene *Star*, a putative E3 ubiquitin ligase gene, is involved in late blight resistance and organ development (Wu et al., 2009). The rice ANK-RF protein *OsXB3* plays a role in resistance against *Xanthomonas oryzae pv. Oryzae* (Wang et al., 2006).

Soybean (*Glycine max* L.), an important crop providing plant protein and oil, suffers from drought and salt damage with global climate change, especially in China. Previous studies characterized the *ANK* gene families in various plants (Becerra et al., 2004; Huang et al., 2009; Jiang et al., 2013; Yuan et al., 2013; Lopez-Ortiz et al., 2020). In this study, we identified 226 non-redundant soybean *ANK* genes, which were classified into nine subfamilies. An ANK-RF subfamily gene *GmANK114* was significantly induced by drought, salt, and exogenous ABA. We further investigated stress tolerance conferred by *GmANK114* in both *Arabidopsis* and soybean. The functional identification of *GmANK114* will be very helpful for further understanding how ANK proteins in soybean adapt to abiotic stresses.

MATERIALS AND METHODS

Identification of Soybean *ANK* Genes

We obtained the Hidden Markov Model (HMM) profile of the ANK domain (PF00023) from Pfam v29.0.[1] BLAST was used to identify putative *GmANK* with the ANK domain (PF00023) as a query against the Phytozome database (v12.1)[2] of soybean. All hits with expected values less than 1.0 were retrieved and redundant sequences were removed using BLASTclust.[3] Then, all candidate sequences that met the standards were analyzed manually in the Pfam database once more and were checked

[1]http://pfam.sanger.ac.uk

[2]https://phytozome.jgi.doe.gov/pz/portal.html

[3]http://toolkit.tuebingen.mpg.de/blastclust

using the SMART program (Letunic et al., 2009) for the purposes of eliminating any sequences not containing the ANK domain (Liu et al., 2016a). The ExPASy website was used to predict physio-chemical parameters of ANK proteins such as molecular weights (Mw) and theoretical isoelectric points (pI) (Artimo et al., 2012).

Phylogenetic Relationships and Classification of GmANKs

The phylogenetic relationships among ANKs were inferred using Clustal X with a gap opening penalty of 10 and a gap extension penalty of 0.1 (Thompson et al., 1997). A phylogenetic tree was constructed using the neighbor-joining method in MEGA 7 and bootstrap analysis was conducted using 1,000 replications (Tamura et al., 2011). Database tools in SMART were used to analyze their typical functional structure domains. The sample protein structures of each subfamily were drawn manually.

Gene Structure Prediction, Motif Analysis and Promoter Analysis

An exon-intron substructure map was produced by tools online GSDS 2.0 (Gene Structure Display Sever)[4] (Guo et al., 2007). The conserved domain motifs analyze of soybean ANK proteins were conducted by TBtools (Chen et al., 2020), according to the analyzed result from MEME Suite 5.1.1.[5] The motifs number were set for 10. The 2,000 bp region upstream of the initiation codon as the promoter region of the *GmANK-RFs* were selected to identify the *cis*-acting elements by submitting the promoter sequence to the PLACE[6] and PlantCARE[7] databases (Li et al., 2019).

Physical Mapping and Gene Duplication

All non-redundant *ANKs* were mapped on the 20 chromosomes on the basis of information in the soybean database using the MG2C website (MapGene2Chrom web v2)[8] (Liu et al., 2016b). Segmental and tandem duplication events were determined as previously described (Wang et al., 2016; Fan et al., 2019). Gene segmental duplications events were analyzed and visualized by Multiple Collinearity Scan toolkit (MCScanx)[9] and Circos-0.67 program[10] respectively, with a E-value for 10^{-10}. The tandem duplications were characterized as adjacent genes with a distance of less than 200 kb within neighboring intergenic region (Holub, 2001). Tandem duplications were manually marked on the physical map.

Gene Ontology Annotation

The functional annotation for the GmANK genes were conducted by Blast2GO[11] software according to the previous description, including the subsequent analysis of annotation results (Conesa and Gotz, 2008).

Expression Analysis of Soybean *ANK-RF* Genes

Transcriptome data was obtained from the Phytozome database to investigate the expression profile of 17 *ANK-RF* genes in different soybean tissues, including root, root hairs, stem, leaves, nodules, flower, and seed of soybean. These transcriptome data were obtained under normal growing conditions and were not subjected to any stress. RNA-seq data of various abiotic stresses were extracted from our previous research to study the expression of *ANK-RF* genes under drought, NaCl and ABA treatments (Shi et al., 2018). The RNA-seq data were obtained from three biological replicates. Tophat and cufflinks were used to analyze the RNA-seq expression, and the gene expressions were uniformed in fragments per kilobase million (FPKM). The expression of *ANK-RF* genes was extracted from the total expression data. The FPKM values of soybean *ANK-RF* genes in different tissues and under abiotic stress treatments (drought, NaCl and ABA) were shown in **Supplementary Tables 2, 3**. TBtools software was used to generate the heatmap (Chen et al., 2020).

Plant Materials and Stresses Treatment

Seeds of soybean variety Williams 82 were grown in a greenhouse at 28/20°C day/night temperatures, with a photoperiod of 14 h light/10 h dark and 60% relative humidity. For drought treatment, 16-day-old seedlings were placed on filter paper for the induction of rapid drought for 0, 1, 2, 4, 8, 12, and 24 h. For NaCl treatment, 16-day-old seedlings in soil watered with 200 mM NaCl solution. For ABA treatments, the seedlings were exposed to 100 μM ABA. Unstressed plants were maintained as control. After stress treatments, the seedlings were carefully harvested and immediately frozen with liquid nitrogen, and stored at −80°C until RNA isolation.

Wild-type (WT) and T3 transgenic seeds were used to evaluate the drought and salt tolerance. For germination assay, seeds were cultured in the medium with 6 or 9% (w/v) PEG 6000 and 75, 100, and 125 mM NaCl. After 3 days of vernalization, the seeds were transferred to normal conditions for germination. Seeds were considered to be germinated when radicles emerged from the seed coats. The percentage of germinated seeds was calculated based on the number of seedlings at 1, 2, 3, 4, 5, and 6 day. All the experiments were repeated three times.

Agrobacterium rhizogenes-Mediated Transformation of Soybean Hairy Roots

The open reading frame (ORF) of *GmANK114* was amplified and ligated into plant transformation vector pCAMBIA3301 driven by the CaMV35S promoter to generate the pCAMBIA3301-*GmANK114* overexpression vector. The recombinant vectors were introduced into *Agrobacterium rhizogenes* strain K599, and that was used to infect soybean cultivar Williams 82 cotyledonary node by injection as described previously (Kereszt et al., 2007). All experiments have three biological repetitions at least.

[4]http://gsds.cbi.pku.edu.cn/
[5]http://meme-suite.org/tools/meme
[6]http://www.dna.affrc.go.jp/PLACE/
[7]http://bioinformatics.psb.ugent.be/webtools/plantcare/html/
[8]http://mg2c.iask.in/mg2c_v2.0/
[9]http://chibba.pgml.uga.edu/mcscan2/
[10]http://circos.ca/
[11]http://www.blast2go.com

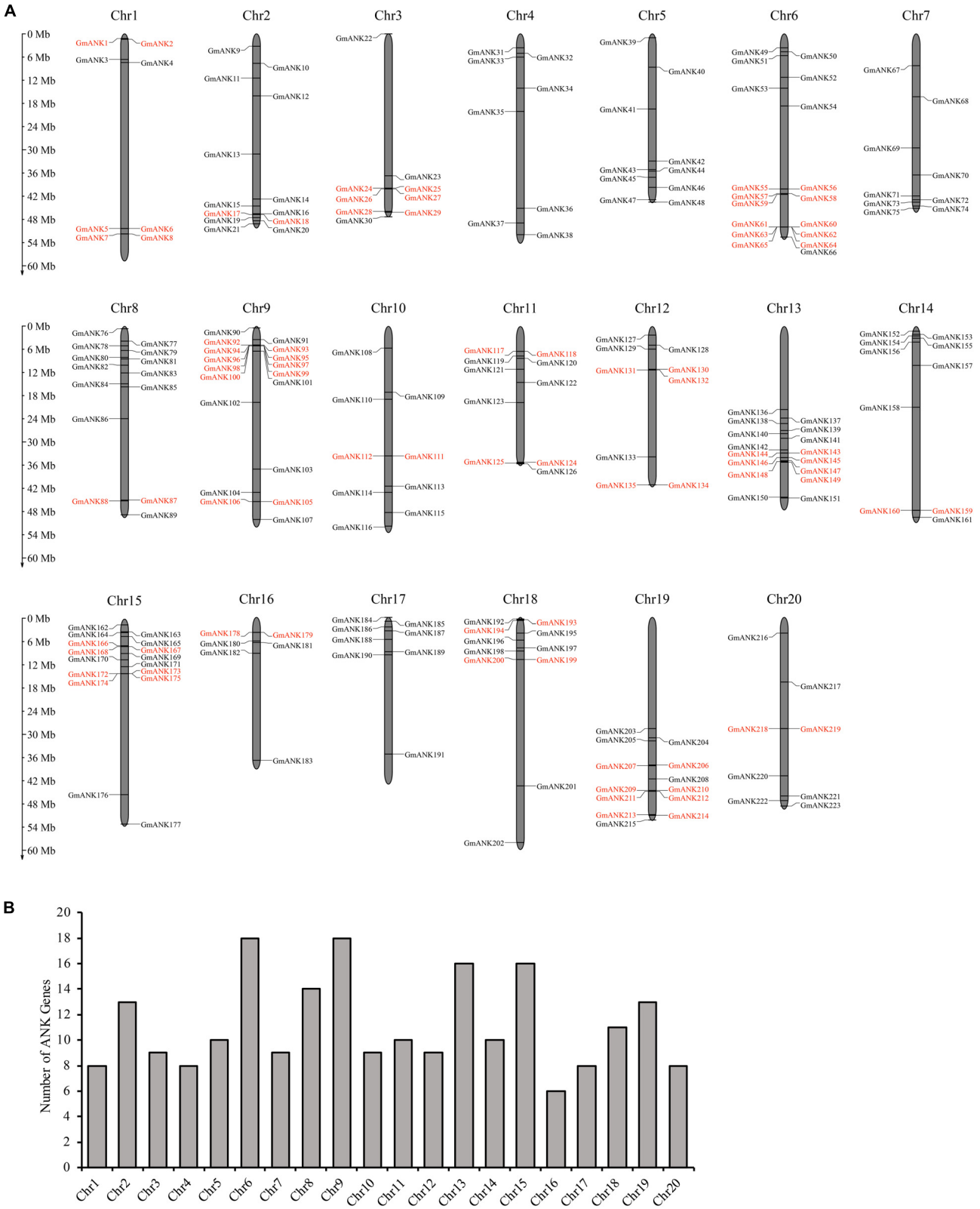

FIGURE 1 | Distribution of 223 *GmANK* genes on the soybean chromosomes. **(A)** The physical location of each member in soybean. The scale on the left is in megabases (Mb). The chromosome number (Chr1–Chr20) is indicated at the top of each chromosome. The tandem duplicated gene clusters are marked by the red rectangle. **(B)** The numbers of *ANK* genes were distributed on 20 chromosomes.

Measurements of Proline, MDA, H_2O_2, and O^{2-} Contents

Before measurements, the transgenic soybean hairy roots were subjected to drought or 200 mM NaCl stress for 5 days, after which the proline (Pro), malondialdehyde (MDA), H_2O_2, and O^{2-} contents of leaves were measured using the corresponding assay kit (Solarbio, Beijing, China) in accordance with the manufacturer's protocol. All measurements were repeated three times.

RNA Extraction and Quantitative Real-Time PCR

Total RNA was isolated using Trizol reagent (TaKaRa, Japan) and treated with RNase-free DNase I (TaKaRa, Japan) to remove genomic DNA contamination. The cDNA synthesis and reverse transcription-PCR were conducted using TransScript All-in One First-Strand cDNA Synthesis SuperMix for qPCR (TRANSGEN, China). Quantitative real-time PCR (qRT-PCR) was performed in three technical replicates using Super Real PreMix Plus (SYBR Green) (TIANGEN, China) with an Applied Biosystems® 7500 Real-Time PCR System. The soybean *CYP2* (Glyma.12g024700) gene was used for normalization (Zhang et al., 2019). The primers used for qRT-PCR are listed in **Supplementary Table 4**.

DAB and NBT Staining

The detached leaves of transgenic soybean were stained separately after stress treatment. For 3,3-diaminobenzidine (DAB) and nitroblue tetrazolium (NBT) staining, the samples were immersed in DAB or NBT solution (Solarbio, China) for 12 h and then transferred to 75% ethanol for decoloring until the leaves became white (Du et al., 2018).

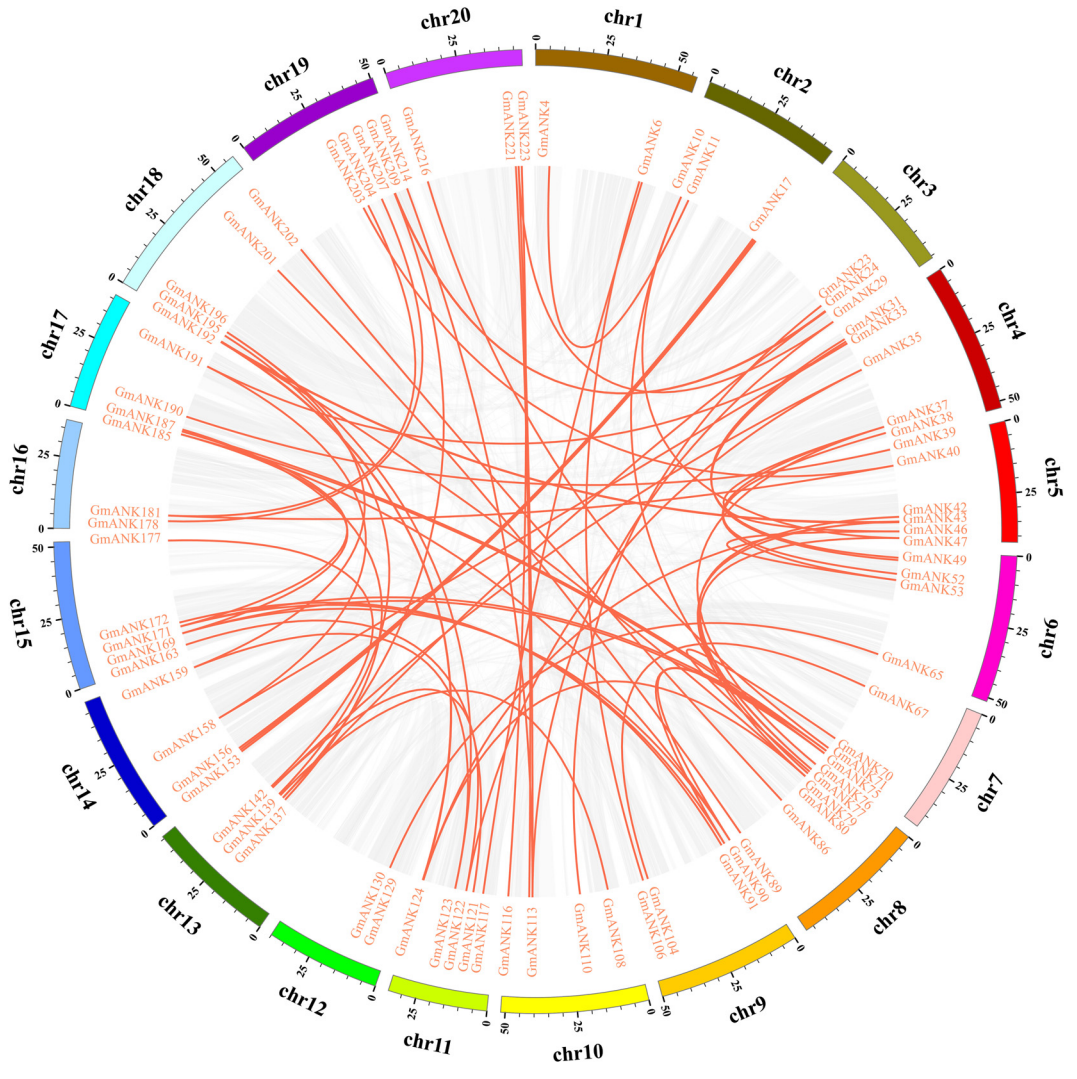

FIGURE 2 | Distribution of segmentally duplication *ANK* genes on soybean chromosomes. Gray lines indicate all synteny blocks in whole soybean genome, and red lines indicate duplicated *ANK* gene pairs.

Statistical Analysis

All experiments above were replicated three times independently. The values are shown as mean ± standard deviation (SD). ANOVA test was used for statistical analyses, and the signifcance was labeled $^{*}P < 0.05$; and $^{**}P < 0.01$.

RESULTS

Identification of Soybean *ANKs*

The ANK domain (PF00023) was used as a query and searched in several databases including Phytozome, NCBI, Pfam, and SMART, a total of 226 genes encoding ANK proteins were identified in soybean. Almost all the *GmANKs* contained introns. The number of introns in these genes ranged from 0 (*GmANK9*, *GmANK12* and *GmANK14*) to 21 (*GmANK53*) (**Supplementary Figure 1**). These results suggested that members of the *GmANK* family might be active and constantly evolving.

The size and physicochemical properties of *GmANKs* varied substantially. The length of GmANK proteins ranged from 133 (GmANK7) to 1,637 (GmANK122) amino acids. The molecular weights of GmANK proteins changed from 14,747.23 Da (GmANK7) to 179,852.44 Da (GmANK122). The characteristic features of GmANK protein sequences are summarized in **Supplementary Table 1**.

Chromosomal Location and Duplication Events Analysis

To determine the genomic distribution of *ANK* genes, chromosomal localization maps were constructed in soybean.

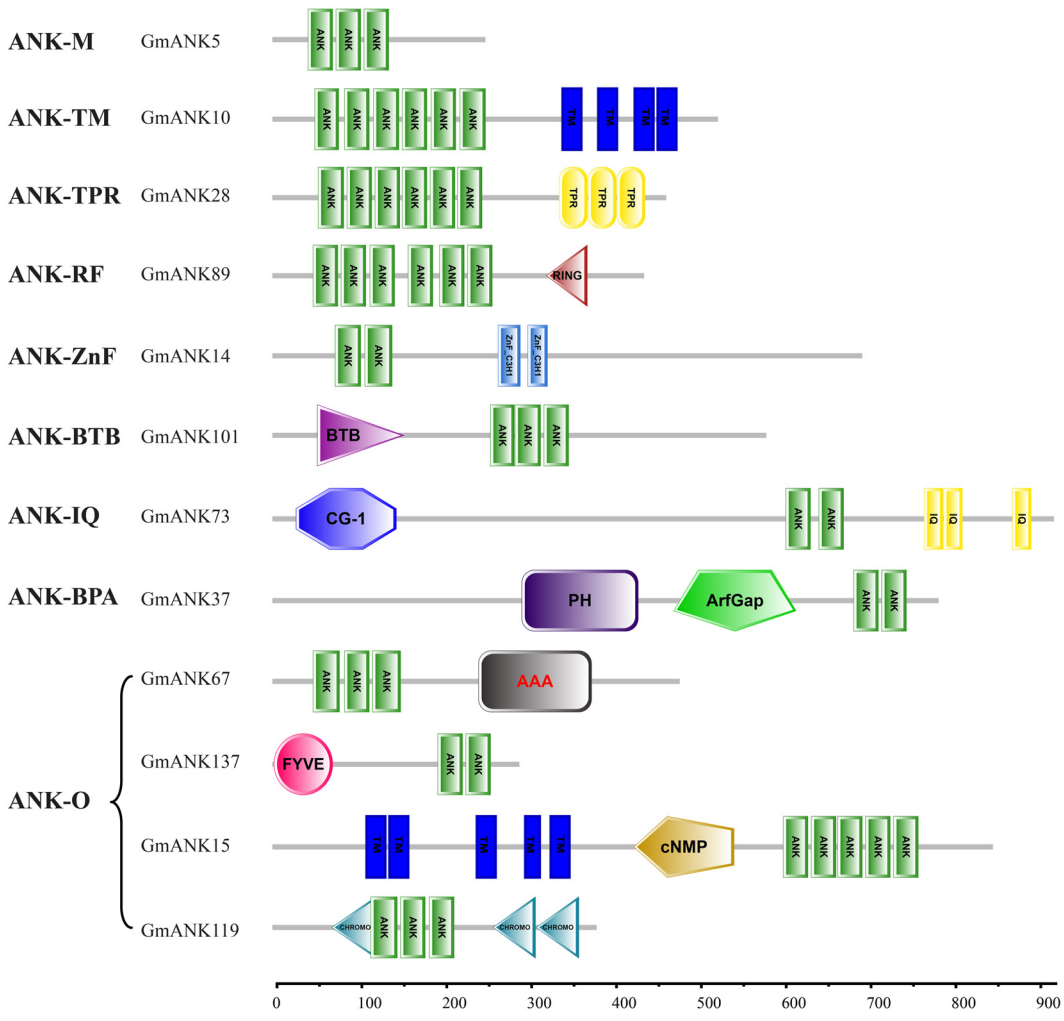

FIGURE 3 | Domain compositions of representative GmANK proteins from each subfamily. The subfamily name of each corresponding protein and gene ID of a representative protein of the family are given on the left. Different domains are indicated with different colors and abbreviations. The length, order and number of domains represent the actual situation in each protein. Domain abbreviations are: ANK, ankyrin repeat domain; TM, transmembrane; TPR, tetratricopeptide repeat domain; RING, ring finger domain; ZnF-C3H1, zinc finger; BTB, BTB/POZ domain; CG-1, calmodulin-binding transcription activator; IQ, calmodulin-binding domain; PH, pleckstrin homology domain; ArfGap, putative GTP-ase activating proteins for the small GTPase; AAA, ATPase family associated with various cellular activities; FYVE, FYVE zinc finger; cNMP, cyclic nucleotide-binding domain; CHROMO, chromatin organization modifier domain.

The precise position (in bp) of each *GmANK* gene on soybean chromosomes is detailed in **Supplementary Table 1**. In total, 223 of the 226 *GmANKs* on chromosomes revealed an uneven distribution in the genome. As shown in **Figure 1**, the number of genes per chromosome ranged from 6 to 18. Chromosomes 6 and 9 had the largest number of *GmANK* genes (18 members), followed by 16 *GmANK* genes on each of chromosomes 13 and 15, while low densities of *GmANK* genes were observed in chromosome 16 (six members).

To elucidate the conceivable mechanism of evolution of *GmANKs*, tandem and segmental duplication events were analyzed. A total of 81 *GmANK* genes were involved in tandem duplications consisting of 34 clusters (**Figure 1**). The distance between these genes ranged from 2.8 to 180.4 kb and five tandemly duplicated *GmANK* sets contained more than three genes. Among them, two tandemly duplicated *GmANK* sets contained three members (*GmANK57/58/59*, *GmANK166/167/168*), one tandemly duplicated *GmANK* set contained four members (*GmANK172/173/174/175*), one tandemly duplicated *GmANK* set contained six members (*GmANK57/58/59/166/167/168*), the maximum tandemly duplicated set contained nine members (*GmANK92/93/94/95/96/97/98/99/100*) and the other tandem duplications contained only two genes. Besides tandem duplication events, we further observed that up to 46% (104 out of 226) of *GmANK* genes were involved in segmental duplication and 36 genes were duplicated more than twice (**Figure 2**). In general, these results show that tandem and segmental duplication may be one of the main contributing factors for the large expansion of *ANK* genes in the soybean genome.

Classification of GmANKs

Based on the domain compositions (Huang et al., 2009), the 226 GmANK proteins were classified into nine subfamilies according to the results of SMART searches (**Figure 3**). In total, 78 members that contained only one ANK domain belonged to subfamily ANK-M, while the remaining 148 proteins contained additional typical domains. Transmembrane domains were found in 78 GmANKs, which were identified as the ANK-TM subfamily. Seventeen members were confirmed as subfamily ANK-RF (ring finger). ANK-BTB subfamily (four members) had broad-complex, tramtrack and bric a brac domains. The other subfamilies included seven members with BAR, PH and ArfGap domains (ANK-BPA subfamily), two with tetratricopeptide repeat domains (ANK-TPR subfamily), 13 with zinc-finger domain (ANK-ZnF), and 11 contained conserved CG-1 (Calmodulin-binding Transcription Activator) and IQ (Calmodulin-binding motif) domains (ANK-IQ subfamily). ANK-O subfamily (16 members) contained other domains including FYVE, AAA, cNMP and CHROMO (**Table 1**).

Phylogenetic Analysis of GmANK Proteins and Conserved Motif Analysis

To understand the evolutionary relationships of GmANKs, an unrooted phylogenetic tree was constructed using the neighbor-joining method. The phylogenetic analysis categorized all GmANKs into six discrete groups (Group I–VI) comprising 41, 52, 50, 28, 16, and 39 proteins, respectively (**Figure 4**). Classification based on the phylogenetic tree and domain composition were consistent in general but not quite, such as for GmANK122 and GmANK142. Phylogenetic analysis reveals well-supported bootstrap values between GmANK122 and GmANK142 (Group III). However, GmANK122 has a RING domain (ANK-RF) but GmANK142 belongs to the ANK-M subfamily.

To better understand the function of each GmANKs subgroups, the motifs analysis of GmANKs family were conducted using MEME and TBtools software with default parameters (**Supplementary Figure 2**). The sizes of these conserved motifs ranged from 15 to 50 amino acids (**Table 2**). In general, the motifs structures in each subgroup of GmANK family were highly consistent and different combination of motifs represented different subgroups of GmANK family according to the analysis results of **Supplementary Figure 2**, which may account for the special biological functions of each groups and further confirmed their phylogenetic relationships.

TABLE 1 | Number of *ANK* genes in different subgroups classified by the domains that they contained.

Subfamily	Detail information	Soybean	Maize	Rice	*Arabidopsis*	Tomato
ANK-M	Proteins with only ankyrin repeat	78	30	73	18	26
ANK-TM	Ankyrin-transmembrane proteins	78	15	37	40	25
ANK-TPR	Protein with tetratricopeptide repeats	2	2	22	1	4
ANK-RF	Proteins with Ring finger proteins	17	9	9	5	7
ANK-ZnF	Proteins with Zinc-finger proteins	13	3	7	6	8
ANK-BTB	Proteins with BTB domain	4	2	6	7	7
ANK-IQ	Proteins with calmodulin biding motif-containing protein	11	1	4	4	7
ANK-PK	Proteins with protein kinases	-	4	4	7	9
ANK-BPA	Proteins with BAR, PH and ArfGTPase-activating domain	7	2	3	4	4
ANK-IT	Protein with K^+ channel protein	-	-	-	6	7
ANK-GPCR	Protein with GPCR-chaperone1 domain	-	-	-	-	4
ANK-MS	Protein with motile-sperm domain	-	-	1	-	4
ANK-O	Proteins with other domains	16	3	9	7	15
Total		226	71	175	105	130

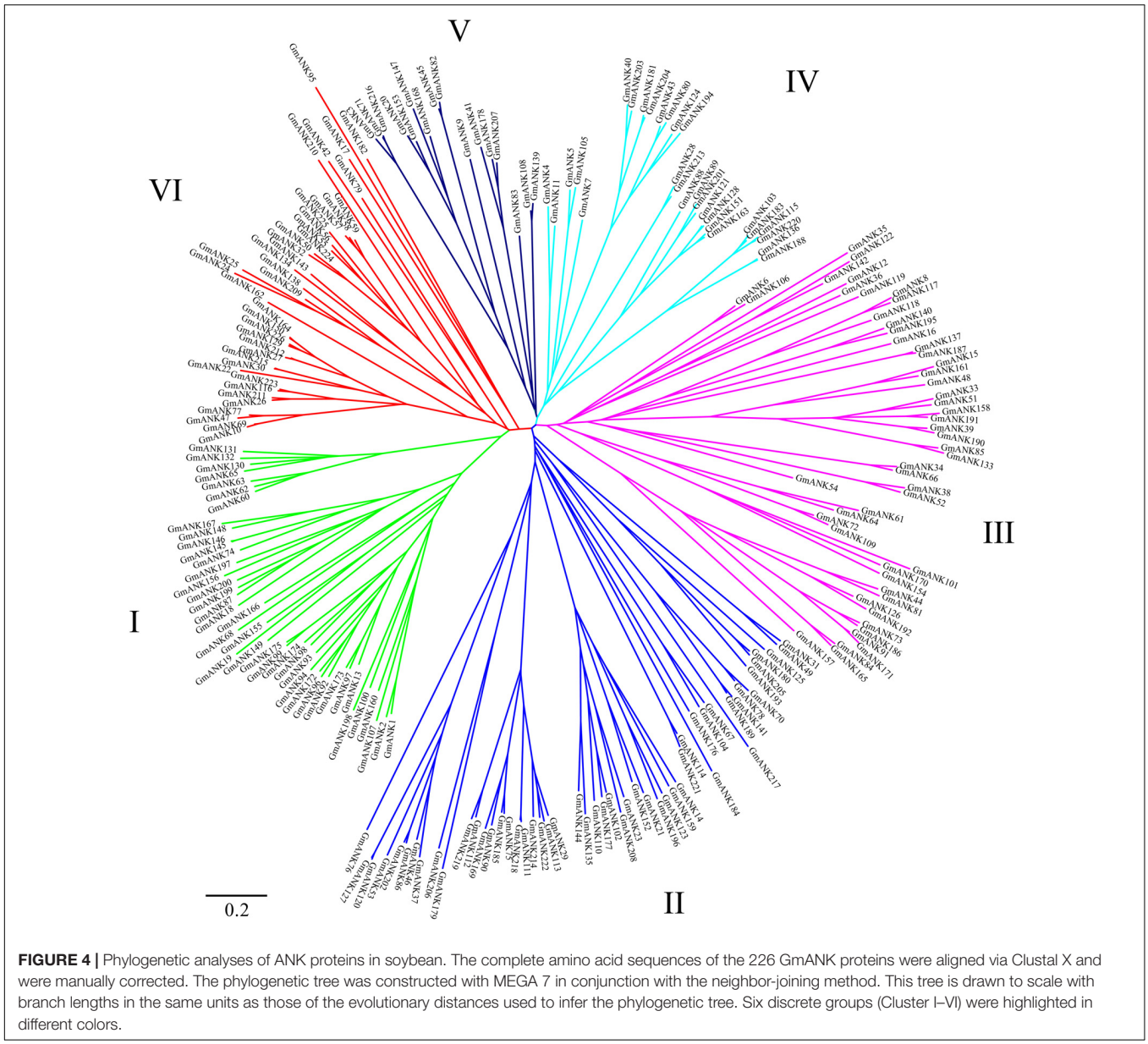

FIGURE 4 | Phylogenetic analyses of ANK proteins in soybean. The complete amino acid sequences of the 226 GmANK proteins were aligned via Clustal X and were manually corrected. The phylogenetic tree was constructed with MEGA 7 in conjunction with the neighbor-joining method. This tree is drawn to scale with branch lengths in the same units as those of the evolutionary distances used to infer the phylogenetic tree. Six discrete groups (Cluster I–VI) were highlighted in different colors.

TABLE 2 | List of the identified motifs of GmANK proteins.

motifs	BEST POSSIBLE MATCH	width
1	IRDSDGRTPLHJAARRGHVEV	21
2	KNTANSCTVVATLIATVAFAAAFTVPGGV	29
3	GNTALHLAVRKGHVEVVKLLL	21
4	FRMYSFKVRPCSRAYSHDWTECPFVHPGENARRRDPRKYHYSCVPCPEFR	50
5	LFISLAVVVVQTSVVVIETKAKKQVVAVINKLMWLACVCIS	41
6	MFLSILTSRYAEEDFLKSLPLKLJFGLVTLFISIASMMVAF	41
7	ISGAALQMQWELKWFEEVKKJMPPSFIERKNSDGKTAREJFTEEHKELLK	50
8	TPLHVAAANGHVEVV	15
9	ELKQTVSDIKHEVHSQLEQTRQTRKRVQGIAKEJKKLHREG	41
10	GRTALHVAVRGGHSSVVKLJL	15

Gene Ontology Annotation

To better understand the possible biological function of *GmANK* genes, Blast2GO software were used to performed the Gene Ontology (GO) annotation (**Supplementary Figure 3**). According to the GO annotation results, there were a total of 62 GmANK proteins were annotated in various biological processes, including signal transduction, regulation of membrane potential, positive regulation of transcription from RNA polymerase II promoter, regulation of proteolysis and S-adenosylmethionine metabolic process. There were 59 GmANK proteins were predicted to be related to molecular functions, such as transcriptional activator activity, RNA polymerase II core promoter proximal region sequence-specific binding, voltage-gated potassium channel activity, ubiquitin protein ligase binding, zinc ion binding and metal ion binding. Finally, 138 GmANK proteins were belonged to cellular components, which were located to membrane, integral component of membrane, cytoplasm, integral component of plasma membrane and ubiquitin ligase complex respectively. With the help of GO analysis results, we could primarily confirm the functional characteristics of GmANK proteins, like biological processes, molecular functions and cellular components, and will be very useful for its future functional researches in soybean.

GmANK-RFs Promoters Contain Various Stress-Responsive Elements

Promoter sequences were analyzed by PlantCARE and some *cis*-acting elements were revealed in all *ANK-RFs* promotor regions, such as ABRE (response to ABA), MYB (response to drought), MYB-like (response to drought), MBS (involvement in drought-inducibility), MYC (response to drought and salt) and LTR (response to low-temperature). In addition, an auxin-responsive element (TGA-element) and a MeJA-responsive element (CGTCA-motif and TGACG-motif) were also identified (**Table 3**). This result indicated that the *GmANK-RFs* genes may be involved in abiotic stresses, especially in drought.

Tissue-Specific Expression Patterns of *GmANK-RF* Genes

The expression abundance among different tissues and development stages may show diversity of different genes to adapt to various biological processes. To gain insights into the expression of *ANK-RF* genes in seven soybean tissues and organs, gene chip data were downloaded using publicly available RNA-seq data from the soybean genome database (**Supplementary Table 2**). The heatmap showed that 17 members of the ANK-RF subfamily were expressed in root, root hairs, stem, leaves, nodules, flowers and seeds (**Figure 5**). Among these *ANK-RF* genes, *GmANK89* and *GmANK201* had the highest expression in all tissues and organs, while *GmANK88* was only weakly expressed in root and *GmANK121* was slightly expressed in root hairs. Additionally, the expression patterns were different between *ANK-RF* genes in the same tissues. For example, the expression of *GmANK151* and *GmANK63* were at the highest level in stem, but *GmANK220* was expressed most strongly in flowers; *GmANK136* transcription had higher enrichment in root and *GmANK163* had stronger accumulation in root hairs. These transcriptional patterns suggested that the expression of these genes might be governed by diverse and potentially tissue-dependent regulatory mechanisms. *GmANK89* and *GmANK201* had extremely high expression in all tissues indicating that they may play specific roles in growth and development of soybean.

GmANK-RF Genes Were Involved in Various Abiotic Stresses

Extensive studies have shown that ANK-RF subfamily genes may be involved in responding to various abiotic stresses in some species (Nodzon et al., 2004; Seong et al., 2007a,b; Yang et al., 2008). According to our previous research, RNA-seq was performed using soybean seedlings under drought, NaCl and ABA treatments (Shi et al., 2018). RNA-seq data indicated that 17 *GmANK-RFs* responded differently to drought, NaCl, and ABA treatments (**Figure 6**). Among them, several genes induced expressed under drought stress, such as *GmANK103*, *GmANK114*, *GmANK136*, and *GmANK220*. *GmANK114* were also specifically induced by NaCl. Under ABA stress, *GmANK183* and *GmANK188* showed down-regulated expression.

Based on the results of RNA-seq, we examined the expression patterns of 17 *GmANK-RF* genes during various abiotic stresses and phytohormone treatments by qRT-PCR (**Figure 7**). Quantitative real-time PCR results were roughly consistent with RNA-seq data. The expression levels of candidate genes varied in response to drought, NaCl, and ABA for 1, 2, 4, 8, 12, 24 h compared to untreated control samples. Under drought treatment, the expression of all *GmANK-RF* genes was increased, especially *GmANK103*, *GmANK114*, *GmANK201*, and *GmANK221*, which were induced more than 30-fold. For salt treatment, the peaks of *GmANK114*, *GmANK151*, and *GmANK163* transcription were increased to 15-fold. *GmANK89*, *GmANK114*, *GmANK151*, *GmANK163*, and *GmANK221* were also induced by ABA, however, the level of *GmANK115*, *GmANK121*, *GmANK128*, and *GmANK220* barely changed compared with 0 h. Through our transcriptional analysis of *GmANK-RF* genes, we found that the expression of *GmANK114* was significantly up-regulated under drought, salt, and ABA stress conditions (**Figure 7**). Therefore, *GmANK114* was selected for further verification.

GmANK114 Conferred Drought and Salt Tolerance in *Arabidopsis*

GmANK114 under the control of CaMV35S were transformed into *Arabidopsis* plants and T3 transgenic seeds were selected for tolerance identification. For drought treatment, the transgenic and WT seeds were germinated on Murashige and Skoog (MS) medium containing various concentrations of PEG6000 (**Figure 8A**). The transgenic and WT plants had no significant differences under the standard conditions in growth and morphology (**Figure 8B**), suggesting that over-expression of *GmANK114* genes might not affect plant growth and development under normal conditions. However, the germination percentage of transgenic plants was higher than the wild type in the presence of 6 and 9% PEG (**Figures 8C,D**). In

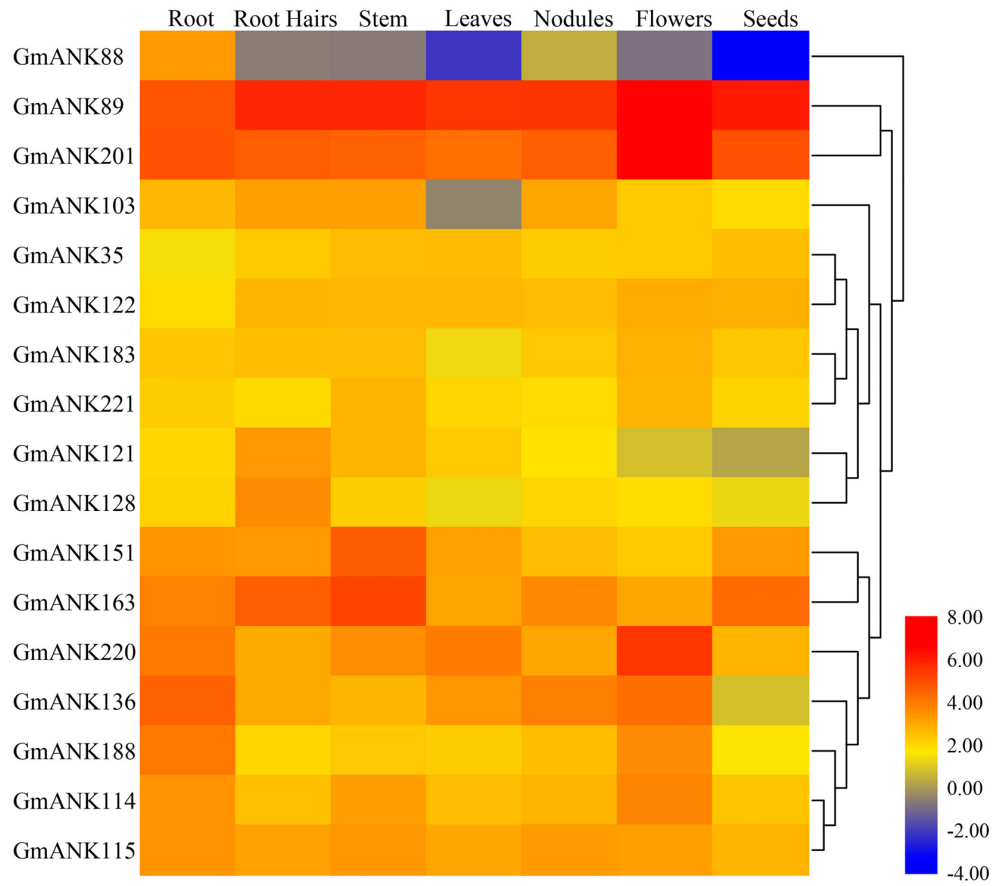

FIGURE 5 | Heat map of expression profiles (in log2-based FPKM) of soybean *ANK-RF* subgroup genes in different tissues (root, root hairs, stem, leaf, nodules, flower and seed). The gene names are on the left and the tissue names are on the top of the figure, and the expression abundance of each transcript is represented by the color bar: Red, higher expression; blue, lower expression.

growth medium with 9% PEG, 51.7, 48.9, and 46.2% of seeds germinated from three transgenic lines whereas only 40.1% of wild type germinated within 3 days (**Figure 8D**).

To further investigate the role of *GmANK114* under high salt, we observed the germination of overexpression *GmANK114* transgenic *Arabidopsis* seeds grown on medium containing various salt concentrations. For the germination assay, seeds of transgenic lines and WT were germinated on 75, 100, and 125 mM NaCl (**Figure 9A**), and the germination rates of both WT and transgenic seeds were determined. There was no difference in germination rate between transgenic lines and WT seeds in MS medium (**Figure 9B**), but the germination time and the germination rate in transgenic lines was earlier and higher than that in WT when treated with NaCl, especially for 125 mM NaCl (**Figures 9C–E**).

GmANK114 Improved Drought and Salt Tolerance in Transgenic Soybean Hairy Roots

The function of *GmANK114* in drought and salt tolerance was further investigated by performing similar abiotic stress assays in *Agrobacterium rhizogenes*-mediated soybean hairy roots. Quantitative real-time PCR analysis showed that the expression level of *GmANK114* was significantly higher in hairy roots overexpressing *GmANK114* (OE) compared with the empty vector (3301) control (**Figure 10C**). For drought treatment, all hairy root seedlings including control grew in soil with no water for 2 weeks, and then rewatered for one week. Morphologically, no significant differences were observed for all experimental plants under normal growth conditions. Drought treatment caused obvious differences in growth and physiology between *GmANK114* overexpression lines and 3301-control. The leaves of all hairy root plants gradually yellowed and wilted with the drought treatment going on, but the control was more sensitive compared with the plants carrying the *GmANK114* under drought treatment after 7 days (**Figure 10A**). After rewatered for 7 days, 66.7% of the transgenic plants were still alive, while the control plants had a survival rate of only 22.2% (**Figure 10D**). The same phenomenon occurred with NaCl treatment and the survival rate in transgenic hairy roots was higher than that in control (**Figures 11A,C**).

In order to analyze the mechanism in improving drought resistance of *GmANK114*, MDA and Pro contents were

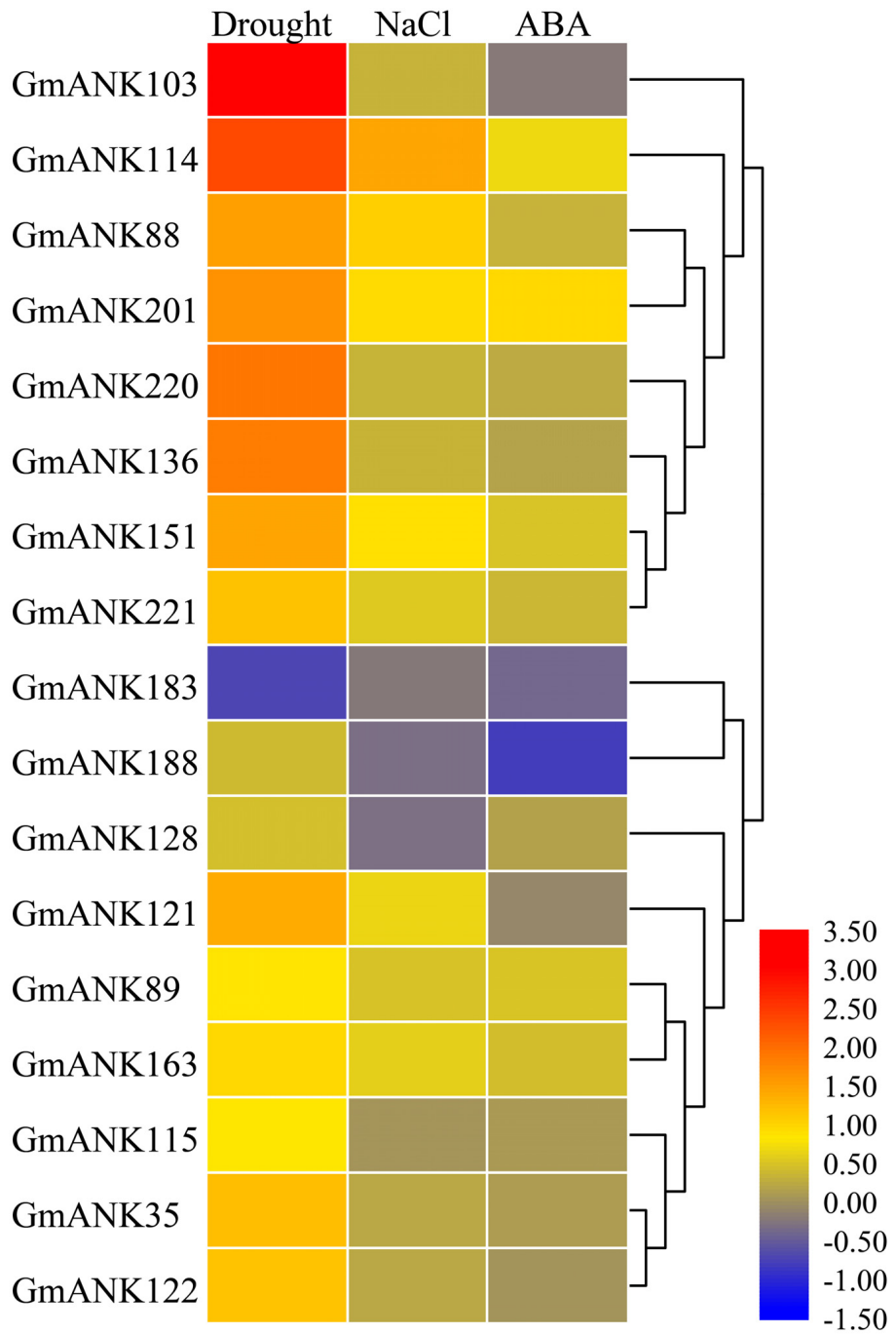

FIGURE 6 | Transcriptome analysis-based soybean RNA sequencing data under drought, NaCl, and ABA. The expression abundance of each transcript is represented by the color bar: Red, higher expression; blue, lower expression.

determined under normal growth and stress conditions. Under normal growth conditions, the MDA content, which were 31.5 and 29.2 nmol/g in transgenic lines and 3301, respectively, did not differ among all plants. While under drought conditions, the MDA content in transgenic soybean was 45.2 nmol/g, significantly lower than that in control (59.3 nmol/g) (**Figure 10E**). The same results were obtained with salt treatment: the MDA contents in transgenic hairy root and CK were 30.9 and 48.4 nmol/g, respectively (**Figure 11D**). Under both drought and salt treatments, the Pro content in transgenic lines was higher than that in CK. By contrast, there was no significant difference in the Pro contents between transgenic lines and control under normal condition (**Figures 10F**, **11E**).

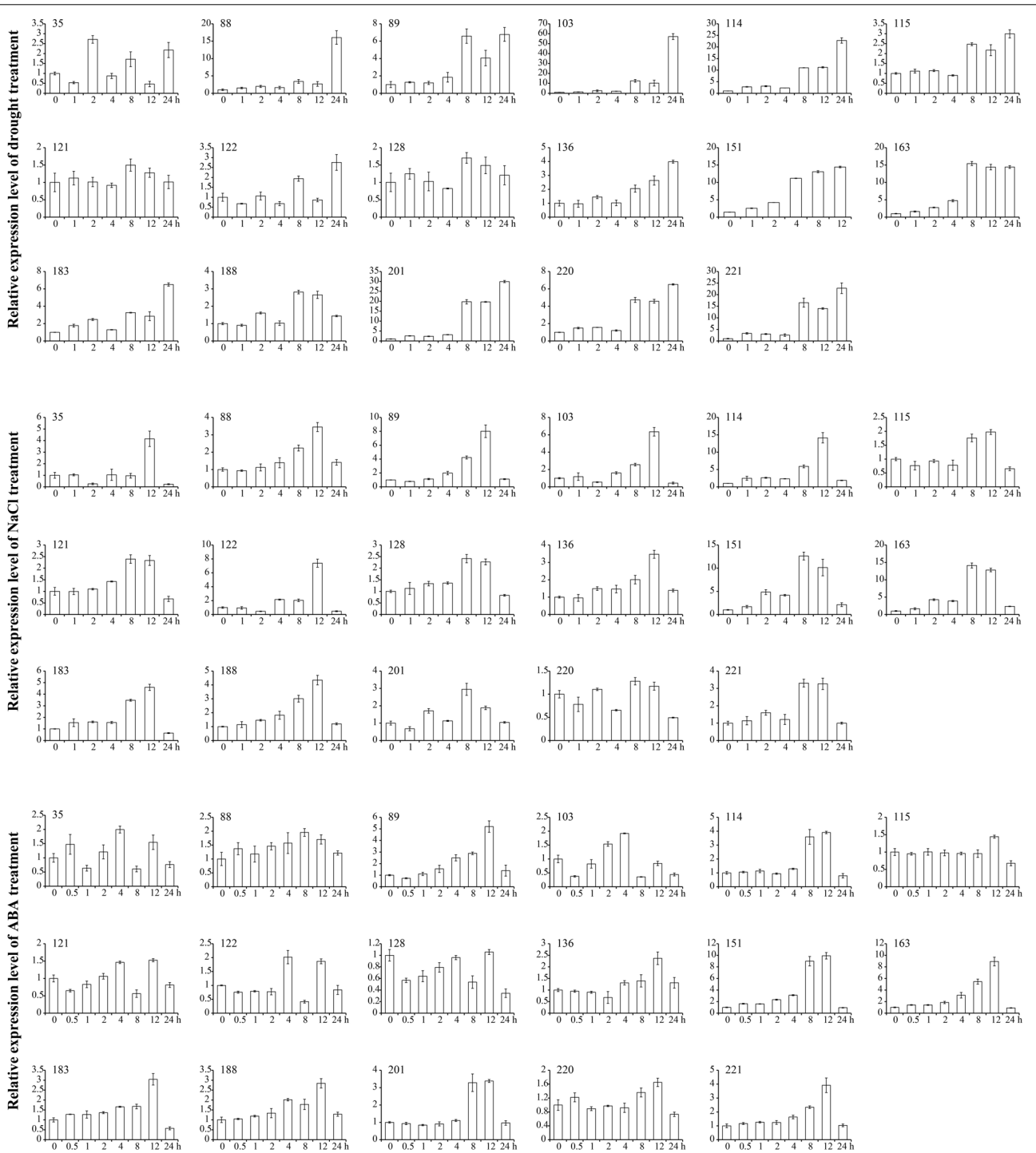

FIGURE 7 | qRT-PCR analysis of 17 soybean *ANK-RF* genes under drought, NaCl and ABA treatments. The expression levels were normalized to that of *CYP2*. The mean and SD calculated from three biological replicates.

Abiotic stress leads to the accumulation of reactive oxygen species (ROS), which can affect plant growth and development. Soybean leaves were stained with DAB and NBT to detect hydrogen peroxide (H_2O_2) and superoxide (O^{2-}) contents in 3301 and OE. Under normal growth condition, no significant difference was observed in all plant leaves between the 3301-control and *GmANK114*-OE. However, the color depth of the transgenic hairy root leaves was significantly lower than that of the 3301 plants under drought and salt treatments (**Figures 10B**, **11B**). The contents of O^{2-} and H_2O_2 in leaves

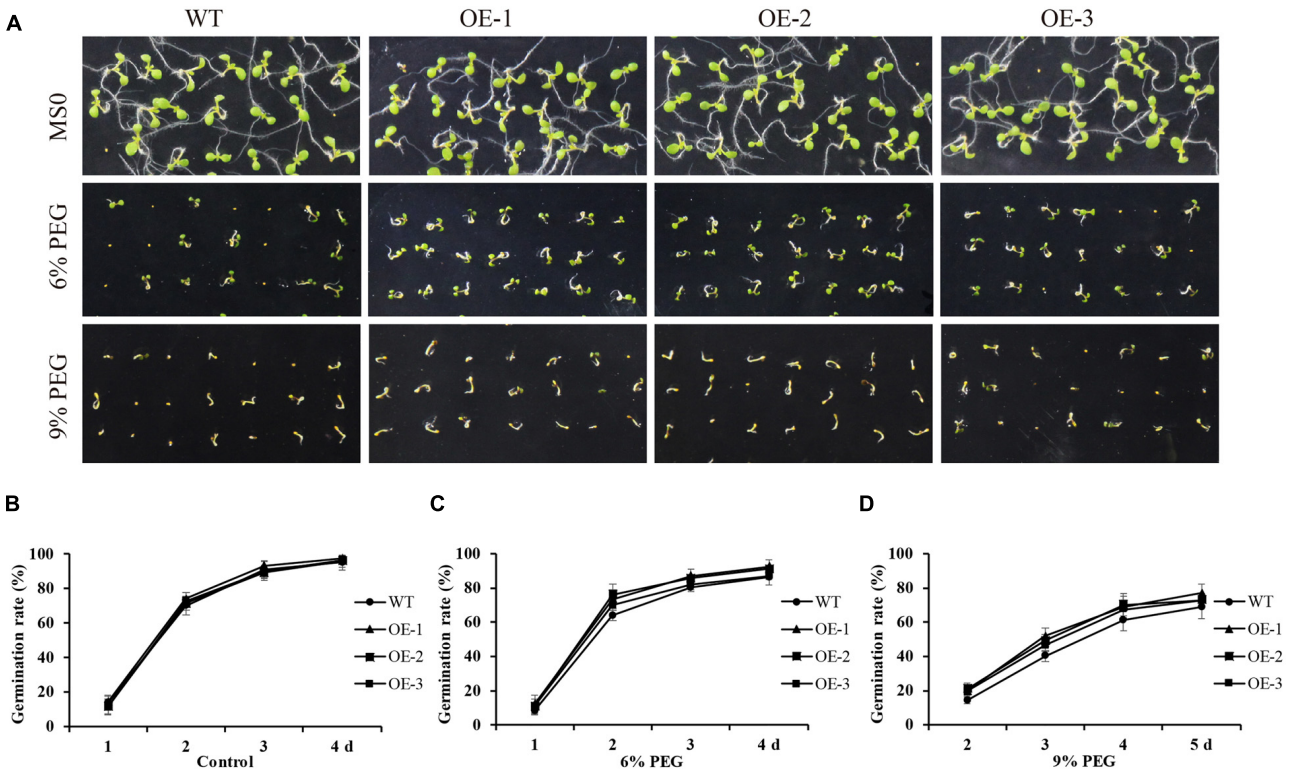

FIGURE 8 | Overexpression of *GmANK114* enhanced seed germination rates under PEG6000 treatment. **(A)** Seed germination analysis of different lines seeds under 6% and 9% PEG6000 to simulated drought treatment. **(B–D)** Seed germination rates of WT and *GmANK114* transgenic *Arabidopsis* seeds at different time points. Date for each time point are means of three independent replicates.

were also measured and the results were consistent with the staining of DAB and NBT. Meanwhile, we found that the leaves of overexpressed *GmANK114* plants produced lower levels of free oxygen radicals with drought and NaCl treatments (**Figures 10G,H**, **11F,G**). These results indicated that *GmANK114* positively regulated tolerance to drought and salt stresses in transgenic soybean hairy roots.

GmANK114 Activated Transcripts of Stress-Responsive Genes in Soybean

To investigate the possible tolerance mechanisms, several drought- and salt-related genes were analyzed in transgenic soybean hairy roots under normal and stress conditions (**Figure 12**). When grown in normal conditions, we found that there were no significant differences in the expression level of these genes between 3301 and *GmANK114* OE lines by qRT-PCR. Under drought condition, the expression of *bZIP1* (Gao et al., 2011) had no clear difference, whereas transcript levels of the other genes in OE lines were higher than that in the 3301 control, including *WRKY13* (Zhou et al., 2008), *NAC11* (Hao et al., 2011), *DREB2* (Chen et al., 2007), *MYB84* (Wang et al., 2017), and *bZIP44* (Liao et al., 2008). Similarly, overexpression of *GmANK114* regulated transcripts of *WRKY13*, *NAC11*, *DREB2*, *MYB84*, and *bZIP44* under salt stress. These results indicated that *GmANK114* may be a key signaling molecule regulating plant drought and salt responses.

DISCUSSION

Drought and salt are the important factors that seriously affect the production and quality for soybean, especially for China which possess a population base. The ANK protein containing several conserved ankyrin repeats (2 to over 20) are important connexins protein that links membrane proteins and signaling molecules to the components of the underlying cytoskeleton (Li and Chye, 2004; Voronin and Kiseleva, 2008; Cunha and Mohler, 2009). ANK protein plays a key role in various cellular processes, participates in plant growth, development, intracellular protein transport, signal transduction, and stress responses (Wu et al., 2009; Brestic et al., 2015; Popescu et al., 2017). The study on the function of ANK protein will help to elucidate the mechanism that plants respond to environmental stresses, and provide the theoretical basis for environmental adaptation in plants.

Recently, the number of ANK proteins have been found is 105, 175, 130, and 71 in *Arabidopsis*, rice, tomato, and maize, respectively (Becerra et al., 2004; Huang et al., 2009; Jiang et al., 2013; Yuan et al., 2013). Although, it has been previously reported that 162 ankyrin repeats genes

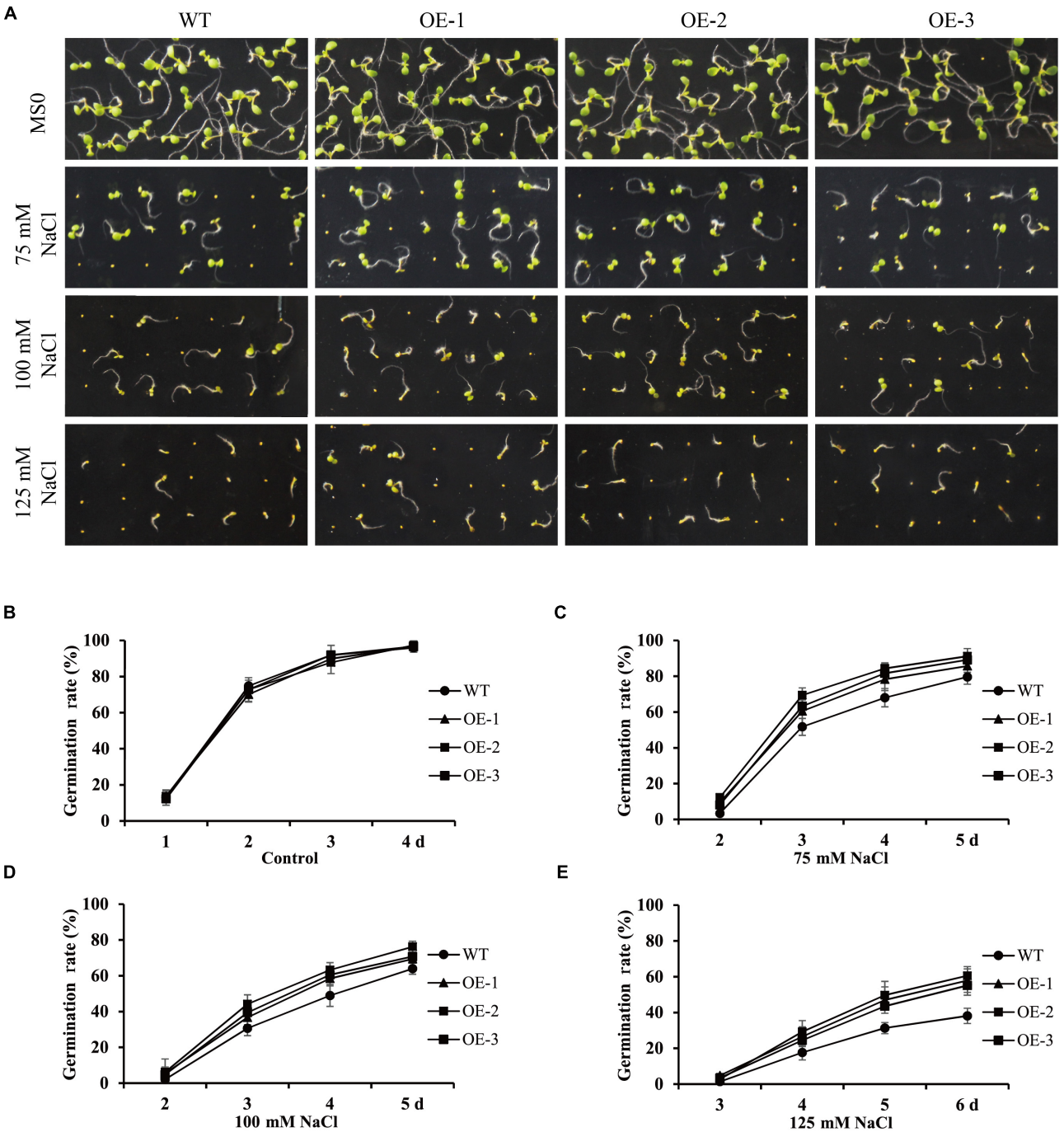

FIGURE 9 | Germination rates of seeds in the presence or absence of NaCl in transgenic *Arabidopsis*. Values are means from three experiments. **(A)** Seed germination analysis of different lines seeds under 75, 100 and 125 mM NaCl to simulated salt treatment. **(B–E)** Seed germination rates of WT and *GmANK114* transgenic *Arabidopsis* seeds at different time points. Date for each time point are means of three independent replicates. The error bars indicate SD.

were found in soybean (Zhang et al., 2016), we identified 226 *ANK* genes in soybean and classified them into nine subfamilies. This difference maybe resulted from constantly updated in soybean genome database in recent years. The same subfamilies were found in *Arabidopsis*, rice, maize and soybean based on the domain compositions (**Table 1**), we inferred that these kinds of subfamilies were relatively conserved and they will take the similar functions in plants. The ANK-GPCR subfamily (protein with GPCR-chaperone1 domain) only found in tomato, but not in *Arabidopsis*, rice, maize and soybeans. Due to the differences in morphological structure, lifestyle and growth environment of plants evolution, some

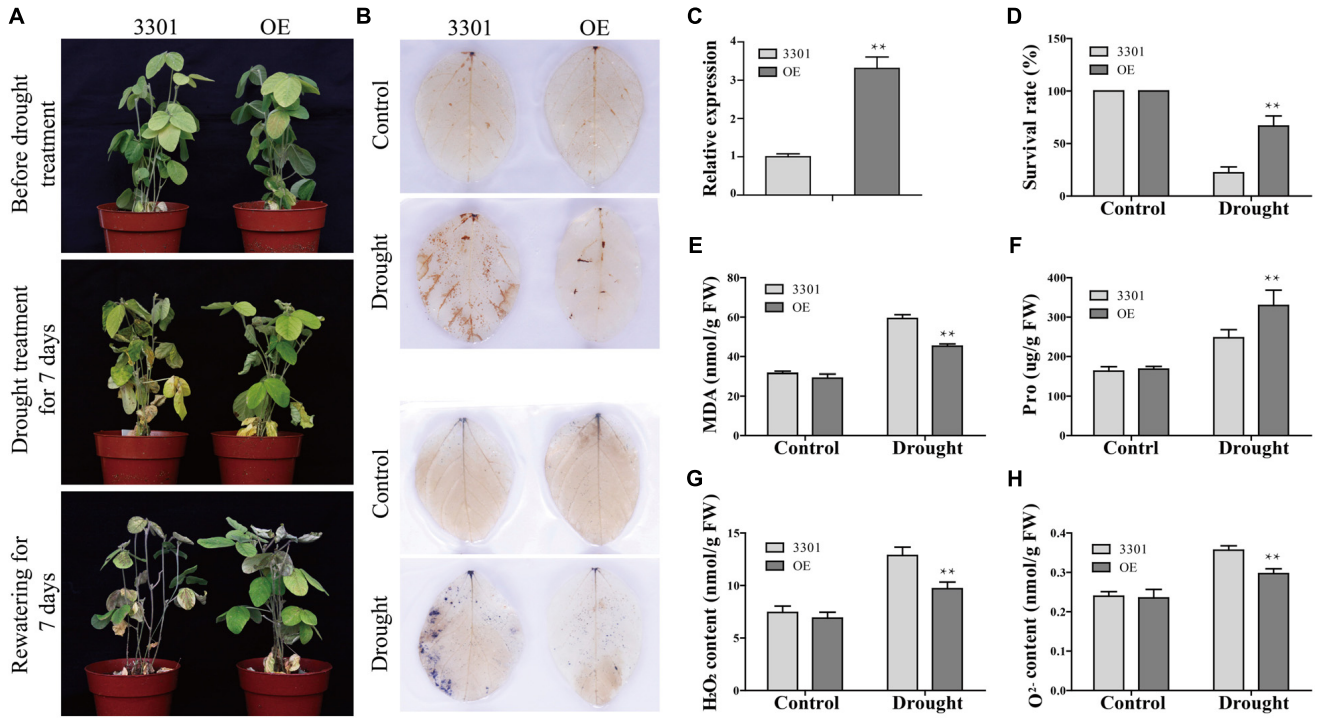

FIGURE 10 | *GmANK114* improves drought stress tolerance in transgenic soybean hairy roots. **(A)** Phenotypes of *GmANK114*-overexpression and 3301-control transgenic soybean plants under before and after drought treatment. **(B)** DAB (top) and NBT (bottom) staining of OE and 3301 plant leaves under drought treatments. **(C)** Relative *GmANK114* expression in hairy roots of overexpressing *GmANK114* and control as shown by qRT-PCR. **(D)** Survival rate of normal and drought-stressed plants. **(E)** MDA and **(F)** proline content were detected in OE and 3301 plants under drought or normal growth condition. **(G)**The content of H_2O_2 and **(H)** O^{2-} in the leaves of *GmANK114*-OE and 3301-control plants after drought or normal condition for one week. The data were means ± SDs of three experiments. ANOVA test demonstrated that OE were significant differences (*$P < 0.05$ and **$P < 0.01$) compared with the corresponding controls.

conserved subfamily genes have been retained to exercise the common physiological functions of plants, and specific genes have been developed to meet their own functional needs. ANK-GPCR subfamily genes may perform specific functions in tomato.

Several *ANK* genes may participate in responses to biotic and abiotic stresses. The expression of tobacco *NEIP2* was induced in the first few hours by treatment with salt and ethylene and further enhances plant performance under salt and oxidative stresses (Cao et al., 2015). ANK domain are crucial for YrU1 resistance to stripe rust in wheat (Wang et al., 2020). Based on this evidence, it was speculated that the soybean *ANK* genes probably involved in biotic and abiotic stress responses.

When plants are subjected to environmental stress, the second messenger perceives the stimulus in the environment and then modulates intracellular Ca^{2+} levels. The change of Ca^{2+} concentration often initiates a protein phosphorylation cascade that finally transfers to transcription factors controlling specific stress-regulated genes (Xiong et al., 2002). Transcription factors regulate the expression of target genes by binding to downstream gene promoters, thereby enabling plants to adapt to changes in the external environment. *ANK-RFs* were previously reported to be related to pathogen defense, plant growth and development, such as *XA21* and *XB3* (Wang et al., 2006). In this study, multiple *cis*-elements were found in the promoter region of *GmANK-RF* genes, including MeJA-responsive element (CGTCA-motif and TGACG-motif), which showed that *GmANK-RF* genes could function in defense responses. In addition, a number of stress response elements were also identified in the *ANK-RF* genes promoter region, such as drought response element MYB, MYB-like, MBS, salt response element MYC, low temperature element LTR, and ABA response element ABRE (**Table 3**). This indicates that *GmANK-RFs* might participate in multiple abiotic and biotic stress responses.

In the present study, the soybean *ANK-RF* gene *GmANK114* was shown to improve drought and salt tolerance in plants (**Figures 10**, **11**). Proline functions in lowering the cellular osmotic potential and restoring intracellular solute concentrations, which prevents water loss from cells (Cui et al., 2018). MDA can inhibit the activity of cellular protective enzymes and reduce antioxidant content (Del Rio et al., 2005). When the enzyme and membrane system of plant tissues are destroyed, MDA content will be greatly increased (Tsikas, 2017). Therefore, MDA reflects the antioxidant capacity of plant tissues and can also be used as an indicator to measure the resistance of plants against external stress (Yang et al., 2019). Under drought and salt stresses, the differences of Pro and MDA contents between transgenic lines and controls

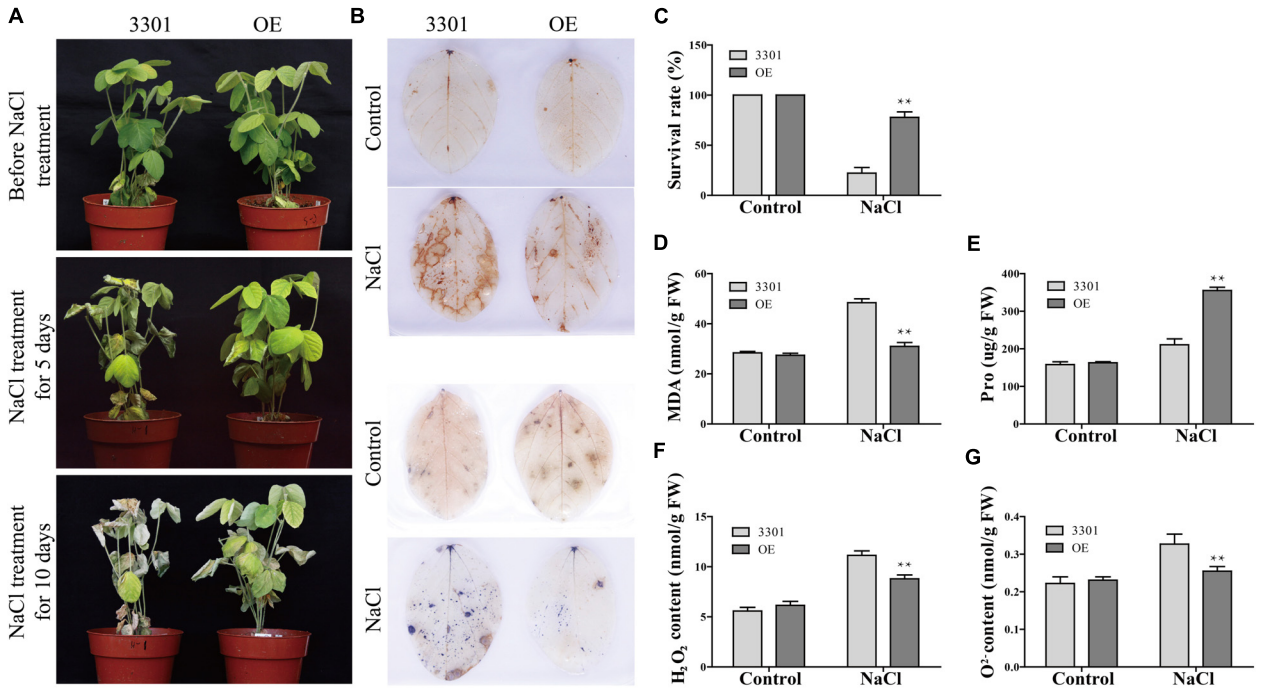

FIGURE 11 | Phenotype and physiological indexes analysis of *GmANK114* transgenic soybean hairy roots under salt stress. **(A)** Phenotypes was evaluated in transgenic soybean plants after NaCl treatment. **(B)** DAB (top) and NBT (bottom) staining of leaves of OE and 3301 plants under NaCl treatments. **(C)** Survival rate of soybean hairy roots grown with salt treatment. **(D–G)** MDA, proline, H_2O_2 and O^{2-} contents in leaves of plants with transgenic hairy roots were measured under salt treatment for 7 days. All values are represented means for three biological replicates (n = 18). The error bars indicate SD. Significant differences ($^*P < 0.05$ and $^{**}P < 0.01$) are indicated by asterisks above the columns.

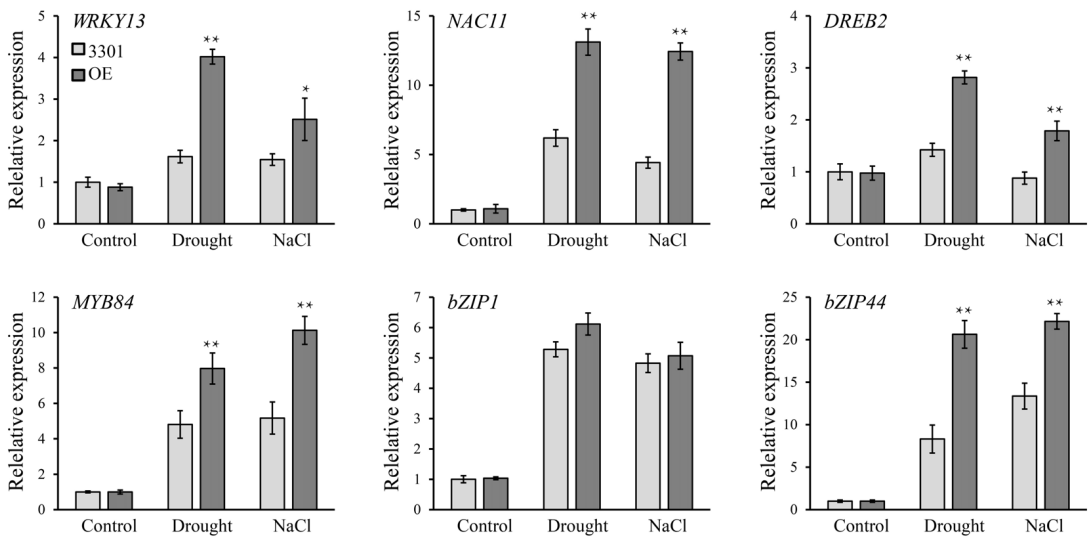

FIGURE 12 | The relative transcript levels of *WRKY13*, *NAC11*, *DREB3*, *MYB84*, *bZIP1* and *bZIP44* in transgenic *GmANK114* and 3301 soybeans. qRT-PCR was used to detect expression levels under normal and stress treatment and *GmCYP2* was used as an internal control. Values are means and SD obtained from three biological replicates. The asterisks indicate a statistical significance ($^*P < 0.05$ and $^{**}P < 0.01$) compared with the corresponding controls.

showed that *GmANK114* could confer tolerance of soybean to drought and salinity. The intracellular ROS content affects plant growth and development. H_2O_2 and O^{2-} are the main sources of ROS, and can lead to the oxidative destruction of cells (Mittler et al., 2004). The contents of H_2O_2 and O^{2-} in leaves of transgenic soybean were significantly lower than that in control. This indicates that *GmANK114* gives soybean the ability to remove ROS. These results show that

TABLE 3 | cis-acting elements of *GmANK-RFs* promoter region in soybean.

	Gene Name	ABRE	MYB	MYB-like	MBS	MYC	LTR	CGTCA -motif	TGACG -motif	TCA -element	TGA -element
1	GmANK35	3	5	1		2	2	1	1	1	1
2	GmANK88	3	7	2	3	7	1	1	1		
3	GmANK89	1	1			3	3	2	2		1
4	GmANK103	1	3	1		7		2	2	1	2
5	GmANK114	1	6	2		4		1	1		
6	GmANK115	2	6	3		6	1				
7	GmANK121	4	2		2	4					
8	GmANK122	4	3	2		4	1				1
9	GmANK128	5	1			5		4	4		
10	GmANK136	2	10	2	1	5	2	2	2	1	1
11	GmANK151	1	4	2	1	6		1	1	2	1
12	GmANK163		2			5	1			3	
13	GmANK183	2	5	3		3		4	4	1	4
14	GmANK188	4	6	1	1	8	1				1
15	GmANK201	2	2		1	5	3	3	3		1
16	GmANK220	1	4	1		5	1	1	1		
17	GmANK221	5	4	1		6	1	1	1		

the *GmANK114* gene is involved in abiotic stresses and can scavenge ROS.

Plants have developed flexibly molecular and cellular mechanisms to fight against various abiotic stresses. *GmANK114* was induced by drought, NaCl, and ABA. To further explain the molecular mechanism of *GmANK114* participating in abiotic stresses, the expression levels of drought- and salt-related marker genes were tested by qRT-PCR. Transcription factor *DREB2* specifically binds DRE element containing core sequence -CCGAC- that is involved in rapid expression of salt and drought stress responsive genes in *Arabidopsis* (Sakuma et al., 2006). bZIP proteins are well known for responding to ABA and stresses signaling. Several bZIP proteins can bind to ABRE (–ACGT–) elements and activate expression of ABRE-driven reporter genes, including *GmbZIP1* and *GmbZIP44* which are induced by drought, NaCl, cold, and ABA (Liao et al., 2008; Gao et al., 2011). Besides, *WRKY13, NAC11*, and *MYB84* are also involved in stress responses. Compared with controls, the expression profiles of stresses target genes have obvious differences in *GmANK114* transgenic hairy roots under drought and salt stresses, especially for *WRKY13, NAC11, DREB2, MYB84*, and *bZIP44* which were significantly up-regulated (**Figure 12**). This result suggest that *GmANK114* could change the expression of drought- and salt-related marker genes. That's probably because *ANK114* indirectly affects the expression of these genes by affecting the function of other genes. However, it is not clear how *ANK114* affects the function of other genes to enhance stress resistance in soybean. Therefore, further studies are necessary to clarify the mechanism of the *GmANK114* participating in abiotic stresses.

CONCLUSION

A total of 226 *ANK* genes were identified from the soybean genome. A member of the ANK-RF subfamily, *GmANK114*, improved tolerance against drought and salt stresses. This study provides important clues for future functional analysis of *ANK-RFs* in regulating of drought- and salt-related signal pathways in soybean.

DATA AVAILABILITY STATEMENT

The datasets presented in this study can be found in online repositories. The names of the repository/repositories and accession number(s) can be found in the article/ **Supplementary Material**.

AUTHOR CONTRIBUTIONS

Z-SX and D-HM coordinated the project, conceived and designed the experiments, and edited the manuscript. J-YZ performed the experiments and wrote the first draft. Z-WL and YS conducted the bioinformatic work and performed the experiments. Z-WF, JC, Y-BZ, and MC contributed with valuable discussions. Y-ZM coordinated the project. All authors have read and agreed to the published version of the manuscript.

FUNDING

This research was financially supported by the National Natural Science Foundation of China (31871624), the National Transgenic Key Project of the Chinese Ministry of Agriculture (2016ZX08002002-010), the Fundamental Research Funds for Central Non-Profit Institute of Crop Sciences, Chinese Academy of Agricultural Sciences (Y2020PT12 and S2020ZC02), and the Programme of Introducing Talents of Innovative Discipline to Universities (Project 111) from the State Administration of Foreign Experts Affairs (#B18042) "Crop breeding for disease resistance and genetic improvement".

ACKNOWLEDGMENTS

We are grateful to Dr. Lijuan Qiu from Crop Science, Chinese Academy of Agricultural Sciences for providing the soybean seeds.

SUPPLEMENTARY MATERIAL

The Supplementary Material for this article can be found online at: https://www.frontiersin.org/articles/10.3389/fpls.2020.584167/full#supplementary-material

Supplementary Figure 1 | Gene structure analysis of the 226 *GmANK* genes. Untranslated regions (upstream/downstream) are displayed by blue box. Introns and exons are shown by black lines and yellow boxes, respectively. The lengths of introns and exons of each gene were displayed proportionally.

Supplementary Figure 2 | Putative motifs of each soybean ANK proteins.

Supplementary Figure 3 | Gene Ontology (GO) annotation for the GmANK proteins. BP: biological processes; MF: molecular functions; CC: cellular components.

Supplementary Figure 4 | Sequence alignment of ANK-RF proteins in soybean.

Supplementary Figure 5 | Germination rates of seeds in transgenic *Arabidopsis* under PEG6000 and NaCl treatments.

Supplementary Table 1 | Description of soybean *ANK* genes.

Supplementary Table 2 | FPKM values of different tissues of soybean *ANK-RF* genes.

Supplementary Table 3 | FPKM values under drought, NaCl, and ABA treatment of soybean *ANK-RF* genes.

Supplementary Table 4 | Primers used in this study.

Supplementary Table 5 | Gene Ontology (GO) annotation for the GmANK proteins.

REFERENCES

Albert, S., Després, B., Guilleminot, J., Bechtold, N., Pelletier, G., Delseny, M., et al. (1999). The *EMB506* gene encodes a novel ankyrin repeat containing protein that is essential for the normal development of *Arabidopsis embryos*. *Plant J.* 17, 169–179. doi: 10.1046/j.1365-313x.1999.00361.x

Artimo, P., Jonnalagedda, M., Arnold, K., Baratin, D., Csardi, G., de Castro, E., et al. (2012). ExPASy: SIB bioinformatics resource portal. *Nucleic Acids Res.* 40, W597–W603. doi: 10.1093/nar/gks400

Becerra, C., Jahrmann, T., Puigdomenech, P., and Vicient, C. M. (2004). Ankyrin repeat-containing proteins in *Arabidopsis*: characterization of a novel and abundant group of genes coding ankyrin-transmembrane proteins. *Gene* 340, 111–121. doi: 10.1016/j.gene.2004.06.006

Berrocal-Lobo, M., Stone, S. L., Yang, X., Antico, J., Callis, J., Ramonell, K. M., et al. (2010). ATL9, a RING zinc finger protein with E3 ubiquitin ligase activity implicated in chitin- and NADPH oxidase-mediated defense responses. *PLoS One* 5:e14426. doi: 10.1371/journal.pone.0014426

Brestic, M., Zivcak, M., Kunderlikova, K., Sytar, O., Shao, H., Kalaji, H. M., et al. (2015). Low PSI content limits the photoprotection of PSI and PSII in early growth stages of chlorophyll b-deficient wheat mutant lines. *Photosynth. Res.* 125, 151–166. doi: 10.1007/s11120-015-0093-1

Cao, Y. R., Chen, H. W., Li, Z. G., Tao, J. J., Ma, B., Zhang, W. K., et al. (2015). Tobacco ankyrin protein NEIP2 interacts with ethylene receptor NTHK1 and regulates plant growth and stress responses. *Plant Cell Physiol.* 56, 803–818. doi: 10.1093/pcp/pcv009

Carvalho, S. D., Saraiva, R., Maia, T. M., Abreu, I. A., and Duque, P. (2012). XBAT35, a novel *Arabidopsis* RING E3 ligase exhibiting dual targeting of its splice isoforms, is involved in ethylene-mediated regulation of apical hook curvature. *Mol. Plant* 5, 1295–1309. doi: 10.1093/mp/sss048

Chen, C., Chen, H., Zhang, Y., Thomas, H. R., Frank, M. H., He, Y., et al. (2020). TBtools – an integrative toolkit developed for interactive analyses of big biological data. *Mol. Plant* 13:116. doi: 10.1016/j.molp.2020.06.009

Chen, M., Wang, Q. Y., Cheng, X. G., Xu, Z. S., Li, L. C., Ye, X. G., et al. (2007). *GmDREB2*, a soybean DRE-binding transcription factor, conferred drought and high-salt tolerance in transgenic plants. *Biochem. Biophys. Res. Commun.* 353, 299–305. doi: 10.1016/j.bbrc.2006.12.027

Chen, T. H., and Murata, N. (2011). Glycinebetaine protects plants against abiotic stress: mechanisms and biotechnological applications. *Plant Cell Environ.* 34, 1–20. doi: 10.1111/j.1365-3040.2010.02232.x

Conesa, A., and Gotz, S. (2008). Blast2GO: a comprehensive suite for functional analysis in plant genomics. *Int. J. Plant Genomics* 2008:619832. doi: 10.1155/2008/619832

Cui, X. Y., Du, Y. T., Fu, J. D., Yu, T. F., Wang, C. T., Chen, M., et al. (2018). Wheat CBL-interacting protein kinase 23 positively regulates drought stress and ABA responses. *BMC Plant Biol.* 18:93. doi: 10.1186/s12870-018-1306-5

Cunha, S. R., and Mohler, P. J. (2009). Ankyrin protein networks in membrane formation and stabilization. *J. Cell. Mol. Med.* 13, 4364–4376. doi: 10.1111/j.1582-4934.2009.00943.x

Del Rio, D., Stewart, A. J., and Pellegrini, N. (2005). A review of recent studies on malondialdehyde as toxic molecule and biological marker of oxidative stress. *Nutr. Metab. Cardiovasc. Dis.* 15, 316–328. doi: 10.1016/j.numecd.2005.05.003

Du, Y. T., Zhao, M. J., Wang, C. T., Gao, Y., Wang, Y. X., Liu, Y. W., et al. (2018). Identification and characterization of *GmMYB118* responses to drought and salt stress. *BMC Plant Biol.* 18:320. doi: 10.1186/s12870-018-1551-7

Elenbaas, B., Dobbelstein, M., Roth, J., Shenk, T., and Levine, A. J. (1996). The MDM2 oncoprotein binds specifically to RNA through its RING finger domain. *Mol. Med.* 2, 439–451. doi: 10.1007/bf03401903

Fan, K., Yuan, S., Chen, J., Chen, Y., Li, Z., Lin, W., et al. (2019). Molecular evolution and lineage-specific expansion of the PP2C family in Zea mays. *Planta* 250, 1521–1538. doi: 10.1007/s00425-019-03243-x

Freemont, P. S., Hanson, I. M., and Trowsdale, J. (1991). A novel gysteine-rich sequence motif. *Cell* 64, 483–484. doi: 10.1016/0092-8674(91)90229-R

Gao, S. Q., Chen, M., Xu, Z. S., Zhao, C. P., Li, L., Xu, H. J., et al. (2011). The soybean *GmbZIP1* transcription factor enhances multiple abiotic stress tolerances in transgenic plants. *Plant Mol. Biol.* 75, 537–553. doi: 10.1007/s11103-011-9738-4

Garcion, C., Guilleminot, J., Kroj, T., Parcy, F., Giraudat, J., and Devic, M. (2006). AKRP and EMB506 are two ankyrin repeat proteins essential for plastid differentiation and plant development in *Arabidopsis*. *Plant J.* 48, 895–906. doi: 10.1111/j.1365-313X.2006.02922.x

Guo, A.-Y., Zhu, Q.-H., Chen, X., and Luo, J.-C. (2007). GSDS: a gene structure display server. *Yi Chuan* 29, 1023–1026. doi: 10.1360/yc-007-1023

Hao, Y. J., Wei, W., Song, Q. X., Chen, H. W., Zhang, Y. Q., Wang, F., et al. (2011). Soybean *NAC* transcription factors promote abiotic stress tolerance and lateral root formation in transgenic plants. *Plant J.* 68, 302–313. doi: 10.1111/j.1365-313X.2011.04687.x

Hasanuzzaman, M., Hossain, M. A., da Silva, J. T., and Fujita, M. (2012). "Plant response and tolerance to abiotic oxidative stress: antioxidant defense is a key factor," in *Crop Stress and its Management: Perspectives and Strategies*, eds B. Venkateswarlu, A. Shanker, C. Shanker, and M. Maheswari (Dordrecht: Springer), 261–315. doi: 10.1007/978-94-007-2220-0_8

Holub, E. B. (2001). The arms race is ancient history in *Arabidopsis*, the wildflower. *Nat. Rev. Genet.* 2, 516–527. doi: 10.1038/35080508

Huang, J., Chen, F., Del Casino, C., Autino, A., Shen, M., Yuan, S., et al. (2006). An ankyrin repeat-containing protein, characterized as a ubiquitin ligase, is closely associated with membrane-enclosed organelles and required for pollen germination and pollen tube growth in lily. *Plant Physiol.* 140, 1374–1383. doi: 10.1104/pp.105.074922

Huang, J., Zhao, X., Yu, H., Ouyang, Y., Wang, L., and Zhang, Q. (2009). The ankyrin repeat gene family in rice: genome-wide identification, classification

and expression profiling. *Plant Mol. Biol.* 71, 207–226. doi: 10.1007/s11103-009-9518-6

Jiang, H., Wu, Q., Jin, J., Sheng, L., Yan, H., Cheng, B., et al. (2013). Genome-wide identification and expression profiling of ankyrin-repeat gene family in maize. *Dev. Genes Evol.* 223, 303–318. doi: 10.1007/s00427-013-0447-7

Kereszt, A., Li, D., Indrasumunar, A., Nguyen, C. T., Nontachaiyapoom, S., Kinkema, M., et al. (2007). *Agrobacterium rhizogenes*-mediated transformation of soybean to study root biology. *Nat. Protoc.* 2, 948–952. doi: 10.1038/nprot.2007.141

Letunic, I., Doerks, T., and Bork, P. (2009). SMART 6: recent updates and new developments. *Nucleic Acids Res.* 37, D229–D232. doi: 10.1093/nar/gkn808

Li, B., Liu, Y., Cui, X. Y., Fu, J. D., Zhou, Y. B., Zheng, W. J., et al. (2019). Genome-wide characterization and expression analysis of soybean *TGA* transcription factors identified a novel TGA gene involved in drought and salt tolerance. *Front. Plant Sci.* 10:549. doi: 10.3389/fpls.2019.00549

Li, H.-Y., and Chye, M.-L. (2004). *Arabidopsis* Acyl-CoA-binding protein ACBP2 interacts with an ethylene-responsive element-binding protein, AtEBP, via its ankyrin repeats. *Plant Mol. Biol.* 54, 233–243. doi: 10.1023/b:plan.0000028790.75090.ab

Liao, Y., Zou, H. F., Wei, W., Hao, Y. J., Tian, A. G., Huang, J., et al. (2008). Soybean *GmbZIP44*, *GmbZIP62* and *GmbZIP78* genes function as negative regulator of ABA signaling and confer salt and freezing tolerance in transgenic *Arabidopsis*. *Planta* 228, 225–240. doi: 10.1007/s00425-008-0731-3

Liu, J. M., Xu, Z. S., Lu, P. P., Li, W. W., Chen, M., Guo, C. H., et al. (2016a). Genome-wide investigation and expression analyses of the pentatricopeptide repeat protein gene family in foxtail millet. *BMC Genomics* 17:840. doi: 10.1186/s12864-016-3184-2

Liu, J. M., Zhao, J. Y., Lu, P. P., Chen, M., Guo, C. H., Xu, Z. S., et al. (2016b). The E-subgroup pentatricopeptide repeat protein family in *Arabidopsis thaliana* and confirmation of the responsiveness *PPR96* to abiotic stresses. *Front. Plant Sci.* 7:1825. doi: 10.3389/fpls.2016.01825

Lopez-Ortiz, C., Pena-Garcia, Y., Natarajan, P., Bhandari, M., Abburi, V., Dutta, S. K., et al. (2020). The ankyrin repeat gene family in capsicum spp: genome-wide survey, characterization and gene expression profile. *Sci. Rep.* 10:4044. doi: 10.1038/s41598-020-61057-4

Lorick, K. L., Jensen, J. P., Fang, S., Ong, A. M., Hatakeyama, S., and Weissman, A. M. (1999). RING fingers mediate ubiquitin-conjugating enzyme (E2)-dependent ubiquitination. *Proc. Natl. Acad. Sci. U.S.A.* 96, 11364–11369. doi: 10.1073/pnas.96.20.11364

Lu, H., Liu, Y., and Greenberg, J. T. (2005). Structure-function analysis of the plasma membrane- localized *Arabidopsis* defense component ACD6. *Plant J.* 44, 798–809. doi: 10.1111/j.1365-313X.2005.02567.x

Lu, H., Rate, D. N., Song, J. T., and Greenberg, J. T. (2003). ACD6, a novel ankyrin protein, is a regulator and an effector of salicylic acid signaling in the *Arabidopsis* defense response. *Plant Cell* 15, 2408–2420. doi: 10.1105/tpc.015412

Lyzenga, W. J., Booth, J. K., and Stone, S. L. (2012). The *Arabidopsis* RING-type E3 ligase XBAT32 mediates the proteasomal degradation of the ethylene biosynthetic enzyme, 1-aminocyclopropane-1-carboxylate synthase 7. *Plant J.* 71, 23–34. doi: 10.1111/j.1365-313X.2012.04965.x

Michaely, P., and Bennett, V. (1992). The ANK repeat: a ubiquitous motif involved in macromolecular recognition. *Trends Cell Biol.* 2, 127–129. doi: 10.1016/0962-8924(92)90084-z

Miles, M. C., Janket, M. L., Wheeler, E. D., Chattopadhyay, A., Majumder, B., Dericco, J., et al. (2005). Molecular and functional characterization of a novel splice variant of ANKHD1 that lacks the KH domain and its role in cell survival and apoptosis. *FEBS J.* 272, 4091–4102. doi: 10.1111/j.1742-4658.2005.04821.x

Mittler, R., Vanderauwera, S., Gollery, M., and Van Breusegem, F. (2004). Reactive oxygen gene network of plants. *Trends Plant Sci.* 9, 490–498. doi: 10.1016/j.tplants.2004.08.009

Mosavi, L. K., Cammett, T. J., Desrosiers, D. C., and Peng, Z.-y (2004). The ankyrin repeat as molecular architecture for protein recognition. *Protein Sci.* 13, 1435–1448. doi: 10.1110/ps.03554604

Nodzon, L. A., Xu, W. H., Wang, Y., Pi, L. Y., Chakrabarty, P. K., and Song, W. Y. (2004). The ubiquitin ligase XBAT32 regulates lateral root development in *Arabidopsis*. *Plant J.* 40, 996–1006. doi: 10.1111/j.1365-313X.2004.02266.x

Popescu, S. C., Brauer, E. K., Dimlioglu, G., and Popescu, G. V. (2017). Insights into the structure, function, and ion-mediated signaling pathways transduced by plant integrin-linked kinases. *Front. Plant Sci.* 8:376. doi: 10.3389/fpls.2017.00376

Prasad, M. E., Schofield, A., Lyzenga, W., Liu, H., and Stone, S. L. (2010). *Arabidopsis* RING E3 ligase XBAT32 regulates lateral root production through its role in ethylene biosynthesis. *Plant Physiol.* 153, 1587–1596. doi: 10.1104/pp.110.156976

Qi, J., Song, C. P., Wang, B., Zhou, J., Kangasjarvi, J., Zhu, J. K., et al. (2018). Reactive oxygen species signaling and stomatal movement in plant responses to drought stress and pathogen attack. *J. Integr. Plant Biol.* 60, 805–826. doi: 10.1111/jipb.12654

Sakuma, Y., Maruyama, K., Osakabe, Y., Qin, F., Seki, M., Shinozaki, K., et al. (2006). Functional analysis of an *Arabidopsis* transcription factor, *DREB2A*, involved in drought-responsive gene expression. *Plant Cell* 18, 1292–1309. doi: 10.1105/tpc.105.035881

Sedgwick, S. G., and Smerdon, S. J. (1999). The ankyrin repeat: a diversity of interactions on a common structural framework. *Trends Biochem. Sci.* 24, 311–316. doi: 10.1016/s0968-0004(99)01426-7

Seong, E. S., Cho, H. S., Choi, D., Joung, Y. H., Lim, C. K., Hur, J. H., et al. (2007a). Tomato plants overexpressing *CaKR1* enhanced tolerance to salt and oxidative stress. *Biochem. Biophys. Res. Commun.* 363, 983–998. doi: 10.1016/j.bbrc.2007.09.104

Seong, E. S., Choi, D., Cho, H. S., Lim, C. K., Cho, H. J., and Wang, M. H. (2007b). Characterization of a stress-responsive ankyrin repeat containing zinc finger protein of *capsicum annuum* (CaKR1). *J. Biolchem. Mol. Biol.* 40, 952–958. doi: 10.5483/bmbrep.2007.40.6.952

Shi, W. Y., Du, Y. T., Ma, J., Min, D. H., Jin, L. G., Chen, J., et al. (2018). The WRKY transcription factor *GmWRKY12* confers drought and salt tolerance in soybean. *Int. J. Mol. Sci.* 19:4087. doi: 10.3390/ijms19124087

Stone, S. L., Hauksdottir, H., Troy, A., Herschleb, J., Kraft, E., and Callis, J. (2005). Functional analysis of the RING-type ubiquitin ligase family of *Arabidopsis*. *Plant Physiol.* 137, 13–30. doi: 10.1104/pp.104.052423

Tamura, K., Peterson, D., Peterson, N., Stecher, G., Nei, M., and Kumar, S. (2011). MEGA5: molecular evolutionary genetics analysis using maximum likelihood, evolutionary distance, and maximum parsimony methods. *Mol. Biol. Evol.* 28, 2731–2739. doi: 10.1093/molbev/msr121

Thompson, J. D., Gibson, T. J., Plewniak, F., Jeanmougin, F., and Higgins, D. G. (1997). The CLUSTAL_X windows interface: flexible strategies for multiple sequence alignment aided by quality analysis tools. *Nucleic Acids Res.* 25, 4876–4882. doi: 10.1093/nar/25.24.4876

Tsikas, D. (2017). Assessment of lipid peroxidation by measuring malondialdehyde (MDA) and relatives in biological samples: analytical and biological challenges. *Anal. Biochem.* 524, 13–30. doi: 10.1016/j.ab.2016.10.021

Veatch-Blohm, M. E. (2007). Principles of plant genetics and breeding. *Crop Sci.* 47:385. doi: 10.2135/cropsci2007.05.0002br

Voronin, D. A., and Kiseleva, E. V. (2008). Functional role of proteins containing ankyrin repeats. *Cell Tissue Biol.* 2, 1–12. doi: 10.1134/s1990519x0801001x

Wang, F., Chen, H. W., Li, Q. T., Wei, W., Li, W., Zhang, W. K., et al. (2015). GmWRKY27 interacts with GmMYB174 to reduce expression of *GmNAC29* for stress tolerance in soybean plants. *Plant J.* 83, 224–236. doi: 10.1111/tpj.12879

Wang, H., Zou, S., Li, Y., Lin, F., and Tang, D. (2020). An ankyrin-repeat and WRKY-domain-containing immune receptor confers stripe rust resistance in wheat. *Nat. Commun.* 11:1353. doi: 10.1038/s41467-020-15139-6

Wang, M., Yue, H., Feng, K., Deng, P., Song, W., and Nie, X. (2016). Genome-wide identification, phylogeny and expressional profiles of mitogen activated protein kinase kinase kinase (MAPKKK) gene family in bread wheat (*Triticum aestivum* L.). *BMC Genomics* 17:668. doi: 10.1186/s12864-016-2993-7

Wang, N., Zhang, W., Qin, M., Li, S., Qiao, M., Liu, Z., et al. (2017). Drought tolerance conferred in soybean (*Glycine max.* L) by *GmMYB84*, a novel R2R3-MYB transcription factor. *Plant Cell Physiol.* 58, 1764–1776. doi: 10.1093/pcp/pcx111

Wang, Y.-S., Pi, L.-Y., Chen, X., Chakrabarty, P. K., Jiang, J., De Leon, A. L., et al. (2006). Rice XA21 binding protein 3 is a ubiquitin ligase required for full Xa21-mediated disease resistance. *Plant Cell* 18, 3635–3646. doi: 10.1105/tpc.106.046730

Wu, T., Tian, Z., Liu, J., Yao, C., and Xie, C. (2009). A novel ankyrin repeat-rich gene in potato, *Star*, involved in response to late blight. *Biochem. Genet.* 47, 439–450. doi: 10.1007/s10528-009-9238-2

Xiong, L., Schumaker, K. S., and Zhu, J. K. (2002). Cell signaling during cold, drought, and salt stress. *Plant Cell* 14, S165–S183. doi: 10.1105/tpc.000596

Yang, R., Chen, M., Sun, J. C., Yu, Y., Min, D. H., Chen, J., et al. (2019). Genome-wide analysis of LIM family genes in foxtail millet (*Setaria italica* L.) and characterization of the role of *SiWLIM2b* in drought tolerance. *Int. J. Mol. Sci.* 20:1303. doi: 10.3390/ijms20061303

Yang, X., Sun, C., Hu, Y., and Lin, Z. (2008). Molecular cloning and characterization of a gene encoding RING zinc finger ankyrin protein from drought-tolerant *Artemisia desertorum*. *J. Biosci.* 33, 103–112. doi: 10.1007/s12038-008-0026-7

Yang, Y., and Guo, Y. (2018). Unraveling salt stress signaling in plants. *J. Integr. Plant Biol.* 60, 796–804. doi: 10.1111/jipb.12689

Yuan, X., Zhang, S., Qing, X., Sun, M., Liu, S., Su, H., et al. (2013). Superfamily of ankyrin repeat proteins in tomato. *Gene* 523, 126–136. doi: 10.1016/j.gene.2013.03.122

Zhang, D., Wan, Q., He, X., Ning, L., Huang, Y., Xu, Z., et al. (2016). Genome-wide characterization of the ankyrin repeats gene family under salt stress in soybean. *Sci. Total Environ.* 568, 899–909. doi: 10.1016/j.scitotenv.2016.06.078

Zhang, H., Scheirer, D. C., Fowle, W. H., and Goodman, H. M. (1992). Expression of antisense or sense RNA of an ankyrin repeat-containing gene blocks chloroplast differentiation in *Arabidopsis*. *Plant Cell* 4, 1575–1588. doi: 10.1105/tpc.4.12.1575

Zhang, X. Z., Zheng, W. J., Cao, X. Y., Cui, X. Y., Zhao, S. P., Yu, T. F., et al. (2019). Genomic analysis of stress associated proteins in soybean and the role of GmSAP16 in abiotic stress responses in *Arabidopsis* and soybean. *Front. Plant Sci.* 10:1453. doi: 10.3389/fpls.2019.01453

Zhou, Q. Y., Tian, A. G., Zou, H. F., Xie, Z. M., Lei, G., Huang, J., et al. (2008). Soybean WRKY-type transcription factor genes, *GmWRKY13*, *GmWRKY21*, and *GmWRKY54*, confer differential tolerance to abiotic stresses in transgenic *Arabidopsis* plants. *Plant Biotechnol. J.* 6, 486–503. doi: 10.1111/j.1467-7652.2008.00336.x

Zhu, J. K. (2016). Abiotic stress signaling and responses in plants. *Cell* 167, 313–324. doi: 10.1016/j.cell.2016.08.029

Conflict of Interest: The authors declare that the research was conducted in the absence of any commercial or financial relationships that could be construed as a potential conflict of interest.

frontiers in Plant Science

REVIEW
published: 12 November 2020
doi: 10.3389/fpls.2020.565339

Root Adaptation via Common Genetic Factors Conditioning Tolerance to Multiple Stresses for Crops Cultivated on Acidic Tropical Soils

Vanessa A. Barros[1,2†], Rahul Chandnani[3†], Sylvia M. de Sousa[1†], Laiane S. Maciel[1,3†], Mutsutomo Tokizawa[3†], Claudia T. Guimaraes[1], Jurandir V. Magalhaes[1,2] and Leon V. Kochian[3*]*

[1] Embrapa Maize and Sorghum, Sete Lagoas, Brazil, [2] Departamento de Biologia Geral, Universidade Federal de Minas Gerais, Belo Horizonte, Brazil, [3] Global Institute for Food Security, University of Saskatchewan, Saskatoon, SK, Canada

OPEN ACCESS

Edited by:
Manny Delhaize,
Plant Industry (CSIRO), Australia

Reviewed by:
Roberto Tuberosa,
University of Bologna, Italy
Harsh Raman,
New South Wales Department of Primary Industries, Australia

***Correspondence:**
Leon V. Kochian
leon.kochian@gifs.ca
Jurandir V. Magalhaes
jurandir.magalhaes@embrapa.br

† These authors have contributed equally to this work

Specialty section:
This article was submitted to Plant Abiotic Stress, a section of the journal Frontiers in Plant Science

Received: 24 May 2020
Accepted: 20 October 2020
Published: 12 November 2020

Citation:
Barros VA, Chandnani R, de Sousa SM, Maciel LS, Tokizawa M, Guimaraes CT, Magalhaes JV and Kochian LV (2020) Root Adaptation via Common Genetic Factors Conditioning Tolerance to Multiple Stresses for Crops Cultivated on Acidic Tropical Soils. Front. Plant Sci. 11:565339. doi: 10.3389/fpls.2020.565339

Crop tolerance to multiple abiotic stresses has long been pursued as a Holy Grail in plant breeding efforts that target crop adaptation to tropical soils. On tropical, acidic soils, aluminum (Al) toxicity, low phosphorus (P) availability and drought stress are the major limitations to yield stability. Molecular breeding based on a small suite of pleiotropic genes, particularly those with moderate to major phenotypic effects, could help circumvent the need for complex breeding designs and large population sizes aimed at selecting transgressive progeny accumulating favorable alleles controlling polygenic traits. The underlying question is twofold: do common tolerance mechanisms to Al toxicity, P deficiency and drought exist? And if they do, will they be useful in a plant breeding program that targets stress-prone environments. The selective environments in tropical regions are such that multiple, co-existing regulatory networks may drive the fixation of either distinctly different or a smaller number of pleiotropic abiotic stress tolerance genes. Recent studies suggest that genes contributing to crop adaptation to acidic soils, such as the major Arabidopsis Al tolerance protein, AtALMT1, which encodes an aluminum-activated root malate transporter, may influence both Al tolerance and P acquisition via changes in root system morphology and architecture. However, *trans*-acting elements such as transcription factors (TFs) may be the best option for pleiotropic control of multiple abiotic stress genes, due to their small and often multiple binding sequences in the genome. One such example is the C2H2-type zinc finger, AtSTOP1, which is a transcriptional regulator of a number of Arabidopsis Al tolerance genes, including *AtMATE* and *AtALMT1*, and has been shown to activate *AtALMT1*, not only in response to Al but also low soil P. The large WRKY family of transcription factors are also known to affect a broad spectrum of phenotypes, some of which are related to acidic soil abiotic stress responses. Hence, we focus here on signaling proteins such as TFs and protein kinases to identify, from the literature, evidence for

unifying regulatory networks controlling Al tolerance, P efficiency and, also possibly drought tolerance. Particular emphasis will be given to modification of root system morphology and architecture, which could be an important physiological "hub" leading to crop adaptation to multiple soil-based abiotic stress factors.

Keywords: acid soils, aluminum toxicity, aluminum tolerance, phosphorus deficiency, phosphorus efficiency, drought resistance, transcription factor, signaling

INTRODUCTION

Acidic soils (soils pH < 5.5) are quite extensive worldwide, comprising up to 50% of the world's potentially arable lands (Von Uexküll and Mutert, 1995). As the acidic weathered soils are particularly prominent in the humid tropics and subtropics where many developing countries in sub-Saharan Africa and Asia are located, and food production must keep pace with population growth (Godfray et al., 2010), acidic soils are a major constraint for developing world agriculture The two most significant limitations to crop production on acid soils from the plant nutrition perspective are aluminum (Al) toxicity and phosphorus (P) deficiency (Kochian et al., 2015). Both arise from the unique chemical properties of highly weathered acid soils. Aluminum is the most abundant metal in the earth's crust as it is a major component of clays, as aluminosilicates. At soil pH values of pH 5.5 and below, Al^{3+} ions are solubilized into the soil solution. Al^{3+} is quite toxic to roots, inhibiting both root elongation and root meristem cell division (see, for example, Kochian, 1995; Ma et al., 2001; Kobayashi et al., 2013b, and references therein). This results in major reductions in yields due to insufficient water and mineral nutrient uptake by the root systems. Low-P soil levels and availability also arise from the chemical properties of acidic soils as soil weathering exposes Al and Fe oxides/hydroxides on the surface of clay minerals, which bind soil P (as the phosphate anion) tightly, reducing its bioavailability (Marschner, 1995). Soils with low P availability will be designated henceforth as low-P soils for brevity. The third related stress we address in this review is drought stress, which is found on all soil types, including acidic soils. The unique aspect to acidic soils is that crop adaptation to drought on those soils requires that the plants be both Al tolerant to maintain a healthy root system to facilitate water absorption, along with specific adaptations to drought which are ubiquitously found in crop species on all soil types. Because crops acidic soils have had to adapt to all three stresses simultaneously, it is not surprising that especially in recent literature common features in adaptation to these three abiotic stresses are being uncovered. This is the theme we address in this review.

In searching for classes of genes involved in mediating resistance concurrently to these three stresses, it is more likely that "upstream" genes that control regulatory and signaling networks such as transcription factors (TFs), kinases and phosphatases would be more likely candidates than structural genes such as root plasma membrane transporters that mediate efflux of Al-binding organic acid anions that have been shown to be involved in crop Al tolerance (Ma et al., 2001; Ryan et al., 2001; Kochian et al., 2004, 2015). Regulatory genes, such as transcription factors, bind to very small *cis* elements in the promoter region. Depending also on more complex aspects such as chromatin structure, this gives TFs potential for promiscuous binding to many targets, giving rise to complex regulatory circuits. A good example of how the promiscuity of TF binding sites can impact evolutionary adaptation is presented in Pougach et al. (2014), where they show that duplication of a transcription factor gene allowed the emergence of two independent regulatory circuits in yeast. Since TFs are often regulators of response to multiple stresses, they are excellent candidates for breeding programs searching for pleiotropic control of co-existing stresses in acidic soils such as Al toxicity, low P availability, and drought (Baillo et al., 2019).

In this review, we have focused on signaling/regulatory proteins such as TFs and protein kinases to identify, from the literature, evidence for unifying regulatory networks controlling Al tolerance, P efficiency and also possibly drought tolerance. Particular emphasis will be given to modification of root system morphology and architecture, which could be an important physiological "hub" leading to crop adaptation to multiple soil-based abiotic stress factors.

ALUMINUM TOXICITY AND TOLERANCE

Transcriptional Regulation Involved in Al Tolerance

Aluminum (Al) on acidic soils intoxicates root regions involved in root growth (meristem and elongation zone). Cells in these regions are subject to rapid alterations in Al-induced transcription, resulting in the induction of expression of several Al tolerance genes associated with root tip Al exclusion and detoxification mechanisms (Kochian et al., 2015).

Several TFs (TFs) have been reported to be involved in crop Al tolerance, and the majority of these TFs belong to zinc finger and WRKY transcription factor families. Among them, *STOP1* in Arabidopsis and *ART1* in rice are the best characterized TFs regulating Al tolerance. STOP1, a C2H2-type zinc finger transcription factor, was identified via positional cloning of a low-pH-sensitive Arabidopsis mutant. Although *AtSTOP1* expression is not induced by Al, the *stop1*-mutant is also Al hypersensitive (Iuchi et al., 2007). AtSTOP1 has four functional zinc finger domains that bind to a 15-bp long sequence in the *AtALMT1* promoter. *AtALMT1* is the major Arabidopsis Al tolerance gene (Hoekenga et al., 2006), closely related to the primary wheat Al tolerance gene, *TaALMT1* (Sasaki et al., 2004). These two ALMT genes and similar ones in other plant species encode root

cell plasma membrane Al-activated malate efflux transporters that are one of the key genes involved in root Al exclusion via release of Al-binding organic acid anions. Mutations in the STOP1 binding sites and in AtSTOP1 zinc finger domains critically suppress *AtALMT1* expression, indicating that STOP1 binding is essential for *AtALMT1* expression and Al tolerance in Arabidopsis (Tokizawa et al., 2015). Furthermore, AtSTOP1 also regulates the expression of other transporters required for Al tolerance in Arabidopsis, including *AtMATE* (Al-activated citrate transporter) and *AtALS3* (ABC transporter-like protein) (Liu et al., 2009; Sawaki et al., 2009).

AtSTOP1 is ubiquitously expressed in the root with higher expression in the root tip, and its expression is not affected by Al stress. In turn, AtSTOP1 downstream genes (*AtALMT1*, *AtMATE*, and *AtALS3*) are induced by Al (Liu et al., 2009; Sawaki et al., 2009). These findings suggest that Al might induce *AtSTOP1* regulation at the post-transcriptional/-translational level. Recently, an F-box protein that regulates the level of AtSTOP1 protein, RAE1, was identified in Arabidopsis (Zhang Y. et al., 2019). The authors showed that RAE1 interacts with SKP1, a protein involved in ubiquitination and subsequent proteasomal degradation of target proteins. These two proteins interact to form a functional SCF-type E3 ligase complex, physically binding to STOP1 and driving its degradation via the ubiquitin 26S proteasome. As such, *AtALMT1* and other STOP1 regulated genes, including *AtMATE* and *AtALS3*, are overexpressed in the *rae1* mutant. Interestingly, AtSTOP1 binds to the *RAE1* promoter and positively regulates its expression, indicating that there is a negative feedback loop between *AtSTOP1* and *RAE1*. Finally, the authors suggest that the feedback loop might be important in controlling AtSTOP1 homeostasis, enabling the degradation of accumulated AtSTOP1 after Al stress.

The transcriptional regulation of *AtALMT1* expression by STOP1 is fairly well characterized. However, as stated in Tokizawa et al. (2015), the structure of the *AtALMT1* promoter indicates that other factors may be acting on its expression. The authors identified several *cis*-elements in the *ALMT1* promoter related to: (1) Al-induced early and late expression; (2) root tip-specific expression; and (3) repression of *ALMT1* expression. In addition, it was reported that the transcription factor, *CAMTA2* (Calmodulin binding *trans*-activator 2), binds to the *AtALMT1* promoter at a *cis*-element in a different binding region than STOP1, and appears to be involved in induction of *AtALMT1* expression only in late Al stress. Previously, it was also demonstrated that AtWRKY46 binds to W-box sequences in the *AtALMT1* promoter, repressing its expression in the absence of Al (Ding et al., 2013), indicating that regulation of *AtALMT1* is not restricted to STOP1.

Sharing 41.2% sequence identity with AtSTOP1, the rice homolog, OsART1, was identified by map-based cloning of an Al-sensitive rice mutant. ART1 is also a C2H2-type zinc finger transcription factor involved in the regulation of a number of rice Al responsive genes, but, unlike *AtSTOP1*, it is not responsive to low pH. Microarray analyses showed that OsART1 regulates at least 31 downstream genes in response to Al (Yamaji et al., 2009). This transcription factor directly binds to a GGNVS core sequence in the *OsSTAR1* promoter, which is present in 29 of the 31 ART1-regulated genes (Tsutsui et al., 2011). Some of the ART1-regulated genes have been functionally characterized as being involved in Al tolerance, including a number of transporters mediating Al uptake into the root and the vacuole, a Mg uptake transporter, and an ABC transporter that helps mediate the release of UDP-glucose into the cell wall to possibly minimize Al binding (Huang et al., 2009, 2012; Xia et al., 2010, 2013; Yokosho et al., 2011; Chen et al., 2012). Interestingly, the GGNVS core promoter sequence is also found in the promoter of genes regulated by AtSTOP1, suggesting that STOP1 and ART1 recognize similar DNA sequences (Tokizawa et al., 2015).

STOP1/ART1-like proteins, and their function in the regulation of Al tolerance genes, are broadly conserved among land plant species, including dicots, monocots, woody plants, and even bryophytes (Chen et al., 2013; Sawaki et al., 2014; Fan et al., 2015; Daspute et al., 2018; Huang et al., 2018; Wu et al., 2018; Ito et al., 2019; Kundu et al., 2019). The genome of the moss, *Physcomitrella patens* has a functional STOP1-like protein, and knock out of *PpSTOP1* results in an Al sensitive phenotype, suggesting that plants acquired *STOP1* at a very early time during land adaptation of plants, protecting roots from toxic environments including Al and low pH (Ohyama et al., 2013).

In addition to OsART1, OsWRKY22 also regulates the Al-induced expression of *OsFRDL4*, which encodes the rice root plasma membrane citrate efflux transporter. *OsWRKY22* is rapidly induced by Al and works as a transcriptional activator of the *OsFRDL4* expression via binding to W-box *cis*-elements in the *FRDL4* promoter. OsWRKY22 has not been shown to regulate other *ART1*-regulated genes, however, OsWRKY22 and OsART1 are essential for the full activation of Al-induced *FRDL4* expression and root citrate secretion in rice (Li et al., 2018).

Recently, through QTL mapping, GWAS, and functional analyses, two novel TFs in sorghum were identified, SbWRKY1 and SbZNF1, which positively regulate *SbMATE* expression (Melo et al., 2019). Previously, it was reported that miniature inverted-repeat transposable elements (MITE) in the *SbMATE* promoter play a critical role in its expression, and the number of MITE repeats is strongly correlated with *SbMATE* expression level and Al tolerance in sorghum (Magalhaes et al., 2007), which is consistent with the findings of (Salvi et al., 2007) showing that allelic polymorphisms due to MITE insertions can affect the transcription of regulated genes. These two TFs directly bind to sequences flanking the transposable element and, according to the proposed model, the expanded number of MITE repeats found in Al-tolerant genotypes provides an increased number of binding sites for SbWRKY1 and SbZNF1, resulting in higher sorghum *SbMATE* expression and Al tolerance (Melo et al., 2019). Similar to *SbMATE*, other studies have shown that the diversity of the promoter structures contributes to differences in Al tolerance between tolerant and sensitive genotypes in several crops. Al responsive genes of tolerant accessions of wheat (*TaALMT1*), *Holcus lanatus* (*HlALMT1*) and rice (*OsFRDL4*) carry more STOP1/ART1 binding sites in their promoters and exhibit higher expression levels than the same genes in the respective sensitive accessions (Chen et al., 2013; Tokizawa et al., 2015; Yokosho et al., 2016). These findings indicate that the enrichment of transcription factor binding sites in Al-tolerance gene promoters

leads to enhanced transcription factor recruitment, which might explain, at least partially, Al tolerance in several crop species.

In addition to zinc-finger and WRKY TFs, *ASR1* and *ASR5* (Abscisic acid, Stress and Ripening protein 1 and 5) are involved in Al tolerance in rice (Arenhart et al., 2013, 2014, 2016). *ASR5* is induced by Al and binds to the *OsSTAR1* promoter and functions together with OsART1 as transcriptional activators of the *OsSTAR1* expression. This study also demonstrated that *ASR5*-silenced plants impair the expression of two other rice Al tolerance genes, *OsNrat1* and *OsFRDL4*, suggesting that ASR5 is also involved in their transcriptional regulation (Arenhart et al., 2014). Subsequently, it was reported that *ASR5*-silenced plants exhibited a similar Al tolerance phenotype as wild type plants. This was attributed to the transcription factor *ASR1*, which, under the silencing of *ASR5*, is highly induced and regulates ASR5-target genes, including *STAR1*, in a non-preferential manner.

Recently, studies searching for novel regulators of Al resistance have identified TFs related to the modification of the cell wall properties (Li C.X. et al., 2019; Lou et al., 2020). In Arabidopsis, it was found that the *wrky47* mutant has reduced Al tolerance and altered subcellular Al distribution, i.e., increased Al accumulation in symplast, and decreased Al content in the root apoplast. According to the authors (Li C.X. et al., 2019), these effects occur due to the reduction of cell wall Al-binding capacity, conferred by decreased hemicellulose-I cell wall content in the mutant. It was demonstrated that AtWRKY47 directly binds to and activates the expression of genes encoding *EXTENSIN-LIKE PROTEIN (ELP)* and *XYLOGLUCAN ENDOTRANSGLUCOSYLASE-HYDROLASES17 (XTH17)*, that are involved in cell wall modification. Within those, XTH17 works in modifying hemicellulosic polymers during cell expansion (Zhu et al., 2014), and ELP is involved in cell wall extension (Li C.X. et al., 2019). These findings indicate that *WRKY47* is involved in Al resistance by increasing cell wall bind of the rhizotoxic Al^{3+} ion, minimizing its effect on the cell wall and also reducing uptake into the root cytoplasm (Li C.X. et al., 2019). Another study showed that *VuNAR1* (*Vigna umbellata NAC-type Al Responsive1*), a rice bean *NAC* transcription factor, is up-regulated by Al in the root apex (Lou et al., 2020). In this paper, it was demonstrated that VuNAR1 binds to the *AtWAK1* (Arabidopsis wall-associated receptor kinase 1) and *VuWAKL1* (*Vigna umbellata WAK1-like*) promoters, positively regulating their expression (Lou et al., 2020). In Arabidopsis, *WAK1* is rapidly induced by Al, and the *AtWAK1* overexpression increases Al tolerance (Sivaguru et al., 2003). Lou et al. (2020) showed that the phenotype of the *Atwak1* mutant is higher root cell wall pectin content under Al stress, and it is believed that the binding of Al ions to the negatively charged carboxylic acid residues in pectin is involved in one of the components of Al rhizotoxicity, with methylation of the pectin carboxyl groups correlating with reduced Al toxicity (Yang et al., 2008).

Other Signaling Molecules

We still don't know how plants sense Al ions to trigger Al-dependent gene regulation. However, several signaling molecules have been identified that appear to be involved in initiating Al-induced transcriptional regulation. For example, Al-induced changes in cytosolic Ca^{2+} and pH (H^+), have been implicated as sensing/signaling molecules in Al signaling [see review by Kochian et al. (2015) and references therein]. In addition to these ions, several other endogenous species, reactive oxygen species (ROS), phytohormones, and the phosphatidylinositol pathway, appear to be involved in Al signal transduction.

Reactive Oxygen Species

Reactive oxygen species including peroxides, superoxide, hydroxyl radical, singlet oxygen are produced in response to a range of stress responses (Banti et al., 2010; Miller et al., 2010; Shahid et al., 2014; Hieno et al., 2019). Biomolecules including lipids, proteins, and DNA/RNA are oxidized by ROS, and this oxidative damage leads to organelle disfunction and programmed cell death (PCD) (Van Breusegem and Dat, 2006; Mittler, 2017). To protect the oxidative stress, plants activate antioxidant systems (i.e., ROS scavenging pathways) and also induce/activate a series of heat shock proteins (HSPs, e.g., molecular chaperon) (Sharma et al., 2012; Driedonks et al., 2015; Mishra et al., 2018; Waszczak et al., 2018). Al toxicity has been shown to trigger ROS, including hydrogen peroxides (H_2O_2), and Al/H_2O_2-mediated PCD was reported in various plant species (Yamamoto et al., 2002; Sivaguru et al., 2013; Huang et al., 2014). To protect against this, Al induces multiple genes associated with antioxidant production, such as peroxidase and superoxide dismutase, and they play a likely secondary role in Al tolerance (Ezaki et al., 2000; Basu et al., 2001). On the other hand, ROS also can act as signal molecules with the best characterized of these involved in plant defenses against pathogens and pests (see review by Bhattacharjee, 2012, and references therein). With regards to plant Al toxicity and tolerance, Sivaguru et al. (2013) showed there is a strong correlation between Al-induced ROS production and *SbMATE* expression, both temporally and spatially in the sorghum root tip. Subsequently, Kobayashi et al. (2013a) showed that *AtALMT1* and *AtMATE* expression are induced by H_2O_2 without Al. However, H_2O_2 cannot activate malate release from the roots, suggesting that protein activation of ALMT1 is regulated by a H_2O_2-independent pathway. In addition, several proteome analyses of Al stress revealed that several heat shock proteins (HSPs) are induced by Al stress (Zhen et al., 2007; Jiang et al., 2015), and the ER resident chaperon, *AtBIP3*, was identified as a possible Al-tolerance gene which is highly expressed in Al tolerant Arabidopsis accessions (Kusunoki et al., 2017). Interestingly, Enomoto et al. (2019) recently reported that AtSTOP1 directly regulates *AtHSF2A*, which is a master regulator of a series of HSPs, under hypoxic conditions. It is known that hypoxia stress involves ROS-mediated oxidative stress (Blokhina et al., 2003; Schmidt et al., 2018). These results suggest that activation of chaperon proteins including HSPs might be involved in signaling leading to tolerance of Al-induced oxidative stress in plants.

Nitric oxide (NO) is also induced by Al and has been suggested to be involved as a signaling molecule in Al signal transduction. There are several reports describing that Al-induced root growth inhibition is alleviated by application of the NO donor, sodium

nitroprusside (Wang and Yang, 2005; Zhang et al., 2011; He et al., 2012). More detailed research into the mechanistic basis for NO-regulated Al stress alleviation is still needed, but it may involve Al tolerance based on the following findings: (1) NO enhancement of antioxidant systems to prevent Al-induced oxidative stress (Wang and Yang, 2005; He et al., 2019), (2) NO modulation of OA metabolism and secretion under Al stress (Yang et al., 2012a,b), and (3) Al induction of endogenous ABA that may be a positive regulator of Al resistance (see phytohormone section below) (He et al., 2012).

Phytohormones

The root apex is the primary site of Al toxicity, and one of most active sites in the plant for phytohormone signaling (Ryan et al., 1993; Jung and McCouch, 2013). Auxin (i.e., Indole-3-acetic acid [IAA]) is a key regulator for plant root growth and development (Overvoorde et al., 2010). An appropriate auxin gradient with a maximal auxin gradient in the root apex are essential for continuous root growth (Petersson et al., 2009). Several membrane-localized PIN-FORMED (PIN) proteins, which are auxin-efflux transport proteins, play a major role in the regulation of the formation and maintenance of this gradient (Wiśniewska et al., 2006; Grieneisen et al., 2007). Al toxicity disturbs this auxin gradient in the root apex (Kollmeier et al., 2000; Shen et al., 2008); moreover, Al interferes with the appropriate membrane localization of PIN2 in Arabidopsis root tip cells (Shen et al., 2008). In addition, Al sensitivity was altered by knock-out or over-expression *PIN* genes in rice and Arabidopsis (Sun et al., 2010; Wu et al., 2014, 2015). These results suggest that abnormal PIN-mediated auxin flux in the root apex under Al stress is one of reasons for Al-induced root growth inhibition. Additionally, several Al-inducible IAA synthesizing genes, *AtTAA1* and *AtYUCCA*, encode proteins that regulate IAA accumulation in the root transition zone (TZ) which is located between the root meristem and zone of elongation (Yang et al., 2014; Liu et al., 2016). These genes are specifically induced in the TZ in response to Al, and activate IAA biosynthesis, resulting in root growth inhibition. Lastly, a recent study showed that the multidrug and toxic compound extrusion transporter, DETOXIFICATION 30 (DEX30), regulates auxin homeostasis in the TZ under Al stress, and contributes to Arabidopsis Al tolerance (Upadhyay et al., 2020).

Abscisic acid (ABA) also appears to be involved in Al signaling. Similar to several other phytohormones, endogenous ABA levels are upregulated under Al stress (see, for example, Kasai et al., 1995). However, unlike auxin and ethylene, ABA positively regulates Al tolerance. Al-induced root growth inhibition is alleviated by exogenous ABA application in barley, soybean, and buckwheat (Kasai et al., 1993; Shen et al., 2004; Hou et al., 2010; Reyna-Llorens et al., 2015). Additionally, co-treatment of ABA and Al induce greater root tip organic acid release than Al alone in soybean (Shen et al., 2004). In addition, ABA induces *AtALMT1* and *AtMATE* expression and malate release without Al in Arabidopsis (Kobayashi et al., 2013a). Therefore, Al-induced ABA production may contribute to the activation of OA transporter expression and increased OA release, which leads to Al resistance. Interestingly, IAA also induces *AtALMT1* expression, but it cannot activate malate release from roots without Al. This result is consistent with the finding that IAA treatment does not enhance Arabidopsis Al resistance.

Phosphatidylinositol

Recently, Wu et al. (2019) reported that blockade of phosphatidylinositol (PI) signaling, especially the Phosphatidylinositol 4-kinase (PI4K) and phospholipase C (PLC) pathways, leads to down-regulation of a number of Al-inducible genes, including *ALMT1*. PI and its derivatives are membrane lipids and conserved as signaling molecules among eukaryotes, and are involved in various important biological process such as membrane trafficking, root hair and pollen tube tip growth, and stress responses in plants (Meijer and Munnik, 2003; Thole and Nielsen, 2008; Ischebeck et al., 2010; Hou et al., 2016). In the screening, PIK-75 (Inhibitor for phosphatidylinositol 3-kinase [PI3K] in human) was identified that inhibits Al-induced malate secretion due to reduction of *ALMT1* expression. *In silico* docking analysis suggested that PIK-75 can interact with PI3K and PI4K in Arabidopsis. They confirmed that the PI4K and the subsequent PLC pathways play critical roles in Al-inducible *ALMT1* expression. Additionally, the blocking of the PI4K/PLC pathways significantly suppresses several Al-inducible genes, including STOP1-dependent target genes. The PI3K inhibitor does not affect Al-induced gene expression, suggesting that the PI4K/PLC pathways uniquely regulate signaling pathways associated with Al-inducible gene expression. However, PI3K is involved in plant Al signal transduction, because the PI3K inhibitor reduces root malate exudation via activation of the ALMT1 protein. More than 20 years ago, (Jones and Kochian, 1995) already speculated that the relationship between Al toxicity and membrane lipids included phosphatidylinositol. They found that Al directly and strongly binds to several plasma membrane lipids. PI(4,5)P2, the intermediate product between the PI4K and PLC pathways, has highest binding affinity with Al^{3+}. In addition, inositol trisphosphate, which is one of final products in the PI4K/PLC pathways, is transiently accumulated in culture coffee cells under Al stress (Poot-Poot and Teresa Hernandez-Sotomayor, 2011). These findings suggest that Al alters PI signaling/metabolism, and this could be a possible sensing mechanism for Al stress in plants.

P DEFICIENCY STRESS AND RESPONSES

Root system architecture (RSA) alterations leading to longer and thinner ageotropic lateral roots in the topsoil (where P levels are highest) is essential for the plants to more effectively forage for P in the soil, increasing P acquisition under low soil P availability (Lynch, 2011). The main processes that affect RSA and increase root exploration capacity stem from cell division in the root pericycle ahead of generation of lateral root meristems, which allows for indeterminate growth, and the formation of seminal and lateral roots arising from lateral meristem initials in the pericycle of the root stele (López-Bucio et al., 2003).

Root remodeling in soils with low-P availability is related to two types of signaling pathways. Local signaling is associated with RSA modifications regulated by changes in the rhizosphere P concentration in the soil, with the root apical meristem (RAM) being the site sensing the P changes in the soil (Chien et al., 2018). Under low-P conditions, the differentiation of meristematic and stem cells especially in the pericycle, where lateral roots arise, are triggered (Sánchez-Calderón et al., 2005; López-Bucio et al., 2019; Wang et al., 2019). The second P signaling pathway is systemic signaling, where low soil P availability results in lower shoot P availability, triggering systemic responses transmitted to the root to reprogram root processes enhancing P acquisition. The primary conduit for these systemic responses is the phloem, which in addition to sugars produced by photosynthesis in mature leaves, also contains hundreds or thousands of different RNA species and proteins that can serve as signaling molecules for plant responses.

The best example of this is plant response to P deficiency, which triggers massive changes in the phloem transcriptome and proteome (Zhang et al., 2016; Zhang Z. et al., 2019). The first example of P deficiency systemic signaling involves the *microRNA 399* (*mirR399*), which is induced early in the low-P response in leaves and moves to the root in the phloem to interact with its target, the *PHO2* gene (Fujii et al., 2005; Chiou et al., 2006; Hu et al., 2015). The transcription factor AtMYB2 acts as a direct transcriptional activator of *miR399* (Baek et al., 2013), and *miR399* then can directly cleave *PHOSPHATE 2* (*PHO2*) mRNA in some species (Bari et al., 2006; Ramírez et al., 2013; Ouyang et al., 2016). PHO2 is a ubiquitin-conjugating E2 enzyme (UBC24) that negatively regulates P transporters, inhibiting P uptake and root-to-shoot translocation under sufficient P conditions (Aung et al., 2006; Bari et al., 2006). Subsequent studies showed that PHO2 targets proteins that are involved in expression of the root high affinity uptake transport genes, *Pht1;8* and *Pht1;9*. *miR399* is strongly induced by P deficiency in source leaves and then loaded into the phloem, where it is translocated to the root and silences *PHO2*, which in turn allows high expression of *Pht1;8/Pht1;9* and increased root P uptake (Fujii et al., 2005; Bari et al., 2006; Chiou et al., 2006; Hsieh et al., 2009). In the Zhang et al. (2016) paper cited above, the authors directly identified and quantified mRNAs that move from the shoot toward the root in the phloem, and whose abundance are altered by P deficiency. They used the appearance of *miR399* in the phloem as a bioassay for the plant perceiving P deficiency in the shoot and found it appeared in the lower source leaf phloem rapidly, within 12 h after withholding P from the roots. In this study they found that imposition of Pi stress induced large and rapid changes in the mRNA population in the phloem, and grafting studies demonstrated that many hundreds of phloem-mobile mRNAs are delivered to specific sink tissues, including the root. From these findings the authors proposed that the shoot vascular system acts as the site of perception for root-derived Pi stress signals, and the phloem delivers a cascade of signals to the different plant sinks, in order to coordinate P status throughout the plant. The molecular mechanisms for both local and systemic signaling that orchestrate P sensing and activation of pathways induced by low-P availability are not fully understood. The cross-talk between regulatory networks certainly occurs, but the information available is still fragmented, so this topic will focus on the transcriptional networks and molecules involved in P response and root remodeling.

MicroRNA 399 plays this key role in Pi-starvation signaling network in many plant species other than Arabidopsis. Its rice homolog, *LEAF TIP NECROSIS1* (*LTN1*), is associated with root morphology changes under low-P, and the lack of function *ltn1* mutant exhibits elongation of primary and adventitious roots under P starvation. In rice, *LTN1* is a key component downstream of *miR399* in the P starvation response (Hu et al., 2011). In maize, *miR399* transcripts are strongly induced in maize by P deficiency. Moreover, lines overexpressing *MIR399b* accumulated more P in their shoots, showing P-toxicity phenotypes and presented significantly lower abundance of the long-noncoding RNA1 (*PILNCR1*) in P-efficient lines, indicating that the interaction between *PILNCR1* and *miR399* is important for tolerance to low-P (Du et al., 2018). Finally, the overexpression of the transcription factor, *WRKY74*, in rice led to a larger root system phenotype, enhanced P acquisition and grain yield (Dai et al., 2016). These authors also showed that OsWRKY74 likely is a positive regulator of *miR399*.

PHOSPHORUS-STARVATION TOLERANCE 1 (PSTOL1) genes

To date, there are not many genes that directly link root morphology and P acquisition, particularly in crop species cultivated in soils with low-P availability. A receptor-like cytoplasmic kinase gene named *PHOSPHORUS-STARVATION TOLERANCE 1* (*PSTOL1*) described by Gamuyao et al. (2012), is the first candidate P efficiency (tolerance to low soil P) gene identified. This gene encodes a receptor-like kinase and is responsible for a major quantitative trait locus for rice root P uptake (Wissuwa et al., 2002). Rice lines overexpressing *PSTOL1* showed greater root total length and root surface area (Gamuyao et al., 2012), and enhanced phosphorus uptake and grain yield under low-P conditions compared to the control. PSTOL1 is expressed in the crown root primordial and parenchymatic cells located outside of the peripheral vascular cylinder, where crown roots are formed in rice (Gamuyao et al., 2012). Although P-starvation induced (*PSI*) genes were not differentially regulated by PSTOL1, constitutive genes with regards to P supply, such as HOX1 (Scarpella et al., 2005), a transcription factor that is a positive regulator of root cell differentiation, was up regulated in lines overexpressing *PSTOL1* in the Gamuyao et al. (2012) study, which is consistent with the proposed role of PSTOL1 in regulating early crown root development and root growth in rice.

In sorghum, multiple homologs of *OsPSTOL1* were shown by candidate gene association mapping to be associated with P efficiency in the field (grain yield and P uptake on low-P soil) and/or in the lab (changes in root topology and growth, and P uptake; Hufnagel et al., 2014). In this study, these sorghum *SbPSTOL1* genes appear to modify root system morphology and architecture, leading to increases in grain yield in field studies on a low-P Brazilian soil, and also exhibited enhanced

biomass accumulation and P content in sorghum landraces from West Africa using native soils. These data suggest a stable effect of the target alleles across environments and sorghum genetic backgrounds (Hufnagel et al., 2014; Bernardino et al., 2019). In maize, homologs of *OsPSTOL1* that were preferentially expressed in roots and co-localized with QTLs associated with root morphology and P acquisition traits (Azevedo et al., 2015), mapped in the same region as QTLs for grain yield on a low-P soil (Mendes et al., 2014).

TFs Involved in Plant Low-P Response/P Efficiency

The maize transcription factor (TF) ROOTLESS CONCERNING CROWN AND SEMINAL ROOTS (RTCS) has been shown to be involved in altering root development and architecture (Hetz et al., 1996; Taramino et al., 2007). More recently, Salvi et al. (2016) also reported co-mapping of a quantitative trait loci controlling the number of seminal roots in maize, with the *RTCS* gene. RTCS contains a Lateral Organ Boundaries (LOB) domain, LBD, that is induced by auxin. RTCS acts downstream of ARF34 (and is responsible for the initiation of embryonic seminal and postembryonic shoot-borne roots (Xu et al., 2015). Other RTCS LBD proteins are involved in several developmental processes; for example, Arabidopsis LBD16/ASYMMETRIC LEAVES18 (ASL18) is involved in the regulation of lateral root formation, downstream of ARF7 and ARF19 TF's (Lee et al., 2009). RTCS was highly expressed in a P efficient maize genotype under low-P conditions when compared to a P inefficient genotype (De Sousa et al., 2012), indicating that is modulated by maize P status.

The TF *PTF1* (*phosphorus starvation transcription factor*) is a member of the *BASIC HELIX-LOOP-HELIX* (*bHLH*) family of TF's and plays a role in low-Pi tolerance response in rice, maize and soybean (Yi et al., 2005; Li et al., 2011; Li Z. et al., 2019). In maize, ZmPTF1 is involved in the promotion of lateral root development and also binds to the promoter and positively regulates the transcription of a number of other TF's including *9-cis-epoxycarotenoid dioxygenase (NCED)*, *C-repeat-binding factor (CBF4)*, *ATAF2/NAC081*, and *NAC30*. RNA-seq data showed that genes related to the auxin signaling pathway are also up-regulated in *ZmPTF1* overexpression lines (Li Z. et al., 2019). These authors suggested that ZmPTF1 acts upstream of signaling pathways related to biosynthesis and activation of phytohormones such as ABA and auxin, which are associated with root system development and the Pi starvation and drought tolerance responses.

There are a number of other WRKY TFs involved in P deficiency stress. One of these is WRKY6, which negatively regulates *PHO1* expression under normal, sufficient P conditions. PHO1 is the phosphate efflux transporter that mediates xylem loading of Pi in the roots. When the plant experiences P deficiency, WRKY6 is degraded via 26S proteasome-mediated proteolysis (Chen et al., 2009). Its homolog in Arabidopsis, WRKY42, also negatively regulates *PHO1* transcription under P sufficiency, but under the same plant P status, it positively regulates expression of the gene encoding the root Pi uptake transporter, PHT1;1 (Chen et al., 2009; Su et al., 2015). Under P deficiency, like WRKY6, WRKY42 is also degraded by the 26S proteasome. Another related TF, *WRKY45*, whose expression is root-specific, binds to two W box elements in the promoter of *PHT1* and regulates its transcription (Wang et al., 2014). WRKY75 appears to play dual roles in P deficiency responses. It is an activator of expression of a number of P deficiency induced genes, including phosphatases and P transporters (Devaiah et al., 2007). But it also is a negative regulator of root development associated with P deficiency. That is, when it is knocked out, lateral root length and number, and root hair density, were significantly increased. Hence, *WRKY75* is the first WRKY transcription factor to be shown to regulate both a nutrient deficiency response and root development and architecture.

Major Al Tolerance Genes That Are Also Involved in P Deficiency Stress Pathways

As plants that have adapted to highly acidic soils have had to deal with the dual stresses of Al toxicity and low soil P availability/high P fixation (Kochian et al., 2015), it is not surprising researchers have recently begun to discover that what were believed to solely be Al tolerance genes also can be involved in P deficiency responses and possibly P efficiency. These findings come from research on Arabidopsis, and the three key players in this scenario are STOP1, the TF that regulates Al-induced expression of a number of Al tolerance genes (Iuchi et al., 2007), and two of the genes regulated by STOP. These are *ALMT1*, the root tip PM malate anion channel that is activated by Al and releases Al chelating malate into the acid soil rhizosphere (Hoekenga et al., 2006), and *ALS3*, whose function is more varied and puzzling. ALS3 was first shown by Larsen et al. (2005) to be an Al tolerance gene that encodes an ABC transporter that in the shoots, is localized to the vasculature and hydathodes. The authors showed in the shoot it was PM-localized and speculated it could confer Al tolerance by loading Al into the phloem, thus moving it away from the site of toxicity in the root tip.

More recently, Dong et al. (2017) found that in Arabidopsis roots, knockout of *ALS3* results in hypersensitivity to low-P. In this study, ALS3 was found to be part of a root tonoplast ABC transporter complex with AtSTAR1, which is the counterpart of rice OsSTAR1, which in rice pairs with OsSTAR2 (the rice counterpart of ALS3) to form a cytoplasmic vesicle ABC transporter involved in rice Al tolerance (Huang et al., 2009). The Arabidopsis ALS3/AtSTAR1 transporter complex was shown to mediate electrogenic transport in oocytes (transports net charge across the membrane), but it is not clear what solute AtSTAR1/ALS3 transports across the root-cell tonoplast. This study is one of several (the others being; Müller et al., 2015; Balzergue et al., 2017; Mora-Macías et al., 2017) that together explain the primary Arabidopsis P deficiency response, which is inhibition of primary root growth and continued lateral root growth under low-P growth conditions. This response involves the genes initially shown to be involved in Al tolerance, *ALS3*, *ALMT1* and *STOP1*. The low-P inhibition of primary root growth requires Fe to occur, and under low-P conditions, Fe

accumulation both into the root symplasm and the cell wall is increased. The path of events that start with P deficiency under sufficient/high Fe growth conditions and end with inhibition of Arabidopsis primary root growth are both elegant and relatively complex. These events are summarized here:

(1) P deficiency inhibition of Arabidopsis primary root growth requires available Fe in order to occur.
(2) Under P deficiency, STOP1 induces *ALMT1* gene expression; subsequently the ALMT1 protein releases malate into the root tip apoplast and rhizosphere where it increases Fe availability in the apoplast via chelation of Fe^{3+} from the rhizosphere.
(3) At the same time, P deficiency induces the release of the multicopper ferroxidase, LPR1, from the ER to the cell wall of RAM cells surrounding stem cells in the RAM. LPR1-mediated reduction/oxidation of ferric/ferrous ions in this cell wall region generates peroxide, which catalyzes lignification and cell wall stiffening, accounting for the initial rapid inhibition of root growth.
(4) Concurrently, the ROS generation from LPR1-mediated ferroxidase activity triggers callose formation in this region of the RAM, which blocks plasmodesmata between the stem cells and cells surrounding the stem cell niche.
(5) This prevents for cell-to-cell transport of the TF, SHORT-ROOT, which is essential for stem cell division. This inhibition of stem cell division exhausts the meristem, resulting in the slower inhibition and termination of primary root growth.

The way that cells in the RAM perceive P deficiency is not understood, however, it is known that the accumulation of AtSTOP1 in the nucleus is the on-off switch for the regulatory mechanisms involved in the inhibition of primary root growth associated with P deficiency and Fe accumulation. Wang et al. (2019), building upon the research presented in Dong et al. (2017), showed that STOP1, ALMT1, and LPR1 act downstream of ALS3/STAR1 in controlling Arabidopsis primary root growth in response to P deficiency. Furthermore, they found that the tonoplast ABC transporter, ALS3/STAR1, represses STOP1 protein accumulation in the nucleus, thus inhibiting *ALMT1* transcriptional activation. They suggested that an unknown metabolite or ion is sequestered in the vacuole by ALS3/AtSTAR1, and this metabolite or ion is necessary for STOP1 accumulation in the nucleus. Subsequently, Godon et al. (2019) found that the stability of AtSTOP1 in the nucleus is triggered by Fe^{3+} accumulated in root cells under P deficiency, and not the decrease in P itself. They also found that Al^{3+} had the same effect as Fe on stimulating STOP1 accumulation in the nucleus, which is consistent with the abundance of toxic Al^{3+} ions in acidic soils. The authors suggested that the AtALS3/AtSTAR1 transporter may be mediating the accumulation of either ionic Fe or Al, or Fe/Al chelates in the vacuole, and in the case of P deficiency, this transporter controls cytoplasmic Fe homeostasis via the stability of AtSTOP1 in the nucleus under low-P conditions.

Involvement of Posttranslational Modification in P Deficiency Responses

SUMO E3 LIGASE (SIZ1) is responsible for post-translational modifications based on the addition of small Ubiquitin-like Modifier (or SUMO) proteins, which can affect protein function (Gareau and Lima, 2010). The MYB-like transcription factor, PHOSPHATE STARVATION RESPONSE1 (PHR1), which modulates RSA under P starvation, is one example of a protein modified by sumoylation (Miura et al., 2011). In rice, OsMYB2P-1 positively regulates P starvation signaling and lines overexpressing this gene have a longer primary root and more lateral roots compared to the wild type under low-P conditions (Dai et al., 2012). PHR1 and its homolog PHL1 (PHR1-Like1) directly bind to the *cis*-element, P1BS (Rubio et al., 2001), which is prevalent in the promoters of many P starvation induced genes, including *PHO1*, *miR399*, *IPS1* (*INDUCED BY PHOSPHATE STARVATION1*), and *RNS1* (*RIBONUCLEASE1*) (Poirier et al., 1991; Bariola et al., 1994; Martín et al., 2000; Bari et al., 2006). PHR1 has also been found to be sequestered from the nucleus in a P-dependent manner by SPX1, a nucleus-localized SYG/PHO81/XPR1 domain protein, inhibiting PHR1 activity (Puga et al., 2014). In rice, SPX4 negatively regulates *PHR2*; under low-P, *SPX4* degradation is accelerated through the 26S proteasome pathway, releasing PHR2 into the nucleus and activating the expression of *PSI* genes (Lv et al., 2014). Getting back to sumoylation, a loss-of-function *siz1* mutant exhibited reduced primary root growth and increased lateral root and root hair length and density, which is apparently independent from the PHR1/SIZ1 signaling pathway (Miura et al., 2011). SIZ1 is also involved in the negative regulation of auxin patterning to modulate RSA in response to low-P (Miura et al., 2011).

This *siz1* mutation also revealed a dual role of the SIZ1 E3 ligase in the regulation of P homeostasis in rice. In *siz1* rice plants grown under P deficiency, two root high-affinity P transporter genes, *OsPT1* and *OsPT8*, were more highly expressed compared to the WT, whereas *OsPT2* and *OsPT6* (which are expressed in both roots and shoots) were down-regulated (Wang et al., 2015). OsPT2 and OsPT8 are phosphorylated by CASEIN KINASE2 (CK2), which inhibits their interaction with PHOSPHATE TRANSPORTER TRAFFIC FACILITATOR1 (OsPHF1) under normal conditions. OsPHF1 is a SEC protein that facilitates the trafficking of Pi transporters from the ER to the PM (González et al., 2005). The retained phosphorylated phosphate transporters in the endoplasmic reticulum lead to a reduced P absorption from the rhizosphere (Chen et al., 2015). Also, rice PROTEIN PHOSPHATASE95 (OsPP95), a PP2C protein phosphatase negatively regulated by OsPHO2, positively regulates P homeostasis and remobilization, through the interaction with OsPT2 and OsPT8. OsPP95 acts antagonistically with CK2 to regulate the reversible phosphorylation of phosphate transporters (Yang et al., 2020b).

Another transcriptional factor with a role in P homeostasis is WRKY6, which was shown to negatively regulate the expression of *PHO1* (Chen et al., 2009), which is a phosphate efflux transporter localized to the Arabidopsis root vasculature and

is key in loading Pi absorbed by roots from the soil into the xylem for translocation to the shoot (Hamburger et al., 2002). Its closest Arabidopsis homolog, WRKY42, also negatively regulates *PHO1* transcription under P starvation, (Chen et al., 2009; Su et al., 2015). Interestingly, under Pi-sufficient conditions, WRKY42 positively regulates *PHT1;1* expression, which is a root high and low affinity Pi uptake transporter in Arabidopsis (Shin et al., 2004). WRKY42 accomplishes this by binding directly to the *PHT1;1* promoter, and this binding is abolished by low-Pi stress. During Pi starvation, the WRKY42 protein is degraded through the 26S proteasome pathway. These results show that AtWRKY42 modulates Pi homeostasis by regulating the expression of *PHO1* and *PHT1;1* to adapt to environmental changes in Pi availability.

Members of the Proteaceae Family Have Evolved Unique Adaptations to Acquire P From Low-P Soils

Some plant species of the Proteaceae family develop cluster or proteoid roots in response to growth on low-P soils. Cluster roots are specialized primary lateral roots that develop one or more clusters of rootlets along their axes. Cluster roots synthesize large amounts of organic acid, such as citrate and malate, which are subsequently released into the rhizosphere to increase P availability by chelating metals such as Fe, Al, and Ca that are fixing the phosphate anions in the soil (Keerthisinghe et al., 1998; Neumann et al., 2000; Peñaloza et al., 2002). A number of genes are involved in the developmental and biochemical responses in cluster roots. These include upregulation of the root high-affinity phosphate transporters, LaPT1, and phosphoenolpyruvate carboxylase 3 (LaPEPC3) under P deficiency. Also, it was found that white lupine homologs of the Arabidopsis SCARECROW (AtSCR), LaSCR and LaSCR1 are localized to the root endodermis and presumably help drive the developmental processes that result in these impressive clusters of laterals, which play such an important role in lupine adaptation to low-P soils (Peñaloza et al., 2005; Sbabou et al., 2010).

Recently, a cultivated accession of white lupin was sequenced and de novo assemblies of a landrace and a wild relative were also performed (Hufnagel et al., 2020). The modern accession displays an increased soil exploration capacity through early establishment of lateral and cluster roots (Hufnagel et al., 2020). The authors identified the presence of AP2/EREBP, a large multigene family that is key to control of lateral root development. They also identified several mature microRNAs expressed in cluster root sections and related to P deficiency responses, such as *miRNA156*, *miRNA166*, *miRNA211139*, and members of *miRNA399* family, that were not detected previously in white lupin. Moreover, Hufnagel et al. (2020) identified five genes that are targets of the detected miRNAs, including the TFs *LaWRKY* (*Lalb_Chr07g0182001*) and *LaPUCHI*-3 (*Lalb_Chr18g0055601*). Activation of key regulatory genes may trigger the early establishment of the root system, and consequently P-uptake and P efficiency (increased grain yield on low-P soils).

DROUGHT STRESS AND TOLERANCE

Drought stress is the most widespread abiotic stress affecting crop yield and quality. Due to the sessile nature of plants, evolutionary adaptations have enabled plants to develop sophisticated mechanisms to tolerate or avoid drought. When plants sense water deficit in the surrounding environment, it leads to the generation of drought stress signals (Blackman and Davies, 1985; Kuromori et al., 2014; Batool et al., 2019). These primary and secondary drought response signals are perceived by receptor molecules which leads to direct changes in the expression of genes or expression of TFs that regulate expression drought-responsive genes, which ultimately leads to drought adaptation (Kuromori et al., 2014). Drought signaling networks are presumably complex and to date poorly understood, but it is clear they involve both intercellular and intracellular signaling (Kuromori et al., 2014). Because this review focuses on root adaption to multiple stresses, here we will focus on the role of drought-related communication between the roots and shoots involving intercellular signaling networks and TFs responsive to drought.

Drought Signaling Molecules

Hormones

Several studies have shown that phytohormones act as signaling molecules in response to drought. ABA is one of the most widely studied phytohormones in part because of its role in regulating stomatal conductance in response to different related abiotic stresses that impact plant water status including drought, salinity, high and low temperatures. Jones and Mansfield (1970) showed that external application of ABA to roots led to a reduction in stomatal aperture suggesting that ABA was involved in regulation of stomatal conductance. This led a number of researchers to conduct plant water stress studies investigating the hypothesis that root-derived ABA is a primary candidate for root to shoot drought signaling. It had been generally accepted that stomatal closure in response to drought was triggered by reductions in leaf water potential due to the drought conditions. A key finding in changing thinking about drought signaling came from the work of Blackman and Davies (1985), which showed that reduced water content in roots in response to drought led to stomatal closing or reduction in stomatal aperture without changes in leaf water potential. This indicated that a signal was likely traveling from the root to leaves to help induce stomatal closure. As described above regarding the earlier work of Jones and Mansfield (1970), ABA was already known to decrease stomatal opening and thus it became a logical candidate for a drought-induced root signal transmitted to leaves. Subsequently, it was shown that upon soil drying, the ABA concentration was increased in maize roots and xylem sap (Zhang and Davies, 1989, 1990a), and these findings further strengthened the idea of ABA as a key drought induced signal in root to shoot signaling. Subsequent work with a number of plant species, including maize, sycamore, lupin, wheat, castor bean and grapevine (Loveys and Kriedemann, 1974; Zhang et al., 1987; Henson et al., 1989; Zhang and Davies, 1990b) all showed that soil water deficit induced ABA synthesis in roots, and the newly synthesized ABA was then translocated to leaves via the xylem to induce stomatal closure.

Drought stress can cause arrested shoot growth; however, it has been shown that under those conditions root elongation can continue due to ABA-mediated plant adaptations (Sharp and Davies, 1989; Saab et al., 1990; Sharp et al., 1994) observed that primary root elongation was maintained under water limited conditions, and in subsequent work it was suggested that increased ABA accumulation in the root under drought conditions (water potential [ψ_w] of −1.6 MPa) might play a key role in the prevention of root growth elongation inhibition under drought stress (Saab et al., 1990). In the Saab et al. (1990) study, two treatments were employed. These involved both the root application of fluridone, an inhibitor of carotenoid biosynthesis that provides the precursors for ABA biosynthesis, and the use of the *vp5* mutant that is deficient in carotenoids that leads to reduced ABA synthesis. They showed that in both of these treatments, the roots did not maintain continued root elongation at a lower water potential compared to wild type maize plants. They also conducted these experiments in a dark environment with saturated humidity to rule out the indirect effects of ABA deficiency on photosynthesis and/or alterations in stomatal control. Subsequently, Sharp et al. (1994) confirmed the role of ABA in maintenance of tap root growth under water limited conditions by applying exogenous ABA, which recovered the wild type root growth phenotype in both the *vp5* mutant and fluridone-treated plants under drought. Based on an earlier report by Wright (1980) on the interaction between ABA and ethylene, researchers from the Sharp lab also investigated whether ABA-dependent inhibition of ethylene synthesis was involved in the maintenance of root elongation under water limited conditions (Spollen et al., 2000). In this study, wild type root growth elongation was recovered by applying ethylene synthesis and action inhibitors in the vp5 mutant and in fluridone-treated maize plants, suggesting that the ability of root growth to better tolerate drought compared to shoot growth does involve interactions between ABA and ethylene.

Despite this body of work supporting the hypothesis of root to shoot translocation of ABA in response to drought, other studies suggesting the importance of leaf ABA synthesis have been carried out in a number of labs using reciprocal grafting between wild type and ABA deficient mutants in tomato, Arabidopsis, and sunflower. In these studies, drought stress was imposed on the wild type shoot/mutant roots and mutant shoots/wild type roots grafting combinations. When these different grafted "genotypes" were water stressed, the shoot genotype was shown to control stomatal behavior, suggesting that shoot-derived ABA was also important drought response (Jones et al., 1987; Fambrini et al., 1995; Holbrook et al., 2002; Christmann et al., 2007; Dodd et al., 2009). In summary, despite the general acceptance in the plant water relations that the primary mode of ABA signaling occurs via root ABA synthesis, followed by translocation via xylem to the leaves, it is clear that the field of plant ABA signaling is not unified behind this hypothesis. As supported by the findings reported in the publications summarized in this section of the review, ABA signaling may involve both roots and leaves, with a systemic response involving ABA that is made in roots under drought and transported to leaves, and a more local response within the drought-stressed leaf.

The ABA signaling pathway has been studied extensively in the model plant, *Arabidopsis thaliana*. ABA receptors have been identified in Arabidopsis, and during ABA signaling, ABA has been shown to bind to intracellular ABA receptors from the PYR/PYL/RCAR family, triggering a signal cascade that results in ABA-mediated stomatal closure (Fujii et al., 2009; Nishimura et al., 2009; Santiago et al., 2009; Cutler et al., 2010; Gonzalez-Guzman et al., 2012). The binding of ABA to its receptor leads to interactions with a Type 2C protein phosphatase (PP2C), which inhibits PP2C-mediated activation of an OST (Open stomata) 1 kinase. This kinase is responsible for stomatal opening by controlling anion channels in the guard cell plasma membrane, and blocking its activation results in stomatal closure (Ma et al., 2009; Park et al., 2009; Hauser et al., 2017). Hence, PP2C is a negative regulator of the ABA signaling pathway, resulting in stomatal closure. Interesting recent findings from Belda-Palazon et al. (2018) showed that the PYL8 ABA receptor is responsible for root perception of ABA though a non-cell-autonomous mechanism. In this study the PYL8 transcript was localized to the root meristem epidermis and stele, while the PYL8 protein was also found in adjacent tissues. The authors go on to show that both inter- and intracellular trafficking of PYL8 appears to occur in the RAM. This study shows that ABA receptors can interact with ABA in the root. It doesn't appear that this interaction plays a role in drought signaling to the shoot. Instead the authors hypothesize that the binding of ABA to the PYL8 receptor in the root may be involved in well documented roles of ABA in root function including root growth associated with hydrotropism and salt stress, and root plasticity in response to variation in nutrient availability (Barberon et al., 2016; Feng et al., 2016; Dietrich et al., 2017).

There are a number of published papers indicating that ABA biosynthesis occurs in both shoots and roots, and this occurs first via biosynthetic processes in plastids, and then the ABA precursors made in the plastid are transported to the cytosol, where they are converted to ABA (Thompson et al., 2007; Fujii et al., 2009; Nishimura et al., 2009; Santiago et al., 2009; Cutler et al., 2010). With regards to drought signaling regulation of stomatal function, cytosolic ABA has been found to bind to PYR1-type ABA receptors also located in the cytoplasm (Fujii et al., 2009; Nishimura et al., 2009; Santiago et al., 2009; Cutler et al., 2010). Based on the findings presented above for (Belda-Palazon et al., 2018), it is clear that ABA receptors are both functioning in the root and the leaf. In the studies showing that ABA binds to PYR1-type ABA receptors in leaf tissue, although not directly stated, the clear implication is that this ABA interaction with its receptor occurs in the guard cell cytoplasm, although that has not yet been shown.

Components of the ABA signaling pathway that are involved in moving ABA either into guard cells or from roots to leaves have been found. Kuromori et al. (2010) identified an ABC (ATP binding cassette) efflux transporter gene *AtABCG25* that encodes an ABC transport protein localized in the root vascular parenchyma plasma membrane. This transporter exports ABA accumulated in root xylem parenchyma cells into xylem vessels

in response to drought stress. Studies also showed that transgenic Arabidopsis plants overexpressing *AtABCG25* had higher leaf temperatures and lower transpirational loss of water from detached leaves, compared to wild type plants. This is consistent with more ABA being provided to guard cells from the root, leading to stomatal closure. Furthermore, Kang et al. (2010) has identified an ABA uptake transporter, AtABCG40 (also known as Pleiotropic drug resistance transporter PDR12). This ABC transporter is localized to the plasma membrane and predominantly expressed in leaf guard cells, where it acts to transport ABA that is delivered via the xylem, into guard cells. In summary, many of the structural components of the root to shoot ABA signaling network are being identified, including root-localized ABA biosynthetic pathways, transporters involved in xylem translocation of ABA to the shoot, and transporters in the leaf moving ABA into guard cells.

Another hormone that appears to be involved in drought signaling is cytokinin. Reduced maize stomatal aperture due to exposure to dry soil was reversed by the application of cytokinin to the roots (Blackman and Davies, 1985). Whereas xylem levels of ABA are increased in response to drought treatment of rice seedlings, cytokinin levels are decreased under the same drought conditions (Bano et al., 1993). These findings suggest that both hormones are involved in drought signaling, acting antagonistically to more finely regulate stomatal aperture related to plant water status (Blackman and Davies, 1985; Bano et al., 1993).

Peptide Hormones

The CLE (CLAVATA3/EMBRYO-SURROUNDING REGION) family of peptides are small peptides that function as plant hormones via release from cells into the extracellular space, where they function as intercellular signaling molecules. They have been shown to bind to receptor-like proteins at the outer surface of the plant cell plasma membrane to help mediate signal transmission. CLE peptides have been shown to regulate a range of physiological and developmental processes, including drought responses. CLE proteins have recently been shown to be a mobile signal transmitted from roots to shoots and involved in increased ABA biosynthesis after dehydration stress (Takahashi et al., 2018). In this study, synthetic isotope-labeled CLE25 was externally applied to roots and its accumulation was detected in leaves of treated plants using nanoscale nLC-MS/MS. The CLE25 peptide has been shown to be involved in regulation of ABA biosynthesis in leaves after the roots sense drought conditions in the soil (Takahashi et al., 2018). CLE25 is expressed in vascular tissues and its expression is induced in response to drought. Subsequently, the CLE25 peptide moves from the roots to leaves, where it enhances ABA synthesis and accumulation, helping trigger stomatal closure. It does this by binding to BARELY ANY MERISTEM (BAM) receptors in leaves. It is possible that CLE25 plays a role in the leaf-mediated regulation of stomatal function described above from the earlier publications reporting on the physiology of drought induced stomatal closure. If this is the case, then CLE2 could be a second root-to-shoot drought signal (the other being ABA itself) that triggers leaf-localized ABA regulation of stomatal responses to drought.

Other Signals

Plant cellular and apoplastic pH has been proposed to be another signaling factor that could play a role in stomatal aperture regulation (Hartung et al., 1998; Wilkinson, 1999). Drought stress has been shown to trigger an increase in xylem sap pH (Gollan et al., 1992; Wilkinson and Davies, 1997; Hartung et al., 1998). Under these conditions, Wilkinson and Davies (1997) found that this led to an increase in apoplastic ABA in the leaves. They hypothesized that as drought increases ABA concentrations in the xylem sap, and are then transported to the leaves, the higher apoplastic (xylem) pH will deprotonate acid groups in the ABA molecules and the increased charge of the ABA anion will reduce passive ABA flux through the lipid bilayer of the leaf cell plasma membrane. Hence, they speculated that extracellular ABA may be important in triggering stomatal closure. This is a topic that will require more research to more clearly define both the role of xylem pH in drought signaling and the role of apoplastic ABA in directly regulating stomatal response to drought.

Recent studies have identified specific microRNAs that are responsive to drought stress (Bakshi and Oelmüller, 2014; Bakhshi et al., 2016; Aravind et al., 2017) and this could be part of another drought signaling mechanism, as microRNAs can regulate genes post-transcriptionally (Aukerman and Sakai, 2003). Bakhshi et al. (2016) identified 61 known and 11 novel microRNAs involved in drought signaling in rice by performing experiments with a divided root system where half of the root system was water stressed and the other half kept well-watered. They identified miRNAs that exhibited differential expression when the entire root system is exposed to drought stress, along with miRNAs whose expression was altered in response to divided root system drought versus well-watered signaling. The results for differential expression of many of the miRNAs were validated via qRT-PCR. Furthermore, *in silico* target analysis led to the identification of two to three hundred novel target genes for the drought stress response of the entire root system, along with responses of the divided root system to drought and well-watered conditions. From the target analysis, the authors proposed these miRNAs could be involved in a number of drought response pathways, including ABA and calcium signaling, detoxification of free radicals induced by drought, and stimulation of lateral root initiation and growth, which could lead to bigger and deeper root systems that could more effectively acquire water located deeper in the soil profile under drought.

TFs Responsive to Drought

It is well known that transcription factor (TF) proteins can play major roles in regulatory and signaling networks, and plant drought response is no exception. A number of recent studies have been conducted to identify TFs responsive to drought and in some these studies, the function of the identified TFs has been elucidated (He et al., 2016; Lee et al., 2016, 2017; Chen Y. et al., 2018; Kumar et al., 2019). TFs responsive to drought are members of several different TF families including: (1) the AREB/ABF (ABA responsive binding or ABRE binding factor) family; (2) the AP2/ERF (ethylene response element binding factor) family; (3) the bZIP (the basic leucine zipper) family; (4) the NAC (NAM,

ATAF1,2, CUC2) family; and (5) the WRKY transcription factor family (Joshi et al., 2016).

With regards to a TF in the AREB/ABF family involved in drought signaling, Marinho et al. (2016) showed that soybean transgenic lines overexpressing *AtAREB1* exhibited enhanced performance under drought without any penalty on yield. From changes in expression profiles for phosphatases (PP2C) and kinases (SnRK2) in the *AtAREB1*-overexpressing transgenic plants, the authors noted that the observed lower expression of phosphatases and higher expression of kinases are known to be linked to ABA-dependent stomatal closure, and the resulting reduced stomatal conductance to water in the OE lines could explain the observed drought resistance. This overexpression line also had a higher leaf area index and elevated intrinsic water use in subsequent research by Fuganti-Pagliarini et al. (2017). In rice, overexpression of *OsERF71* altered expression of genes that regulate lignin biosynthesis and cell wall loosening enzymes, leading to increased root radial growth, more cell layers in the vasculature, and increased root aerenchyma, and these root structural changes were associated with reduced water transpiration and increased drought tolerance (Lee et al., 2016). OsERF71 belongs to the AP2/ERF TF family and is mainly expressed in the root endodermis, meristem and pericycle tissues. It was not clear how these root structural changes confer drought resistance, but the authors noted that increased radial growth has been observed in other studies in response to drought. The authors pointed out that in these previous studies, it has been suggested that observed increases in aerenchyma could reduce the carbon cost required to produce bigger root systems (Zhu et al., 2010). In the *OsERF71* overexpressing lines, the putative lignin biosynthesis genes, cinnamoyl-coenzyme was expressed ten-fold higher than in wild type plants. This was associated with quantification of higher lignin accumulation in roots tissues by phloroglucinol staining in the transgenic plants. Increased lignin biosynthesis might be required for additional root layer formation for wider radial root growth to accommodate larger aerenchyma.

NAC TFs have been characterized in transgenic wheat and it was reported that *TaRNAC1*-overexpressing lines exhibited changes in root growth and structure, which resulted in larger and deeper root systems and increased performance under drought, presumably due to enhanced water acquisition (Chen D. et al., 2018). Finally, He et al. (2016) evaluated Arabidopsis transgenic lines overexpressing the wheat *TaWRKY33* transcription factor for drought tolerance. They observed that *TaWRKY33* overexpression was associated with increased expression of *ABI5*, which encodes a basic leucine zipper transcription factor that in involved in the regulation of seed germination and early seedling growth under abiotic stress conditions that involve ABA. It has been shown that ABI5 is involved in the receptor-mediated ABA signaling described above (PYR/PYL/RCAR ABA receptors, PP2C phosphatases and SnRK2 kinases), through its interaction with ABSCISIC ACID RESPONSE ELEMENT (ABRE) motifs in target gene promoters. Hence, ABI5 has been shown or proposed to be involved in many ABA-related activities, including seed germination, seedling stress tolerance, integration of hormone interactions, and ABA biosynthesis (for a review, Skubacz et al., 2016).

In the He et al. (2016) publication, the authors suggested that the TaWRKY-mediated increase in *ABI5* expression was likely central to the observed improved performance under drought, possibly due to increased ABA synthesis under drought conditions. In the OE lines they also observed reduced transpirational loss of water from excised leaves, which would correlate with increased ABA accumulation resulting in greater stomatal closure.

ERECTA- A Leucine Rich Repeat Receptor-Like Kinase

The *ERECTA* gene has been shown to be involved in the regulation of leaf transpirational water loss through stomata by altering leaf anatomy (Masle et al., 2005). Leaf carbon isotope discrimination, which is due to the discrimination against the naturally occurring carbon isotope, ^{13}C, in favor of the more abundant ^{12}C isotope during photosynthetic CO_2 fixation by the rate-limiting enzyme, Rubisco, is negatively related to leaf transpiration efficiency (ratio between transpirational water loss and photosynthetic CO_2 assimilation). Hence, leaf isotope C discrimination can be used as a proxy phenotype for transpirational efficiency. Using this approach, leaf isotope C discrimination was used to phenotype an Arabidopsis Col-4 x Ler RIL population. Genetic analysis of the data yielded a significant QTL for transpirational efficiency for leaf isotope C discrimination that was then fine mapped on chromosome 2 (48.96–51.02 cM) and explained up to 64% of the phenotypic variation for this trait in the RIL population. The population parents, Col and Ler, contain *ERECTA (ER)* and *er1* alleles, respectively. Upon screening of candidate genes residing in that region, they found that the *ERECTA* gene was located in the center of the QTL interval. They also observed contrasting values of leaf isotope C discrimination for individuals with the *ER* or *er1* alleles. For functional validation of the candidate gene for transpirational efficiency, multiple ERECTA mutants were compared with near-isogenic lines containing *ERECTA* allele homozygotes. They observed that all of the *er* mutants exhibited higher leaf isotope C discrimination and therefore lower transpirational efficiency than lines homozygous for *ERECTA* allele. Further, in transgenic lines which complemented the mutation with the *ERECTA* allele, they confirmed the identity of *ERECTA* as a transpirational efficiency gene. By dissecting leaf anatomical features, lower stomatal conductance because of lower stomatal density caused by epidermal cell expansion, was observed as the anatomical effect of the *ERECTA* gene. Loosely packed fewer and smaller mesophyll cells were also observed, and it was concluded that all of these phenotypes collectively are affecting transpirational efficiency. These anatomical phenotypic traits were maintained under drought stress which suggests that the *ERECTA* gene could be an important genetic tool to increase transpirational efficiency in crops in drought stress environments.

Zheng et al. (2015) also showed that the expression of two wheat *TaER* genes were positively correlated with

transpiration efficiency and yield traits. Gene sequences for ERECTA orthologs in wheat were identified by Linzhou et al. (2013) using a homology-based cloning approach. Zheng et al. (2015) subsequently found the physical chromosomal location of these genes on chromosomes 6 and 7 by using *in silico* approaches to compare *TaER* cDNA sequences to a wheat genome sequence database. The authors also observed significant variation in expression of these genes among 48 wheat varieties in the flag leaves at grain filling and at the heading growth stages. There was a significant positive correlation in TaER expression with water use efficiency, flag leaf area and yield traits (biomass and gain yield), whereas the rate of transpiration, stomatal density and rate of photosynthesis were negatively correlated. These results were consistent with Masle et al. (2005) and further strengthened the role of ER genes in regulation of transpiration efficiency. In addition to the above studies, Li H. et al. (2019) also showed increased drought resistance in Arabidopsis and maize plants by overexpressing the sorghum *ER* (*SbER2-1*) gene and the transgenic overexpression lines exhibited increased rates of photosynthesis and water use efficiency.

POSSIBLE COMMON DETERMINANTS OF AL TOLERANCE, P EFFICIENCY AND DROUGHT TOLERANCE

C2H2 TFs

Water deficit may disrupt the lipid bilayer in cell membranes, triggering protein denaturation and accumulation of cellular electrolytes, which may lead to osmotic imbalance in plant cells (Fernando and Schroeder, 2016). Hence, osmotic adjustments play a role in plant adaptation to dehydration via turgor maintenance and by the production of osmoprotectants that maintain proper cellular function (Blum, 2017). Cys2/His2-type (C2H2), zinc fingers are known to play a role in plant abiotic stresses tolerance and emerge as a possible hub controlling tolerance to Al toxicity, low-P and also drought stress. Possible mechanisms whereby C2H2 zinc fingers influence drought tolerance have been recently reviewed by Han et al. (2020). Those mechanisms involve the biosynthesis of solutes in the cell leading to osmotic adjustments, reactive oxygen species scavenging via enhanced antioxidant enzyme activity and ABA-dependent signaling pathways.

As previously described, there is evidence linking the C2H2 transcription factor, STOP1, to both Al tolerance and P deficiency tolerance (see section "Major Al Tolerance Genes That Are Also Involved in P Deficiency Stress Pathways"). This emerging pleiotropic role of STOP1 in abiotic stress tolerance has been further supported by the recent finding that *stop1* knockout lines showed enhanced drought tolerance in Arabidopsis (Sadhukhan et al., 2019). Among the genes suppressed in the *stop1* mutant was the *CBL-interacting protein kinase 23* (*CIPK23*), which may be involved in K^+/Na^+ homeostasis via regulation of K^+ transporters. In agreement with K^+ involvement in stomatal opening (Munemasa et al., 2015), further complementation experiments suggested that the STOP1 function in drought tolerance occurs via ABA-mediated stomatal closure elicited by CIPK23. A protein phosphatase 2C-family protein, PP2C61, was also repressed in the *stop1* mutant, which provides further indication of ABA-dependency for STOP1. This scenario points toward a highly pleiotropic nature of the transcription factor *STOP1*. In this context, STOP1 enhances *AtMATE*- and *AtALMT1*-mediated Al tolerance (see section "Transcriptional Regulation Involved in Al Tolerance"), inhibits primary root growth and enhances lateral root proliferation under P deficiency, possibly favoring P acquisition via Fe-mediated RAM exhaustion (see section "Major Al Tolerance Genes That Are Also Involved in P Deficiency Stress Pathways"). In addition, STOP1 may also influence both salt and drought tolerance (Sadhukhan et al., 2019). However, STOP1 was suggested to negatively impact drought tolerance in Arabidopsis (Sadhukhan et al., 2019), which may conflict with a possible general role of STOP1 in crop adaptation to acidic, tropical soils, where Al toxicity, P deficiency and drought stress usually co-exist.

NAC and bHLH Transcription Factors

There are many reports linking NAC TFs including NAM, ATAF, and CUC TFs with drought tolerance (Nakashima et al., 2012), which largely involves ABA-dependent pathways. However, some NAC TFs show very early responses to ABA treatment, probably before endogenous ABA accumulates (Tran et al., 2004). Hence, some NACs are also thought to function through ABA-independent pathways (Singh and Laxmi, 2015), at least to some extent. Mutant analysis targeting class III SnRK2 protein kinase genes resulted in repression of the NAC gene, *RD26*, indicating that the expression of stress-inducible NACs is under control of the central ABA perception and signaling module (Nakashima et al., 2012; Fernando and Schroeder, 2016). Overexpression of the stress responsive, NAC gene, *SNAC1*, has been reported to lead to salt and drought tolerance in rice without a penalty in yield (Hu et al., 2006). SNAC1 was shown to bind to the promoter of the stress-induced gene, early responsive to drought 1 (*OsERD1*), and many stress-related genes were up-regulated in the *SNAC1*-overexpressing rice plants. The transgenic lines were also more sensitive to ABA and showed reduced water loss due to enhanced stomatal closing (with apparent no effect in photosynthesis), possibly by drought induction of *SNAC1* in guard cells (Hu et al., 2006). Also, OsNAC5 has been found to improve drought tolerance in rice via up-regulation of stress-inducible genes, and both OsNAC6 and OsNAC10 may also improve rice drought tolerance (reviewed by Nakashima et al., 2014; Singh and Laxmi, 2015).

Basic helix-loop-helix (bHLH) TFs have been implicated in drought regulation of stress-related genes via a wide-range of possible tolerance mechanisms, including stomatal development, ABA signaling, trichome and root hair development, osmoregulation, photosynthesis and growth regulation, in addition to ROS scavenging (reviewed by Castilhos et al., 2015; Sun et al., 2018). For example, AtMYC2 (bHLH) and AtMYB2 (MYB) TFs interact with *cis* elements in the promoter of the dehydration-responsive gene, *rd22*, to function

as transcriptional activators in ABA-inducible gene expression under drought stress in Arabidopsis (Abe et al., 2003). However, strong alterations of stomatal development elicited by some bHLH TFs may hinder their practical application in cultivar development (Castilhos et al., 2015).

The bHLH family member, PTF1, has been found to play a role in low-Pi tolerance in rice, maize and soybean (see section "TFs Involved in Plant Low-P response/P Efficiency"). In maize, ZmPTF1 was also shown to enhance lateral root development and confer drought tolerance (Li Z. et al., 2019). Enhanced drought tolerance in the *ZmPTF1*-overexpression lines might be a result of activation of ABA and auxin signaling pathways and enhanced lateral root growth, which may be at least in part caused by up-regulation of NAC TFs. In fact, ZmPTF1 was shown to bind to the promoter of *NAC30* and other TFs, acting as a positive regulator of those genes (Li Z. et al., 2019). Thus, a possible connection between NAC-mediated tolerance to both drought and low-P conditions may be mediated at some extent via bHLH-dependent regulation of NAC TFs.

Interestingly, NAC TFs may also connect with Al tolerance based on up-regulation of *VuNAR1* in the *Vigna umbellata* root apex (Lou et al., 2020) and Al inducibility of other NACs (Escobar-Sepúlveda et al., 2017; Jin et al., 2020). Since VuNAR1 was shown to bind to the promoters of wall-associated receptor kinase genes, this NAC gene may confer Al tolerance through regulation of cell wall pectin metabolism (Lou et al., 2020). Interestingly, this mechanism could possibly feedback on P acquisition, since wall-associated kinases have been shown to affect root growth (Kanneganti and Gupta, 2008, 2011; Kaur et al., 2013).

MYB TFs

Transcription factors possessing a conserved MYB domain involved with DNA binding are important players in abiotic stress tolerance and are intimately involved in cross-talk between different types of abiotic stresses. MYB TFs may influence drought tolerance via regulation of root growth and development, leaf development, stomatal movement in response to drought, cell wall biosynthesis, cuticle and suberin biosynthesis, and antioxidant activity via accumulation of flavonoids (reviewed by Baldoni et al., 2015). MYB TFs are also closely associated with changes in root morphology, which involves rather complex responses to different hormones. MYB77 has been implicated in auxin signaling via interaction with auxin response factors (ARFs), changing lateral root growth (Shin et al., 2007). MYB involvement with ABA signaling stems from the interaction between the ABA sensing gene, PLY8, and MYB77 (Zhao et al., 2014). By increasing auxin signaling, this interaction leads to a recovery of lateral root growth following inhibition by ABA. An important role for MYB TFs in abiotic stress cross-talk is also suggested by the joint role of AtMYB60 (Oh et al., 2011) and AtMYB96 in both stomatal movement and lateral root growth, with an integrative role in ABA and auxin signaling being proposed for AtMYB96 (Baldoni et al., 2015). Another MYB transcription factor working in a similar way is SiMYB75, which function in an ABA-dependent manner to promote root growth and drought tolerance, which results from enhanced stomatal closure to reduce water loss (Dossa et al., 2020).

By far the most compelling case of a MYB transcription factor jointly modulating drought stress and P deficiency tolerance arises from AtMYB2 regulation of *miR399* (Baek et al., 2016, 2017). As previously described (Section 3), *miR399* is a key component in P homeostasis (Fujii et al., 2005; Baek et al., 2013). Baek et al. (2016) have shown that AtMYB2 regulation of miR399 is involved in drought responses, with transgenic Arabidopsis plants overexpressing *miR399f* exhibiting ABA resistance and drought hypersensitivity. This response is thought to be a consequence of ABA-signaling, with *miR399* targeting CSP41B and ABF3 (Baek et al., 2016).

WRKY TFs

WRKY TFs can act both as activators or repressors of gene expression and are involved both with abiotic and biotic stress responses (Bakshi and Oelmüller, 2014). The function of WRKY genes in drought tolerance is closely related to ABA signaling, which gives rise to a multi-pronged mode of action on plant performance under drought including stomatal closure and changes in RSA. Studies with a promoter::reporter gene construct for the sorghum member of the WRKY family, SbWRKY30, indicated that the *SbWRKY30* promoter responds to different phytohormones such as ABA, GA and Me-JA (Yang et al., 2020a). Expressed both in the tap root and leaf, *SbWKRY30* was induced by drought stress and conferred drought tolerance both in Arabidopsis and rice by affecting RSA. This drought tolerance response may also be a result of enhanced ROS scavenging elicited by SbWRKY30. This transcription factor was also found to influence the transcription of a number of stress-responsive genes, including *SbRD29* (Yang et al., 2020a).

Among other WRKY proteins, AtWRKY40 has been shown to interact with the C-terminal of the ABA receptor ABAR, with ABA acting to remobilize AtWRKY40 from the nucleus to the cytoplasm (reviewed by Rushton et al., 2012). Since AtWRKY40, AtWRKY18 and AtWRKY60 are negative regulators of ABA signaling, this mechanism leads to de-repression of ABA-dependent pathways and, hence, induction of ABA-responsive genes (Shang et al., 2010). With ABA sensing by its receptors, ABI5 is de-repressed and activates AtWRKY63, which activates stress-inducible genes such as *RD29* and *COR47* (Ren et al., 2010; Rushton et al., 2012).

Although there are many reports of WRKY TFs influencing drought responses (Rushton et al., 2012; Rabara et al., 2014; Singh and Laxmi, 2015), examples of common WRKY proteins also acting on Al tolerance and P deficiency tolerance are rather scarce, which might merely reflect less research focus on the involvement of WRKY TFs in abiotic stresses other than drought. Transgenic Arabidopsis with constitutive expression of the stress-response transcriptional coactivator, *multiprotein bridging factor 1c* (*MBF1c*), were more tolerant to bacterial infection, heat, and osmotic stress (Suzuki et al., 2005). *AtWRKY46* expression was found to be elevated in the transgenic lines, albeit only slightly, suggesting that AtWRKY46 could possibly be involved with stress tolerance in the *MBF1c* lines. Somewhat more compelling is the observation that *AtWRKY46* was induced by drought,

salt and oxidative stress (Ding et al., 2014). AtWRKY46 was expressed in guard cells and may regulate stomatal opening and drought stress. Additionally, AtWRKY46 was found to regulate lateral root development in osmotic and salt stress conditions, possibly via ABA-signaling (in part via ABI4 regulation) and auxin homeostasis (Ding et al., 2015).

This suggests that AtWRKY46 could act on stress tolerance beyond its repressor role on the expression of the Al tolerance

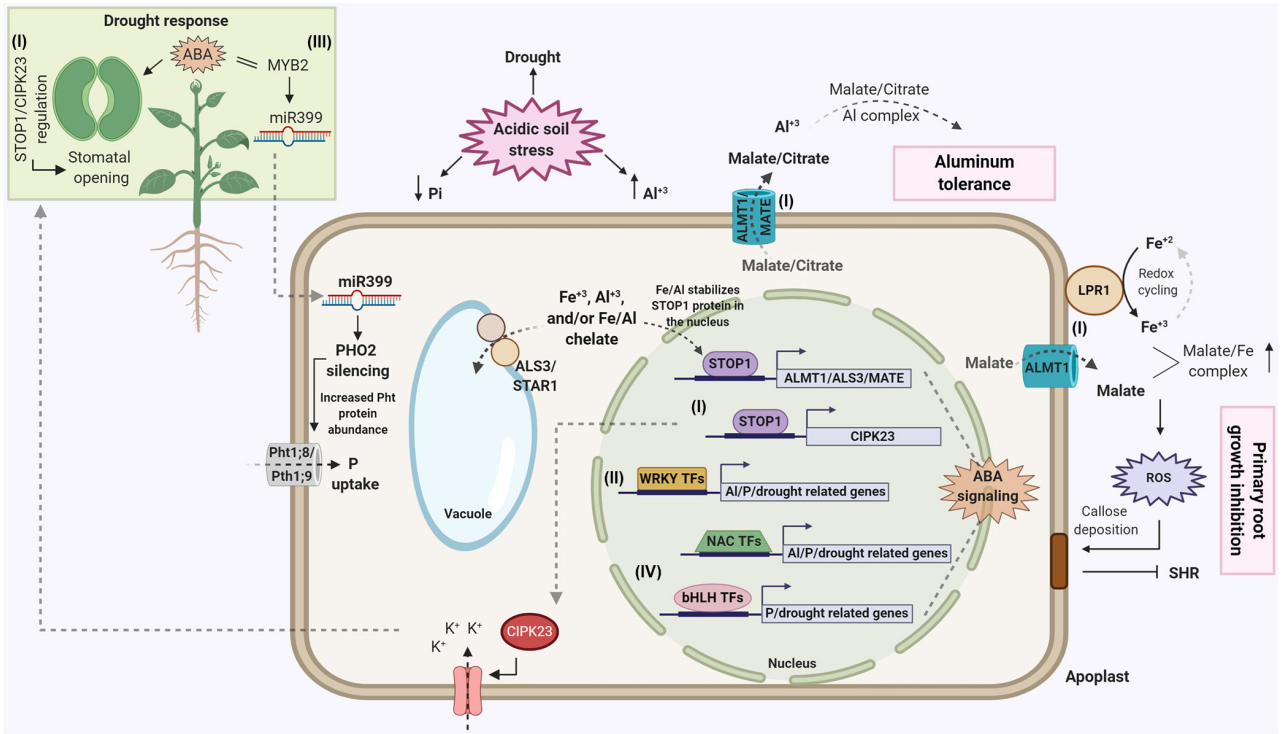

FIGURE 1 | Model for cross-talk between Al toxicity, low-P availability and drought stress. Four transcriptional regulatory networks are highlighted that we identified in this review that may be involved with plant responses to these three abiotic stresses. **(I)** The *SENSITIVE TO PROTON RHIZOTOXICITY 1* (*STOP1*) transcription factor is involved in Al tolerance, P deficiency and drought stress. In addition to *AtMATE*, *STOP1* transcriptionally activates the *ALUMINUM ACTIVATED MALATE TRANSPORTER1* (*ALMT1)* which encodes the root PM anion channel that mediates Al activated malate release from roots, detoxifying Al in the rhizosphere. P deficiency induces the release of the multicopper ferroxidase (LPR1) that reduces/oxidizes Fe. P deficiency also induces expression of *ALMT1*, and the malate released via the ALMT1 protein chelates and facilitates accumulation of Fe in the cell wall where its oxidoreduction is catalyzed by LPR1, generating peroxides, which triggers lignification and cell wall stiffening, and rapid inhibition of root growth. At the same time, ROS generated from oxidoreduction of Fe triggers callose formation, which blocks plasmodesmata between stem cell initials and cells of the RAM outside the stem cell niche. This blockage of the plasmodesmata prevents cell-to-cell transport of the transcription factor, *SHORT-ROOT*, which is needed to drive stem cell division. This exhausts the RAM and terminates primary root growth. The Fe accumulated in the cell wall also drives increased Fe influx into the cytoplasm of RAM and the increased Fe helps stabilize and enhance STOP1 accumulation in the nucleus. Under P sufficient conditions, the tonoplast ABC transporter, ALS3/STAR1, is hypothesized to transport the Fe or Al (depending on soil conditions) or possibly Fe/Al-chelates into the vacuole and the reduction of Fe/Al levels in the cytoplasm and nucleus represses STOP1 protein accumulation in the nucleus, inhibiting *ALMT1,* transcriptional activation. With regards to STOP1's involvement in drought response, *STOP1* also transcriptionally activates *CBL-INTERACTING PROTEIN KINASE 23* (*CIPK23*) expression, and the CIPK23 protein is an activator of high affinity K^+ transporters in the root and possibly the shoot, which could result in enhanced stomatal opening and a reduction in drought tolerance due to increased transpirational water loss. **(II)** A second family of candidate TFs are the large WRKY family. There are several WRKY transcription factor family members involved in responses to drought and Al toxicity. For example, *AtWRKY46* represses *ALMT1* expression in the absence of Al and also is expressed in guard cells in response to drought stress; although its role in drought response remains to be elucidated **(III)** The AtMYB2 transcription factor co-regulates P efficiency and is involved in drought response via regulation of *miR399*. AtMYB2 induces *miR399* in response to ABA and salt stress, and overexpression of *miR399* results in salt and ABA tolerance but interestingly, is associated with drought sensitivity. *miR399* plays a well-documented role in long distance P deficiency signaling in the phloem as it is synthesized in response to P deficiency in mature source leaves and is translocated in the phloem to the root, where it silences *PHOSPHATE 2* (*PHO2)*, which encodes a ubiquitin-conjugating E2 enzyme that negatively regulates P transporters under P sufficiency. **(IV)** NAC and Basic helix-loop-helix (bHLH) transcriptional factors have been implicated in drought regulation of stress-related genes via a wide-range of possible tolerance mechanisms, which involves ABA-dependent and independent pathways. The bHLH family member, PTF1, plays a role in low P tolerance, enhancing lateral root development. ZmPTF1 bind to the promoter of NAC30 and other TFs, acting as a positive regulator of those genes. Thus, a possible connection between NAC-mediated tolerance to both drought and low-P conditions may be mediated at some extent via bHLH-dependent regulation of NAC TFs. NAC TFs may also connect with Al tolerance based on up-regulation of VuNAR1 root apex and Al inducibility of other NACs. VuNAR1 also binds to the promoters of wall-associated receptor kinase genes, conferring Al tolerance through regulation of cell wall pectin metabolism. Although there is no evidence for direct interaction of STOP1, *AtMATE1* and *AtALS3* promoters, it is clear that STOP1 is crucial for induction of these genes. Not shown here is a possible link between Al tolerance and drought tolerance via ERF transcription factors, whose supporting evidence is more limited and preliminary. The figure was created with BioRender.com.

gene, *AtALMT1* (Ding et al., 2013), possibly influencing P acquisition and tolerance to drought stress. While enhanced lateral roots by AtWRKY46 might be expected to lead to enhanced P acquisition on low-P conditions, the nature of the impact of AtWRKY46 on drought tolerance, whether negative or positive, is yet to be unraveled in detail. Another possible case of cross-talk between drought stress tolerance and tolerance to low-P conditions involves WRKY45. Arabidopsis lines overexpressing *OsWRKY45* showed enhanced disease resistance and drought tolerance, possibly via ABA-mediated stomatal closure and induction of stress-related genes (Qiu and Yu, 2009). In Arabidopsis, *AtWRKY45* is induced by low-P, regulates *PSI* genes and is involved with changes in RSA that are apparently P-independent (see section "TFs Involved in Plant Low-P response/P Efficiency"; Devaiah et al., 2007). Also, AtWRKY45 participates in P responses by binding to the *PHT1;1* promoter and regulating its transcription, thereby enhancing P uptake (see section "TFs Involved in Plant Low-P response/P Efficiency"; Wang et al., 2014). These reports suggest that WRKY45 could have a pleiotropic effect, enhancing both drought tolerance and P acquisition in low-P conditions.

Ethylene Response Factors (ERFs)

Ethylene response factors are TFs in the AP2/ERF superfamily, which are involved in tolerance to multiple abiotic stresses (Debbarma et al., 2019). Well-known members of this family include the Dehydration Responsive Element Binding (DREB) factors, which are frequently involved in the ABA-independent regulation of drought responsive genes (Singh and Laxmi, 2015), possibly involving ethylene signaling (Leng and Zhao, 2019). However, in some cases, DRE elements on some promoters are involved in both ABA-dependent and ABA-independent abiotic stresses (Agarwal et al., 2017). Overexpression of DREB TFs has resulted in increased drought tolerance, but with occasional deleterious side-effects (Agarwal et al., 2017). Chen Y. et al. (2018) identified in *Jatropha curcas* a P starvation responsive AP2/ERF transcription factor, *JcERF035*, which was downregulated under -P conditions. Overexpression of this P-starvation responsive AP2/ERF in Arabidopsis resulted in enhanced root hairs but reduced number and length of lateral roots, which was apparently independent from P supply. Recently, overexpression of *ERF74* in Arabidopsis was shown to enhance tolerance to a variety of stress factors, including drought, high light, heat and Al toxicity, whereas the *erf74* mutant displayed higher sensitivity to these stresses. Like many other abiotic stresses, Al toxicity, generates ROS (see Section 2.2a), which may both be a toxic product and also can be a signal. Yao et al. (2017) showed that the *erf74* mutant lacked the reactive oxygen species burst often seen in the early stages of various stresses, which was due to lower expression level *of RESPIRATORY BURST OXIDASE HOMOLOG D (RbohD*) in the *erf74* mutant. Possibly this is part of a ROS signaling pathway conditioning tolerance to stresses such as Al toxicity, drought and temperature extremes, which may be related to ROS signals (Yao et al., 2017). While these studies with JcERF35 and AtERF74 suggest that some ERF transfactors might be involved in plant responses to P, Al and drought stress, this area awaits considerable further investigation. Also, given the involvement of ABA as a positive regulator of Al tolerance, including induction of *AtALMT1* and *AtMATE* expression (see Section 2.2b), other, yet unidentified factors may connect drought and Al tolerance via ABA-dependent pathways.

CONCLUSION

In this review, we examined the literature for common elements shared between the three major stresses that often co-occur on acidic soils: Al toxicity, low P availability and drought, with a focus on genes/proteins involved in signaling and/or regulatory pathways and networks controlling plant responses and adaptations to these three abiotic stresses. In general, research on crop adaptation to acidic soils has focused on one of the two primary stresses resulting from the unique chemistry of acidic soils, Al toxicity or P deficiency. But as this field has advanced and matured, we showed here that quite recently, a number of genes have been identified that are involved both in Al resistance and adaptation to P deficiency. The very broad field of research on crop adaptations to drought, on the other hand, has not focused much on the possible role of drought resistance mechanisms in adaptations to acidic soils. This is primarily because drought, by its very nature, occurs on all types of soils in many different eco-agricultural systems. Nonetheless, in this review we did identify several genes and the proteins they encode that could play a role in adaptation to all three of these abiotic stresses. At the beginning of this review, we speculated that genes involved in signaling/regulatory networks might be the best source for candidates involved in crop adaptation to all three stresses. This turned out to be the case as we identified transcription factors from several TF families that could play this pleiotropic role. These TF's are summarized here and a model of the function of the best candidate TF's in the three abiotic stresses is presented in **Figure 1**.

(1) STOP1, a C2H2 Zinc Finger Transcription Factor: This is probably the most interesting candidate as it has been shown to clearly be a key Al tolerance gene, regulating the Al-induced transcriptional activation of a number of Al tolerance genes in Arabidopsis, including the major Al tolerance gene, *ALMT1* (Iuchi et al., 2007). STOP1 also plays a key role in Arabidopsis root response to P deficiency, as under low P STOP1 again activates *ALMT1* expression, enhancing the production of the *ALMT1* anion channel that facilitates root malate release, which is central to the root apex Fe accumulation needed to exhaust the primary root RAM and root growth (Müller et al., 2015; Balzergue et al., 2017; Mora-Macías et al., 2017). The loss of primary root apical dominance then appears to lead to enhanced lateral root growth which could confer enhanced P acquisition in low P soil. Additionally, there is a reasonable amount of circumstantial evidence implicating STOP1 in several drought responses. This includes the recent finding that

stop1 knockout lines showed enhanced drought tolerance in Arabidopsis (Sadhukhan et al., 2019), suggesting that STOP1 is a negative regulator of drought tolerance. These authors also found that the STOP1 regulated the expression of the gene encoding the CBL-interacting protein kinase 23 (CIPK23), and complementation of the *stop1* mutant with CIPK23 reversed the drought phenotype (back to drought sensitivity). Furthermore, in a heterologous system, *Xenopus* oocytes, CIPK23 can activate via phosphorylation the guard cell PM anion channel, SLAC1 (SLOW ANION CHANNEL-ASSOCIATED 1) (Maierhofer et al., 2014), the direct link between this process and drought physiology involving stomatal closure is still unclear. Nevertheless, these findings all point toward the highly pleiotropic nature of the transcription factor, *STOP1*.

(2) WRKY Transcription factors: We found different members of the WRKY TF family that were involved in all three stresses, but did not identify a single WRKY member clearly influencing all stresses. One possibility is AtWRKY46, which is involved in Al tolerance where it represses *ALMT1* expression in the absence of Al (Ding et al., 2013). Additionally, it was shown to be involved in drought response, as it is expressed in guard cells and this expression is induced by drought, salt and oxidative stress (Ding et al., 2014). Additionally, AtWRKY46 was found to enhance lateral root development in response to osmotic and salt stress conditions, possibly via ABA-signaling and auxin homeostasis (Ding et al., 2015). It would be interesting to find out if this increased lateral root development and growth could also play a role in improved P efficiency.

(3) AtMYB2 Regulation of *miR399*: There is good evidence for this MYB transcription factor co-regulating P efficiency and drought tolerance via regulation of *miR399* (Baek et al., 2016, 2017). As detailed above, *miR399* is an important player in P homeostasis via a long distance systemic signaling system in the phloem translocating *miR399* from mature source leaves to the root, where it silences *PHO2*, the ubiquitin-conjugating E2 enzyme that negatively regulates P transporters under P sufficiency (Fujii et al., 2005; Baek et al., 2013). It was also shown that AtMYB2 regulation of *miR399* is also involved in plant responses to abscisic acid (ABA), and to salt and drought (Baek et al., 2016). Salt and ABA treatment induced the expression of *miR399*, and overexpression of *miR399* resulted in enhanced salt tolerance and interestingly, hypersensitivity to drought. Hence the pleiotropic nature of AtMYB regulation of *miR399* spanning low P and drought stress is apparent, although the functional basis of its impact on drought responses remains to be elucidated.

In conclusion, there are tantalizing links in the literature between the regulation of plant adaptation and responses to Al toxicity, P deficiency and drought stress. To provide the readers with a summary of the work reviewed in this paper, we have included **Supplementary Table 1** (Gene families possibly involved in pleiotropic mechanisms) resulting in multiple stress tolerances (tolerance to Al toxicity, P deficiency and drought) which contains lists of members of five gene families (*WRKY*, *STOP1*, *MYB*, *bHLH*, and *NAC*) involved in Al toxicity, drought stress and P deficiency. However more research is needed to say with certainty that the same factors can regulate tolerance to all three stresses. If that is the case, it will be quite intriguing to determine if these genes would be useful in a plant breeding program for multiple environmental stresses. Within a scenario where the same genes in some way influence tolerance to multiple stresses, instances of conflicting effects may be foreseen, as previously discussed. If the same gene acts simultaneously as positive and negative regulators of tolerance to different stresses, this may cancel its final effect in phenotypic expression or even be detrimental to crop performance on acidic soils. Within the context of molecular breeding strategies targeting quantitative traits such as genomic selection, these and other negative effects may be filtered out along the selection process via genomic estimation of breeding values. However, transgenic approaches may be more sensitive to this problem. In that regard, gene editing has emerged as a powerful approach to fine tune gene expression, which could help circumvent negative effects coming from pleiotropy or epistasis. This approach has proven useful in bypassing negative epistasis effects on yield in tomato (Soyk et al., 2017) and to tackle quantitative trait variation (Rodríguez-Leal et al., 2017). Particularly to deal with possible hurdles when exploring pleiotropy in crop adaption to acidic soils, it is more than certain that in-depth knowledge of the physiological and genetic underpinnings of multiple stress tolerance will be required.

AUTHOR CONTRIBUTIONS

JM and LK also handled the revising and editing of the full version of the manuscript. All authors contributed by conducting literature research and writing of different parts of the text.

FUNDING

We acknowledge support from the Canada Excellence Research Chairs program and the Global Institute for Food Security to LK, the Fundação de Amparo a Pesquisa do Estado de Minas Gerais (FAPEMIG), the National Council for Scientific and Technological Development (CNPq) and the Embrapa Macroprogram to JM, and from Coordenação de Aperfeiçoamento de Pessoal de Nível Superior - Brasil (CAPES) – Finance Code 001 (to VB).

SUPPLEMENTARY MATERIAL

The Supplementary Material for this article can be found online at: https://www.frontiersin.org/articles/10.3389/fpls.2020.565339/full#supplementary-material

REFERENCES

Abe, H., Urao, T., Ito, T., Seki, M., and Shinozaki, K. (2003). Arabidopsis AtMYC2 (bHLH) and AtMYB2 (MYB) function as transcriptional activators in abscisic acid signaling. *Society* 15, 63–78. doi: 10.1105/tpc.006130.salt

Agarwal, P. K., Gupta, K., Lopato, S., and Agarwal, P. (2017). Dehydration responsive element binding transcription factors and their applications for the engineering of stress tolerance. *J. Exp. Bot.* 68, 2135–2148. doi: 10.1093/jxb/erx118

Aravind, J., Rinku, S., Pooja, B., Shikha, M., Kaliyugam, S., Mallikarjuna, M. G., et al. (2017). Identification, characterization, and functional validation of drought-responsive microRNAs in subtropical maize inbreds. *Front. Plant Sci.* 8:941. doi: 10.3389/fpls.2017.00941

Arenhart, R. A., Bai, Y., Valter De Oliveira, L. F., Bucker Neto, L., Schunemann, M., Maraschin, F. D. S., et al. (2014). New insights into aluminum tolerance in rice: the ASR5 protein binds the STAR1 promoter and other aluminum-responsive genes. *Mol. Plant* 7, 709–721. doi: 10.1093/mp/sst160

Arenhart, R. A., De Lima, J. C., Pedron, M., Carvalho, F. E. L., Da Silveira, J. A. G., Rosa, S. B., et al. (2013). Involvement of ASR genes in aluminium tolerance mechanisms in rice. *Plant Cell Environ.* 36, 52–67. doi: 10.1111/j.1365-3040.2012.02553.x

Arenhart, R. A., Schunemann, M., Bucker Neto, L., Margis, R., Wang, Z. Y., and Margis-Pinheiro, M. (2016). Rice ASR1 and ASR5 are complementary transcription factors regulating aluminium responsive genes. *Plant Cell Environ.* 39, 645–651. doi: 10.1111/pce.12655

Aukerman, M. J., and Sakai, H. (2003). Regulation of flowering time and floral organ identity by a microRNA and its APETALA2-like target genes. *Plant Cell* 15, 2730–2741. doi: 10.1105/tpc.016238

Aung, K., Lin, S.-I., Wu, C.-C., Huang, Y.-T., Su, C., and Chiou, T.-J. (2006). pho2, a phosphate overaccumulator, is caused by a nonsense mutation in a microRNA399 target gene. *Plant Physiol.* 141, 1000–1011. doi: 10.1104/pp.106.078063

Azevedo, G. C., Cheavegatti-Gianotto, A., Negri, B. F., Hufnagel, B., da Silva, L. C. E., Magalhaes, J. V., et al. (2015). Multiple interval QTL mapping and searching for PSTOL1 homologs associated with root morphology, biomass accumulation and phosphorus content in maize seedlings under low-P. *BMC Plant Biol.* 15:172. doi: 10.1186/s12870-015-0561-y

Baek, D., Chun, H. J., Kang, S., Shin, G., Park, S. J., Hong, H., et al. (2016). A role for arabidopsis miR399f in salt, drought, and ABA signaling. *Mol. Cells* 39, 111–118. doi: 10.14348/molcells.2016.2188

Baek, D., Chun, H. J., Yun, D. J., and Kim, M. C. (2017). Cross-talk between phosphate starvation and other environmental stress signaling pathways in plants. *Mol. Cells* 40, 697–705. doi: 10.14348/molcells.2017.0192

Baek, D., Kim, M. C., Chun, H. J., Kang, S., Park, H. C., Shin, G., et al. (2013). Regulation of miR399f transcription by AtMYB2 affects phosphate starvation responses in *Arabidopsis*. *Plant Physiol.* 161, 362–373. doi: 10.1104/pp.112.205922

Baillo, E. H., Kimotho, R. N., Zhang, Z., and Xu, P. (2019). Transcription factors associated with abiotic and biotic stress tolerance and their potential for crops improvement. *Genes (Basel)* 10, 1–23. doi: 10.3390/genes10100771

Bakhshi, B., Fard, E. M., Nikpay, N., Ebrahimi, M. A., Bihamta, M. R., Mardi, M., et al. (2016). MicroRNA signatures of drought signaling in rice root. *PLoS One* 11:e0156814. doi: 10.1371/journal.pone.0156814

Bakshi, M., and Oelmüller, R. (2014). Wrky transcription factors jack of many trades in plants. *Plant Signal. Behav.* 9:e27700. doi: 10.4161/psb.27700

Baldoni, E., Genga, A., and Cominelli, E. (2015). Plant MYB transcription factors: Their role in drought response mechanisms. *Int. J. Mol. Sci.* 16, 15811–15851. doi: 10.3390/ijms160715811

Balzergue, C., Dartevelle, T., Godon, C., Laugier, E., Meisrimler, C., Teulon, J. M., et al. (2017). Low phosphate activates STOP1-ALMT1 to rapidly inhibit root cell elongation. *Nat. Commun.* 8, 1–16. doi: 10.1038/ncomms15300

Bano, A., Dorffling, K., Bettin, D., and Hahn, H. (1993). Abscisic acid and cytokinins as possible root-to-shoot signals in xylem sap of rice plants in drying soil. *Funct. Plant Biol.* 20, 109–115. doi: 10.1071/pp9930109

Banti, V., Mafessoni, F., Loreti, E., Alpi, A., and Perata, P. (2010). The heat-inducible transcription factor HsfA2 enhances anoxia tolerance in *Arabidopsis*. *Plant Physiol.* 152, 1471–1483. doi: 10.1104/pp.109.149815

Barberon, M., Vermeer, J. E. M., De Bellis, D., Wang, P., Naseer, S., Andersen, T. G., et al. (2016). Adaptation of root function by nutrient-induced plasticity of endodermal differentiation. *Cell* 164, 447–459. doi: 10.1016/j.cell.2015.12.021

Bari, R., Pant, B. D., Stitt, M., and Scheible, W. R. (2006). PHO2, microRNA399, and PHR1 define a phosphate-signaling pathway in plants. *Plant Physiol.* 141, 988–999. doi: 10.1104/pp.106.079707

Bariola, P. A., Howard, C. J., Taylor, C. B., Verburg, M. T., Jaglan, V. D., and Green, P. J. (1994). The *Arabidopsis* ribonuclease gene RNS1 is tightly controlled in response to phosphate limitation. *Plant J.* 6, 673–685. doi: 10.1046/j.1365-313X.1994.6050673.x

Basu, U., Good, A. G., and Taylor, G. J. (2001). Transgenic *Brassica napus* plants overexpressing aluminium-induced mitochondrial manganese superoxide dismutase cDNA are resistant to aluminium. *Plant. Cell Environ.* 24, 1269–1278.

Batool, A., Cheng, Z.-G., Akram, N. A., Lv, G.-C., Xiong, J.-L., Zhu, Y., et al. (2019). Partial and full root-zone drought stresses account for differentiate root-sourced signal and yield formation in primitive wheat. *Plant Methods* 15:75.

Belda-Palazon, B., Gonzalez-Garcia, M.-P., Lozano-Juste, J., Coego, A., Antoni, R., Julian, J., et al. (2018). PYL8 mediates ABA perception in the root through non-cell-autonomous and ligand-stabilization–based mechanisms. *Proc. Natl. Acad. Sci. U.S.A.* 115, E11857—E11863.

Bernardino, K. C., Pastina, M. M., Menezes, C. B., De Sousa, S. M., Maciel, L. S., Geraldo Carvalho, G. C., et al. (2019). The genetic architecture of phosphorus efficiency in sorghum involves pleiotropic QTL for root morphology and grain yield under low phosphorus availability in the soil. *BMC Plant Biol.* 19:87. doi: 10.1186/s12870-019-1689-y

Bhattacharjee, S. (2012). The language of reactive oxygen species signaling in plants. *J. Bot.* 2012, 985298.

Blackman, P. G., and Davies, W. J. (1985). Root to shoot communication in maize plants of the effects of soil drying. *J. Exp. Bot.* 36, 39–48. doi: 10.1093/jxb/36.1.39

Blokhina, O., Virolainen, E., and Fagerstedt, K. V. (2003). Antioxidants, oxidative damage and oxygen deprivation stress: a review. *Ann. Bot.* 91, 179–194. doi: 10.1093/aob/mcf118

Blum, A. (2017). Osmotic adjustment is a prime drought stress adaptive engine in support of plant production. *Plant Cell Environ.* 40, 4–10. doi: 10.1111/pce.12800

Castilhos, G., Lazzarotto, F., Spagnolo-Fonini, L., Bodanese-Zanettini, M. H., and Margis-Pinheiro, M. (2015). Possible roles of basic helix-loop-helix transcription factors in adaptation to drought. *Plant Sci.* 235:130. doi: 10.1016/j.plantsci.2015.03.012

Chen, D., Chai, S., McIntyre, C. L., and Xue, G.-P. (2018). Overexpression of a predominantly root-expressed NAC transcription factor in wheat roots enhances root length, biomass and drought tolerance. *Plant Cell Rep.* 37, 225–237. doi: 10.1007/s00299-017-2224-y

Chen, J., Wang, Y., Wang, F., Yang, J., Gao, M., Li, C., et al. (2015). The rice CK2 kinase regulates trafficking of phosphate transporters in response to phosphate levels. *Plant Cell* 27, 711–723. doi: 10.1105/tpc.114.135335

Chen, Y., Wu, P., Zhao, Q., Tang, Y., Chen, Y., Li, M., et al. (2018). Overexpression of a phosphate starvation response ap2/erf gene from physic nut in arabidopsis alters root morphological traits and phosphate starvation-induced anthocyanin accumulation. *Front. Plant Sci.* 9:1186. doi: 10.3389/fpls.2018.01186

Chen, Y. F., Li, L. Q., Xu, Q., Kong, Y. H., Wang, H., and Wu, W. H. (2009). The WRKY6 transcription factor modulates PHOSPHATE1 expression in response to low pi stress in arabidopsis. *Plant Cell* 21, 3554–3566. doi: 10.1105/tpc.108.064980

Chen, Z. C., Yamaji, N., Motoyama, R., Nagamura, Y., and Ma, J. F. (2012). Up-regulation of a magnesium transporter gene osmgt1 is required for conferring aluminum tolerance in rice. *Plant Physiol.* 159, 1624–1633. doi: 10.1104/pp.112.199778

Chen, Z. C., Yokosho, K., Kashino, M., Zhao, F. J., Yamaji, N., and Ma, J. F. (2013). Adaptation to acidic soil is achieved by increased numbers of cis-acting elements regulating ALMT1 expression in *Holcus lanatus*. *Plant J.* 76, 10–23. doi: 10.1111/tpj.12266

Chien, P. S., Chiang, C. P., Leong, S. J., and Chiou, T. J. (2018). Sensing and signaling of phosphate starvation: from local to long distance. *Plant Cell Physiol.* 59, 1714–1722. doi: 10.1093/pcp/pcy148

Chiou, T.-J., Aung, K., Lin, S.-I., Wu, C.-C., Chiang, S.-F., and Su, C. (2006). Regulation of phosphate homeostasis by microRNA in *Arabidopsis*. *Plant Cell* 18, 412–421. doi: 10.1105/tpc.105.038943

Christmann, A., Weiler, E. W., Steudle, E., and Grill, E. (2007). A hydraulic signal in root-to-shoot signalling of water shortage. *Plant J.* 52, 167–174. doi: 10.1111/j.1365-313x.2007.03234.x

Cutler, S. R., Rodriguez, P. L., Finkelstein, R. R., and Abrams, S. R. (2010). Abscisic acid: emergence of a core signaling network. *Annu. Rev. Plant Biol.* 61, 651–679. doi: 10.1146/annurev-arplant-042809-112122

Dai, X., Wang, Y., Yang, A., and Zhang, W. H. (2012). OsMYB2P-1, an R2R3 MYB transcription factor, is involved in the regulation of phosphate-starvation responses and root architecture in rice. *Plant Physiol.* 159, 169–183. doi: 10.1104/pp.112.194217

Dai, X., Wang, Y., and Zhang, W. H. (2016). OsWRKY74, a WRKY transcription factor, modulates tolerance to phosphate starvation in rice. *J. Exp. Bot.* 67, 947–960. doi: 10.1093/jxb/erv515

Daspute, A. A., Kobayashi, Y., Panda, S. K., Fakrudin, B., Kobayashi, Y., Tokizawa, M., et al. (2018). Characterization of CcSTOP1; a C2H2-type transcription factor regulates Al tolerance gene in pigeonpea. *Planta* 247, 201–214. doi: 10.1007/s00425-017-2777-6

De Sousa, S. M., Clark, R. T., Mendes, F. F., Carlos De Oliveira, A., Vilaça De Vasconcelos, M. J., Parentoni, S. N., et al. (2012). A role for root morphology and related candidate genes in P acquisition efficiency in maize. *Funct. Plant Biol.* 39, 925–935. doi: 10.1071/FP12022

Debbarma, J., Sarki, Y. N., Saikia, B., Boruah, H. P. D., Singha, D. L., and Chikkaputtaiah, C. (2019). Ethylene Response Factor (ERF) family proteins in abiotic stresses and CRISPR–Cas9 genome editing of ERFs for multiple abiotic stress tolerance in crop plants: a review. *Mol. Biotechnol.* 61, 153–172. doi: 10.1007/s12033-018-0144-x

Devaiah, B. N., Karthikeyan, A. S., and Raghothama, K. G. (2007). WRKY75 transcription factor is a modulator of phosphate acquisition and root development in *Arabidopsis*. *Plant Physiol.* 143, 1789–1801. doi: 10.1104/pp.106.093971

Dietrich, D., Pang, L., Kobayashi, A., Fozard, J. A., Boudolf, V., Bhosale, R., et al. (2017). Root hydrotropism is controlled via a cortex-specific growth mechanism. *Nat. Plants* 3:17057.

Ding, Z. J., Yan, J. Y., Li, C. X., Li, G. X., Wu, Y. R., and Zheng, S. J. (2015). Transcription factor WRKY46 modulates the development of *Arabidopsis* lateral roots in osmotic/salt stress conditions via regulation of ABA signaling and auxin homeostasis. *Plant J.* 84, 56–69. doi: 10.1111/tpj.12958

Ding, Z. J., Yan, J. Y., Xu, X. Y., Li, G. X., and Zheng, S. J. (2013). WRKY46 functions as a transcriptional repressor of ALMT1, regulating aluminum-induced malate secretion in *Arabidopsis*. *Plant J.* 76, 825–835. doi: 10.1111/tpj.12337

Ding, Z. J., Yan, J. Y., Xu, X. Y., Yu, D. Q., Li, G. X., Zhang, S. Q., et al. (2014). Transcription factor WRKY46 regulates osmotic stress responses and stomatal movement independently in *Arabidopsis*. *Plant J.* 79, 13–27. doi: 10.1111/tpj.12538

Dodd, I. C., Theobald, J. C., Richer, S. K., and Davies, W. J. (2009). Partial phenotypic reversion of ABA-deficient flacca tomato (*Solanum lycopersicum*) scions by a wild-type rootstock: normalizing shoot ethylene relations promotes leaf area but does not diminish whole plant transpiration rate. *J. Exp. Bot.* 60, 4029–4039. doi: 10.1093/jxb/erp236

Dong, J., Piñeros, M. A., Li, X., Yang, H., Liu, Y., Murphy, A. S., et al. (2017). An *Arabidopsis* ABC transporter mediates phosphate deficiency-induced remodeling of root architecture by modulating iron homeostasis in roots. *Mol. Plant* 10, 244–259. doi: 10.1016/j.molp.2016.11.001

Dossa, K., Mmadi, M. A., Zhou, R., Liu, A., Yang, Y., Diouf, D., et al. (2020). Ectopic expression of the sesame MYB transcription factor SiMYB305 promotes root growth and modulates ABA-mediated tolerance to drought and salt stresses in *Arabidopsis*. *AoB Plants* 12, 1–14. doi: 10.1093/aobpla/plz081

Driedonks, N., Xu, J., Peters, J. L., Park, S., and Rieu, I. (2015). Multi-level interactions between heat shock factors, heat shock proteins, and the redox system regulate acclimation to heat. *Front. Plant Sci.* 6:999. doi: 10.3389/fpls.2015.00999

Du, Q., Wang, K., Zou, C., Xu, C., and Li, W.-X. (2018). The PILNCR1-miR399 regulatory module is important for low phosphate tolerance in maize. *Plant Physiol.* 177, 1743–1753. doi: 10.1104/pp.18.00034

Enomoto, T., Tokizawa, M., Ito, H., Iuchi, S., Kobayashi, M., Yamamoto, Y. Y., et al. (2019). STOP1 regulates the expression of HsfA2 and GDH s that are critical for low-oxygen tolerance in *Arabidopsis*. *J. Exp. Bot.* 70, 3297–3311. doi: 10.1093/jxb/erz124

Escobar-Sepúlveda, H. F., Trejo-Téllez, L. I, García-Morales, S., and Gómez-Merino, F. C. (2017). Expression patterns and promoter analyses of aluminum-responsive NAC genes suggest a possible growth regulation of rice mediated by aluminum, hormones and NAC transcription factors. *PLoS One* 12:e0186084. doi: 10.1371/journal.pone.0186084

Ezaki, B., Gardner, R. C., Ezaki, Y., and Matsumoto, H. (2000). Expression of aluminum-induced genes in transgenic *Arabidopsis* plants can ameliorate aluminum stress and/or oxidative stress. *Plant Physiol.* 122, 657–666. doi: 10.1104/pp.122.3.657

Fambrini, M., Vernieri, P., Toncelli, M. L., Rossi, V. D., and Pugliesi, C. (1995). Characterization of a wilty sunflower (*Helianthus annuus* L.) mutant: III. Phenotypic interaction in reciprocal grafts from wilty mutant and wild-type plants. *J. Exp. Bot.* 46, 525–530. doi: 10.1093/jxb/46.5.525

Fan, W., Lou, H. Q., Gong, Y. L., Liu, M. Y., Cao, M. J., Liu, Y., et al. (2015). Characterization of an inducible C2H2-type zinc finger transcription factor Vu STOP 1 in rice bean (*Vigna umbellata*) reveals differential regulation between low pH and aluminum tolerance mechanisms. *New Phytol.* 208, 456–468. doi: 10.1111/nph.13456

Feng, W., Lindner, H., Robbins, N. E., and Dinneny, J. R. (2016). Growing out of stress: the role of cell-and organ-scale growth control in plant water-stress responses. *Plant Cell* 28, 1769–1782. doi: 10.1105/tpc.16.00182

Fernando, V. C. D., and Schroeder, D. F. (2016). "Role of ABA in *Arabidopsis* salt, drought, and desiccation tolerance," in *Abiotic and Biotic Stress in Plants-Recent Advances and Future Perspectives*, eds A. Shanker and C. Shanker (London: IntechOpen).

Fuganti-Pagliarini, R., Ferreira, L. C., Rodrigues, F. A., Molinari, H. B. C., Marin, S. R. R., Molinari, M. D. C., et al. (2017). Characterization of soybean genetically modified for drought tolerance in field conditions. *Front. Plant Sci.* 8:448. doi: 10.3389/fpls.2017.00448

Fujii, H., Chinnusamy, V., Rodrigues, A., Rubio, S., Antoni, R., Park, S.-Y., et al. (2009). In vitro reconstitution of an abscisic acid signalling pathway. *Nature* 462, 660–664. doi: 10.1038/nature08599

Fujii, H., Chiou, T. J., Lin, S. I, Aung, K., and Zhu, J. K. (2005). A miRNA involved in phosphate-starvation response in *Arabidopsis*. *Curr. Biol.* 15, 2038–2043. doi: 10.1016/j.cub.2005.10.016

Gamuyao, R., Chin, J. H., Pariasca-Tanaka, J., Pesaresi, P., Catausan, S., Dalid, C., et al. (2012). The protein kinase Pstol1 from traditional rice confers tolerance of phosphorus deficiency. *Nature* 488, 535–539. doi: 10.1038/nature11346

Gareau, J. R., and Lima, C. D. (2010). The SUMO pathway: emerging mechanisms that shape specificity, conjugation and recognition. *Nat. Rev. Mol. Cell Biol.* 11, 861–871. doi: 10.1038/nrm3011

Godfray, H. C. J., Beddington, J. R., Crute, I. R., Haddad, L., Lawrence, D., Muir, J. F., et al. (2010). Food security: the challenge of feeding 9 billion people. *Science* 327, 812–818. doi: 10.1126/science.1185383

Godon, C., Mercier, C., Wang, X., David, P., Richaud, P., Nussaume, L., et al. (2019). Under phosphate starvation conditions, Fe and Al trigger accumulation of the transcription factor STOP1 in the nucleus of *Arabidopsis* root cells. *Plant J.* 99, 937–949. doi: 10.1111/tpj.14374

Gollan, T., Schurr, U., and Schulze, E.-D. (1992). Stomatal response to drying soil in relation to changes in the xylem sap composition of *Helianthus annuus*. I. The concentration of cations, anions, amino acids in, and pH of, the xylem sap. *Plant. Cell Environ.* 15, 551–559. doi: 10.1111/j.1365-3040.1992.tb01488.x

González, E., Solano, R., Rubio, V., Leyva, A., and Paz-Ares, J. (2005). PHOSPHATE TRANSPORTER TRAFFIC FACILITATOR1 is a plant-specific SEC12-related protein that enables the endoplasmic reticulum exit of a high-affinity phosphate transporter in *Arabidopsis*. *Plant Cell* 17, 3500–3512. doi: 10.1105/tpc.105.036640

Gonzalez-Guzman, M., Pizzio, G. A., Antoni, R., Vera-Sirera, F., Merilo, E., Bassel, G. W., et al. (2012). *Arabidopsis* PYR/PYL/RCAR receptors play a major role in quantitative regulation of stomatal aperture and transcriptional response to abscisic acid. *Plant Cell* 24, 2483–2496. doi: 10.1105/tpc.112.098574

Grieneisen, V. A., Xu, J., Marée, A. F. M., Hogeweg, P., and Scheres, B. (2007). Auxin transport is sufficient to generate a maximum and gradient guiding root growth. *Nature* 449, 1008–1013. doi: 10.1038/nature06215

Hamburger, D., Rezzonico, E., Petétot, J. M.-C., Somerville, C., and Poirier, Y. (2002). Identification and characterization of the *Arabidopsis* PHO1 gene involved in phosphate loading to the xylem. *Plant Cell* 14, 889–902. doi: 10.1105/tpc.000745

Han, G., Lu, C., Guo, J., Qiao, Z., Sui, N., Qiu, N., et al. (2020). C2H2 Zinc finger proteins: master regulators of abiotic stress responses in plants. *Front. Plant Sci.* 11:115. doi: 10.3389/fpls.2020.00115

Hartung, W., Wilkinson, S., and Davies, W. J. (1998). Factors that regulate abscisic acid concentrations at the primary site of action at the guard cell. *J. Exp. Bot.* 49, 361–367. doi: 10.1093/jexbot/49.suppl_1.361

Hauser, F., Li, Z., Waadt, R., and Schroeder, J. I. (2017). SnapShot: abscisic acid signaling. *Cell* 171:1708. doi: 10.1016/j.cell.2017.11.045

He, G.-H., Xu, J.-Y., Wang, Y.-X., Liu, J.-M., Li, P.-S., Chen, M., et al. (2016). Drought-responsive WRKY transcription factor genes TaWRKY1 and TaWRKY33 from wheat confer drought and/or heat resistance in *Arabidopsis*. *BMC Plant Biol.* 16:116. doi: 10.1186/s12870-016-0806-4

He, H., Oo, T. L., Huang, W., He, L.-F., and Gu, M. (2019). Nitric oxide acts as an antioxidant and inhibits programmed cell death induced by aluminum in the root tips of peanut (*Arachis hypogaea* L.). *Sci. Rep.* 9, 1–12.

He, H.-Y., He, L.-F., Gu, M.-H., and Li, X.-F. (2012). Nitric oxide improves aluminum tolerance by regulating hormonal equilibrium in the root apices of rye and wheat. *Plant Sci.* 183, 123–130. doi: 10.1016/j.plantsci.2011.07.012

Henson, I. E., Jensen, C. R., and Turner, N. C. (1989). Leaf gas exchange and water relations of lupins and wheat. III. Abscisic acid and drought-induced stomatal closure. *Funct. Plant Biol.* 16, 429–442. doi: 10.1071/pp9890429

Hetz, W., Hochholdinger, F., Schwall, M., and Feix, G. (1996). Isolation and characterization of rtcs, a maize mutant deficient in the formation of nodal roots. *Plant J.* 10, 845–857. doi: 10.1046/j.1365-313X.1996.10050845.x

Hieno, A., Naznin, H. A., Inaba-Hasegawa, K., Yokogawa, T., Hayami, N., Nomoto, M., et al. (2019). Transcriptome analysis and identification of a transcriptional regulatory network in the response to H2O2. *Plant Physiol.* 180, 1629–1646. doi: 10.1104/pp.18.01426

Hoekenga, O. A., Maron, L. G., Piñeros, M. A., Cançado, G. M. A., Shaff, J., Kobayashi, Y., et al. (2006). AtALMT1, which encodes a malate transporter, is identified as one of several genes critical for aluminum tolerance in Arabidopsis. *Proc. Natl. Acad. Sci. U. S. A.* 103, 9738–9743. doi: 10.1073/pnas.0602868103

Holbrook, N. M., Shashidhar, V. R., James, R. A., and Munns, R. (2002). Stomatal control in tomato with ABA-deficient roots: response of grafted plants to soil drying. *J. Exp. Bot.* 53, 1503–1514. doi: 10.1093/jexbot/53.373.1503

Hou, N., You, J., Pang, J., Xu, M., Chen, G., and Yang, Z. (2010). The accumulation and transport of abscisic acid insoybean (*Glycine max* L.) under aluminum stress. *Plant Soil* 330, 127–137. doi: 10.1007/s11104-009-0184-x

Hou, Q., Ufer, G., and Bartels, D. (2016). Lipid signalling in plant responses to abiotic stress. *Plant. Cell Environ.* 39, 1029–1048. doi: 10.1111/pce.12666

Hsieh, L.-C., Lin, S.-I., Shih, A. C.-C., Chen, J.-W., Lin, W.-Y., Tseng, C.-Y., et al. (2009). Uncovering small RNA-mediated responses to phosphate deficiency in *Arabidopsis* by deep sequencing. *Plant Physiol.* 151, 2120–2132. doi: 10.1104/pp.109.147280

Hu, B., Wang, W., Deng, K., Li, H., Zhang, Z., Zhang, L., et al. (2015). MicroRNA399 is involved in multiple nutrient starvation responses in rice. *Front. Plant Sci.* 6:188. doi: 10.3389/fpls.2015.00188

Hu, B., Zhu, C., Li, F., Tang, J., Wang, Y., Lin, A., et al. (2011). Leaf tip necrosis1 plays a pivotal role in the regulation of multiple phosphate starvation responses in rice. *Plant Physiol.* 156, 1101–1115. doi: 10.1104/pp.110.170209

Hu, H., Dai, M., Yao, J., Xiao, B., Li, X., Zhang, Q., et al. (2006). Overexpressing a NAM, ATAF, and CUC (NAC) transcription factor enhances drought resistance and salt tolerance in rice. *Proc. Natl. Acad. Sci. U.S.A.* 103, 12987–12992. doi: 10.1073/pnas.0604882103

Huang, C. F., Yamaji, N., Chen, Z., and Ma, J. F. (2012). A tonoplast-localized half-size ABC transporter is required for internal detoxification of aluminum in rice. *Plant J.* 69, 857–867. doi: 10.1111/j.1365-313X.2011.04837.x

Huang, C. F., Yamaji, N., Mitani, N., Yano, M., Nagamura, Y., and Ma, J. F. (2009). A bacterial-type ABC transporter is involved in aluminum tolerance in rice. *Plant Cell* 21, 655–667. doi: 10.1105/tpc.108.064543

Huang, S., Gao, J., You, J., Liang, Y., Guan, K., Yan, S., et al. (2018). Identification of STOP1-like proteins associated with aluminum tolerance in sweet sorghum (*Sorghum bicolor* L.). *Front. Plant Sci.* 9:258. doi: 10.3389/fpls.2018.00258

Huang, W.-J., Oo, T. L., He, H.-Y., Wang, A.-Q., Zhan, J., Li, C.-Z., et al. (2014). Aluminum induces rapidly mitochondria-dependent programmed cell death in Al-sensitive peanut root tips. *Bot. Stud.* 55:67.

Hufnagel, B., de Sousa, S. M., Assis, L., Guimaraes, C. T., Leiser, W., Azevedo, G. C., et al. (2014). Duplicate and conquer: Multiple homologs of PHOSPHORUS-STARVATION TOLERANCE1 enhance phosphorus acquisition and sorghum performance on low-phosphorus soils. *Plant Physiol.* 166, 659–677. doi: 10.1104/pp.114.243949

Hufnagel, B., Marques, A., Soriano, A., Marquès, L., Divol, F., Doumas, P., et al. (2020). High-quality genome sequence of white lupin provides insight into soil exploration and seed quality. *Nat. Commun.* 11:492. doi: 10.1038/s41467-019-14197-9

Ischebeck, T., Seiler, S., and Heilmann, I. (2010). At the poles across kingdoms: phosphoinositides and polar tip growth. *Protoplasma* 240, 13–31. doi: 10.1007/s00709-009-0093-0

Ito, H., Kobayashi, Y., Yamamoto, Y. Y., and Koyama, H. (2019). Characterization of NtSTOP1-regulating genes in tobacco under aluminum stress. *Soil Sci. Plant Nutr.* 65, 251–258. doi: 10.1080/00380768.2019.1603064

Iuchi, S., Koyama, H., Iuchi, A., Kobayashi, Y., Kitabayashi, S., Kobayashi, Y., et al. (2007). Zinc finger protein STOP1 is critical for proton tolerance in *Arabidopsis* and coregulates a key gene in aluminum tolerance. *Proc. Natl. Acad. Sci. U.S.A.* 104, 9900–9905. doi: 10.1073/pnas.0700117104

Jiang, H.-X., Yang, L.-T., Qi, Y.-P., Lu, Y.-B., Huang, Z.-R., and Chen, L.-S. (2015). Root iTRAQ protein profile analysis of two *Citrus* species differing in aluminum-tolerance in response to long-term aluminum-toxicity. *BMC Genomics* 16:949. doi: 10.1186/s12864-015-2133-9

Jin, J. F., Wang, Z. Q., He, Q. Y., Wang, J. Y., Li, P. F., Xu, J. M., et al. (2020). Genome-wide identification and expression analysis of the NAC transcription factor family in tomato (*Solanum lycopersicum*) during aluminum stress. *BMC Genomics* 21:288. doi: 10.1186/s12864-020-6689-7

Jones, D. L., and Kochian, L. V. (1995). Aluminum inhibition of the inositol 1, 4, 5-trisphosphate signal transduction pathway in wheat roots: a role in aluminum toxicity? *Plant Cell* 7, 1913–1922. doi: 10.1105/tpc.7.11.1913

Jones, H. G., Sharp, C. S., and Higgs, K. H. (1987). Growth and water relations of wilty mutants of tomato (*Lycopersicon esculentum* Mill.). *J. Exp. Bot.* 38, 1848–1856. doi: 10.1093/jxb/38.11.1848

Jones, R. J., and Mansfield, T. A. (1970). Suppression of stomatal opening in leaves treated with abscisic acid. *J. Exp. Bot.* 21, 714–719. doi: 10.1093/jxb/21.3.714

Joshi, R., Wani, S. H., Singh, B., Bohra, A., Dar, Z. A., Lone, A. A., et al. (2016). Transcription factors and plants response to drought stress: current understanding and future directions. *Front. Plant Sci.* 7:1029. doi: 10.3389/fpls.2016.01029

Jung, J. K. H. M., and McCouch, S. R. M. (2013). Getting to the roots of it: genetic and hormonal control of root architecture. *Front. Plant Sci.* 4:186. doi: 10.3389/fpls.2013.00186

Kang, J., Hwang, J.-U., Lee, M., Kim, Y.-Y., Assmann, S. M., Martinoia, E., et al. (2010). PDR-type ABC transporter mediates cellular uptake of the phytohormone abscisic acid. *Proc. Natl. Acad. Sci. U.S.A.* 107, 2355–2360. doi: 10.1073/pnas.0909222107

Kanneganti, V., and Gupta, A. K. (2008). Wall associated kinases from plants—an overview. *Physiol. Mol. Biol. Plants* 14, 109–118. doi: 10.1007/s12298-008-0010-6

Kanneganti, V., and Gupta, A. K. (2011). RNAi mediated silencing of a wall associated kinase, OsiWAK1 in *Oryza sativa* results in impaired root development and sterility due to anther indehiscence. *Physiol. Mol. Biol. Plants* 17, 65–77. doi: 10.1007/s12298-011-0050-1

Kasai, M., Sasaki, M., Tanakamaru, S., Yamamoto, Y., and Matsumoto, H. (1993). Possible involvement of abscisic acid in increases in activities of two vacuolar H+-pumps in barley roots under aluminum stress. *Plant Cell Physiol.* 34, 1335–1338.

Kasai, M., Sasaki, M., Yamashita, K., Yamamoto, Y., and Matsumoto, H. (1995). "Increase of ATP-dependent H+ pump activity of tonoplast of barley roots by aluminium stress: possible involvement of abscisic acid for the regulation," in *Plant-Soil Interactions at Low pH: Principles and Management*, eds R. A. Date, N. J. Grundon, G. E. Rayment, and M. E. Probert (Dordrecht: Springer), 341–344. doi: 10.1007/978-94-011-0221-6_48

Kaur, R., Singh, K., and Singh, J. (2013). A root-specific wall-associated kinase gene, HvWAK1, regulates root growth and is highly divergent in barley and other cereals. *Funct. Integr. Genomics* 13, 167–177. doi: 10.1007/s10142-013-0310-y

Keerthisinghe, G., Hocking, P. J., Ryan, P. R., and Delhaize, E. (1998). Effect of phosphorus supply on the formation and function of proteoid roots of white lupin (*Lupinus albus* L.). *Plant. Cell Environ.* 21, 467–478. doi: 10.1046/j.1365-3040.1998.00300.x

Kobayashi, Y., Kobayashi, Y., Sugimoto, M., Lakshmanan, V., Iuchi, S., Kobayashi, M., et al. (2013a). Characterization of the complex regulation of AtALMT1 expression in response to phytohormones and other inducers. *Plant Physiol.* 162, 732–740. doi: 10.1104/pp.113.218065

Kobayashi, Y., Kobayashi, Y., Watanabe, T., Shaff, J. E., Ohta, H., Kochian, L. V., et al. (2013b). Molecular and physiological analysis of Al3+ and H+ rhizotoxicities at moderately acidic conditions. *Plant Physiol.* 163, 180–192. doi: 10.1104/pp.113.222893

Kochian, L. V. (1995). Cellular mechanisms of aluminum toxicity and resistance in plants. *Annu. Rev. Plant Biol.* 46, 237–260. doi: 10.1146/annurev.pp.46.060195.001321

Kochian, L. V., Hoekenga, O. A., and Pineros, M. A. (2004). How do crop plants tolerate acid soils? Mechanisms of aluminum tolerance and phosphorous efficiency. *Annu. Rev. Plant Biol.* 55, 459–493. doi: 10.1146/annurev.arplant.55.031903.141655

Kochian, L. V., Piñeros, M. A., Liu, J., and Magalhaes, J. V. (2015). Plant adaptation to acid soils: the molecular basis for crop aluminum resistance. *Annu. Rev. Plant Biol.* 66, 571–598. doi: 10.1146/annurev-arplant-043014-114822

Kollmeier, M., Felle, H. H., and Horst, W. J. (2000). Genotypical differences in aluminum resistance of maize are expressed in the distal part of the transition zone. Is reduced basipetal auxin flow involved in inhibition of root elongation by aluminum? *Plant Physiol.* 122, 945–956. doi: 10.1104/pp.122.3.945

Kumar, M., Chauhan, A. S., Yusuf, M. A., Sanyal, I., and Chauhan, P. S. (2019). Transcriptome sequencing of chickpea (Cicer arietinum l.) genotypes for identification of drought-responsive genes under drought stress condition. *Plant Mol. Biol. Rep.* 37, 186–203. doi: 10.1007/s11105-019-01147-4

Kundu, A., Das, S., Basu, S., Kobayashi, Y., Kobayashi, Y., Koyama, H., et al. (2019). GhSTOP1, a C2H2 type zinc finger transcription factor is essential for Aluminum and proton stress tolerance and lateral root initiation in cotton. *Plant Biol.* 21, 35–44. doi: 10.1111/plb.12895

Kuromori, T., Miyaji, T., Yabuuchi, H., Shimizu, H., Sugimoto, E., Kamiya, A., et al. (2010). ABC transporter AtABCG25 is involved in abscisic acid transport and responses. *Proc. Natl. Acad. Sci. U.S.A.* 107, 2361–2366. doi: 10.1073/pnas.0912516107

Kuromori, T., Mizoi, J., Umezawa, T., Yamaguchi-Shinozaki, K., and Shinozaki, K. (2014). Drought stress signaling network. *Mol. Biol.* 2, 383–409. doi: 10.1007/978-1-4614-7570-5_7

Kusunoki, K., Nakano, Y., Tanaka, K., Sakata, Y., Koyama, H., and Kobayashi, Y. (2017). Transcriptomic variation among six *Arabidopsis thaliana* accessions identified several novel genes controlling aluminium tolerance. *Plant. Cell Environ.* 40, 249–263. doi: 10.1111/pce.12866

Larsen, P. B., Geisler, M. J. B., Jones, C. A., Williams, K. M., and Cancel, J. D. (2005). ALS3 encodes a phloem-localized ABC transporter-like protein that is required for aluminum tolerance in *Arabidopsis*. *Plant J.* 41, 353–363. doi: 10.1111/j.1365-313X.2004.02306.x

Lee, D.-K., Chung, P. J., Jeong, J. S., Jang, G., Bang, S. W., Jung, H., et al. (2017). The rice OsNAC 6 transcription factor orchestrates multiple molecular mechanisms involving root structural adaptions and nicotianamine biosynthesis for drought tolerance. *Plant Biotechnol. J.* 15, 754–764. doi: 10.1111/pbi.12673

Lee, D.-K., Jung, H., Jang, G., Jeong, J. S., Kim, Y. S., Ha, S.-H., et al. (2016). Overexpression of the OsERF71 transcription factor alters rice root structure and drought resistance. *Plant Physiol.* 172, 575–588. doi: 10.1104/pp.16.00379

Lee, H. W., Kim, N. Y., Lee, D. J., and Kim, J. (2009). LBD18/ASL20 regulates lateral root formation in combination with LBD16/ASL18 downstream of ARF7 and ARF19 in *Arabidopsis*. *Plant Physiol.* 151, 1377–1389. doi: 10.1104/pp.109.143685

Leng, P., and Zhao, J. (2019). Transcription factors as molecular switches to regulate drought adaptation in maize. *Theor. Appl. Genet.* 133, 1455–1465. doi: 10.1007/s00122-019-03494-y

Li, C. X., Yan, J. Y., Ren, J. Y., Sun, L., Xu, C., Li, G. X., et al. (2019). A WRKY transcription factor confers aluminum tolerance via regulation of cell wall modifying genes. *J. Integr. Plant Biol.* 62, 1176–1192. doi: 10.1111/jipb.12888

Li, G. Z., Wang, Z. Q., Yokosho, K., Ding, B., Fan, W., Gong, Q. Q., et al. (2018). Transcription factor WRKY22 promotes aluminum tolerance via activation of OsFRDL4 expression and enhancement of citrate secretion in rice (*Oryza sativa*). *New Phytol.* 219, 149–162. doi: 10.1111/nph.15143

Li, H., Han, X., Liu, X., Zhou, M., Ren, W., Zhao, B., et al. (2019). A leucine-rich repeat-receptor-like kinase gene SbER2–1 from sorghum (*Sorghum bicolor* L.) confers drought tolerance in maize. *BMC Genomics* 20:737. doi: 10.1186/s12864-019-6143-x

Li, Z., Gao, Q., Liu, Y., He, C., Zhang, X., and Zhang, J. (2011). Overexpression of transcription factor ZmPTF1 improves low phosphate tolerance of maize by regulating carbon metabolism and root growth. *Planta* 233, 1129–1143. doi: 10.1007/s00425-011-1368-1

Li, Z., Liu, C., Zhang, Y., Wang, B., Ran, Q., Zhang, J., et al. (2019). The bHLH family member ZmPTF1 regulates drought tolerance in maize by promoting root development and abscisic acid synthesis. *J. Exp. Bot.* 70, 5471–5486. doi: 10.1093/jxb/erz307

Linzhou, H., Yasir, T. A., Phillips, A. L., and Hu, Y.-G. (2013). Isolation and characterization of ERECTA genes and their expression patterns in common wheat (*Triticum aestivum* L.). *Aust. J. Crop Sci.* 7, 381–390.

Liu, G., Gao, S., Tian, H., Wu, W., Robert, H. S., and Ding, Z. (2016). Local transcriptional control of YUCCA regulates auxin promoted root-growth inhibition in response to aluminium stress in *Arabidopsis*. *PLoS Genet.* 12:e1006360. doi: 10.1371/journal.pgen.1006360

Liu, J., Magalhaes, J. V., Shaff, J., and Kochian, L. V. (2009). Aluminum-activated citrate and malate transporters from the MATE and ALMT families function independently to confer *Arabidopsis aluminum* tolerance. *Plant J.* 57, 389–399. doi: 10.1111/j.1365-313X.2008.03696.x

López-Bucio, J., Cruz-Ramírez, A., and Herrera-Estrella, L. (2003). The role of nutrient availability in regulating root architecture. *Curr. Opin. Plant Biol.* 6, 280–287. doi: 10.1016/S1369-5266(03)00035-9

López-Bucio, J. S., Salmerón-Barrera, G. J., Ravelo-Ortega, G., Raya-González, J., León, P., de la Cruz, H. R., et al. (2019). Mitogen-activated protein kinase 6 integrates phosphate and iron responses for indeterminate root growth in *Arabidopsis thaliana*. *Planta* 250, 1177–1189. doi: 10.1007/s00425-019-03212-4

Lou, H. Q., Fan, W., Jin, J. F., Xu, J. M., Chen, W. W., Yang, J. L., et al. (2020). A NAC-type transcription factor confers aluminium resistance by regulating cell wall-associated receptor kinase 1 and cell wall pectin. *Plant Cell Environ.* 43, 463–478. doi: 10.1111/pce.13676

Loveys, B. R., and Kriedemann, P. E. (1974). Internal control of stomatal physiology and photosynthesis. I. Stomatal regulation and associated changes in endogenous levels of abscisic and phaseic acids. *Funct. Plant Biol.* 1, 407–415. doi: 10.1071/pp9740407

Lv, Q., Zhong, Y., Wang, Y., Wang, Z., Zhang, L., Shi, J., et al. (2014). SPX4 negatively regulates phosphate signaling and homeostasis through its interaction with PHR2 in rice. *Plant Cell* 26, 1586–1597. doi: 10.1105/tpc.114.123208

Lynch, J. P. (2011). Root phenes for enhanced soil exploration and phosphorus acquisition: tools for future crops. *Plant Physiol.* 156, 1041–1049. doi: 10.1104/pp.111.175414

Ma, J. F., Ryan, P. R., and Delhaize, E. (2001). Aluminium tolerance in plants and the complexing role of organic acids. *Trends Plant Sci.* 6, 273–278. doi: 10.1016/s1360-1385(01)01961-6

Ma, Y., Szostkiewicz, I., Korte, A., Moes, D., Yang, Y., Christmann, A., et al. (2009). Regulators of PP2C phosphatase activity function as abscisic acid sensors. *Science* 324, 1064–1068.

Magalhaes, J. V., Liu, J., Guimarães, C. T., Lana, U. G. P., Alves, V. M. C., Wang, Y. H., et al. (2007). A gene in the multidrug and toxic compound extrusion (MATE) family confers aluminum tolerance in sorghum. *Nat. Genet.* 39, 1156–1161. doi: 10.1038/ng2074

Maierhofer, T., Diekmann, M., Offenborn, J. N., Lind, C., Bauer, H., Hashimoto, K., et al. (2014). Site-and kinase-specific phosphorylation-mediated activation of SLAC1, a guard cell anion channel stimulated by abscisic acid. *Sci. Signal.* 7:ra86. doi: 10.1126/scisignal.2005703

Marinho, J. P., Kanamori, N., Ferreira, L. C., Fuganti-Pagliarini, R., Carvalho, J., de, F. C., et al. (2016). Characterization of molecular and physiological responses under water deficit of genetically modified soybean plants overexpressing the

AtAREB1 transcription factor. *Plant Mol. Biol. Report.* 34, 410–426. doi: 10.1007/s11105-015-0928-0

Marschner, H. (1995). Adaptation of plants to adverse chemical soil conditions. *Marschners Miner. Nutr. High. Plants* 2012, 409–472. doi: 10.1016/b978-0-12-384905-2.00017-0

Martín, A. C., Del Pozo, J. C., Iglesias, J., Rubio, V., Solano, R., De La Peña, A., et al. (2000). Influence of cytokinins on the expression of phosphate starvation responsive genes in *Arabidopsis*. *Plant J.* 24, 559–567. doi: 10.1046/j.1365-313X.2000.00893.x

Masle, J., Gilmore, S. R., and Farquhar, G. D. (2005). The ERECTA gene regulates plant transpiration efficiency in *Arabidopsis*. *Nature* 436, 866–870. doi: 10.1038/nature03835

Meijer, H. J. G., and Munnik, T. (2003). Phospholipid-based signaling in plants. *Annu. Rev. Plant Biol.* 54, 265–306.

Melo, J. O., Martins, L. G. C., Barros, B. A., Pimenta, M. R., Lana, U. G. P., Duarte, C. E. M., et al. (2019). Repeat variants for the SbMATE transporter protect sorghum roots from aluminum toxicity by transcriptional interplay in cis and trans. *Proc. Natl. Acad. Sci. U.S.A.* 116, 313–318. doi: 10.1073/pnas.1808400115

Mendes, F. F., Guimarães, L. J. M., Souza, J. C., Guimarães, P. E. O., Magalhaes, J. V., Garcia, A. A. F., et al. (2014). Genetic architecture of phosphorus use efficiency in tropical maize cultivated in a low-P soil. *Crop Sci.* 54, 1530–1538. doi: 10.2135/cropsci2013.11.0755

Miller, G. A. D., Suzuki, N., Ciftci-Yilmaz, S., and Mittler, R. O. N. (2010). Reactive oxygen species homeostasis and signalling during drought and salinity stresses. *Plant. Cell Environ.* 33, 453–467. doi: 10.1111/j.1365-3040.2009.02041.x

Mishra, D., Shekhar, S., Singh, D., Chakraborty, S., and Chakraborty, N. (2018). "Heat shock proteins and abiotic stress tolerance in plants," in *Regulation of Heat Shock Protein Responses*, eds A. Asea and P. Kaur (Cham: Springer), 41–69. doi: 10.1007/978-3-319-74715-6_3

Mittler, R. (2017). ROS are good. *Trends Plant Sci.* 22, 11–19. doi: 10.1016/j.tplants.2016.08.002

Miura, K., Lee, J., Gong, Q., Ma, S., Jin, J. B., Yoo, C. Y., et al. (2011). SIZ1 Regulation of phosphate starvation-induced root architecture remodeling involves the control of auxin accumulation. *Plant Physiol.* 155, 1000–1012. doi: 10.1104/pp.110.165191

Mora-Macías, J., Ojeda-Rivera, J. O., Gutiérrez-Alanís, D., Yong-Villalobos, L., Oropeza-Aburto, A., Raya-González, J., et al. (2017). Malate-dependent Fe accumulation is a critical checkpoint in the root developmental response to low phosphate. *Proc. Natl. Acad. Sci. U.S.A.* 114, E3563–E3572. doi: 10.1073/pnas.1701952114

Müller, J., Toev, T., Heisters, M., Teller, J., Moore, K. L., Hause, G., et al. (2015). Iron-dependent callose deposition adjusts root meristem maintenance to phosphate availability. *Dev. Cell* 33, 216–230. doi: 10.1016/j.devcel.2015.02.007

Munemasa, S., Hauser, F., Park, J., Waadt, R., Brandt, B., and Schroeder, J. I. (2015). Mechanisms of abscisic acid-mediated control of stomatal aperture. *Curr. Opin. Plant Biol.* 28, 154–162. doi: 10.1016/j.pbi.2015.10.010

Nakashima, K., Takasaki, H., Mizoi, J., Shinozaki, K., and Yamaguchi-Shinozaki, K. (2012). NAC transcription factors in plant abiotic stress responses. *Biochim. Biophys. Acta Gene Regul. Mech.* 1819, 97–103. doi: 10.1016/j.bbagrm.2011.10.005

Nakashima, K., Yamaguchi-Shinozaki, K., and Shinozaki, K. (2014). The transcriptional regulatory network in the drought response and its crosstalk in abiotic stress responses including drought, cold, and heat. *Front. Plant Sci.* 5:170. doi: 10.3389/fpls.2014.00170

Neumann, G., Massonneau, A., Langlade, N., Dinkelaker, B., Hengeler, C., Römheld, V., et al. (2000). Physiological aspects of cluster root function and development in phosphorus-deficient white lupin (*Lupinus albus* L.). *Ann. Bot.* 85, 909–919. doi: 10.1006/anbo.2000.1135

Nishimura, N., Hitomi, K., Arvai, A. S., Rambo, R. P., Hitomi, C., Cutler, S. R., et al. (2009). Structural mechanism of abscisic acid binding and signaling by dimeric PYR1. *Science* 326, 1373–1379. doi: 10.1126/science.1181829

Oh, J. E., Kwon, Y., Kim, J. H., Noh, H., Hong, S. W., and Lee, H. (2011). A dual role for MYB60 in stomatal regulation and root growth of *Arabidopsis thaliana* under drought stress. *Plant Mol. Biol.* 77, 91–103. doi: 10.1007/s11103-011-9796-7

Ohyama, Y., Ito, H., Kobayashi, Y., Ikka, T., Morita, A., Kobayashi, M., et al. (2013). Characterization of AtSTOP1 orthologous genes in tobacco and other plant species. *Plant Physiol.* 162, 1937–1946. doi: 10.1104/pp.113.218958

Ouyang, X., Hong, X., Zhao, X., Zhang, W., He, X., Ma, W., et al. (2016). Knock out of the PHOSPHATE 2 gene TaPHO2-A1 improves phosphorus uptake and grain yield under low phosphorus conditions in common wheat. *Sci. Rep.* 6:29850. doi: 10.1038/srep29850

Overvoorde, P., Fukaki, H., and Beeckman, T. (2010). Auxin control of root development. *Cold Spring Harb. Perspect. Biol.* 2:a001537.

Park, S.-Y., Fung, P., Nishimura, N., Jensen, D. R., Fujii, H., Zhao, Y., et al. (2009). Abscisic acid inhibits type 2C protein phosphatases via the PYR/PYL family of START proteins. *Science* 324, 1068–1071.

Peñaloza, E., Corcuera, L. J., and Martinez, J. (2002). Spatial and temporal variation in citrate and malate exudation and tissue concentration as affected by P stress in roots of white lupin. *Plant Soil* 241, 209–221. doi: 10.1023/A:1016148222687

Peñaloza, E., Muñoz, G., Salvo-Garrido, H., Silva, H., and Corcuera, L. J. (2005). Phosphate deficiency regulates phosphoenolpyruvate carboxylase expression in proteoid root clusters of white lupin. *J. Exp. Bot.* 56, 145–153. doi: 10.1093/jxb/eri008

Petersson, S. V., Johansson, A. I., Kowalczyk, M., Makoveychuk, A., Wang, J. Y., Moritz, T., et al. (2009). An auxin gradient and maximum in the Arabidopsis root apex shown by high-resolution cell-specific analysis of IAA distribution and synthesis. *Plant Cell* 21, 1659–1668. doi: 10.1105/tpc.109.066480

Poirier, Y., Thoma, S., Somerville, C., and Schiefelbein, J. (1991). A mutant of *Arabidopsis* deficient in xylem loading of phosphate. *Plant Physiol.* 97, 1087–1093. doi: 10.1104/pp.97.3.1087

Poot-Poot, W., and Teresa Hernandez-Sotomayor, S. M. (2011). Aluminum stress and its role in the phospholipid signaling pathway in plants and possible biotechnological applications. *IUBMB Life* 63, 864–872. doi: 10.1002/iub.550

Pougach, K., Voet, A., Kondrashov, F. A., Voordeckers, K., Christiaens, J. F., Baying, B., et al. (2014). Duplication of a promiscuous transcription factor drives the emergence of a new regulatory network. *Nat. Commun.* 5, 1–12.

Puga, M. I., Mateos, I., Charukesi, R., Wang, Z., Franco-Zorrilla, J. M., De Lorenzo, L., et al. (2014). SPX1 is a phosphate-dependent inhibitor of Phosphate Starvation response 1 in Arabidopsis. *Proc. Natl. Acad. Sci. U.S.A.* 111, 14947–14952. doi: 10.1073/pnas.1404654111

Qiu, Y., and Yu, D. (2009). Over-expression of the stress-induced OsWRKY45 enhances disease resistance and drought tolerance in *Arabidopsis*. *Environ. Exp. Bot.* 65, 35–47. doi: 10.1016/j.envexpbot.2008.07.002

Rabara, R. C., Tripathi, P., and Rushton, P. J. (2014). The potential of transcription factor-based genetic engineering in improving crop tolerance to drought. *Omi. A J. Integr. Biol.* 18, 601–614. doi: 10.1089/omi.2013.0177

Ramírez, M., Flores-Pacheco, G., Reyes, J. L., Álvarez, A. L., Drevon, J. J., Girard, L., et al. (2013). Two common bean genotypes with contrasting response to phosphorus deficiency show variations in the microRNA 399-mediated PvPHO2 regulation within the PvPHR1 signaling pathway. *Int. J. Mol. Sci.* 14, 8328–8344. doi: 10.3390/ijms14048328

Ren, X., Chen, Z., Liu, Y., Zhang, H., Zhang, M., Liu, Q., et al. (2010). ABO3, a WRKY transcription factor, mediates plant responses to abscisic acid and drought tolerance in *Arabidopsis*. *Plant J.* 63, 417–429. doi: 10.1111/j.1365-313X.2010.04248.x

Reyna-Llorens, I., Corrales, I., Poschenrieder, C., Barcelo, J., and Cruz-Ortega, R. (2015). Both aluminum and ABA induce the expression of an ABC-like transporter gene (FeALS3) in the Al-tolerant species *Fagopyrum esculentum*. *Environ. Exp. Bot.* 111, 74–82. doi: 10.1016/j.envexpbot.2014.11.005

Rodríguez-Leal, D., Lemmon, Z. H., Man, J., Bartlett, M. E., and Lippman, Z. B. (2017). Engineering quantitative trait variation for crop improvement by genome editing. *Cell* 171, 470–480. doi: 10.1016/j.cell.2017.08.030

Rubio, V., Linhares, F., Solano, R., Martín, A. C., Iglesias, J., Leyva, A., et al. (2001). A conserved MYB transcription factor involved in phosphate starvation signaling both in vascular plants and in unicellular algae. *Genes Dev.* 15, 2122–2133. doi: 10.1101/gad.204401

Rushton, D. L., Tripathi, P., Rabara, R. C., Lin, J., Ringler, P., Boken, A. K., et al. (2012). WRKY transcription factors: Key components in abscisic acid signalling. *Plant Biotechnol. J.* 10, 2–11. doi: 10.1111/j.1467-7652.2011.00634.x

Ryan, P. R., Delhaize, E., and Jones, D. L. (2001). Function and mechanism of organic anion exudation from plant roots. *Annu. Rev. Plant Biol.* 52, 527–560.

Ryan, P. R., Ditomaso, J. M., and Kochian, L. V. (1993). Aluminium toxicity in roots: an investigation of spatial sensitivity and the role of the root cap. *J. Exp. Bot.* 44, 437–446. doi: 10.1093/jxb/44.2.437

Saab, I. N., Sharp, R. E., Pritchard, J., and Voetberg, G. S. (1990). Increased endogenous abscisic acid maintains primary root growth and inhibits shoot

growth of maize seedlings at low water potentials. *Plant Physiol.* 93, 1329–1336. doi: 10.1104/pp.93.4.1329

Sadhukhan, A., Enomoto, T., Kobayashi, Y., Watanabe, T., Iuchi, S., Kobayashi, M., et al. (2019). Sensitive to Proton Rhizotoxicity1 regulates salt and drought tolerance of Arabidopsis thaliana through transcriptional regulation of CIPK23. *Plant Cell Physiol.* 60, 2113–2126. doi: 10.1093/pcp/pcz120

Salvi, S., Giuliani, S., Ricciolini, C., Carraro, N., Maccaferri, M., Presterl, T., et al. (2016). Two major quantitative trait loci controlling the number of seminal roots in maize co-map with the root developmental genes rtcs and rum1. *J. Exp. Bot.* 67, 1149–1159. doi: 10.1093/jxb/erw011

Salvi, S., Sponza, G., Morgante, M., Tomes, D., Niu, X., Fengler, K. A., et al. (2007). Conserved noncoding genomic sequences associated with a flowering-time quantitative trait locus in maize. *Proc. Natl. Acad. Sci. U.S.A.* 104, 11376–11381. doi: 10.1073/pnas.0704145104

Sánchez-Calderón, L., López-Bucio, J., Chacón-López, A., Cruz-Ramírez, A., Nieto-Jacobo, F., Dubrovsky, J. G., et al. (2005). Phosphate starvation induces a determinate developmental program in the roots of *Arabidopsis thaliana*. *Plant Cell Physiol.* 46, 174–184. doi: 10.1093/pcp/pci011

Santiago, J., Dupeux, F., Round, A., Antoni, R., Park, S.-Y., Jamin, M., et al. (2009). The abscisic acid receptor PYR1 in complex with abscisic acid. *Nature* 462, 665–668. doi: 10.1038/nature08591

Sasaki, T., Yamamoto, Y., Ezaki, B., Katsuhara, M., Ahn, S. J., Ryan, P. R., et al. (2004). A wheat gene encoding an aluminum-activated malate transporter. *Plant J.* 37, 645–653. doi: 10.1111/j.1365-313X.2003.01991.x

Sawaki, Y., Iuchi, S., Kobayashi, Y., Kobayashi, Y., Ikka, T., Sakurai, N., et al. (2009). Stop1 regulates multiple genes that protect arabidopsis from proton and aluminum toxicities. *Plant Physiol.* 150, 281–294. doi: 10.1104/pp.108.134700

Sawaki, Y., Kobayashi, Y., Kihara-Doi, T., Nishikubo, N., Kawazu, T., Kobayashi, M., et al. (2014). Identification of a STOP1-like protein in Eucalyptus that regulates transcription of Al tolerance genes. *Plant Sci.* 223, 8–15. doi: 10.1016/j.plantsci.2014.02.011

Sbabou, L., Bucciarelli, B., Miller, S., Liu, J., Berhada, F., Filali-Maltouf, A., et al. (2010). Molecular analysis of SCARECROW genes expressed in white lupin cluster roots. *J. Exp. Bot.* 61, 1351–1363. doi: 10.1093/jxb/erp400

Scarpella, E., Simons, E. J., and Meijer, A. H. (2005). Multiple regulatory elements contribute to the vascular-specific expression of the rice HD-zip gene Oshox1 in *Arabidopsis*. *Plant Cell Physiol.* 46, 1400–1410. doi: 10.1093/pcp/pci153

Schmidt, R. R., Weits, D. A., Feulner, C. F. J., and van Dongen, J. T. (2018). Oxygen sensing and integrative stress signaling in plants. *Plant Physiol.* 176, 1131–1142. doi: 10.1104/pp.17.01394

Shahid, M., Pourrut, B., Dumat, C., Nadeem, M., Aslam, M., and Pinelli, E. (2014). "Heavy-metal-induced reactive oxygen species: phytotoxicity and physicochemical changes in plants," in *Reviews of Environmental Contamination and Toxicology*, Vol. 232, ed. D. Whitacre (Cham: Springer), 1–44. doi: 10.1007/978-3-319-06746-9_1

Shang, Y., Yan, L., Liu, Z. Q., Cao, Z., Mei, C., Xin, Q., et al. (2010). The Mg-chelatase H subunit of Arabidopsis antagonizes a group of WRKY transcription repressors to relieve ABA-responsive genes of inhibition. *Plant Cell* 22, 1909–1935. doi: 10.1105/tpc.110.073874

Sharma, P., Jha, A. B., Dubey, R. S., and Pessarakli, M. (2012). Reactive oxygen species, oxidative damage, and antioxidative defense mechanism in plants under stressful conditions. *J. Bot.* 2012:217037.

Sharp, R. E., and Davies, W. J. (1989). "Regulation of growth and development of plants growing with a restricted supply of water," in *Plants Under Stress: Biochemistry, Physiology and Ecology and Their Application to Plant Improvement Society for Experimental Biology Seminar Series*, eds H. G. Jones, T. J. Flowers, and M. B. E. Jones (Cambridge: Cambridge University Press), 71–94. doi: 10.1017/CBO9780511661587.006

Sharp, R. E., Wu, Y., Voetberg, G. S., Saab, I. N., and LeNoble, M. E. (1994). Confirmation that abscisic acid accumulation is required for maize primary root elongation at low water potentials. *J. Exp. Bot.* 45, 1743–1751. doi: 10.1093/jxb/45.special_issue.1743

Shen, H., Hou, N., Schlicht, M., Wan, Y., Mancuso, S., and Baluska, F. (2008). Aluminium toxicity targets PIN2 in Arabidopsis root apices: effects on PIN2 endocytosis, vesicular recycling, and polar auxin transport. *Chin. Sci. Bull.* 53:2480. doi: 10.1007/s11434-008-0332-3

Shen, H., Ligaba, A., Yamaguchi, M., Osawa, H., Shibata, K., Yan, X., et al. (2004). Effect of K-252a and abscisic acid on the efflux of citrate from soybean roots. *J. Exp. Bot.* 55, 663–671. doi: 10.1093/jxb/erh058

Shin, H., Shin, H.-S., Dewbre, G. R., and Harrison, M. J. (2004). Phosphate transport in *Arabidopsis*: Pht1; 1 and Pht1; 4 play a major role in phosphate acquisition from both low-and high-phosphate environments. *Plant J.* 39, 629–642.

Shin, R., Burch, A. Y., Huppert, K. A., Tiwari, S. B., Murphy, A. S., Guilfoyle, T. J., et al. (2007). The Arabidopsis transcription factor MYB77 modulates auxin signal transduction. *Plant Cell* 19, 2440–2453. doi: 10.1105/tpc.107.050963

Singh, D., and Laxmi, A. (2015). Transcriptional regulation of drought response: a tortuous network of transcriptional factors. *Front. Plant Sci.* 6:895. doi: 10.3389/fpls.2015.00895

Sivaguru, M., Ezaki, B., He, Z. H., Tong, H., Osawa, H., Baluška, F., et al. (2003). Aluminum-induced gene expression and protein localization of a cell wall-associated receptor kinase in *Arabidopsis*. *Plant Physiol.* 132, 2256–2266. doi: 10.1104/pp.103.022129

Sivaguru, M., Liu, J., and Kochian, L. V. (2013). Targeted expression of Sb MATE in the root distal transition zone is responsible for sorghum aluminum resistance. *Plant J.* 76, 297–307.

Skubacz, A., Daszkowska-Golec, A., and Szarejko, I. (2016). The role and regulation of ABI5 (ABA-Insensitive 5) in plant development, abiotic stress responses and phytohormone crosstalk. *Front. Plant Sci.* 7:1884. doi: 10.3389/fpls.2016.01884

Soyk, S., Lemmon, Z. H., Oved, M., Fisher, J., Liberatore, K. L., Park, S. J., et al. (2017). Bypassing negative epistasis on yield in tomato imposed by a domestication gene. *Cell* 169, 1142–1155. doi: 10.1016/j.cell.2017.04.032

Spollen, W. G., LeNoble, M. E., Samuels, T. D., Bernstein, N., and Sharp, R. E. (2000). Abscisic acid accumulation maintains maize primary root elongation at low water potentials by restricting ethylene production. *Plant Physiol.* 122, 967–976. doi: 10.1104/pp.122.3.967

Su, T., Xu, Q., Zhang, F. C., Chen, Y., Li, L. Q., Wu, W. H., et al. (2015). WRKY42 modulates phosphate homeostasis through regulating phosphate translocation and acquisition in *Arabidopsis*. *Plant Physiol.* 167, 1579–1591. doi: 10.1104/pp.114.253799

Sun, P., Tian, Q.-Y., Chen, J., and Zhang, W.-H. (2010). Aluminium-induced inhibition of root elongation in Arabidopsis is mediated by ethylene and auxin. *J. Exp. Bot.* 61, 347–356. doi: 10.1093/jxb/erp306

Sun, X., Wang, Y., and Sui, N. (2018). Transcriptional regulation of bHLH during plant response to stress. *Biochem. Biophys. Res. Commun.* 503, 397–401. doi: 10.1016/j.bbrc.2018.07.123

Suzuki, N., Rizhsky, L., Liang, H., Shuman, J., Shulaev, V., and Mittler, R. (2005). Enhanced tolerance to environmental stress in transgenic plants expressing the transcriptional coactivator multiprotein bridging factor 1c. *Plant Physiol.* 139, 1313–1322. doi: 10.1104/pp.105.070110

Takahashi, F., Suzuki, T., Osakabe, Y., Betsuyaku, S., Kondo, Y., Dohmae, N., et al. (2018). A small peptide modulates stomatal control via abscisic acid in long-distance signalling. *Nature* 556, 235–238. doi: 10.1038/s41586-018-0009-2

Taramino, G., Sauer, M., Stauffer, J. L., Multani, D., Niu, X., Sakai, H., et al. (2007). The maize (Zea mays L.) RTCS gene encodes a LOB domain protein that is a key regulator of embryonic seminal and post-embryonic shoot-borne root initiation. *Plant J.* 50, 649–659. doi: 10.1111/j.1365-313X.2007.03075.x

Thole, J. M., and Nielsen, E. (2008). Phosphoinositides in plants: novel functions in membrane trafficking. *Curr. Opin. Plant Biol.* 11, 620–631. doi: 10.1016/j.pbi.2008.10.010

Thompson, A. J., Mulholland, B. J., Jackson, A. C., McKee, J. M. T., Hilton, H. W., Symonds, R. C., et al. (2007). Regulation and manipulation of ABA biosynthesis in roots. *Plant. Cell Environ.* 30, 67–78. doi: 10.1111/j.1365-3040.2006.01606.x

Tokizawa, M., Kobayashi, Y., Saito, T., Kobayashi, M., Iuchi, S., Nomoto, M., et al. (2015). Sensitive to Proton Rhizotoxicity1, calmodulin binding transcription activator2, and other transcription factors are involved in Aluminum-Activated Malate Transporter1 expression. *Plant Physiol.* 167, 991–1003. doi: 10.1104/pp.114.256552

Tran, L. S. P., Nakashima, K., Sakuma, Y., Simpson, S. D., Fujita, Y., Maruyama, K., et al. (2004). Isolation and functional analysis of arabidopsis stress-inducible NAC transcription factors that bind to a drought-responsive cis-element in the early responsive to dehydration stress 1 promoter. *Plant Cell* 16, 2481–2498. doi: 10.1105/tpc.104.022699

Tsutsui, T., Yamaji, N., and Ma, J. F. (2011). Identification of a cis-acting element of ART1, a C2H2-type zinc-finger transcription factor for aluminum tolerance in rice. *Plant Physiol.* 156, 925–931. doi: 10.1104/pp.111.175802

Upadhyay, N., Kar, D., and Datta, S. (2020). A multidrug and toxic compound extrusion (MATE) transporter modulates auxin levels in root to regulate root development and promotes aluminium tolerance. *Plant. Cell Environ.* 43, 745–759. doi: 10.1111/pce.13658

Van Breusegem, F., and Dat, J. F. (2006). Reactive oxygen species in plant cell death. *Plant Physiol.* 141, 384–390.

Von Uexküll, H. R., and Mutert, E. (1995). Global extent, development and economic impact of acid soils. *Plant Soil* 171, 1–15. doi: 10.1007/bf00009558

Wang, H., Sun, R., Cao, Y., Pei, W., Sun, Y., Zhou, H., et al. (2015). OsSIZ1, a SUMO E3 ligase gene, is involved in the regulation of the responses to phosphate and nitrogen in rice. *Plant Cell Physiol.* 56, 2381–2395. doi: 10.1093/pcp/pcv162

Wang, H., Xu, Q., Kong, Y. H., Chen, Y., Duan, J. Y., Wu, W. H., et al. (2014). Arabidopsis WRKY45 transcription factor activates Phosphate transporter1;1 expression in response to phosphate starvation. *Plant Physiol.* 164, 2020–2029. doi: 10.1104/pp.113.235077

Wang, X., Wang, Z., Zheng, Z., Dong, J., Song, L., Sui, L., et al. (2019). Genetic dissection of Fe-Dependent signaling in root developmental responses to phosphate deficiency. *Plant Physiol.* 179, 300–316. doi: 10.1104/pp.18.00907

Wang, Y.-S., and Yang, Z.-M. (2005). Nitric oxide reduces aluminum toxicity by preventing oxidative stress in the roots of *Cassia tora* L. *Plant Cell Physiol.* 46, 1915–1923. doi: 10.1093/pcp/pci202

Waszczak, C., Carmody, M., and Kangasjärvi, J. (2018). Reactive oxygen species in plant signaling. *Annu. Rev. Plant Biol.* 69, 209–236.

Wilkinson, S. (1999). pH as a stress signal. *Plant Growth Regul.* 29, 87–99.

Wilkinson, S., and Davies, W. J. (1997). Xylem sap pH increase: a drought signal received at the apoplastic face of the guard cell that involves the suppression of saturable abscisic acid uptake by the epidermal symplast. *Plant Physiol.* 113, 559–573. doi: 10.1104/pp.113.2.559

Wiśniewska, J., Xu, J., Seifertová, D., Brewer, P. B., Ružička, K., Blilou, I., et al. (2006). Polar PIN localization directs auxin flow in plants. *Science* 312:883. doi: 10.1126/science.1121356

Wissuwa, M., Wegner, J., Ae, N., and Yano, M. (2002). Substitution mapping of Pup1: a major QTL increasing phosphorus uptake of rice from a phosphorus-deficient soil. *Theor. Appl. Genet.* 105, 890–897. doi: 10.1007/s00122-002-1051-9

Wright, S. T. C. (1980). The effect of plant growth regulator treatments on the levels of ethylene emanating from excised turgid and wilted wheat leaves. *Planta* 148, 381–388. doi: 10.1007/bf00388127

Wu, D., Shen, H., Yokawa, K., and Baluška, F. (2014). Alleviation of aluminium-induced cell rigidity by overexpression of OsPIN2 in rice roots. *J. Exp. Bot.* 65, 5305–5315. doi: 10.1093/jxb/eru292

Wu, D., Shen, H., Yokawa, K., and Baluška, F. (2015). Overexpressing OsPIN2 enhances aluminium internalization by elevating vesicular trafficking in rice root apex. *J. Exp. Bot.* 66, 6791–6801. doi: 10.1093/jxb/erv385

Wu, L., Sadhukhan, A., Kobayashi, Y., Ogo, N., Tokizawa, M., Agrahari, R. K., et al. (2019). Involvement of phosphatidylinositol metabolism in aluminum-induced malate secretion in *Arabidopsis*. *J. Exp. Bot.* 70, 3329–3342. doi: 10.1093/jxb/erz179

Wu, W., Lin, Y., Chen, Q., Peng, W., Peng, J., Tian, J., et al. (2018). Functional conservation and divergence of soybean GmSTOP1 members in proton and aluminum tolerance. *Front. Plant Sci.* 9:570. doi: 10.3389/fpls.2018.00570

Xia, J., Yamaji, N., Kasai, T., and Ma, J. F. (2010). Plasma membrane-localized transporter for aluminum in rice. *Proc. Natl. Acad. Sci. U.S.A.* 107, 18381–18385. doi: 10.1073/pnas.1004949107

Xia, J., Yamaji, N., and Ma, J. F. (2013). A plasma membrane-localized small peptide is involved in rice aluminum tolerance. *Plant J.* 76, 345–355. doi: 10.1111/tpj.12296

Xu, C., Tai, H., Saleem, M., Ludwig, Y., Majer, C., Berendzen, K. W., et al. (2015). Cooperative action of the paralogous maize lateral organ boundaries (LOB) domain proteins RTCS and RTCL in shoot-borne root formation. *New Phytol.* 207, 1123–1133. doi: 10.1111/nph.13420

Yamaji, N., Huang, C. F., Nagao, S., Yano, M., Sato, Y., Nagamura, Y., et al. (2009). A zinc finger transcription factor ART1 regulates multiple genes implicated in aluminum tolerance in rice. *Plant Cell* 21, 3339–3349. doi: 10.1105/tpc.109.070771

Yamamoto, Y., Kobayashi, Y., Devi, S. R., Rikiishi, S., and Matsumoto, H. (2002). Aluminum toxicity is associated with mitochondrial dysfunction and the production of reactive oxygen species in plant cells. *Plant Physiol.* 128, 63–72. doi: 10.1104/pp.010417

Yang, J. L., Li, Y. Y., Zhang, Y. J., Zhang, S. S., Wu, Y. R., Wu, P., et al. (2008). Cell wall polysaccharides are specifically involved in the exclusion of aluminum from the rice root apex. *Plant Physiol.* 146, 602–611. doi: 10.1104/pp.107.111989

Yang, L.-T., Chen, L.-S., Peng, H.-Y., Guo, P., Wang, P., and Ma, C.-L. (2012a). Organic acid metabolism in *Citrus grandis* leaves and roots is differently affected by nitric oxide and aluminum interactions. *Sci. Hortic.* 133, 40–46. doi: 10.1016/j.scienta.2011.10.011

Yang, L.-T., Qi, Y.-P., Chen, L.-S., Sang, W., Lin, X.-J., Wu, Y.-L., et al. (2012b). Nitric oxide protects sour pummelo (*Citrus grandis*) seedlings against aluminum-induced inhibition of growth and photosynthesis. *Environ. Exp. Bot.* 82, 1–13. doi: 10.1016/j.envexpbot.2012.03.004

Yang, Z., Chi, X., Guo, F., Jin, X., Luo, H., Hawar, A., et al. (2020a). SbWRKY30 enhances the drought tolerance of plants and regulates a drought stress-responsive gene, SbRD19, in sorghum. *J. Plant Physiol.* 246–247, 153142. doi: 10.1016/j.jplph.2020.153142

Yang, Z., Yang, J., Wang, Y., Wang, F., Mao, W., He, Q., et al. (2020b). PROTEIN PHOSPHATASE95 regulates phosphate homeostasis by affecting phosphate transporter trafficking in rice. *Plant Cell* 32, 740–757. doi: 10.1105/tpc.19.00685

Yang, Z.-B., Geng, X., He, C., Zhang, F., Wang, R., Horst, W. J., et al. (2014). TAA1-regulated local auxin biosynthesis in the root-apex transition zone mediates the aluminum-induced inhibition of root growth in *Arabidopsis*. *Plant Cell* 26, 2889–2904. doi: 10.1105/tpc.114.127993

Yao, Y., He, R. J., Xie, Q. L., Zhao, X. H., Deng, X. M., He, J. B., et al. (2017). ETHYLENE RESPONSE FACTOR 74 (ERF74) plays an essential role in controlling a respiratory burst oxidase homolog D (RbohD)-dependent mechanism in response to different stresses in *Arabidopsis*. *New Phytol.* 213, 1667–1681. doi: 10.1111/nph.14278

Yi, K., Wu, Z., Zhou, J., Du, L., Guo, L., Wu, Y., et al. (2005). OsPTF1, a novel transcription factor involved in tolerance to phosphate starvation in rice. *Plant Physiol.* 138, 2087–2096. doi: 10.1104/pp.105.063115

Yokosho, K., Yamaji, N., Fujii-Kashino, M., and Ma, J. F. (2016). Retrotransposon-mediated aluminum tolerance through enhanced expression of the citrate transporter OsFRDL4. *Plant Physiol.* 172, 2327–2336. doi: 10.1104/pp.16.01214

Yokosho, K., Yamaji, N., and Ma, J. F. (2011). An Al-inducible MATE gene is involved in external detoxification of Al in rice. *Plant J.* 68, 1061–1069. doi: 10.1111/j.1365-313X.2011.04757.x

Zhang, J., and Davies, W. J. (1989). Abscisic acid produced in dehydrating roots may enable the plant to measure the water status of the soil. *Plant. Cell Environ.* 12, 73–81. doi: 10.1111/j.1365-3040.1989.tb01918.x

Zhang, J., and Davies, W. J. (1990a). Changes in the concentration of ABA in xylem sap as a function of changing soil water status can account for changes in leaf conductance and growth. *Plant. Cell Environ.* 13, 277–285. doi: 10.1111/j.1365-3040.1990.tb01312.x

Zhang, J., and Davies, W. J. (1990b). Does ABA in the xylem control the rate of leaf growth in soil-dried maize and sunflower plants? *J. Exp. Bot.* 41, 1125–1132. doi: 10.1093/jxb/41.9.1125

Zhang, J., Schurr, U., and Davies, W. J. (1987). Control of stomatal behaviour by abscisic acid which apparently originates in the roots. *J. Exp. Bot.* 38, 1174–1181. doi: 10.1093/jxb/38.7.1174

Zhang, Y., Zhang, J., Guo, J., Zhou, F., Singh, S., Xu, X., et al. (2019). F-box protein RAE1 regulates the stability of the aluminum-resistance transcription factor STOP1 in Arabidopsis. *Proc. Natl. Acad. Sci. U.S.A.* 116, 319–327. doi: 10.1073/pnas.1814426116

Zhang, Z., Wang, H., Wang, X., and Bi, Y. (2011). Nitric oxide enhances aluminum tolerance by affecting cell wall polysaccharides in rice roots. *Plant Cell Rep.* 30:1701. doi: 10.1007/s00299-011-1078-y

Zhang, Z., Zheng, Y., Ham, B.-K., Chen, J., Yoshida, A., Kochian, L. V., et al. (2016). Vascular-mediated signalling involved in early phosphate stress response in plants. *Nat. Plants* 2, 1–9. doi: 10.1081/e-epcs-120010640

Zhang, Z., Zheng, Y., Ham, B.-K., Zhang, S., Fei, Z., and Lucas, W. J. (2019). Plant lncRNAs are enriched in and move systemically through the phloem in response to phosphate deficiency. *J. Integr. Plant Biol.* 61, 492–508. doi: 10.1111/jipb.12715

Zhao, Y., Xing, L., Wang, X., Hou, Y.-J., Gao, J., Wang, P., et al. (2014). The ABA receptor PYL8 promotes lateral root growth by enhancing MYB77-dependent transcription of auxin-responsive genes. *Sci. Signal.* 7, ra53—ra53.

Zhen, Y., Qi, J.-L., Wang, S.-S., Su, J., Xu, G.-H., Zhang, M.-S., et al. (2007). Comparative proteome analysis of differentially expressed proteins induced by Al toxicity in soybean. *Physiol. Plant* 131, 542–554. doi: 10.1111/j.1399-3054.2007.00979.x

Zheng, J., Yang, Z., Madgwick, P. J., Carmo-Silva, E., Parry, M. A. J., and Hu, Y.-G. (2015). TaER expression is associated with transpiration efficiency traits and yield in bread wheat. *PLoS One* 10:e0128415. doi: 10.1371/journal.pone.0128415

Zhu, J., Brown, K. M., and Lynch, J. P. (2010). Root cortical aerenchyma improves the drought tolerance of maize (Zea mays L.). *Plant Cell Environ.* 33, 740–749.

Zhu, X. F., Wan, J. X., Sun, Y., Shi, Y. Z., Braam, J., Li, G. X., et al. (2014). Xyloglucan endotransglucosylase-hydrolase17 interacts with xyloglucan endotransglucosylase-hydrolase31 to confer xyloglucan endotransglucosylase action and affect aluminum sensitivity in arabidopsis. *Plant Physiol.* 165, 1566–1574. doi: 10.1104/pp.114.243790

Conflict of Interest: The authors declare that the research was conducted in the absence of any commercial or financial relationships that could be construed as a potential conflict of interest.

Advantages of publishing in Frontiers

OPEN ACCESS
Articles are free to read for greatest visibility and readership

FAST PUBLICATION
Around 90 days from submission to decision

HIGH QUALITY PEER-REVIEW
Rigorous, collaborative, and constructive peer-review

TRANSPARENT PEER-REVIEW
Editors and reviewers acknowledged by name on published articles

Frontiers
Avenue du Tribunal-Fédéral 34
1005 Lausanne | Switzerland

Visit us: www.frontiersin.org
Contact us: frontiersin.org/about/contact

REPRODUCIBILITY OF RESEARCH
Support open data and methods to enhance research reproducibility

DIGITAL PUBLISHING
Articles designed for optimal readership across devices

FOLLOW US
@frontiersin

IMPACT METRICS
Advanced article metrics track visibility across digital media

EXTENSIVE PROMOTION
Marketing and promotion of impactful research

LOOP RESEARCH NETWORK
Our network increases your article's readership